Christoph Rapp

Hydraulics in Civil Engineering

A Course with Experiments and Open-Source-Codes

OPEN ACCESS

Springer

Hydraulics in Civil Engineering

Christoph Rapp

Hydraulics in Civil Engineering

A Course with Experiments and Open-Source-Codes

Springer

Christoph Rapp
Munich, Germany

ISBN 978-3-031-54859-8 ISBN 978-3-031-54860-4 (eBook)
https://doi.org/10.1007/978-3-031-54860-4

German Edition published by Springer Vieweg
Translation from the German language edition: “Hydraulik für Ingenieure und Naturwissenschaftler” by Christoph Rapp, © Springer Fachmedien Wiesbaden 2021. Published by Springer Vieweg. All Rights Reserved.

This Springer imprint is published by the registered company Springer Nature Switzerland AG
The registered company address is: Gewerbestrasse 11, 6330 Cham, Switzerland

Dedicated to the future generations confronted with increasingly severe water-related challenges. Being part of a demanding society, my concern is about what we leave behind for our loved ones. In this light, being called "Gagiua" by my daughters (the greatest dad on the planet) is the recognition that means everything to me.

Antonia and Carlotta, and naturally, my wife Julia, you are wonderful.

Preamble

This book is the result of nine years of teaching at the Technical University of Munich (Technische Universität München), eleven years of professional practice, including several lectureships at international universities. This book is based on a number of exercises, practical experiments and lectures by means of which I aim to clearly explain what are at times very complex hydromechanical relationships. In this vein, it is important that the reader is able to conceptualise a phenomenon in a similar way as a scientist would. In an article in the magazine *Hydrolink* of the IAHR (International Association for Hydro-Environment Engineering and Research), this approach, which was awarded the Ernst Otto Fischer Award, was described as follows:

> A discovery starts with an observation. The best evidence for this thesis is the endlessly cited story of the apple falling on Isaac Newton's head. Newton, it is said, started asking why such things happen and, from there, eventually derived the laws of mechanics. Tracing the train of thought even further back, it was Plato who deduced the concept of anamnesis. He stated that the immortal soul already knows everything but forgets it all upon its birth. Humans must recall their original notions through external triggers – percipience. Indeed, without ever taking notice of the stars, mankind would never have discovered the heliocentric system and the orbits. Hence, education in natural sciences should always start with observing or sensing, in general, the phenomena. Through a notion of what is going on, one comprehends and deduces interrelated theories. The findings must be thoroughly questioned and finally applied to certain problems [44]. This goes along with a constant comparison of experiments and theory [46].

It is my desire to make the fascinating topic of water attractive to you. Therefore, before we deal with hydraulics, we will start with a teaser – the chapter titled "About water" (see Chapter 1). I'm sure you will gradually overcome any inhibitions you may have concerning differential equations and programming. However, you should also be fully aware of the fact that the requirements you'll be asked to meet are quite high.

In Part I of the book you have before you, the relevant physical relationships are derived such that they are – hopefully – logical and comprehensive. This is why each single step of the calculations is explained in detail, perhaps in too much detail for some of you! Whenever possible, illustrative experiments will be used for explanation, some of which you may carry out yourself using the simplest means.

The second part of the book is dedicated to the explanation of one-dimensional hydraulics – again by means of several experiments. Part II is supported by programming examples

in Octave, the freely available and open-source MATLAB® variant[A]. Therefore, it is advisable to immediately download Octave at:

https://www.gnu.org/software/octave/download.html

The accompanying open-source codes may be obtained from:

https://github.com/christophrapp/hydraulics

By the way, the programming examples provided throughout the book are presented in similar blue boxes as above.
In Part III, the topics are taught by means of sample tests with explanations of their solutions. No pianist or guitarist, no soccer player or skier, can learn the skills required to perform their passions just by reading a book or learning a theory by heart. Remember: Practice – and more practice still – makes perfect.
Part IV rounds off the teaching content by covering elaborate practical examples. These examples include the water-level optimisation of a run-of-river power plant, the determination of the forces and moments acting on a weir system and on a hydropower penstock, and the determination of the necessary pipe diameters for a wastewater system. The Appendix is a supplement to those sections that would have become too extensive or too detailed in the main parts.
The book does not claim to fully describe all mathematical and physical principles. In particular, you will not find any shape parameter or loss coefficient tables or implementation instructions in this book. Instead, this book is intended to help its readers comprehend hydraulic phenomena as well as to critically question problems and to project the gained insights onto other complex interrelations.

Flow is from left to right unless indicated differently. Calculations in the book were conducted with the codes provided, therefore the accuracy of the used numbers can be slightly different from the rounded ones printed in the book.

For the provision of materials, I wish to thank SWM Services GmbH, Wasser- und Schifffahrtsamt Heidelberg, Kreuzinger + Manhart Turbulenz GmbH as well as Hamburg-Wasser. My sincerest thanks go to my colleagues Dr Florian Schwertfirm, Dr Andreas Zeiselmair, Dr Florian Mintgen and Dipl.-Ing. Andrés Botero Halblaub for their invaluable remarks, improvements and corrections. Brita Baumgärtel translated the book, which was originally written in German, with the support of Steven McAllister. A very special thanks goes to David Magallanes at Proofed for giving it the finaly touch. Thank you all very much!
The open access publication of this book was made possible by the Verein zur Förderung des internationalen Wissensaustauschs e.V. (knowledgExchange.org) through the generous support of the Cordes & Graefe Stiftung. Many thanks!
If any errors survived, despite the most scrutinous checks, please send details of these to rapp@knowledgExchange.org.
I hope you enjoy the book.

Yours, Christoph Rapp

[A] I advise you to use the open source software Octave. Admittedly, as a student with a free MATLAB® licence, you get used to the user-friendly interface and will later have to pay licence fees.

Contents

List of Figures

Nomenclature

Mathematical operators

d	(total) derivative of a quantity, infinitesimal quantity
∂	partial derivative, differentiation with respect to a single quantity only
Δ	difference of two values of a quantity
∇	nabla operator, gradient
∇^2	Laplace operator, second derivative
rot	rotation
lim	limit function

General

$\vec{x}$	vectorial or tensorial quantity
$\langle \quad \rangle$	ensemble averaging, time averaged
$\overline{\quad}$	spatial filtering, spatial averaged
$\tilde{}$	subfilter
$'$	fluctuation
*	dimensionless quantity

Greek upper case letters

Γ	$[\mathrm{m}^2/\mathrm{s}]$	vorticity
$\Gamma(x)$	[various]	general function
$\Omega(k)$	$\left[\frac{\mathrm{rad}}{\mathrm{s}}\right]$	angular frequency of the wave number k
$\Phi(x,y)$	$[\mathrm{m}^2/\mathrm{s}]$	potential function
$\Phi(x)$	[various]	general function
$\Psi(x,y)$	$[\mathrm{m}^2/\mathrm{s}]$	stream function
Ξ	[m]	amplitude

Latin upper case letters

A	$[\mathrm{m}^2]$	area
B	[m]	width
C	[various]	integration constant
C	[mol/L]	concentration
C^+	[m/s]	characteristic
C^-	[m/s]	characteristic
D	[m]	diameter
E	$[\mathrm{N/m}^2]$	modulus of elasticity
EGL	[m]	energy grade line
$F(x)$	[ ]	antiderivative
F	[N]	force
F_B	[N]	buoyancy force
F_F	[N]	friction force
F_G	[N]	gravity force
F_I	[N]	inertia force
F_P	[N]	pressure force
Fr	[ ]	Froude number
H	[m]	energy head
$H_{\min}$	[m]	minimum energy head of an open channel flow
HGL	[m]	hydraulic grade line
I	[N s]	momentum
J	[ ]	slope
J_B	[ ]	slope of the bed
J_E	[ ]	slope of the energy grade line
J_{WS}	[ ]	slope of the water surface
K	[ ]	minor (local) loss coefficient
K_0	$\left[\mathrm{m}^{\frac{1}{2}}/\mathrm{s}\right]$	constant for the determination of the Manning coefficient n
K^+	[m]	constant of the C^+ characteristic
K^-	[m]	constant of the C^- characteristic
L	[m]	length
M	[N m]	moment of force
P	[W]	power
P	[m]	wetted perimeter
P_P	[W]	power of a pump
P_T	[W]	power of a turbine
Q	$[\mathrm{m}^3/\mathrm{s}]$	discharge
R	[m]	radius
R_{hy}	[m]	hydraulic radius
Re	[ ]	Reynolds number
SUPER		supercritical flow
SUB		subcritical flow
T	[°C], [K]	temperature
V	$[\mathrm{m}^3]$	volume
W	[N m] = [J]	work

Latin lower case letters

a	$[\mathrm{m/s^2}]$	acceleration
a	$[\mathrm{m/s}]$	propagation velocity
a	$[\,]$	parabola factor
b	$[\mathrm{m}]$	width
c	$[\mathrm{m/s}]$	relative propagation velocity
c_{abs}	$[\mathrm{m/s}]$	absolute propagation velocity
d	$[\mathrm{m}]$	diameter
Δe	$[\mathrm{N\,m}] = [\mathrm{J}]\,, [\mathrm{m}]$	dissipated energy of a flow, head loss
e_{ij}	$[1/\mathrm{s}]$	antisymmetrical part of the velocity gradient tensor
$f(x)$	$[\,]$	function
f_{D}	$[\,]$	friction coefficient
g	$[\mathrm{m/s^2}]$	gravitational acceleration
h	$[\mathrm{m}]$	height
h_p	$[\mathrm{m}]$	piezometric pressure head
Δh_{max}	$[\mathrm{m}]$	Joukowsky surge
h'	$[\mathrm{m}]$	local coordinate (downwards from water surface)
i, j	$[\,]$	index
k	$[\,]$	wave number
$k = \frac{v^2}{2g}$	$[\mathrm{m}]$	velocity head
k_f	$[\mathrm{m/s}]$	permeability coefficient
k_s	$[\mathrm{m}]$	equivalent sand grain roughness
l	$[\mathrm{m}]$	length
l_v	$[\mathrm{m}]$	turbulent length scale
m	$[\mathrm{kg}]$	mass
m	$[\mathrm{m^3/s}]$	dipole intensity
m	$[\,]$	lateral gradient of a trapezoid
$\vec{n}$	$[\,]$	normal vector
n	$\left[\mathrm{s/m^{\frac{1}{3}}}\right]$	Manning coefficient
o	$[\mathrm{m}]$	coordinate normal to s
p	$[\mathrm{N/m^2}] = [\mathrm{Pa}]$	pressure
p_{atm}	$[\mathrm{N/m^2}] = [\mathrm{Pa}]$	atmospheric pressure
p_v	$[\mathrm{N/m^2}] = [\mathrm{Pa}]$	vapour pressure
q	$[\mathrm{m^3/(s\,m)}]$	discharge per unit width
q	$[\mathrm{m}]$	coordinate binormal to s
r	$[\mathrm{m}]$	radial coordinate
r_s	$[\,]$	relative roughness
s	$[\mathrm{m}]$	coordinate (along the streamline $\vec{s}$)
s_{ij}	$[1/\mathrm{s}]$	symmetrical part of the velocity gradient tensor
t	$[\mathrm{s}]$	time
$\overline{u}$	$[\mathrm{m/s}]$	spatial filtered velocity
$\tilde{u}$	$[\mathrm{m/s}]$	subfilter velocity
u'	$[\mathrm{m/s}]$	velocity fluctuations
u_τ	$[\mathrm{m/s}]$	shear stress velocity
u, v, w	$[\mathrm{m/s}]$	velocity component in the x, y, z direction
x, y, z	$[\mathrm{m}]$	coordinate

v	[m/s]	velocity
v_f	[m/s]	Darcy velocity, filter velocity
y_+	[ ]	wall distance, inner coordinates
y	[m]	flow depth
y_c	[m]	critical flow deph
y_N	[m]	normal water depth
w	[m]	weir height
w	[m]	wall thickness

Greek lower case letters

$\alpha, \beta, \delta, \gamma, \varepsilon$	[°], [rad]	angle
$\gamma(x)$	[various]	general function
ε	[ ]	deformation
δ_{ij}	[ ]	Kronecker delta
δ_ν	[m]	thickness of the viscous sublayer
η	[m]	Kolmogorov scale
η	$[\mathrm{N\,s/m^2}]$	dynamic viscosity
η	[ ]	efficiency factor
κ	[ ]	von Kármán constant
λ	[m]	wave length
μ	[ ]	discharge coefficient
μ_L	[ ]	lateral contraction coefficient
μ_V	[ ]	valve loss coefficient
ν	$[\mathrm{m^2/s}]$	kinematic viscosity
ν_r	$[\mathrm{m^2/s}]$	turbulent viscosity
ω	[1/s]	angular frequency
$\vec{\omega}$	[1/s]	rotation vector
ϕ	[ ]	friction coefficient
$\phi(x)$	[various]	general function
ψ	[ ]	contraction coefficient
ψ	[ ]	loss coefficient (derivation normal water conditions)
ρ	$[\mathrm{kg/m^3}]$	density
σ	$[\mathrm{N/m^2}]$	stress
σ_S	[N/m]	surface tension
τ	$[\mathrm{N/m^2}]$	stress
τ_w	$[\mathrm{N/m^2}]$	wall shear stress
τ_{ij}	$[\mathrm{N/m^2}]$	stress tensor
τ_{ij}^s	$[\mathrm{N/m^2}]$	subgrid-scale stress
$\xi(x,t)$	[m]	height of wave at place x and instant of time t
ξ	[m]	local coordinate
ζ	[m]	local coordinate

Chapter 1
About water

1.1 On origins

According to the equations of the general theory of relativity, the universe is either expanding or contracting [17]. In order to circumvent the unthinkable, Einstein introduced a factor to keep the size constant. Some 20 years later, however, Hubble, who gave his name to the telescope, discovered that the universe is actually expanding. He did this by proving that the color spectrums of far stars change as a result of their motion. This frequency shift, also referred to as the Doppler effect, occurs if a source moves relative to a receiver (as in the case of a police car siren). This evidence confirmed that a continuous expansion must take place. The Big Bang theory was born, and it is still the most probable scenario of the origin of the universe. The age of our universe could be quantified as 13.8 billion years. We'll never know what, and indeed if, anything came before that.

Water is the material source of all things. We often come across this quote by Thales of Miletus (624 to 546 BCE). The considerations that led to it will remain a secret despite countless interpretations. However, when van Helmont planted a young tree into a pot 2,000 years later for a scientific experiment and only watered it, he saw a considerable increase in weight five years later, thus confirming Thales' thesis [2]. At that time, nothing was known about the conversion of light energy to chemical energy, the so-called phenomenon known as photosynthesis.

It wasn't until the 18th century that the Greek theory of the four basic elements (fire, water, earth, air) led to the chemical elements we know today as a result of research conducted by Lavoisier (1743 to 1794). He performed an experiment to demonstrate that burning "two parts inflammable air and one part life air" produces water [2]. He presented the results on June 25, 1783, at the Académie des Sciences. This not only revealed the chemical origin of water but also established stoichiometry, which then contributed to the well-known periodic table of the elements. At that time, oxygen – from the Greek "oxys" (acid) and "gen" (create), i. e. acid-former – was a known element, and it was Lavoisier who introduced hydrogène (hydrogen), the water-former. Though it is not possible to deduce the generation of the simplest element, hydrogen, with only one proton and one electron, it is known that it can be created at a temperature of 3700 °C by the combination of the elementary particles. The other heavier elements such as oxygen stemmed from nuclear fusion of the hydrogen atoms during the birth of stars, as Rutherford proved in 1917. Thereby, the creation of water is certainly obvious: It is the combination of the two most-prevalent reactive elements in the universe – hydrogen and oxygen – that makes life

C. Rapp, *Hydraulics in Civil Engineering*,
https://doi.org/10.1007/978-3-031-54860-4_1

possible: H_2O. One water molecule comprises two hydrogen atoms and one oxygen atom. The oxygen atom "borrows" one electron from each of the two hydrogen atoms in order to assume a lower energy state – this is the atom's mission. The hydrogen, too, benefits from this liaison because the oxygen also shares one of its desired electrons with each of the hydrogen atoms. Two other electron pairs of the oxygen, so-called valence electrons, are moved to the opposite sides such that the molecule spans a tetrahedron (derived from the Greek words for "four" and "surface"). The oxygen now subjects the shared electron pairs to a little more stress such that the two hydrogen atoms form slightly positively charged points and the valence electrons slightly negatively charged corners. This results in what are known as hydrogen bridge bonds, wherein the molecules unite with approximately one tenth of the force of the atomic bonds as the positively charged hydrogen corners are attracted to the negatively charged corners of the oxygen atoms of other molecules. These hydrogen bridge bonds, which are broken and re-formed repeatedly, give water many of its characteristic properties. They are also responsible for the so-called density anomaly, e. g. they are the reason why ice floats. Water may assume three different phases, which are primarily dependent on two state variables: the temperature and the pressure (please scroll to Figure 3.3 on page 31).

Reducing the phase diagram of water to one dimension reflects exactly what everybody experiences in their daily life. Cold water is in the solid phase, very hot water in the gaseous phase, and in between, water is liquid. The known transition values, $0\,°C$ between solid and liquid and $100\,°C$ between liquid and gas, are, however, applicable at atmospheric pressure ($1013\,mbar$). It is also generally known that eggs must be boiled for a longer time on a mountain to make them hard, a fact that this example easily explains. A lower air pressure results in a lower boiling point of water, which is why liquid water cannot be heated to $100\,°C$ on a mountain. The eggs boil at lower temperatures than in the valley. At a pressure as low as $6.12\,mbar$, all three conditions may simultaneously occur at $0.01\,°C$, while liquid water below this pressure does not exist at all. Here, there is a direct transition between solid and gas. This is referred to as sublimation and conversely as re-sublimation.

According to some scientists, water was brought to the newly born earth by comets (they consist of approximately 20 % frozen water, Halley's comet even of 80 %). According to other scientists, the water was brought by asteroids that showered our celestial body with water during its wild youth. If we actually look at the facts, there should be no water on earth due to its proximity to the sun and the resulting heat.

The heavy elements sank into the core of the young earth and the light ones rose to the surface; water, carbon dioxide and nitrogen evaporated, forming the atmosphere. Enormous heat developed in the core and the greenhouse gases, water vapour and carbon dioxide prevented the planet from cooling. The water vapour condensed in the atmosphere, precipitated and evaporated immediately when it hit the hot ground. The torrential rain lasted for ages and flushed out the CO_2 from the atmosphere, reducing the greenhouse effect. The earth cooled down, the water no longer evaporated immediately from the ground but instead flowed off, further reducing the greenhouse effect. CO_2 combined with volcanic rock and transformed with sodium to soda, which in turn became lime and with calcium chloride common salt. The carbon was bound in this way and the ocean slowly but surely became saltier [2].

Nowadays, approximately 97 % of the water on earth is saline, while 77 % of the remaining 3 % is fresh water that is bound as ice in glaciers. Furthermore, 22 % of the fresh water is deep groundwater and barely accessible to humans, meaning that the 1 % of the fresh water that inland waters carry appears almost inexhaustible in view of the huge quantities

of water in the Amazon, Yangtze and Nile Rivers in addition to the Great Lakes or Lake Victoria. Merely 0.01 % of fresh water is in the atmosphere – just 4×10^{15} kg, i. e. a 4 followed by 15 zeroes. Despite these unimaginable masses, water supply has always been one of the central problems of mankind. As 1.2 billion people do not have access to clean drinking water, the UN General Assembly declared the period between 2005 and 2015 the International Decade for Action "Water for Life". In 2010 a resolution was passed which declared access to water and basic sanitary supplies a human right.

1.2 On the origin of life

There is no element more closely linked to life than water. The first living beings developed in the sea before the land was populated, and the origin of each human life is also located in water. Embryos grow in the seawater-like amniotic fluid, so it is no surprise that three quarters of the mass of a newly born child is H_2O-molecules. Although men consist of 55 % water and women of "only" 50 % water, water is the basis for the function of vital organs such as the kidneys (81 %), heart (79 %) and brain (76 %). At the same time, water is the breeding ground for numerous pathogens (e. g. malaria) because of its life-giving power and through its function as a transport medium serving as a carrier for many diseases (e. g. cholera) [31].

As far back as 3.8 billion years ago, amino acids, i. e. components of the proteins that are the elementary constituents of all cells, originated in the primeval ocean. At great depths, far more complex amino acid structures formed because, at that time, the water blocked out harmful UV radiation, as the ozone layer had not yet formed. Approximately 3.5 billion years ago, cyano-bacteria, also known as blue-green algae, used the high reaction potential of water, combining it with carbon dioxide and light to form glucose and oxygen. Thus, they "invented" the metabolism that we now know as photosynthesis, so called due to the use of light as energy source. These blue-green algae that, in a similar form, still occur in Australia, are procaryotes, which means they do not have defined areas, so-called organelles, or even an encapsulated nucleus. Nevertheless, they are able to reproduce, which makes them the first living beings on this planet. Within their cell membranes, which consist of the simplest fats, desoxyribonucleic and ribonucleic acids float in the cell liquid. These acids are the carriers and the multipliers of genetic information.

When the primeval ocean no longer contained the iron that reacted with the oxygen released by the cyano-bacteria to form iron ore – a process which, after all, lasted two billion years – the contamination of the atmosphere by toxic O_2 began. In the present tropopause, about 15 km above the earth's surface, a portion of the oxygen was transformed to ozone, which protected the organisms against harmful UV radiation. About 1.5 billion years ago, eukaryotes, which safeguard the genetic information in a nucleus, developed.

Higher life started to develop following the Cambrian explosion, which took place approximately 540 million years ago. When, after 100 million years, flora and fauna populated the land, this was only achieved thanks to solvent (intracellular) and carrier liquid (intercellular) waters. Water fills the spaces in a cell and therefore about 80 % of the volume. Intercellular water is present primarily in the blood, the brain, the stomach and the intestines. As water is essential for our metabolism, we should drink at least three litres of water per day – a deciduous tree requires 250 L per day.

However, we humans consume, or rather use, much more water – virtual water. The production of one kilogram of tea requires 37 000 L or kg of water. Imagine a room with a

floor space of $15\,m^2$ that is filled with water up to the ceiling. That's what is needed for a single kilogram of tea. Coffee isn't much better. For one kilogram of coffee, the room would be half-filled; for one kilogram of beef, it is one-third full. And even if a rice field required a water depth of $2\,m$ until the harvest, a carnivore consumes twice the amount of virtual water as a vegetarian. For each milk bottle you buy, imagine the additional 800 bottles of water that were needed to produce the milk. And this does not include the several cubic metres of this most precious resource that are necessary for the production of the technical equipment for filling and distribution.
Wildlife is also very eager to gain access to the basis of life, i. e. water. The characteristic features of various animal species, are well known. Camels, for instance, have oval-shaped red blood cells, enabling them to absorb great amounts of water in a very short time without risking water intoxication. As another example, frogs mix their body fluid with glucose prior to hibernation in order to lower its freezing point and to therefore prevent an expansion of their volume when the temperature drops below $0\,°C$. The scarab is a particularly innovative desert inhabitant that seems to have assimilated the phase diagram of water. It places itself against the wind in such a way that the water vapour condenses on its hydrophilic humps due to the wind pressure, thereby letting droplets flow directly into its mouth.
Humans are unable to contort themselves like this in order to obtain this most precious good. In the course of our development, however, we have left no stone unturned in order to gain control of the elixir of life.

1.3 On the origin of civilisation

In regions where water is scarce and not readily available, humans have put much of their energy into storing and accessing it. Early civilisations developed in precisely those regions where creativity was essential to provide people with water. It was here that the inhabitants of the Fertile Crescent excelled, irrigating their fields by means of sophisticated systems. In Mesopotamia, the Tigris and the Euphrates Rivers carry water mainly in springtime, which is too early for the summer harvest but too late for the winter harvest; further south, a most impressive culture developed by exploiting the dangerous Nile floods in a country that is 96 % desert. These ambitious hydraulic structures, which six to three thousand years later still reflect the social importance of water, brought forth crop surpluses and allowed people to do more than just worry about surviving. Culture began to develop, professions began to emerge, and people began to travel and share their knowledge. And in view of the complexity and the might of the structures created to harness it, historians wonder whether it was the administration of water that gave rise to the state [21].
According to a recognised historical theory, the power of the Egyptian pharaoh dynasties stemmed from local rulers who administered the irrigation channels. In wars that took place in approximately 3000 BCE, Menes ("he, who builds the channels") emerged victorious and became the first pharaoh. The tax paid to the rulers in the form of a portion of the harvest was set by means of so-called nilometres. The Roman poet Pliny referred to this unit in his *Naturalis Historia* (Natural History). "Twelve cubits meant hunger, thirteen sufficiency, fourteen joy, fifteen security and sixteen surplus." Heavier floods, which invariably occurred in July, meant catastrophe. Records show that about every five years,

either too much or too little water flowed in the Nile. Hydrologists who could predict such events were worshipped at that time as high priests.
Hammurabi, the sixth king of the first Babylonian dynasty (18th century BCE), wrote one of the world's first extensive legal codes, which included the control and management of water. Paragraph 53 reads:

> He who opens the floodgates but whose dams are not strong enough and so cause flood shall compensate the proprietor for his loss. This shall be determined on the basis of the harvests of the neighbouring fields.

Irrigation became increasingly sophisticated and more voluminous. From 702 to 688 BCE, the Assyrian king Sennacherib built an impressive water supply system with 150 km of channels, several tunnels, aqueducts and weirs. He himself searched for springs and initiated the construction of a new supply for Nineveh. A river was completely blocked by a dam 50 km northeast of the town in order to provide the people with water. To this end, rocks had to be removed over a distance of 35 km and an aqueduct 280 m long and 22 m wide was built near Jerwan. The inscription there reads:

> Sennacherib, the king of the world, the king of Assyria: I initiated the construction of a channel from the Hazur River over a long distance. I built aqueducts from limestone blocks. Said water was carried through them.

For the Romans, the handling of water, both its supply and disposal, was the dominant issue in the planning of their metropolises. The most impressive building is certainly the Pont du Gare near Nîmes. Jacques Rousseau described his impressions of this structure in his *Confessions* as follows:

> I expected to see a monument, worthy of the hands which built it. But this work exceeded my expectation; and that was the first time in my life. [...] I roamed the three levels of this majestic building which I hardly dared to enter. The echo of my steps under these immense arches made me believe to hear the powerful voices of those who built them. I was lost like an insect in this immensity.

The discharge of wastewater has been of major importance ever since people began living together in larger settlements, or even in cities. In Munich, it wasn't until the second half of the 19th century CE that the hygienist Max von Pettenkofer was able to convince the city council to construct a central sewage system whose prime aim was to contain cholera epidemics. But the examples of Tepe Gawra, Uruk or Habuba Kabira show that the relation between the contamination of the wells by wastewater and rapidly spreading diseases was already known by 4000 BCE. In Babylon, around 1300 BCE, King Adad-Nirari I immortalised himself on a brick of an underground sewer to the Tigris. The cross-section of this brick-built vault was two metres high and 1.8 m wide.
Examples of how we have engaged with water over the ages can be found across the globe. The Mayan dam in Tikal (about 300 CE), the 5000-year-old irrigation system used to grow rice in the present-day Kingdom of Cambodia, which expanded to the spectacular terraces in Yunnan and East Timor, and the Swiss *suons* (water-carrying channels in Valais from about 1000 CE) are further witnesses of the past. Additional elaborations will be omitted here, although other achievements of former generations have been just as outstanding.

1.4 On the origin and source of industry

Humans made use of the power of water long before that of the wind. But the first power unit that was not driven by water or wind was only able to function by using water: the steam engine that Thomas Newcomen designed in 1712. Since then, power plants have seen continuous improvements, and Newcomen's efficiency of 0.5 % has been increased by a factor of 100. New technologies have been developed, but even nuclear power plants cannot generate electricity without water. Today, technological progress is not only based on petroleum as the supplier of energy; $400\,m^3$ of water are required for the production of one car, while a single CD requires 200 L. In addition, there is the supply of food – and water – to the world's current eight billion people. For example, one of the largest (underground) reservoirs in the world is in the Great Plains. It has a surface area of $450\,000\,km^2$ and is now technically capable of being pumped empty in order to stay the appetite of progress. Twenty-five times more water is withdrawn than flows in, which is not in agreement with the idea of sustainability propagated by Hans Carl von Carlowitz (1645 – 1714). The consequences for future generations are not taken into consideration. In most countries, the water used for industrial purposes is still fed impurified into the rivers and finally transported into the oceans. The contaminants join the food chain either by the irrigation of plants or via the sea fish that eat them and land up on our tables. This also applies to the heavy metals from a carelessly discarded cigarette butt, for example, which, if dissolved in one litre of water, is lethal for most fish because of the nicotine and the arsenic content.

As was the case at the onset of civilisation, great efforts are taken, particularly where water is scarce, to provide sufficient quantities of good-quality water. In Singapore, known for its electronic goods, which can only be produced using huge amounts of the purest water, every effort is made to ensure the supply of H_2O. Although it rains considerably in the tiny city-state, every single drop counts in this metropolis that has a population density of more than 7000 people per square kilometre (Germany: 230) and more than 5 million inhabitants. The supply of drinking water from Malaysia creates a high political dependency, meaning that the Singaporean people resort to three water taps for their uses: one dispenses desalinated water, which is obtained using enormous quantities of energy; the second one provides reconditioned wastewater ($2.5 \times 10^6\,m^3$ daily, i. e. 16 times the consumption of all Munich households); and the third one administers rain water. With the aid of adequate water technologies, such as efficient washing machines and dishwashers, lavatory cisterns and so-called droplet irrigation, the precious – and here actually in the economic sense – good water can be saved and used where it's most needed. The relationship between water and technological progress, and between water and the industrial revolution, will not be elaborated on further, but their consequences will be. It is ironic that the properties that make water the central element of life also play a major role in climate change. Water in its three phases – gas, liquid, and solid – has a significant impact on the climate of our planet. The oceans absorb CO_2 (as the primeval ocean did). Water vapour is the number one greenhouse gas, and the ice-albedo effect has the most dramatic impact of all climate feedback loops. However, it is much more important that increasing temperatures significantly influence the hydrologic cycle. Higher temperatures lead to higher humidity in the air, and this increases the probability of disastrous thunderstorms and floods as well as water shortages due to rare rainfall. The Intergovernmental Panel on Climate Change (IPCC) predicted in 2007 that by 2020, there would be an anthropogenic temperature increase of 1 °C and 400 to 800 million people

living in regions of water scarcity; by 2050, there will be 1.5 billion people experiencing water shortages with a temperature increase of 1 °C to 2 °C, or even 2.4 to 3.5 billion if temperature rises by 2.5 °C [9]. And for 2020 they were right.

1.5 To the origin

When viewed from an evolutionary biology standpoint, water plays a key role in the creation theories of religions. In several religions of North Asia, North America, India and Russia, a deity descended to the bottom of the primeval ocean to bring up an earth seed. In Hindu mythology, the voice that embodied Brahma first became water and wind from which the net of the world was woven. For the Maya in Central America, the deity Hurakan called forth the land out of an ocean of darkness and water. The Hebrew God moved upon the water before he divided the water from the land. In Islam, water symbolises creation, security, healing and the connection to something divine. And in the Bible in Genesis, the first book of Moses, it is written:

> (1) In the beginning God created the heavens and the earth. And the earth was without form, and void; and darkness was upon the face of the deep. And the Spirit of God moved upon the face of the waters. [...] (9) And God said, let the waters under the sky be gathered together unto one place, and let the dry land appear: and it was so. (10) And God called the dry land "earth"; and the gathering of waters he called "seas".

Part I
Fundamentals and derivations

Chapter 2
Essential mathematics

2.1 Conventions

The coordinate system shown in Figure 2.1 is used in this book. Here, the z-axis points upwards against the force of gravity. The velocity components in the x-, y- and z-directions are identified by the variables u, v and w, respectively. Later, the so-called index notation will also be used with the three spatial directions described by the indices 1, 2 and 3. The following notation applies: $x_1 = x$, $x_2 = y$, $x_3 = z$ and $u_1 = u$, $u_2 = v$, and $u_3 = w$.

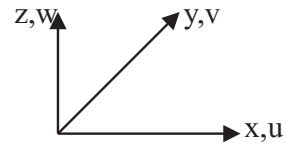

Figure 2.1: Coordinate system with the positive x-direction to the right (direction of flow), the positive y-direction into the drawing plane and the positive z-direction opposite to the force of gravity.

2.2 Physical quantities and their mathematical descriptions

2.2.1 Scalar

A scalar is a non-directed physical quantity. For example, a certain temperature T or concentration C of a substance prevails at a specific point in space. These two physical quantities have no direction. This also applies to density or pressure. A scalar quantity is a function of position and time expressed as $f(x, y, z, t)$.

C. Rapp, *Hydraulics in Civil Engineering*,
https://doi.org/10.1007/978-3-031-54860-4_2

2.2.2 Vector

A vector is a directed physical quantity; forces and velocities have a specific direction in three-dimensional space. In a game of tug-of-war, for example, one team pulls in one direction with a certain force, while the other team – if they are balanced to the same norm – pulls in the opposite direction. The norm $|\vec{X}|$ is referred to as the undirected length of a vector. In this chapter, vectors will be depicted with vector arrows for developing a sense to distinguish between scalar and vectorial quantities.

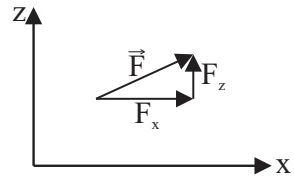

Figure 2.2: Example of a force with two components in the x- and z-directions.

In Figure 2.2, F_x and F_z identify the force components in the x- and in the z-direction, while the arrow $\vec{F}$ reflects just this vectorial property. The vertical bars about $\vec{F}$ in Equation 2.2 represent the norm of that vector. The underlying mathematic operation, the calculation of the hypotenuse using the legs of the right triangle, is written on the right side of the equals sign.

$$\vec{F} = \begin{pmatrix} F_x \\ F_z \end{pmatrix} \tag{2.1}$$

$$|\vec{F}| = \sqrt{F_x^2 + F_z^2} \tag{2.2}$$

2.2.3 Tensor

The meaning of tensors can be illustrated with an infinitesimally small, i. e. minuscule, cube-shaped element (see Figure 5.4). This cube has six surfaces in three-dimensional space with three pairs of normal vectors; each normal vector has got an opponent pointing in the opposite direction (this means that there are three sets of pairs of surfaces that are parallel). Forces may now be applied to these minute surfaces, again in all three spatial directions (positively or negatively). To illustrate this, place your hand on the tabletop in front of you and push your hand away from yourself. You're applying shear stress to this surface in the y plane, which extends perpendicularly to the z plane. This is how you create shear stress τ_{zy}. If you move your hand to the right on the tabletop, then you will induce shear stress on the z surface in the x plane; accordingly, the associated component of the stress tensor is τ_{zx}. Palm pressure applied vertically onto the tabletop corresponds to a stress in the z plane, which is represented by the component τ_{zz}. These three components τ_{zx}, τ_{zy} and τ_{zz} indicate the stresses on the surface in the z plane. In the negative coordinate direction (you move your hand on the tabletop to the left), the stresses assume negative signs. But the stresses could just as well be applied on the surface extending in the x or y plane. When we shrink the cube to one point, this results in what

is known as the stress tensor τ with its nine entries; the main diagonal elements indicate the normal stresses, while the secondary diagonal elements indicate the shear stresses.

$$\tau = \begin{pmatrix} \tau_{xx} & \tau_{xy} & \tau_{xz} \\ \tau_{yx} & \tau_{yy} & \tau_{yz} \\ \tau_{zx} & \tau_{zy} & \tau_{zz} \end{pmatrix} \tag{2.3}$$

2.2.4 Scalar product

The scalar product links two vectors to one scalar value (see Equation 2.4). The projection of $\vec{a}$ onto $\vec{b}$ and the projection of $\vec{b}$ onto $\vec{a}$ are designated by $\vec{a_b}$ and $\vec{b_a}$, respectively (see Figure 2.3). In the scalar product, the projected length of one vector is multiplied by the length of the other.

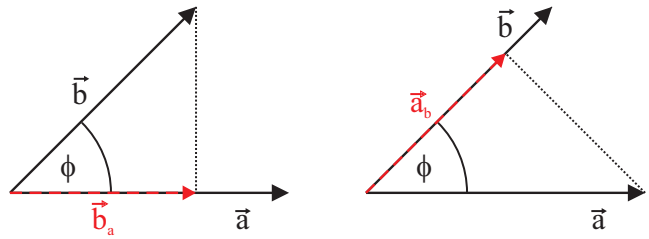

Figure 2.3: Scalar product of two vectors; $\vec{b}$ projected onto the direction of the vector $\vec{a}$ (left) and $\vec{a}$ projected onto the direction of the vector $\vec{b}$, (right).

In Figure 2.3, the arrows with the red broken lines indicate the oriented length of the projection of $\vec{b}$ onto $\vec{a}$ and of $\vec{a}$ onto $\vec{b}$, respectively. The scalar product is positive if $\vec{b}$ points in the same direction as $\vec{a}$; otherwise, it is negative. This is the case if $90° < \phi < 270°$ or $\cos\phi < 0$. We will use the scalar product later for calculating the components of fluxes that are parallel to a line of action (e. g. normal to a surface).

$$\vec{a} \circ \vec{b} = |\vec{a}| \cdot \left|\vec{b}\right| \cdot \cos\phi = \left|\vec{b}\right| \cdot |\vec{a}| \cdot \cos\phi \tag{2.4}$$

Since the lengths of the two vectors $|\vec{a}|$ and $\left|\vec{b}\right|$ are multiplied (and this product, of course, by $\cos\phi$), it does not matter whether $\vec{a} \circ \vec{b}$ or $\vec{b} \circ \vec{a}$ is calculated (commutative law). For vectors in space, the scalar product may be determined according to Equation 2.5.

$$\vec{a} \circ \vec{b} = \begin{pmatrix} a_1 \\ a_2 \\ a_3 \end{pmatrix} \circ \begin{pmatrix} b_1 \\ b_2 \\ b_3 \end{pmatrix} = a_1 \cdot b_1 + a_2 \cdot b_2 + a_3 \cdot b_3 \tag{2.5}$$

2.2.5 Cross product

The result of a cross product of two vectors ($\vec{a} \times \vec{b}$) is a third vector that is perpendicular to the area formed by $\vec{a}$ and $\vec{b}$ (see Figure 2.4). We can find the calculation rules e. g. in [8, p. 192].

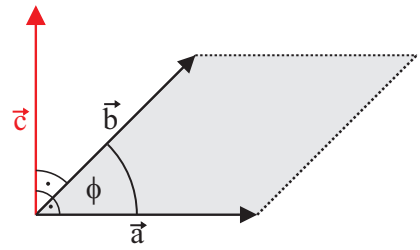

Figure 2.4: Cross product of two vectors $\vec{a} \times \vec{b}$.

$$\vec{c} = \vec{a} \times \vec{b} = \begin{pmatrix} a_2 b_3 - a_3 b_2 \\ a_3 b_1 - a_1 b_3 \\ a_1 b_2 - a_2 b_1 \end{pmatrix} \tag{2.6}$$

The absolute value of $\vec{c}$ represents the area of the parallelogram spanned by $\vec{a}$ and $\vec{b}$.

$$|c| = \left| \vec{a} \times \vec{b} \right| = |\vec{a}| \left| \vec{b} \right| \sin \phi \tag{2.7}$$

2.3 Euler vs. Lagrange

The creation of field theory was just one of Leonhard Euler's outstanding achievements. For the development of fluid mechanics, however, it was essential. But hydraulics would not be complete without the description of movement according to Lagrange's approach.

2.3.1 Lagrange's perspective

The Lagrangian[A] model is based on the perception of movement by the moving individual. Imagine a soccer player running back and forth on the pitch (see Figure 2.5). At kick-off ($t = 0\,\text{min}$), he is located approximately at the centre of the circle ($\vec{s}(t = 0) = \text{centre of circle}$). Maybe he scores a goal from the penalty area in the 23rd minute ($t = 23\,\text{min}$) and ($\vec{s}(t = 23) = \text{penalty box}$) and is substituted in the 68th minute ($t = 68\,\text{min}$) and ($\vec{s}(t = 68) = \text{substitution bench}$). At different times, the player is in different positions on the field $\vec{s}(t)$. Sometimes he sprints faster, sometimes slower ($\vec{v} = \frac{\mathrm{d}\vec{s}}{\mathrm{d}t}$) and in different directions which, however, are always indicated along his trajectory $\vec{s}$

[A] Joseph-Louis Lagrange, ∗1736, Turin, Italy, †1813, Paris, France

(see also Chapter 2.4.1). And he is subjected to accelerations because his velocity varies at any moment ($\vec{a} = f(t) = \frac{d\vec{v}}{dt} = \frac{d^2\vec{s}}{dt^2}$).

Figure 2.5: Lagrangian way of viewing a football match – recorded by a GoPro camera of a red player (not shown in the photo).

We would have to prepare further individual travel directions for all other players and the referee in order to reproduce the events on the football pitch. Being in the thick of it rather than a mere bystander is what Lagrange is all about.

2.3.2 Euler's perspective

The description of the same situation as in the previous Chapter 2.3.1 looks different from Euler's point of view (see Figure 2.6). Euler[B] takes the position of the coach, an outside observer. He permanently monitors the entire field and watches the actions of each player at each moment. Mathematically, this situation can be expressed as follows:

$$\vec{s}(t) = \begin{pmatrix} x \\ y \end{pmatrix} = f(t) \tag{2.8}$$

$$\vec{v}(t) = \begin{pmatrix} u \\ v \end{pmatrix} = f(x,y,t) \tag{2.9}$$

The acceleration of the goal scorer in the above example may of course also be expressed on the Euler field. However, reference has first to be made to Chapters 2.4.1.2 and 5.2.

2.4 Functions

Functions describe dependencies of physical quantities. An example would be the height of a human being during his lifetime, which is written mathematically as $L = f(t)$ (see

[B] Leonhard Euler, ∗1707, Basel, Switzerland, †1783, Saint Petersburg, Russia

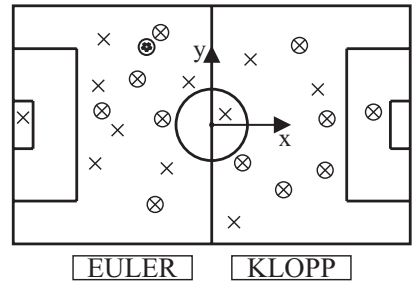

Figure 2.6: Euler's view of a soccer match.

Figure 2.7). In the early months and years, his height (L) will increase rapidly until he is grown up.

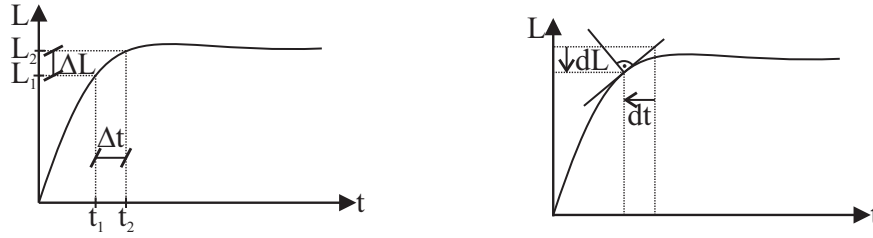

Figure 2.7: Course of a human's height over his/her lifetime.

2.4.1 Derivations

Let's stay with the example of Figure 2.7. During childhood, a person grows rapidly. During youth, growth is slower. As adults, humans no longer grow or might even shrink a little. The change in a quantity with respect to a variable on which it is dependent is known as a derivative, which is obtained by the process of differentiation. When measuring the height of a person e. g. on the same day one year apart ($\Delta t = t_2 - t_1$), we will determine a change in height of $\Delta L = L_2 - L_1$. By means of the quotient $\frac{\Delta L}{\Delta t}$, the mean increase over the course of this year is determined.
In the derivative $\frac{\mathrm{d}L}{\mathrm{d}t}$, we shrink the distance of the measuring points towards zero ($\Delta t \to 0$) and thereby determine the slope of the tangent line at this point.
A function may also be derived several times with respect to the same variable. The second derivative, which indicates the curvature of the function, is written as $\frac{\mathrm{d}^2 f(x)}{\mathrm{d}x^2}$.

2.4.1.1 Partial derivative

There are physical quantities that depend on several variable quantities, as was already stated above. Let's look at the air temperature while we imagine travelling from Munich to Rome. Apart from crossing the Brenner Pass, it will most likely get warmer during

our journey ($T = f(\vec{s})$, see Figure 2.8 (right)). If we stay at home, get up at 6 a.m. and go to sleep at 10 p.m., we will likewise experience a change in temperature ($T = f(t)$, see Figure 2.8 (left)). In a partial derivative, which, by the way, is expressed by a ∂, only the change in a variable as a function of a certain physical quantity is of interest.

Figure 2.8: Temperature variation over the day (left) and temperature variation between Munich and Rome (right).

The change in temperature as a function of time is written as the partial derivative $\frac{\partial T}{\partial t}$. This, in turn, allows the units to be expressed as °C/s or K/s. The change in temperature with respect to position is described by the partial derivative $\frac{\partial T}{\partial \vec{s}}$, the units of which result from the numerator and denominator: °C/m or K/m.

2.4.1.2 Total derivative

The total derivative is defined by the derivative of a physical quantity with respect to another quantity. Contrary to the partial derivative, all functional relationships are taken into consideration. Let's return to the journey from Munich to Rome in our example: the temperature changes over time and distance ($T = f(t, \vec{s}(t))$). When we move, we change our position $\vec{s}$ in the course of time t. Thus, the position $\vec{s}$ is again dependent on time t. The total differential $\frac{\mathrm{d}T}{\mathrm{d}t}$ describes the movement of a Lagrangian observer in the Euler field. This very context is expressed in Equation 2.10.

$$\frac{\mathrm{d}T}{\mathrm{d}t} = \frac{\partial T}{\partial t} + \frac{\partial T}{\partial \vec{s}} \frac{\mathrm{d}\vec{s}}{\mathrm{d}t} = \frac{\partial T}{\partial t} + \vec{v} \frac{\partial T}{\partial \vec{s}} \tag{2.10}$$

This means that the faster we drive to Rome, the faster it gets warmer. The change in temperature is as dependent on the velocity and the change in velocity as a function of distance $\vec{s}$ as it is on warming over the course of the day. The first term on the right side of the equation is the partial derivative of the temperature with respect to time; this is also referred to as a local derivative. We are interested in the change of temperature T with respect to time t; however, T changes with respect to the position function $\vec{s}$, which also depends on the time ($\frac{\mathrm{d}\vec{s}}{\mathrm{d}t}$). This consideration is the basis for the second term, the convective derivative. We form the velocity $\vec{v}$ from the derivative of the position function with respect to time $\frac{\mathrm{d}\vec{s}}{\mathrm{d}t}$.

2.4.2 Integration

Integration is the reverse of the mathematical operation of differentiation. Bronstein and Semendjajew [8, S. 443] state: "While in differential calculus, the derivative of a given function has to be determined, in integral calculus a function is to be found for a given derivative, whose derivative corresponds to the pregiven one."
Imagine again our journey from Munich to Rome, in which we are at position $\vec{s}(t)$ (position vector) at a point of time t. We also already know that the derivative of the position function with respect to time corresponds to the velocity:

$$\vec{v} = \frac{\mathrm{d}\vec{s}}{\mathrm{d}t} \tag{2.11}$$

Our speed is shown in Figure 2.9. We start slowly and accelerate on the highway, take a break and start again for the last stage of the trip.

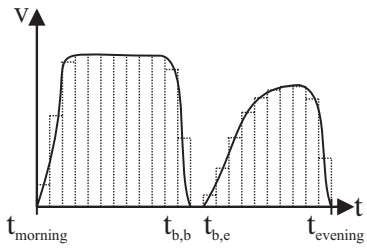

Figure 2.9: Cruising speed as a function of time.

Using integration, we will now calculate the distance travelled. Based on the units alone, it is obvious that our position (or the distance travelled) may be determined by multiplying the velocity $\vec{v}$ by the time t, during which we travel at exactly that velocity. In a purely formal manner, this is done by integrating the velocity over time, which corresponds to the area under the curve in the graph.

$$\vec{s} = \int_{t_{\mathrm{morning}}}^{t_{\mathrm{b,b}}} \vec{v}(t)\,\mathrm{d}t + \int_{t_{\mathrm{b,e}}}^{t_{\mathrm{evening}}} \vec{v}(t)\,\mathrm{d}t \tag{2.12}$$

On the basis of our example, we obtain the position $\vec{s}(t = \text{evening}) = 914\,\mathrm{km}$ (or the norm of the vector as the distance travelled), if the origin of our coordinate system is in Munich.

2.5 Kinematics

In kinematics, deformations are described without considering the forces that cause them. A volume, or two-dimensionally, a surface, may alter its appearance in various ways. While in solid mechanics, deformations and stresses are correlated, it is the deformation speed and the stresses that are correlated in fluid mechanics (see Chapter 5.5). Therefore, in the following discussion, the deformations of a fluid element will be described – for better presentability – in two-dimensional space.

Imagine the area shown in Figure 2.10 as a flexible square whose corners are held by the students Andreas (A), Bernd (B), Claus (C) and Dennis (D). If all four students move at the same velocity, i. e. at the same velocity norm in the same direction (x in this case), the shape of the area is maintained. Here, the velocity in the y direction is zero and changes neither in the x- nor in the y-direction ($v = 0$; $\frac{\partial v}{\partial x} = 0$; $\frac{\partial v}{\partial y} = 0$); a velocity in the x-direction prevails which is constant in all directions ($u = \text{const.}$; $\frac{\partial u}{\partial x} = 0$; $\frac{\partial u}{\partial y} = 0$).

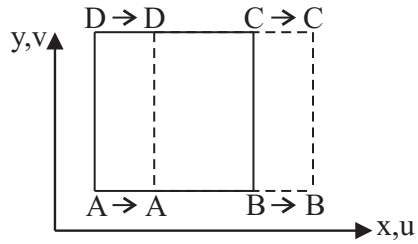

Figure 2.10: Deformation of an element in case of equal velocities at the corners.

2.5.1 Dilatation

Figure 2.11 shows how the element is deformed if an acceleration of the velocity component u occurs along the x-direction. Andreas and Dennis, who are standing at the same horizontal distance x, move more slowly than Bernd and Claus. The u component increases along the x-axis to the right ($\frac{\partial u}{\partial x} \neq 0$). Since Andreas and Dennis move at the same velocity, and Bernd and Claus also each move at the same velocity, though faster than Andreas and Dennis, the element is simply stretched[C]. The change in area (or volume, in three dimensions) represents the trace (i. e. the sum of the main diagonal elements) of the velocity gradient tensor (see Chapter 2.5.4 and Equation 2.16).

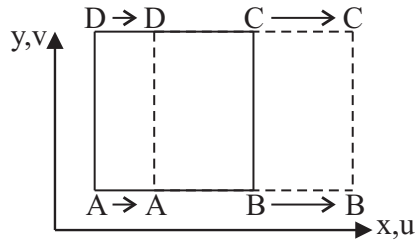

Figure 2.11: Dilatation / stretching of an element.

[C] The increase in area would correspond to an increase in volume in three-dimensional space which, due to the incompressibility of water, is not possible (see Chapter 3.4.10). The element would have to become thinner in the third spatial direction.

2.5.2 Shearing

We will now take our example further. An Audi and a BMW drive in the right lane, and a Citröen and a Dodge in the fast (left) lane of the highway. All four cars are driving in the same direction (x), with the Audi and the BMW at a lower velocity. Since the imaginarily spanned area created by the distances travelled by the four cars is sheared (see Figure 2.12), the square becomes diamond-shaped. In this case, a change of the x velocity component u at two different values of y is given (the Audi and the BMW are at the same y-value; the Citröen and the Dodge are driving at a higher value of y in the fast lane). This relation is mathematically described by the velocity derivative $\frac{\partial u}{\partial y} \neq 0$. None of the cars accelerate or brake, so that the change of the velocity component in the x-direction is zero: $\frac{\partial u}{\partial x} = 0$. The velocity component v (in the y-direction) is zero and does not change, neither in the x-direction nor in the y-direction; i. e. all cars remain in their lanes: $\frac{\partial v}{\partial x} = 0$ and $\frac{\partial v}{\partial y} = 0$.

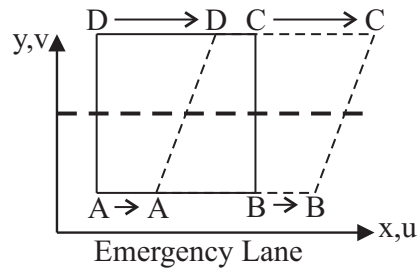

Figure 2.12: Shearing of an element.

2.5.3 Rotation

In our "student" example, the positive x-direction will now be identified by $+x$ and the negative y direction by $-y$. If Andreas moves one step in $-y$ and one step in $+x$, Bernd simultaneously in $+x$ and $+y$, Claus in $+y$ and $-x$ and Dennis in $-x$ and $-y$, then our square is not deformed but rotated. This is referred to as a rotation (see Figure 2.13). We see that Andreas and Bernd each move one step to the right, i. e. that the velocity component u along the x-direction does not change. The same applies to Claus and Dennis, whose steps to the left also do not allow a change of the u-component along the x-direction. Thus: $\frac{\partial u}{\partial x} = 0$. But at the same time, we learn that there is definitely a change of the u-component in the y-direction, because while Andreas and Bernd go to the right, Claus and Dennis, who have a higher y-position, take one step to the left, which results in $\frac{\partial u}{\partial y} \neq 0$. The same applies to the v-component. Andreas and Dennis, who are situated along the same x-position, move one step downward while Bernd and Claus move upward. Thus, the v-component does not change in the y-direction, but it does in the x-direction ($\frac{\partial v}{\partial y} = 0$, $\frac{\partial v}{\partial x} \neq 0$). We will return to this later in Chapter 2.5.4.
The x-, y-, and z-components of the rotation vector correspond to the vectors that are normal to the plane of rotation. For example, the x-component of the rotation vector

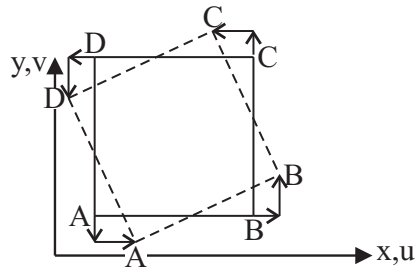

Figure 2.13: Rotation of an element.

describes the rotation in the *y*-*z* plane. The rotation vector, for whose direction of rotation the "right hand rule" applies, is:

$$\vec{\omega} = \begin{pmatrix} \frac{\partial w}{\partial y} - \frac{\partial v}{\partial z} \\ \frac{\partial u}{\partial z} - \frac{\partial w}{\partial x} \\ \frac{\partial v}{\partial x} - \frac{\partial u}{\partial y} \end{pmatrix} \tag{2.13}$$

If you memorise "*wuv*, or better wuff wuff ;-)", as the sequence of the velocity components which are derived to the remaining spatial direction and subtract the elements mirrored on the main diagonal from this, it is quite easy to remember the rotation vector. The rotation vector can also be written as the cross product of the nabla operator ∇ and the velocity vector $\vec{u}$ (see Chapter 2.2.5 or Equation 2.6):

$$\mathrm{rot}\,\vec{u} = \nabla \times \vec{u} = \begin{pmatrix} \frac{\partial}{\partial x} \\ \frac{\partial}{\partial y} \\ \frac{\partial}{\partial z} \end{pmatrix} \times \begin{pmatrix} u \\ v \\ w \end{pmatrix} = \begin{pmatrix} \frac{\partial w}{\partial y} - \frac{\partial v}{\partial z} \\ \frac{\partial u}{\partial z} - \frac{\partial w}{\partial x} \\ \frac{\partial v}{\partial x} - \frac{\partial u}{\partial y} \end{pmatrix} \tag{2.14}$$

2.5.4 Velocity gradient tensor

The variations of the velocities on a field as explained above may be represented by the so-called velocity gradient tensor $\nabla\vec{u}$. This tensor includes the superpositioning of shearing, dilatation and rotation of an element. The tensor in three-dimensional space is written as:

$$\nabla\vec{u} = \begin{pmatrix} \frac{\partial u}{\partial x} & \frac{\partial u}{\partial y} & \frac{\partial u}{\partial z} \\ \frac{\partial v}{\partial x} & \frac{\partial v}{\partial y} & \frac{\partial v}{\partial z} \\ \frac{\partial w}{\partial x} & \frac{\partial w}{\partial y} & \frac{\partial w}{\partial z} \end{pmatrix} \tag{2.15}$$

The meaning of the elements of this tensor may be explained by means of the following example: Elementary deformations may be described via the decomposition of the velocity gradient tensor (see Equation 2.15) into a symmetric (s_{ij}, Equation 2.16) and an antisymmetric part (e_{ij}, Equation 2.17). In turn, the sum of s_{ij} and e_{ij} results in $\nabla\vec{u}$.

$$s_{ij} = \frac{1}{2} \begin{pmatrix} \frac{\partial u}{\partial x} + \frac{\partial u}{\partial x} & \frac{\partial u}{\partial y} + \frac{\partial v}{\partial x} & \frac{\partial u}{\partial z} + \frac{\partial w}{\partial x} \\ \frac{\partial v}{\partial x} + \frac{\partial u}{\partial y} & \frac{\partial v}{\partial y} + \frac{\partial v}{\partial y} & \frac{\partial v}{\partial z} + \frac{\partial w}{\partial y} \\ \frac{\partial w}{\partial x} + \frac{\partial u}{\partial z} & \frac{\partial w}{\partial y} + \frac{\partial v}{\partial z} & \frac{\partial w}{\partial z} + \frac{\partial w}{\partial z} \end{pmatrix} \tag{2.16}$$

$$e_{ij} = \frac{1}{2}\begin{pmatrix} 0 & \frac{\partial u}{\partial y} - \frac{\partial v}{\partial x} & \frac{\partial u}{\partial z} - \frac{\partial w}{\partial x} \\ \frac{\partial v}{\partial x} - \frac{\partial u}{\partial y} & 0 & \frac{\partial v}{\partial z} - \frac{\partial w}{\partial y} \\ \frac{\partial w}{\partial x} - \frac{\partial u}{\partial z} & \frac{\partial w}{\partial y} - \frac{\partial v}{\partial z} & 0 \end{pmatrix} \tag{2.17}$$

The main diagonal elements of the tensor ($\frac{\partial u}{\partial x}$, $\frac{\partial v}{\partial y}$, $\frac{\partial w}{\partial z}$), which are also found in the symmetric part, specify the dilatation.
The off-diagonal elements are responsible for shearing and rotation. If both $\frac{\partial u}{\partial y}$ and $\frac{\partial v}{\partial x}$ are positive, the element is sheared and becomes diamond-shaped. The right-hand lower corner moves upward because $\frac{\partial v}{\partial x} > 0$. The left-hand upper corner moves to the right due to $\frac{\partial u}{\partial y} > 0$. For the right-hand upper corner, both changes apply, and the corner moves to the right and upward. You will find the summation of the secondary diagonal elements in the symmetric part of the velocity gradient tensor $\frac{1}{2}\left(\frac{\partial u}{\partial y} + \frac{\partial v}{\partial x}\right)$, which indicates shearing.
The antisymmetric part of the velocity gradient tensor (Equation 2.17) indicates the rotation of an element in the flow (see Figure 2.13). If the norms of $\frac{\partial u}{\partial y}$ and $\frac{\partial v}{\partial x}$ are equal, but have opposite signs, then the element rotates without deformations occurring.

2.5.5 Divergence

The divergence of the velocity vector is the sum of the main diagonal elements of the velocity gradient tensor (i. e. its trace); divergence corresponds to the change in volume:

$$\operatorname{div} \vec{u} = \frac{\partial u}{\partial x} + \frac{\partial v}{\partial y} + \frac{\partial w}{\partial z} \tag{2.18}$$

For an incompressible fluid (see Chapter 3.4.10), i. e. a medium whose density does not change upon the application of pressure, the constant mass is equivalent to the constant volume. Therefore, the following applies to incompressible fluids: $\operatorname{div} \vec{u} = 0$.

2.6 Einstein summation convention

The Einstein[D] summation convention is a notation which is often used for expressing three-dimensional equations. In this context, [8, p. 271] reads:

> The summation convention generally stipulates that if an index occurs twice in an expression, the expression is summed over all provided values of this index. If an index occurs once in the expressions, ..., this means that the relevant equation applies to all values that may be passed by this index.

With the indices used in this book, the equation for $i = j = 1, 2, 3$ in the above-mentioned source becomes:

$$\tilde{x_i} = a_{ij} x_j \tag{2.19}$$

[D] Albert Einstein, ∗1879, Ulm, Germany, †1955, Princeton, USA

$$\begin{aligned} \tilde{x_1} &= a_{11}x_1 + a_{12}x_2 + a_{13}x_3 \\ \tilde{x_2} &= a_{21}x_1 + a_{22}x_2 + a_{23}x_3 \\ \tilde{x_3} &= a_{31}x_1 + a_{32}x_2 + a_{33}x_3 \end{aligned} \tag{2.20}$$

We will use the Einstein summation convention in the description of the fundamental equations.

2.7 Elementary fluid mechanic terms

Table 2.1 summarises elementary fluid mechanics terms. The following figures in Table 2.2 illustrate these relationships.

Table 2.1: Elementary fluid mechanics terms.

steady	$\frac{\partial \vec{u}}{\partial t} = 0$	the local velocity does **not** change as a function of time
unsteady	$\frac{\partial \vec{u}}{\partial t} \neq 0$	the local velocity changes as a function of time
uniform	$\frac{\partial \vec{u}}{\partial \vec{s}} = 0$	the velocity does **not** change as a function of place
non-uniform	$\frac{\partial \vec{u}}{\partial \vec{s}} \neq 0$	the velocity changes with place
continuous	$\frac{\partial Q}{\partial \vec{s}} = 0$	the flow rate does **not** change as a function of place
discontinuous	$\frac{\partial Q}{\partial \vec{s}} \neq 0$	the flow rate changes as a function of place

Table 2.2: Examples of flow types.

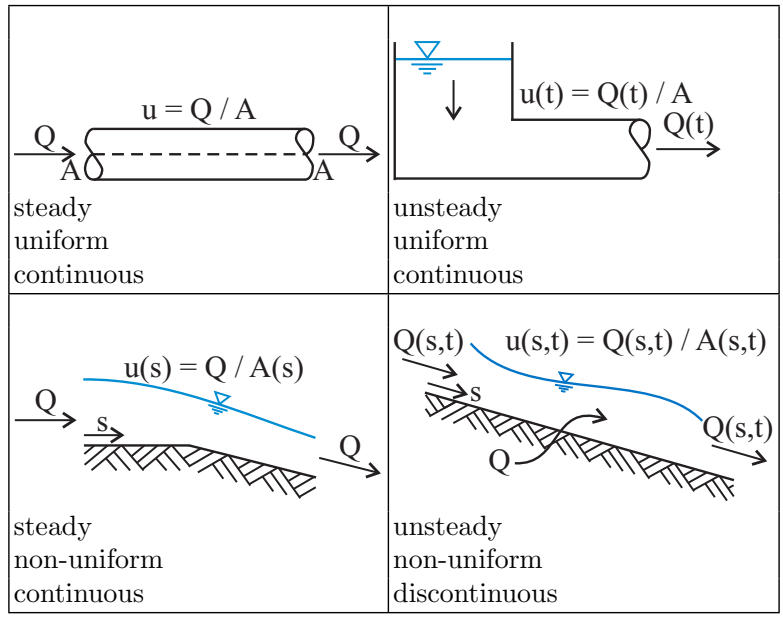

The upper left-hand figure in Table 2.2 does not show any time dependency. Therefore, the flow is steady. The discharge cross-section does not change, which is why the flow velocity does not change. Thus, the flow is uniform. As no fluid is added or leaked, the flow is continuous.
In Table 2.2, top right, a time dependency is indicated by $Q(t)$. The container fluid is discharged. Thus, the flow is unsteady. Because of the lack of any extra inflow or outflow, the flow is to be identified as continuous. And because the cross-section does not vary along the length of the pipe, the flow is uniform.
In Table 2.2, bottom left, no time dependency is discernible; therefore, the flow is to be termed as steady. Not a single drop of fluid leaves the water body except for the outlet cross-section, and nothing may enter it except for the inlet cross-section; therefore, the flow is continuous. However, the flow velocity varies along the streamwise direction $\vec{s}$ due to the variable cross-section. Thus, the flow in the bottom-left figure is non-uniform.
Table 2.2, bottom right, illustrates where the velocity changes as a function of time and place. In addition, a lateral inflow is identified. The flow is unsteady, non-uniform and discontinuous.

2.8 Selected flow lines

2.8.1 Streakline

A streakline is the trace connecting all fluid particles that have passed a prescribed point. Imagine a marathon refreshment station. The trace connecting all runners with cups is a streakline. Figure 2.14 shows water vapour from a chimney of a power station. The current connection of all particles that have passed the chimney tip carries the water vapour as tracer, while the other particles do not.

Figure 2.14: Example of a streakline. The addition of water vapour occurs at the chimney, the point source. The vapour cloud shows the trace connecting all particles that were at this point.

2.8.2 Streamline

Streamlines are tangents of the flow vectors. Figure 2.15 shows streamlines as they develop with the selected flow configuration over the time average. The fluid flows over periodically arranged hills. Similar to a ski jumper, the flow lifts off the hill in time average and only attaches again at approximately $\frac{x}{h} \approx 4$. The space between hill and reattachment point is filled by a so-called recirculation zone. On the right-hand side, the acceleration of the fluid due to the reduction of the outlet cross-section may be seen from the decreasing distances between the streamlines.

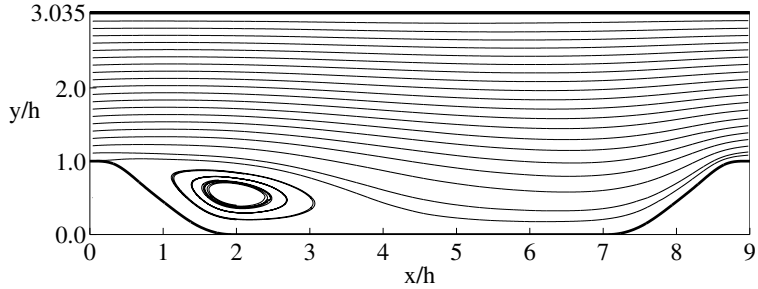

Figure 2.15: Streamlines of a flow over periodically arranged hills.

2.8.3 Pathline

A pathline is the connection of those locations that were touched by a fluid element. A comet with its tail would be a suitable image for a pathline. Or perhaps you may recall the story of Hänsel and Gretel who dropped breadcrumbs (which were subsequently eaten by birds) to mark their path. The crumbs represent the places where the two children had been (see Figure 2.16).

Figure 2.16: Hänsel and Gretel mark their pathline with bread crumbs. Charity stamp of the Deutsche Bundespost, issued 02.10.1961. Circulation 9750000, Michel No. 369, design Bert Jäger.

2.8.4 Streamtube

A surrounding bundle of streamlines is referred to as a streamtube; no fluid bale leaks through its lateral surface. Therefore, the volume flow, which may also be referred to as flow rate or discharge, may be designated as a scalar product between the velocity vector $\vec{u}$ and the cross-sectional vector area $\vec{n}\,\mathrm{d}A$ as:

$$Q = \int \vec{u} \circ \vec{n}\,\mathrm{d}A \tag{2.21}$$

In the case of laminar flows (see Chapter 6), streamlines, streaklines and pathlines are identical.

2.9 Selected cross-sections

In hydraulics, a clear distinction is made between flows under pressure (pipe hydraulics) and flows with free surfaces (open channel hydraulics). Sometimes these conditions alternate over time, e. g. in a sewage system, which exhibits a free water level and flow during dry weather and a discharge under pressure in case of flood.
In this chapter, the most common cross-sections will be discussed with respect to their characteristic quantities. From the continuity condition (Equation 5.2), it becomes apparent that the area A plays a major role in hydraulics due to its linear relationship with the flow velocity. Another quantity, whose impact we will only become acquainted with in Chapter 13.9, is the so-called wetted perimeter P. This is the area where the flow is in contact with the boundary, i. e. where external friction occurs. In a riverbed, these are the bank slopes and the base, in a circular cross-section the circular arc from the bottom to the water level. We may generally assume that the friction between water and air is negligible. The flow area and the wetted perimeter are linked via the so-called hydraulic radius $R_{\mathrm{hy}} = \frac{A}{P}$ (see Figure 13.22). Table 2.3 displays the area, the wetted perimeter and the width of the water surface of selected cross-sections.

Table 2.3: Characteristic values of selected cross-sections.

sketch	area $[m^2]$	wetted perimeter [m]	width water surface [m]
completely filled circular pipe 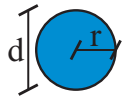	$A = r^2\pi = \frac{d^2\pi}{4}$	$P = 2r\pi = d\pi$	———
completely filled rectangular pipe 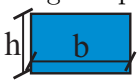	$A = bh$	$P = 2(b+h)$	———
rectangular cross-section 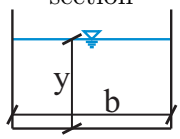	$A = by$	$P = b+2y$	$b_{WS} = b$
trapezoidal cross-section 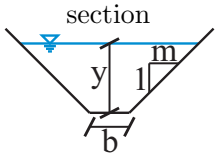	$A = (b+my)\,y$	$P = b+2y\sqrt{1+m^2}$	$b_{WS} = b+2my$
partially filled circular pipe 	$\alpha = 2\,\text{acos}\left(1-\frac{y}{r}\right)$; $A = \frac{1}{2}r^2(\alpha - \sin(\alpha))$	$P = r\cdot\alpha$	$b_{WS} = d\cdot\sin\left(\frac{\alpha}{2}\right)$

Chapter 3
Essential physics

3.1 Aggregate states

3.1.1 Solid

In a solid body, the molecules have a fixed, unalterable order as long as the stress remains under the yield point (σ see Chapter 3.4.7). When stress is applied, the object will consequently be deformed (ε see Chapter 3.4.8), and when stress is released, the solid body will return to its original shape (elastic behaviour; see Figure 3.1). With twice the stress applied, the deformation will be doubled (linear elastic behaviour). If a solid body is subjected to plastic deformation, then the molecular structure will be irreversibly altered at one place.

Figure 3.1: Stress/deformation behaviour of an elastic solid body.

Take a ruler and apply a stress by bending it. When the stress is released, the ruler returns to its original unbent state. The ruler exhibits an elastic behaviour. Then get an ice lolly and suck it until only the stick remains. Now repeat the same experiment with the lolly stick, but this time, apply sufficient stress to break the stick. In this case, the lolly stick shows a plastic deformation behaviour.

C. Rapp, *Hydraulics in Civil Engineering*,
https://doi.org/10.1007/978-3-031-54860-4_3

3.1.2 Liquid

Liquids and gases are referred to as fluids. The molecular structure is not fixed; the molecules are able to move in space. If a stress is temporarily applied to a fluid, the fluid is deformed but does not return to its original condition upon stress release. This behaviour is depicted in Figure 3.2. In any given space, liquids gather at the bottom, like water in a glass, for example.

Figure 3.2: Stress/deformation behaviour of a fluid.

Take a glass filled with water and apply a stress by emptying it. When you release the stress, i. e. put the emptied glass back on the table, the liquid will not return into the glass. The deformation ε is maintained.

3.1.3 Gaseous

Gases have properties similar to those of liquids; the molecules are able to move freely. However, it is much easier to compress gases (see Chapter 3.4.10), which have a much lower density (see Chapter 3.4.6) than liquids. The number of particles of an ideal gas is constant in a certain volume at the same pressure (see Chapter 3.4.9) and same temperature and thus independent of the particle mass or the particle type.

As in the case of fluids, gases do not return to their original state when stress is released. Think about cigarette smoke that is exhaled; it does not enter the lungs when the stress is released. In order to breath in again, stress must be applied anew.

3.1.4 Aggregate states of water

The three states of water – solid, liquid, gaseous – are best explained by means of the phase diagram (see Figure 3.3).
By plotting the pressure vertically upwards and the temperature to the right, a sort of "y" forms between the regions of the three phases of water. On the left at low temperatures, water is solid; in the centre, it is liquid; and at high temperatures, it is gaseous. At a low pressure, water exists only in a solid or gaseous state, and the transition from one to the other state is called (re-)sublimation. We all have often experienced phase changes

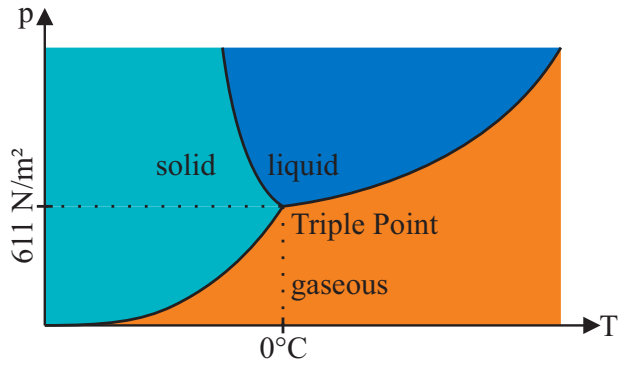

Figure 3.3: Phase diagram of water.

between the solid, liquid and gaseous phases and are made aware of them by changing temperatures. When it gets warm in springtime, the snow melts; the frozen water becomes liquid again. When boiling pasta, some of the water evaporates and becomes gaseous. The dependence on pressure is not something we come across often. When boiling eggs on a mountain where the air pressure is lower, the phase transition occurs at a lower temperature. Water changes its state on the right branch of the "y" further down and thus at a lower temperature. In order to be cooked to perfection, the eggs must be boiled for a longer period at the lower evaporation temperature.

3.2 Quantities and their units

In physics, quantities without units are meaningless. When choosing the right means of transport to cover a distance specified as 600, it is crucial that we know whether we are referring to metres or kilometres. When working with international teams or on international projects, it is necessary to agree on a system being used: the "Système international d'unités" (SI) or the Anglo-Saxon "Imperial System". In our field of science, this applies in particular to the local (Gauß-Krüger coordinates, UTM, etc.) and altitude indications (metres above sea level based on the sea level of the North Sea or the Mediterranean Sea). In science, the SI (also known as the metric system) units have prevailed due to their practicality. The SI system is built on seven basic units. These are summarised in Table 3.1. In the context of hydraulics, we will deal with the first four basic units and derive all the other ones from them.

3.3 Newton's axioms

Generally speaking, the entire contents of this book are based on Newtonian mechanics and its fundamental statements on the motions of bodies. Dialectically, it is necessary to differentiate between verifiable laws and axioms, i. e. "statements of a mathematical theory, from which the other [statements] may logically be derived" [7]. The axiom itself cannot be substantiated within a system but is fundamental to it.

Table 3.1: SI basic units.

quantity	symbol	unit	unit symbol
length	L	metre	m
mass	m	kilogram	kg
time	T	second	s
temperature	T	kelvin	K
current	I	ampere	A
amount of substance	N	mol	mol
luminous intensity	J	candela	cd

3.3.1 Lex prima – inertial law

A body remains in a state of rest or uniform translation unless applied forces cause a change in this state of motion.

$$\vec{v} = \text{const.} \quad \text{for } \vec{F} = 0 \tag{3.1}$$

In other words, if a body must change its state of motion, forces must act on it.

3.3.2 Lex secunda – basic equation of mechanics

The change in motion is proportional to the magnitude of the applied force and takes place in the direction of the straight line along which the force is acting.

The change in momentum over time results from the acting forces. On this subject, Grehn et al [15] offer the following summary:

The force $\vec{F}$ which imparts the acceleration $\vec{a}$ on a body with the mass m is the product of this mass m and the acceleration $\vec{a}$.

$$\vec{F} = m\vec{a} = m\frac{\mathrm{d}\vec{v}}{\mathrm{d}t} \tag{3.2}$$

3.3.3 Lex tertia - "actio = reactio"

Forces always occur in pairs.

When a body A applies the force $\vec{F}_A$ on a body B (actio), then B also applies on A the force $\vec{F}_B$, referred to as counterforce (reactio), which is opposed and its absolute value equal to the first force [15]. For a one-dimensional problem we can write:

$$\vec{F}_A = -\vec{F}_B \tag{3.3}$$

3.4 Principal physical quantities

3.4.1 Force

A force $\vec{F}$ is equivalent to the product of mass and acceleration:

$$\vec{F} = m\vec{a} \quad [\mathrm{N}] = \left[\mathrm{kg\,m/s^2}\right] \tag{3.4}$$

A beer crate containing 20 bottles with the mass

$$m = 20 \cdot 0.5\,\mathrm{L} \cdot 1\,\mathrm{kg/L} + 20 \cdot m_{\mathrm{bottle}} + m_{\mathrm{crate}} \tag{3.5}$$

has a weight force of:

$$F_{G,\text{beer crate}} = (20 \cdot 0.5\,\mathrm{L} \cdot 1\,\mathrm{kg/L} + 20 \cdot m_{\mathrm{bottle}} + m_{\mathrm{crate}})\,g \tag{3.6}$$

3.4.2 Momentum

A force is the change in momentum $\vec{I}$ over time, which corresponds to Newton's second axiom.

$$\vec{F} = \frac{\mathrm{d}\vec{I}}{\mathrm{d}t} = m\frac{\mathrm{d}\vec{v}}{\mathrm{d}t} \quad \text{with } \vec{I}\ [\mathrm{N\,s}] \tag{3.7}$$

In order to change the momentum of a beer crate, i. e. in order to bring it from the rest state into motion, a force must be applied.

$$F_x = m_{\text{beer crate}}\frac{\mathrm{d}u}{\mathrm{d}t} \tag{3.8}$$

$$\mathrm{d}t = m_{\text{beer crate}}\frac{\mathrm{d}u}{F_x} \tag{3.9}$$

If the beer crate with the mass $m_{\text{beer crate}} = 12\,\mathrm{kg}$ is to be accelerated from the rest state to the velocity $u = 0.2\,\mathrm{m/s}$ in the x-direction, then a force of $F_x = 1.0\,\mathrm{N}$ over $\mathrm{d}t = \frac{12\,\mathrm{kg}\cdot 0.2\,\mathrm{m/s}}{1\,\mathrm{N}} = 2.4\,\mathrm{s}$ must be applied.

3.4.3 Work

In physics, work W corresponds to a force which is applied over a certain displacement. Work is the scalar product of the vectorial quantities force and displacement.

$$W = \vec{F} \circ \vec{x} \quad [\mathrm{N\,m}] \tag{3.10}$$

Work due to lifting, acceleration, clamping and friction can be done on a body. In the case of work due to lifting, a body with a weight F_G is lifted by a distance Δh. If a body is subjected to a force with a component along the displacement vector $\vec{s}$, it is accelerated and then possesses the kinetic energy $\frac{1}{2}mv^2$ (see Chapter 3.4.4). Work may, for example,

also be done by tightening a spring or compressing a fluid. Friction work must be done in order to overcome the force due to friction F_R along a distance $\vec{s}$. If you lift a beer crate from the floor onto a table that is 70 cm[A] high, you did the following lifting work:

$$W = m_{\text{crate}} \cdot \vec{g} \circ \vec{s} = F_{G,\text{crate}} \cdot h_{\text{table}} = 12\,\text{kg} \cdot 9.81\,\text{m/s}^2 \cdot 0.7\,\text{m} = 82.4\,\text{N m} \tag{3.11}$$

The scalar product ensures that only the displacement parallel to the gravity vector $\vec{g}$, where $\vec{g} \circ \vec{s} = h_{\text{table}}$, is accounted for. Work may be doubled by either lifting two beer crates onto the table or one crate twice as high.

3.4.4 Energy

In [15], the following definition of energy can be found:

> The energy of a body or a system is a property whose change Δe equals the work W which is (externally) done on the body or the system.

If work is done on a body, its energy is increased; if the body or the system does work externally, the body's or the system's energy decreases [15]:

$$\Delta e = W \quad [\text{N m}] = [\text{J}] \tag{3.12}$$

By lifting the beer crate, we have increased its energy by $\Delta e = F_G \cdot h_{\text{table}}$. When pulling the crate over the floor, we carry out friction work. The energy which was applied as force $\vec{F}$ over the length of the displacement vector $\vec{s}$ was converted to heat (beer crate and floor). A body can be accelerated by the application of energy and will then possess kinetic energy $\frac{1}{2}mv^2$. If, for example, a piston is pushed with a force $\vec{F}$ along the path $\vec{s}$ within a closed cylinder, the medium in the cylinder is compressed, and upon stress release, the work done becomes free again[B]. The so-called first law of thermodynamics states that the energy in a closed system remains constant (see e. g. [15]):

> The sum of energies within a system is constant.

3.4.5 Power

Power P corresponds to work per unit time.

$$P = \frac{W}{t} \quad [\text{N m/s}] = [\text{W}] \tag{3.13}$$

Don't be confused. W is the abbreviation for work as well as for the unit of power – Watt. A person who can place the beer onto the table quickly demonstrates considerable power. Even if two people carry out the same work by lifting 10 beer crates 70 cm and placing them onto the table, the one who needed only 1 min for this task performed twice the power of the other one who took 2 min.

[A] Do not fail to use the correct SI units from the very beginning; i. e. insert 0.70 m rather than 70 cm.

[B] Compressed air storage reservoirs utilise what is known as compression energy.

3.4.6 Density

The density ρ of a homogenous body corresponds to the quotient of mass and volume $\rho = \frac{m}{V}$ and has the unit $\mathrm{kg/m^3}$.

Determine the density of water by weighing a measuring cylinder, filling it, and determining its mass again. If possible, check the indicated volume of the measuring cylinder by measuring its height and radius.
Now you can add salt, for example, to the content of the container and check both the level and weight. Make sure that the salt is dissolved.
What are your findings?
The density of water amounts to approximately $1000\,\mathrm{kg/m^3}$. It increases with the addition of salt.

3.4.7 Stress

Stress σ or τ is a "generally non-isotropic [i. e. of different magnitudes in the spatial directions] reaction force, related to an area in elastic bodies when deformed by external forces" [7]. In fluid mechanics, normal stresses, i. e. stresses acting perpendicularly on a particular surface, are referred to as pressure p (see Chapter 3.4.9) and surface parallel stresses are known as shear stresses τ. In Chapter 2, a tensor was already explained by means of the stress example (see Equation 2.3). From the definition of stress, its units $\mathrm{N/m^2}$ follow. In mechanics, tensile stresses are generally defined positively and compression stresses negatively. In hydromechanics, no tensile stresses occur, which is why the pressure always has a positive sign. It is only in the relative reference system (see Chapter 8.7) that water pressure may take negative values.

At first sight, surface tensions (see Chapter 3.4.12) have nothing to do with the stress described here; this also becomes clear from their respective units.

3.4.8 Deformation (rate)

In the case of a solid body, stress and elongation describe elastic behaviour (see Figure 3.1). When the elastic stress is released, the solid body returns to its initial state. Deformation is indicated as $\varepsilon = \frac{\Delta l}{l}$.
In fluids, applied stresses cause a deformation as long as they are maintained (see Figure 3.2). Therefore, stress is responsible for the deformation rate of a fluid. This deformation rate is described by the velocity gradient tensor (see Equation 2.15).

3.4.9 Pressure

Pressure p corresponds to the "force per unit area of a surface" [7]. Everybody is probably familiar with it as a scalar quantity, though a watertight definition sounds quite clumsy.

Instead, let's take a look at the human pyramid in Figure 3.4. While no pressure acts on Andreas, Alexander and Anton from above, Bernd, Bastian, Bruno and Benedikt have to carry the upper three. Carsten, Christian and Claus are even worse off because they not only have to carry Andreas, Alexander and Anton but also the additional load of Bernd, Bruno and Benedikt. Dominik, Ditmar, Daniel and Detlef bear the pressure of the three rows above them. The pressure perceived by a particular row depends upon the weight of the people stacked above and whether the human pyramid is built on the Moon or on the Earth because of the magnitude of the gravitational constant $\vec{g}$. In correct physical terms, the pressure depends on the density of the continuum, the gravity and on the overlying medium.

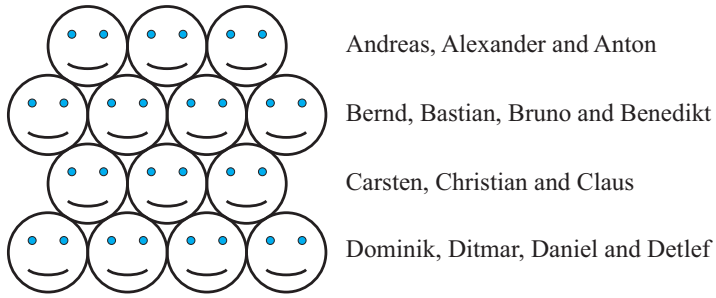

Figure 3.4: Illustration of the pressure that is linearly dependent on the overlying medium.

$$p = \rho g h \quad \text{for} \, \rho = \text{const.} \tag{3.14}$$

When stacking humans of identical density in our example, the linear dependence of pressure on depth can already be seen. This will be discussed in detail in Chapter 7. The pressure reflects normal stress, which means that it acts perpendicularly to the surface surrounding the medium.
At this point, it makes sense to differentiate and clarify the concepts of absolute und relative pressure in detail.

3.4.9.1 Absolute pressure

The term "absolute pressure" is understood to be the sum of air and water pressure. When we are at sea level, the ambient air has a pressure of approximately $p_{\text{atm}} = 1013\,\text{mbar}$. Then, if we dive $h = 10\,\text{m}$ into the sea, we are subjected to the pressure $p(h) = p_{\text{atm}} + \rho_{\text{seawater}} \cdot g \cdot h$.
Due to the fact that in nearly all hydromechanical applications the atmospheric pressure acts from all sides, we may always calculate – aside from one exception – the relative pressure. When considering closed air volumes (see Chapter 7.9), we must use the absolute pressure.

3.4.9.2 Relative pressure

The relative pressure is related to the ambient pressure p_{atm}. Relative to it, the pressure increases to $p(h) = \rho_{\text{seawater}} \cdot g \cdot h$ during our dive into the sea.

3.4.10 Compressibility

The compressibility of a body indicates the change in volume when a stress is applied. Compressibility is described as the ratio between the pressure applied to a volume and the change in volume:

$$E = -\frac{\Delta pV}{\Delta V} \tag{3.15}$$

Thus, the modulus of elasticity (also known as Young's modulus) has the same units as pressure $\left[\mathrm{N/m^2}\right]$. The minus sign is due to the fact that the volume becomes smaller ΔV, i. e. negative, when pressure is applied.

You may demonstrate compressibility by using a syringe – without the needle. Draw air up into the syringe and seal the opening with your finger. If you now push the piston down, the air volume is compressed. The piston is moving until the air cannot be compressed any further. Repeat the experiment with water as the test medium and make sure that no air is trapped. You will not be able to push the piston into the shaft of the syringe because water is much less compressible than air; therefore, it has a greater modulus of elasticity.

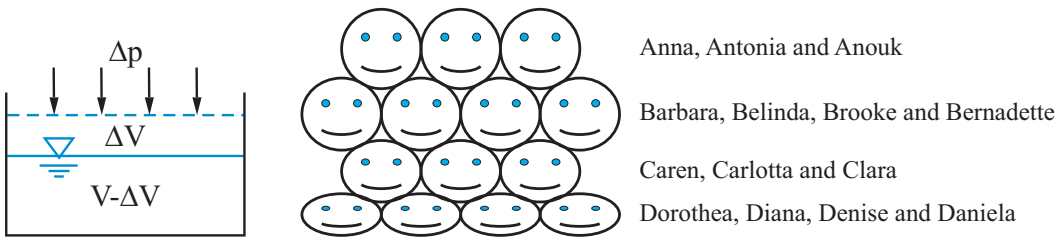

Figure 3.5: Compression of a fluid volume (left) and explanation of the pressure distribution with compressible media (right).

If we think back to the example in Figure 3.4, we assumed that the humans were not squeezed together by the overlying load. On the right-hand side of Figure 3.5, the lower rows are compressed due to the load. Here, the initial mass of a human (or molecule) is constant, the height or the volume in three-dimensional space is reduced; because $\rho = \frac{m}{V}$, this leads to an increase in density as depth increases. Our human pyramid is compressible. Compressibility is an inherent property of gases and leads to the air pressure increasing in a non-linear manner with overlying medium (see Figure 3.6). For compressible fluids, the pressure must be calculated by Equation 3.16:

$$p_{\text{compressible fluids}} = \int \rho(h) g \, \mathrm{d}h \tag{3.16}$$

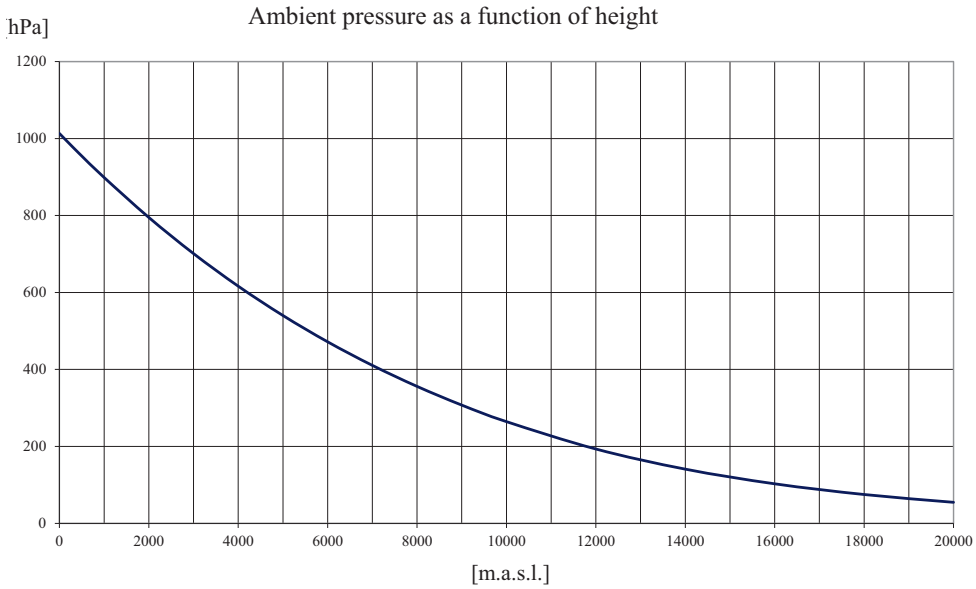

Figure 3.6: Atmospheric pressure as a function of height above sea level.

Climb a mountain and take a plastic bottle (bottled water) with you. At the summit, empty the bottle and seal it tightly before hiking down again.
What happens?
When you are back at the bottom, the bottle will have shrivelled up. The reason is quite simple. The air pressure at the summit is lower than in the valley. When the bottle was sealed, the bottle filled with air was subjected to the pressure prevalent at the mountain top. At the summit, air exerts the same external pressure against the bottle wall as it exerts from inside. While descending, the air pressure outside the bottle increases but the air pressure inside remains constant because the bottle is firmly sealed. Eventually, the bottle no longer withstands the pressure difference between outside and inside and shrivels up.

3.4.11 Viscosity

Viscosity describes the resistance to movement of one layer of fluid over another. Figure 3.7 shows two plates with a fluid in between. By applying a force, one plate is offset relative to the other one. Due to the adhesion condition (the molecules closest to the wall are "glued" onto the wall), the velocity of the fluid directly at the boundary is equal to that of the plate. The velocity gradient, i. e. the change in velocity between the two plates, is indicated by $\frac{\mathrm{d}v}{\mathrm{d}n}$. The force which is required to impose this velocity gradient is dependent on the so-called dynamic viscosity η $\left[\mathrm{Ns/m^2}\right]$ and the area A: $F = -\eta A \frac{\mathrm{d}v}{\mathrm{d}n}$.

$$\sigma = -\eta \frac{\mathrm{d}v}{\mathrm{d}n} \tag{3.17}$$

With what are known as Newtonian fluids, the ratio between applied force (or stress) and the velocity gradient is linear. In fluid mechanics, the kinematic viscosity $\nu = \frac{\eta}{\rho}$ $\left[\mathrm{m}^2/\mathrm{s}\right]$ is often used.

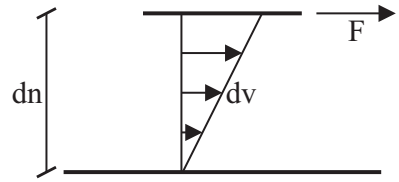

Figure 3.7: Two plates with a fluid in between are offset relative to each other.

In non-Newtonian fluids, on the other hand, the ratio between force and velocity gradient is not linear.

Take two bowls and pour water into one of them. Put corn starch into the second bowl and dissolve it in water. Then stick a finger, first slowly then quickly, into the water bowl and pull the finger out, again slowly then quickly. Repeat the experiment with the corn starch mixture. What are your findings?

We are lucky because we work with water. The characteristics of a Newtonian fluid makes things a lot easier.

3.4.12 Surface tension

The surface tension σ_S is a quantity that may virtually always be neglected. It plays a role only in ground water and in very thin containers or small tubes (capillaries). Its effect can be seen when water is dripped onto a table. The water does not spread over the entire tabletop, but the individual drops remain unaffected and form a curved surface. The contact angle with the limiting medium (i. e. the tabletop) is to be identified by ϕ. Surface tension has the effect of causing water in a capillary to move upwards against gravity. With the balance of the capillary ($F_C = \sigma_S 2r\pi\cos\phi$) and the gravity force ($F_G = \rho g h r^2 \pi$), the rise h, which is primarily dependent on the diameter of the capillary, may be calculated: $h = \frac{2\sigma_S \cos\phi}{\rho g r}$. By the way, the capillary force shows that the surface tension is effective along the boundary $2r\pi$ and therefore has – as the only stress – the unit $\mathrm{N/m}$. The contact angle ϕ between the water and the glass amounts to approximately 20°, so that water rises approximately 2.8 cm in a 1.0 mm thick capillary.

The effects of surface tension are best observed by means of a sand-filled bowl with a perforated bottom (or with at least a few holes). If this bowl is placed in a bed of water, the sand will be soaked far higher than the actual water level.

3.4.13 Discharge

Discharge, which is sometimes also referred to as volume flow rate, is the fluid volume that travels through a flow cross-section within a certain time unit. Formally, the discharge may be described as the integral of the velocity with respect to the cross-sectional area. Since the surface is oriented in a particular direction according to its normal vector, the only velocity component occurring in this direction is multiplied by the flow area in order to obtain the discharge. Mathematically, the scalar product of the velocity $\vec{v}$ and the normal vector $\vec{n}$ is integrated over the surface area $\mathrm{d}A$.

$$Q = \frac{\mathrm{d}V}{\mathrm{d}t} = \int \vec{v} \circ \vec{n} \, \mathrm{d}A \quad \left[\mathrm{m}^3/\mathrm{s}\right] \tag{3.18}$$

3.5 Properties of water

The properties of water, which are relevant to hydraulics, are listed in Table 3.2 for various temperatures.

Boil an egg and remove it from the pot using a spoon. What do you see?
It takes only a few seconds until the egg is completely dry.
The high temperature of the boiled egg heats the air in its vicinity. The water evaporates because the air can absorb more water when the temperature is higher.

Next, take a cold beer from the fridge (I think you deserved it.). What happens?
The beer bottle mists up immediately, and water drops run down it.
Why does this happen? The air temperature directly adjacent to the bottle cools down. At lower temperatures, the air holds less vapour. The water condenses on the bottle and forms drops.

Table 3.2: Properties of liquid water.

temperature	density	dyn. viscosity	kin. viscosity	vapour pressure
T	ρ	η	ν	p_v
[°C]	$[\mathrm{kg/m^3}]$	$10^{-3}\,[\mathrm{Ns/m^2}]$	$10^{-6}\,[\mathrm{m^2/s}]$	$10^{3}\,[\mathrm{N/m^2}]$
0	999.840	1.7921	1.7924	0.6112
5	999.964	1.5108	1.5189	0.8725
10	999.700	1.3077	1.3081	1.2280
15	999.101	1.1404	1.1414	1.7053
20	998.206	1.0050	1.0068	2.3385
30	995.650	0.8007	0.8042	4.2452
40	992.219	0.6560	0.6611	7.3813
50	988.050	0.5494	0.5560	12.334
60	983.210	0.4688	0.4768	19.933
70	977.790	0.4061	0.4153	31.177
80	971.830	0.3565	0.3668	47.375
90	965.320	0.3165	0.3279	70.119
100	958.350	0.2838	0.2961	101.33

Chapter 4
Introduction to potential theory

4.1 Introduction to potential theory

Potential theory is a mathematical construct for describing frictionless and rotationless flows. It is applied to laminar flow around bodies, beyond the boundary layer in aerodynamics and in groundwater hydraulics (see Chapter 15). It is performed analogously in electrical engineering, where a parallel plate capacitor represents a potential field perpendicular to which electrons are travelling. Magnetic field lines are also consistent with this concept. In the context of this book, potential flow is formulated two-dimensionally.
Rotationless flows may be described via a scalar function Φ, the so-called potential function. We set – in a purely mathematical way – the two velocity components equal to the partial derivatives of this potential function:

$$\begin{aligned} u &= \frac{\partial \Phi}{\partial x} \\ v &= \frac{\partial \Phi}{\partial y} \end{aligned} \tag{4.1}$$

When inserting the gradient of the potential function into the two-dimensional continuity condition $\frac{\partial u}{\partial x} + \frac{\partial v}{\partial y} = 0$ (see Equation 2.18), it follows that

$$\frac{\partial u}{\partial x} + \frac{\partial v}{\partial y} = \frac{\partial^2 \Phi}{\partial x^2} + \frac{\partial^2 \Phi}{\partial y^2} = 0 \tag{4.2}$$

This differential equation, which may be found in [8, page 689], is also known as Laplace's[A] equation. The second derivative is therefore represented by what is known as the Laplace operator ∇^2.
We will now pursue the idea that streamlines reflect the tangents of the velocity vectors (see Chapter 2.8 and Figure 4.1). This means that the gradient of the stream function corresponds to the ratio of the velocity components $\frac{\mathrm{d}y}{\mathrm{d}x} = \frac{v}{u}$. The equation is rearranged as follows:

$$u\,\mathrm{d}y - v\,\mathrm{d}x = 0 \tag{4.3}$$

[A] Pierre-Simon Laplace, ∗1749, Beaumont-en-Auge, France, †1827, Paris, France

C. Rapp, *Hydraulics in Civil Engineering*,
https://doi.org/10.1007/978-3-031-54860-4_4

This shows that we can generate a stream function Ψ whose gradient for y results in the component u and whose gradient for x results in the component $-v$:

$$\begin{aligned} u &= \frac{\partial \Psi}{\partial y} \\ v &= -\frac{\partial \Psi}{\partial x} \end{aligned} \tag{4.4}$$

When inserting these expressions for u and v into the condition for the freedom of rotation $\mathrm{rot}\,\vec{v} = \frac{\partial v}{\partial x} - \frac{\partial u}{\partial y} = 0$, (see Chapter 2.5.3), it can be seen that the stream function, as well as the potential function, satisfies Laplace's equation.

$$\begin{aligned} \mathrm{rot}\,\vec{v} = \frac{\partial v}{\partial x} - \frac{\partial u}{\partial y} = -\frac{\partial^2 \Psi}{\partial x^2} - \frac{\partial^2 \Psi}{\mathrm{d}y^2} = 0 \quad \text{and therefore:} \\ \frac{\partial^2 \Psi}{\partial x^2} + \frac{\partial^2 \Psi}{\partial y^2} = 0 \end{aligned} \tag{4.5}$$

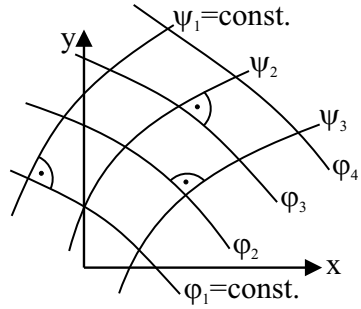

Figure 4.1: Potential- and streamlines in a field.

At this point, let's go back again to the potential function Φ and form the total differential, which must be zero along a potential line:

$$\begin{aligned} &\frac{\mathrm{d}\Phi}{\mathrm{d}x_i} = \frac{\partial \Phi}{\partial x} + \frac{\partial \Phi}{\partial y} = 0 \\ &\mathrm{d}\Phi = \frac{\partial \Phi}{\partial x}\,\mathrm{d}x + \frac{\partial \Phi}{\partial y}\,\mathrm{d}y = u\,\mathrm{d}x + v\,\mathrm{d}y = 0 \\ &\frac{\mathrm{d}y}{\mathrm{d}x} = -\frac{u}{v} \end{aligned} \tag{4.6}$$

Two functions $f_1(x_i)$ and $f_2(x_i)$ are perpendicular to each other at one point, if[B]:

$$\frac{\mathrm{d}f_1(x_i)}{\mathrm{d}x_i} = c; \text{ and } \frac{\mathrm{d}f_2(x_i)}{\mathrm{d}x_i} = -\frac{1}{c} \tag{4.7}$$

[B] Just test this relationship by inserting $c = 1, 2$ and 3 and entering the gradients into a Cartesian coordinate system.

Since exactly this condition is met for Equations 4.3 and 4.6, stream- and potential lines are perpendicular to each other at every point of the flow field.
Several solutions exist for Laplace's equation. There are also several solutions for basic types of flow which may be arbitrarily superimposed. These basic solutions are indicated in Table 4.1. Superposition makes it possible to describe nearly any flow field from these elementary solutions.

4.2 Parallel flow

The description of a parallel potential flow is almost trivial. The potential function Φ differentiated with respect to x yields u and differentiated with respect to y results in v. Because the velocity in a parallel flow does not change, the components are generally indicated by u_0 and v_0. Thus:

$$\begin{aligned} u &= \frac{\partial \Phi}{\partial x} \quad u = \frac{\partial \Psi}{\partial y} \\ v &= \frac{\partial \Phi}{\partial y} \quad v = -\frac{\partial \Psi}{\partial x} \end{aligned} \tag{4.8}$$

Upon the integration of the equations ($\int u\,\mathrm{d}x = \int \frac{\partial \Phi}{\partial x}\,\mathrm{d}x$ and $\int u\,\mathrm{d}y = \int \frac{\partial \Psi}{\partial y}\,\mathrm{d}y$), the two functions may be expressed as:

$$\begin{aligned} \Phi &= u_0 x + C_1 \\ \Psi &= u_0 y + C_2 \end{aligned} \tag{4.9}$$

The integration constants can be determined from the velocity component in the y-direction, v, as both ways must lead to the stream and potential function. Therefore we find $C_1 = v_0 y$ and $C_2 = -v_0 x$. You can try it out by inserting C_1 and C_2 into Equations 4.9 and deriving them with respect to x and y, which yields again Equation set 4.8.

4.3 Source and sink flow

In potential theory, sources and sinks are singular points; here, the equations are consequently invalid. These basic flows not only enable the description of, for example, groundwater withdrawals or returns via discharge wells but also describe boundaries of bodies through a skilful arrangement via the so-called boundary streamline. Let us examine sources.
A water quantity $q\left[\mathrm{m}^2/\mathrm{s}\right]$ shall be supplied to the environment of the source at point $(0,0)$. The unit in the two-dimensional representation of potential theory as formulated herein corresponds to the depth-related discharge. Because of the radial flow of the water, the velocity decreases towards the outside. The tangential component u_t does not exist. The velocity follows from the continuity condition as the quotient of the depth-related discharge and the circumference:

$$\begin{aligned} u_r &= \frac{q}{2\pi r} \\ u_t &= 0 \end{aligned} \tag{4.10}$$

In Cartesian coordinates, the components are described via trigonometric functions. By multiplying the expression for u_r by one in the form of $\frac{r}{r}$, the denominator includes r^2, which according to Pythagoras corresponds to x^2+y^2. In the numerator, $r\cos\alpha$ becomes x and $r\sin\alpha$ becomes y:

$$\begin{aligned} u = u_r\cos\alpha &= \frac{q}{2\pi r}\cos\alpha = \frac{q}{2\pi r}\left(\frac{r}{r}\right)\cos\alpha = \frac{q}{2\pi}\left(\frac{x}{x^2+y^2}\right) = \frac{\partial\Phi}{\partial x} = \frac{\partial\Psi}{\partial y} \\ v = u_r\sin\alpha &= \frac{q}{2\pi r}\sin\alpha = \frac{q}{2\pi r}\left(\frac{r}{r}\right)\sin\alpha = \frac{q}{2\pi}\left(\frac{y}{x^2+y^2}\right) = \frac{\partial\Phi}{\partial y} = -\frac{\partial\Psi}{\partial x} \end{aligned} \tag{4.11}$$

In order to arrive at the potential and stream functions, Equation set 4.11 must be integrated. Consult a pocketbook of mathematics, e. g. [8, p. 447], or a table of integrals. There you will find a general solution for the special form of the integrand:

$$\int \frac{f'(x)}{f(x)}\,\mathrm{d}x = \ln|f(x)| + C \tag{4.12}$$

Taking the derivative of the denominator (within the brackets) with respect to x (top equation) or y (bottom equation) in the set of Equations 4.11 yields $2x$ or $2y$, respectively, which corresponds to twice the numerator. With the application of the rule 4.12, the integrand (bracketed factor in Equations 4.11) may therefore be written as $\frac{1}{2}\ln|f(x)|$. The following is obtained for the potential function Φ:

$$\Phi = \frac{q}{2\pi}\frac{1}{2}\ln\left|x^2+y^2\right| = \frac{q}{2\pi}\frac{1}{2}\ln\left(x^2+y^2\right) \tag{4.13}$$

As x^2+y^2 must be positive, we may as well do without the vertical bars. When leafing through school texts or having [8, p. 9] at hand, the next sleight of hand may be understood.

> Definition: The logarithm of a number $x>0$ to the base $b>0, b\neq 1, \ldots$ is to be understood as the exponent of the power to which b is to be raised in order to obtain the number x.

Under the logarithm, the factor $\frac{1}{2}$ becomes the power $\frac{1}{2}$, which leads to $\ln\sqrt{x^2+y^2}$ and eventually results in:

$$\Phi = \frac{q}{2\pi}\frac{1}{2}\ln\left(x^2+y^2\right) = \frac{q}{2\pi}\ln\left(x^2+y^2\right)^{\frac{1}{2}} = \frac{q}{2\pi}\ln r \tag{4.14}$$

For the derivation of the stream function, a mathematical formulary will again be helpful. In the table for integrals of elementary functions, e. g. [8, p. 445], one reads as follows:

$$\int \frac{\mathrm{d}x}{a^2+x^2} = \frac{1}{a}\operatorname{atan}\frac{x}{a} \tag{4.15}$$

First, let's write down the integral for the stream function from Formulas 4.11.

$$\Psi = \int \frac{q}{2\pi}\left(\frac{x}{x^2+y^2}\right)\mathrm{d}y \tag{4.16}$$

With the aid of the solution from the table, we let $a = x$ and $\mathrm{d}x = \mathrm{d}y$ so that we can solve for Ψ:

$$\Psi = \frac{q}{2\pi} x \int \frac{\mathrm{d}y}{x^2 + y^2} = \frac{q}{2\pi} \frac{x}{x} \operatorname{atan} \frac{y}{x} = \frac{q}{2\pi} \operatorname{atan} \frac{y}{x} \tag{4.17}$$

4.4 Potential vortex

Freedom of rotation and potential vortex? How, indeed, can these go together? Well, the potential vortex is a very special vortex. A minute particle, that is in it, does not rotate. As an example, the circuit of the gondolas of a Ferris wheel may essentially be seen as movement in a potential vortex. Though moving in circles, the cabins always remain oriented in the same direction. In fluid mechanics, this will only work if no shear stresses are in effect, i. e. if the flow is frictionless. Movement, e. g. in a Rhön wheel that rotates as a solid body (see Figure 4.2), presents itself quite differently. Thus, the solid body vortex cannot be described by potential theory.

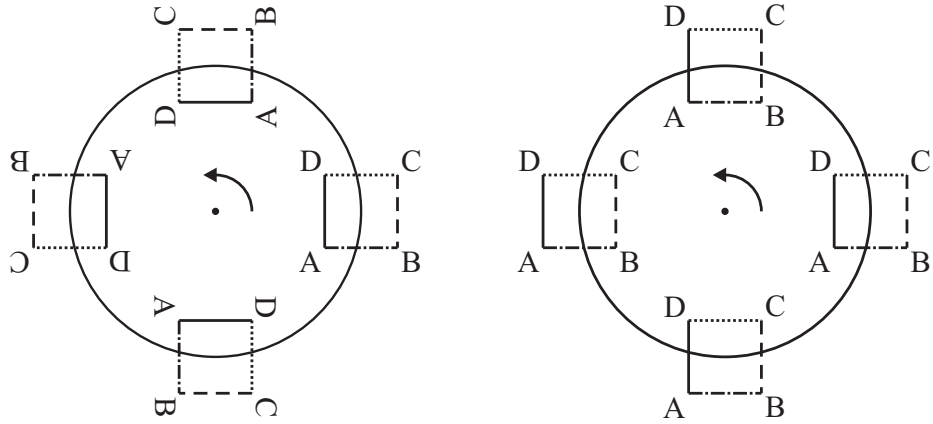

Figure 4.2: Solid body rotation (left) and potential vortex (right).

Let's leave the image of the Ferris wheel and consider how the nature of the circular flow might be such that an entrained particle does not change its orientation. We have already defined the rotation of a particle via the velocity gradients in Chapter 2.5. For the rotation in the $x-y$ plane, the following applies: $\mathrm{rot} u_z = \frac{\partial v}{\partial x} - \frac{\partial u}{\partial y}$.

For a particle to maintain its orientation on a circular path (see Figure 4.2 right), the flow on the outer path must be slower than on the inside. In the case that $\frac{\partial v}{\partial x} = \frac{\partial u}{\partial y}$, we deal with a rotationless flow.

For the description of the potential vortex, we refer to the derivations of the source and sink flow and exchange stream- and potential lines. For the radial velocity component u_r, we have distributed the discharge per unit depth q along the circumference $2\pi r$. Since stream- and potential lines are perpendicular to each other and are to be exchanged, this can be achieved by setting $u_r = 0$ and $u_t = \frac{\Gamma}{2\pi r}$. Here, Γ identifies the vorticity that indicates to some extent the discharge per unit depth on the radius element r.

As with the source and sink flow, the decomposition of the velocity components in the x- and y-direction is performed via the sine and cosine functions, which along with the tangential component yield the following expressions:

$$\begin{aligned} u &= -u_t \sin\alpha = -\frac{\Gamma}{2\pi r}\sin\alpha = -\frac{\Gamma}{2\pi r}\left(\frac{r}{r}\right)\sin\alpha = -\frac{\Gamma}{2\pi}\left(\frac{y}{x^2+y^2}\right) = \frac{\partial\Phi}{\partial x} = \frac{\partial\Psi}{\partial y} \\ v &= u_t \cos\alpha = \frac{\Gamma}{2\pi r}\cos\alpha = \frac{\Gamma}{2\pi r}\left(\frac{r}{r}\right)\cos\alpha = \frac{\Gamma}{2\pi}\left(\frac{x}{x^2+y^2}\right) = \frac{\partial\Phi}{\partial y} = -\frac{\partial\Psi}{\partial x} \end{aligned} \tag{4.18}$$

The signs result from the mathematical definition of the angle α originating at the positive x-axis and sweeping anti-clockwise towards the positive y-axis. In the first quadrant, for example, where x and y are positive, the velocity component u_t is directed opposite the positive x-direction. Let's find out whether the rotation is actually zero and calculate $\mathrm{rot}u_z = \frac{\partial v}{\partial x} - \frac{\partial u}{\partial y}$ by first differentiating the two components with respect to x or y according to the quotient rule [8, p. 396].

$$\begin{aligned} \frac{\partial v}{\partial x} &= \frac{\partial}{\partial x}\frac{\Gamma}{2\pi}\frac{x}{x^2+y^2} = \frac{\Gamma}{2\pi}\frac{\left(x^2+y^2\right)-x\cdot 2x}{\left(x^2+y^2\right)^2} = \frac{\Gamma}{2\pi}\frac{y^2-x^2}{\left(x^2+y^2\right)^2} \\ \frac{\partial u}{\partial y} &= \frac{\partial}{\partial y}\left(-\frac{\Gamma}{2\pi}\frac{y}{x^2+y^2}\right) = -\frac{\Gamma}{2\pi}\frac{\left(x^2+y^2\right)-y\cdot 2y}{\left(x^2+y^2\right)^2} = -\frac{\Gamma}{2\pi}\frac{x^2-y^2}{\left(x^2+y^2\right)^2} \\ &= \frac{\Gamma}{2\pi}\frac{y^2-x^2}{\left(x^2+y^2\right)^2} \end{aligned} \tag{4.19}$$

It follows that $\mathrm{rot}u_z = \frac{\partial v}{\partial x} - \frac{\partial u}{\partial y} = 0$. Thus, a potential vortex is rotationless. The centre of the vortex, like a source or sink, is a mathematical singularity where the equations do not apply. There, because $r = 0$, $u = v = \infty$.

4.5 Summary of the elementary solutions

Table 4.1 summarises the derived elementary solutions of Laplace's equation[C]. In the description of groundwater flows, we will return to potential theory.

[C] The extensive derivation for the dipole, which is hardly relevant in our field, was moved into the Appendix A.1.

Table 4.1: Solutions of Laplace's equation for selected elementary flows.

	parallel flow	source/sink	potential vortex	dipole
streamlines $\Psi = \text{const.}$	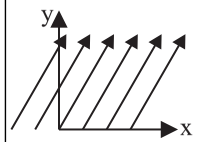	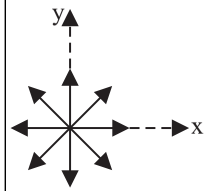	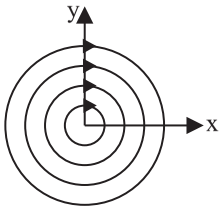	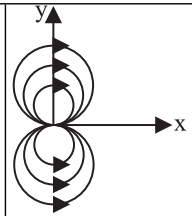
potential function $\Phi(x,y)$	$u_0 \cdot x + v_0 y$	$\frac{q}{2\pi}\ln r = \frac{q}{2\pi}\ln\sqrt{x^2+y^2}$	$-\frac{\Gamma}{2\pi}\operatorname{atan}\left(\frac{y}{x}\right)$	$\frac{m}{2\pi}\frac{x}{x^2+y^2}$
stream function $\Psi(x,y)$	$u_0 \cdot y - v_0 x$	$\frac{q}{2\pi}\alpha = \frac{q}{2\pi}\operatorname{atan}\frac{y}{x}$	$\frac{\Gamma}{2\pi}\ln\sqrt{x^2+y^2}$	$-\frac{m}{2\pi}\frac{y}{x^2+y^2}$
$u(x,y)$	u_0	$\frac{q}{2\pi}\frac{x}{x^2+y^2}$	$-\frac{\Gamma}{2\pi}\frac{y}{x^2+y^2}$	$\frac{m}{2\pi}\frac{y^2-x^2}{(x^2+y^2)^2}$
$v(x,y)$	v_0	$\frac{q}{2\pi}\frac{y}{x^2+y^2}$	$\frac{\Gamma}{2\pi}\frac{x}{x^2+y^2}$	$-\frac{m}{2\pi}\frac{2xy}{(x^2+y^2)^2}$
$\lvert\vec{v}(x,y)\rvert$	$\sqrt{u_0^2+v_0^2}$	$\frac{q}{2\pi r}$	$\frac{\Gamma}{2\pi r}$	$\frac{m}{2\pi r^2}$

Chapter 5
Basic equations

5.1 Continuity condition

We have already mentioned the continuity condition (i. e. the law of conservation of mass) in kinematics (see Chapter 2.5). It would be best to picture a fluid parcel with the dimensions $\mathrm{d}x, \mathrm{d}y, \mathrm{d}z$; its centre of gravity moves with velocity u while its edges may generally have quite different velocities from each other, in which case the element undergoes deformation. At the same time, the density of the fluid parcel may change. First, we will look at this matter two-dimensionally (see Figure 5.1).

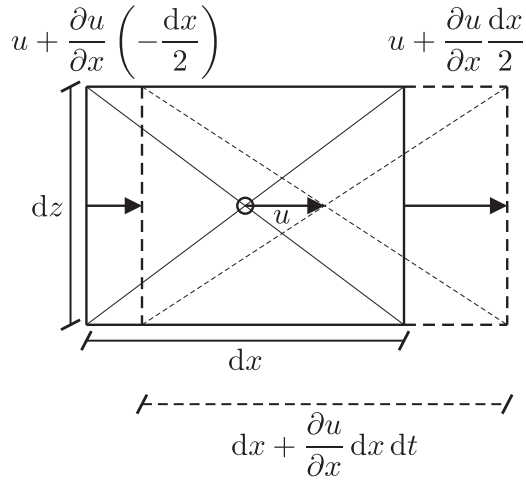

Figure 5.1: Fluid element whose centre of gravity moves with velocity u.

While the centre of gravity of the two-dimensional element travels with velocity u in the x-direction, the left border has a velocity of $u_{\mathrm{left}} = u + \frac{\partial u}{\partial x}\left(-\frac{\mathrm{d}x}{2}\right)$ and the right-hand edge has velocity $u_{\mathrm{right}} = u + \frac{\partial u}{\partial x}\frac{\mathrm{d}x}{2}$. Thus, the velocity difference between front and rear (or between the right and left sides) amounts to $u_{\mathrm{right}} - u_{\mathrm{left}} = \frac{\partial u}{\partial x}\mathrm{d}x$. The change in length of the element is obtained by multiplying the velocity difference with the time $\mathrm{d}t$ during which this difference prevails, i. e. $\frac{\partial u}{\partial x}\mathrm{d}x\,\mathrm{d}t$. If one length of a cube changes by this value, then the effects on its volume are determined by the multiplication with the surface element

C. Rapp, *Hydraulics in Civil Engineering*,
https://doi.org/10.1007/978-3-031-54860-4_5

$\mathrm{d}y\,\mathrm{d}z$. This becomes somewhat more complex in three-dimensional space. We describe the change of mass of the volume with respect to time as follows:

$$\begin{aligned}\frac{\mathrm{d}m}{\mathrm{d}t} &= \frac{\mathrm{d}(\rho \cdot V)}{\mathrm{d}t} = V\frac{\mathrm{d}\rho}{\mathrm{d}t} + \rho\frac{\mathrm{d}V}{\mathrm{d}t} = V\frac{\partial\rho}{\partial t} + \rho\left[\left(\frac{\partial u}{\partial x}\left(\frac{\mathrm{d}x}{2}\right) - \left(\frac{\partial u}{\partial x}\left(-\frac{\mathrm{d}x}{2}\right)\right)\right)\mathrm{d}y\,\mathrm{d}z\right. \\ &\left. + \left(\frac{\partial v}{\partial y}\left(\frac{\mathrm{d}y}{2}\right) - \left(\frac{\partial v}{\partial y}\left(-\frac{\mathrm{d}y}{2}\right)\right)\right)\mathrm{d}x\,\mathrm{d}z + \left(\frac{\partial w}{\partial z}\left(\frac{\mathrm{d}z}{2}\right) - \left(\frac{\partial w}{\partial z}\left(-\frac{\mathrm{d}z}{2}\right)\right)\right)\mathrm{d}x\,\mathrm{d}y\right] \\ &= \frac{\partial\rho}{\partial t}\,\mathrm{d}x\,\mathrm{d}y\,\mathrm{d}z + \rho\left[\left(\frac{\partial u}{\partial x}\,\mathrm{d}x\right)\mathrm{d}y\,\mathrm{d}z + \left(\frac{\partial v}{\partial y}\,\mathrm{d}y\right)\mathrm{d}x\,\mathrm{d}z + \left(\frac{\partial w}{\partial z}\,\mathrm{d}z\right)\mathrm{d}x\,\mathrm{d}y\right] \\ &= \frac{\partial\rho}{\partial t}\,\mathrm{d}x\,\mathrm{d}y\,\mathrm{d}z + \rho\left[\frac{\partial u}{\partial x} + \frac{\partial v}{\partial y} + \frac{\partial w}{\partial z}\right]\mathrm{d}x\,\mathrm{d}y\,\mathrm{d}z = 0\end{aligned} \tag{5.1}$$

If the volume actually grows (because of the net growths in the three spatial directions), the density would have to decrease correspondingly during the same time interval $\frac{\partial\rho}{\partial t}\,\mathrm{d}x\,\mathrm{d}y\,\mathrm{d}z$ in order to satisfy the constancy of mass. With an incompressible medium, which generally applies to water, the derivative of the density $\frac{\partial\rho}{\partial t}$ disappears (the first term). Therefore, the conservation of mass with such media corresponds to the constancy of volume. When dividing Equation 5.1 by the density and the volume, we obtain the divergence described in Chapter 2.5, which becomes zero for an incompressible medium.

$$\mathrm{div}\,\vec{u} = \frac{\partial u_i}{\partial x_i} = \frac{\partial u}{\partial x} + \frac{\partial v}{\partial y} + \frac{\partial w}{\partial z} = 0 \tag{5.2}$$

Take a balloon and fill it with water to prepare a water bomb. There must be no air in the bomb. You will certainly agree with me that the water mass in the closed balloon is constant. Play around a little with the water bomb without bursting it. You observe that it must become thicker on one side if the other side becomes thinner. When you stretch it, it becomes thinner in the other two coordinate directions.
The same applies to the fluid parcel even though it is located within a flow. Simply ignore the surrounding balloon.

Or we can take a PE bottle and cut it open. We mark the positions on a balloon with a B and on the bottle with an F. Then we pull the balloon through the cone and find that the balloon becomes longer where the cross-section is smaller (the distance between the Bs increases). This means that the fluid element must move faster when the cross-section decreases.

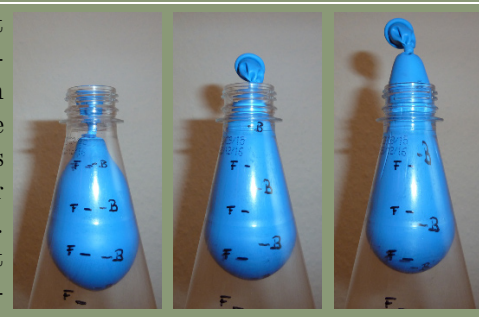

We will demonstrate what our theoretical considerations mean in practice by means of the flow through a contraction, as shown in Figure 5.2. For this purpose, we integrate the divergence of the velocity field over the volume of the contraction $\int \mathrm{div}\,\vec{u}\,\mathrm{d}V$; for an incompressible medium, this integral must have a value of zero.
According to [8, p. 685], the Gaussian integral theorem (Equation 5.3) to which we refer again for the derivation of the law of momentum in Chapter 5.8 provides the "connection

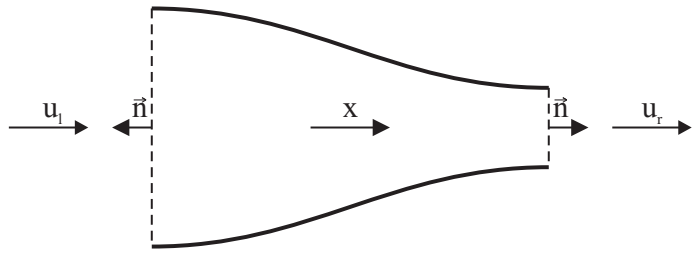

Figure 5.2: Flow in a contraction.

between a volume integral over a volume V which is interspersed by a field $\vec{u}$, and a surface integral over the area A encompassing this volume. The orientation of the surface is such that the outside is the positive side[A]. Let $\vec{u}$ be a continuous vector field with its first partial derivatives existing and continuous."

$$\int \operatorname{div} \vec{u} \, \mathrm{d}V = \int \vec{u} \circ \vec{n} \, \mathrm{d}A \tag{5.3}$$

In our example, there are only two surfaces, left and right, through which a medium flows; on the left, fluid flows opposite the normal vector, and on the right, it flows in the same direction as the normal vector, which is the reason for the opposite signs on the right side of Equation 5.4. Here – but only here – we refer to $\overline{u}$ as the averaged velocity over the cross-section. Mathematically, $\overline{u}$ corresponds to $\frac{1}{A}\int u \, \mathrm{d}A$.

$$\int \operatorname{div} \vec{u} \, \mathrm{d}V = \int \vec{u} \circ \vec{n} \, \mathrm{d}A = \int \vec{u_l} \circ \vec{n} \, \mathrm{d}A_l + \int \vec{u_r} \circ \vec{n} \, \mathrm{d}A_r = \overline{u_l}\,(-1) A_l + \overline{u_r}\,(+1) A_r \tag{5.4}$$

With $\operatorname{div} \vec{u} = 0$ (see Equation 5.2), Equation 5.5 ultimately shows that the mean velocity, multiplied by the cross-section, i. e. the discharge, remains constant.

$$\overline{u_l} A_l = \overline{u_r} A_r; \text{ therefore } Q = uA = \text{const.} \tag{5.5}$$

5.2 Cauchy equation

The Cauchy equation is based on Newton's second axiom, which states that the momentum of a mass may be changed only if a force is acting on this mass (see Equation 5.6). Since in the incompressible flows with which we deal (with the exception of Chapter 12) the mass in a volume cannot change because of the constancy of density, the description of force is expressed in terms of a change in velocity with respect to time.

$$\vec{F} = \frac{\mathrm{d}\vec{I}}{\mathrm{d}t} = \frac{\mathrm{d}(m\vec{v})}{\mathrm{d}t} = m\frac{\mathrm{d}\vec{v}}{\mathrm{d}t} = m \cdot \vec{a} \tag{5.6}$$

A commonly known formula says that a force is determined by mass multiplied by acceleration.

[A] At another place of the same source, it reads [8, p. 500] that the normal vector points outward with outside defined as positive.

Consider an accelerated differential cube element with the edge length $\mathrm{d}x \cdot \mathrm{d}y \cdot \mathrm{d}z$ and the density ρ. In order to accelerate the mass $\rho \cdot \mathrm{d}x \cdot \mathrm{d}y \cdot \mathrm{d}z$, a force must act on it according to Newton's second axiom. In the Euler context (see Chapter 2.3.2), the acceleration of the mass is described via the total derivative (see Chapter 2.4.1.2). With Einstein's sum convention (see Chapter 2.6), the following expression results:

$$a_i = \frac{\partial u_i}{\partial t} + u_j \frac{\partial u_i}{\partial x_j} \tag{5.7}$$

For the acceleration in the three spatial directions i, three equations are obtained, each containing the local derivative $\frac{\partial u_i}{\partial t}$ and the sum over the convective derivatives. Let's write the equations again in their full lengths to become familiar with the sum convention. The velocity components in the x-, y- and z-directions are identified by the variable names u, v and w, respectively.

$$\begin{aligned} a_x &= \frac{\partial u}{\partial t} + u\frac{\partial u}{\partial x} + v\frac{\partial u}{\partial y} + w\frac{\partial u}{\partial z} \\ a_y &= \frac{\partial v}{\partial t} + u\frac{\partial v}{\partial x} + v\frac{\partial v}{\partial y} + w\frac{\partial v}{\partial z} \\ a_z &= \frac{\partial w}{\partial t} + u\frac{\partial w}{\partial x} + v\frac{\partial w}{\partial y} + w\frac{\partial w}{\partial z} \end{aligned} \tag{5.8}$$

From the previous considerations, we can conclude that there are three relevant forces in fluid mechanics: volume, planar and linear forces. Fortunately, we don't have to worry about any other forces such as magnetism. We have already mentioned surface tension as a linear force. As the surface tension is, in general, negligibly small and plays a role only in small capillaries, we will concentrate on the volume and planar forces in this book.
Let's go back to our balloon fluid volume. Figures 5.3, 5.5 and 5.6 on the following pages are included to assist in understanding the concept.

Figure 5.3: Fluid volume under the influence of gravity.

The force of gravity is considered a volume force that acts on the cube: $F_G = \rho \cdot \mathrm{d}x \cdot \mathrm{d}y \cdot \mathrm{d}z \cdot \vec{g}$. Therein, $\vec{g}$ is a vector which, according to the convention stated in Chapter 2.1, has a component in the negative z-direction as a sole element:

$$\vec{g} = \begin{pmatrix} 0 \\ 0 \\ -9.81 \end{pmatrix} \tag{5.9}$$

Due to $\vec{g}$, the element is accelerated opposite to the positive z-direction (see Figure 5.3). Let's derive the planar forces by means of Figure 5.4. To be prepared for Einstein's sum convention, the spatial directions x, y and z are identified by indices 1, 2 and 3. Therein, the first index represents the surface normal, and the second index the direction of action of the stress $\tau_{\text{normal,direction of stress}}$. This is done in accordance with relevant works (e. g. [60]).
The stresses act on the opposite surfaces in the opposite direction according to the free body principle. We will see immediately that the individual stresses cancel each other and that only their variations are effective.
But slow down: the following planar forces are acting in the x-direction (that is x_1):

$$\begin{aligned} F_x = {} & \tau_{xx}\,\mathrm{d}y\,\mathrm{d}z + \frac{\partial \tau_{xx}}{\partial x}\frac{\mathrm{d}x}{2}\,\mathrm{d}y\,\mathrm{d}z - \left[\tau_{xx}\,\mathrm{d}y\,\mathrm{d}z + \frac{\partial \tau_{xx}}{\partial x}\left(-\frac{\mathrm{d}x}{2}\right)\mathrm{d}y\,\mathrm{d}z\right] \\ & + \tau_{yx}\,\mathrm{d}x\,\mathrm{d}z + \frac{\partial \tau_{yx}}{\partial y}\frac{\mathrm{d}y}{2}\,\mathrm{d}x\,\mathrm{d}z - \left[\tau_{yx}\,\mathrm{d}x\,\mathrm{d}z + \frac{\partial \tau_{yx}}{\partial y}\left(-\frac{\mathrm{d}y}{2}\right)\mathrm{d}x\,\mathrm{d}z\right] \\ & + \tau_{zx}\,\mathrm{d}x\,\mathrm{d}y + \frac{\partial \tau_{zx}}{\partial z}\frac{\mathrm{d}z}{2}\,\mathrm{d}x\,\mathrm{d}y - \left[\tau_{zx}\,\mathrm{d}x\,\mathrm{d}y + \frac{\partial \tau_{zx}}{\partial z}\left(-\frac{\mathrm{d}z}{2}\right)\mathrm{d}x\,\mathrm{d}y\right] \\ = {} & \frac{\partial \tau_{xx}}{\partial x}\,\mathrm{d}x\,\mathrm{d}y\,\mathrm{d}z + \frac{\partial \tau_{yx}}{\partial y}\,\mathrm{d}y\,\mathrm{d}x\,\mathrm{d}z + \frac{\partial \tau_{zx}}{\partial z}\,\mathrm{d}z\,\mathrm{d}x\,\mathrm{d}y \end{aligned} \tag{5.10}$$

The stress in the x-direction acting on the surface varies along this direction and is expressed as $\frac{\partial \tau_{xx}}{\partial x}$. After traversing the distance $\mathrm{d}x$, it takes on the value $\frac{\partial \tau_{xx}}{\partial x}\mathrm{d}x$. This stress, which has changed compared to that of the opposite surface, acts on the surface area with size $\mathrm{d}y \cdot \mathrm{d}z$. The resulting force is obtained by the product of stress and surface area, i. e. $\frac{\partial \tau_{xx}}{\partial x}\mathrm{d}x\,\mathrm{d}y\,\mathrm{d}z$. Since the effect of this stress points in the same direction as the surface normal vector, it is referred to as the normal stress. Figure 5.5 shows what happens when a normal stress acting on our element in the x-direction is greater on the left than on the right. The element moves to the right.
But at the other surfaces, shear stresses also point in the x-direction, and we must include these in our force balance. The surfaces oriented in the y-direction exhibit a stress difference, expressed as $\frac{\partial \tau_{yx}}{\partial y}\mathrm{d}y$, in the x-direction. This stress difference acts on the surface with an extension in the x- and z-directions. The proportion of the force component in the x-direction at the free body planes whose normal vectors point in the y-direction is therefore $\frac{\partial \tau_{yx}}{\partial y}\mathrm{d}y\,\mathrm{d}x\,\mathrm{d}z$. The same consideration applies to the two remaining surfaces of the cube whose normal vectors extend parallel to the z-axis: $\frac{\partial \tau_{zx}}{\partial z}\mathrm{d}z\,\mathrm{d}x\,\mathrm{d}y$. In Figure 5.6, the fluid element is moved to the right by the shear stress τ_{zx}.
Using the index notation with the differential volume $\mathrm{d}V = \mathrm{d}x\,\mathrm{d}y\,\mathrm{d}z = \mathrm{d}x_1\,\mathrm{d}x_2\,\mathrm{d}x_3$, the following results are given for the x-component of the force:

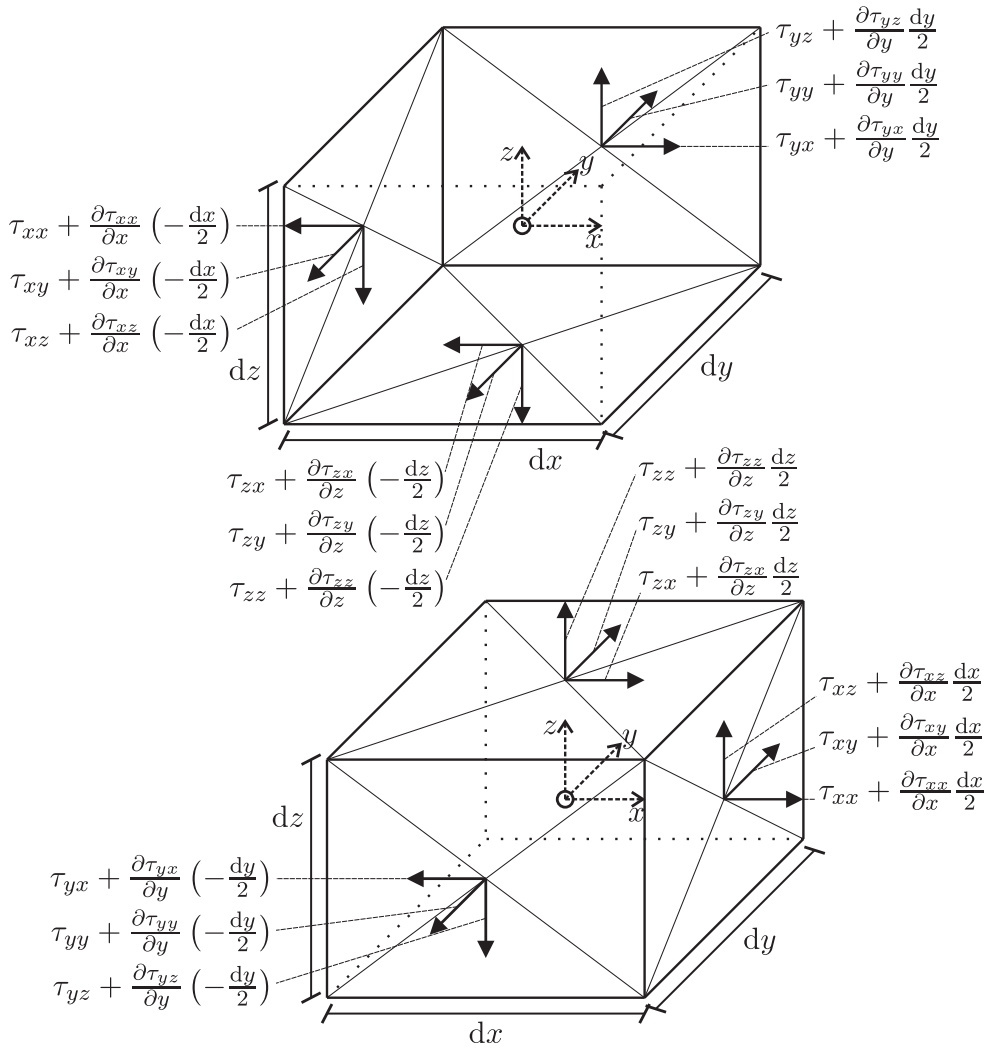

Figure 5.4: Stresses at the differential element, rear part of the cube on the top, front part on the bottom.

$$F_x = \frac{\partial \tau_{11}}{\partial x_1}\,\mathrm{d}x_1\,\mathrm{d}x_2\,\mathrm{d}x_3 + \frac{\partial \tau_{21}}{\partial x_2}\,\mathrm{d}x_2\,\mathrm{d}x_1\,\mathrm{d}x_3 + \frac{\partial \tau_{31}}{\partial x_3}\,\mathrm{d}x_3\,\mathrm{d}x_1\,\mathrm{d}x_2 \tag{5.11}$$

The force components for the three spatial directions may be written with Einstein's sum convention as follows:

$$F_i = \frac{\partial \tau_{ji}}{\partial x_j}\,\mathrm{d}V \tag{5.12}$$

Thus, Equation 5.12 applies to the directions i, wherein the partial derivatives must be summed up over j (see Equation 5.11).
The principle of conservation of angular momentum allows the exchange of the indices because $\tau_{ij} = \tau_{ji}$. For more details, see [16, p. 192] or the Appendix in Chapter A.2.
Back to the consideration of forces acting on the differential element, we write at first the sum over the forces acting in the x-direction only:

Figure 5.5: Fluid volume under normal stress.

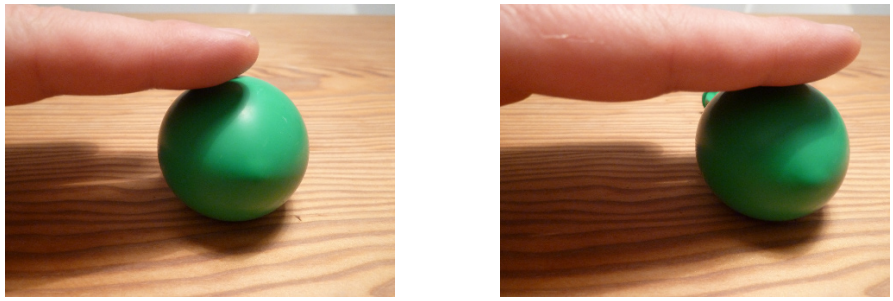

Figure 5.6: Fluid volume under the influence of shear stress.

$$\mathrm{d}V\,\rho\frac{\mathrm{d}u}{\mathrm{d}t}=\mathrm{d}V\left(\frac{\partial\tau_{xx}}{\partial x}+\frac{\partial\tau_{yx}}{\partial y}+\frac{\partial\tau_{zx}}{\partial z}\right) \tag{5.13}$$

The mass $\rho\,\mathrm{d}V$ is accelerated by $\frac{\mathrm{d}u}{\mathrm{d}t}$ in the x-direction if the respective stresses act in this direction. When writing Equation 5.13 with Einstein's sum convention for the three spatial directions, one must not forget the force of gravity ($F_G=\rho\,\mathrm{d}V\,g_z$) acting in the (negative) z-direction. Moreover, we divide by $\mathrm{d}V$ and insert the density into the derivative, so that Equation 5.14, which is also known as Cauchy equation, is also formally applicable to compressible media:

$$\frac{\partial\left(\rho u_i\right)}{\partial t}+u_j\frac{\partial\left(\rho u_i\right)}{\partial x_j}=\rho g_i+\frac{\partial\tau_{ij}}{\partial x_j} \tag{5.14}$$

Of course, Equation 5.14 satisfies Newton's third axiom. The mass on the left side is accelerated (reactio) when the forces on the right side act on this mass (actio).

5.3 Constitutive equation

The Cauchy equation (see Equation 5.14) describes the acceleration of an element due to generally applied surface and volume forces, irrespective of the type of mass in question. The constitutive equation (the Latin word constitutive means determining) describes the material properties. Specifically, it concerns the formulation of how an element is deformed in relation to an applied stress. In Chapter 3.1, we have basically considered the behaviour of solid bodies and fluids; the deformation of a fluid element was already

described in Chapter 2.5. The viscosity was discussed as a substance property of a fluid in Chapter 3.4.11. We will now combine our thoughts.
First, we divide the tensor τ_{ij} into a pressure component and the rest. This sleight of hand will later allow us to establish simple equations in hydrostatics. The pressure is a scalar quantity acting in the same manner in all spatial directions (1, 2 and 3, or x, y and z, respectively). To add the scalar pressure to the stress tensor, we use the so-called Kronecker delta δ_{ij}:

$$\delta_{ij} = \begin{bmatrix} 1 & 0 & 0 \\ 0 & 1 & 0 \\ 0 & 0 & 1 \end{bmatrix} \tag{5.15}$$

The pressure in the stresses corresponds to $-p\delta_{ij}$; we call the rest, which contains contributions of the viscosity, σ_{ij} [60].

$$\tau_{ij} = -p\delta_{ij} + \sigma_{ij} \tag{5.16}$$

The pressure always acts in a direction opposite to the normal vector of the surface, which leads to a prefixed negative sign. It is obvious that an element is not deformed upon translation or rotation (see Chapter 2.5 again). The deformation, or the deformation rate of the element merely reflects the symmetrical proportion of the velocity gradient tensor s_{ij}.
Let's go back to Equation 3.17 in Chapter 3.4.11. There, we found for Newtonian fluids that the dynamic viscosity as a proportionality factor links stress and the linear velocity gradient. Equation 3.17, with the spatial directions in index notation, generally reads as:

$$\sigma_{ij} = \kappa_{ijmn} s_{mn} \tag{5.17}$$

Therein, κ_{ijmn} is a fourth level tensor that linearly links each stress component of σ_{ij} with one of the possible velocity gradients, or rather, with the symmetric proportion s_{mn} [18, p. 63][B].
Next, we will focus on the description of κ and try to trim this giant monster a little. Due to isotropy (stress in the Newtonian fluid has no preferred direction – see above), the stress/expansion ratio is independent of the rotation of the coordinate system. All isotropic tensors of even order consist of products with the Kronecker delta δ. Therefore, a fourth-level tensor may be written via a sum of scalars λ, η, γ, multiplied by the Kronecker delta [50, p. 507]:

$$\kappa_{ijmn} = \lambda\,\delta_{ij}\delta_{mn} + \eta\,\delta_{im}\delta_{jn} + \gamma\delta_{in}\delta_{jm} \tag{5.18}$$

Since σ_{ij} is symmetrical (see Chapter A.2), it follows that κ_{ijmn} must also be symmetrical in i and j, which is only the case if $\gamma = \eta$[C]. Transferred into Equation 5.17, these considerations result in:

[B] Actually, Formula 5.17 comprises nothing other than Equation 3.15, which describes the ratio of stress and strain (or pressure and compressibility) via the modulus of elasticity. However, here we have an individual proportionality factor κ, i. e. a construct of $9 \times 9 = 81$ elements for any combination of σ_{ij} and s_{ij}. We are already anticipating that this κ has something to do with viscosity (see Chapter 3.4.11).

[C] Check it! For any (i, j), the entries at $m = i$ and $n = j$ are 1, which follows from the multiplications of the Kronecker deltas for $\delta_{im}\delta_{jn}$. If, however, $\delta_{in}\delta_{jm}$ is calculated, then the entry 1 will be found at $m = j$ and $n = i$, i. e. mirrored relative to the first term on the principal diagonal. The remaining matrix elements are filled with zeros. Since the mutually symmetrical elements are multiplied by η and γ, η and γ must be equal so that the matrix in turn becomes symmetrical.

$$\begin{aligned}\sigma_{ij} = \kappa_{ijmn} s_{mn} &= \lambda\,\delta_{ij}\delta_{mn}s_{mn} + \eta\,\delta_{im}\delta_{jn}s_{mn} + \gamma\delta_{in}\delta_{jm}s_{mn} \\ &= \lambda\,\delta_{ij}s_{mm} + \eta\,s_{ij} + \gamma s_{ij} = \lambda\,\delta_{ij}s_{mm} + 2\eta\,s_{ij}\end{aligned} \tag{5.19}$$

Therein, s_{mm} represents the divergence of the velocity field[D] $s_{mm} = s_{11} + s_{22} + s_{33} = \operatorname{div}\vec{u}$. By inserting Equation 5.19 into 5.16, the following expression is obtained:

$$\tau_{ij} = -p\delta_{ij} + 2\eta s_{ij} + \lambda\,\delta_{ij}s_{mm} \tag{5.20}$$

For an incompressible fluid, such as water with its high modulus of elasticity ($E_{\text{water}} = 2.1 \times 10^9\,\text{N/m}^2$), the last term is omitted because $s_{mm} = \operatorname{div}\vec{u} = 0$. Therefore, the randomly selected factors λ and γ become irrelevant. It is obvious that η corresponds to the dynamic viscosity, which also becomes apparent from the unit ($[\text{Ns/m}^2] \times [\text{m/(s m)}] = [\text{N/m}^2]$). Accordingly, this yields the constitutive equation for an incompressible fluid:

$$\tau_{ij} = -p\delta_{ij} + 2\eta s_{ij} \tag{5.21}$$

5.4 Euler equation

In Euler's lifetime, the viscous term in the constitutive equation (5.21) was still unknown. For this reason, the Euler equation describes only frictionless flows. The derivation starts with the Cauchy equation (see Chapter 5.2).

$$\frac{\partial u_i}{\partial t} + u_j\frac{\partial u_i}{\partial x_j} = \frac{1}{\rho}\frac{\partial \tau_{ij}}{\partial x_j} + g_i \tag{5.22}$$

When inserting the constitutive equation (see Chapter 5.3), a description for the stresses τ is obtained. The constitutive equation for an incompressible and frictionless flow (where $\eta = 0$) reads:

$$\tau_{ij} = -p\delta_{ij} + 2\eta s_{ij} = -p\delta_{ij} \tag{5.23}$$

In the Euler equation (5.24), only normal stresses, i. e. the pressure, are considered. We obtain it by inserting Equation 5.23 into Equation 5.14:

$$\frac{\partial u_i}{\partial t} + u_j\frac{\partial u_i}{\partial x_j} = \frac{1}{\rho}\frac{\partial\,(-p\delta_{ij})}{\partial x_j} + g_i = -\frac{1}{\rho}\frac{\partial p}{\partial x_i} + g_i \tag{5.24}$$

5.5 Navier-Stokes equation

The mathematically correct description of friction is attributed to Henri Navier[E] and Gabriel Stokes[F], who worked independently of each other. These so-called Navier-Stokes equations (5.29 and 5.30) fully describe flows by means of momentum and mass conservation.

[D] See Einstein's sum convention in Chapter 2.6: the sum over the indices appears twice.

[E] Henri Navier, ∗1785, Dijon, France, †1836, Paris, France

[F] Gabriel Stokes, ∗1819, Skreen, Ireland, †1903, Cambridge, England

In this case, too, the derivation starts with the general equation of motion, which is named after Cauchy:

$$\frac{\partial u_i}{\partial t} + u_j \frac{\partial u_i}{\partial x_j} = \frac{1}{\rho} \frac{\partial \tau_{ij}}{\partial x_j} + g_i \tag{5.25}$$

However, the constitutive equation (5.21), including the viscous term $\tau_{ij} = -p\delta_{ij} + 2\eta s_{ij}$, is inserted here for the stresses. As in the derivation of the Euler equation, the Kronecker delta δ_{ij} reduces the dimension of the pressure derivative.

$$\begin{aligned} \frac{\partial u_i}{\partial t} + u_j \frac{\partial u_i}{\partial x_j} &= \frac{1}{\rho} \frac{\partial \left(-p\delta_{ij} + 2\eta s_{ij}\right)}{\partial x_j} + g_i = -\frac{1}{\rho} \frac{\partial p\delta_{ij}}{\partial x_j} + \frac{1}{\rho} \frac{\partial}{\partial x_j} \left(2\eta s_{ij}\right) + g_i \\ &= -\frac{1}{\rho} \frac{\partial p}{\partial x_i} + \frac{1}{\rho} \frac{\partial}{\partial x_j} \left(2\eta s_{ij}\right) + g_i \end{aligned} \tag{5.26}$$

In the derivation of the kinematic relations, the velocity gradient tensor $\operatorname{grad} \vec{u}$ was divided into a symmetric ($s_{ij} = \frac{1}{2}\left(\frac{\partial u_i}{\partial x_j} + \frac{\partial u_j}{\partial x_i}\right)$) and an antisymmetric ($e_{ij}$) part (see also Chapter 2.5.4). Let's have a closer look at it:

$$2s_{ij} = \begin{pmatrix} \frac{\partial u}{\partial x} + \frac{\partial u}{\partial x} & \frac{\partial u}{\partial y} + \frac{\partial v}{\partial x} & \frac{\partial u}{\partial z} + \frac{\partial w}{\partial x} \\ \frac{\partial v}{\partial x} + \frac{\partial u}{\partial y} & \frac{\partial v}{\partial y} + \frac{\partial v}{\partial y} & \frac{\partial v}{\partial z} + \frac{\partial w}{\partial y} \\ \frac{\partial w}{\partial x} + \frac{\partial u}{\partial z} & \frac{\partial w}{\partial y} + \frac{\partial v}{\partial z} & \frac{\partial w}{\partial z} + \frac{\partial w}{\partial z} \end{pmatrix} \tag{5.27}$$

If only small temperature differences are allowed, the location-specific viscosity η may be separated from the derivative and written before it. With the kinematic viscosity $\nu = \frac{\eta}{\rho}; \left[\mathrm{m^2/s}\right]$, the viscous term, as it is known, reads:

$$\frac{1}{\rho} \frac{\partial}{\partial x_j} \left(2\eta s_{ij}\right) = \frac{\eta}{\rho} \frac{\partial}{\partial x_j} \frac{\partial u_i}{\partial x_j} = \nu \frac{\partial^2 u_i}{\partial x_j^2} \tag{5.28}$$

Thus, the Navier-Stokes equation for viscous, incompressible (see Chapter 3.4.10) flows is:

$$\frac{\partial u_i}{\partial t} + u_j \frac{\partial u_i}{\partial x_j} = -\frac{1}{\rho} \frac{\partial p}{\partial x_i} + g_i + \nu \frac{\partial^2 u_i}{\partial x_j^2} \tag{5.29}$$

This equation is also referred to as the momentum equation. It is an aspect of forces with the unit $\mathrm{m/s^2}$. The unit for force N is obtained by integrating the equation over the volume in question and the prevailing density. Together with the continuity condition (Equation 5.30[G]), which was already derived as divergence via the kinematic relations in Chapter 2.5.5, the Navier-Stokes equations fully describe flows of incompressible fluids.

$$\frac{\partial u_i}{\partial x_i} = 0 \tag{5.30}$$

In its written form, the continuity equation (5.30) has the unit 1/s. In this case, too, one would have to integrate over the volume and the density in order to obtain the rate of mass change in kg/s.

[G] In the continuity condition, summation is also carried out over the duplicate index so that the equation reads as follows: $\frac{\partial u}{\partial x} + \frac{\partial v}{\partial y} + \frac{\partial w}{\partial z} = 0$.

5.6 Dimensionsless Navier-Stokes equation

Flows behave similarly if they are geometrically and dynamically similar [10]. The geometric comparability is achieved by scaling the lengths, e. g. as for the scale of a road map. The dynamic similarity is given with the identical dimensionless Navier–Stokes equation (5.29). For writing the equation in a dimensionless form, the following reference quantities $l_{\mathrm{ref}}, u_{\mathrm{ref}}$ and ρ are defined:

$$x_i^* = \frac{x_i}{l_{\mathrm{ref}}}; u_i^* = \frac{u_i}{u_{\mathrm{ref}}}; t^* = t\frac{u_{\mathrm{ref}}}{l_{\mathrm{ref}}}; p^* = \frac{p}{\rho u_{\mathrm{ref}}^2} \tag{5.31}$$

Thus, we may write:

$$\begin{aligned} \frac{\partial u_i^*}{\partial t^*} + u_j^* \frac{\partial u_i^*}{\partial x_j^*} &= -\frac{\partial p^*}{\partial x_i^*} + \frac{g_i x_{\mathrm{ref}}}{u_{\mathrm{ref}}^2} + \frac{\nu}{u_{\mathrm{ref}} x_{\mathrm{ref}}} \frac{\partial^2 u_i^*}{\partial x_j^{*2}} \\ \frac{\partial u_i^*}{\partial x_i^*} &= 0 \end{aligned} \tag{5.32}$$

The dimensionless form of the Navier-Stokes equations is obtained with the Froude number[H] $\mathrm{Fr} = \frac{u_{\mathrm{ref}}}{\sqrt{g_i x_{\mathrm{ref}}}}$ as the ratio of the inertia forces to the mass forces, and with the Reynolds number[I] $\mathrm{Re} = \frac{u_{\mathrm{ref}} x_{\mathrm{ref}}}{\nu}$ as the ratio of the inertia forces to the viscous forces.

$$\begin{aligned} \frac{\partial u_i^*}{\partial t^*} + u_j^* \frac{\partial u_i^*}{\partial x_j^*} &= -\frac{\partial p^*}{\partial x_i^*} + \frac{1}{\mathrm{Fr}^2} + \frac{1}{\mathrm{Re}} \frac{\partial^2 u_i^*}{\partial x_j^{*2}} \\ \frac{\partial u_i^*}{\partial x_i^*} &= 0 \end{aligned} \tag{5.33}$$

The dynamic similarity is given only if the Froude number[J] and the Reynolds number are equal. This is generally not possible in scaled experiments. Therefore, compromises must be found and the law of similarity must be met as far as possible. In pipe flows, it is mostly the viscous forces that are significant; channel flows are generally highly turbulent, and the mass forces are dominant.

5.7 Bernoulli equation

The Bernoulli[K] equation is derived from the Euler equation (see Chapter 5.4). The Euler equation reads:

$$\frac{\partial u_i}{\partial t} + u_j \frac{\partial u_i}{\partial x_j} = -\frac{1}{\rho}\frac{\partial p}{\partial x_i} + g_i \tag{5.34}$$

As already mentioned above, the Euler equation has no viscosity term, which is why the Bernoulli equation also describes only frictionless flows. For gravity, the sole force acting

[H] William Froude, ∗1810, Dartington, England, †1879, Simonstown, South Africa

[I] Osbourne Reynolds, ∗1842, Belfast, Northern Ireland, †1912, Watchet, England

[J] Fr is defined only for flows with free surfaces.

[K] Daniel Bernoulli, ∗1700, Groningen, the Netherlands, †1782, Basel, Switzerland

on the volume, only that component of the motion that is in the z-direction is relevant. In our case of the upward-pointing z-coordinate, gravity acts against it; therefore, the term has a negative sign.

$$g_i = -\frac{\partial gz}{\partial x_i} = -g\frac{\partial z}{\partial x_i} \quad \text{with } g \approx 9.807\,\mathrm{m/s^2} \tag{5.35}$$

You certainly recognize Equation 5.35 as the downhill-slope force. $\frac{\partial z}{\partial x_i}$ indicates the slope in the three spatial directions. The following is the Euler equation in a different notation:

$$\frac{\partial u_i}{\partial t} + u_j\frac{\partial u_i}{\partial x_j} = -\frac{1}{\rho}\frac{\partial p}{\partial x_i} - \frac{\partial gz}{\partial x_i} \tag{5.36}$$

Before arriving at Bernoulli's stroke of genius, let's take a little time for a short anecdote. Daniel Bernoulli, after whom the equation was named, was born into a dynasty of mathematicians. His father, Johann I. Bernoulli, was a mathematics professor and taught amongst others the highly talented boy Leonhard Euler. Daniel, who was seven years older, at first studied medicine and practiced in Venice before he was appointed as professor of physics at Saint Petersburg University. After the death of his brother Nikolaus II Bernoulli, who also held a professorship in mathematics there, Daniel Bernoulli appointed Leonhard Euler as his brother's successor. When Daniel Bernoulli returned to Basel in 1733, Euler took over the professorship in physics. It is not unlikely that the development of this basic equation of fluid mechanics was at least fostered by the relationship between the two men that was initiated during their childhood.

We will now turn to the glorious idea that relates only to the convective acceleration $u_j\frac{\partial u_i}{\partial x_j}$. First, we subtract the term $u_j\frac{\partial u_j}{\partial x_i}$ therefrom and add it again directly. The operation reads as follows:

$$u_j\frac{\partial u_i}{\partial x_j} = u_j\left(\frac{\partial u_i}{\partial x_j} - \frac{\partial u_j}{\partial x_i}\right) + u_j\frac{\partial u_j}{\partial x_i} \tag{5.37}$$

The first term on the right of the equals sign is already known from the kinematic relations (see Chapter 2.5). $\frac{\partial u_i}{\partial x_j} - \frac{\partial u_j}{\partial x_i}$ describes the rotation, though with negative sign. The prefixed u_j of the second term on the right side may be drawn into the derivative because they have the same indices, which leads to $\frac{1}{2}\frac{\partial u_j u_j}{\partial x_i}$[L]. The extended Euler equation is as follows:

$$\frac{\partial u_i}{\partial t} + \frac{\partial}{\partial x_i}\left(\frac{1}{2}u_j^2\right) + \frac{1}{\rho}\frac{\partial p}{\partial x_i} + \frac{\partial gz}{\partial x_i} = u_j\left(\frac{\partial u_i}{\partial x_j} - \frac{\partial u_j}{\partial x_i}\right) \tag{5.38}$$

The derivative with respect to the coordinate x_i is obviously present in three of the terms, so these terms are bracketed. Additionally, the local acceleration $\frac{\partial u_i}{\partial t}$ is omitted for a steady flow[M].

$$\frac{\partial}{\partial x_i}\left[\frac{1}{2}u_j^2 + \frac{p}{\rho} + gz\right] = u_j\left(\frac{\partial u_i}{\partial x_j} - \frac{\partial u_j}{\partial x_i}\right) \tag{5.39}$$

[L] The explanation for $\frac{1}{2}$ is quite simple, because when u_j is drawn into the derivative, the multiplication by the already existing ∂u_j yields a ∂u_j^2; hence, the factor 2, which previously had not existed, originates from the differentiation.

[M] However, we will insert it again later in the same form.

The term on the right side, $u_j \left(\frac{\partial u_i}{\partial x_j} - \frac{\partial u_j}{\partial x_i} \right)$, vanishes if we describe the flow along a streamline $\vec{s}$ (see Chapter 2.8) and integrate the equation along it[N]. The bracketed expression on the right side can be written as $\operatorname{rot} \vec{u}$ so that the whole term reads $\vec{u} \times \operatorname{rot} \vec{u}$. Regarding a streamline (by definition, $\vec{u} \parallel \mathrm{d}\vec{s}$), the vector of the cross product is perpendicular to $\mathrm{d}\vec{s}$; hence, the right side of the equation becomes zero[O].

$$\int \frac{\partial}{\partial s} \left[\frac{1}{2} u_s^2 + \frac{p}{\rho} + gz \right] \mathrm{d}s = \frac{1}{2} u^2 + \frac{p}{\rho} + gz + \text{const.} = 0 \tag{5.40}$$

The equation has the unit $\mathrm{m}^2/\mathrm{s}^2$; only by multiplication of the fluid mass in the area of interest (by multiplication of the density integrated over the volume), the generally known unit of energy Joule $\left[\mathrm{J} = \mathrm{kg\,m}^2/\mathrm{s}^2 \right]$ is obtained. With division by the gravitational constant, the equation is converted to the unit metre; the integration constant on the other side of the equals sign is referred to as energy head H. In the flow, the three types of energy (velocity, pressure and geodetic height) may vary randomly; it is merely their sum which remains constant. Energy is conserved.

$$H = \frac{u^2}{2g} + \frac{p}{\rho g} + z \tag{5.41}$$

In particular with the unit metre, the Bernoulli equation (5.41) is very clear. The effects of the individual terms may be demonstrated by simple experiments (see Chapter 8).

5.8 Momentum equation

As mentioned above, the Cauchy equation (see Chapter 5.2) is based on Newton's treatment of forces and is generally applicable. With the law of momentum, the Cauchy equation is applied to a fluid volume fixed in space (see Figure 5.7). Since the derivatives of the density for an incompressible fluid disappear, we may write:

$$\rho \frac{\partial u_i}{\partial t} + \rho u_j \frac{\partial u_i}{\partial x_j} = \rho g_i + \frac{\partial \tau_{ij}}{\partial x_j} \tag{5.42}$$

The Cauchy equation (5.14) is first formally integrated over the spatial volume:

$$\int \rho \frac{\partial u_i}{\partial t} \mathrm{d}V + \int \rho u_j \frac{\partial u_i}{\partial x_j} \mathrm{d}V = \int \rho g_i \mathrm{d}V + \int \frac{\partial \tau_{ij}}{\partial x_j} \mathrm{d}V \tag{5.43}$$

[N] This holds of course for potential flows (see Chapter 4) too, as $\operatorname{rot} \vec{u} = 0$.

[O] Let's place a local coordinate system on the streamline $\vec{s}$ such that the x-direction coincides with the s-direction. Hence, with the cross product (see Equation 2.6) and the rotation $\nabla \times \vec{u}$ in Equation 2.14, it follows that for the components u, v and w in the three spatial directions x, y and z, respectively:

$$(\vec{u} \times \operatorname{rot} \vec{u}) \circ \mathrm{d}\vec{s} = \begin{pmatrix} u \\ v \\ w \end{pmatrix} \times \begin{pmatrix} \frac{\partial w}{\partial y} - \frac{\partial v}{\partial z} \\ \frac{\partial u}{\partial z} - \frac{\partial w}{\partial x} \\ \frac{\partial v}{\partial x} - \frac{\partial u}{\partial y} \end{pmatrix} \circ \mathrm{d}\vec{s} = \begin{pmatrix} v\left(\frac{\partial v}{\partial x} - \frac{\partial u}{\partial y} \right) - w\left(\frac{\partial u}{\partial z} - \frac{\partial w}{\partial x} \right) \\ w\left(\frac{\partial w}{\partial y} - \frac{\partial v}{\partial z} \right) - u\left(\frac{\partial v}{\partial x} - \frac{\partial u}{\partial y} \right) \\ u\left(\frac{\partial u}{\partial z} - \frac{\partial w}{\partial x} \right) - v\left(\frac{\partial w}{\partial y} - \frac{\partial v}{\partial z} \right) \end{pmatrix} \circ \mathrm{d}\vec{s} = \begin{pmatrix} 0 \\ u\frac{\partial u}{\partial y} \\ u\frac{\partial u}{\partial z} \end{pmatrix} \circ \begin{pmatrix} \mathrm{d}s \\ 0 \\ 0 \end{pmatrix} = 0$$

Next we will deal with steady flows for which $\frac{\partial u_i}{\partial t} = 0$ and look at Figure 5.7, that shows a sketch of a vertical cross-section of a free body fluid volume.

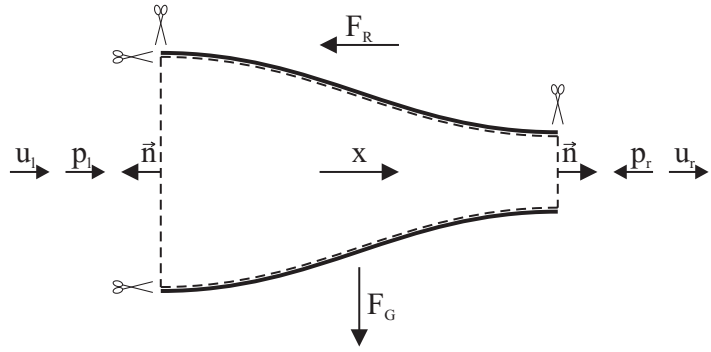

Figure 5.7: Vertical cross-section of a free body fluid volume.

Fluid enters on the left side with velocity u_l in the x-direction and exits on the right side with velocity u_r. It is evident that the fluid does not voluntarily undergo deformation of the kind shown in Figure 5.7. To this effect, an external force, which will be referred to as reaction force F_R, must be applied. Remember how we set up the Cauchy equation. We stated that a fluid mass is accelerated (left side of the equation) when volume and surface forces (on the right side) act on it, which corresponds to the principle in mechanics "actio = reactio" (or, as we have written, "reactio = actio"). If we want to include external forces and account for the "internal forces" of the flow, it is worthwhile to rearrange the equation correspondingly. In Figure 5.7, F_R enters opposite the x-direction; the reaction of the fluid as force in the x-direction is on the right of the equals sign.

$$F_R = -\int \rho u_j \frac{\partial u_i}{\partial x_j} \mathrm{d}V + \int \rho g_i \mathrm{d}V + \int \frac{\partial \tau_{ij}}{\partial x_j} \mathrm{d}V \tag{5.44}$$

We will now analyse Equation 5.44 term by term; let's begin with the convective derivative $\int \rho u_j \frac{\partial u_i}{\partial x_j} \mathrm{d}V$[P]. Formally, we find it difficult at first to integrate the convective part of the velocity derivative with the Gaussian theorem (see also Chapter 5.1) over our volume fixed in space, because unfortunately, the term reads $\frac{\partial u_i}{\partial x_j} = \frac{\partial u}{\partial x} + \frac{\partial u}{\partial y} + \frac{\partial u}{\partial z}$ and not $\mathrm{div}\,\vec{u} = \frac{\partial u_i}{\partial x_i} = \frac{\partial u}{\partial x} + \frac{\partial v}{\partial y} + \frac{\partial w}{\partial z}$.
We will leave the Cartesian coordinate system and formulate Equation 5.44 for a stream-tube along the coordinate s which coincides with the streamline $\vec{s}$ (see Chapter 2.8). Therein, o is normal, and q is binormal to s; o and q each span the three-dimensional space perpendicular to s, and the velocity components u_s, u_o and u_q are defined. The convective acceleration integrated over the control volume reads as follows:

$$\int \rho u_j \frac{\partial u_i}{\partial x_j} \mathrm{d}V = \int \rho \left(u_s \frac{\partial u_s}{\partial s} + u_o \frac{\partial u_s}{\partial o} + u_q \frac{\partial u_s}{\partial q} \right) \mathrm{d}V \tag{5.45}$$

[P] The convective acceleration $\frac{\partial u}{\partial x}\frac{\mathrm{d}x}{\mathrm{d}t} = u\frac{\partial u}{\partial x}$ was already discussed in Chapter 2.4.1.2. The velocity field varies in the x-direction ($\frac{\partial u}{\partial x}$), and a fellow traveller notices this acceleration earlier if he moves faster (with velocity u) in exactly this direction (x).

From now on, we assume a uniform velocity profile in the cross-section. Then $\frac{\partial u_s}{\partial o} = \frac{\partial u_s}{\partial q} = 0$ and Equation 5.45 reads:

$$\int \rho u_j \frac{\partial u_i}{\partial x_j} \, \mathrm{d}V = \int \rho \left(u_s \frac{\partial u_s}{\partial s} + 0 + 0 \right) \mathrm{d}V = \int \rho u_s \frac{\partial u_s}{\partial s} \, \mathrm{d}V \tag{5.46}$$

This corresponds almost exactly with the formulation of the continuity condition in a streamtube (Equation 5.4); therefore, we may write down the partial derivative in the convective acceleration with the Gaussian integral theorem as follows:

$$\int \frac{\partial u_s}{\partial s} + \frac{\partial u_o}{\partial o} + \frac{\partial u_q}{\partial q} \, \mathrm{d}V = \int \frac{\partial u_s}{\partial s} + 0 + 0 \, \mathrm{d}V = \int \vec{u} \circ \vec{n} \, \mathrm{d}A \tag{5.47}$$

The scalar product of the normal and velocity vectors ensures that only the component of the velocity vector that is perpendicular to the sectional surface, entering or exiting, is considered for the discharge $Q = \int \vec{u} \circ \vec{n} \, \mathrm{d}A$. Finally, the convective acceleration is obtained:

$$\int u_j \frac{\partial u_i}{\partial x_j} \, \mathrm{d}V \overset{\text{uniform}}{=} \int u_s \frac{\partial u_s}{\partial s} + u_o \frac{\partial u_s}{\partial o} + u_q \frac{\partial u_q}{\partial s} \, \mathrm{d}V = \int \vec{u} \circ (\vec{u} \circ \vec{n}) \, \mathrm{d}A \tag{5.48}$$

The signs of the terms are hard to understand, and that is why we will take a meticulous look at them. On the left side, where the fluid flows in, the normal vector $\vec{n}$ points opposite the flow direction (which is in the positive x-direction) and is therefore negative. For the term on the left side of the control volume, which is referred to as entering net rate of momentum, or entering momentum flux[Q], we obtain (back at Equation 5.46):

$$\int \rho \vec{u_l} \circ (\vec{u_l} \circ \vec{n}) \, \mathrm{d}A_l = \int \rho \vec{u_l} \circ (\vec{u_l} (-1)) \, \mathrm{d}A_l \tag{5.49}$$

For the same quantity on the right side, also known as leaving momentum flux, the following results:

$$\int \rho \vec{u_r} \circ (\vec{u_r} \circ \vec{n}) \, \mathrm{d}A_r = \int \rho \vec{u_r} \circ (\vec{u_r} (+1)) \, \mathrm{d}A_r \tag{5.50}$$

Let's go on with the other terms. By integration of the density ρg_i over the volume, the weight as volume force is obtained.

$$\int \rho g_i \, \mathrm{d}V = \rho g_i V \tag{5.51}$$

The volume integral over the derivative of the stresses with respect to position again becomes a surface integral via the Gaussian theorem:

$$\int \frac{\partial \tau_{ij}}{\partial x_j} \, \mathrm{d}V \overset{\text{Gauss-theorem}}{=} \int \tau_{ij} \circ \vec{n} \, \mathrm{d}A \tag{5.52}$$

Due to the multiplication by the normal vector, the only thing that matters here is the proportion of the stress tensor that acts perpendicularly to this surface, i. e. the pressure $\int -p \vec{n} \, \mathrm{d}A$ as negative stress τ_{ii}. Analogous to the momentum fluxes entering (left) and

[Q] The quantity is a momentum per unit time, which is, according to Newton's second axiom (see Chapter 3.3), changed by the forces applied.

leaving (right) the control volume, we define the pressure as negative stress (see Chapter 5.3) at the free body surfaces. For the left side where the fluid enters, the expression reads as follows:

$$\int -p_l \vec{n} \, \mathrm{d}A_l = \int -p_l \, (-1) \, \mathrm{d}A_l = \int p_l \, \mathrm{d}A_l \tag{5.53}$$

The normal vector points to the left, opposite to the positive x-axis, and is therefore negative. The right side may be written as follows:

$$\int -p_r \vec{n} \, \mathrm{d}A_r = \int -p_r \, (+1) \, \mathrm{d}A_r = -\int p_r \, \mathrm{d}A_r \tag{5.54}$$

The findings are now combined in Equation 5.44:

$$F_R = -\int \rho \, \vec{u} \circ (\vec{u} \circ \vec{n}) \, \mathrm{d}A + \rho g_i V + \int -p \vec{n} \, \mathrm{d}A \tag{5.55}$$

And further:

$$\begin{aligned} F_R &= -\left(\int \rho \vec{u_l} \circ (\vec{u_l} \circ \vec{n}) \, \mathrm{d}A_l + \int \rho \vec{u_r} \circ (\vec{u_r} \circ \vec{n}) \, \mathrm{d}A_r \right) + \rho g_i V \\ &+ \left(\int -p_l \vec{n} \, \mathrm{d}A_l + \int -p_r \vec{n} \, \mathrm{d}A_r \right) \\ &= -\left(-\int \rho \vec{u_l} \circ (\vec{u_l}) \, \mathrm{d}A_l + \int \rho \vec{u_r} \circ (\vec{u_r}) \, \mathrm{d}A_r \right) + \rho g_i V + \int p_l \, \mathrm{d}A_l - \int p_r \, \mathrm{d}A_r \end{aligned} \tag{5.56}$$

Equation 5.56 may now be simplified for uniform conditions at the sectional surfaces. With a constant velocity distribution over the cross-section, we obtain:

$$\int \rho \vec{u_l} \circ (\vec{u_l} \circ \vec{n}) \, \mathrm{d}A_l = \int \rho \vec{u_l} \circ (\vec{u_l} \, (-1)) \, \mathrm{d}A_l = -\rho Q u_l \tag{5.57}$$

$$\int \rho \vec{u_r} \circ (\vec{u_r} \circ \vec{n}) \, \mathrm{d}A_r = \int \rho \vec{u_r} \circ (\vec{u_r} \, (+1)) \, \mathrm{d}A_r = \rho Q u_r \tag{5.58}$$

The following results are obtained for a uniform pressure distribution:

$$\int -p_l \vec{n} \, \mathrm{d}A_l = \int -p_l \, (-1) \, \mathrm{d}A_l = \int p_l \, \mathrm{d}A_l = p_l A_l \tag{5.59}$$

$$\int -p_r \vec{n} \, \mathrm{d}A_r = \int -p_r \, (+1) \, \mathrm{d}A_r = \int -p_r \, \mathrm{d}A_r = -p_r A_r \tag{5.60}$$

Equation 5.56 may thus be simplified as follows:

$$\begin{aligned} F_R &= -\left(-\rho Q u_l + \rho Q u_r\right) + \rho g_i V + \int p_l \, \mathrm{d}A_l - \int p_r \, \mathrm{d}A_r \\ &= +\rho Q u_l + p_l A_l - \rho Q u_r - p_r A_r + \rho g_i V \end{aligned} \tag{5.61}$$

From Equation 5.61, it can be seen that both the pressure force and the momentum flux on both sides point in towards the control volume, irrespective of how the cross-sectional boundaries of the free body are oriented. This is plausible for the pressure force on the right side. For the momentum fluxes, it is conceivable that the fluid on the other side of the right sectional surface of the free body must push off from the control volume and therefore the force also points in towards the volume. Here, the formula is again "actio =

reactio" (see Chapter 3.3). In our case (see Figure 5.7), the reaction force was applied in the negative x-direction, which is why it has the same sign as the forces on the right side, which also point to the left.
Over the lateral surface, no flow takes place; however, the pressure force must be relieved over this surface. This is calculated in a pipe by means of what is known as Barlow's formula (12.17).
Generally speaking, because of the law of momentum, the conditions shown in Figure 5.8 result:

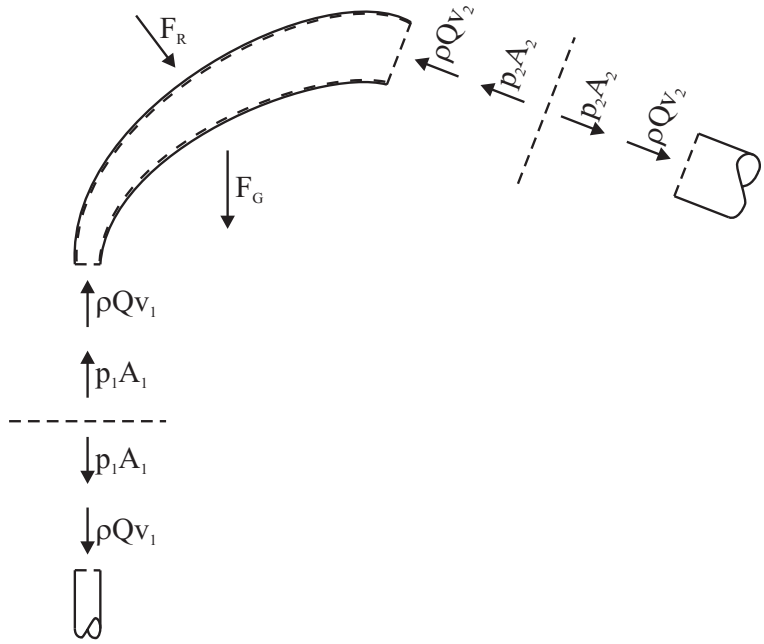

Figure 5.8: Free body fluid volume with spatial curvature.

Ludwig Prandtl, probably Germany's most famous fluid mechanics scientist, classified the law of momentum in his "Führer durch die Strömungslehre" (Guide through Fluid Dynamics) as follows [32]:

> "The value of these laws of momentum is that they merely include statements on conditions at the boundaries of an area, and that it is therefore possible to draw conclusions on details of processes which one does not completely control."

5.9 Summary of the basic equations

Figure 5.9 summarises the derivations of the basic equations with the specified conditions. Applications and experiments will be explained in Part II.

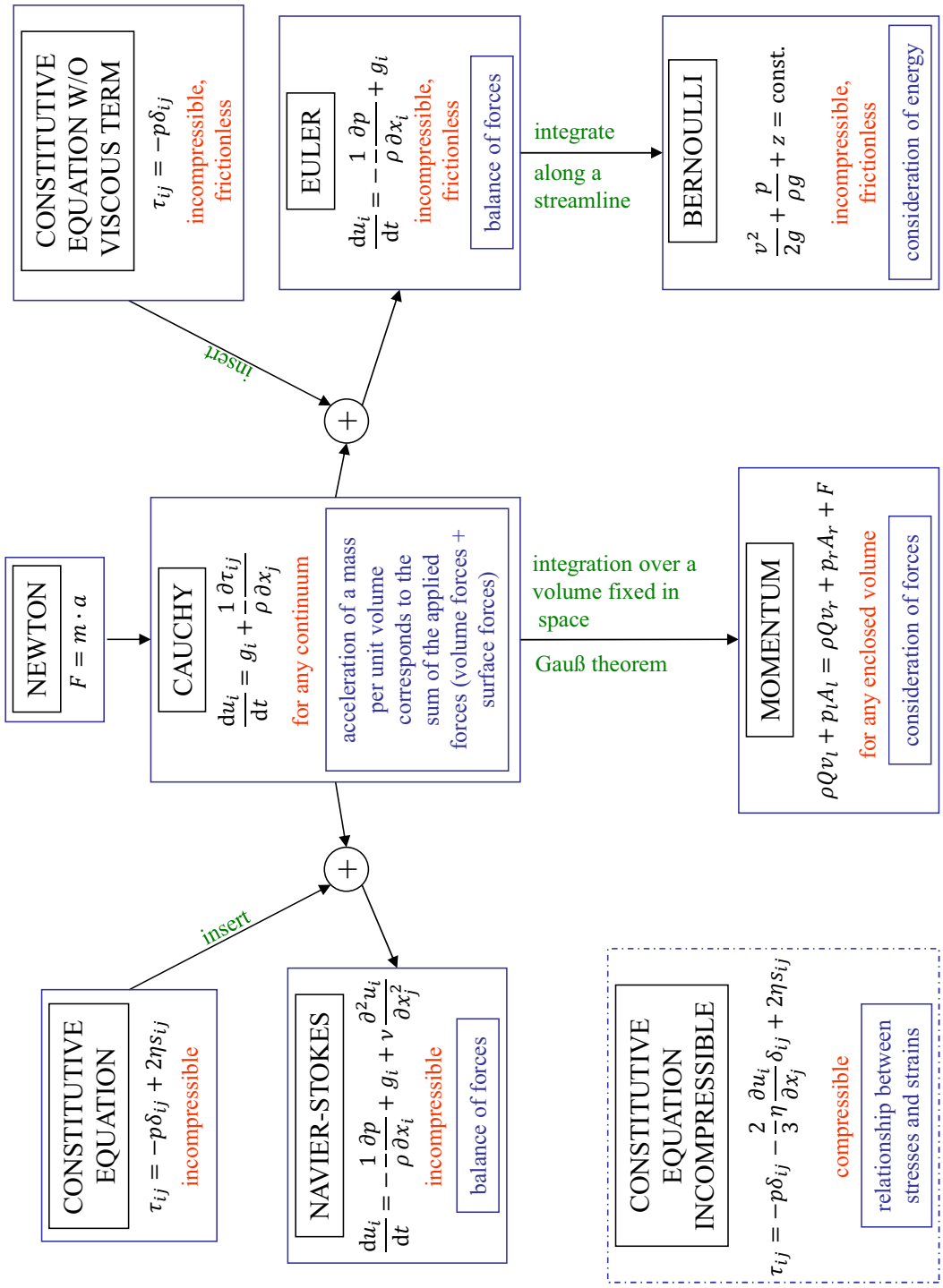

Figure 5.9: Basis equations according to [40].

Chapter 6
Turbulence and its modelling

6.1 Introduction to turbulence

[A]Flows are generally divided into laminar and turbulent flows, with the latter exhibiting a chaotic character. Turbulent flows are *irregular*, *swirled*, *random*, *unsteady* and *unpredictable* and are therefore primarily time-dependent. The Brockhaus der Naturwissenschaften und der Technik [7] states under the term *Strömungslehre* (fluid mechanics): "At laminar flows (...), the layers of different velocities pass each other without the generation of eddies. With an increase in flow velocity in a pipe, the initially laminar movement suddenly changes to a statistically disordered, *turbulent flow*. The cause is that the flow near the wall becomes unstable."
Since this phenomenon is so hard to grasp, Kundu and Cohen [25] refer to a quotation by Lesieur (1987):

> "Turbulence is a dangerous topic which is at the origin of serious fights in scientific meetings since it represents extremely different points of view, all of which have in common their complexity as well as an inability to solve the problem. It is even difficult to agree on what exactly the problem to be solved is."

Pope [34], however, recommends that turbulent flows be observed by means of, for example, replica of Osborne Reynolds' legendary dye experiment. Figure 6.1 shows the streakline (see Chapter 2.8), i. e. the connection of all fluid elements which have passed the point where the tracer was injected. With the laminar flow, a clear line is perceptible; during transition, this line is broken by the onset of eddies and the chaotic character of turbulent flow leads to a blurred image of the dye.
At $\mathrm{Re} = \frac{uD}{\nu} \approx 2300$, a laminar pipe flow changes to a turbulent flow (see Chapter 5.6). The following thought experiment (see Figure 6.2) is intended to clarify the difference between the two fundamentally different types of flow [43]:

> When offering pedestrians at 3 a.m. on a Saturday night an incentive of approximately $\Delta e = 0.10\,€$ for walking from Marienplatz to Stachus, one can convince probably only a few to do so. The few who can be persuaded will purposefully start without abrupt changes in direction. When repeating the experiment on a Saturday afternoon at 3 p.m. and offering $\Delta e = 50\,€$ for walking the same distance, people will fight. Everybody wants to get hold of the money, which means that Neuhauser Straße, which connects Marienplatz and Stachus, will be overcrowded. There will be pushing and elbowing, and bunches of several dozens of people will be the play ball in the chaos of the mass. Because of the crowd, the boundary becomes

[A] This chapter is taken almost word for word from Rapp [44].

C. Rapp, *Hydraulics in Civil Engineering*,
https://doi.org/10.1007/978-3-031-54860-4_6

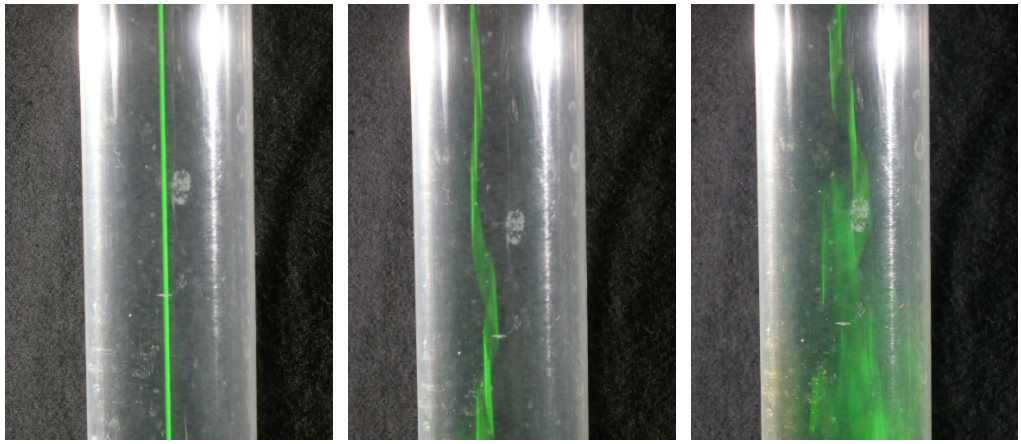

Figure 6.1: A replica of Reynolds' dye experiment for exemplifying the laminar (left) and the turbulent flow (right). The transition between laminar and turbulent is shown in the centre.

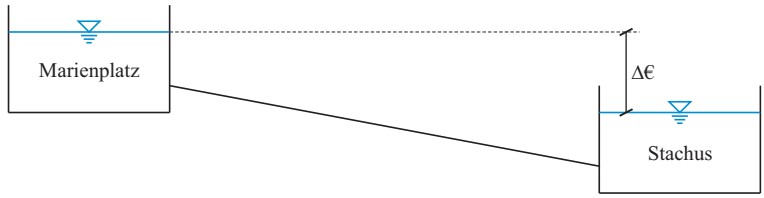

Figure 6.2: Thought experiment Marienplatz - Stachus (Munich's main pedestrian zone) [43].

> increasingly important since people will also be pushed to the boundary where open store doors and market stalls do not allow frictionless passing. Many more people will probably arrive at Stachus, but they will be much more exhausted than the night owls. Their energy will not be dissipated by the large structures, even when they move together with dozens of neighbours, e. g. perpendicularly to the main flow direction. Their energy will be dissipated as they elbow their immediate neighbours who do not take the same direction.[B]

The Brockhaus der Technik [7] lists this important characteristic under the keyword *turbulente Bewegung* (turbulent movement):

> "Irregular movement of a flow, wherein flow energy is dissipated through the formation of eddies and their collapse to new, still finer eddies. (. . .)"

6.2 Cursory approach to numerics

For the calculation of flows, the Navier–Stokes equations (5.29 and 5.30) must be discretised in terms of time and space; likewise, boundary conditions must be set at the boundaries of the domain. This means that the partial differential continuous equations are transformed to an algebraic form [54]. Thus, the equations must be formulated at distinct points (method of finite differences) or control volumes (method of finite volumes) in the flow area in order to be able to obtain the space and time derivatives. These points

[B] This metaphoric paraphrasing is inadequate solely because turbulence is a three-dimensional (and not a two-dimensional) phenomenon.

or volumes may be arranged in space in various ways. Figure 6.3 is an illustration of an example of a two-dimensional numerical grid that may be used for the simulation of flows.

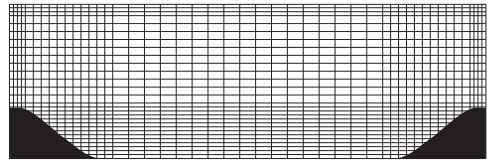

Figure 6.3: Example of a two-dimensional cartesian calculation grid for numeric simulations according to [6].

In the discrete formulation, the gradients in the equations require a corresponding numeric approximation; in this case, too, there are various common methods available. For instance, in the method of central differences (of second order), the pressure gradient in the z-direction at point i can be approximated by the two points $i-1$ and $i+1$, which are spaced apart by Δz:

$$\frac{\partial p}{\partial z} \approx \frac{p_{i+1} - p_{i-1}}{2 \cdot \Delta z} \tag{6.1}$$

The result is that a turbulent flow cannot be calculated exactly. But the finer the resolution, the smaller the approximation error. Moreover, there is the phenomenon, described above, of the small eddies being mainly responsible for the friction losses in the flow. To represent these small eddies, an adequately fine discretisation is necessary; therefore, the Navier–Stokes equations must be solved at numerous points or volumes. Because of the time dependency of a turbulent flow, a very high resolution of time is also required to represent these small eddies. Another property complicates life (or the solution of the equations). Eddies become smaller with an increasing degree of turbulence, which is characterised by the Reynolds number. According to the Kolmogorov[C] similarity hypothesis, the lengths of the greatest to the smallest eddies scale with $\mathrm{Re}^{\frac{3}{4}}$ [34]. This means that the spatial discretisation must increase by $\left(\mathrm{Re}^{\frac{3}{4}}\right)^3 = \mathrm{Re}^{\frac{9}{4}}$.

6.3 Direct Numerical Simulation

When a flow is discretised in terms of time and space in such a manner that all length and time scales are completely resolved, this is referred to as a direct numerical simulation (DNS). The Navier–Stokes equations (5.29 and 5.30) describe the flow comprehensively, so in this case no turbulence model is required. With correctly set boundary conditions, the results correspond to the physically correct solution. However, the numeric cost due to the spatial discretisation increases by $\mathrm{Re}^{\frac{9}{4}}$. Apart from the spatial resolution, the time step must be reduced at higher Reynolds numbers, so that according to Fröhlich [14] the CPU (central processor unit) time increases proportionally to Re^3. Because of this, the DNSs, which must be simulated on supercomputers, are limited to academic cases with relatively low Reynolds numbers.

[C] Andrei Nikolajewitsch Kolmogorow, ∗1903, Tambow, Russia, †1987, Moscow, Russia

6.4 Reynolds Averaged Navier–Stokes Simulation

Although the quantities described in the Navier–Stokes equation (5.29 and 5.30) are at an instant of time of random character, they converge to an average value of statistically steady-state flows with associated variance. Therefore, Osbourne Reynolds suggested that instantaneous values be split into their average and fluctuation values ($u_i(x,t) = \langle u_i(x)\rangle + u_i'(x,t)$). The Reynolds equation reads:

$$\frac{\partial \langle u_i\rangle}{\partial t} + \langle u_j\rangle \frac{\partial \langle u_i\rangle}{\partial x_j} = -\frac{1}{\rho}\frac{\partial \langle p\rangle}{\partial x_i} + g_i + \nu \frac{\partial^2 \langle u_i\rangle}{\partial x_j^2} - \frac{\partial \langle u_i' u_j'\rangle}{\partial x_j} \tag{6.2}$$

Compared to the Navier–Stokes equation, the Reynolds equation (6.2) has another six unknowns in the form of the so-called Reynolds stress tensor $\rho\langle u_i' u_j'\rangle$ or rather its partial derivative with respect to position for an incompressible fluid $\rho\frac{\partial \langle u_i' u_j'\rangle}{\partial x_j}$. The system with four equations (the momentum equation holds for the three spatial directions; the fourth equation is the continuity condition) is based on a total of ten unknowns; this is referred to as the closure problem of turbulence. In Reynolds Averaged Navier–Stokes (RANS) simulations, it is this tensor that is modelled. More detailed explanations may be taken from the relevant literature, e. g. [48], [34] or [25].
In an example illustrating an approach flow in a hydropower plant, Figure 6.4 shows the norm of the mean velocity vector resulting from a RANS simulation. This simulation strategy yields results only for the time-averaged conditions.

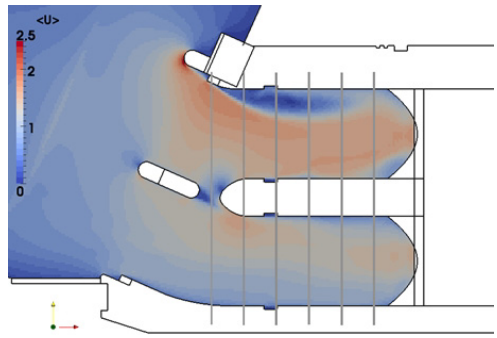

Figure 6.4: Mean flow velocity in a sectional plane through a three-dimensional calculation domain from a Reynolds Averaged Navier–Stokes simulation.

Because of the relatively low CPU costs, RANS simulations often lend themselves as the method of choice.

6.5 Large Eddy Simulation

In large eddy simulations (LES), structures carrying high energy are resolved by selected discretisation, while small, energy-dissipating eddies are modelled [14]. If the velocity is divided into a proportion $\bar{u}$ that is represented by discretisation and a proportion $\tilde{u}$ that

is not resolved by the grid, the non-linearity of the convection term $u_j \frac{\partial u_i}{\partial x_j}$ leads to what are known as subgrid stresses τ_{ij}^s. These stresses result from the fact that the momentum transport of the eddies, which are smaller than the spatial discretisation, is not mapped numerically. They are calculated as follows: $\tau_{ij}^s = \rho\,(\overline{u_i u_j} - \tilde{u}_i \tilde{u}_j)$. The Navier–Stokes equations (5.29 and 5.30) are extended to the filtered Navier–Stokes equations by the gradient of the subgrid stresses (the partial derivative of the subgrid stresses with respect to position):

$$\frac{\mathrm{d}u_i}{\mathrm{d}t} = -\frac{1}{\rho}\frac{\partial p}{\partial x_i} + g_i + \nu \frac{\partial^2 u_i}{\partial x_j^2} - \frac{1}{\rho}\frac{\partial \tau_{ij}^s}{\partial x_j} \tag{6.3}$$

The term $\frac{\partial \tau_{ij}^s}{\partial x_j}$, which is also referred to as a subfilter term, must be mapped via an adequate model.
Figure 6.5 is an illustration of an example of the current velocity field of a flow through a hydropower plant screen. Contrary to the average values in Figure 6.4, the resulting plot exhibits sharp boundaries of the colour-marked instantaneous velocities.

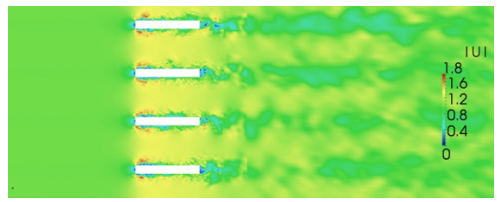

Figure 6.5: Flow velocity at a distinct time in a sectional plane through a three-dimensional computation domain from a large eddy simulation.

6.6 Shallow Water Equations

In depth-averaged shallow water equations, the momentum in the vertical direction is neglected and, as the name suggests, averaging of the velocity over the flow depth is carried out [3]. The momentum balance in the z-direction is integrated into the description of the hydrostatic pressure. This is why the Navier–Stokes equations are simplified in such a manner that they are also applicable to the solution of large computation domains. However, the conditions for the scope of application of these equations, hydrostatic pressure distribution and a w-component that is very much smaller than u and v, must be met. Equation 6.4 comprises the shallow water equations for the three spatial directions. The bar signifies the spatial averaging of the respective quantity; the stresses τ must be introduced empirically.

$$\begin{aligned}
\frac{\partial h\bar{u}}{\partial t} + \frac{\partial h\bar{u}\bar{u}}{\partial x} + \frac{\partial h\bar{u}\bar{v}}{\partial y} &= -\frac{g}{2}\frac{\partial h^2}{\partial x} - gh\frac{\partial z_s}{\partial x} - \frac{\tau_{sx}}{\rho} + \frac{\partial h\bar{\tau}_{xx}/\rho}{\partial x} + \frac{\partial h\bar{\tau}_{xy}/\rho}{\partial y} \\
\frac{\partial h\bar{v}}{\partial t} + \frac{\partial h\bar{v}\bar{u}}{\partial x} + \frac{\partial h\bar{v}\bar{v}}{\partial y} &= -\frac{g}{2}\frac{\partial h^2}{\partial y} - gh\frac{\partial z_s}{\partial y} - \frac{\tau_{sy}}{\rho} + \frac{\partial h\bar{\tau}_{yx}/\rho}{\partial x} + \frac{\partial h\bar{\tau}_{yy}/\rho}{\partial y} \\
0 &= -\frac{1}{\rho}\frac{\partial p}{\partial z} - g
\end{aligned} \tag{6.4}$$

Mass conservation becomes:

$$\frac{\partial h}{\partial t} + \frac{\partial h\overline{u}}{\partial x} + \frac{\partial h\overline{v}}{\partial y} = 0 \tag{6.5}$$

Especially for the calculation of the flow in natural channels, where there are no exact geometrical and hydrological data available or measurable, this strategy yields sufficient and useful information. Figure 6.6 shows a colour-marked flow depth map, obtained from such a 2D computation, in a floodplain. One can easily imagine that the resolution of

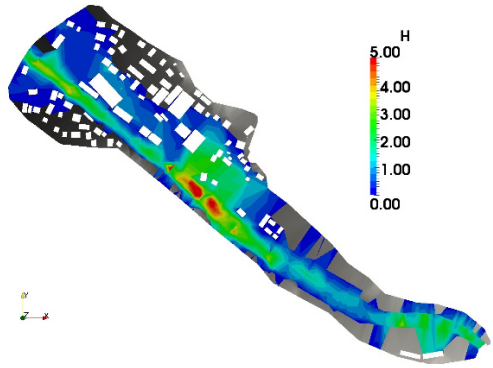

Figure 6.6: Flow depth of the Dornbirner Ache in Vorarlberg, Austria, from [55].

the smallest eddy structures in a computation domain of several square kilometres is impossible. A true-to-detail description of the boundary cannot be given, nor can the necessary computer power for the computation be provided. However, in this case, the precise knowledge of individual structures and flow separations is not the subject of the investigation. Rather, the rough determination of inundation areas in case of flood events is of interest.

6.7 Final considerations on turbulence

Turbulence is a complicated topic that, in most cases, makes the accurate computation of flows impossible. And although the images resulting from three-dimensional simulations are so beautifully coloured and convincing, they should nevertheless be critically questioned. Fortunately, the exact solution of flow problems is not even necessary in most cases. As an engineer, one would normally like to know whether components are able to withstand a certain load or whether, for example, areas will be flooded or not. For such issues, boundary conditions such as river topography and precipitation are associated with high uncertainties. Therefore, the one-dimensional approaches that will be discussed in the following part are far more than a rough estimation of the conditions. In any case, they are often – together with the experiments – the only possibility of comprehending these complex flows and verifiably estimating their consequences.

Part II
Applied hydraulics

Chapter 7
Hydrostatics

7.1 General information on hydrostatics

Hydrostatics is a special field of hydromechanics and thus of the Navier-Stokes equations (5.29 and 5.30). Because the fluid is stationary, all velocities and their gradients become zero. The only acting forces originate from pressure and gravity.
When inserting 0 into the Navier-Stokes equation for the velocities and their derivatives in a static system, Equation 7.1 is obtained.

$$0 = -\frac{1}{\rho}\frac{\partial p}{\partial z} + g \tag{7.1}$$

7.2 Hydrostatic pressure

According to Chapter 3.4.9, the pressure, being a scalar quantity, is not directed. However, the individual molecules bear against one another. A fluid boundary, e. g. a wall, has to absorb the pressure. The pressure always acts perpendicularly to the wall, regardless of its inclination. This fact can be comprehended as follows: As we agreed at the beginning of this chapter, the fluid is stationary in hydrostatics. Take your mobile phone and put it on a table. Now apply a normal stress with your hand (press perpendicularly to the tabletop). Then try to apply a horizontal stress on the phone's surface. You will succeed only if you move your hand (and thus the phone) along the table plane. However, this is not in accordance with the rules of hydrostatics! This means that the pressure can act only perpendicularly to the boundary.
As explained in Chapter 3.4.9, the pressure in an incompressible fluid increases linearly as a function of depth (see Figure 7.1). Equation 7.1 in the integral form reads:

$$\int_{z=\mathrm{WS}-h}^{z=\mathrm{WS}} \frac{1}{\rho}\frac{\partial p}{\partial z}\,\mathrm{d}z = \int_{z=\mathrm{WS}-h}^{z=\mathrm{WS}} g\,\mathrm{d}z \tag{7.2}$$

This becomes

$$\frac{p}{\rho} = [gz]_{z=\mathrm{WS}-h}^{z=\mathrm{WS}} + \mathrm{const.} = g\,[z_{\mathrm{WS}} - z_{\mathrm{WS}-h}] + \mathrm{const.} \tag{7.3}$$

and solved for p:

C. Rapp, *Hydraulics in Civil Engineering*,
https://doi.org/10.1007/978-3-031-54860-4_7

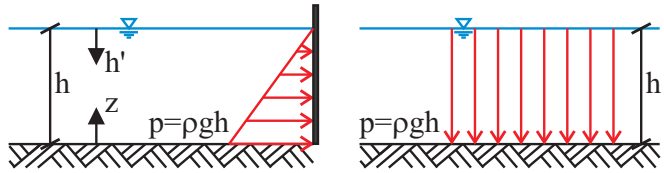

Figure 7.1: Pressure acting on a vertical wall (left) or on the bottom of a container (right).

$$p = \rho g h + C \tag{7.4}$$

First, let's go through the individual calculation steps. We integrate the partial derivative of the pressure which depends on the coordinate direction z over exactly this coordinate direction. Needless to say, as a result, just this derivative vanishes. Since the left side of the equation is not dependent on z, the integration limits $z = \mathrm{WS} - h$ and $z = \mathrm{WS}$ are meaningless. However, the gravity constant g on the right side is integrated with respect to z, which results in gz. The integration limits are set from the lower to the higher value of z (see also e. g. [8, p. 457]). The integral is then written for the function $f(x)$ whose antiderivative $F(x)$ is written as:

$$\int_{\mathrm{from}}^{\mathrm{to}} f(x) = [F(x)]_{\mathrm{from}}^{\mathrm{to}} = F(x = \mathrm{to}) - F(x = \mathrm{from}) \tag{7.5}$$

The solution of a definite integral (an integral with integration limits) implies the addition of an integration constant C which satisfies the boundary condition. In our case, this constant is the pressure at the water surface, i. e. the atmospheric pressure p_{atm}, which we will examine closer later in Chapter 7.9 in the context of relative and absolute pressure. The constant is zero in the case of relative pressure.
In the integration of Equation 7.1, nothing is done formally other than adding the load of the respective overlying molecules. From Equation 7.1, the relationship between fluid depth and pressure follows, which was already described in Chapter 3.4.9. Equation 7.1, which is based on the Navier-Stokes equation, already includes the incompressibility of water via the constitutive equation (5.21). p is linearly dependent on z. In the coordinate system defined in Figure 2.1, the z-axis points upwards; the gravity g is directed in the negative z-direction. When introducing the auxiliary coordinate h' from the water surface in a downward direction, the water pressure increases linearly with $\rho g h'$. When the depth is identified by h, then the description of the pressure, which everybody has to know by heart even while sleeping, is:

$$p = \rho g h \tag{7.6}$$

The unit of the pressure can be derived from this equation:

$$\mathrm{kg/m^3 \cdot m/s^2 \cdot m = kg/(m\,s^2) = N/m^2} \tag{7.7}$$

The right side of Figure 7.1 depicts the pressure at the bottom of a container which is a function of depth h' and can be written as $p = \rho g h$. On the left side of the figure, the effect of the pressure on a vertical wall is depicted. The pressure increases linearly with depth and reaches the value $p = \rho g h$ at the bottom.
Here, we should recall that the pressure is scalar, i. e. not directed. Within the fluid, i. e. somewhere in the middle of the water column in Figure 7.1, the individual water molecules

under pressure can bear against one another. They simply transmit the pressure. At the boundary, they bear against the wall.

7.3 Pressure force

The pressure force on the wall in Figure 7.1 results from the integration of the pressure over the area. At every single tiny bit of the wall, the pressure $p = \rho g h'$ prevails. Imagine numerous single arrows that increase from 0 at the water surface to $\rho g h$ at the bottom. Each of them acts on an infinitesimally small area. Thus, the pressure force is obtained by multiplying the pressure with the infinitesimally small areas $\mathrm{d}A$:

$$F_{\text{pressure}} = \int p \, \mathrm{d}A \tag{7.8}$$

For the wall:

$$\int_b \int_0^h \rho g h' \, \mathrm{d}h' \, \mathrm{d}b = \rho g b \frac{h^2}{2} \tag{7.9}$$

The pressure force acting on the vertical wall can thus be calculated by multiplying the pressure on the surface's centre of gravity with the surface area. This issue will be taken up further below.

$$F_{\text{pressure}} = h_{\text{CG}} \rho g A \tag{7.10}$$

7.4 Buoyancy

Why is a stone under water lighter than above water? Before asking this question, we take a pebble with a diameter of approximately 5 cm and carry it to a completely filled wash basin. We feel the stone's weight in the hand and then immerse it into the basin. What do you feel? Does the stone really become lighter?

Now, follow an experiment in which the forces are measured:

Experiment

Buoyancy of a stone

This experiment (see Figure 7.2) is simple but nonetheless valuable. The stone is suspended on a spring balance and has a weight of $F_{\text{above water}} = 16.5\,\text{N}$. When the stone is immersed under water, the spring balance indicates a force of $F_{\text{under water}} = 10.6\,\text{N}$. The difference is due to the so-called buoyancy force. It results from the pressure difference between the upper and the lower surfaces of the stone, which, when integrated over the area on which this pressure difference acts, becomes the buoyancy force.
Let's look more closely at the situation (Figures 7.2 and 7.3). When diving from the water surface by h_1 to the upwardly directed surface of the stone, the water exerts a pressure

of $\rho g h_1$ on this surface. This pressure prevails on the entire upwardly directed surface of the stone (A_{stone}), which leads to a downward force $F_{\downarrow} = \rho g h_1 A_{\text{stone}}$.
The pressure increases from $\rho g h_1$ to $\rho g h_2$ downwards along the side wall of the stone. At the same time, we observe that the pressure increase is the same on all sides and the pressure forces acting on the sides of the stone sum up to zero. The stone is neither pushed to the left nor to the right, nor to the front nor rear. It remains in its horizontal position. However, at the downwardly directed surface at the bottom of the stone, the pressure force $F_{\uparrow} = \rho g h_2 A_{\text{stone}}$ acts upwards – perpendicular to the directed boundary.
The vertical force results as the sum of the upwardly- and downwardly directed forces:

$$F_{\text{buoyancy}} = F_{\uparrow} - F_{\downarrow} = \rho g h_2 A_{\text{stone}} - \rho g h_1 A_{\text{stone}} = \rho g (h_2 - h_1) A_{\text{stone}} \tag{7.11}$$

When $h_{\text{stone}} = h_2 - h_1$ and $V_{\text{displacement}} = A_{\text{stone}} \cdot h_{\text{stone}}$, the buoyancy force can be expressed as:

$$F_{\text{buoyancy}\uparrow} = \rho g h_{\text{stone}} A_{\text{stone}} = \rho g V_{\text{displacement}} \tag{7.12}$$

With the stone immersed into the container ($d = 0.293\,\text{m}$), the water surface has risen by $9\,\text{mm}$. Since the water surrounds the stone entirely, the difference in the water levels multiplied by the area of the water surface of the cylindrical container corresponds to the volume of the stone. The displaced water volume is calculated as $V_{\text{displacement}} = \Delta h_{\text{WS}} \cdot A_{\text{vessel}} = 0.009 \cdot 0.293^2 \frac{\pi}{4} = 6.07 \times 10^{-4}\,\text{m}^3$. By multiplying this displaced volume by ρg, the buoyancy force $F_{\text{buoyancy}} = 5.95\,\text{N}$ ($F_{\text{above water}} - F_{\text{under water}}$) is obtained. The calculated buoyancy corresponds to the difference between the weight forces of the stone above and below water, which explicitly demonstrates the relationship.

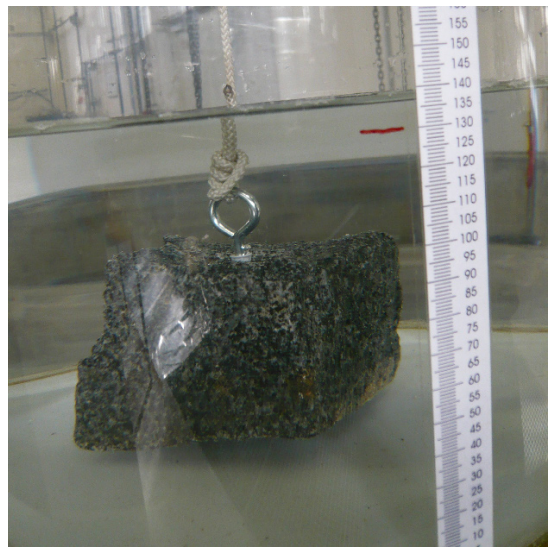

Figure 7.2: Stone subject to buoyancy.

Of course, the mass of the stone remains constant throughout the experiment $m_{\text{stone}} = \rho_{\text{stone}} \cdot V_{\text{stone}} = \rho_{\text{stone}} \cdot V_{\text{displacement}}$. By the way, the density of the stone can also be calculated with $F_{\text{above water}}$ from $\rho_{\text{stone}} = \frac{m_{\text{stone}}}{V_{\text{stone}}}$.

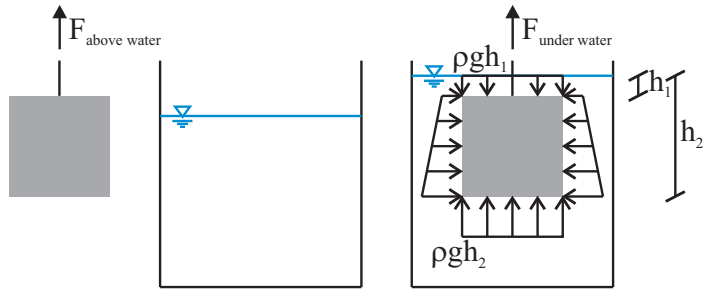

Figure 7.3: Stone subject to buoyancy – pressure distribution.

You can easily carry out the experiment yourself by means of a spring balance from a DIY shop.

7.5 Pressure diagrams

7.5.1 Pressure diagrams with application of pressure on both sides

There is water on both sides of the separating wall in Figure 7.4. The pressure acting on the wall can be visualised by means of a pressure diagram, which we will explore together. We start where the conditions are known. Atmospheric pressure prevails at the wall directly at the water surface, i. e. the water pressure is 0. When we move downwards on the left side of the wall, the pressure increases linearly until we reach the pressure $p = \rho g h_1$ at the bottom. On the right side, we also start where the pressure is known: at the water surface. We start at zero pressure and move downwards along the wall. We reach the bottom already after traversing the distance h_2, where the pressure $\rho g h_2$ prevails. The gradient of the two triangles is ρg, so that the resulting pressure distribution in the region with water on the left and right side is constant.

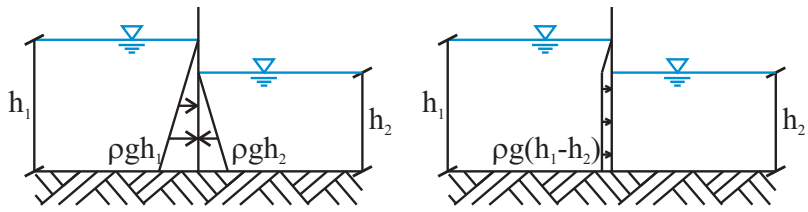

Figure 7.4: There is water on both sides of the separating wall. The resulting pressure diagram is depicted on the right.

7.5.2 Fluids with different densities

The behaviour of pressure in the case of two liquids with different densities is discussed with reference to Figure 7.5. Due to its lower density (Figure 7.5 left), oil ($\rho_{\text{oil}} \approx 800\,\text{kg/m}^3$) floats on water (for more details, see Chapter 7.4). Though oil has a somewhat smaller modulus of elasticity than water ($E_{\text{oil}} \approx \frac{1}{2} E_{\text{water}}$), it can nevertheless be considered incompressible like water. Therefore, the pressure increases linearly with depth from the oil surface by $\rho_{\text{oil}} g$ and reaches the value $p = \rho_{\text{oil}} g h_1$ at the water surface. The uppermost water molecules are already subjected to exactly this pressure, which is why the pressure diagram of the water begins with the value $p = \rho_{\text{oil}} g h_1$. From there, the pressure from the water increases along the wall by $\rho_{\text{water}} g$; due to the higher density of water, the rate of change of pressure is greater than it is with oil. At the bottom, the water pressure reaches $p_{\text{water,bottom}} = \rho_{\text{water}} g h_2$; the total pressure amounts to $p_{\text{total}} = \rho_{\text{oil}} g h_1 + \rho_{\text{water}} g h_2$.

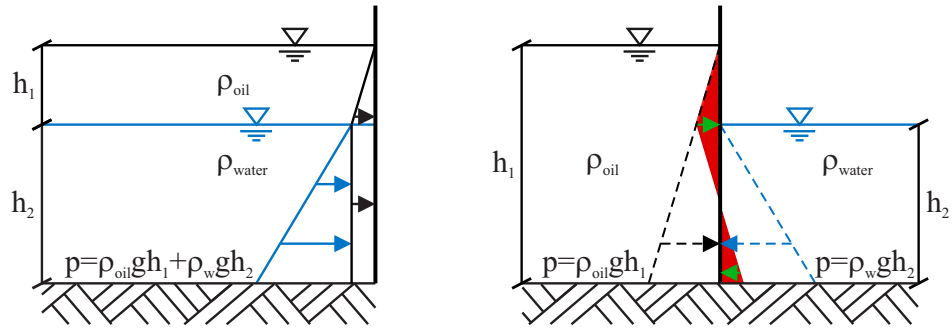

Figure 7.5: In the left figure, oil floats on water. The right figure shows a separating wall, with oil on the left side and water on the right side.

You can derive the pressure diagram in Figure 7.5 (right) yourself from the above. The oil pressure increases to $p = \rho_{\text{oil}} g h_1$ at the bottom; on the right side of the separating wall, the water pressure increases to $p = \rho_{\text{water}} g h_2$ at the bottom. The resulting pressure diagram is colored red in Figure 7.5. Whether the lowermost component of the resulting pressure acts to the left or right depends on the density and height ratios. In our example, it acts to the left as long as $\rho_{\text{oil}} g h_1' < \rho_{\text{water}} g h_2'$ applies. As soon as the water pressure upwards along the wall becomes smaller than the oil pressure at the same level, the resulting pressure direction changes. With tasks like this, it is recommended that you calculate and sum up the individual forces for the calculation of the resulting force acting on the wall. Thus, the following is obtained for the pressure force per unit width of oil in two-dimensional space:

$$F_{\text{pressure,oil}} = \frac{1}{2} \rho_{\text{oil}} g h_1^2 \quad [\text{N/m}] \tag{7.13}$$

and from the water:

$$F_{\text{pressure,water}} = \frac{1}{2} \rho_{\text{water}} g h_2^2 \quad [\text{N/m}] \tag{7.14}$$

7.5.3 Water pressure on inclined flat objects

From an example, we can learn that the pressure force on a flat object at any inclination can be calculated by multiplying the pressure at the centre of gravity with the surface area. For the determination of the pressure force, the pressure as a function of depth in the liquid is integrated over the area.

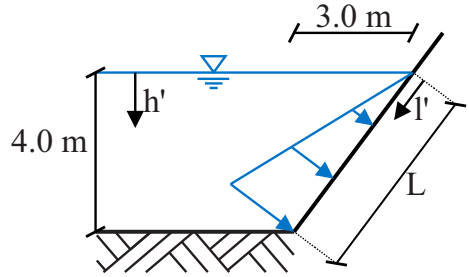

Figure 7.6: Water pressure on an oblique wall at a lake.

When diving along the wall shown in Figure 7.6 to the bottom of the lake, the pressure increases only as a function of depth in the liquid h'. The pressure which prevails at this depth acts perpendicularly to each of these infinitesimally small bits of the wall. At the water surface, the pressure 0 prevails, and at the lake bottom it is ρgh. In between, the pressure increases linearly (the linear increase of pressure with depth was discussed in Chapter 3.4.9), which leads to the pressure diagram drawn in Figure 7.6. For calculating the pressure force on the wall, the pressure is integrated along the boundary. For this purpose, we define the coordinate h' from the water surface vertically downwards and l' from the water surface along the boundary downwards.

$$F_{\text{pressure}} = \int p \, \mathrm{d}A = \int \int \rho g h'(l') \, \mathrm{d}b \, \mathrm{d}l' \tag{7.15}$$

With $\mathrm{d}b = 1\,\mathrm{m}$ or rather as a force per unit width in two-dimensional space as well as with $L = \sqrt{3^2 + 4^2} = 5$, $\frac{h}{L} = \frac{4.0}{\sqrt{3^2+4^2}} = \frac{4}{5}$ the pressure force follows:

$$F_{\text{pressure}} = \int_0^L \rho g \frac{4}{5} l' \, \mathrm{d}l' = \rho g \frac{4}{5} \frac{L^2}{2} \tag{7.16}$$

The direction of the force extends perpendicularly to the wall. The line of action lies in the centre of gravity of the pressure diagram, which can be demonstrated via force × lever arm. This is because the resulting pressure force at the point of the applied force must yield the same moment as the integral over the differential area $\mathrm{d}A$ with its respective lever arm $l'(\mathrm{d}A)$. The centre of gravity follows from the integration of the pressure ($\rho gh' = \rho g \frac{4}{5} l'$) acting at each point with its respective lever arm l' perpendicularly on the boundary $\mathrm{d}l'$ and division by the pressure force:

$$l_{\text{CG}} = \frac{\int_0^L \rho g \frac{4}{5} l' l' \, \mathrm{d}l'}{\rho g \frac{4}{5} L \frac{L}{2}} = \frac{\rho g \frac{4}{5} \frac{L^3}{3}}{\frac{1}{2} \rho g \frac{4}{5} L^2} - 0 = \frac{2}{3} L \tag{7.17}$$

Thus, the line of action is located $\frac{2}{3}L$ from the coordinate origin at the water surface. Here, the coordinate direction l' along the boundary and the direction of the force perpendicular to the wall are to be taken into consideration. In our specific example, it follows for the pressure force per unit width on the wall:

$$F_{\text{pressure}} = \frac{1}{2}\rho g \frac{4}{5}L^2 \quad [\text{N/m}] \tag{7.18}$$

The clockwise rotating moment about the base of the wall is:

$$M_{\circlearrowright} = \frac{1}{2}\rho g \frac{4}{5}L^2 \frac{1}{3}L \quad [\text{N m/m}] \tag{7.19}$$

7.5.4 Decomposition

For certain tasks, it is advisable to divide forces into their components. In the case of pressure as a scalar quantity, the horizontal component is always exactly the same as the vertical one, i. e. $\rho g h'$. In Figure 7.7, the two components increase from 0 at the water surface to $\rho g \cdot 4.0$ at the bottom. However, in the pressure diagrams on the left side of Figure 7.7 it is evident that the vertical component of the pressure force increases over a length of 3.0 m, whereas the horizontal component increases over 4.0 m. According to Pythagoras, the length of the wall under water follows as $L = \sqrt{3.0^2 + 4.0^2} = 5.0\,\text{m}$ from the ratios. The force components in the horizontal and in the vertical direction also follow these ratios exactly, as is obvious from the right side of Figure 7.7.

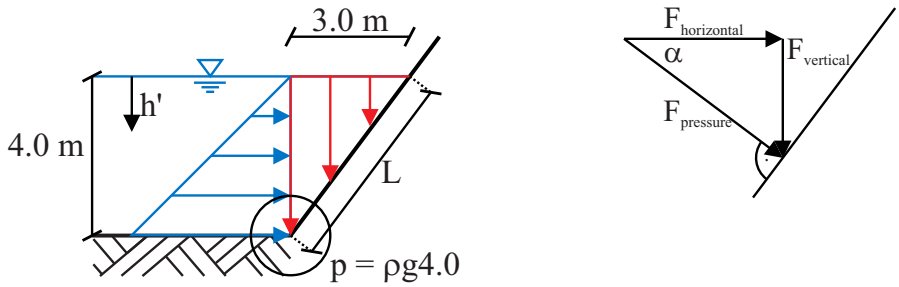

Figure 7.7: Decomposition of the pressure force on an oblique wall.

The surface area (or, in three-dimensional space, the volume) of the vertical pressure diagram multiplied by the density and gravity results in the vertical pressure force.

$$F_{\text{vertical}} \overset{2D}{=} \rho g A_{\text{pressure diagram vertical}} \quad [\text{N/m}] \tag{7.20}$$

This statement also applies to the horizontal force.

$$F_{\text{horizontal}} \overset{2D}{=} \rho g A_{\text{pressure diagram horizontal}} \quad [\text{N/m}] \tag{7.21}$$

7.5.5 Lines of action of resulting horizontal forces

We can determine the lines of action of the resulting horizontal pressure forces by recalling that these forces, just as the pressure $\rho g h'$, act on the individual, infinitesimally small surface elements $\mathrm{d}A = \mathrm{d}b\,\mathrm{d}h'$ with their respective lever arms h' (see Figure 7.8). The following is the result:

$$h_{\text{line of action horizontal}} = \frac{\int_0^h \rho g h' h' \,\mathrm{d}h'}{\rho g h \frac{h}{2}} = \frac{\rho g \frac{h^3}{3}}{\frac{1}{2}\rho g h^2} - 0 = \frac{2}{3}h = h_{\text{CG pressure diagram}} \qquad (7.22)$$

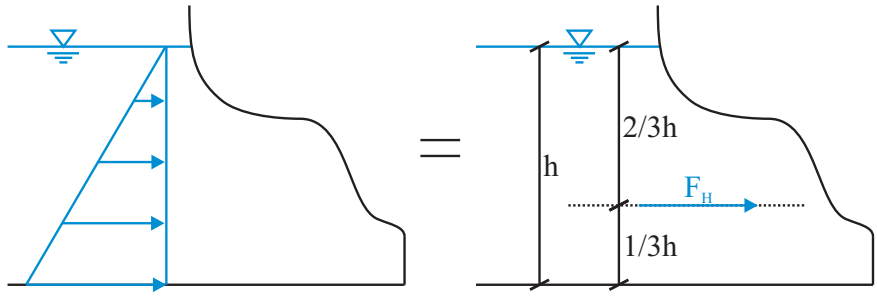

Figure 7.8: Line of action, or point of application of force, of the resulting horizontal pressure force.

7.5.6 Lines of action of resulting vertical forces

For the vertical pressure diagrams also, the resulting force together with the lever arm of the point of application of force must result in the same moment as the individual, infinitesimally small pressure forces $p\,\mathrm{d}A$ with their respective lever arms, which are expressed by the horizontal auxiliary coordinate x. With the resulting vertical force per unit

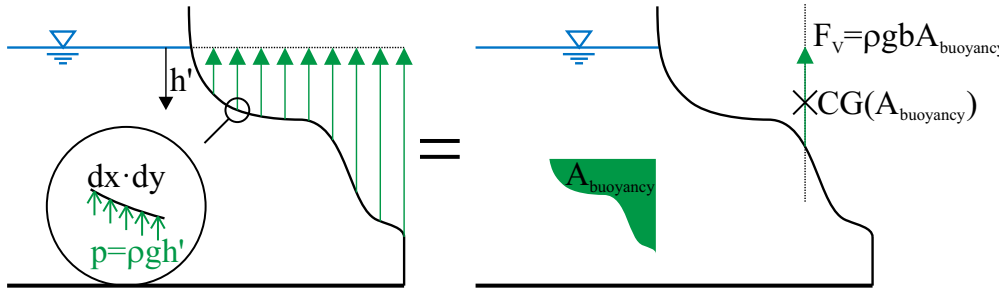

Figure 7.9: Line of action, or point of application of force, respectively, of the resulting vertical pressure force.

width $F_V = \rho g A_{\text{buoyancy}}$ in [N/m], we can write:

$$\rho g A_{\text{buoyancy}} \cdot l_{\text{lever}} = \int \rho g h'(x) x \, \mathrm{d}x \tag{7.23}$$

By rearranging Equation 7.23:

$$l_{\text{lever}} = \frac{\int \rho g h'(x) x \, \mathrm{d}x}{\rho g A_{\text{buoyancy}}} = \frac{\int h'(x) x \, \mathrm{d}x}{A_{\text{buoyancy}}} \tag{7.24}$$

The expression (7.24) can be found slightly modified in [8, p. 493] titled 'Coordinates of the centre of gravity in a homogenous plane figure'. The point of application of the resulting vertical force F_V is also the centre of gravity of the buoyancy area.
Let's focus again on the context with reference to Figure 7.10. Four slim girls are enjoying themselves (to represent the relatively low pressure on the left of Figure 7.9) on the left side of a seesaw and two well-fed boys sit on the right side (representing the high pressures there). If the resulting vertical force from the seesawing kids (including the dead load of the seesaw) passes exactly through the support, or if the support is located exactly at the centre of gravity of the seesawing persons, then the equilibrium of moments exists. Thus, the centre of gravity (or the vertical centroidal axis), together with the resulting vertical force, represents the pressure distribution at the boundary surface.

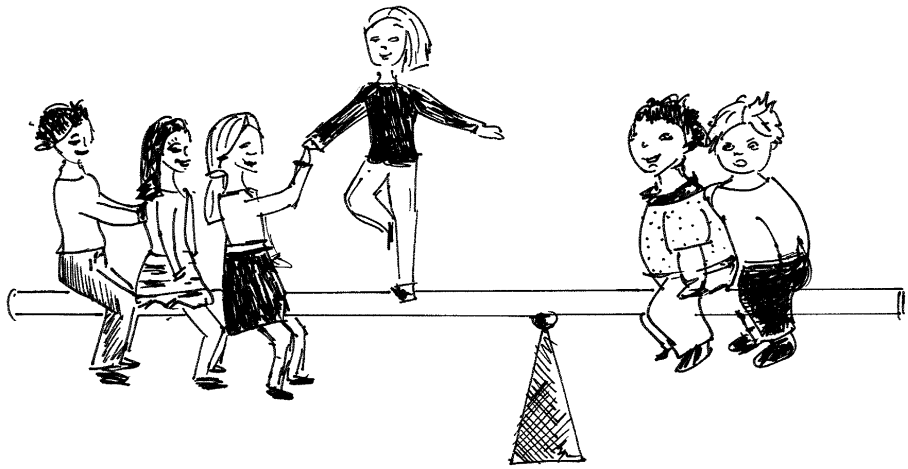

Figure 7.10: Seesaw as an example depicting the resulting vertical pressure force and its line of application. Design: Julia Rüping.

Experiment

Water pressure on an articulated plate

The test rig illustrated in Figure 7.11 serves to demonstrate the water pressure on a flat plate. On the right side of the separating wall, water is poured in until the equilibrium of moments at a water surface of $h = 0.085\,\mathrm{m}$ about the joint of the plate is reached and the flap tilts to the left. The forces and their lever arms are marked directly at the test rig.

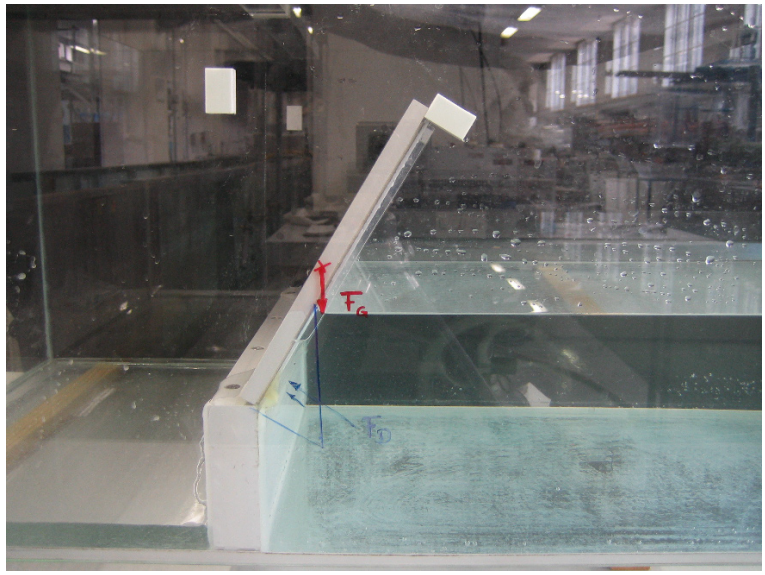

Figure 7.11: Water pressure on an articulated plate.

The plate has a thickness of $w = 0.01\,\mathrm{m}$, a length of $l = 0.2\,\mathrm{m}$ and a width of $b = 0.388\,\mathrm{m}$. The density of PVC is $\rho_{\mathrm{PVC}} = 1450\,\mathrm{kg/m^3}$, so that the resulting weight of the flap is:

$$F_G = w \cdot b \cdot l \cdot \rho_{\mathrm{PVC}} \cdot g = 11.04\,\mathrm{N} \tag{7.25}$$

The line of action of the weight force of the flap extends through its centre of gravity, i. e. through its centre. Therefrom the lever arm with respect to the tilting point can be determined for the plate at an inclination of 30° relative to the vertical direction (see also Figure 7.12):

$$x_1 = \frac{l}{2}\sin 30^\circ - \frac{w}{2}\cos 30^\circ = 0.0457\,\mathrm{m} \tag{7.26}$$

The resulting pressure force is calculated via the integral of the pressure over the surface area on which it is acting. The triangular-shaped pressure distribution acts along the wetted section $\frac{h}{\cos 30^\circ}$.

$$F = \int p\,\mathrm{d}A = \frac{1}{2}\rho \cdot g \cdot h \cdot \frac{h}{\cos 30^\circ} \cdot b = 15.87\,\mathrm{N} \tag{7.27}$$

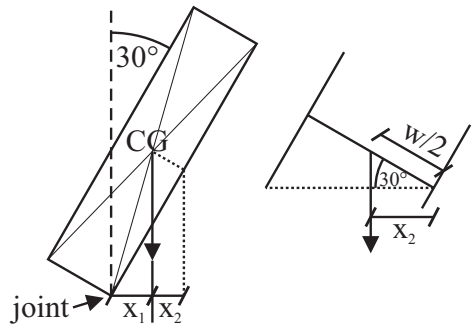

Figure 7.12: Lever arm of the articulated plate.

The lever arm of this force is located at one third of the wetted section, i. e. at $\frac{h}{3\cos 30°} = 3.27\,\text{cm}$, so that the equilibrium of moments about the tilting point can be calculated as:

$$\sum M_{\circlearrowleft} = 11.04 \cdot 0.0457 - 15.9 \cdot 0.0327 = 0.505 - 0.519 \approx 0 \tag{7.28}$$

Just when the moment from the water pressure exceeds the moment from the dead weight of the plate, the plate tilts.

7.5.7 'Base point line'

A 'base point line' can be used to determine the vertical pressure force component. As described in Chapter 7.5.4, the pressure diagram can be divided into a horizontal and a vertical component. In most cases, the horizontal component can be easily drawn, because it invariably increases linearly from the water surface to the bottom (see Figure 7.13).

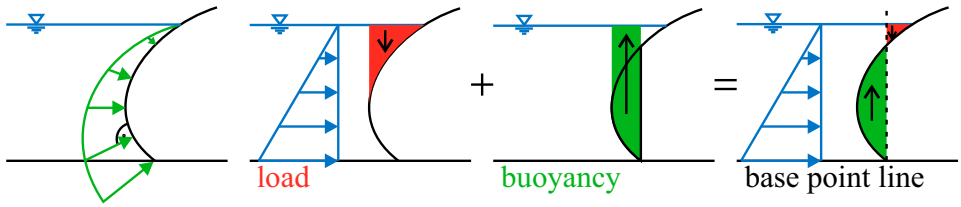

Figure 7.13: Pressure on a curved wall, divided into horizontal and vertical components of the pressure diagram.

The explanation of the vertical load starts directly at the water surface on the curved wall, where the water pressure is zero. When moving along the wall to the left, the pressure increases with the depth of the fluid, until it acts only in the horizontal direction at a point with a vertical tangent. Along this just-described line, the water pressure $\rho g h'$ as a scalar quantity is equal both in the vertical and in the horizontal direction. We can also see that, shortly before reaching the vertical tangent, the vertical component of the pressure acts downwards on the wall. With the length of the arrow h' from the water

surface to the wall, the red-coloured pressure diagram in Figure 7.13 is obtained. This pressure diagram acts downwards.
When following the contour beyond the vertical tangent, we find that the direction of the arrow has reversed. The vertical component, which acts from the scalar pressure at the boundary, is directed upwards. This direction of action does not change along the wall to the bottom. Analogous to our previous approach, we draw arrows in the vertical pressure diagram, which extend from the boundary of the curved surface to the water surface, because here as well the pressure is dependent on the depth within the liquid h'[A]. The portion of the vertical pressure diagram with the upwardly directed action is referred to as buoyancy; we colour it green in our sketch. In doing so, we detect that part of the load region is also occupied by the buoyancy region. Both components cancel each other out so that the pressure diagram in the lower region of Figure 7.13 (rightmost part), remains. This pressure diagram is also obtained by drawing a vertical line from the foot of the wall (i. e. from where the wall on the water side touches the bottom) to the water surface. When there is water between this vertical line and the wall, then this area (in three dimensional space, the volume) is to be referred to as load; it acts downwards. With air between the 'base point line' and the wall, this area (or volume) is included as buoyancy in the balance of forces; the buoyancy force acts upwards.
Thus, we obtain a lens-shaped buoyancy area at the left of the 'base point line', and, at its right side in the upper region, a quasi-triangular-shaped load area.

Example

Horizontal and vertical pressure diagrams

We will perform the entire process by means of an example. The wall depicted in the following Figure 7.14 is filled from both sides.

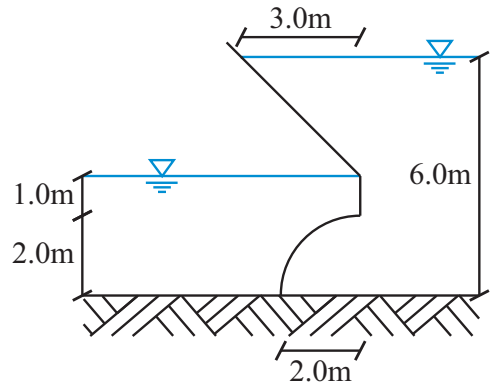

Figure 7.14: Example for pressure diagrams.

[A] The wall above does not change this fact. Those who question this should dive downwards approximately at the position where the horizontal pressure diagram is drawn. The pressure increases with the depth of the liquid h'. At the bottom, one can move in the horizontal plane on the isosurface of the pressure without perceiving a pressure change. In this manner, one advances under the wall, where the pressure ρgh prevails at the bottom.

Let's start with the horizontal pressure diagrams on the right and left side. On the left, the pressure increases from the water surface to the bottom to $p_{\text{bottom,left}} = \rho g \cdot 3.0$; on the right, up to $p_{\text{bottom,right}} = \rho g \cdot 6.0$. The result is a trapezoid acting to the left which linearly increases from the water surface on the right side to the water level on the left. From there to the bottom, the increase on the right side is equal to that on the left side so that they neutralise each other. The resulting pressure on the wall in the lower region remains constant.
It would be best if you follow the sketches in Figure 7.15. For the vertical pressure diagram, we proceed successively and first look at the load from the water pressure on the left side. At the upper right corner of the quarter circle, a pressure head of $1.0\,\text{mH}_2\text{O}$ or a pressure of $\rho g \cdot 1.0$ acts downwards on the wall. The pressure then increases to $\rho g \cdot 3.0$ to the base point. Advantageously, we draw the pressure arrows again from the water surface to the boundary which is defined by the quadrant. The area marked in red in Figure 7.15 at the top right consisting of a rectangle minus a quadrant:

$$A_{\text{load,left}} = 3.0 \cdot 2.0 - \frac{1}{4} 2.0^2 \cdot \pi = 2.86\,\text{m}^2 \tag{7.29}$$

This results in a downwardly directed vertical force per unit width.

$$F_{\text{vertical,left}} = A_{\text{load,left}} \rho g \tag{7.30}$$

Now we will turn to the right side. When again moving downwards from the water surface, the pressure increases to the corner up to $\rho g \cdot 3.0$. Of course, the vertical part of the wall is not subjected to any vertical pressure component. The water-filled quadrant adjoins below, where the vertical pressure component points upwards; filled from the right side, the quadrant is subjected to buoyancy. Here, the pressure increases from $\rho g \cdot 4.0$ to $\rho g \cdot 6.0$. When drawing the pressure arrows, it is noticeable that a part of the load-triangle is now also subjected to buoyancy. When superposed, the area (with the load under positive sign) of the vertical pressure diagram on the right side is calculated as follows:

$$A_{\text{right}} = \frac{1}{2} 3.0 \cdot 3.0 - \left(6.0 \cdot 2.0 - \frac{1}{4} 2.0^2 \cdot \pi \right) = -4.36\,\text{m}^2 \tag{7.31}$$

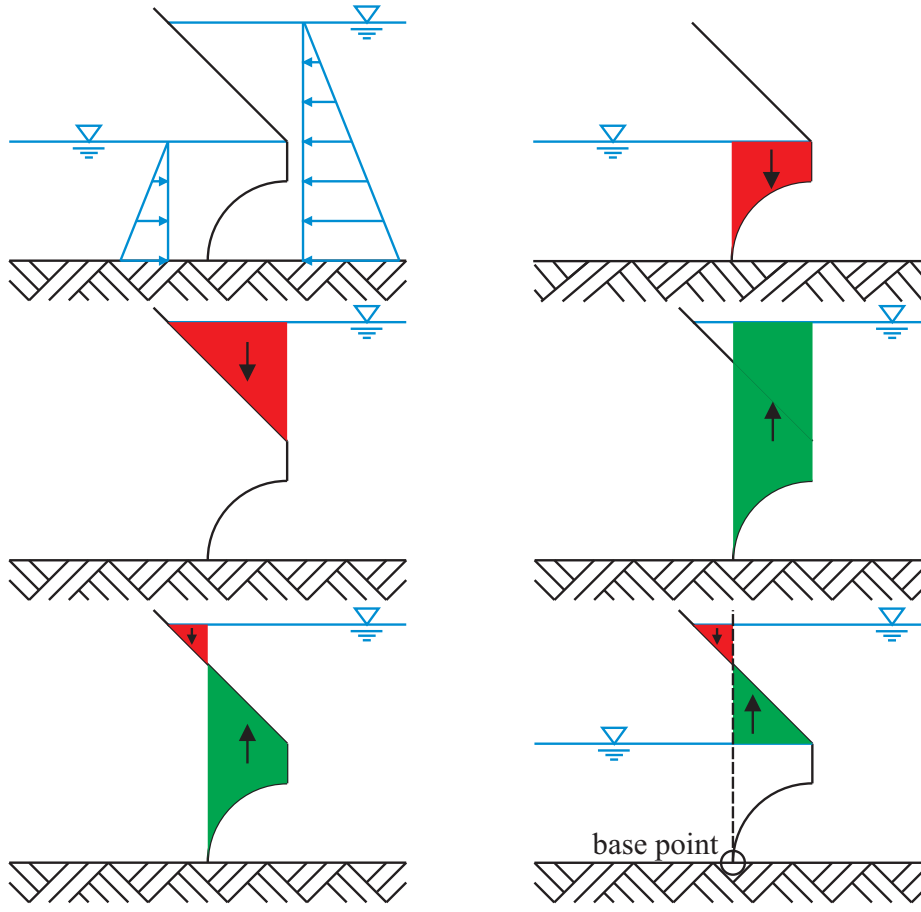

Figure 7.15: Pressure diagrams for the illustrated retaining wall: top left: horizontal pressure forces; top right: vertical pressure force for the water pressure on the left of the wall; centre left: vertical pressure diagram for the upper part of the wall (water application on the right); centre right: vertical pressure diagram for the lower part of the wall (water application right); bottom left: resulting vertical pressure diagram for water application right; bottom right: resulting vertical pressure diagram for two-sided water application by means of the 'base point line'.

It takes significantly less effort to draw a vertical line from the base, i. e. from the wet part of the wall, that connects to the bottom, to the uppermost water surface. If air is present between that vertical line and the wall, this area (volume, in three-dimensional space) is under buoyancy. If the areas/volumes are filled with water, then there is a load condition.
Up to the water surface on the left side of the wall, the areas are under buoyancy or load, depending on whether the filling on the right or the left is considered. The triangle above is under buoyancy because air is present between the 'base point line' and the wall. Another triangle follows along the 'base point line' to the water surface which is on the right side of the wall. Between this vertical line and the wall there is water; consequently, a load condition is present here. In total, a buoyancy force per unit width acts:

$$F_{\uparrow} = \left(A_{\text{buoyancy}} - A_{\text{load}}\right) \rho g = (4.36 - 2.86)\, \rho g = 14715\,\text{N/m} \tag{7.32}$$

7.6 Hydrostatic paradox

Actually, the hydrostatic paradox is no paradox; rather it is obvious by consistent implementation of the physical findings. In fact, it stipulates that the pressure solely depends on the depth of immersion in the liquid. Figure 7.16 shows various containers, all of which are standing on the same horizontal plane; the water surfaces in the different containers are at the same level. At the bottom of all the containers, the same pressure ρgh prevails. Imagine that you dive four meters deep at a corner of a swimming pool. You feel the pressure $p = \rho g 4.0$ as a load on your body. Then you swim to the other three corners of the pool and dive again four meters deep. Which pressure do you feel there? Of course, $\rho g 4.0$ again. Wherever you dive four meters deep, this pressure will prevail. Thus, we can state that in hydrostatics, horizontal planes are isosurfaces of the pressure. Regardless of which container we dive to the bottom, or whether we swim back and forth at the bottom – the pressure there is ρgh.

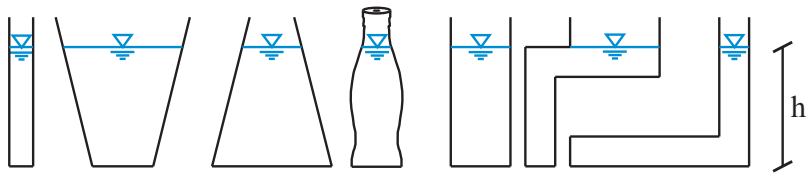

Figure 7.16: Containers with the same pressure prevailing at the bottom (ρgh).

To comprehend this phenomenon, we have to engage in some dialectic and define terminology. The force that results from the pressure at the bottom is not the same for the different containers because it refers to the bottom area: $F_{\text{bottom pressure}} = \rho g h A_{\text{bottom}}$.
The total vertical force that the bottom has to absorb corresponds to the weight of the water body (at this point, we neglect the weight of the container): $F_{\text{vertical,total}} = \int \rho g \, \mathrm{d}V = \rho g V_{\text{water}}$.
When referring to the force by which the container has to be held together in the vertical direction as flange force, then this comes full circle.

Example

Hydrostatic paradox

To demonstrate that the hydrostatic paradox is actually not a paradox, we take a rotation-symmetrical container (see Figure 7.17).

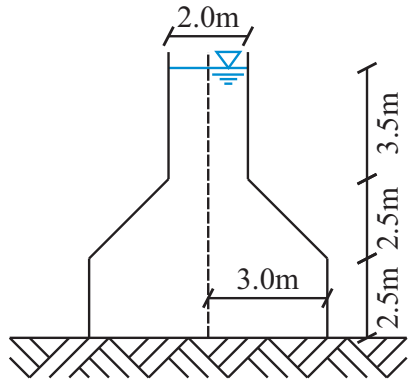

Figure 7.17: Rotation-symmetrical container to illustrate the hydrostatic paradox.

The calculation of the force that results from the pressure at the bottom is easiest because it consists of the pressure at the bottom and the bottom area:

$$F_{\text{bottom pressure}} = \rho g h A_{\text{bottom}} = \rho g \cdot 8.50 \cdot 3^2 \pi = 2.358 \times 10^6\,\text{N} \tag{7.33}$$

We can determine the volume under buoyancy by means of a table value for the volume of a truncated cone, where $R_1 = 1.0\,\text{m}$, $R_2 = 3.0\,\text{m}$, $L_1 = 3.5\,\text{m}$ and $L_2 = 2.5\,\text{m}$:

$$V_{\text{buoyancy}} = R_2^2 \pi \cdot (L_1 + L_2) - \left[R_1^2 \pi \cdot L_1 + \frac{L_2 \pi}{3} \cdot \left(R_1^2 + R_1 \cdot R_2 + R_2^2 \right) \right] = 124.62\,\text{m}^3 \tag{7.34}$$

The buoyancy results from:

$$F_{\text{buoyancy}} = \rho g V_{\text{buoyancy}} = 1.223 \times 10^6\,\text{N} \tag{7.35}$$

For the total vertical force, we use the water volume with $L_3 = 2.5\,\text{m}$:

$$V_{\text{water}} = R_1^2 \pi \cdot L_1 + \frac{L_2 \pi}{3} \cdot \left(R_1^2 + R_1 \cdot R_2 + R_2^2 \right) + R_2^2 \pi \cdot L_3 = 115.72\,\text{m}^3 \tag{7.36}$$

The water volume multiplied by the density and gravity constant results in the total vertical force:

$$F_{\text{vertical,total}} = \rho g V_{\text{water}} = 1.135 \times 10^6\,\text{N} \tag{7.37}$$

We will note immediately that the sum of the force that results from the pressure at the bottom and the buoyancy results in the total vertical force $F_{\downarrow\text{bottom pressure}} + F_{\uparrow\text{buoyancy}} = F_{\downarrow\text{vertical,total}}$. That is logical, since the buoyancy is transmitted to the bottom of the

container via the flange between the wall and the bottom. It's not that paradox, the 'Paradox'.

7.7 Water pressure on arbitrarily inclined flat objects

Generally speaking, we obtain the pressure force on an oblique surface via the integral of the pressure over this surface or via the pressure at the centre of gravity p_{CG} times the area A:

$$F_P = \int p \, \mathrm{d}A = p_{\mathrm{CG}} A \tag{7.38}$$

To find the point of application of the resulting pressure force F_P, we calculate the moment about the point of intersection of the auxiliary coordinate ζ with the water surface (see Figure 7.18). Within the integral, $\rho g h'$ is the pressure at the respective height, which can be expressed as $\rho g \zeta \sin\varepsilon$.

$$M = \int \rho g h' \zeta \, \mathrm{d}A = \int \rho g \zeta \sin\varepsilon \zeta \, \mathrm{d}A = \rho g \sin\varepsilon \int \zeta^2 \, \mathrm{d}A \tag{7.39}$$

The last term $\int \zeta^2 \, \mathrm{d}A$ is the geometrical moment of inertia I_ξ about the ξ-axis, which points to the drawing plane and lies on the water surface. When we refer to the point of application of the pressure force as ζ_P, the resulting pressure force times this lever arm must result in the previously calculated moment.

$$M = \rho g \zeta_{\mathrm{CG}} \sin\varepsilon A \zeta_P = \rho g z_{\mathrm{CG}} A \zeta_P \tag{7.40}$$

By equating the terms (7.39) and (7.40), the point of application of the pressure force follows as:

$$\zeta_P = \frac{\rho g \sin\varepsilon \int \zeta^2 \, \mathrm{d}A}{\rho g \zeta_{\mathrm{CG}} \sin\varepsilon A} = \frac{\int \zeta^2 \, \mathrm{d}A}{\zeta_{\mathrm{CG}} A} = \frac{I_\xi}{\zeta_{\mathrm{CG}} A} \tag{7.41}$$

With Steiner's theorem (see e. g. [52, p. 4.29]) the geometrical moment of inertia can be moved to the centre of gravity; it applies $\xi \parallel y$, i. e. the direction remains constant:

$$I_\xi = I_{y,\mathrm{CG}} + \zeta_{\mathrm{CG}}^2 A \tag{7.42}$$

For ζ_P it follows:

$$\zeta_P = \frac{I_{y,\mathrm{CG}} + \zeta_{\mathrm{CG}}^2 A}{\zeta_{\mathrm{CG}} A} = \zeta_{\mathrm{CG}} + \frac{I_{y,\mathrm{CG}}}{\zeta_{\mathrm{CG}} A} \tag{7.43}$$

When we apply the finding e. g. to a trapezoid with the parameters from Figure 7.18[B], we obtain the following equation for the area $A_{\mathrm{trapezoid}} = (b_1 + b_2)\,\frac{h}{2}$ and $I_{y,\mathrm{CG,trapezoid}} = h^3 \frac{(b_1+b_2)^2 + 2b_1 b_2}{36(b_1+b_2)}$:

[B] Note that here h identifies the height of the body and not the depth of the water. This is not intended to create confusion but rather to simplify the handling of pertinent table values (e. g. [52]), which always specify the geometrical moments of inertia with the variables b and h.

$$\begin{aligned}\zeta_{P,\text{trapezoid}} &= \zeta_{CG} + \frac{1}{\zeta_{CG}\,(b_1+b_2)\,\frac{h}{2}} h^3 \frac{(b_1+b_2)^2+2b_1b_2}{36\,(b_1+b_2)} \\ &= \zeta_{CG} + \frac{h^2}{\zeta_{CG}} \frac{(b_1+b_2)^2+2b_1b_2}{18\,(b_1+b_2)^2} = \zeta_{CG} + \frac{h^2}{18\zeta_{CG}} \left(1 + \frac{2b_1b_2}{(b_1+b_2)^2}\right)\end{aligned} \tag{7.44}$$

Franke [13, S. 43] expresses the same context as follows:

$$\begin{aligned}\zeta_{P,\text{trapezoid}} &= \zeta_2 - \frac{\zeta_1\,(2b_1+b_2) + \frac{h}{2}\,(b_1+b_2)}{\frac{3}{h}\zeta_1\,(b_1+b_2) + (b_1+2b_2)} \\ &= \zeta_2 - \frac{\zeta_2\,(2b_1+b_2) - \frac{h}{2}\,(3b_1+b_2)}{\frac{3}{h}\zeta_2\,(b_1+b_2) - (2b_1+b_2)}\end{aligned} \tag{7.45}$$

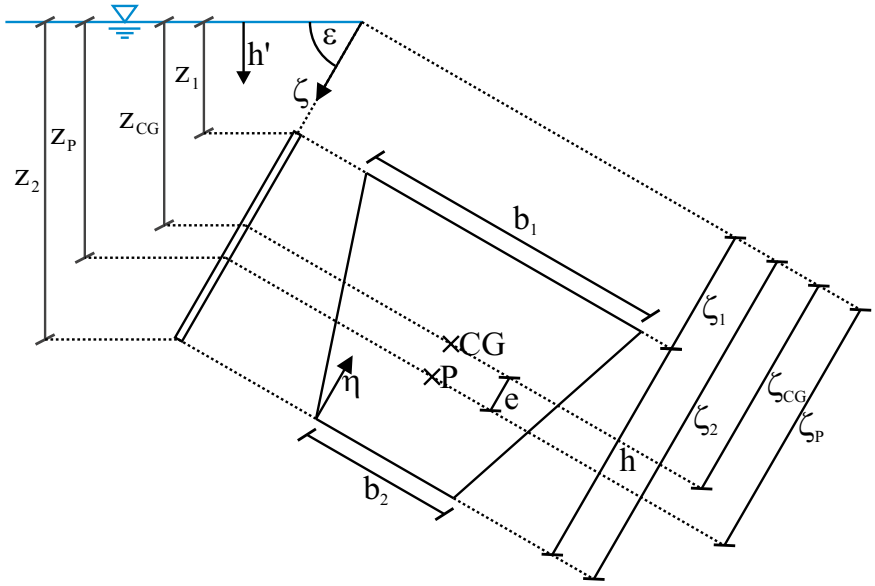

Figure 7.18: Water pressure on arbitrarily inclined surfaces.

Before we practice arithmetic, I suggest you switch on the computer. Open Octave and compare the results for the point of application of the resulting pressure force on a trapezoid by inserting any values for the terms in Equations 7.44 and 7.45.

```
1> b1 = 3
2> b2 = 5
3> h = 4
4> zeta1 = 1.5
5> zeta2 = zeta1 + h
6> zetaCG = zeta2 - h/3*(2*b1 + b2)/(b1 + b2)
7> zetaP = zetaCG + h^2/(18*zetaCG)*(1 + 2*b1*b2/(b1 + b2)^2)
8> zetaP = zeta2 - (zeta1*(2*b1 + b2) + h/2*(b1 + b2))/...
> (3/h*zeta1*(b1 + b2) + (b1 + 2*b2))
9> zetaP = zeta2 - (zeta2*(2*b1 + b2) - h/2*(3*b1 + b2))/...
> (3/h*zeta2*(b1 + b2) - (2*b1 + b2))
```

Explanation of the individual lines `n>`

`1> % We define the width b1 (see sketch 7.18) as 3.0 m and confirm by` Enter . `By the way, by typing ';' at the end of the line, you can suppress the output of the results. This is reasonable in particular with complex calculations because the screen display negatively influences performance.`

`2> % Let the width b2 (see sketch 7.18) be 5.0 m.`

`3> % The height of the trapezoidal surface is 4.0 m (see sketch 7.18).`

`4> % The board is immersed 1.5 m along the` ζ `coordinate.`

`5> % According to sketch 7.18,` ζ_2 `lies below` ζ_1 `(by` h `in the` ζ`-direction). After typing, we start the computation by pressing the` Enter `key.`

`6> % For the centre of gravity of the trapezoid, we enter the corresponding formula from Table 7.1 and confirm by` Enter . `Octave immediately shows the result.`

`7> % With our Equation 7.44, entered with the above defined variables, we obtain the point of application of the resulting pressure force as a function of the coordinate` ζ`.`

`8> % Alternatively, we can use the corresponding equation from Table 7.1, that is the first expression of Equation 7.45. Octave is informed by the ... followed by` Enter `that the equation is continued in the next line.`

`> % The equation is completed with the denominator and the computation is started by` Enter . `The equation in the expression 7.45 provides the same result.`

`9> % At least for the presentation in this book, a line with ... and` Enter `is necessary here as well.`

`> % With the second expression in Equation 7.45, we obtain the same result for` $\zeta_{P,\mathrm{trapezoid}}$`.`

Why not repeat steps 1–9 with different values?

We can determine the point of application of the pressure force on a rectangle from Equation 7.45 with $b_1 = b_2 = b$:

$$\begin{aligned}\zeta_{P,\text{rectangle}} &= \zeta_2 - \frac{\zeta_1(2b+b)+\frac{h}{2}(b+b)}{\frac{3}{h}\zeta_1(b+b)+(b+2b)} = \zeta_2 - \frac{\zeta_1 3b+\frac{h}{2}2b}{\frac{3}{h}\zeta_1 2b+3b} = \zeta_2 - \frac{3\zeta_1+h}{\frac{6\zeta_1}{h}+3} \\ &= \zeta_2 - \frac{3\zeta_1 h+h^2}{6\zeta_1+3h} = \zeta_2 - \frac{\zeta_1 h+\frac{h^2}{3}}{2\zeta_1+h} = \zeta_2 - \frac{h}{3}\cdot\frac{3\zeta_1+h}{2\zeta_1+h}\end{aligned} \tag{7.46}$$

For $b_2 = 0$, the point of application of the pressure force for a triangle with its tip pointing downwards follows:

$$\begin{aligned}\zeta_{P,\text{triangle}} &= \zeta_2 - \frac{\zeta_1(2b_1+0)+\frac{h}{2}(b_1+0)}{\frac{3}{h}\zeta_1(b_1+0)+(b_1+0)} = \zeta_2 - \frac{\zeta_1 2b_1+\frac{h}{2}b_1}{\frac{3}{h}\zeta_1 b_1+b_1} = \zeta_2 - \frac{2\zeta_1+\frac{h}{2}}{\frac{3}{h}\zeta_1+1} \\ &= \zeta_2 - \frac{2\zeta_1 h+\frac{h^2}{2}}{3\zeta_1+h} = \zeta_2 - \frac{h}{2}\cdot\frac{4\zeta_1+h}{3\zeta_1+h}\end{aligned} \tag{7.47}$$

For a circle with $I_y = \frac{r^4\pi}{4}$, we obtain:

$$\zeta_{P,\text{circle}} = \zeta_{\text{CG}} + \frac{r^4\pi}{4\zeta_{\text{CG}} r^2\pi} = \zeta_{\text{CG}} + \frac{r^2}{4\zeta_{\text{CG}}} \tag{7.48}$$

In Figure 7.18 and Table 7.1, the centres of gravity and points of application of the pressure force are indicated for various surfaces. In addition, the distances between the centre of gravity and point of application e are indicated; these are to be derived from Equation 7.41[C].

[C] E. g. for a rectangle where the geometrical moment of inertia is related to the centre of gravity: $e = \frac{bh^3}{12bh\zeta_P} = \frac{h^2}{12z_{\text{CG}}}\sin\varepsilon$

Table 7.1: Pressure force and point of application at arbitrarily inclined surfaces. Here, h designates the height of the object, not the depth of the water measured from the surface (see also Figure 7.18).

Shape	$\frac{F}{\rho g}$ respectively $z_{\mathrm{CG}}A$	ζ_P	ζ_{CG}	e
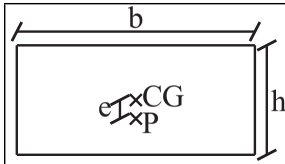	$bh\left(z_1+\frac{h}{2}\sin\varepsilon\right)$	$\zeta_2-\frac{h}{3}\cdot\frac{3\zeta_1+h}{2\zeta_1+h}$	$\zeta_2-\frac{h}{2}$	$\frac{h^2}{12\zeta_{\mathrm{CG}}}$
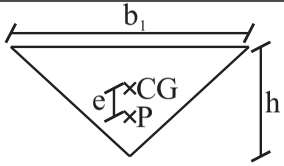	$\frac{bh}{2}\left(z_1+\frac{h}{3}\sin\varepsilon\right)$	$\zeta_2-\frac{h}{2}\cdot\frac{4\zeta_1+h}{3\zeta_1+h}$	$\zeta_2-\frac{2}{3}h$	$\frac{h^2}{18\zeta_{\mathrm{CG}}}$
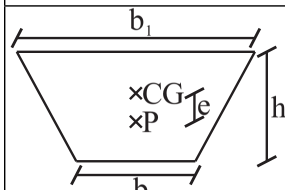	$\frac{h}{2}z_1\left(b_1+b_2\right)+\frac{h^2}{6}\sin\varepsilon\left(b_1+2b_2\right)$	$\zeta_2-\frac{\zeta_1(2b_1+b_2)+\frac{h}{2}(b_1+b_2)}{\frac{3}{h}\zeta_1(b_1+b_2)+(b_1+2b_2)}$	$\zeta_2-\frac{h}{3}\frac{2b_1+b_2}{b_1+b_2}$	$\frac{h^2}{18}\frac{(b_1+b_2)^2+2b_1b_2}{\zeta_{\mathrm{CG}}(b_1+b_2)^2}$
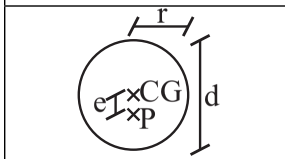	$r^2\pi\left(z_1+r\sin\varepsilon\right)$	$\zeta_1+r+\frac{r^2}{4\cdot(\zeta_1+r)}$	ζ_2-r	$\frac{r^2}{4\zeta_{\mathrm{CG}}}$

7.8 Moving liquids

Hydrostatics in moving liquids? How can that go together: static and at the same time moving? In this chapter, we will address questions concerning liquids that are stationary in a moving reference system. Imagine a glass of beer in a bistro aboard a fast train.
This chapter, wherein the z-axis points downwards from the water surface, is almost completely described by the following sentence: The water surface is always perpendicular to the acceleration. In the case of a lake without outflow or a filled glass, we are quite sure that the water surface is horizontal. When looking at the Pacific Ocean, it also seems to be logical that the water surface is perpendicular to the acceleration vector – gravity. This also holds true with moving fluids, though we are now considering accelerations that additionally occur in the x- and y-directions. Perhaps you have encountered a situation where you spilled water when driving a car or going by train. We take a look (in anticipation of the next experiment) at Figure 7.19 to see why that is.

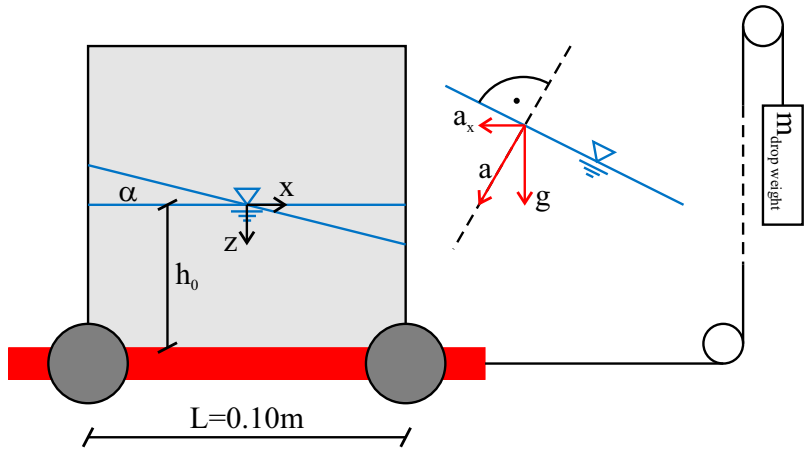

Figure 7.19: Glass of water on an accelerated car in anticipation of the next experiment.

The water surface is a level surface where the water pressure is zero. The change of the pressure on it equals zero, i. e. $\mathrm{d}p = 0$.
In the case of moving liquids too, the Navier-Stokes equation (5.29) must be valid. Since the fluid in the moving reference system is and remains stationary, the local $(\frac{\partial u_i}{\partial t})$ and convective acceleration $(u_j \frac{\partial u_i}{\partial x_j})$ are both zero. If the molecules are not displaced with respect to each other, friction is also non-existent $(\nu \frac{\partial^2 u_i}{\partial x_j^2} = 0)$. The relationship stipulated at the beginning of the chapter remains, whereas here, the acceleration vector also comprises components in the horizontal directions x and y:

$$-\frac{1}{\rho}\frac{\partial p}{\partial x_i} + g_i = 0 \tag{7.49}$$

We rearrange Equation 7.49 and multiply by $\mathrm{d}x_i$:

$$\frac{\partial p}{\partial x_i}\,\mathrm{d}x_i = \rho g_i\,\mathrm{d}x_i \tag{7.50}$$

With $g = (a_x\ a_y\ a_z)^T$ and $\frac{\partial p}{\partial x_i}\,\mathrm{d}x_i$ being the change of pressure $\mathrm{d}p$ in the direction $\mathrm{d}x_i$, the mathematical result for a level surface in a cartesian coordinate system can be expressed as:

$$\frac{\partial p}{\partial x}\cdot\mathrm{d}x+\frac{\partial p}{\partial y}\cdot\mathrm{d}y+\frac{\partial p}{\partial z}\cdot\mathrm{d}z=\rho\,(a_x\,\mathrm{d}x+a_y\,\mathrm{d}y+a_z\,\mathrm{d}z)=\mathrm{d}p\overset{!}{=}0 \tag{7.51}$$

In cylindrical coordinates, this yields:

$$\rho\left(\frac{\partial u_r}{\partial r}\,\mathrm{d}r+\frac{\partial w}{\partial z}\,\mathrm{d}z\right)=\rho\,(a_r\,\mathrm{d}r+a_z\,\mathrm{d}z)=\mathrm{d}p\overset{!}{=}0 \tag{7.52}$$

Now, what exactly did we do? $\frac{\partial p}{\partial x_i}$ is the change of the pressure p as a function of location x_i. If we want to know the extent of pressure change after we have travelled along the differential path $\mathrm{d}x_i$, then we have to multiply the change of the pressure $\frac{\partial p}{\partial x_i}$ by exactly this path $\mathrm{d}x_i$[D]. Of course, the other term of Equation 7.49 has to be multiplied by $\mathrm{d}x_i$, and, because a level surface is defined exactly so that the pressure change is zero, we may write $\mathrm{d}p\overset{!}{=}0$. We can comprehend the meaning of Equations 7.51 and 7.52 by looking at a stationary system that does not exhibit any acceleration in the x- and y-directions or in the radial direction ($a_x = a_y = 0$, $a_r = 0$). With gravity $a_z = 9.81\,\mathrm{m/s^2}$ (... with the sign convention described above) said equations can only be fulfilled if $\mathrm{d}z = 0$, i. e. if we move in the horizontal plane.

7.8.1 Acceleration along a straight line

When moving a container from the stationary condition in the x-direction, the acceleration acts in the opposite direction. You can check this in an elevator when moving upwards – you feel heavier. When moving down, you feel lighter, which is due to d'Alembert's inertial force.

Experiment

Acceleration of a water-filled car

We look at a small experiment where a rectangular container ($0.1\,\mathrm{m}\times 0.1\,\mathrm{m}\times 0.1\,\mathrm{m}$) is half filled and mounted on a car (see Figures 7.19 and 7.20). The car is connected to a drop weight via a rope which runs over two rollers. Upon releasing the car's brake, it will be constantly accelerated by the drop weight in the x-direction. Thereby, the water surface tilts in such a manner that it rises at the rear and drops at the front.
The acceleration of the car in the horizontal direction is obtained via the quotient of the drop weight and the total mass which has to be accelerated by this drop weight: $a_x = -g\frac{m_{\text{drop weight}}}{m_{\text{car}}+m_{\text{water}}+m_{\text{drop weight}}} = -9.81\frac{0.50}{2.0+0.5+0.5} = -1.635\,\mathrm{m/s^2}$. The weight cannot simply drop freely but must accelerate the mass of the car together with the water. The water surface, being a level surface, extends perpendicularly to the resulting acceler-

[D] Please note the explanations for partial derivatives and differential quantities in Part 1 of this book.

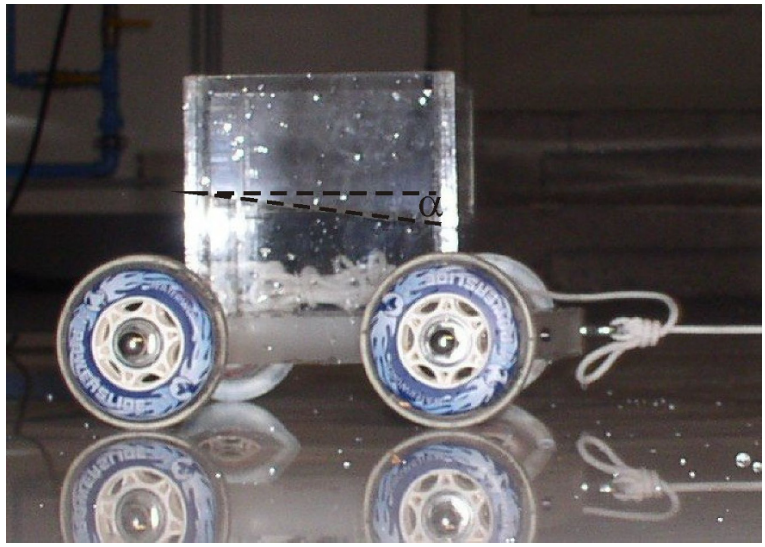

Figure 7.20: Constantly accelerated container.

ation. The tilt angle can be calculated via the arctangent of the acceleration ratios: $\alpha = \arctan\frac{-1.635}{9.81} = -9.46°$. The comparison with the snapshot that shows ($\alpha \approx 8°$) reveals a small difference, which can be explained by friction losses.
Now, the question concerning the pressure in this container becomes exciting. As described above, the water surface is a level surface where the water pressure is 0. Thus, we can determine the pressure in the container in two ways. In either case, we have to measure the water depth in the direction of the acceleration vector:

1. By means of the vertical cover at this location and gravity.
2. Via the resulting acceleration vector and the prevailing cover along its line of action.

Due to the conservation of mass, the water surface at the tilt point in the middle of the container remains at the same level $h_0 = 0.05\,\mathrm{m}$. With a computational angle of 9.46°, the pressure in the rear bottom corner for variant 1 is:

$$p = \rho g \left(h_0 + \arctan 9.46° \cdot \frac{L}{2} \right) = 570.8\,\mathrm{N/m^2} \tag{7.53}$$

The water depth along the resulting acceleration vector can be calculated with the depth at the rear container wall $\left(h_0 + \arctan 9.46° \cdot \frac{L}{2}\right)$ via the cosine:

$$h_{\perp a} = \cos 9.46° \left(h_0 + \arctan 9.46° \cdot \frac{L}{2} \right) \tag{7.54}$$

For the pressure in the bottom rear corner, it follows that:

$$\begin{aligned} p = \rho a h_{\perp a} &= \rho a \cos 9.46° \left(h_0 + \arctan 9.46° \cdot \frac{L}{2} \right) \\ &= \rho \sqrt{-1.635^2 + 9.81^2} \cos 9.46° \left(h_0 + \arctan 9.46° \cdot \frac{L}{2} \right) = 570.8\,\mathrm{N/m^2} \end{aligned} \tag{7.55}$$

7.8.2 Acceleration along a circular path

A rotating container is based on the same principle as the constantly accelerated car. Here, the liquid rotates with the same constant angular velocity ω as the container due to the adhesive forces; consequently, this is a hydrostatic phenomenon in the moving reference system. The surface or the level surface with the (relative) pressure 0 is parabolically shaped because the water surface always adjusts perpendicularly to the acceleration; the centripetal acceleration (or the centrifugal acceleration which is of opposite sign) increases quadratically with the radius. The level line (that is, the water surface) can be calculated by means of Equation 7.52 and the continuity condition.

Experiment

Rotating container

Figure 7.21 shows an example of a rotating cylinder. The coordinate origin is again located at the height of the water surface and the z-axis is directed downwards.

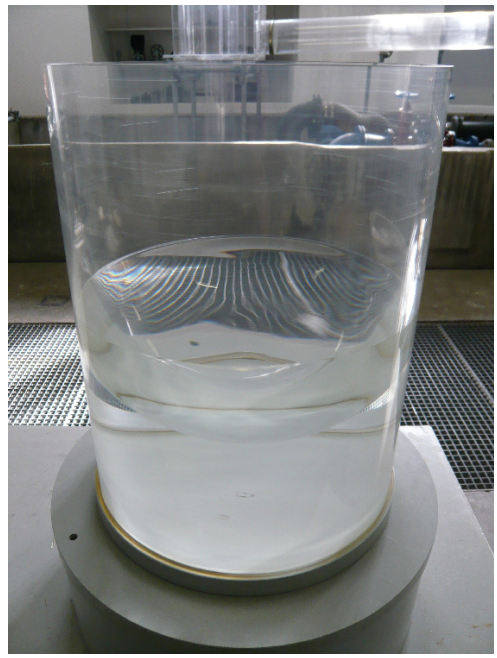

Figure 7.21: Image of the rotating container with the forming parabolic water surface.

With the accelerations in the radial direction $a_r = \omega^2 r$ and $a_z = g$, the equation for the level line follows from Equation 7.52:

$$\int a_r \,\mathrm{d}r + \int a_z \,\mathrm{d}z = \int \omega^2 r \,\mathrm{d}r + \int g \,\mathrm{d}z = \frac{r^2}{2}\omega^2 + gz + c_1 = 0 \tag{7.56}$$

First, we divide the equation by g and solve for the water surface z, which defines the constant c_1 anew and designates it as the initial value at the coordinate origin at $r = 0$ as z_0.

$$z(r) = -\frac{\omega^2 r^2}{2g} + z_0 \tag{7.57}$$

With the container in the stationary condition, we mark the water surface. When rotated, the water surface in the centre of the container drops while it rises at the wall. It is evident that the water mass that was in the centre of the container is now present in the outer region. When placing the coordinate origin on the water surface with the container being stationary ($z = 0$), the volume integral $\int_{\phi=0}^{2\pi}\int_{r=0}^{r=R} z(r) r\,\mathrm{d}r\,\mathrm{d}\phi$ must be zero, even with the container in rotation. Take into account the Jacobi determinant r, which has to be given in the integration of the surface in cylindrical coordinates. When inserting $z(r)$, it follows that:

$$\begin{aligned}\int_{\phi=0}^{2\pi}\int_{r=0}^{r=R} z(r) r\,\mathrm{d}r\,\mathrm{d}\phi &= \int_{r=0}^{r=R}\left(-\frac{\omega^2 r^2}{2g} + z_0\right) r\,\mathrm{d}r = \int_{r=0}^{r=R} -\frac{\omega^2 r^3}{2g} + z_0 r\,\mathrm{d}r \\ &= \left[-\frac{\omega^2 r^4}{2g\cdot 4} + z_0\frac{r^2}{2}\right]_{r=0}^{r=R} + c_2 = -\frac{\omega^2 R^4}{2g\cdot 4} + z_0\frac{R^2}{2} + c_2 \overset{!}{=} 0\end{aligned} \tag{7.58}$$

The integration constant c_2 is, of course, zero because for $\omega = 0$, $z_0 = 0$ (the water surface in the centre remains at the coordinate origin when the container is not rotating) and Equation 7.58 can only be satisfied with $c_2 = 0$. Since the volume integral (and thus the right side of our equation) is zero, we can divide by 2π immediately after the integration with respect to ϕ and the insertion of the interval limits $(2\pi;\, 0)$; it disappears. According to the integration rules which can be found in e. g. [8, p. 457], the upper integration limit is inserted into the antiderivative (i. e. into the integrated function), and the antiderivative with the inserted lower integration limit is deducted therefrom (see Equation 7.5). Since $r = 0$, nothing needs to be deducted. Solving for z_0, we obtain:

$$z_0 = \frac{\omega^2 R^4}{2g\cdot 4}\cdot\frac{2}{R^2} = \frac{\omega^2 R^2}{4g} \tag{7.59}$$

When z_0 is inserted into the above Equation 7.57, we obtain the following for the water surface in a rotating cylinder:

$$z(r) = -\frac{\omega^2 r^2}{2g} + \frac{\omega^2 R^2}{4g} \tag{7.60}$$

In our example, with $R = 0.147\,\mathrm{m}$ and the angular velocity $\omega = 2\pi f = 2\pi\cdot 2 = 12.57\,\mathrm{Hz}$, the calculation for the height of the outer water surface gives the result $z(r = R) = z_{\mathrm{outer}} = -\frac{12.57^2 R^2}{2g} + \frac{12.57^2 R^2}{4g} = -0.087\,\mathrm{m}$ with respect to the original level (the z-axis points downwards from the water surface). In the centre of the container, we obtain $z(r = 0) = z_{\mathrm{centre}} = -\frac{12.57^2 0^2}{2g} + \frac{12.57^2 R^2}{4g} = 0.087\,\mathrm{m}$.

7.9 Boyle-Mariotte law

You probably remember the Boyle-Mariotte law from school. It states that the product of volume and pressure in a gas is constant if the temperature also remains constant (see Equation 7.61). This is referred to as adiabatic process.

$$p \cdot V = \text{const.} \quad \text{for } T = \text{const.} \tag{7.61}$$

At this point, we shall recall (see Chapter 3.4.9) that we generally have to distinguish between the absolute and relative water pressure (see Figure 7.22).

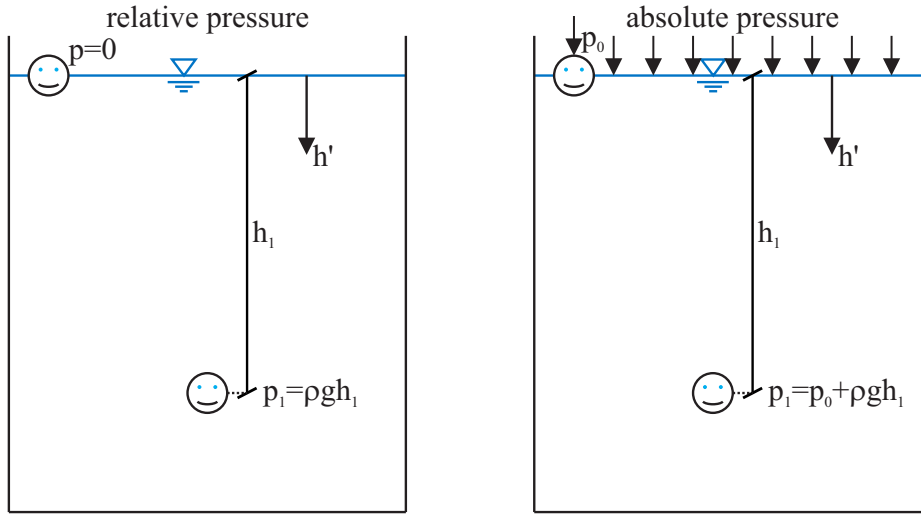

Figure 7.22: Relative and absolute pressure.

For some questions in engineering, the scrupulous application of this law is essential, which is why we should deal with it in more detail. Help yourself to a drink and immerse a transparent drinking straw into it. The liquid level in the straw is the same as it is in the glass. Remove the straw, seal it airtightly at the upper end and immerse it again. What do you detect? The liquid level rises a little in the straw, but certainly not up to the water surface in the glass. What could be the reason?

You can carry out another depictive test with the aid of a straw:
Place the straw into the glass of water and close the open end with the tip of your finger. When you remove the straw from the glass, you see that it remains partly filled with water. Why is that[a]?

[a] When removing the straw from the water, part of the water flows out whereby the air volume increases. According to Boyle-Mariotte, the pressure in the air volume must decrease; it drops below the atmospheric pressure. The pressure increases linearly with the water depth as measured from the water surface (where the air pressure in the straw prevails) until an equilibrium between the atmospheric pressure and air pressure in the straw plus the water pressure at the bottom end of the straw is established. The air pressure in the straw therefore corresponds to $p_{\text{straw}} = p_0 - \rho g h_{\text{water in straw}}$.

Before we explore the reasons together in a cool experiment, you have to promise the following:

With **enclosed air volumes**, we must **always** calculate with the **absolute pressure**, i. e. the sum of air and water pressure (see Figure 7.22).

Experiment

Determination of the height above sea level by means of a Coke bottle

We fix a straw in the opening of a Coke bottle and seal it with a rubber plug in an air-tight manner. Before sealing it, we have to determine the initial air volume. Therefore, we fill the entire Coke bottle and the straw with water, weigh it and by taking the density into account yield $V_0 = 3.573 \times 10^{-4}\,\mathrm{m}^3$. The bottle is then completely emptied and inserted upside-down into a water container. The water surface rises 10.8 cm in the straw which has an inner diameter of 1.0 cm. The original air volume has been reduced by $0.108 \cdot R^2\pi = 8.48 \times 10^{-6}\,\mathrm{m}^3$ (see Figure 7.23).

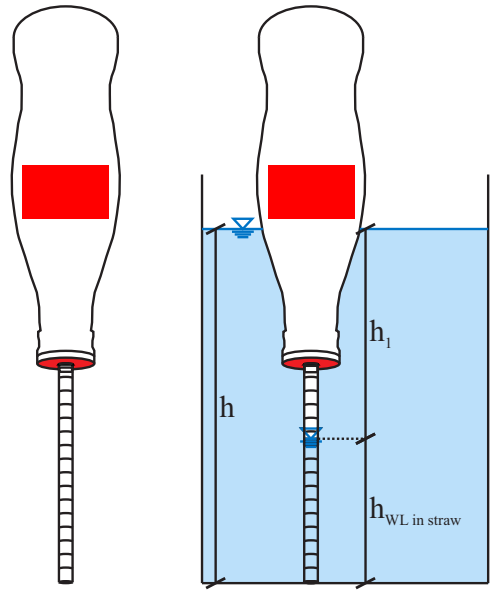

Figure 7.23: Determination of the height above sea level by means of a Coke bottle.

Let's go on a diving tour. We dive to the bottom of the glass and move directly under the straw. We (or the liquid) remain there stationary. At this level, the pressure in the glass is ρgh, and on the other side of the straw wall it is also ρgh. If this was not the case, then liquid would be pressed in or out until equilibrium is achieved. We venture into the straw and slowly move upwards. The surrounding pressure is reduced to the same extent as the depth of the liquid. We remain at the boundary between liquid and air. Here, the same pressure prevails in the straw as in the glass at the same level. It does not matter whether

we resurface in the straw or in the glass; the cover (or the load) from the water molecules above us is reduced to the same extent. We therefore find that the pressure within the straw at the water surface is exactly the same as the pressure outside the straw within the glass at the same height $\rho g h_1$. The total air volume in the straw is now subject to exactly this pressure[E].

At the beginning of the experiment, atmospheric pressure p_0 prevailed in the total volume, V_0, of bottle and straw. Thus, the air pressure in the immersed bottle is calculated as:

$$p_1 = p_0 + \rho g\,(h - h_{\text{WS in straw}}) = p_0 + \rho g\,(0.345 - 0.108) = p_0 + \rho g \cdot 0.237 = p_{\text{atm}} + 2325 \tag{7.62}$$

We obtain the air volume V_1, which prevails after immersing the bottle, by subtracting the water volume that has entered the straw:

$$V_1 = 3.573 \times 10^{-4} - 0.005^2 \pi \cdot 0.108 = 3.488 \times 10^{-4}\,\text{m}^3 \tag{7.63}$$

The initial pressure p_0 is the atmospheric pressure p_{atm} which can be calculated by means of the Boyle-Mariotte equation.

$$p_{\text{atm}} V_0 = (p_{\text{atm}} + 2325)\,V_1 = p_{\text{atm}} V_1 + 2325 \cdot V_1 \tag{7.64}$$

This yields:

$$p_{\text{atm}}\,(V_0 - V_1) = 2325 \cdot V_1 \tag{7.65}$$

We finally obtain:

$$p_{\text{atm}} = 2325 \frac{V_1}{(V_0 - V_1)} = 95\,611\,\text{Pa} \tag{7.66}$$

The height above sea level can then be derived from the barometric formula (7.67) (where $T(h=0) = 288.15\,\text{K}$, $p(h=0) = 1013.25\,\text{hPa}$, $\frac{\text{d}T}{\text{d}h} = 6.5 \times 10^{-3}\,\text{K/m}$) (see also Figure 3.6):

$$p(h) = p_0 \left(1 - \frac{\text{d}T}{\text{d}h} \frac{h}{T(h=0)}\right)^{5.255} \quad [\text{hPa}] \tag{7.67}$$

We obtain 487 m.a.s.l. by means of an equation solver or by trial and error, which is not so bad for the official elevation of Munich (519 m.a.s.l.)[F].

[E] The experiment neither works alone with the Coke bottle nor with the straw. The problem is that the difference of the absolute pressures (barometric pressure vs. air plus water pressure) is so small that the air volume is hardly compressed. The water surface in the straw or in the bottle then rises only insignificantly. It is therefore advantageous to have an additional volume (the bottle body) and a small cross-section at the air-water interface (the straw) so that the water rises noticeably. Just try it with a wine bottle, which has a relatively slim neck and a fat body.

[F] Note: The calculation process is very sensitive, and weather-related deviations of the air pressure from the ideal condition assumed in the barometric formula are not the exception, but the rule.

Experiment

Balloon under water

The Boyle-Mariotte relation between pressure and volume will be explained in another experiment. A blown-up balloon is first pulled just slightly below the water surface (see Figure 7.24). With the water surface marked at the water column and the balloon pulled further downwards, a drop of the water level is to be observed. What could be the reason for this?

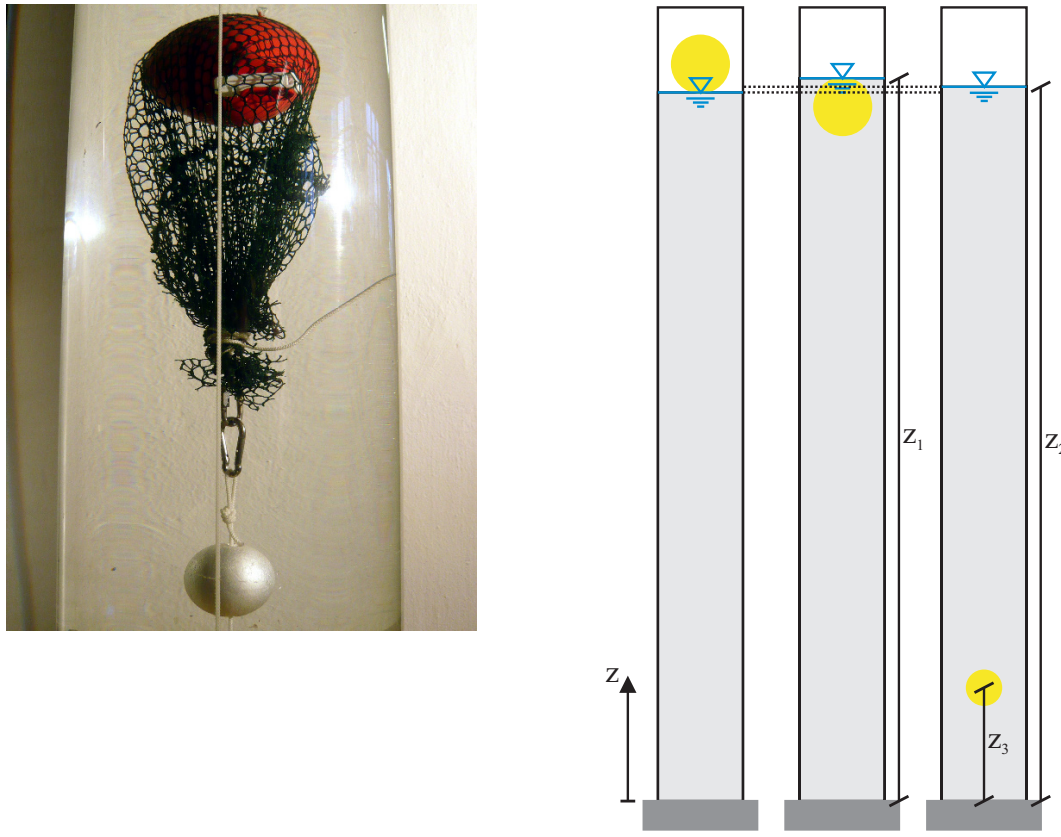

Figure 7.24: Compressed air in a balloon under water.

Quite right, the balloon has shrunk. Due to the higher pressure at a greater depth, the original air volume must become smaller according to $p \cdot V = \text{const}$. An air volume of 5.0 L under atmospheric (that is, absolute) pressure of $101\,000\,\text{N/m}^2$ was pumped into the balloon via a pressure regulator. The water level in the column ($d = 0.293\,\text{m}$), which was determined with the balloon just completely immersed to $z_1 = 2.63\,\text{m}$, dropped to $z_2 = 2.619\,\text{m}$ by the balloon being pulled down. The absolute pressure at the height of the balloon $z_3 = 0.54\,\text{m}$ amounts to $p_3 = p_{\text{atm}} + (z_2 - z_3)\,\rho g = 101\,000 + (2.619 - 0.54)\,\rho g = 121\,395\,\text{N/m}^2$. The air volume of the balloon under pressure can be calculated with these values from Boyle-Mariotte's law, $p_0 V_0 = p_3 V_3$:

$$V_3 = V_0 \frac{p_0}{p_3} = 5.0 \times 10^{-3} \frac{101\,000}{121\,395} = 4.160 \times 10^{-3}\,\mathrm{m}^3 = 4.16\,\mathrm{L} \tag{7.68}$$

Of course, the volume reduction can be calculated via the water surface difference between z_1 and z_2 ($\mathrm{d}V = 0.011 \cdot \frac{0.293^2\pi}{4} = 0.74\,\mathrm{L}$), which is consistent with the result from the Boyle-Mariotte equation.

Chapter 8
Bernoulli equation and energy diagrams

8.1 Classification of the Bernoulli equation

It follows from the equations derived in Chapter 5 that an exact calculation of the flow situation in a pipe section is possible only in exceptional cases of laminar flows. For answering questions that an engineer might have, one-dimensional, steady-state approaches are often sufficient. In the present chapter, we therefore start with loss-free flow, which is described one-dimensionally by the Bernoulli equation (see Equation 5.41 or Chapter 5.7), in which each term has the unit 'metre'. The equation is as follows:

$$H = z + \frac{p}{\rho g} + \frac{v^2}{2g} \tag{8.1}$$

Therein z is the geodetic height, $\frac{p}{\rho g}$ is the pressure height and $\frac{v^2}{2g}$ is the velocity height[A]. Thus, H is the sum of the three forms of energy, which remains constant in a loss-free flow. According to Equation 8.1, in the case of a horizontal pipe expansion where ($z =$ const.), the pressure must increase because the velocity decreases. In the case of tapering, v increases, which, of course, results in an increase of $\frac{v^2}{2g}$. In order to maintain $H =$ const., $\frac{p}{\rho g}$ in turn must become smaller since $z =$ const. That's what it's all about.

8.2 Piezometric pressure height

We will first look at a water container in which hydrostatic conditions prevail; the flow velocity is zero everywhere (see Figure 8.1). When we float on the water surface, no water pressure is acting on us and our velocity is negligibly small. Our total energy is solely the geodetic height z_1; the pressure height $\frac{p_1}{\rho g}$ and the velocity height $\frac{v_1^2}{2g}$ are zero. We now move downwards and remain in position 2, where the geodetic height has decreased to z_2. At the same time, however, the pressure height increased by the same degree to $\frac{p_2}{\rho g}$ (with $p_2 = \rho g h_2$). We therefore find that the sum of z_2 and $\frac{p_2}{\rho g}$ again results in z_1. When we dive deeper to position 3, where the geodetic height is only z_3, the pressure height $\frac{p_3}{\rho g}$ acts on

[A] In the following, v will indicate the mean cross-section velocity.

C. Rapp, *Hydraulics in Civil Engineering*,
https://doi.org/10.1007/978-3-031-54860-4_8

us. No matter how we twist it, the sum of geodetic height z and pressure height $\frac{p}{\rho g}$ is the same everywhere in our system: it corresponds to the height of the water level. As this quantity $(z + \frac{p}{\rho g})$ is widely used, it has been given its own name: piezometric pressure height.

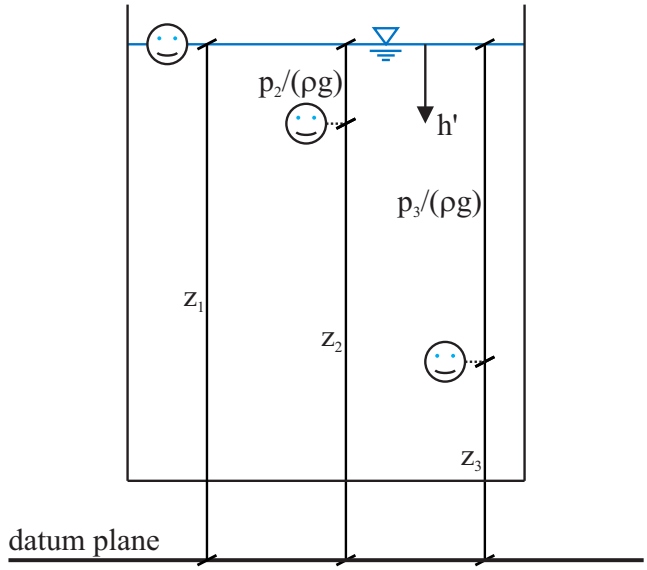

Figure 8.1: Explanations of the piezometric pressure height.

8.3 Excursus: Energy diagram – an introduction

The energy diagram is an important instrument by means of which the hydraulic conditions in pipelines and open channels may be clearly represented. The unit of the terms in the Bernoulli equation (8.1) – metre – is very helpful.
Let's go back again to the example we just discussed. The piezometric pressure height in the container always corresponds to the water level. We indicate the piezometric pressure height with a broken green line (the so-called hydraulic grade line) in the energy diagram (see "HGL" in Figure 8.2 on the left). The so-called energy grade line (EGL) represents the total energy of our system. The energy grade line reflects the sum of geodetic height, pressure height and velocity height. The velocity in the container is $v = 0$ because the water does not move, and the kinetic energy is therefore $\frac{v^2}{2g} = 0$. In the container, the energy height corresponds to the piezometric pressure height $H = z + \frac{p}{\rho g} + \frac{0^2}{2g}$. For our energy diagram, this means that the hydraulic and energy grade lines lie at exactly the same level – the water level (see Figure 8.2 right).
Now, finally, we let the water flow! *Πάντα ῥεῖ*[B]

[B] Quote attributed to Heraclitus of Ephesus (520 - 460 BCE) meaning that "Everything is in a state of flux".

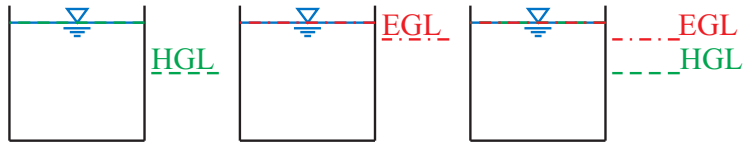

Figure 8.2: Hydraulic grade line, energy grade line and overall energy diagram for a container.

8.4 Bernoulli in pipes

Figure 8.3 shows a glass tube with water flowing through. Moving from left to right it exhibits a gradual expansion and then an abrupt tapering. There are openings to which the tubes are tightly connected on the upper side of the apparatus. Now we focus on the vertically arranged tubes, so-called level gauges, which are identified by numbers 1, 4 and 5[C]. When diving downwards in one of these tubes, the pressure increases linearly and reaches the value $\rho g h'$ at the depth h'. Let's have a look at a water molecule in the area of the level gauge connection. If the pressure from below were higher than that from above, then the molecule would enter the level gauge[D]. Conversely, the molecule would enter the glass tube (through which water is flowing) from the level gauge if the pressure from above were higher. However, it stays in place because the water level in the gauge remains constant. Together with the geodetic height z, which may be related to any level (e. g. the tube axis), the water level in the gauge indicates the so-called piezometric pressure height $z + \frac{p}{\rho g}$.

A wafer-thin tube bent at a 90° angle was tightly inserted into the tube at the third and sixth (last) opening and turned opposite to the flow direction along the axis of the main tube (see Figure 8.4 left). This tube that is directed against the flow is called a Pitot tube. It is named after Henri de Pitot[E], a French hydraulic engineer who worked in the 18th century. We dive again through the tube, along the tube axis opposite the direction of flow, to the opening. In this case, the same pressure prevails on the right and on the left of our sample molecule[F]. However, it can be seen that both Pitot tubes exhibit a higher water level than the neighbouring level gauges. This is the essential finding of the Bernoulli equation. Due to the relatively short length of the glass tube, energy losses may be neglected between cross-sections at the pipes numbered 3 and 4 as well as at those numbered 5 and 6 ($H_3 = H_4$, $H_5 = H_6$). The three forms of energy, geodetic height, pressure height, and velocity height exist in the cross-section of level gauge 5. Note that $H_5 = z_5 + \frac{p_5}{\rho g} + \frac{v_5^2}{2g}$. In the cross-section of Pitot tube 6, the velocity immediately upstream from the wafer-thin tube amounts to zero (water flows neither in nor out); hence $v_6 = 0$ and therefore $H_6 = z_6 + \frac{p_6}{\rho g}$. With $z_5 = z_6$, it follows that:

[C] Because of the non-parallel streamlines below level gauge 2 it is bracketed. We may apply the Bernoulli equation there but we have to be careful with the pressure; for further explanation see Chapter 5.7 and the box on page 118.

[D] Here, water does not behave differently from a crowd of people at a rock concert. If you are jammed in like a sardine attending a Red Hot Chili Peppers' concert and the crowd presses harder from behind than the people in front of you, you will inevitably be pushed forward. On the other hand, if the crowd pressure is reversed, you will be pushed rearward.

[E] Henri de Pitot, (∗1695), Aramon, France (†1771), Aramon, France

[F] Otherwise, more and more water would flow in or out, and thus the water level in the Pitot tube would rise or fall, respectively.

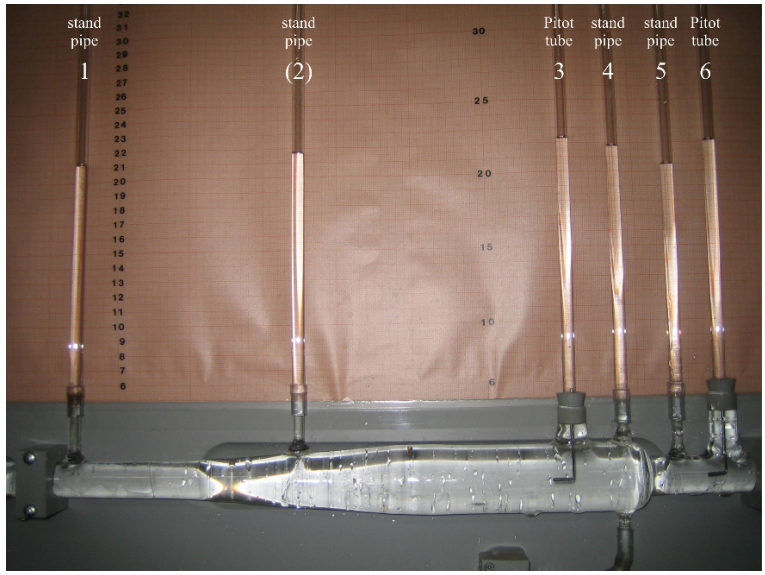

Figure 8.3: Tube experiment for explaining the Bernoulli equation.

$$\frac{p_6}{\rho g} = \frac{p_5}{\rho g} + \frac{v_5^2}{2g} \tag{8.2}$$

Thus, the Pitot tube indicates the sum of the piezometric height $\frac{p}{\rho g} + z$ and the velocity height $\frac{v^2}{2g}$.

8.5 Excursus: Energy diagram – a continuation

The level gauge reflects the piezometric height and the Pitot tube indicates the total energy height. The entirety of flow information may be summarised in an energy diagram (see Figure 8.4, right). Therein, the energy grade line represents the total energy (i. e. the energy height H) at each cross-section, which corresponds exactly to the water level in a Pitot tube attached at a particular location. This also applies to the hydraulic grade line, which indicates the piezometric pressure height, and may be measured via the water level in a level gauge. Together with the height of the tube axis, which corresponds to the geodetic height z, the pressure height $\frac{p}{\rho g}$ may also be determined. Here, the tube axis represents the mean geodetic height of the water which is present in the tube.

Experiment

Discharge in a pipe

The experiment of Figure 8.3 clarifies the Bernoulli relationship between pressure height and velocity height by means of a tube expansion and its tapering. With an increasing

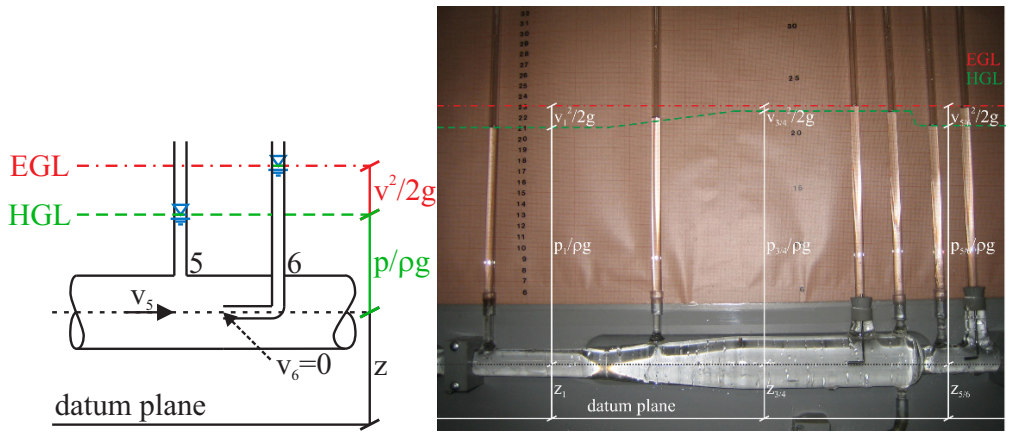

Figure 8.4: Energy diagram for a level gauge and a Pitot tube in a pipe flow (left) as well as for the tube experiment (right) in Figure 8.3.

diameter ($d_1 = 2.0\,\text{cm}$, $d_{3,4} = 4.0\,\text{cm}$), the fluid velocity is reduced, leading to a pressure increase. On the right side, the water once again is accelerated ($d_{5,6} = 2.0\,\text{cm}$); hence, the pressure drops. The total energy is indicated by the height of the water in the Pitot tubes. The 0.016 m difference in water levels between Pitot tube (6) and level gauge (5) corresponds to the velocity height $\frac{v_5^2}{2g}$ (see Figure 8.4, left), from which the discharge may easily be calculated using Equation 8.2: $Q = A\sqrt{\frac{v_5^2}{2g}2g} = 0.01^2\pi\sqrt{0.016 \cdot 2g} = 0.176\,\text{L/s}$.

However, we may also determine the discharge from the level gauges not far upstream or downstream from the tapering. For loss-free flow and $z_4 = z_5$ in the Bernoulli equation, it follows that

$$\frac{p_4}{\rho g} + \frac{v_4^2}{2g} = \frac{p_5}{\rho g} + \frac{v_5^2}{2g} \tag{8.3}$$

and further:

$$\frac{p_4}{\rho g} - \frac{p_5}{\rho g} = \frac{v_5^2}{2g} - \frac{v_4^2}{2g} = \frac{Q^2}{2g}\left(\frac{1}{A_5^2} - \frac{1}{A_4^2}\right) \tag{8.4}$$

The discharge results from the cross-sectional area values and the difference in pressure height $\frac{p_4 - p_5}{\rho g} = 0.013\,\text{m}$, which may be taken from Figure 8.3:

$$Q = \sqrt{\frac{2}{\rho}(p_4 - p_5) \cdot \left(\frac{1}{A_5^2} - \frac{1}{A_4^2}\right)^{-1}} = 0.164\,\text{L/s} \tag{8.5}$$

The discharge obtained from the velocity height agrees sufficiently accurately with the solution from the difference in pressure height.

8.6 Bernoulli and outflows

In preparation for the next steps, we will continue the considerations of Chapter 8.2 and drill a hole into the container wall (see Figure 8.5).

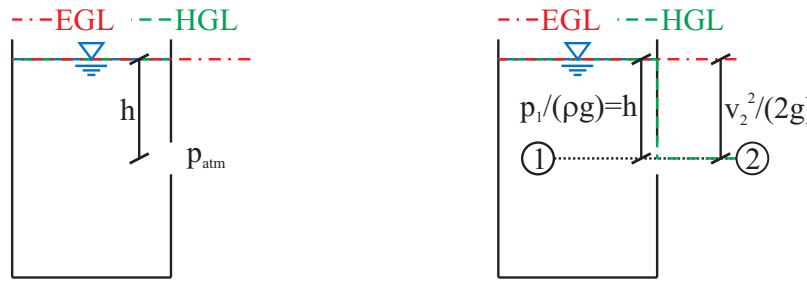

Figure 8.5: Extension of the example in Figure 8.1.

We have certainly dealt extensively with the increase in pressure as a function of depth; everyone will agree that we can describe the pressure in the container at the level of the drilled hole as ρgh. The difference between absolute and relative pressure (see Chapter 3.4.9) should again be discussed briefly. The atmospheric pressure acts on the water surface so that the absolute pressure at the level of the hole is $p_{\text{atm}} + \rho gh$. The atmospheric pressure p_{atm} prevails outside the container. This means that as we drill a hole into the container wall, this pressure acts through the hole against the water. Thus, the atmospheric pressure acts on the fluid particles from both sides so that we may as well safely omit it. The relative (water) pressure outside the container is therefore 0.
The Bernoulli equation was derived by integration along a streamline $\vec{s}$ (see Chapter 5.7) from the Euler equation (5.24), which, contrary to the Navier–Stokes equation (5.29), does not include a viscous (friction) term.
With a hole drilled through the container wall, water will be pressed through it because the pressure on the left side is greater than on the right (by ρgh). Imagine an overcrowded auditorium at the end of the lecture. All students push through a door that is quite narrow. Those at the door are subjected to the pressure of the fellow students from behind while no pressure from the front is counteracting them, and they can freely leave.
Back to the Bernoulli equation, which stipulates that the total energy remains constant. This means that the water, when flowing out of the container, has the same energy height outside, as indicated by the chain-dotted red lines in Figure 8.5.

Take care that the preconditions of the Bernoulli equation prevail! If hydraulic losses are not negligible, you are not allowed to apply it[a]. Where streamlines are bent, the pressure is distributed non-linearly; hence exact knowledge of the local pressure or velocity distribution is essential for statements concerning the entire cross-section of the flow. If possible, balance the three forms of energy at locations where parallel streamlines prevail.

[a] We will see a little later how we can integrate hydraulic losses into the Bernoulli equation.

If we move on a streamline (see dotted line in Figure 8.5) from left to right, then the velocity height $\frac{v_1^2}{2g} = 0$ and the pressure height $\frac{p_1}{\rho g} = h$ are still acting at the starting point[G]. On the right side at cross-section 2, the pressure height (relative to the water pressure) is $\frac{p_2}{\rho g} = 0$. Since $z_1 = z_2$, it follows from the Bernoulli equation that the velocity

[G] ... which is somewhat awkward for me to explain; let's say that v is negligibly small.

height $\frac{v_2^2}{2g}$ must be h. This is exactly what we see when we place a Pitot tube at level $z_1 = z_2$ into the jet. All that remains is to draw the hydraulic grade line at the outflow in its axis, and then our energy diagram will be complete with the corresponding lettering.
You may ask yourself why the hydraulic grade line happens to lie at the level of the outflow. Let's go back to Chapter 8.2. Therein we determined that the hydraulic grade line reflects the piezometric pressure height. It consists of the pressure height (zero at the outflow) and the geodetic height, which is, of course, at the outflow level. If the water does not have at least this energy, which is equivalent to the water level at the opening, then of course nothing can flow out.
For the outflow, we may now establish the Bernoulli equation:

$$z_1 + \frac{p_1}{\rho g} + \frac{v_1^2}{2g} = z_2 + \frac{p_2}{\rho g} + \frac{v_2^2}{2g} = \frac{p_1}{\rho g} = \frac{v_2^2}{2g} \tag{8.6}$$

With $\frac{p_1}{\rho g} = h$ it follows that:

$$v_2 = \sqrt{2gh} \tag{8.7}$$

8.7 Cavitation

Up to now, we've looked at water only as a liquid. We know from Figure 3.3 that water may also exist in other states. And it is this characteristic of water that we should be aware of.
In the Bernoulli equation, z describes the vertical distance from the reference height to the pipe axis, $\frac{p}{\rho g}$ the vertical distance from the pipe axis to the hydraulic grade line, which corresponds to the piezometric pressure height, and $\frac{v^2}{2g}$ the velocity height (see Figure 8.6). If the hydraulic grade line is below the pipe axis, negative pressure prevails, i. e. a pressure lower than the ambient pressure. We take advantage of this fact when we "pull" liquid via a drinking straw out of a glass. The atmospheric pressure is then higher than the pressure within our mouth and therefore "pushes" the liquid upwards against gravity.
We know from Figure 3.3 that water can be gaseous even at relatively low temperatures, namely when the pressure is low. We will have a closer look at this phenomenon in the following experiment, which you can easily carry out yourself.

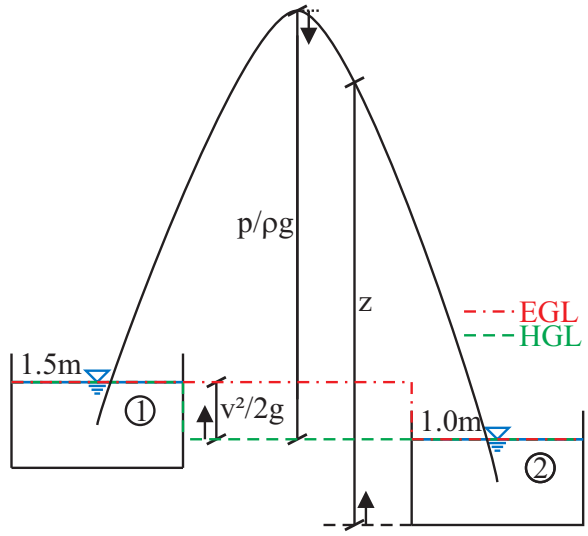

Figure 8.6: Negative pressure in a pipeline system. Please ignore the drop of the energy grade line at the boundary of container 2 (for now).

Experiment

Water vapour in a hose

Given two containers (e. g. buckets), we fill one with water. Then water is sucked from one container into a hose approximately 20 m long and directed into the other container. Then we grip the hose in the middle and pull it upwards while the two ends remain in the containers. Above a height of approximately 8 m, the liquid water in the hose becomes gaseous; this is referred to as a separation of the liquid columns. On the right side of Figure

Figure 8.7: Experiment for the generation of gaseous water in a hose (see also Figure 8.6).

8.7, you see that the water in the upper area of the hose is gaseous. The water cannot flow over this "gas barrier". In order to ensure that the water flows, the pressure must be greater than the vapour pressure. For the temperature-dependent vapour pressure, $-7.5\,\mathrm{mH_2O}$ is generally considered a standard value.
If the pressure drops locally, e. g. in pumps or turbines, under the vapour pressure, H_2O "bubbles" or "voids" develop; these voids implode and become liquid again at places of higher pressure. When they implode, a liquid jet passes through the void at several hundred metres per second. Due to the pressure gradient in a flow adjacent to walls (which will be dealt with later), the jet is always directed against the boundary. No material can withstand these "pinpricks"; therefore, almost any effort is taken to prevent from this phenomenon which is generally known as cavitation.
I think we are now well equipped for more in-depth knowledge of this subject.

Chapter 9
Outflow from openings

9.1 Outflow through openings

In the present chapter, we will extend the considerations concerning the Bernoulli equation to questions that are of interest in filling and emptying large and small containers making use of energy diagrams.

9.2 Torricelli equation

We begin with the derivation of the Torricelli[A] equation. In Chapter 8.6, we derived the relationship between the pressure and velocity of the outflow from a container by means of Figure 8.5 ($h = \frac{v^2}{2g}$). By rearranging, we obtain Equation 9.1:

$$v = \sqrt{2gh} \tag{9.1}$$

Experiment

Water jet

For our experiment, we use a container whose bottom outlet is closed by a ball valve (see Figure 9.1). How far does the jet reach at a pressure height of 2.0 m and a height of the outflow of $h_{\text{outflow}} = 80\,\text{cm}$?
The velocity component in the x-direction u results from the Bernoulli or the Torricelli equation. The velocity is zero in the container, and the pressure height is $h = \frac{p}{\rho g} = 2.0\,\text{m}$ in relation to the outlet opening; downstream from the orifice, atmospheric pressure prevails so that the velocity component u may be calculated:

$$u = \sqrt{2gh} = \sqrt{2 \cdot 9.81 \cdot 2.0} = 6.26\,\text{m/s} \tag{9.2}$$

[A] Evangelista Torricelli, ∗1608, Faenza, Italy, †1647, Florence, Italy

C. Rapp, *Hydraulics in Civil Engineering*,
https://doi.org/10.1007/978-3-031-54860-4_9

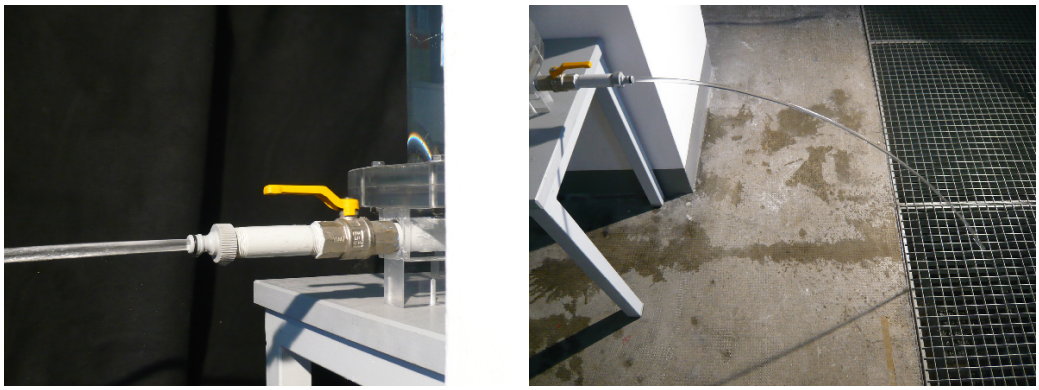

Figure 9.1: Water jet discharged from a container (left); jet with a (meanwhile) lower water level in the container (right).

Immediately downstream from the orifice (or outside the container), the velocity component in the vertical direction is $w = 0$, but the water moves constantly at velocity u in the x-direction and is accelerated downwards by gravity. The time during which the water is in the air is dependent only on the height of the outflow h_{outflow} (and g), which is also known as a horizontal projectile motion. With $h_{\text{outflow}} = \frac{g}{2}t^2$, it follows that $t = \sqrt{\frac{2h_{\text{outflow}}}{g}} = 0.40\,\text{s}$. During this time period, the water moves $x = t \cdot u = 0.40 \cdot 6.26 = 2.53\,\text{m}$ in the horizontal direction.

Returning to the Torricelli equation

We remember that the Bernoulli equation does not include friction; when deriving further formulas therefrom, they will not, then, include any energy losses. We "cheat" by inserting a coefficient of friction, localised for orifices by means of numerous tests, in the range of $\phi = 0.96 \ldots 0.98$ (see Equation 9.1). This means that 2 % to 4 % of the hydraulic energy is lost when fluid flows out of an orifice. We should not yet be concerned that the energy grade line does not actually extend horizontally.
We will now closely look at the outflow. As in the rock concert discussed above, the water molecules push from the container opening to the outside due to the pressure difference. To visualise the conditions at the outlet, it is best to imagine a cyclist who circles into a yard entry. If she approaches perpendicularly, she simply goes straight through. If she approaches the passage in parallel, as illustrated in the following Figure 9.2, and tries to get through the gate, she will not succeed in following exactly the contour of the sharp edge. She turns with the smallest possible radius and approaches the gate. Her streamline is shown as a broken line in the drawing.
Here is where things get exciting with the Bernoulli equation. Although we know that for the boundary streamline the pressure is zero, we are not able to describe the pressure distribution precisely at the opening cross-section. However, it will be zero across the jet where parallel streamlines prevail since no fluid wants "in" or "out" there. At this position, the cross-section of the jet is (A_J), which is smaller than at the container opening (A_O); the jet is subjected to tapering, which is described by the empirically determined contraction coefficient ψ as the ratio of the jet area to the area of the opening.

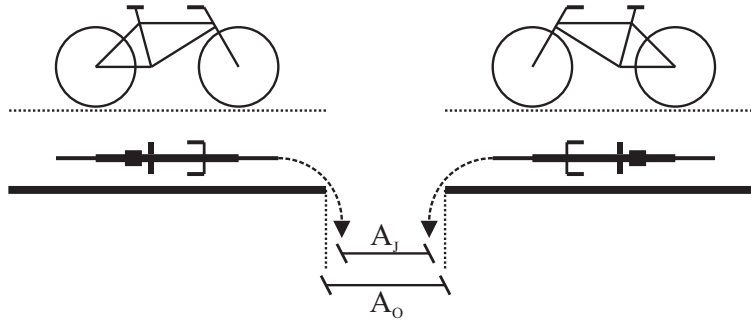

Figure 9.2: Constriction of a jet by the boundary streamline.

$$\psi = \frac{A_J}{A_O} \tag{9.3}$$

With Equation 9.1, we may set up an expression for the outflow Q:

$$Q = \phi \psi A_O \sqrt{2gh} \tag{9.4}$$

The friction coefficient ϕ and the contraction coefficient ψ form the so-called discharge coefficient μ:

$$\mu = \phi \cdot \psi \tag{9.5}$$

From this, the Torricelli equation is obtained (9.6):

$$Q = \mu A_O \sqrt{2gh}, \quad \text{where } \frac{h}{h_O} > 1.5 \tag{9.6}$$

There is one issue with the Torricelli equation (9.6) that we have to watch: if the water at the outflow is not deep enough, air may be sucked in due to eddy generation, which reduces the outlet cross-section so that less water flows out than calculated. You have certainly seen such an air-sucking eddy when emptying a bathtub. For the outflow from container openings, the water depth h should be at least 1.5 times the height of the opening h_O.

9.3 Outflow from a "small" and a "large" opening

Up to now we've withheld the fact that the pressure $\rho g h_T$ at the upper edge of a vertical opening of height h_O is lower than the pressure height ($\rho g h_B$) at the lower edge due to the difference between the heights of the two edges. It follows from the relationship that was derived at the beginning of this chapter that the velocity at the upper end of the orifice is lower than that at the lower end. However, it does not increase linearly over the height of the orifice but rather as $\sqrt{h}$ (see Figure 9.3).
This means specifically that we must integrate the velocity with respect to the height of the orifice in order to determine the discharge and write the Torricelli equation with the width of the opening b as follows (Equation 9.7):

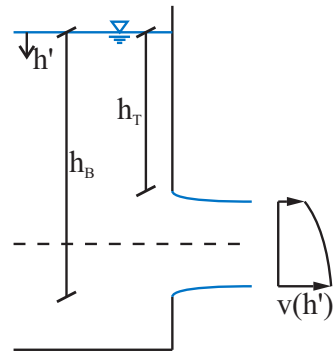

Figure 9.3: Outflow from a "large" opening.

$$Q = \int_{h_T}^{h_B} \mu b \sqrt{2gh'}\, \mathrm{d}h' \tag{9.7}$$

Experiment

Comparison between "small" and "large" opening

We compare the results between a small and a large opening by means of an experiment (see Figure 9.4). Because the container is so large, a constant water level may be assumed during the time of measurement.

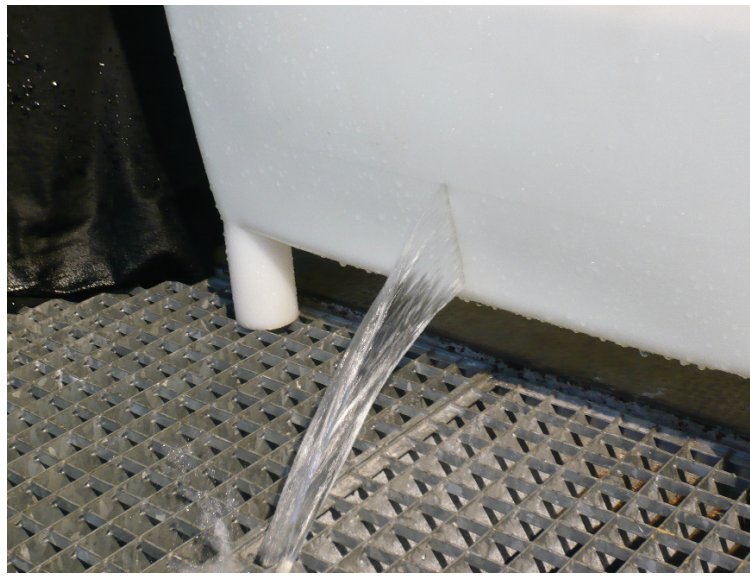

Figure 9.4: Outflow from a container.

- With a mean water depth of $h_m = 0.40\,\mathrm{m}$ at the centre of the opening and an outflow coefficient $\mu = 0.6$, an opening width $b = 5.0\,\mathrm{mm}$ and its height $h_O = 10.0\,\mathrm{cm}$, the discharge is obtained according to Equation 9.6:

$$Q = \mu \cdot b \cdot h_O \sqrt{2gh_m} = 0.6 \cdot 5.0 \times 10^{-3} \cdot 0.10 \sqrt{2g \cdot 0.40} = 0.84\,\mathrm{L/s} \tag{9.8}$$

- For the determination of the discharge by integration of the velocity with respect to the orifice height h_O, we use Equation 9.7. In our case, the outflow velocity is not dependent on the width, but it is dependent on the water depth at the opening. We therefore integrate the outflow velocity, which is dependent on the water depth h', with respect to the same $\mathrm{d}h'$. The constant values such as μ, $\sqrt{2g}$ and b may be written before the integral.

$$Q = \mu b \sqrt{2g} \int_{h_T}^{h_B} \sqrt{h'}\,\mathrm{d}h' = 0.0133 \cdot \frac{2}{3} \left[h_B^{\frac{3}{2}} - h_T^{\frac{3}{2}} \right] = 0.84\,\mathrm{L/s} \tag{9.9}$$

  With these ratios of water depth and height of the orifice, the difference is negligible. By the way, in the experiment, the discharge was determined with a bucket that was filled with water from the jet for approximately 5 s. The water volume in the bucket was determined by weighing the bucket before and after filling; the results of three measurements were between 3.95 and 4.4 L, i. e. between 0.79 and 0.88 L/s.

Example

Outflow from a triangular opening

Now we go to another degree of complication, but don't worry, everything will be discussed in a relaxed manner.
Here, we look at the outflow through a triangular opening from the container seen in Figure 9.5. The opening angle, 2α, is 60°. Half of this opening angle, α, is therefore 30°; $h_T = 1.0\,\mathrm{m}$ and $h_B = 1.4\,\mathrm{m}$. When using the Torricelli equation for the determination of the outflow, we must take into account that the width of the opening depends on h', i. e. $b = f(h')$.
First, let's find out how we might describe the area. The width of the triangle at the height h_T may be expressed via the tangent:

$$\tan\alpha = \frac{\frac{b}{2}}{h_B - h_T} \tag{9.10}$$

When we describe the width of the opening as a function of the coordinate h', which we must do (unfortunately), we may solve the previous equation for b. b is described as a function of h' and the concrete value h_T is replaced by the coordinate h'. We must not forget that the following equation is applicable only for the range $h_T \le h' \le h_B$.

$$b(h') = 2\tan\alpha \left(h_B - h'\right) \quad \text{where } h_T \le h' \le h_B \tag{9.11}$$

We test the equation for the two extreme values:

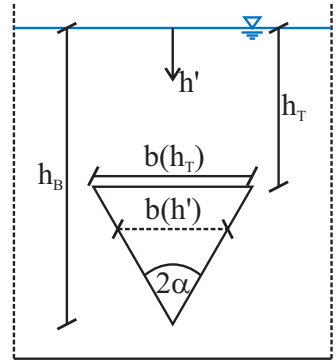

Figure 9.5: Outflow from a triangular opening.

$$b(h_T) = 2\tan\alpha\,(h_B - h_T) = 2\tan 30^\circ \cdot 0.4\,\mathrm{m} = 0.462\,\mathrm{m} \tag{9.12}$$

$$b(h_B) = 2\tan\alpha\,(h_B - h_B) = 2\tan 30^\circ \cdot 0\,\mathrm{m} = 0\,\mathrm{m} \tag{9.13}$$

It seems to work! Therefore, $b(h')$ is inserted into Equation 9.14 in such a manner that width $b(h')$ is not before the integral as a constant but rather is inside it.

$$Q = \mu \int_{h_T}^{h_B} b(h')\sqrt{2gh'}\,\mathrm{d}h' = \mu \int_{h_T}^{h_B} 2\tan\alpha\,\left(h_B - h'\right)\sqrt{2gh'}\,\mathrm{d}h' \tag{9.14}$$

The job is already half done. First, we place the constants before the integral and combine them into a single constant C:

$$Q = \mu \cdot \sqrt{2g} \cdot 2\tan\alpha \int_{h_T}^{h_B} \left(h_B - h'\right)\sqrt{h'}\,\mathrm{d}h' = C \cdot \int_{h_T}^{h_B} h_B \cdot \sqrt{h'} - h' \cdot \sqrt{h'}\,\mathrm{d}h' \tag{9.15}$$

Next, the constant C may be directly calulated: $C = 3.0688\,\mathrm{m}^{\frac{1}{2}}/\mathrm{s}$. The unit $\mathrm{m}^{\frac{1}{2}}/\mathrm{s}$ comes from the root of the gravity constant. From the integration of $\int h_B \cdot \sqrt{h'}\,\mathrm{d}h'$, it follows that $\frac{2}{3} \cdot h_B \cdot h'^{\frac{3}{2}}$. Also, $\int h' \cdot \sqrt{h'}\,\mathrm{d}h' = \int h'^{\frac{3}{2}}\,\mathrm{d}h' = \frac{2}{5} \cdot h'^{\frac{5}{2}}$. Now, let's insert the limits of the definite integral:

$$\begin{aligned} Q &= 3.0688 \left[\frac{2}{3} \cdot h_B \cdot h'^{\frac{3}{2}} - \frac{2}{5} \cdot h'^{\frac{5}{2}}\right]_{h_T}^{h_B} = \\ &= 3.0688 \left[\left(\frac{2}{3} \cdot 1.4 \cdot 1.4^{\frac{3}{2}} - \frac{2}{5} \cdot 1.4^{\frac{5}{2}}\right) - \left(\frac{2}{3} \cdot 1.4 \cdot 1.0^{\frac{3}{2}} - \frac{2}{5} \cdot 1.0^{\frac{5}{2}}\right)\right] = \\ &= 3.0688 \cdot 0.0851 = 0.261\,\mathrm{m}^3/\mathrm{s} = 261\,\mathrm{L/s} \end{aligned}$$

Phew, that was tough. Let's recall what we learnt in Chapter 7.3: the pressure force is the result of the multiplication of the pressure at the centre of gravity by the area. For the outflow from openings, the pressure at the centre of gravity is used in the calculation for the discharge velocity. The equation for the above example with $A_\nabla = \frac{1}{2} \cdot 0.462 \cdot 0.40 = 0.0924\,\mathrm{m}^2$ reads as follows:

$$Q = \mu \cdot A_\nabla \sqrt{2gh_{\mathrm{CG}}} = 0.6 \cdot 0.0924\sqrt{2g \cdot 1.133} = 0.261\,\mathrm{m}^3/\mathrm{s} = 261\,\mathrm{L/s} \tag{9.16}$$

Perhaps you ask yourselves: "What was this stress good for?" The only answer I have is: "For the sake of knowledge". Seriously though, there are cases in which the error of approximation is not tolerable and that require an analytically correct solution.
Let's take a break!

9.4 Outflow at a variable water level

Back at the desk now, we concentrate on a question that is primarily of interest in the context of reservoirs. It is a matter of determining the outflow when the water level is variable. This must be done when filling and emptying rainwater retention basins or basins of dams. So off we go.

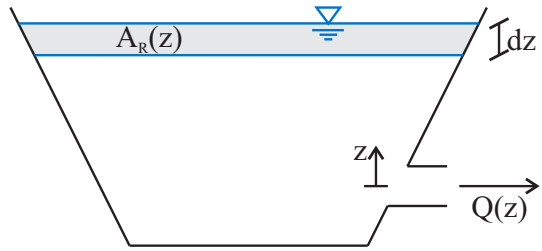

Figure 9.6: Outflow from a container in which the water level is variable; the area of the reservoir is indicated as A_R.

Figure 9.6 shows a container with a dropping water level during an outflow. For the sake of simplicity, we position the origin of the z-axis such that z increases positively upwards in the centre of the opening. In order to be able to calculate the duration of the outflow, we use a brilliant idea: the volume V that flows out over a certain time period t corresponds exactly to the volume that is missing in the container. Logical, isn't it?
The volume that flows out is obtained via the integral of the discharge with respect to time. This becomes obvious when considering the units. The discharge that is dependent on z has the unit $\left[\mathrm{m}^3/\mathrm{s}\right]$ which, multiplied by the unit of time [s], results in the unit of volume $\left[\mathrm{m}^3\right]$. Hence, the volume that flows out may be represented as follows:

$$V = \int Q(z)\,\mathrm{d}t \tag{9.17}$$

The water volume that is missing in the container is generally described by the integration of the area with respect to the height:

$$V = \int A_\mathrm{R}(z)\,\mathrm{d}z \tag{9.18}$$

When setting up the continuity equation, attention must be paid to the coordinate direction. During the outflow of the container, the water level sinks, causing z to decrease, which would lead to a negative volume with the above equation. Make sure that the integral $\int_{z_T}^{z_B}$ reads "from top to bottom" with the integration limits in the proper order. Thus, we write:

$$V = \int_{t(z_T)}^{t(z_B)} Q(z)\,\mathrm{d}t = -\int_{z_T}^{z_B} A_\mathrm{R}(z)\,\mathrm{d}z \tag{9.19}$$

For the calculation of the outflow duration, Equation 9.19 is rearranged to solve for $\mathrm{d}t$. By integration, t remains on the left side, and the resulting z-dependent terms are written on the right side and integrated:

$$t = \int_{z_T}^{z_B} -\frac{A_\mathrm{R}(z)}{Q(z)}\,\mathrm{d}z \tag{9.20}$$

In order to carry out such tasks, one must first formulate the discharge and the outflow area as a function of z. Let's risk looking at a first example; later, things will get somewhat more complicated with an experiment.

Example

Outflow from a container with a sinking water level

In this example, the area of the container $A_\mathrm{C} = 3.0\,\mathrm{m}^2$ is independent of z (see Figure 9.7), which makes things easier. The water level is assumed to drop from $z_T = 4.0\,\mathrm{m}$ to $z_B = 2.0\,\mathrm{m}$. The height of the opening ($A_O = 7.854 \times 10^{-3}\,\mathrm{m}^2$; $\mu = 0.65$) is at $z_\mathrm{opening} = 0\,\mathrm{m}$. How long does it take for the water level to drop from 4.0 m to 2.0 m?

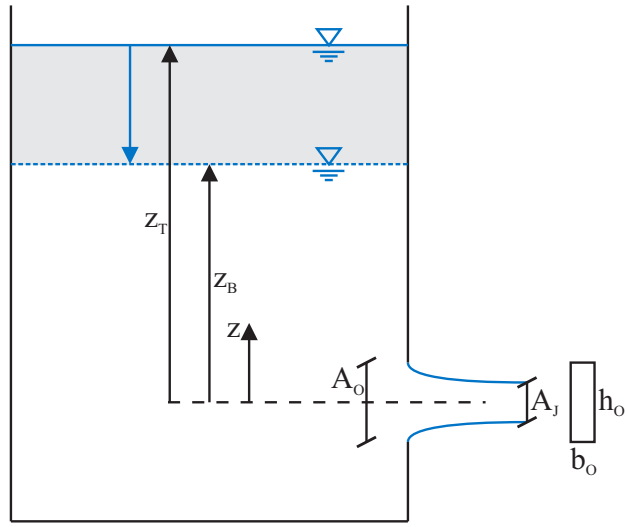

Figure 9.7: Outflow from a container with a variable water level.

Since the container area is independent of z, it may be placed before the integral. It follows that:

$$t = -A_\mathrm{C} \int_{z_T}^{z_B} \frac{1}{Q(z)}\,\mathrm{d}z \tag{9.21}$$

The z-dependent outflow is described by Equation 9.22:

$$Q(z) = \mu A_O \sqrt{2gz} \tag{9.22}$$

Constants μ, A_O and $\sqrt{2g}$ may again be inserted before the integral so that the result is:

$$t = -\frac{A_C}{\mu A_O \sqrt{2g}} \int_{4.0}^{2.0} \frac{1}{\sqrt{z}} \, dz \tag{9.23}$$

The integration of $\int z^{-\frac{1}{2}} \, dz$ yields $2 \cdot z^{\frac{1}{2}}$ and thus:

$$t = -2\frac{A_C}{\mu A_O \sqrt{2g}} \left[\sqrt{z}\right]_{4.0}^{2.0} = -2\frac{A_C}{\mu A_O \sqrt{2g}} \left[\sqrt{2.0} - \sqrt{4.0}\right] = 155.43\,\text{s} \tag{9.24}$$

The units may serve as a plausibility check of the integration[B]:

$$[\text{s}] = \frac{\left[\text{m}^2\right]}{\left[\text{m}^2 \cdot \text{m}^{\frac{1}{2}}/\text{s}\right]} \left[\text{m}^{\frac{1}{2}}\right] = [\text{s}] \tag{9.25}$$

That looks quite okay. We will still check whether we would have obtained a similar result with a mean depth of 3.0 m: The outflow volume is $V = A_C \cdot \Delta z = 3.0\,\text{m}^2 \cdot 2.0\,\text{m} = 6.0\,\text{m}^3$. The discharge Q with a mean depth of $z = 3.0\,\text{m}$ yields $Q = \mu A_O \sqrt{2gz} = \mu A_O \sqrt{2g \cdot 3.0} = 0.0392\,\text{m}^3/\text{s}$. An outflow duration of 153.19 s results from computing $t = \frac{V}{Q}$, which seems to confirm the result from the more complex solution by integration.
Are you feeling well prepared for the ultimate challenge in this chapter? If so, then we can tackle the following experiment.

Experiment

Outflow from an inverted pyramid

During the outflow from the inverted pyramid depicted in Figure 9.9 the cross-sectional area changes with the water depth. In the calculation of the outflow duration, the container area $A(z)$, which is dependent on z, must also be integrated. When carrying out the experiment, it may be observed that at first the water level sinks slowly despite a considerable water depth and later sinks faster. First, we set up the equation for the container area. The wall angle on all four sides of the pyramid is 26.6° relative to vertical; the area of the base of the pyramid is that of a square. Use a pocket calculator and determine the tangent of 26.6°; it is very close to $\frac{1}{2}$ so that we will proceed with a value of 0.5. The following Figure 9.8, which you are advised to draw, clarifies the relationships:
The container wall is inclined sideways by $0.5z$, which leads to a pyramid base edge length of $2 \cdot 0.5z + b_O$. Figure 9.8 (left) depicts this. The result is a container area that is a function of z:

$$A(z) = (b_O + z)^2 \tag{9.26}$$

[B] The observant reader may have noted that the integration constant was withheld. We may of course insert constants and relate them with the limits of a specific datum. It is certainly more reasonable to choose the starting time of the emptying process, which of course means that the constant is 0 s.

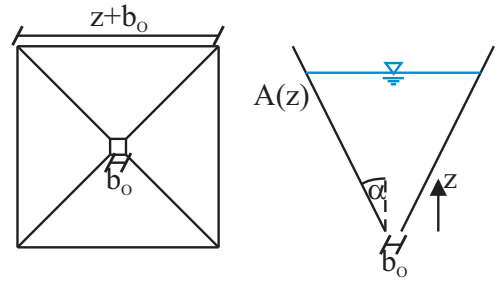

Figure 9.8: Geometric considerations concerning the outflow from an inverted pyramid.

In this case, it follows that for Equation 9.20, with $b_O = 1.0\,\text{cm}$ and $\mu = 0.9$[C]:

$$\begin{aligned} t = -\int_{z_T}^{z_B} \frac{A(z)}{Q(z)}\,\mathrm{d}z &= \frac{1}{\mu A_O\sqrt{2g}}\int_{z_B}^{z_T}\frac{(b_O+z)^2}{\sqrt{z}}\,\mathrm{d}z = \\ &= \frac{1}{0.9\times 10^{-4}\sqrt{2g}}\int_{z=0}^{z=0.48} b_O^2 z^{-\frac{1}{2}} + 2b_O z^{\frac{1}{2}} + z^{\frac{3}{2}}\,\mathrm{d}z = \\ &= 2508.5\left[2b_O z^{\frac{1}{2}} + \frac{4}{3}b_O z^{\frac{3}{2}} + \frac{2}{5}z^{\frac{5}{2}}\right]_{z=0}^{z=0.48} = 171.6\,\text{s} \end{aligned} \tag{9.27}$$

Figure 9.9: Outflow from an inverted pyramid.

By comparison, the outflow duration that was measured by means of a stopwatch is a little shorter at 162 s, which can be explained by the quite arbitrary choice of the discharge coefficient μ.
For those who still aren't tired, the show goes on. The others may feel free to skip the rest and go on to Chapter 10.

[C] In Bronstein and Semendjajew [8, page 457] we again look up the integration limits. We integrate from z_T (lower integration limit) to z_B (upper limit). In the next step, we swap the limits, which is why the minus sign is omitted.

Caution! For the mathematically experienced persons only!
Reality is even somewhat more complicated. Do you remember the derivation of the Bernoulli equation in Chapter 5.7? The local derivative $\frac{\partial u}{\partial t}$ of the Euler equation (5.24) was set to zero right at the first step. Since then, we have ignored nonstationary phenomena. If we want to do it exactly, we must consider the acceleration of the water level. This can be achieved as follows:

We integrate the local acceleration of the water level $a_l(z)$ as well as the remaining terms of the Euler equation (5.24) in the derivation of the steady-state Bernoulli equation along the streamline $\vec{s}$ (see Equation 9.28). We make an approximation and replace the streamline with the vertical coordinate z.

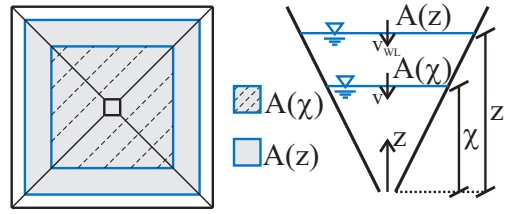

Figure 9.10: Schematic diagram for calculating the influence of the local acceleration.

At exactly the surface of the water, the very thin slice exhibits the area $A(z)$ but measures only $A(\chi)$ at its bottom during the outflow (see Figure 9.10); thereby, the water surface is accelerated [59, S. 368]. Thus, we integrate $\frac{\partial v}{\partial t}$ along the streamline of the accelerated water surface χ.

$$\int a_l(z)\,\mathrm{d}\chi = \int_{\chi=0}^{z} \frac{\partial v}{\partial t}\,\mathrm{d}\chi \tag{9.28}$$

We may express the velocity v at the bottom of the slice χ using the sinking velocity of the water level and the continuity condition:

$$v = v_{\mathrm{WL}} \cdot \frac{A(z)}{A(\chi)} \tag{9.29}$$

We substitute this expression for v in the integral of the previous equation and place that part independent of χ outside the integral. The velocity of the water level is replaced by the derivative of its position with respect to time.

$$\int a_l(z)\,\mathrm{d}\chi = A(z)\frac{\mathrm{d}v_{\mathrm{WL}}}{\mathrm{d}t}\int_{\chi=0}^{z}\frac{\mathrm{d}\chi}{A(\chi)} = A(z)\frac{\mathrm{d}^2 z}{\mathrm{d}t^2}\int_{\chi=0}^{z}\frac{\mathrm{d}\chi}{A(\chi)} \tag{9.30}$$

Let us focus on the term before the integral. Here, we rearrange the continuity condition (9.20) and write:

$$\frac{\mathrm{d}z}{\mathrm{d}t} = -\frac{Q(z)}{A(z)} = -\frac{\mu A_O\sqrt{2gz}}{(b_O+z)^2} \tag{9.31}$$

We form the second derivative of position with respect to time $\frac{\mathrm{d}^2 z}{\mathrm{d}t^2}$ by taking the derivative of Equation 9.31 first with respect to $\mathrm{d}z$ and then in turn $\mathrm{d}z$ to $\mathrm{d}t$. In the following equation, we can substitute the expression for $\frac{\mathrm{d}z}{\mathrm{d}t}$, seen in Equation 9.31.

$$\begin{aligned}\frac{\mathrm{d}^2 z}{\mathrm{d}t^2} &= \frac{\mathrm{d}}{\mathrm{d}t}\left(-\frac{Q(z)}{A(z)}\right) = \frac{\mathrm{d}}{\mathrm{d}z}\left(-\frac{Q(z)}{A(z)}\right)\frac{\mathrm{d}z}{\mathrm{d}t} \\ &= -\mu A_O\sqrt{2g}\frac{\mathrm{d}}{\mathrm{d}z}\left(\frac{\sqrt{z}}{(b_O+z)^2}\right)\cdot(-1)\,\frac{\mu A_O\sqrt{2gz}}{(b_O+z)^2}\end{aligned} \tag{9.32}$$

With

$$\frac{\mathrm{d}}{\mathrm{d}z}\frac{\sqrt{z}}{(b_O+z)^2} = \frac{\frac{1}{2}z^{-\frac{1}{2}}(b_O+z)^2 - 2(b_O+z)\sqrt{z}}{(b_O+z)^4} \tag{9.33}$$

it follows that:

$$\frac{\mathrm{d}^2 z}{\mathrm{d}t^2} = \left(\mu A_O\sqrt{2g}\right)^2\frac{\sqrt{z}}{(b_O+z)^6}\left(\frac{(b_O+z)^2}{2\sqrt{z}} - 2(b_O+z)\sqrt{z}\right) \tag{9.34}$$

All that remains is the integral of $\frac{1}{A(\chi)}$ with respect to χ.

$$\int_{\chi=0}^{z}\frac{\mathrm{d}\chi}{A(\chi)} = \int_{\chi=0}^{z}\frac{\mathrm{d}\chi}{(b_O+\chi)^2} = \left[\frac{-1}{b_O+\chi}\right]_0^z = -\frac{1}{b_O+z} + \frac{1}{b_O+0} \tag{9.35}$$

Substituting, we may write the acceleration integrated along the sinking water level from Equation 9.30 as follows:

$$\int a_l(z)\,\mathrm{d}\chi = A(z)\cdot\left(\mu A_O\sqrt{2g}\right)^2\frac{\sqrt{z}}{(b_O+z)^6}\left(\frac{(b_O+z)^2}{2\sqrt{z}} - 2(b_O+z)\sqrt{z}\right)\cdot\left(\frac{1}{b_O} - \frac{1}{b_O+z}\right) \tag{9.36}$$

The outflow in Equation 9.27 was based on the Torricelli (or the Bernoulli) equation. Its derivation yielded the terms $\frac{1}{2}v^2$, $\frac{p}{\rho}$ and gz. For an outflow $\frac{p}{\rho} = 0$ applies and gz is converted to $\frac{1}{2}v^2$. It is therefore evident to normalize the error, that arises by neglecting the local acceleration, by gz.

$$\frac{1}{gz}\int a_l(z)\,\mathrm{d}\chi = A(z)\frac{1}{gz}\cdot\left(\mu A_O\sqrt{2g}\right)^2\frac{\sqrt{z}}{(b_O+z)^6}\left(\frac{(b_O+z)^2}{2\sqrt{z}} - 2(b_O+z)\sqrt{z}\right)\cdot\left(\frac{1}{b_O} - \frac{1}{b_O+z}\right) \tag{9.37}$$

Table 9.1 lists this relative error for various z coordinates. The choice of the outflow

Table 9.1: Relative error due to neglecting the local acceleration of the outflow from the inverted pyramid.

z coordinate [m]	0.48	0.24	0.12	0.06	0.02
error	-2.01×10^{-5}	-1.47×10^{-4}	-9.93×10^{-4}	-5.73×10^{-3}	-5.00×10^{-2}

coefficient μ has a significantly greater impact. By the way, the maximum error of 5 % in the last row of the table is related to a much shorter time period than that with the container almost full (the little amount of water left flows out rapidly). We might combine the influence of the acceleration of the water surface with the outflow duration in order to determine the total duration. But even I have had enough of this topic for now.

Chapter 10
Momentum equation

10.1 Classification of the law of momentum

The law of momentum was derived in Chapter 5 by means of integration of the Cauchy equation of motion over a control volume (see Figure 5.9). The internal forces that act upon the control volume are in equilibrium with the reaction force. In the following experiments, we will find out more about the secrets of the law of momentum.

10.2 Flow forces in open channel flows

We will investigate the force conditions in an open channel with a sluice gate in an illustrative experiment.

Experiment

Force acting on a plane sluice gate

A sluice gate is mounted on a cart that is placed on an open channel in a laboratory flume. The cart is held by means of a spring balance (see Figure 10.1). When switching on the pump, the open channel is flooded, and the cart moves in the direction of flow until an equilibrium between the flow forces in the x-direction and the spring force is obtained. We make use of the free body method and mark the forces acting on the plexiglass wall of the flume (see Figure 10.2). The gravitational force acts in the vertical direction, and the channel bottom acts against it. In the horizontal direction, the pressure force, i. e. the integral of the pressure with respect to the area $\int p\,\mathrm{d}A$ and the momentum flux $\rho Q v$, are entered at the interfaces pointing into the control volume. In the horizontal direction, the resulting reaction force is the spring force F_H, which maintains the volume in the depicted shape in space.
In the experiment shown in Figure 10.1, an upstream flow depth $y_{\mathrm{left}} = 17.6\,\mathrm{cm}$, as well as the depth $y_{\mathrm{right}} = 2.0\,\mathrm{cm}$ at the smallest cross-section of the jet, were measured in the open channel of width $b = 20\,\mathrm{cm}$ at a discharge of $Q = 5.7\,\mathrm{L/s}$.

C. Rapp, *Hydraulics in Civil Engineering*,
https://doi.org/10.1007/978-3-031-54860-4_10

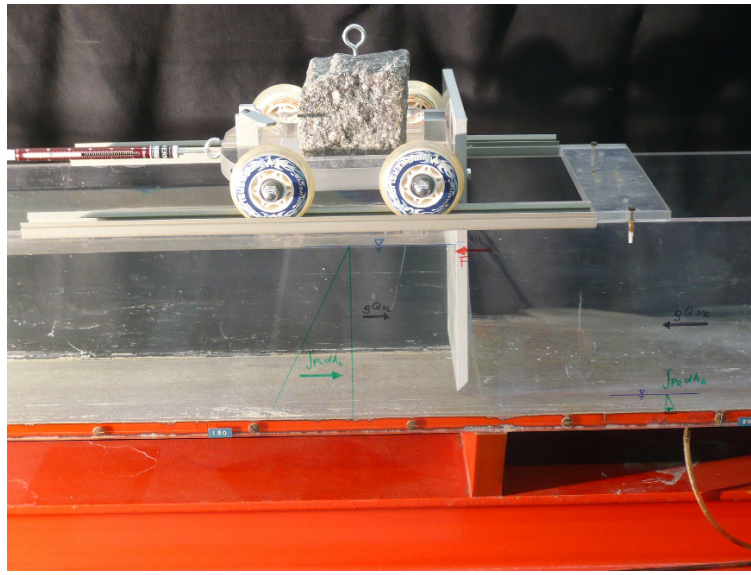

Figure 10.1: Force acting on a sluice gate.

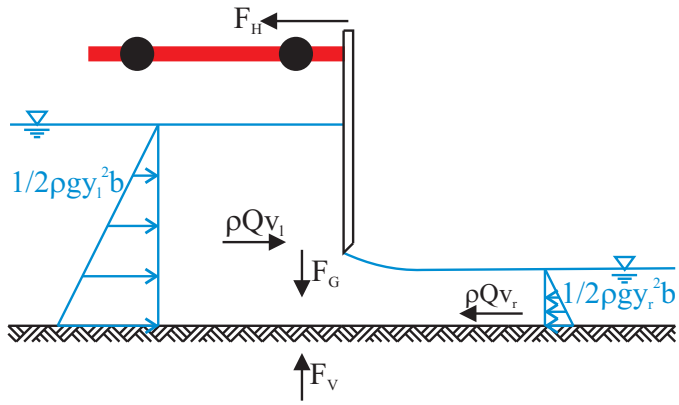

Figure 10.2: Law of momentum for determining the force acting on a sluice gate.

$$\int p_{\text{left}}\,\mathrm{d}A_{\text{left}} + \rho Q v_{\text{left}} = \int p_{\text{right}}\,\mathrm{d}A_{\text{right}} + \rho Q v_{\text{right}} + F_H \tag{10.1}$$

$$\frac{1}{2}\rho g y_{\text{left}}^2 b + \rho Q v_{\text{left}} = \frac{1}{2}\rho g y_{\text{right}}^2 b + \rho Q v_{\text{right}} + F_H \tag{10.2}$$

$$\frac{1}{2}\rho g \cdot 0.176^2 \cdot 0.2 + \rho \frac{Q^2}{0.176 \cdot 0.20} = \frac{1}{2}\rho g \cdot 0.020^2 \cdot 0.2 + \rho \frac{Q^2}{0.020 \cdot 0.20} + F_H \tag{10.3}$$

$$30.387 + 0.923 = 0.392 + 8.123 + F_H \tag{10.4}$$

This results in a horizontal force of $F_H = 22.8\,\text{N}$, whereas the spring balance indicates a force of approximately 21 N. The difference between measurement and calculation arises from the friction force of the cart and the friction associated with the flow; both forces are included in the resultant force F_H.

10.3 Fastening and flange force at a hose with nozzle

The following experiment clarifies how the flow forces are absorbed by a load-carrying structure.

Experiment

Holding force for a hose with nozzle

This experiment is a hiding place for the pitfalls of the law of momentum. One must always be extremely aware of which forces are acting, which forces conceal themselves in the resultant one and, above all, how these forces are absorbed by the surrounding structure.
Perhaps you once happened to lose your grip on a pressurised garden hose and could not catch the dancing nozzle until you finally turned off the tap. With the present experiment, we determine the holding force for the hose (see Figure 10.3). For this purpose, we open the water tap and see that the cart moves backwards until equilibrium is established between the flow forces and the measured spring force of approximately 3.0 N.

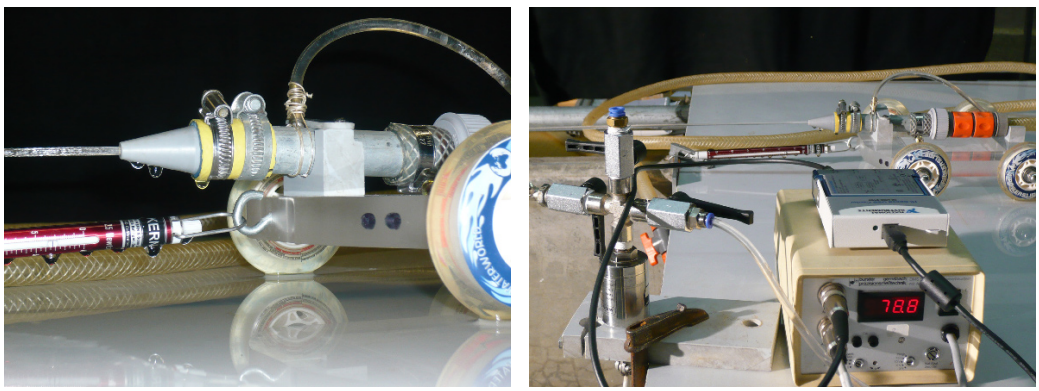

Figure 10.3: Nozzle fastened on a cart with pressure connection (left). Detail of the experimental arrangement with cart, pressure connection, pressure sensor, amplifier and display (right).

To solve the problem we would reflexively form a control volume around the nozzle and mark the pressure force and the momentum flux at the hose and the momentum flux with the velocity at the nozzle (the pressure is zero due to the ambient air downstream from the nozzle). Though the entering momentum flux $\rho Q v_{\text{hose}}$ and the pressure force $p_{\text{hose}} A_{\text{hose}}$ in the interior of the hose are counteracting the leaving momentum flux, they cannot be absorbed by the hose, transferred into the ground and released there; the force is simply passed on by the fluid. The hose is not able to absorb forces radially to its axis. You may try it out by means of a hose bent at an angle of 90°, which may be accomplished by sliding the ends against each other. We take this consideration as the basis for our free body, i. e. the control volume (see Figure 10.4).

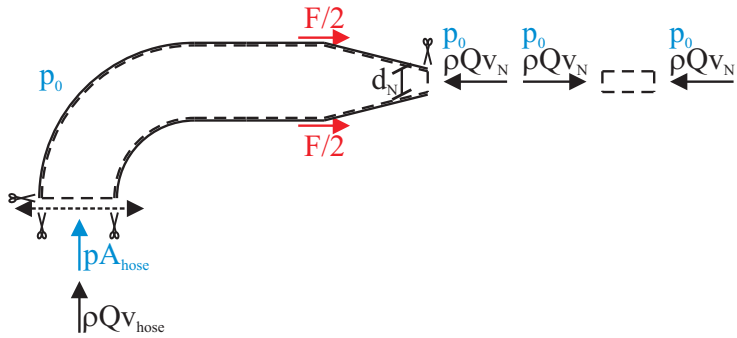

Figure 10.4: Free body of hose and nozzle.

Only the momentum flux $\rho Q v_{\text{nozzle}}$ leaving the control volume through the nozzle and the holding force of the spring balance F act along the axis of the jet. The exiting jet is also counteracted by the atmospheric pressure, however, it also acts on the hose in the opposite direction; hence, these pressure forces cancel each other out (see Figure 10.5).

Figure 10.5: Detail of the forces due to atmospheric pressure; these forces cancel each other out.

With the nozzle diameter $d_{\text{nozzle}} = 0.0035\,\text{m}$ and the measured discharge $Q = 0.17\,\text{L/s}$, the horizontal reaction force follows:

$$F_R = \frac{\rho Q^2}{A_{\text{nozzle}}} = \rho \frac{\left(0.17 \times 10^{-3}\right)^2}{\frac{\left(3.5 \times 10^{-3}\right)^2 \pi}{4}} = 3.0\,\text{N} \tag{10.5}$$

The hose must be held against the leaving momentum flux $\rho Q v_{\text{nozzle}} = 3.0\,\text{N}$, which is also evident by the volume of the free jet shown on the right in Figure 10.4. The result is confirmed by the measurement (see above). The pressure must be released via the surface area of the control volume. The pressure was measured by means of a sensor. The display in Figure 10.3 (right) indicated the pressure in percent of 2.0 bar. Accordingly, a pressure of $p_{\text{hose}} = 0.788 \cdot 2.0\,\text{bar} = 1.576 \times 10^5\,\text{N/m}^2$ was present at the moment of the recording. For the hose with a wall thickness of $w = 3.0\,\text{mm}$, a radial stress of

$$\sigma_r = \frac{p \cdot d_{\text{hose}}}{2w} = \frac{1.576 \times 10^5 \cdot 0.015}{2 \cdot 3.0 \times 10^{-3}} = 3.94 \times 10^5\,\text{N/m}^2 \tag{10.6}$$

is obtained with the so-called Barlow's formula (also see Equation 12.17). In addition, the force of gravity must be released into the ground. It corresponds to the sum of the weights of the cart ($F_{G,\text{cart}}$), the hose and the nozzle ($F_{G,\text{hose+nozzle}}$), and of the water within the hose ($\rho g V_{\text{water}}$).
In the following discussion, the force that is required to keep the fluid volume within its shape is determined.

Fastening force for a nozzle at a hose

The fastening force of the nozzle shown in Figure 10.3 at the hose is also relevant. Imagine that you hold the hose in your left hand and the nozzle in your right hand. If you try placing the nozzle on the hose from which water is flowing, you must press it firmly against the end of the hose. If you let go of the nozzle, then the water jet carries it away. To determine the fastening force, we must therefore fit the control volume such that the interface is between nozzle and hose (see Figure 10.6).

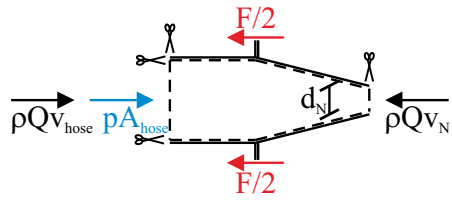

Figure 10.6: Fastening force of a nozzle on a hose.

The force with which the nozzle must be pressed against the hose corresponds to the reaction force of the flow forces. On the left, the pressure force and the momentum flux with v_{hose} act. On the right, the pressure height is zero because the atmospheric pressure prevails at the outflow. The pressure within the hose upstream from the nozzle amounts to $1.576 \times 10^5\,\text{N/m}^2$ (see above) with a hose diameter of $d_{\text{hose}} = 0.015\,\text{m}$.

$$p_{\text{hose}} A_{\text{hose}} + \rho \frac{Q^2}{A_{\text{hose}}} = \rho \frac{Q^2}{A_{\text{nozzle}}} + F \tag{10.7}$$

$$1.576 \times 10^5 \frac{0.015^2 \pi}{4} + \rho \frac{\left(0.17 \times 10^{-3}\right)^2}{\frac{0.015^2 \pi}{4}} = \rho \frac{\left(0.17 \times 10^{-3}\right)^2}{\frac{\left(3.5 \times 10^{-3}\right)^2 \pi}{4}} + F \tag{10.8}$$

$$27.85 + 0.164 = 3.00 + F \tag{10.9}$$

$$F = 25.01\,\text{N} \tag{10.10}$$

Thus, the connection between nozzle and hose must withstand at least 25 N. Here again, a radial stress of $3.94 \times 10^5\,\text{N/m}^2$ to be absorbed by the hose jacket is obtained from the Barlow's formula (see Equation 12.17).

Chapter 11
Steady pipe flow

11.1 Dynamic similarities of pipe flows

The Navier–Stokes equations (5.29 and 5.30), which are written in dimensionless form in Chapter 5.6, are essential for all flows. Flows behave similarly only if Froude and Reynolds numbers are identical. For pipe flows, the Froude number is not defined since these flows do not have free surfaces. A pipe flow is driven by the pressure gradient and the viscous forces are dominating which is why the Reynolds number is used for the comparability of such flows (see Chapter 5.6 and Equation 11.1). Generally, the Reynolds number is related to the kinematic viscosity ν, the pipe diameter d and the mean flow velocity v.

$$\mathrm{Re} = \frac{u_{\mathrm{ref}} x_{\mathrm{ref}}}{\nu} = \frac{vd}{\nu} \tag{11.1}$$

11.2 Description of laminar flows

The Navier–Stokes equations (5.29 and 5.30) may be solved exactly for some laminar flows, e. g. in straight pipelines where $\mathrm{Re} < 2300$. The so-called Couette[A]-Poiseuille[B] flow is widely described as a simple solution. We roll up our sleeves and determine the velocity profile in a plane entirely filled channel of height B that extends infinitely in the x- and y-directions. The bottom remains stationary, whereas the lid moves with velocity $u(z = B) = u_B$. We write down the Navier–Stokes equation for the x-component. Remember, we are dealing with a laminar flow.

$$\frac{\partial u}{\partial t} + u\frac{\partial u}{\partial x} + v\frac{\partial u}{\partial y} + w\frac{\partial u}{\partial z} = -\frac{1}{\rho}\frac{\partial p}{\partial x} + \nu\left(\frac{\partial^2 u}{\partial x^2} + \frac{\partial^2 u}{\partial y^2} + \frac{\partial^2 u}{\partial z^2}\right) \tag{11.2}$$

The individual terms are:

- $\frac{\partial u}{\partial t}$ local derivative of the velocity as a function of time. However, the flow is to be steady-state, i. e. it does not change with time. Therefore, the term becomes zero.

[A] Maurice Marie Alfred Couette ∗1858, Tours, France †1943, Angers, France

[B] Jean Léonard Marie Poiseuille ∗1797, Paris, France †1869, Paris, France

C. Rapp, *Hydraulics in Civil Engineering*,
https://doi.org/10.1007/978-3-031-54860-4_11

- $u\frac{\partial u}{\partial x}$: u is definitely not zero; after all, the water is to move in the x-direction. But since the channel is infinitely long in the x-direction, the velocity component will not change in this direction. $\frac{\partial u}{\partial x}$, and thus the entire term, becomes zero.
- $v\frac{\partial u}{\partial y}$: Since the plate channel is infinite in both horizontal spatial directions, the velocity gradient is $\frac{\partial u}{\partial y} = 0$; likewise, the component in the y-direction is $v = 0$.
- The term $w\frac{\partial u}{\partial z}$ also vanishes because the vertical velocity component w in the laminar steady-state flow must be equal to zero (no fluid can flow through the plates).

The left side of the equation is therefore zero.

- However, $-\frac{1}{\rho}\frac{\partial p}{\partial x}$ cannot be omitted because a pressure gradient in the x-direction must exist. How else would the fluid flow?
- If $\frac{\partial u}{\partial x} = 0$, then the second derivative $\frac{\partial^2 u}{\partial x^2}$ must also be zero.
- The above also applies to $\frac{\partial^2 u}{\partial y^2}$.
- However, it is conceivable that u, the velocity component in the x-direction, changes with respect to the channel height. The velocity at the bottom plate is zero and on top it is u_B. The second partial derivative $\frac{\partial^2 u}{\partial z^2}$ also remains. And this is a good thing since otherwise all terms except the pressure term would be zero; in that case, this pressure term would have to disappear as well in order to satisfy the equation - what would imply statics.

Thus, we may set up a significantly simplified Navier–Stokes equation for the x-direction:

$$\nu\frac{\partial^2 u}{\partial z^2} = \frac{1}{\rho}\frac{\partial p}{\partial x} \tag{11.3}$$

In order to obtain the velocity profile in the z-direction, the equation must be integrated twice with respect to z. Here we go:

$$\int\int \nu\frac{\partial^2 u}{\partial z^2}\,\mathrm{d}z\,\mathrm{d}z = \int\int \frac{1}{\rho}\frac{\partial p}{\partial x}\,\mathrm{d}z\,\mathrm{d}z \tag{11.4}$$

On the left side, the second derivative is reduced to the first derivative, and on the right side, the resulting constant is multiplied by z. In addition, the integration constant must be added. Simultaneously, we divide by ν and note that $\eta = \nu \cdot \rho$.

$$\int \frac{\partial u}{\partial z}\,\mathrm{d}z = \int \left(\frac{1}{\eta}\frac{\partial p}{\partial x}z + C_1\right)\mathrm{d}z \tag{11.5}$$

In the next integration step, the integral of z becomes $\frac{z^2}{2}$ and the integration constant from the first step C_1 is also integrated; moreover, the constant from this calculation step is included. We obtain a preliminary description of the velocity profile:

$$u(z) = \frac{1}{\eta}\frac{\partial p}{\partial x}\frac{z^2}{2} + C_1 z + C_2 \tag{11.6}$$

With the above boundary conditions, the constants may be determined. For $z = 0$, $u = 0$ since $u(z = 0) = 0$. The equation reduces to $0 = 0 + 0 + C_2$. This means that the game is over for C_2: $C_2 = 0$. C_1, however, requires more effort. We insert $u(z = B) = u_B$ into Equation 11.6:

$$u_B = \frac{1}{\eta}\frac{\partial p}{\partial x}\frac{B^2}{2} + C_1 B \tag{11.7}$$

This becomes

$$C_1 = \frac{u_B}{B} - \frac{1}{\eta}\frac{\partial p}{\partial x}\frac{B}{2} \tag{11.8}$$

which again, inserted into 11.6, results in:

$$u(z) = \frac{1}{\eta}\frac{\partial p}{\partial x}\frac{z^2}{2} + \frac{u_B}{B}z - \frac{1}{\eta}\frac{\partial p}{\partial x}\frac{B}{2}z = \frac{u_B}{B}z + \frac{1}{\eta}\frac{\partial p}{\partial x}\frac{z}{2}(z-B) \tag{11.9}$$

Thus, we obtain a parabolic velocity profile for the channel. Let's find out what this means.

Type the lines below into an editor and save the file with the extension .m in a directory of your choice. You may ignore the comments after the % sign.

```
eta=1e-3; % [kg/(ms)]
resolution=1000; % number of calculation points
B=input(Enter the width of channel B: '); % [m]
dpdx=input(Enter the pressure gradient dp/dx: '); % [N/m3]
uB=input(Enter the velocity of the upper plate: '); % [m/s]
z=(0:B/resolution:B)'; % defines the nodes where u is to be calcu-
lated
u=uB/B.*z+1/eta*dpdx.*z/2.*(z-B); % solution of the equation for
the individual z values
plot(u,z) % draw function u(z)
print('velocityProfile.png','-dpng') % save the figure in the
present directory as .png
```

With `cd` in the Octave command line, go into the directory with the saved file (e. g. `cd D:\octave`). The file may be executed when entering the filename (without .m) into the command line and confirming it by pressing Enter. You are asked to enter the values for B, $\frac{\partial p}{\partial x}$ and u_B. Octave then computes and draws the velocity profile over the channel height. If you experiment with various parameters, you will certainly note that the flow direction is opposite the pressure gradient. This is comprehensible because only if the pressure on the left is higher than it is on the right, then the water flows to the right. The pressure gradient is negative from left to right because the pressure decreases in that direction.

For $\frac{\partial p}{\partial x} = 0$, a linear velocity profile of a so-called Couette flow results from any given u_B. With $u_B = 0$, the so-called Poiseuille flow results for a random pressure gradient whose maximum velocity is obtained by taking the derivative of Equation 11.9 with respect to z and setting it to zero:

$$\frac{\mathrm{d}u(z)}{\mathrm{d}z} = \frac{1}{\mathrm{d}z}\left(\frac{1}{2\eta}\frac{\partial p}{\partial x}z(z-B)\right) \stackrel{!}{=} 0 \tag{11.10}$$

The product rule leads to:

$$\frac{1}{2\eta}\frac{\partial p}{\partial x}(z-B) + \frac{1}{2\eta}\frac{\partial p}{\partial x}z = \frac{1}{2\eta}\frac{\partial p}{\partial x}(2z-B) \stackrel{!}{=} 0 \tag{11.11}$$

It can be clearly seen from $2z - B = 0$ that the coordinate corresponding to the maximum velocity is $z = \frac{B}{2}$. With $z = \frac{B}{2}$ inserted into Equation 11.9, the maximum velocity of a Poiseuille flow is finally obtained:

$$u_{\max} = \frac{1}{2\eta}\frac{\partial p}{\partial x}\frac{B}{2}\left(\frac{B}{2} - B\right) = -\frac{1}{8\eta}\frac{\partial p}{\partial x}B^2 \tag{11.12}$$

The mean cross-sectional velocity $\bar{u}$ of a Poiseuille flow (noting that $u_B = 0$) is obtained by the integration of Equation 11.9 with respect to the channel height and the division by B:

$$\begin{aligned}\bar{u} &= \frac{1}{B}\int u(z)\,\mathrm{d}z = \frac{1}{B}\int_0^B \frac{1}{2\eta}\frac{\partial p}{\partial x}\left(z^2 - Bz\right)\mathrm{d}z = \frac{1}{2B\eta}\frac{\partial p}{\partial x}\int_0^B \left(z^2 - Bz\right)\mathrm{d}z \\ &= \frac{1}{2B\eta}\frac{\partial p}{\partial x}\left[\frac{z^3}{3} - \frac{Bz^2}{2}\right]_0^B + C\end{aligned} \tag{11.13}$$

With $C = 0$, it follows that $\frac{\partial p}{\partial x} = 0$, since otherwise water would flow without a driving force. We obtain:

$$\bar{u} = \frac{1}{2B\eta}\frac{\partial p}{\partial x}\left[\frac{z^3}{3} - \frac{Bz^2}{2}\right]_0^B = \frac{1}{2B\eta}\frac{\partial p}{\partial x}\left[\frac{2B^3}{6} - \frac{3B^3}{6}\right] = -\frac{1}{12\eta}\frac{\partial p}{\partial x}B^2 \tag{11.14}$$

Thus, the mean velocity corresponds to $\bar{u} = \frac{2}{3}u_{\max}$.

11.3 Wall shear stress in pipe flows

In Chapter 5.7, the Bernoulli equation was derived from the Euler equation, which does not contain terms that account for friction. The strength of the Bernoulli equation is evident in that numerous tasks may be solved by simple means via these clear relationships. The Bernoulli equation brings structure to complex fluid-mechanical problems. However, there is no such thing as loss-free flow, and there are very few cases in which friction may be neglected.

The following elaborations are based on the idea that energy losses must be accounted for by another descriptive formula. Thereby, the Bernoulli equation "shrivels" to summing up the energies at various cross-sections of the flow. The introduction of the head loss term $\Delta e = J_E \cdot L$ is connected to the names of Darcy[C] and Weisbach[D]. Therein J_E is the slope of the energy grade line and L the flow distance (see Figure 11.1). For now, we write a relationship between slope of the energy grade line and velocity head and introduce the friction coefficient f_{D}. The explanation will become apparent in the following pages.

$$J_E = \frac{f_{\mathrm{D}}}{D}\frac{u^2}{2g} \tag{11.15}$$

Generally speaking, energy is dissipated in flow direction between two cross-sections, i. e. flow-mechanical energy is converted into heat Δe (see Figure 11.1).

[C] Henry Darcy, ∗1803, Dijon, France †1858, Paris, France

[D] Julius Ludwig Weisbach, ∗1806, Mittelschmiedeberg, Germany †1871, Freiberg, Germany

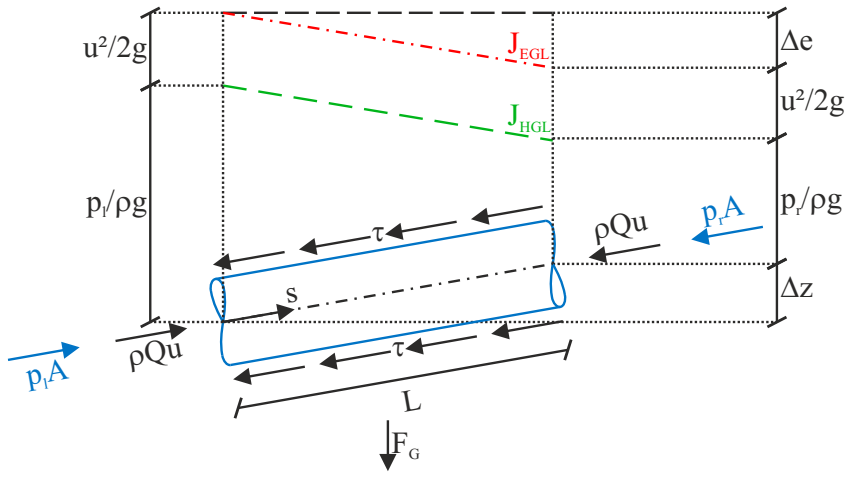

Figure 11.1: Pipe flow considering losses.

We describe the gradient (∇) of the piezometric pressure height (see also Chapter 5.7) along the coordinate s with the slope of the energy grade line J_E[E]:

$$\nabla \frac{p_{\text{piezometric}}}{\rho g} = -J_E = \frac{1}{\rho g}\frac{\mathrm{d}p}{\mathrm{d}s} + \frac{\mathrm{d}z}{\mathrm{d}s} \tag{11.16}$$

The gradient of the piezometric pressure height comprises the variations of pressure and geodetic height. Since the pipe cross-section remains constant, the variation of the velocity height need not be included in the equation. The energy loss Δe is obtained later via multiplication of the slope of the energy grade line by the corresponding flow distance L. Figure 11.1 already indicates the law of momentum. In a pipe with constant diameter, the momentum fluxes on both sides have the same magnitude and are mutually opposed; hence, they cancel each other out. The force balance reads:

$$\rho Qu + \int p\,\mathrm{d}A = \rho Qu + \int \left(p + \frac{\mathrm{d}p}{\mathrm{d}s}\,\mathrm{d}s\right)\mathrm{d}A + \int \rho g \frac{\mathrm{d}z}{\mathrm{d}s}\,\mathrm{d}s\,\mathrm{d}A + \int \tau_W\,\mathrm{d}A_{\text{lateral area}} \tag{11.17}$$

All that remains is the change of the pressure along the flow distance $\mathrm{d}s$. When we set the averaged values over the cross-section $A_{\text{pipe}} = R^2\pi$, or over the lateral area $A_{\text{lateral area}} = 2R\pi\,\mathrm{d}s$, the result is:

$$0 = \frac{\mathrm{d}p}{\mathrm{d}s}\,\mathrm{d}s R^2\pi + \rho g R^2 \pi\,\mathrm{d}s \frac{\mathrm{d}z}{\mathrm{d}s} + \tau_W 2R\pi\,\mathrm{d}s \tag{11.18}$$

In the next step, we divide by $\mathrm{d}s$ and the force balance is written at the differential element:

$$0 = \frac{\mathrm{d}p}{\mathrm{d}s} R^2\pi + \rho g R^2 \pi \frac{\mathrm{d}z}{\mathrm{d}s} + \tau_W 2R\pi \tag{11.19}$$

Now we solve for the wall shear stress τ_W and factor out the area.

$$\tau_W = -\frac{R^2\pi}{2R\pi}\left(\frac{\mathrm{d}p}{\mathrm{d}s} + \rho g \frac{\mathrm{d}z}{\mathrm{d}s}\right) = -\frac{R}{2}\left(\frac{\mathrm{d}p}{\mathrm{d}s} + \rho g \frac{\mathrm{d}z}{\mathrm{d}s}\right) \tag{11.20}$$

[E] The coordinate z points upwards. Therefore, the direction of the slope of the energy grade line is opposite to that of a positive gradient of the geodetic height.

Equation 11.20 may be simplified still further with the Expression 11.16:

$$\tau_W = \rho g \frac{R}{2} J_E \tag{11.21}$$

For now, we have merely established a relation between wall shear stress and slope of the energy grade line. This can be summarised using Formula 11.15 and the substitution $D = 2R$:

$$\tau_W = \rho g \frac{R}{2} \frac{f_D}{D} \frac{u^2}{2g} = \rho g \frac{D}{4} \frac{f_D}{D} \frac{u^2}{2g} = \rho \frac{f_D}{8} u^2 \tag{11.22}$$

11.4 Hydraulic losses of laminar flows

Fundamental differences between laminar and turbulent flows were dealt with in Chapter 6. Newtonian fluids such as water are characterised by the linear relation between velocity gradient and shear stress (see Chapter 3.4.11). This material characteristic has already been included in the Navier–Stokes equation (5.29) with the constitutive equation (5.21). The coefficient that establishes the linear relation between τ and $\frac{\partial u}{\partial n}$ is the so-called dynamic viscosity η. According to Equation 3.17, the following applies to the coordinate direction n, which faces perpendicularly away from the wall:

$$\tau = \eta \frac{\partial u}{\partial n} \tag{11.23}$$

If the radial coordinate r with the origin in the pipe centre is introduced, the Newton's shear stress approach with the direction of r opposite n reads as follows:

$$\tau = -\eta \frac{\partial u}{\partial r} \tag{11.24}$$

This relation is inserted into Equation 11.21, which describes the wall shear stress with $r = R$, so that we obtain:

$$\frac{\partial u}{\partial r} = -\frac{\rho g}{2\eta} r J_E \tag{11.25}$$

Next, we integrate Equation 11.25 with respect to r in order to arrive at the velocity distribution $u(r)$:

$$\int \frac{\partial u}{\partial r} \mathrm{d}r = \int -\frac{\rho g}{2\eta} r J_E \, \mathrm{d}r \tag{11.26}$$

For the velocity component u in the main flow direction, which is dependent on the radial coordinate r, we obtain:

$$u(r) = -\frac{\rho g}{2\eta} \frac{r^2}{2} J_E + C \tag{11.27}$$

At the wall, the no-slip condition applies, i. e. $u(r = R) = 0$; in this way, the integration constant may be determined:

$$C = \frac{\rho g}{2\eta} \frac{R^2}{2} J_E \tag{11.28}$$

Inserted into Equation 11.27, the velocity distribution within the pipe becomes:

$$u(r) = \frac{\rho g}{4\eta}\left(R^2 - r^2\right) J_E \tag{11.29}$$

Expressing the kinematic viscosity as the quotient of dynamic viscosity and density, i. e. $\nu = \frac{\eta}{\rho}$, and substituting this into Equation 11.29, the maximum velocity in the cross-section centre ($r = 0$) is calculated as:

$$u_{\max} = \frac{g}{4\nu} R^2 J_E \tag{11.30}$$

In order to obtain the mean velocity, the velocity distribution must be integrated over the cross-section and divided by the cross-sectional area. Here, the Jacobian factor r (see Equation 7.58) must not be forgotten.

$$\begin{aligned}
\bar{u} &= \frac{1}{R^2\pi}\int_0^{2\pi}\int_0^R u(r) r \,\mathrm{d}r\,\mathrm{d}\phi = \frac{1}{R^2\pi}\int_0^{2\pi}\int_0^R \frac{\rho g}{4\eta}\left(R^2 - r^2\right) J_E r \,\mathrm{d}r\,\mathrm{d}\phi \\
&= \frac{1}{R^2\pi}\frac{g J_E}{4\nu} 2\pi \int_0^R \left(R^2 r - r^3\right)\mathrm{d}r = \frac{1}{R^2}\frac{g J_E}{2\nu}\left[\frac{R^2 r^2}{2} - \frac{r^4}{4}\right]_0^R \\
&= \frac{1}{R^2}\frac{g J_E}{2\nu}\left[\left(\frac{R^2 R^2}{2} - \frac{R^4}{4}\right) - 0\right] = \frac{1}{R^2}\frac{g J_E}{2\nu}\frac{R^4}{4} = \frac{g J_E}{8\nu} R^2
\end{aligned} \tag{11.31}$$

If we solve for J_E and insert the derived relation into the so-called Darcy-Weisbach equation (11.15), we thereby obtain with the mean flow velocity $u = \bar{u}$:

$$\frac{u 8\nu}{g R^2} = \frac{f_{\mathrm{D}}}{D}\frac{u^2}{2g} \tag{11.32}$$

Rearranging for f_{D} yields:

$$f_{\mathrm{D}} = \frac{u 8\nu\,(2g)\,(2R)}{g R^2 u^2} = \frac{32\nu}{Ru} = \frac{64\nu}{Du} \tag{11.33}$$

And finally, substituting the expression for the Reynolds number $\mathrm{Re} = \frac{uD}{\nu}$:

$$f_{\mathrm{D}} = \frac{64}{\mathrm{Re}} \tag{11.34}$$

The friction coefficient f_{D} and the velocity profile of a laminar pipe flow may be derived directly by considering the forces involved.

11.5 Hydraulic losses of turbulent flows

Due to the chaotic properties of turbulent flows (see Chapter 6), the derivation of f_{D} via the linear relation of the wall-normal velocity gradient and shear stress is not possible. Because of velocity fluctuations, stresses also occur within the flow, which, when time-averaged, are referred to as Reynolds stresses. When including these stresses in the law of momentum, a formulation for f_{D} may be set up via what is known as Prandtl's[F] mixing

[F] Ludwig Prandtl, ∗1875, Freising, Germany, †1953, Göttingen, Germany

length approach and the logarithmic law of the wall. For the interested reader, reference is made here to Appendix A.3, though we use the equations ultimately defined by Prandtl and his assistant Nikuradse[G]. We refer to Figure 11.1, which shows the head loss Δe. As depicted therein, we write the terms as a balance between the energy heights on both sides of the equation since the "lengths" on the right and left sides are equal.

$$z_l + \frac{p_l}{\rho g} + \frac{v_l^2}{2g} = z_r + \frac{p_r}{\rho g} + \frac{v_r^2}{2g} + \Delta e \tag{11.35}$$

With $v_l = v_r$, we solve for Δe:

$$\Delta e = z_l - z_r + \frac{p_l}{\rho g} - \frac{p_r}{\rho g} = -\Delta\left(\frac{p}{\rho g} + z\right) \tag{11.36}$$

With a flow through a pipe that has a constant cross-sectional area, the head loss Δe corresponds to the difference between the piezometric pressure heights $-\Delta\left(\frac{p}{\rho g} + z\right)$. As in Chapter 11.4, we express Δe according to Darcy-Weisbach with the friction coefficient f_{D}.

$$\Delta e = \frac{f_{\mathrm{D}} L}{D} \frac{u^2}{2g} \tag{11.37}$$

Measurements have shown that, due to the turbulent fluctuations normal to the flow direction, the velocity profile of a turbulent flow is much wider than in a laminar flow (see also in particular Appendix A.3). Fast fluid goes further toward the wall, which is why the wall itself and the description of the flow at the wall gain importance (see Figure 11.2).

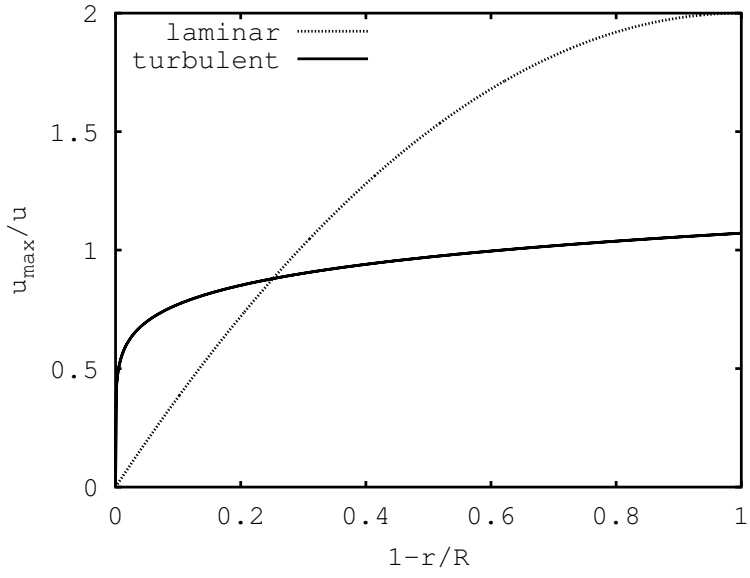

Figure 11.2: Velocity profile of laminar and turbulent (the latter time-averaged) flows, each at mean velocity $\bar{u} = 1$.

[G] Johann Nikuradse, ∗1894, Samtredia, Georgia †1979, Göttingen, Germany

Experiments have shown that a viscous sublayer, as it is called, forms directly on the wall. Figure 11.3 illustrates the context. This viscous sublayer forms a kind of a sliding

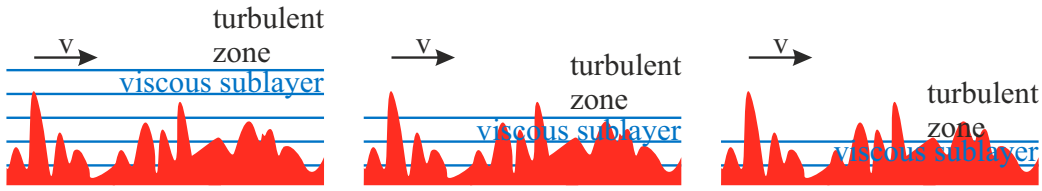

Figure 11.3: Microscopic view of a flow in proximity to the wall. Hydraulically smooth wall on the left, transition region in the middle and rough wall on the right.

surface for the turbulent flow; here, the gaps (possibly microscopically small) between the uneven spots are filled. It is therefore essential to determine, whether or not the velocity fluctuations of the turbulent core zone reach the uneven spots of the wall. In the measurements, the relationship between friction coefficient f_D and relative roughness r_s (determined by the quotient $r_s = \frac{k_s}{D}$), was empirically determined by adhering sand grains of different sizes k_s onto smooth pipe walls[H].

In our thought experiment for turbulence (see Chapter 6), this would mean that people fill the boundary area of the pedestrian zone (with the open doors of the department stores) while they make virtually no progress (see Figure 11.3, left). There is hardly any possibility of changing from one layer to the other. Those in the "turbulent core zone" will not be bothered by the store doors if the thickness of this viscous layer exceeds the projections. We're talking about the smooth wall; here, the friction in the entire cross section is largely dependent on the viscous behaviour close to the wall. The thickness of this viscous layer is determined by the degree of turbulence, i. e. the Reynolds number, since it influences how closely the fluctuations normal to the wall actually approach the wall. You may imagine that the greater the turmoil, the more the people in the turbulent core zone are pushed to the boundary. Therefore, the friction coefficient for smooth walls may be described on the basis of the research by Prandtl and Nikuradse[I].

$$\frac{1}{\sqrt{f_D}} = -2\log\left(\frac{2.5}{\mathrm{Re}\sqrt{f_D}}\right) \tag{11.38}$$

If the viscous layer of people proceeding only at a snail's pace at the boundary of the flow were so thin that even fast runners at the boundary of the turbulent core zone bump against the uneven spots of the wall again and again, we are dealing with a rough boundary (see Figure 11.3, right). The viscosity or the viscous sublayer plays only a minor role. In a flow with a rough boundary, friction is dependent only on the predominant roughness relative to the cross-section[J].

$$\frac{1}{\sqrt{f_D}} = -2\log\left(\frac{k_s}{3.7D}\right) \tag{11.39}$$

[H] The regularity of the uneven spots of the pipe wall has an impact on the resistance behaviour of the flow. In the description of the natural roughness, we still refer to the equivalent sand grain roughness k_s contrary to the actual measurable roughness k. We're not distinguishing further and deal with the equivalent sand grain roughness k_s in the following discussion.

[I] Please see Appendix A.3 for a detailed derivation.

[J] For the derivation, please refer to the Appendix A.3.

Colebrook[K] proposed to introduce a transition region which is pertinent for the most technically relevant flows (see Figure 11.3, centre). Here, both viscosity and roughness influence pipe friction:

$$\frac{1}{\sqrt{f_\mathrm{D}}} = -2\log\left(\frac{2.5}{\mathrm{Re}\sqrt{f_\mathrm{D}}} + \frac{k_s}{3.7D}\right) \tag{11.40}$$

Please note that no explicit solution for f_D is possible in Equations 11.38 and 11.40 and that you must solve them iteratively[L]. The instructions for finding the friction coefficient f_D step-by-step are given in Figure 11.4[M]. The provided code first solves the equation for the transition region and then, if there are hydraulically smooth or rough walls, skips to the associated Equations 11.38 and 11.39. These equations may be applied to arbitrary cross-sections via the introduction of the hydraulic radius, the quotient of area and wetted perimeter.

$$R_\mathrm{hy} = \frac{A}{P} = \frac{D^2\pi}{4D\pi} = \frac{D}{4} \tag{11.41}$$

Figure 11.4 shows the Prandtl–Colebrook algorithm, i. e. the procedure for calculating the friction coefficient according to the above Formulas 11.38 to 11.40. Figure 11.5 shows a simplified Moody diagram to illustrate the relationship between f_D and the Reynolds number Re.

Apart from the derivations, everything in the current discussion relates to the one-dimensional approach; therefore, we will identify the cross-sectional velocity by v.

Example

Calculation of friction coefficients

We switch on the pocket calculator to determine the friction coefficient f_D and the slope of the energy grade line $J_E = \frac{f_\mathrm{D}}{D}\frac{v^2}{2g}$ for four different outflow and pipe configurations. The kinematic viscosity for the various temperatures has already been taken from Table 3.2.

	D [m]	k_s [m]	Q [m^3/s]	T [°C] $\Rightarrow$ ν [m^2/s]
1	0.10	1.0×10^{-6}	5.0×10^{-5}	$10 \Rightarrow 1.3081\times10^{-6}$
2	2.0	1.0×10^{-5}	0.60	$10 \Rightarrow 1.3081\times10^{-6}$
3	1.2	5.0×10^{-4}	1.2	$20 \Rightarrow 1.0068\times10^{-6}$
4	1.2	5.0×10^{-3}	1.2	$20 \Rightarrow 1.0068\times10^{-6}$

In Equations 11.38 and 11.40, f_D occurs both on the left and on the right side of the equals sign. In the initial step 0, we set $f_{\mathrm{D}0} = 0.02$ on the right side and thus obtain f_D

[K] Cyril Frank Colebrook, ∗1910, Swansea, Wales, †1997, Worthing, England

[L] In many standard works, all of which were written long ago, this approach was deemed excessively labor-intensive. Nowadays, every reader of this book has a mobile with a processor that is more powerful than the control chips on the Apollo missions. We therefore do not accept excuses for "more fit for use" formulas.

[M] The open source library also contains, of course, a routine from which the friction coefficient f_D for any parameters may be determined.

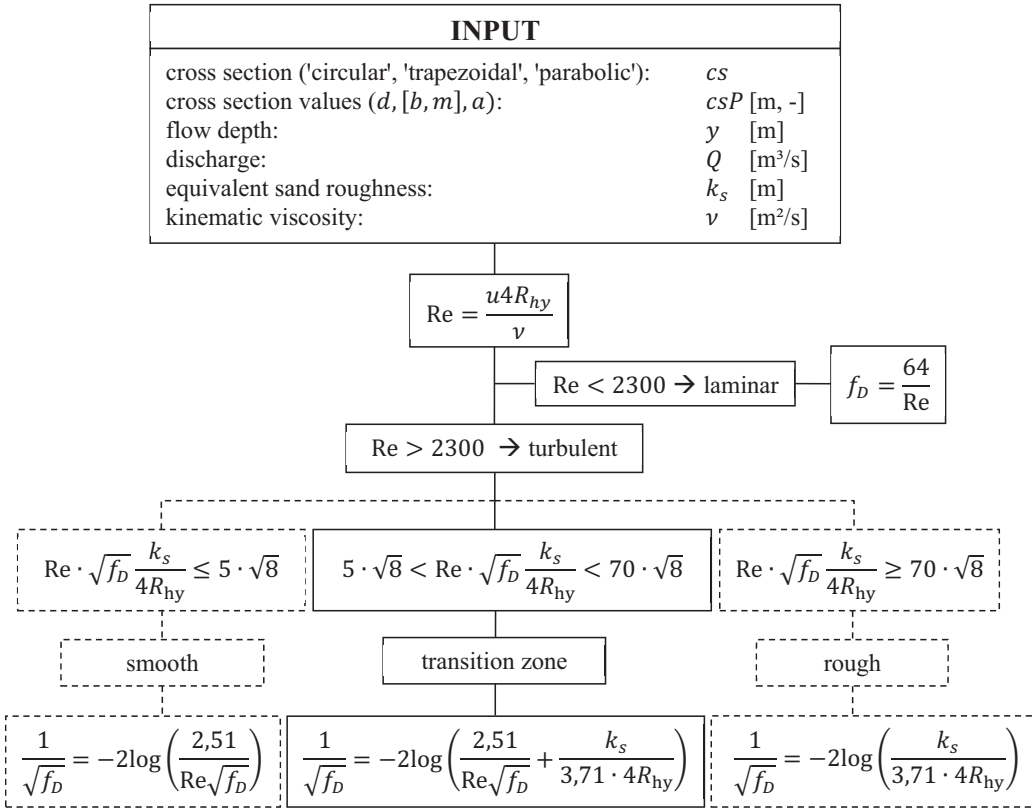

Figure 11.4: Prandtl–Colebrook algorithm for calculating the friction coefficient f_{D}.

on the left side. In the next iterative step, we insert it on the right side and obtain a new result for $f_{\mathrm{D,left}}$, which is inserted on the right until $f_{\mathrm{D,left}} \approx f_{\mathrm{D,right}}$. By processing the individual steps of Figure 11.4, we arrive at the following (intermediate) results:

	Re	f_{D1}	f_{D2}	f_{D3}	comment	J_E
1	487	0.1315	no iteration necessary (laminar)			2.714×10^{-6}
2	2.920×10^5	0.014 12	0.014 64	0.014 58	smooth → 0.014 54	1.352×10^{-5}
3	1.265×10^6	0.016 45	0.016 49	0.016 49		7.885×10^{-4}
4	1.265×10^6	0.028 84	0.028 82	0.028 82	rough → 0.028 74	1.374×10^{-3}

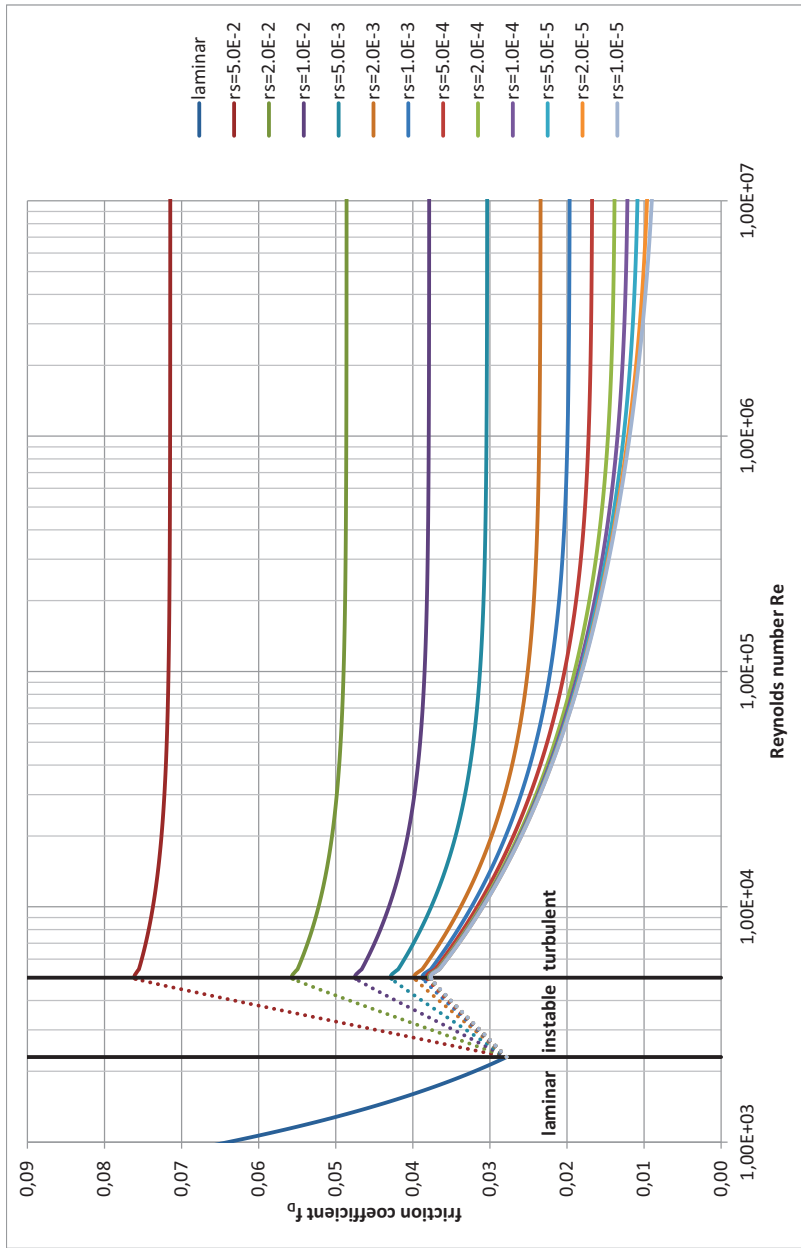

Figure 11.5: Moody diagram – illustration of the relationship between f_{D} and Reynolds number Re.

Example

Free outflow at the end of a pipeline

The purpose of this task is to practice the procedure for determining the discharge in a pipeline system. The following dimensions are given:

$h = 5.0\,\mathrm{m}$	$L = 2500\,\mathrm{m}$	$d = 1.5\,\mathrm{m}$	$k_s = 0.2\,\mathrm{mm}$	$T = 20\,^{\circ}\mathrm{C}$

Figure 11.6 shows a large container with a pipeline that ends with a free outflow. Think about the boundary conditions for the energy diagram. Those who are up to it may sketch it themselves; those who are less sure may follow the descriptions, step-by-step, in Figure 11.7.

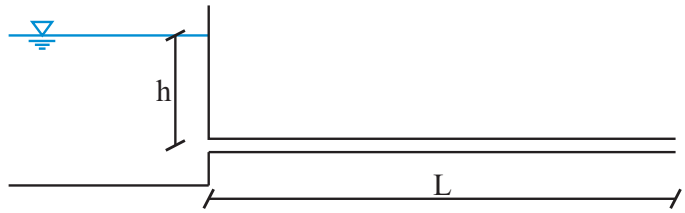

Figure 11.6: Example of pipe flow.

1. The water level in the container indicates the piezometric pressure height; in the container, $v \approx 0 \rightarrow \frac{v^2}{2g} \approx 0$, which is why hydraulic and energy grade line are to be drawn at the water level.
2. We also know the piezometric pressure height at the outflow; it lies in the pipe axis. It's the same as in Figure 8.5. Preferably, we place a small green dot there.
3. At the free end of the pipe, the water has the same velocity as in the middle, which results from the continuity condition. It is mandatory to draw the energy grade line at the end by $\frac{v^2}{2g}$ above the hydraulic grade line.
4. The energy grade line may be connected from there to the energy grade line at the water level of the container since only pipe friction losses occur and the slope of the energy grade line is unchanged.
5. Since $\frac{v^2}{2g}$ is constant throughout the entire pipe, the distance between hydraulic and energy grade line also remains constant. We may therefore draw the hydraulic grade line in parallel with the energy grade line from the pipe's end to the container and enter the individual quantities.
6. At the container, the hydraulic grade line drops downward by $\frac{v^2}{2g}$. A portion of the piezometric pressure energy is converted to kinetic energy, allowing the water to flow.
7. By marking the hydraulic losses Δe at the end of the pipe, the energy diagram is completed.

The energy balance may quite easily be established with the energy diagram from Figure 11.7. The sum of the quantities on the left side of the system (with index l) is identical to the sum of the quantities on the right side (index r).

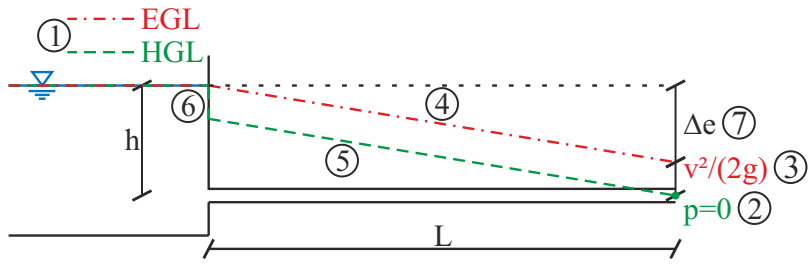

Figure 11.7: Energy diagram for the pipe flow example.

$$z_l + \frac{p_l}{\rho g} + \frac{v_l^2}{2g} = z_r + \frac{p_r}{\rho g} + \frac{v_r^2}{2g} + \Delta e \tag{11.42}$$

With the inserted quantities and $\Delta e = \frac{f_D \cdot L}{d} \frac{v^2}{2g}$, it follows that:

$$5.0 = \frac{v_r^2}{2g} + \frac{f_D \cdot 2500}{1.5} \frac{v_r^2}{2g} \tag{11.43}$$

The equation includes two unknowns; we cannot solve for them directly because we need the velocity v for the Prandtl–Colebrook algorithm. But we will succeed! We estimate $f_D = 0.02$ and calculate a first approximate value for v_r. The equation

$$5.0 = \frac{v_r^2}{2g} \left(1 + \frac{0.02 \cdot 2500}{1.5}\right) \tag{11.44}$$

yields $v_r = 1.69\,\mathrm{m/s}$ and hence $Q = 0.75^2 \cdot \pi \cdot v_r = 2.987\,\mathrm{m^3/s}$. With $d = 1.5\,\mathrm{m}$, $Q = 2.987\,\mathrm{m^3/s}$, $k_s = 2 \times 10^{-4}\,\mathrm{m}$ and $\nu = 1.01 \times 10^{-6}\,\mathrm{m^2/s}$, we obtain $f_D = 0.0132$ at $\mathrm{Re} = 2.52 \times 10^6$ and $\frac{k_s}{d} = 1.33 \times 10^{-4}$ with the equation for the transition region.
Well, the estimate wasn't that bad, but this f_D will certainly yield a quite different flow velocity. We therefore insert the newly obtained f_D into the energy equation.

$$5.0 = \frac{v_r^2}{2g} \left(1 + \frac{0.0132 \cdot 2500}{1.5}\right) \tag{11.45}$$

This results in $v_r = 2.064\,\mathrm{m/s}$, and therefore $Q = 3.648\,\mathrm{m^3/s}$. Well, we have no choice but to completely reprocess the algorithm with this newly found discharge value. We start again at the very top in Figure 11.4 with the same input quantities but with $Q = 3.648\,\mathrm{m^3/s}$.
With the Reynolds number $\mathrm{Re} = 3.08 \times 10^6$ and the equation for the transition region, we obtain $f_D = 0.013\,12$ and $Q = 3.660\,\mathrm{m^3/s}$. In the end, the value for the friction coefficient will converge to $f_D = 0.013\,11$, which confirms the value of f_D obtained above, and the discharge value of $Q = 3.662\,\mathrm{m^3/s}$ subsequently calculated with sufficient accuracy. Those who already feel confident enough may elegantly solve this problem by means of Octave.

Open an editor and create the file `pipe.m` in the directory `D:\myData\OctaveDirectory` where the downloaded calculation routines are saved. The file is to contain the following code:

```
function f=pipe(Q,qs,qsP,y,l,ks,sumK,g,T,dH)
f = -dH+Q^2/(flowArea(qs,qsP,y)^2*2*g)*(sumK+pc(qs,qsP,y,Q,ks,T)*...
l/(4*flowArea(qs,qsP,y)/perimeter(qs,qsP,y)));
endfunction
```

Save the file; the lines mean:

```
The function 'pipe', which must be saved in the directory under
the same name with the extension .m by which it is called, is
dependent on the variables and constants that follow within the
brackets.
Now you recognise the energy equation set equal to 0, which in
turn refers to the provided functions for flow area and perimeter
as well as for the Prandtl-Colebrook algorithm. It is described as
f=, identical with the definition in the first line.
The three dots ... mean that the command is continued on the fol-
lowing line.
endfunction terminates the function.
```

Now type the following commands into the command line of Octave.

```
1> cd D:\myData\OctaveDirectory
2> [Q,fval,info] = ...
> fsolve(@(Q)pipe(Q,'circle',1.5,1.5,2500,2e-4,1,9.81,20,5),3);
```

Explanations of the individual lines `n>`

```
1> % cd means change directory; we change to the directory where
files pipe.m, flowArea.m, perimeter.m and pc.m are saved.
2> % [Q,fval,info] are the output values of the function. The re-
sult is saved in the variable Q.
2> % with fsolve(@(Q)pipe(Q,... the function pipe.m, with variable
Q and the constants that follow, is called. The '3' at the very
end of the command is our assumption for the result, or the start-
ing value of Octave, toward finding the solution.
2> % fval is the actual result of the equation that we had set to
0. For fval, we obtain a very small value (<1E-7).
2> % info indicates how the result was achieved (e. g. 1: con-
verged solution, 0: maximum number of iterations reached, -3: the
confidence interval of the solution is extremely small.)
```

11.6 Minor (local) hydraulic losses

The friction coefficient described above reflects hydraulic losses that occur along pipes. Both in the theoretical derivations in Chapter A.3 and in the underlying physical experiments, a fully developed flow is assumed. This means that no changes in flow direction occur. In a turbulent flow, this happens with a flow distance of approximately $20d$ where d is the pipe diameter.
In practice, extremely few pipelines extend out dead straight; installations such as bends, valves or changes in cross-section are found extensively. This chapter covers these locally limited effects on the hydraulic losses which, due to their squared dependence on kinetic energy, are also related to the velocity height. The individual values will not be listed here. They may be taken from the pertinent tables such as [52, 4, 62] and the technical guidelines of the various associations (IAHR, IWA, etc.). Illustrative sketches associated with the following minor (local) losses may be found in Figure 11.8.

Inflow loss

As already shown in Figure 9.2, the boundary streamline affects the inflow into a pipe. Due to the flow constriction at the start of the pipe, the fluid must be accelerated to a higher velocity than v; the constriction causes recirculation at the wall, which brings about further losses. Only after approximately 20 diameters, the flow is fully developed and the loss may adequately be described via the friction coefficient f_{D}. The energy height that was dissipated up to this point is represented by Δe_I and the dimensionless loss coefficient by K_I.

Outflow loss

With the continuity condition, one may easily deduce that the fluid at the end of a pipeline is still flowing, while $v \to 0$ in the container with a much larger cross-section. Because of the turbulence during mixing in the receiving container, the hydraulic energy is completely dissipated; hence K_O is always set to one. A smaller value may be used in exceptional cases only in very small intermediate containers. But this loss coefficient is essential for the free outflow, too, because at the end of the pipe the kinetic energy still exists; it then dissipates in the free jet.

Bend loss

In flow deflection, losses occur in addition to pipe friction, which are described by coefficient K_B. K_B is dependent not only on the deflection angle but also on the radius of curvature.

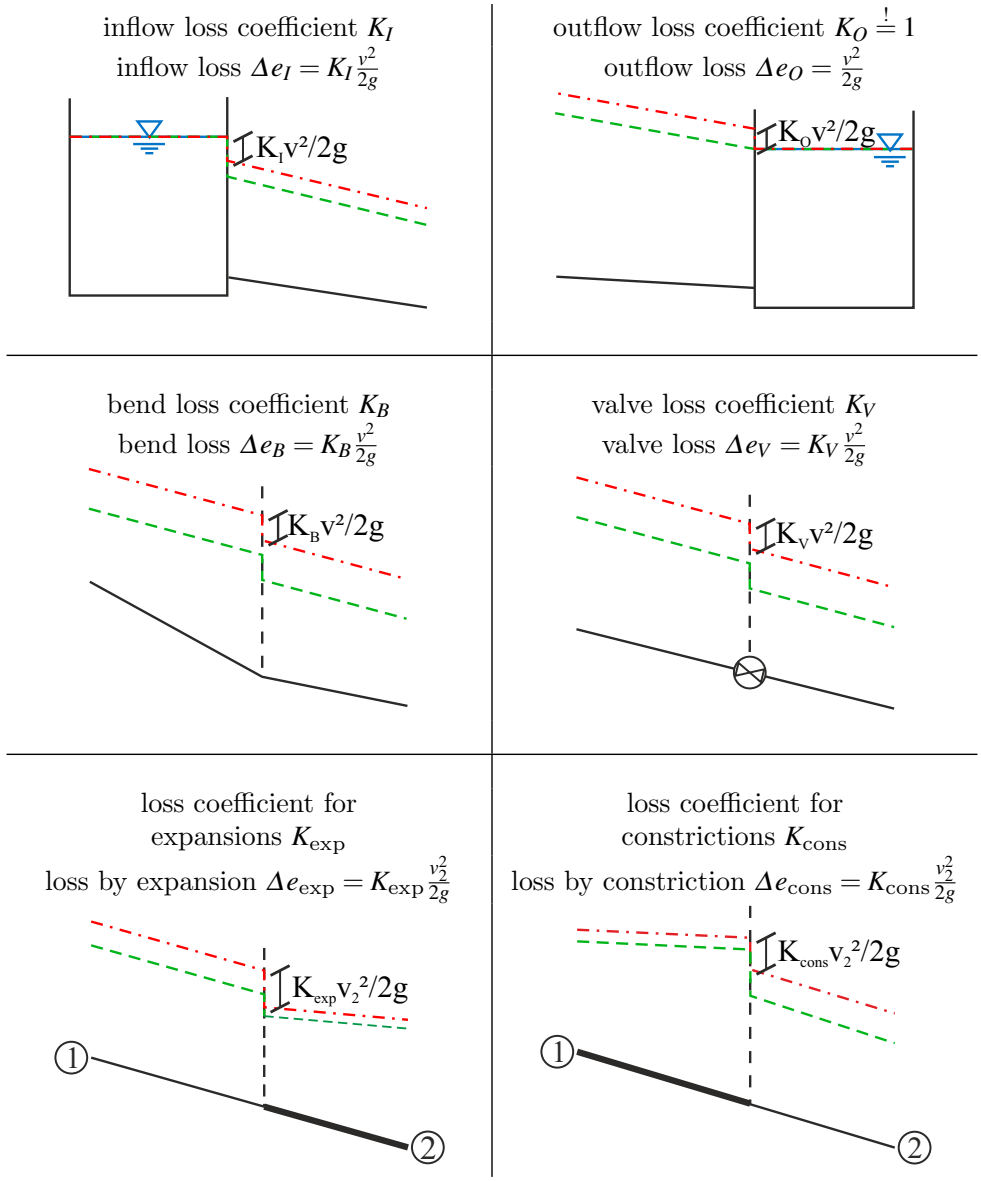

Figure 11.8: Minor (local) loss coefficients.

Valve loss

The word "valve" is a general description for flow control devices. While shut-off valves, such as ball or butterfly valves, are designed for the open or closed state, regulating devices like gate or globe valves may impart variable losses to the flow, thereby adjusting the discharge. Theoretically, the loss coefficient K_V takes values in the range of $0 < K_V < \infty$.

Expansion of cross-section

Minor (local) losses occur in cross-section expansions. The associated equation, with which the energy losses may theoretically be derived via the law of momentum, is attributed to the Frenchmen Borda[N] and Carnot[O]. For the cross-section expansion, it is essential to keep in mind that the loss coefficient K_{exp} is related to the downstream cross-section 2 (see Figure 11.8). These minor (local) losses occur only there.

Constriction of cross-section

In the cross-section constriction, minor losses are of course also pertinent. Imagine the convergence of three highway lanes to a single lane. For the constriction, it must also be kept in mind that the loss coefficient K_{cons} is related to the downstream cross-section 2. In my opinion, you are ready to start a pipeline experiment.

Experiment

Pipe hydraulics

For a clear demonstration of the overall loss-affected pipe flow, we use the test rig of Figure 11.9. The level gauges, which are arranged in the background (the narrow, bright-reddish strip) and connected with the pipe via small holes, allow the tracking of the course of the hydraulic grade line. A magneto-inductive flowmeter is shown in the photo (bottom right). Let's check whether all the equations, pipe friction and minor (local) loss coefficients[P] yield an acceptable result for the discharge.

$H_l = 3.28\,\text{m}$	$H_r = 0.80\,\text{m}$	$l = 4.40\,\text{m}$	$d = 1.5\,\text{cm}$	$k_s = 5.0 \times 10^{-5}\,\text{m}$
$K_I = 0.5$	$K_{B45^\circ} = 0.07$	$K_{B90^\circ} = 0.14$	$T = 20\,^\circ\text{C}$	

First, we draw the energy diagram shown in Figure 11.10. The water levels in the container indicate the piezometric height. The flow velocity in the containers is negligibly low so that the energy grade line (EGL) lies on the water level. The hydraulic grade line (HGL) extends to the container water level at the lower end of the pipe. The EGL may be drawn a distance of $\frac{v^2}{2g}$ above the HGL. This last drop of the EGL to the water level of the lower container represents the outflow loss $K_O \frac{v^2}{2g}$. I recommend that you mark the "height of arrival" of the HGL and EGL at the outflow. The distance between the HGL and EGL is the velocity height $\frac{v^2}{2g}$, which is constant throughout the pipe because the diameter d does not change. Thus, the HGL and EGL must extend in parallel along the pipeline. You may transfer the distance selected to the pipe inlet of the head container. This is to be the start of our journey. At first, there is a downward drop of the EGL by the inflow loss $\Delta e_E = K_I \frac{v^2}{2g}$. Immediately downstream, there awaits the next minor loss, the 45° bend. There is another downward drop of $\Delta e_{B45^\circ} = K_{B45^\circ} \frac{v^2}{2g}$. It doesn't matter how

[N] Jean-Charles de Borda ∗1733, Dax, France †1799, Paris, France

[O] Lazare Nicolas Marguerite Carnot ∗1753, Nolay, France †1823, Magdeburg, Germany

[P] The local loss coefficients are taken from [52].

Figure 11.9: Test rig for pipe hydraulics from [44].

large the drops are shown in the drawing. All that matters is to mentally walk along the pipeline when drawing the energy diagram and to note all conspicuous features. The energy grade line has the same gradient everywhere, because with unchanging boundary conditions for friction (f_D, v and d, see Figure 11.4), the slope of the energy grade line J_E remains constant. The diagram contains another drop for visualising the valve loss which, however, is to be set here with $K_V = 0$ (ball valve completely open). Following the flow with the slope of the energy grade line J_E, the next 45° bend results in another minor loss of $\Delta e_{B45^\circ} = K_{B45^\circ} \frac{v^2}{2g}$, and subsequently of $\Delta e_{B90^\circ} = K_{B90^\circ} \frac{v^2}{2g}$, before the energy grade line drops by $\frac{v^2}{2g}$ to the container water level at the edge of the container. As already mentioned above, the hydraulic grade line (HGL) runs at a constant distance parallel to the energy grade line (EGL).

The problem is actually solved now. From now on, all that must be done is to translate the energy diagram into an adequate formula. Previously, the "lengths" on the left and on the right side have been set equal. We will now try another method and start a mountain hike – in this case, on the path marked in red.

We start our hiking tour at $H_l = 3.28\,\mathrm{m}$, jump downward by Δe_I, descend $\frac{f_D l_1}{d} \frac{v^2}{2g}$ metres along the first path section of length l_1 to the first bend, and then hop down by another $K_{B45^\circ} \frac{v^2}{2g}$ metres. We continue downwards, leaving out the valve loss, until after a path distance of l_2 and a descent of $\frac{f_D l_2}{d} \frac{v^2}{2g}$ metres, the next bend appears. Again, $K_{B45^\circ} \frac{v^2}{2g}$ metres are overcome. The following section has a constant gradient; we descend along

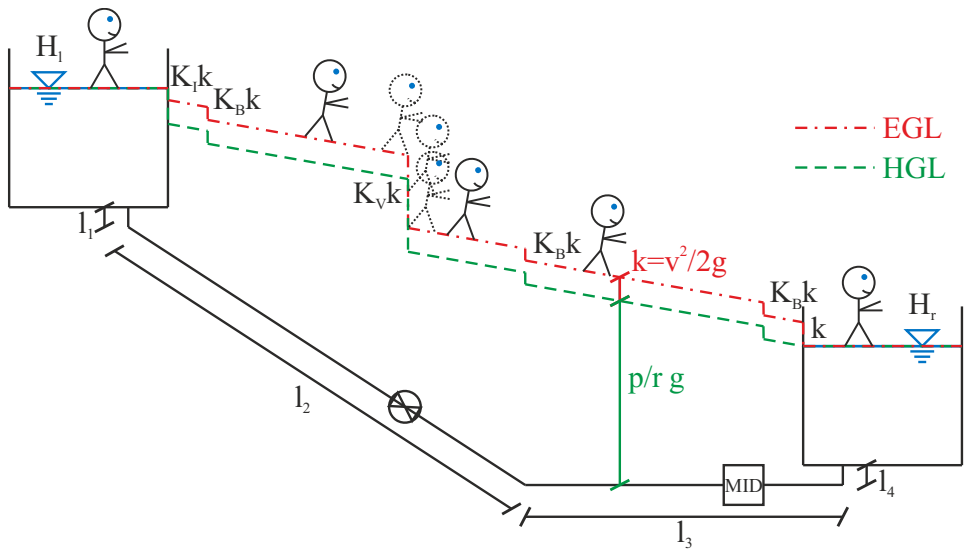

Figure 11.10: Energy diagram for test rig from [44].

this third section by a total of $\frac{f_D l_3}{d}\frac{v^2}{2g}$ metres. A last bend with a height step of $K_{B90°}\frac{v^2}{2g}$ metres follows; then we are on the home stretch of length l_4 at a gradient of $\frac{f_D}{d}\frac{v^2}{2g}$. Arriving at the container, we must jump down by $\frac{v^2}{2g}$ to our target height of $H_r = 0.80\,\mathrm{m}$ above the laboratory floor. Mathematically expressed, our mountain hike reads as follows:

$$H_l - K_I\frac{v^2}{2g} - \frac{f_D l_1}{d}\frac{v^2}{2g} - K_{B45°}\frac{v^2}{2g} - \frac{f_D l_2}{d}\frac{v^2}{2g} - K_{B45°}\frac{v^2}{2g} - \frac{f_D l_3}{d}\frac{v^2}{2g} - K_{B90°}\frac{v^2}{2g} - \frac{f_D l_4}{d}\frac{v^2}{2g} - \frac{v^2}{2g} = H_r \tag{11.46}$$

By combining the pipe friction losses through $l = l_1 + l_2 + l_3 + l_4$ and factoring out the velocity height, Equation 11.46 becomes noticeably clearer:

$$H_l - \frac{v^2}{2g}\left(\frac{f_D l}{d} + K_I + K_{B45°} + K_{B45°} + K_{B90°} + 1\right) = H_r \tag{11.47}$$

With the insertion of the values, Equation 11.47 becomes

$$3.28 - \frac{Q^2}{\left(\frac{d^2\pi}{4}\right)^2 2g}\left(\frac{f_D 4.4}{0.015} + 0.5 + 0.07 + 0.07 + 0.14 + 1\right) = 0.80 \tag{11.48}$$

and further:

$$2.48 - \frac{8Q^2}{0.015^4\pi^2 g}\left(\frac{f_D 4.4}{0.015} + 1.78\right) = 0 \tag{11.49}$$

Equation 11.49 can be rearranged and solved with the initial friction coefficient $f_D = 0.02$:

$$Q = \sqrt{\frac{2.48 \cdot 0.015^4\pi^2 g}{8\left(\frac{0.02 \cdot 4.4}{0.015} + 1.78\right)}} \tag{11.50}$$

This yields $Q = 4.458 \times 10^{-4}\,\mathrm{m^3/s}$, and we start the Prandtl–Colebrook algorithm by running the routine `pc.m`.

```
1> cd D:\myData\OctaveDirectory
2> fD = pc('circle', 1.5e-2, 1.5e-2, 4.458e-4, 5e-5, 20);


Explanations of the individual lines n>
1> % cd means change directory; we change to the directory where
file pc.m is saved.
2> % with pc(qs,qsP,y,Q,ks,T), a function is called; in its first
line, it must be named as follows
2> % function [output1,outputn]=functionname(input1,inputn)
2> % the order of the parameters must be strictly adhered to be-
cause they must be input in the same order that they are called in
the routine.
2> % to be able to calculate outflow values at partial filling,
the flow depth must be entered. Here the pipe is entirely filled
so we enter the diameter.
2> % the function name must be identical to the file name, but
without the extension (here it is 'pc').
2> % the result of the function is assigned to the variable before
the =.
2> % with ; the input is terminated. If it is omitted, Octave
presents the results on the command line.
```

Octave determines a value of 0.0299 for f_D, which is based on a discharge of $Q = 4.458 \times 10^{-4}\,\mathrm{m^3/s}$. We go back to Equation 11.49 and insert $f_\mathrm{D} = 0.0299$.

Those who use the Octave equation solver may once again call the definition of the function (`function H=f(Q)`) by the ↑ key and adjust the value of f_D in `H = 2.48 - 8*Q^2/(0.015^4*pi^2*9.81)*(0.0299*4.4/.015 + 1.78);`. After confirmation by `endfunction`, the call is made yet again by `[Q,fval,info]=fsolve(@f,0.0003)`.

The balancing of the energies results in $Q = 3.795 \times 10^{-4}\,\mathrm{m^3/s}$; however, we do not know if the f_D obtained for $Q = 4.458 \times 10^{-4}\,\mathrm{m^3/s}$ is also valid for $Q = 3.795 \times 10^{-4}\,\mathrm{m^3/s}$. Therefore, we call the Prandtl–Colebrook routine – but now with $Q = 3.795 \times 10^{-4}\,\mathrm{m^3/s}$.

```
1> fD = pc('circle', 1.5e-2, 1.5e-2, 3.795e-4, 5e-5, 20);
```

This time, the equation for the transition region results in $f_\mathrm{D} = 0.0304$, which is very close to the estimate from the previous iteration step where $f_\mathrm{D} = 0.0299$.

We redefine the energy balance by the ↑ key:
`function H=f(Q)`
We insert $f_\mathrm{D} = 0.0304$ into:
`H = 2.48 - 8*Q^2/(0.015^4*pi^2*9.81)*(0.0304*4.4/.015 + 1.78)`
After confirmation by `endfunction`, the call is made again by:
`[Q,fval,info]=fsolve(@f,0.0003)`

The output result is $Q = 3.769 \times 10^{-4}\,\mathrm{m^3/s}$. But we are not yet finished at this point. We still have to prove that f_D holds for this discharge as well.

```
1> fD = pc('circle', 1.5e-2, 1.5e-2, 3.769e-4, 5e-5, 20);
```

The Prandtl–Colebrook algorithm confirms that $f_\mathrm{D} = 0.0304$. This makes the discharge of $Q = 3.769 \times 10^{-4}\,\mathrm{m^3/s}$ official. By the way, the measurement by means of the MID resulted in $0.365\,\mathrm{L/s}$[Q].

11.7 Turbomachines

11.7.1 Pumps

Pumps supply the system with hydraulic energy. Centrifugal pumps that rotate about a motor-driven axis take in water axially at the so-called suction side and increase the pressure level via rotation of the blades. The rotatory motion of the blades pushes the fluid outwards by centrifugal acceleration; the fluid outflows radially. The pressure is further increased by a gradual cross-section expansion at the outlet according to the Bernoulli equation. With the same diameter upstream and downstream from the pump, the pressure increase corresponds to the increase of the total energy H_P. Equation 11.51 specifies the motor power that is required for the supply of Q by H_P (see Chapters 3.4.5 and 3.4.3). Here, the right side of the equation is divided by the efficiency $\eta_P < 1$ because the (electric) power to be provided must compensate for the efficiency loss.

$$P_P = \frac{1}{\eta_P} \rho g Q H_P \quad [\mathrm{W}] \tag{11.51}$$

11.7.1.1 Pipeline characteristic

In a pipe system, the hydraulic losses are a function of discharge. This is referred to as the pipeline characteristic that results from the energy equation taking the losses into account. For the energy diagram in Figure 11.11, left, the equation may be set up as follows if the outflow loss $K_O = 1$ is included in the sum of the minor losses:

$$H_P = (H_r - H_l) + \frac{Q^2}{A^2 2g} \left(\frac{f_\mathrm{D} l}{d} + \sum_{i=1}^{n} K_i \right) \tag{11.52}$$

Figure 11.11, right, shows an example of a pipeline characteristic. The delivery head starts at $H_\mathrm{geo} = H_r - H_l$ for $Q = 0$ and then increases quadratically with Q.

[Q] After the experiment was set up, I could hardly wait to compare the calculated and the measured discharge quantities. But it did not work! I calculated for hours, I doubted the MID and myself. I modified the loss coefficients and changed the roughness of the pipe wall to very smooth. But to no avail. The measured discharge significantly exceeded the calculated one. At some point, I asked the craftsmen whether they really had installed a 0.5 – inch pipe. "Yeah, sure", was their reply; and they were right. Later, I filled such a pipe with water and determined the diameter to be 1.5 cm via its weight. This corresponds to approximately 0.59 – inch which is greater than I expected. Since then, I pay attention to the diameter very carefully...

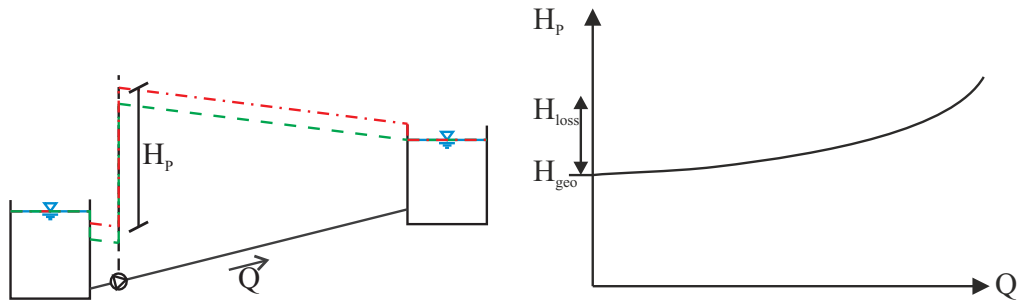

Figure 11.11: Energy diagram of a pipe flow with pump (left) and pipeline characteristic (right).

11.7.1.2 Pump characteristic

The characteristic of a pump shows the relation between delivery head and discharge. It is easy to comprehend that the delivery head of a pump decreases with increasing discharge. Dependencies develop as shown on the left side of Figure 11.12. From the pipeline and the pump characteristic, it follows that one pump in one system can supply only one single discharge; this is referred to as the operating point. Normally, regulation is possible only by imparting additional hydraulic losses to the pipeline characteristic, which should be prevented for reasons of energy efficiency[R]. However, this may be achieved by valves, for example, in which case it must be ensured that they are installed downstream from the pump in order to avoid the risk of cavitation. Initially, it is not a problem for centrifugal pumps to operate against fully closed valves; however, heating of the fluid can lead to trouble. Another possibility for reducing the discharge of a pump is to return a portion of the water via a bypass before the pump. In various pump models, different impellers may be installed in order to realise adjustments to the volume flow. In past years, variable speed pumps that cover a wider outflow spectrum at a concrete delivery head have been developed on a broader scale. The H_P-Q dependencies are represented with their respective efficiencies in what are known as pump characteristic field diagrams (see Figure 11.12, right). Herein H_{NPSH} is the Net Positive Suction Head (NPSH), which depends on the discharge. This value depicts the necessary pressure upstream from the pump in order to prevent cavitation from occurring (see Chapter 8.7).

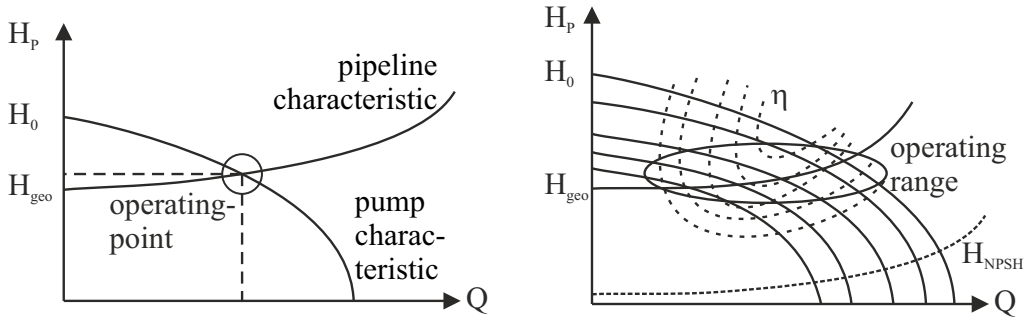

Figure 11.12: Example of a pump characteristic and characteristic field.

[R] Therefore, it is often advisable to have the pumps run only for a certain period of time and to provide a container for inflow and outflow buffering.

Experiment

Determination of a pipeline and a pump characteristic

Anybody who is prepared to pay 20 € for an aquarium pump and a hose may determine the characteristic of a pump in a simple experiment (see Figure 11.13). The hose has a diameter of $d = 11\,\text{mm}$[S] and a length of $l = 2.0\,\text{m}$ with a roughness of $k_s = 5.0 \times 10^{-6}\,\text{m}$. For the temperature, $T = 20\,^{\circ}\text{C}$ may be assumed; for the inflow loss, $K_I = 0.5$ is presumed.

Figure 11.13: Experiment for the determination of a pump characteristic.

The pipeline characteristic is obtained by taking into account the discharge-dependent losses.

$$H_P = H_{\text{geo}} + \frac{Q^2}{\left(\frac{d^2\pi}{4}\right)^2 \cdot 2g}\left(\frac{f_{\text{D}} l}{d} + \sum_{i=1}^{n} K_i\right) = H_{\text{geo}} + \frac{Q^2}{1.772 \times 10^{-7}}\left(181.82 f_{\text{D}} + 1.5\right) \quad (11.53)$$

With the offered Octave-script for calculating the friction coefficient f_{D}, the relation between discharge and head loss listed in Table 11.1 is obtained from the above equation.

Table 11.1: Pipeline characteristic of the hose system from Equation 11.53.

Q [m³/s]	2.0×10^{-5}	4.0×10^{-5}	6.0×10^{-5}	8.0×10^{-5}	10.0×10^{-5}	12.0×10^{-5}
Δe [m]	0.0148	0.0764	0.157	0.262	0.390	0.542

A maximum delivery head of $H_{P,Q=0} = 0.74\,\text{m}$ was measured (82.2 cm from the table top minus the water level of approximately 8 cm in the lower container). The maximum discharge for $H_{\text{geo}} = 0$ was determined, without a hose and by means of a stopwatch and a measuring cup, as $Q_{\max} = \frac{1.0\,\text{L}}{7.5\,\text{s}} = 1.33 \times 10^{-4}\,\text{m}^3/\text{s}$. The discharges at different geodetic

[S] ... though 10 mm is specified...

delivery heads, which were imparted to the system by positioning the outflow increasingly higher, were of course measured with a hose, i. e. including the pipeline characteristic. Table 11.2 lists the measured values of the operating points. The third row shows the hydraulic losses that occurred at the corresponding discharge values (see Formula 11.53); the fourth row shows the sum of head losses and geodetic delivery head. These delivery heads are depicted in Figure 11.14 as small black squares and as a function of discharge. From these so-called operating points, the solid line, which was approximated via a fourth-degree polynomial, specifies the pump characteristic.

Table 11.2: Pump characteristic including the hydraulic losses in the hose system. Measured discharges at different delivery heads.

H_{geo} [m]	0.00	0.08	0.18	0.28	0.38	0.48	0.58	0.68
Q $\left[1 \times 10^{-5}\,\text{m}^3/\text{s}\right]$	13.3	9.80	8.55	7.15	6.17	5.56	3.47	1.92
Δe [m]	0	0.376	0.295	0.214	0.165	0.137	0.060	0.014
$H_{\text{geo}} + \Delta e$ [m]	0	0.456	0.475	0.494	0.545	0.617	0.640	0.694

The various pipeline characteristics are based on the discharge-dependent head losses and on different geodetic delivery heads. The measured operating points lie fairly accurately on the associated characteristics.

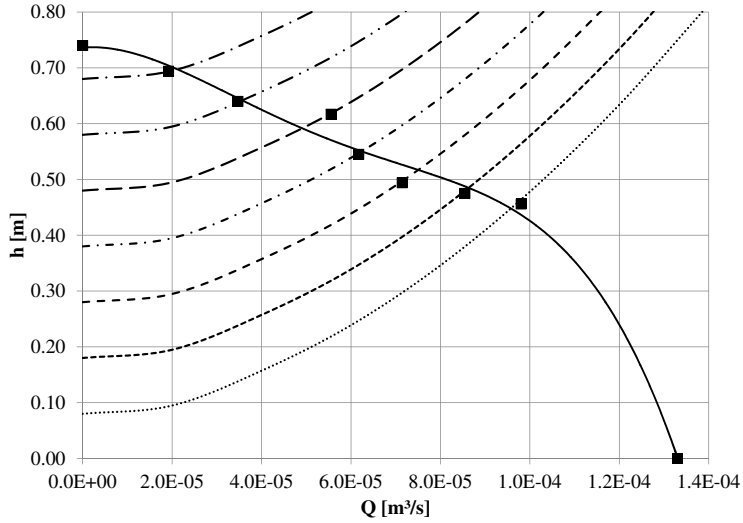

Figure 11.14: Pipeline characteristics for various delivery heads and experimentally determined pump characteristic.

This experiment was intended merely to convey the idea of how a pump that operates at constant capacity behaves in a system with variable boundary conditions (in this case, different delivery heads). A general example with pumps will provide a fitting climax to the practical examples.

11.7.1.3 Parallel pump arrangement

The parallel arrangement of pumps may increase the discharge. However, the pipeline characteristic teaches that doubling the number of pumps does not automatically imply doubling the discharge. Two pumps are often arranged in parallel in order to cover failures or to cope with heavy rainfall events, for example. The parallel arrangement cannot increase the delivery head. The discharges, that are dependent on the delivery heads, are added; that is the pump characteristics are 'added horizontally' (see Figure 11.15).

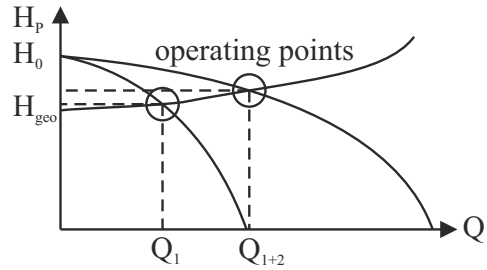

Figure 11.15: Pump characteristic of two parallely arranged identical pumps.

11.7.1.4 Serial pump arrangement

Pumps are serially arranged to increase the delivery head. The discharge cannot be increased by means of this setup. The discharge-dependent delivery heads are added; that is the pump characteristics are "added vertically" (see Figure 11.16).

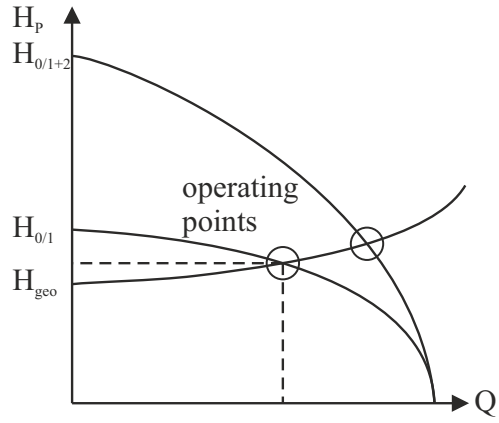

Figure 11.16: Pump characteristic of two serially arranged identical pumps.

11.7.2 Turbines

Turbines are turbomachines that withdraw hydraulic energy from the system and convert it into mechanical energy, which is generally utilised for driving generators to produce electricity. Considering once again the mechanical work that a system performs outwardly, or the work that is done to a system from the outside, the equation for the power of a turbine can easily be derived (see Chapter 3.4.5 and 3.4.3). According to Equation 3.13, power equals work per unit time, which in the case of a turbine is reasonably expressed making use of water mass per unit time (i. e. ρQ). The theoretically available power of a turbine is calculated with the gross head, i. e. the difference of head and tail water levels:

$$P_{T,\text{theoretical}} = \rho g Q H_{\text{gross}} \quad [\text{W}] \tag{11.54}$$

A portion of the originally existing energy (H_{gross}) is dissipated in the penstock by friction; the available head is H_T which is also known as H_{net}. Generally speaking, the net head is the gross head minus the hydraulic losses. The efficiency factor[T] of the turbine $0 < \eta_T < 1$ reduces the power that can be harnessed further.

$$P_T = \eta_T \rho g Q H_T \quad [\text{W}] \tag{11.55}$$

A turbine withdraws energy from the system, which is why it is shown as a drop of the energy grade line by H_T in the energy diagram (see Figure 11.17).

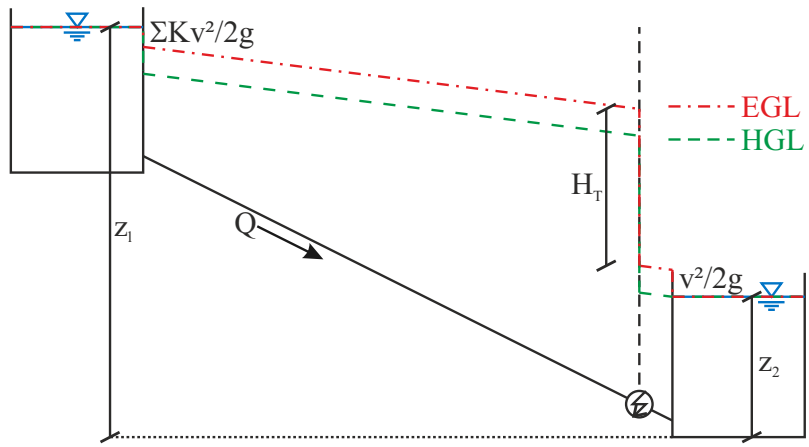

Figure 11.17: Energy diagram of a pipeline system with built-in turbine.

When setting up the energy equation, Formula 11.55 is solved for H_T and inserted.

[T] Hydropower turbines are generally very efficient. They are individually designed for the various configurations. Therefore, they reach efficiency factors in the range of 85 % to 95 %.

Example

Prater hydro power plant in Munich

The Prater hydropower plant in Munich has been operating since 2010 and is completely hidden underground. Its Kaplan turbine has a design discharge of $34\,\mathrm{m^3/s}$. The operation level is at 511.56 m.a.s.l., whereas the tail water may be taken in at 502.06 m.a.s.l.; the head race tunnel of length 170 m has a cross-section of 4.70 m by 4.70 m.
For the calculation of the friction coefficient f_D, we use the hydraulic radius R_hy, which is determined by the quotient of the flow area and the wetted perimeter (see Equation 11.41):

$$R_\mathrm{hy} = \frac{A}{P} = \frac{4.7^2}{4 \cdot 4.7} = 1.175\,\mathrm{m} \tag{11.56}$$

The efficiency of the system (turbine, generator, electrotechnical equipment) is given here as 82 %. Assume that water temperature is $T = 10\,^\circ\mathrm{C}$ and that $k_s = 5\,\mathrm{mm}$. The energy equation, which may be derived from Figure 11.17 with the sum of the individual losses (incl. outflow loss $\sum_{i=1}^{n} K_i = 2.0$), reads:

$$511.56 - \frac{Q^2}{A^2 \cdot 2g}\left(\frac{f_\mathrm{D} L}{4R_\mathrm{hy}} + \sum_{i=1}^{n} K_i\right) - H_T = 502.06 \tag{11.57}$$

$$9.5 - \frac{Q^2}{(4.7 \cdot 4.7)^2 \cdot 2g}\left(\frac{f_\mathrm{D} \cdot 170}{4 \cdot 1.175} + 2.0\right) - H_T = 0 \tag{11.58}$$

With $d = 4R$, we may use the Prandtl–Colebrook algorithm for a square pipe that is entirely filled.

```
1> g = 9.81;
2> Q = 34;
3> ks = 5e-3;
4> A = 4.7*4.7;
5> P = 4*4.7;
6> Rhy = A/P;
7> T = 10;
8> sumK = 2;
9> L = 170;
10> fD = pc('circle',4*Rhy,4*Rhy,Q,ks,T);
11> de = Q^2/(A^2*2*g)*(fD*L/(4*Rhy)+sumK);
```

The following values result for the design discharge of $Q_D = 34\,\mathrm{m^3/s}$: $f_\mathrm{D} = 0.0199$, $\Delta e = 0.329\,\mathrm{m}$, $H_T = 9.500 - 0.329 = 9.171\,\mathrm{m}$. With Equation 11.55, a power of

$$P_T = \eta_T \rho g H_T Q = 0.82 \cdot 1000 \cdot 9.81 \cdot 9.171 \cdot 34 = 2.51 \times 10^6\,\mathrm{W} = 2.51\,\mathrm{MW} \tag{11.59}$$

results. This power is achieved only if a discharge of $34\,\mathrm{m^3/s}$ flows through the turbine at a gross head of 9.50 m. When integrating power with respect to time, one obtains a physical unit of work, either Nm or kWh (see Chapter 3.4.3). The Prater power plant

generates 10.5×10^6 kWh electricity in one average year. At 8760 h/a, this corresponds to a mean power of $\langle P_T \rangle = 1198.6$ kW. By the way, valuable planning instructions may be found in the standard reference work *Low-Head Power Plants* by Mosonyi [30].

11.8 Pipe junctions

At pipe junctions, the flow conditions adjust themselves in such a manner that one single pressure, or a pressure height, is obtained at the junction. We may again recall the previous example of a rock concert. If the hydraulic and energy grade line were to extend in one pipe string so that shortly before the junction a higher pressure prevails than in the node, then the high gradients would result in more water successively flowing out from that string. The higher discharge again leads to greater head losses until equilibrium has been reached. Figure 11.18 shows the flow conditions at a junction by means of an energy diagram[U].

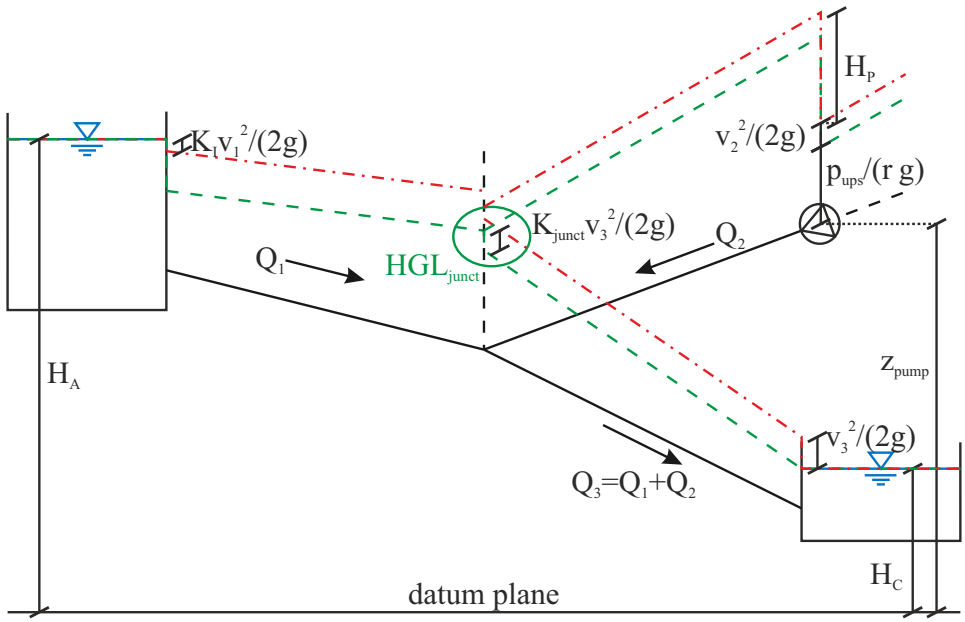

Figure 11.18: Energy diagram of a pipeline system with junction. ©Christoph Rapp 2017. All Rights Reserved.

When setting the pressure height at the junction as a boundary condition, the system of Equations 11.60 to 11.62 is determined. Here, it is of utmost importance to walk along the hydraulic gradient lines in the hiking tour described above. In this way, the outflow loss

[U] In purely mathematical terms, for a theoretically chosen $K_{\text{junct}} = 0$, an upward jump in the energy grade line, in the direction of flow, may occur if the velocity in the converged pipe is higher than in the pipes leading to the node. However, this is not physically possible since no external energy is supplied to the system (see Chapter 3.4.4). However, in reality, hydraulic losses are generated by the junction of the flow and the associated eddies, which must be accounted for.

K_O, i. e. the loss of the velocity height, is already taken into account in the pipe strings upstream from the junction.

$$H_A - \frac{Q_1^2}{A_1^2 2g} K_I - \frac{Q_1^2}{A_1^2 2g} \frac{f_{D1} l_1}{d_1} - \frac{Q_1^2}{A_1^2 2g} = \mathrm{HGL}_{\mathrm{junct}} \tag{11.60}$$

$$z_{\mathrm{pump}} + \frac{p_{\mathrm{ups}}}{\rho g} + \frac{Q_2^2}{A_2^2 2g} + H_P - \frac{Q_2^2}{A_2^2 2g} \frac{f_{D2} l_2}{d_2} - \frac{Q_2^2}{A_2^2 2g} = \mathrm{HGL}_{\mathrm{junct}} \tag{11.61}$$

$$\mathrm{HGL}_{\mathrm{junct}} - \frac{(Q_1 + Q_2)^2}{A_3^2 2g} K_{\mathrm{junct}} - \frac{(Q_1 + Q_2)^2}{A_3^2 2g} \frac{f_{D3} l_3}{d_3} = H_C \tag{11.62}$$

When using the continuity condition, one obtains three equations with the three unknowns $(Q_1, Q_2, \mathrm{HGL}_{\mathrm{junct}})$. Finding the solutions for these unknowns is demonstrated by means of the following example.

Example

Pipeline system with junction

The partial discharges and the pump capacity ($\eta_P = 0.7$) are to be calculated for the illustrated pipeline system when a discharge of $Q_3 = 1.20\,\mathrm{m^3/s}$ is to be attained for maintaining the water supply from the reservoir on the right-hand side.

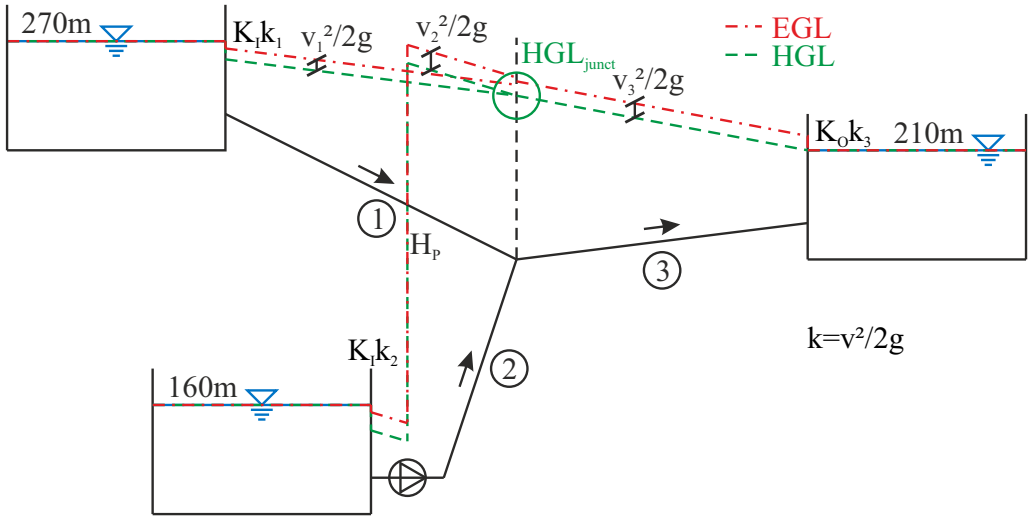

Line data:	Q [m³/s]	l [m]	d [m]	f_D [−]	K_I [−]
1	-	2000	0.60	0.018	0.30
2	-	1800	0.70	0.021	0.30
3	1.20	1300	0.60	0.023	

First, the energy diagram is drawn so that the hydraulic grade lines intersect at one point; the rest is as usual. HGL and EGL lie in the container at the water level. From there, the energy height initially drops precipitously by the inflow loss $K_I k_1 = K_I \frac{Q_1^2}{A_1^2 2g}$, then

continuously with gradient $J_E = \frac{Q_1^2}{A_1^2 2g}\frac{f_{D1}}{d_1}$ over the length l_1. In order to reach the pressure height at the node, a downward drop from the EGL by $k_1 = \frac{Q_1^2}{A_1^2 2g}$ must take place. The following conditional equation results:

$$270 - \frac{Q_1^2}{A_1^2 2g}\left(\frac{f_{D1} l_1}{d_1} + K_I + 1\right) = \mathrm{HGL}_{\mathrm{junct}} \tag{11.63}$$

The equation in the second string looks similar with the exception that, in addition, the pump supplies energy to the system.

$$160 + H_P - \frac{Q_2^2}{A_2^2 2g}\left(\frac{f_{D2} l_2}{d_2} + K_I + 1\right) = \mathrm{HGL}_{\mathrm{junct}} \tag{11.64}$$

Starting from the hydraulic grade line at the junction $\mathrm{HGL}_{\mathrm{junct}}$, the piezometric pressure height gradually declines to the water level of the right-hand container. Since we move from the $\mathrm{HGL}_{\mathrm{junct}}$ along the hydraulic grade line, we arrive exactly at the water level of the container at 210 m.a.s.l. and have no need to drop down by $\frac{v_3^2}{2g}$.

$$\mathrm{HGL}_{\mathrm{junct}} - \frac{(Q_1+Q_2)^2}{A_3^2 2g}\frac{f_{D3} l_3}{d_3} = 210 \tag{11.65}$$

With the known discharge of $Q_3 = 1.20\,\mathrm{m}^3/\mathrm{s}$, the pressure height at the junction may be calculated by the equation for the third string:

$$\begin{aligned}\mathrm{HGL}_{\mathrm{junct}} &= 210 + \frac{(Q_1+Q_2)^2}{A_3^2 2g}\frac{f_{D3} l_3}{d_3} = 210 + \frac{1.2^2}{0.283^2 \cdot 2g}\frac{0.023 \cdot 1300}{0.6} = 210 + 45.751 \\ &= 255.751\,\mathrm{m}\end{aligned} \tag{11.66}$$

The equation that describes the conditions in string 1 (11.63) may now be solved explicitly for Q_1.

$$\begin{aligned}Q_1 &= \sqrt{(270 - \mathrm{HGL}_{\mathrm{junct}})\frac{r_1^4 \pi^2 2g}{\left(\frac{f_{D1} l_1}{d_1} + K_I + 1\right)}} = \sqrt{(270 - 255.751)\frac{0.30^4 \pi^2 2g}{\left(\frac{0.018 \cdot 2000}{0.60} + 0.3 + 1\right)}} \\ &= 0.604\,\mathrm{m}^3/\mathrm{s}\end{aligned} \tag{11.67}$$

From the continuity condition, $Q_2 = Q_3 - Q_1 = 1.20 - 0.604 = 0.596\,\mathrm{m}^3/\mathrm{s}$ follows immediately. When this is inserted into the energy equation for string 2 (11.64), the delivery head and the capacity of the pump may be calculated:

$$\begin{aligned}H_P &= \mathrm{HGL}_{\mathrm{junct}} - 160 + \frac{Q_2^2}{A_2^2 2g}\left(\frac{f_{D2} l_2}{d_2} + K_I + 1\right) = 95.751 + \frac{0.596^2}{0.35^4 \pi^2 2g}\left(\frac{0.021 \cdot 1800}{0.70} + 1.30\right) \\ &= 102.52\,\mathrm{m}\end{aligned} \tag{11.68}$$

The electrical power P_P that is required for driving the pump is obtained by Equation 11.51:

$$P_P = \frac{1}{\eta_P}\rho g Q_2 H_P = \frac{1}{0.70}\rho g \cdot 0.596 \cdot 102.52 = 856.56\,\text{kW} \tag{11.69}$$

11.9 Summary of pipe flow

Figure 11.19 summarises all relevant pipeline system installations in an energy diagram (see also Equation 11.70).

$$\begin{aligned} H_A + H_P - \frac{Q^2}{A_1^2 2g}\left(\frac{f_{\text{D}1} l_1}{d_1} + K_I + K_{B\alpha} + K_V\right) - \frac{Q^2}{A_2^2 2g}\left(\frac{f_{\text{D}2} l_2}{d_2} + K_{\text{exp}}\right) \\ - \frac{Q^2}{A_3^2 2g}\left(\frac{f_{\text{D}3} l_3}{d_3} + K_{\text{cons}} + K_{B\beta} + 1\right) - H_T = H_B \end{aligned} \tag{11.70}$$

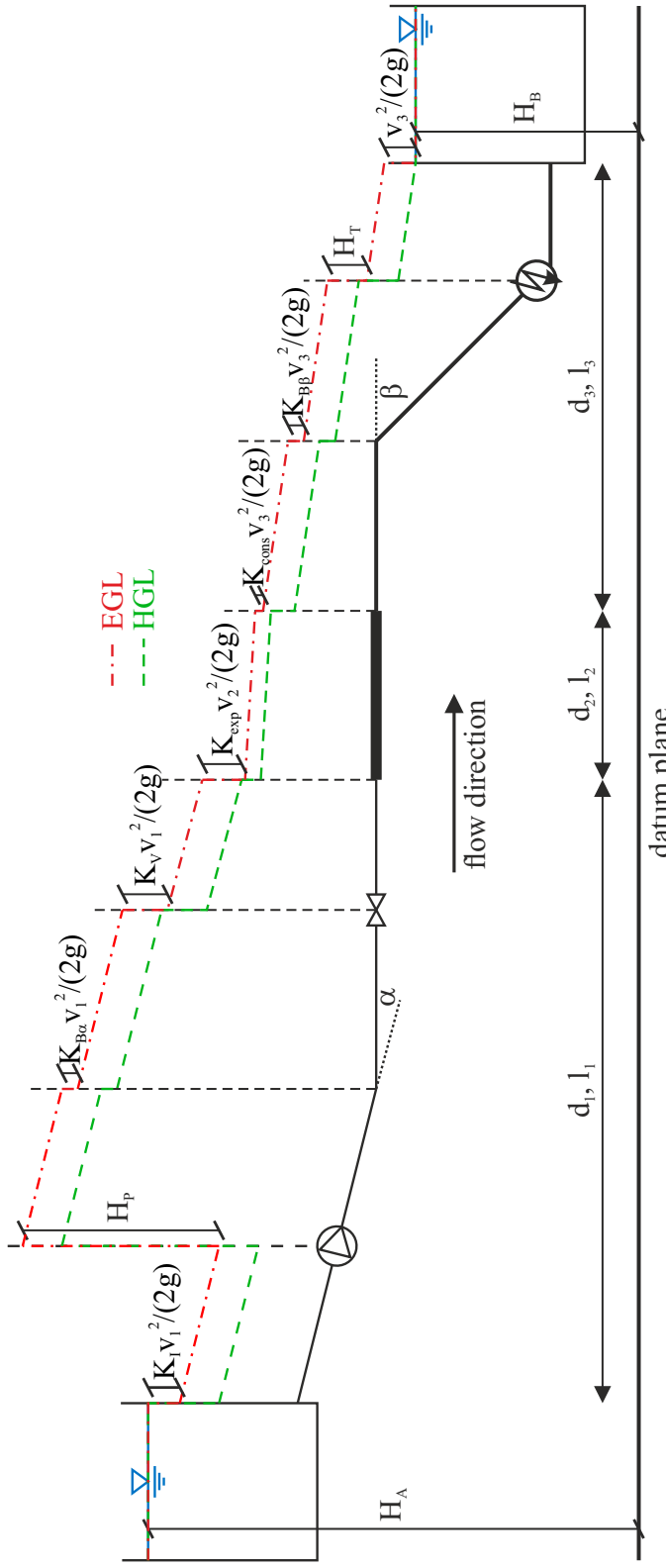

Figure 11.19: Energy diagram of a fictitious pipeline system.

Chapter 12
Unsteady pipe flow

12.1 General remarks on unsteady pipe flows

The pressure surge due to changes in the discharge may be compared to a rear-end collision. When water is abruptly stopped by a valve at the end of a pipeline, this "information" is not yet available at its inlet. At this location, the steady-state condition is still in effect and water continues to flow into the pipeline at that time; the water at the downstream valve is compressed and the pipeline is expanding. The pressure increase resulting from the compression may propagate only as fast as a solid body wave, which leads to oscillatory periods that are not at all negligible, particularly in long pipelines. The analogy of the collision in which a moving mass comes to a sudden standstill is obvious. The "information" about the accident transmitted to the car drivers who are following is delayed by the "reaction time", and so collisions are inevitable.

To illustrate this phenomenon, we consider the spring depicted in Figure 12.1 (which is analogous to the example of Figure 12.13) as an elastic mass that moves to the right due to its momentum (centre top) until it reaches the vicinity of a barrier that is still open (right top)[a]. When closing the barrier rapidly, the mass hits against it; due to inertia, the rear portion is still moving in the original flow direction so that the mass is compressed (left centre)[b] to a degree that is dependent on the modulus of elasticity. Now the spring relaxes in the direction of the free end because the water cannot escape at the valve (centre). The stress in the spring accelerates the water against the original flow direction so that inertia causes an expansion beyond the relaxed condition (right centre). This cycle is repeated until the energy is dissipated by friction i. e. converted to heat (lower row of diagrams).

[a] The water mass is represented by the spring and the valve by the barrier.

[b] Later, in the context of the propagation velocity of disturbances in pressure pipelines, we will find that, depending on the length of the pipeline, it may take several seconds until the inflow into the line subsides. In hydropower plants with discharge magnitudes of $50\,m^3/s$, or even $100\,m^3/s$, an additional several hundred tons of water may flow into the penstock during compression.

C. Rapp, *Hydraulics in Civil Engineering*,
https://doi.org/10.1007/978-3-031-54860-4_12

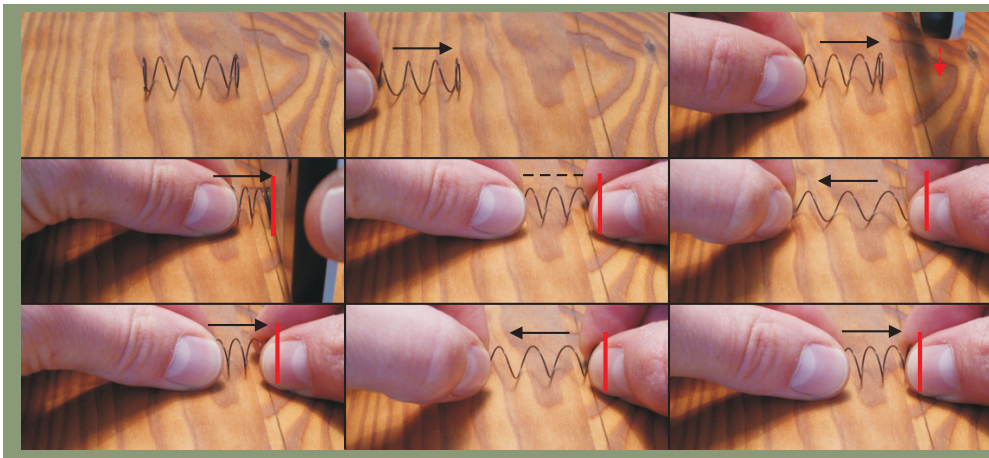

Figure 12.1: Spring stress as analogy to pressure variations in a pipeline due to changes in the discharge.

In pipe hydraulics, the pressure variations due to discharge changes propagate at the speed of sound of the medium and – normally – reach the other end of the pipeline, where there is an open (and unaffected) water surface.
Due to the pressure surge in the pipeline, the pressure gradient reverses when the wave arrives at the reservoir. The compressed water (subjected to stress) flows against the direction of the original pressure gradient from the pipe into the head reservoir. The situation in the pipeline relaxes until the pressure wave – now originating from the reservoir – reaches the closed device. There, however, further relaxation of the water is not possible because the closed valve prevents any further flow of the fluid. Accordingly, the pressure continues to decrease and this information travels upstream at the same velocity. With the lower pressure wave arriving at the upstream reservoir, the cycle reverses since the high-pressure gradient is a strong stimulus for the water to flow into the pipe. The entire process is repeated indefinitely with the Alliévi[A] method, which is based on the continuity condition and the unsteady Bernoulli equation (see Chapter 12.2) due to the conservation of energy. In the method of characteristics, which is based on the continuity and momentum equations, the pressure variations gradually subside (see Chapter 12.7).
Generally speaking, pipelines can cope quite well with the additional radial stresses due to the unsteady pressure increase; in most cases, negative pressure, against which pipelines are defenceless, has more serious consequences.

[A] Lorenzo Alliévi, ∗1856, Milano, Italy †1941, Rome, Italy

You may test this yourselves quite simply. Close a drinking straw with your finger and blow as hard as you can into the other end. The straw's shape remains unchanged. If you suck the air out of the straw, however, it collapses (see Chapter 3.4.9).

Figure 12.2: Positive (left) and negative (right) pressure in a drinking straw.

A good survey of the various methods for calculating the pressure surge is found in Martin and Pohl [29]. At first, we derive the continuity condition and the energy equation for unsteady flows in pipelines that we need for the Alliévi method in order to determine the maximum possible pressure increase known as the Joukowsky surge. Subsequently, the unsteady momentum equation for the pipe flow is derived and applied together with the continuity equation in the method of characteristics. Needless to say, results are compared for illustrative purposes.
I do apologise. This chapter is boring and heavily laden with mathematics. Clench your teeth!

12.2 Continuity condition according to Alliévi

The Alliévi (also known as Alliévi-Riemann) equations are based on a one-dimensional, loss-free approach to the continuity and the energy equations. We start with the derivation of the continuity condition as was done by Siegerstetter [56, page 27], for example.
We describe the change of mass in a pipe section of length $\mathrm{d}x$ as seen in Figure 12.3. Initially, the mass that flows in and out per unit time is $\rho Q = \rho vA$. However, this may change along the flow distance $\mathrm{d}x$; this is referred to as the convective derivative $\frac{\partial(\rho vA)}{\partial x}$. A local change of mass is also possible in that either the density, the volume, and/or the area of a differential disk element increases or decreases $\frac{\partial(\rho A)}{\partial t}$. In other words, if more fluid flows in at the left boundary than flows out on the right (a difference of $\frac{\partial(\rho vA)}{\partial x}\,\mathrm{d}x$), the mass in the volume must have increased by $\frac{\partial(\rho A)}{\partial t}\,\mathrm{d}x$.

$$\rho vA - \frac{\partial(\rho vA)}{\partial x}\frac{\mathrm{d}x}{2} = \rho vA + \frac{\partial(\rho vA)}{\partial x}\frac{\mathrm{d}x}{2} + \frac{\partial(\rho A)}{\partial t}\,\mathrm{d}x \tag{12.1}$$

ρvA can be subtracted from both sides of the equation. Then we divide by $\mathrm{d}xA\rho$ and split the terms of the derivative according to the product rule, i. e. into the convective and local derivatives (see Chapter 5.2).

$$\begin{aligned}\frac{1}{\mathrm{d}xA\rho}\left(\rho v\frac{\partial A}{\partial x}\mathrm{d}x + \rho A\frac{\partial v}{\partial x}\mathrm{d}x + vA\frac{\partial \rho}{\partial x}\mathrm{d}x + \rho\frac{\partial A}{\partial t}\mathrm{d}x + A\frac{\partial \rho}{\partial t}\mathrm{d}x\right)\\ = \frac{v}{A}\frac{\partial A}{\partial x} + \frac{\partial v}{\partial x} + \frac{v}{\rho}\frac{\partial \rho}{\partial x} + \frac{1}{A}\frac{\partial A}{\partial t} + \frac{1}{\rho}\frac{\partial \rho}{\partial t} = 0\end{aligned} \tag{12.2}$$

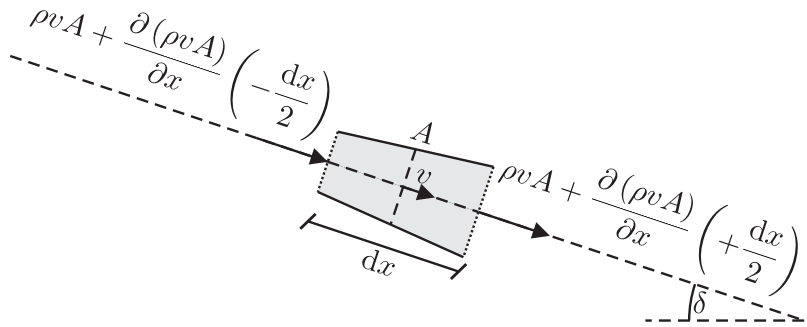

Figure 12.3: Change of mass in a pipe section of length dx.

We may combine the partial derivative of the area and that of the density for the total differential with chain rule (see Chapter 2.4.1.2):

$$\frac{\mathrm{d}A}{\mathrm{d}t} = \frac{\partial A}{\partial x}\frac{\mathrm{d}x}{\mathrm{d}t} + \frac{\partial A}{\partial t} = v\frac{\partial A}{\partial x} + \frac{\partial A}{\partial t} \tag{12.3}$$

$$\frac{\mathrm{d}\rho}{\mathrm{d}t} = \frac{\partial \rho}{\partial x}\frac{\mathrm{d}x}{\mathrm{d}t} + \frac{\partial \rho}{\partial t} = v\frac{\partial A}{\partial x} + \frac{\partial A}{\partial t} \tag{12.4}$$

This allows us to simplify the continuity equation as follows:

$$\frac{1}{\rho}\frac{\mathrm{d}\rho}{\mathrm{d}t} + \frac{1}{A}\frac{\mathrm{d}A}{\mathrm{d}t} + \frac{\partial v}{\partial x} = 0 \tag{12.5}$$

Deformation of the fluid

First, we will deal with the term $\frac{1}{\rho}\frac{\mathrm{d}\rho}{\mathrm{d}t}$, which describes the fluid deformation or compressibility. In a Hooke's medium (see [15, p. 31], for example) there exists a linear relationship between deformation and stress. As a digression, we write the known relationship between the elongation of a bar as the ratio of stress and modulus of elasticity $\frac{\Delta l}{l} = \frac{\sigma}{E}$. Since the pressure is a negative stress in terms of mechanics (i. e. the volume shrinks as pressure increases), the equation involving the fluid volume reads as:

$$\frac{\mathrm{d}V}{V} = -\frac{\mathrm{d}p}{E_\mathrm{F}} \tag{12.6}$$

Solving for the modulus of elasticity, we have:

$$E_\mathrm{F} = -\frac{\mathrm{d}p}{\frac{\mathrm{d}V}{V}} \tag{12.7}$$

However, in any case, mass is conserved and so $\mathrm{d}m = 0$. With $m = \rho V$ and use of the product rule, it follows that

$$\mathrm{d}m = \mathrm{d}\rho V = V\,\mathrm{d}\rho + \rho\,\mathrm{d}V = 0 \tag{12.8}$$

which may be rearranged as:

$$\frac{\mathrm{d}V}{V} = -\frac{\mathrm{d}\rho}{\rho} \tag{12.9}$$

By inserting Equation 12.9 into (12.7), we obtain

$$E_\mathrm{F} = -\frac{\mathrm{d}p}{-\frac{\mathrm{d}\rho}{\rho}} \tag{12.10}$$

or

$$\frac{\mathrm{d}\rho}{\rho} = \frac{\mathrm{d}p}{E_\mathrm{F}} \tag{12.11}$$

which provides us with an expression for the first term of Equation 12.5. Let's focus on the second term.

Deformation of the pipe

The pipe may also undergo deformation. For a circular pipe, $A = \frac{D^2\pi}{4}$ and the derivative of the area with respect to the diameter is $\frac{\mathrm{d}A}{\mathrm{d}D} = \frac{2D\pi}{4} = \frac{D\pi}{2}$. Hence, $\mathrm{d}A$ may be written as follows:

$$\mathrm{d}A = \frac{\pi}{2} D\,\mathrm{d}D \tag{12.12}$$

Thus, it follows for expression $\frac{\mathrm{d}A}{A}$:

$$\frac{\mathrm{d}A}{A} = \frac{\pi}{2} D\,\mathrm{d}D\,\frac{4}{D^2\pi} = \frac{2\,\mathrm{d}D}{D} \tag{12.13}$$

Again, based on Hooke's law, the change of the perimeter is $\frac{\Delta P}{P} = \frac{\Delta\sigma}{E_\mathrm{P}}$, or can be written as $\frac{\Delta P}{P} = \frac{\pi \mathrm{d}D}{\pi D}$. Consequently, $\frac{\mathrm{d}D}{D}$ may be written as done in Equation 12.14:

$$\frac{\mathrm{d}D}{D} = \frac{\mathrm{d}\sigma}{E_\mathrm{P}} \tag{12.14}$$

The relevant stress σ for the volume change comprises the radial component σ_r and the effects of the axial stress in the radial direction $\mu_L\sigma_a$. This influence of axial stresses on the radial direction may be illustrated by a balloon that is stretched (see Figure 12.4). The axial stress influences the radius, which becomes smaller.

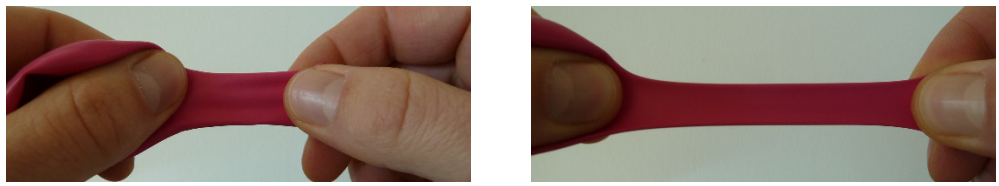

Figure 12.4: Effects of axial and radial stresses. When stretched, the balloon gets narrower.

The stress comprises the radial (σ_r) and the axial component that is multiplied by the lateral contraction number μ_L with values of approximately 0.3 [5, p. 117]:

$$\sigma = \sigma_r - \mu_L \sigma_a \tag{12.15}$$

Since $\sigma_a = \mu_L \sigma_r$, Equation 12.14 may be rewritten using $\sigma = \sigma_r \left(1 - \mu_L^2\right)$.

$$\frac{\mathrm{d}D}{D} = \frac{\mathrm{d}\sigma_r}{E_\mathrm{P}} \left(1 - \mu_L^2\right) \tag{12.16}$$

The change of the radial stress in a pipe with the thin-wall thickness of w is calculated via Barlow's formula (see e. g. [52, p. 13.46]):

$$\mathrm{d}\sigma_r = \frac{\mathrm{d}pD}{2w} \tag{12.17}$$

Equation 12.17, inserted into 12.16, results in:

$$\frac{\mathrm{d}D}{D} = \frac{\mathrm{d}pD}{2wE_\mathrm{P}} \left(1 - \mu_L^2\right) \tag{12.18}$$

For $\frac{\mathrm{d}A}{A}$ we finally obtain the expression:

$$\frac{\mathrm{d}A}{A} = \frac{2\,\mathrm{d}D}{D} = \frac{2\,\mathrm{d}pD}{2wE_\mathrm{P}} \left(1 - \mu_L^2\right) = \frac{\mathrm{d}pD}{wE_\mathrm{P}} \left(1 - \mu_L^2\right) \tag{12.19}$$

Deformation of the system

The total deformation comprises the volume change due to pipe expansion and the compressibility of the fluid. The continuity condition (12.5) for the unsteady flow with the terms for the deformation of the fluid (12.11) and the pipe (12.19) yields:

$$\frac{\partial v}{\partial x} + \frac{1}{E_\mathrm{F}} \frac{\mathrm{d}p}{\mathrm{d}t} + \frac{D}{wE_\mathrm{P}} \left(1 - \mu_L^2\right) \frac{\mathrm{d}p}{\mathrm{d}t} = \frac{\partial v}{\partial x} + \left(\frac{1}{E_\mathrm{F}} + \frac{D}{wE_\mathrm{P}} \left(1 - \mu_L^2\right) \right) \frac{\mathrm{d}p}{\mathrm{d}t} = 0 \tag{12.20}$$

The bracketed expression corresponds to the reciprocal value of the system stiffness, which establishes a relationship between the elastic moduli of the two materials:

$$\frac{1}{E_\mathrm{sys}} = \left(\frac{D}{w} \frac{1}{E_\mathrm{P}} \left(1 - \mu_L^2\right) + \frac{1}{E_\mathrm{F}} \right) \tag{12.21}$$

With $a = \sqrt{\frac{E_\mathrm{sys}}{\rho}}$, the propagation velocity of pressure waves in bars (see e. g. [26, p. 63]), we obtain by substitution

$$a = \sqrt{\frac{E_\mathrm{sys}}{\rho}} = \sqrt{\frac{\frac{1}{\rho}}{\frac{1}{E_\mathrm{F}} + \frac{D}{w} \frac{1}{E_\mathrm{P}} \left(1 - \mu_L^2\right)}} = \sqrt{\frac{\frac{E_\mathrm{F}}{\rho}}{1 + \frac{D}{w} \frac{E_\mathrm{F}}{E_\mathrm{P}} \left(1 - \mu_L^2\right)}} \tag{12.22}$$

and ultimately:

$$\frac{\partial v}{\partial x} + \frac{1}{\rho a^2} \frac{\mathrm{d}p}{\mathrm{d}t} = 0 \tag{12.23}$$

Since disturbances in materials propagate according to the density and the modulus of elasticity, an Indigenous American is capable of hearing an approaching train earlier by

laying his ear on the steel tracks (see Figure 12.5). In our case, with the system consisting of two materials – the (steel) pipe and water – the speed of sound is determined via the system stiffness E_{sys}. By the way, the propagation velocity of disturbances a in steel pipes has a magnitude of approximately $1000\,\text{m/s}$.

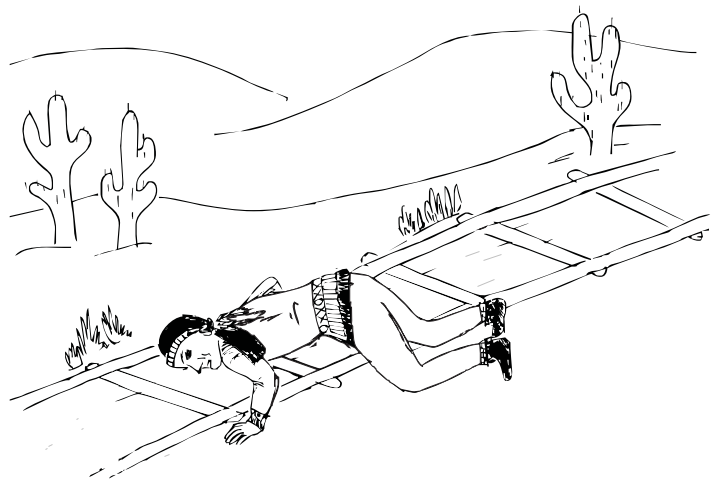

Figure 12.5: An Indigenous American listens to determine whether a train is approaching. Design: Julia Rüping.

In the next step we will use the partial derivatives instead of the total differential:

$$\frac{1}{\rho}\frac{\mathrm{d}p}{\mathrm{d}t} = \frac{1}{\rho}\frac{\partial p}{\partial t} + \frac{1}{\rho}\frac{\partial p}{\partial x}\frac{\mathrm{d}x}{\mathrm{d}t} \tag{12.24}$$

Furthermore, h as piezometric pressure height $h = \frac{p}{\rho g} + z$ can be rearranged as $p = (h-z)\rho g$[B], or $\mathrm{d}p = \rho \cdot g \cdot \mathrm{d}(h-z)$ [5, p. 117]. Finally, with velocity as the derivative of position with respect to time $v = \frac{\mathrm{d}x}{\mathrm{d}t}$, it follows that

$$\frac{1}{\rho}\frac{\mathrm{d}p}{\mathrm{d}t} = \frac{1}{\rho} \cdot \rho \cdot g \cdot \frac{\partial\,(h-z)}{\partial t} + \frac{1}{\rho} \cdot \rho \cdot g \cdot \frac{\partial\,(h-z)}{\partial x} v \tag{12.25}$$

which may be simplified further:

$$\frac{1}{\rho}\frac{\mathrm{d}p}{\mathrm{d}t} = g\left(\frac{\partial\,(h-z)}{\partial t} + v\frac{\partial\,(h-z)}{\partial x}\right) = g\frac{\partial h}{\partial t} + vg\frac{\partial h}{\partial x} - g\frac{\partial z}{\partial t} - vg\frac{\partial z}{\partial x} \tag{12.26}$$

[B] For a better understanding of the situation, refer to the adjacent diagram. In the following discussion, the piezometric pressure height h is used; in order to obtain the pressure height $\frac{p}{\rho g}$, the geodetic height z must be deducted at the corresponding location.

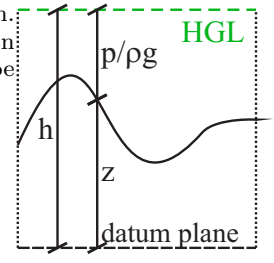

Two issues become evident from Equation 12.26. First, the term $g\frac{\partial z}{\partial t}$ must be zero since otherwise we would face a huge problem. The pipeline should not change its vertical position over time! And second, $\frac{\partial z}{\partial x}$ corresponds to the negative sine of the pipeline angle δ with respect to the horizontal.
The continuity equation (12.23) may ultimately be written as follows:

$$\frac{\partial v}{\partial x} + \frac{g}{a^2}\frac{\partial h}{\partial t} + \frac{vg}{a^2}\frac{\partial h}{\partial x} + \frac{vg}{a^2}\sin\delta = 0 \tag{12.27}$$

12.3 Energy equation according to Alliévi

We derive the unsteady energy equation similarly to the Bernoulli equation (Chapter 5.7), with the exception that the local derivative $\frac{\partial u_i}{\partial t}$ is not set to zero. Since the Bernoulli equation is obtained from the Euler equation by integrating along a streamline, the unsteady term for the streamline in the x-direction is $\frac{1}{g}\frac{\partial v}{\partial t}\,\mathrm{d}x$ (in metres), hence, the Bernoulli equation with the unsteady term, reads

$$z_1 + \frac{p_1}{\rho g} + \frac{v_1^2}{2g} = z_2 + \frac{p_2}{\rho g} + \frac{v_2^2}{2g} + \frac{1}{g}\frac{\partial v}{\partial t}\,\mathrm{d}x \tag{12.28}$$

where the geodetic height and the pressure height may again be rewritten as the piezometric pressure height $h = z + \frac{p}{\rho g}$. With $h_2 - h_1 = \mathrm{d}h$ and $\frac{v_2^2}{2g} - \frac{v_1^2}{2g} = \mathrm{d}\left(\frac{v^2}{2g}\right) = \frac{v}{g}\,\mathrm{d}v$, Equation 12.28 becomes:

$$\mathrm{d}h + \frac{v}{g}\,\mathrm{d}v + \frac{1}{g}\frac{\partial v}{\partial t}\,\mathrm{d}x = 0 \tag{12.29}$$

In the next step, Equation 12.29 is divided by $\mathrm{d}x$.

$$\frac{\mathrm{d}h}{\mathrm{d}x} + \frac{v}{g}\frac{\mathrm{d}v}{\mathrm{d}x} + \frac{1}{g}\frac{\partial v}{\partial t} = 0 \tag{12.30}$$

The disturbance is propagated at $\pm a = \frac{\mathrm{d}x}{\mathrm{d}t}$, which solved for $\mathrm{d}x$ and the result substituted into $\frac{v}{g}\frac{\mathrm{d}v}{\mathrm{d}x}$ yields $\frac{v}{ga}\frac{\partial v}{\partial t}$. However, it must be ensured that the ordinary derivative of the velocity with respect to time becomes the partial one, not to get confused with the total derivative. We can also write the partial derivative for the spatial gradient of the piezometric pressure height. At any rate, it is apparent that division by the very large value ga causes the term to become negligibly small. In addition to the continuity equation (12.27), we thereby obtain Alliévi's second equation:

$$\frac{\partial h}{\partial x} + \frac{1}{g}\frac{\partial v}{\partial t} = 0 \tag{12.31}$$

12.4 Riemann solution of the Alliévi equations

In the continuity condition (12.27) we see the total differential of the piezometric pressure height with respect to time $\frac{g}{a^2}\frac{\partial h}{\partial t} + \frac{vg}{a^2}\frac{\partial h}{\partial x} = \frac{g}{a^2}\frac{\mathrm{d}h}{\mathrm{d}t}$. Via $\mathrm{d}x = a \cdot \mathrm{d}t$ (written as $a \cdot \partial t$ in the partial

differential equation), the convective derivative becomes $\left(\frac{g}{a^2}\right)\frac{v}{a}\frac{\partial h}{\partial t}$, which is negligible since $v \ll a$ (see e. g. [5, p. 118] or [19, p. 252]). Without blinking an eye, we also eliminate the term with the pipeline gradient $vg\frac{\partial z}{\partial x}$ (that is $\frac{vg}{a^2}\sin\delta$ in Equation 12.27) for the same reason. Thus, the coupled Alliévi equations that describe energy (12.32) and continuity (12.33) of an unsteady pipe flow read:

$$\frac{\partial h}{\partial x} + \frac{1}{g}\frac{\partial v}{\partial t} = 0 \tag{12.32}$$

$$\frac{\partial v}{\partial x} + \frac{g}{a^2}\frac{\partial h}{\partial t} = 0 \tag{12.33}$$

For the solution of these differential equations, first, the coordinate $x' = L - x$ is defined; it extends from the valve at the lower reservoir opposite to the flow direction (i. e. in the direction of the negative x-axis) to the upper reservoir (see Figure 12.6). Let's rewrite

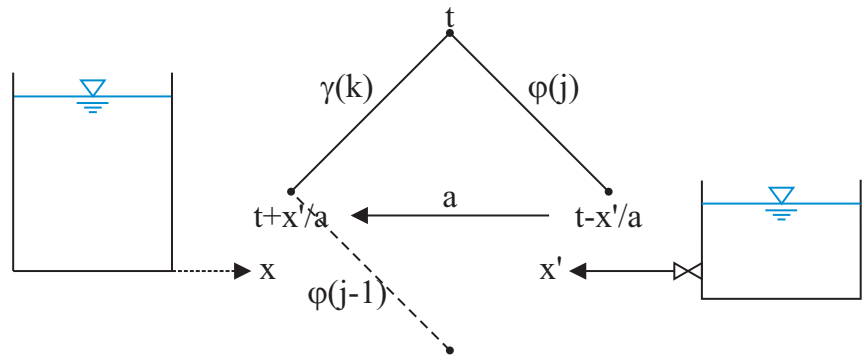

Figure 12.6: Explanations concerning functions $\phi(t-\frac{x'}{a})$ and $\gamma(t+\frac{x'}{a})$.

Equations 12.32 and 12.33 as:

$$\frac{\partial h}{\partial x'} = \frac{1}{g}\frac{\partial v}{\partial t} \tag{12.34}$$

$$\frac{\partial v}{\partial x'} = \frac{g}{a^2}\frac{\partial h}{\partial t} \tag{12.35}$$

We do as Jaeger did [19, page 250 et sqq.] and write down the general solution of the partial differential Equations 12.34 and 12.35 that Riemann[C] found [8, p.s 549-550]. Later we will prove that these are in fact the solutions.

$$h(x',t) = h_0 + \phi(t-\frac{x'}{a}) + \gamma(t+\frac{x'}{a}) \tag{12.36}$$

$$v(x',t) = v_0 - \frac{g}{a}\left[\phi(t-\frac{x'}{a}) - \gamma(t+\frac{x'}{a})\right] \tag{12.37}$$

In Equations 12.36 and 12.37, ϕ and γ are arbitrary integration functions that are determined by their boundary conditions. h_0 and v_0 are the constants of integration, hence

[C] Georg Friedrich Bernhard Riemann, ∗1826, Breselenz, Germany †1866, Lago Maggiore, Italy

the conditions of the steady-state. We can see that the above equations are indeed the solutions of the differential equations when we take the derivative of 12.36 with respect to x' and multiply with $\frac{dt}{dt}$. Again, we substitute $\frac{dx'}{dt} = a$. $\frac{d\phi(t-\frac{x'}{a})}{dx'}$ yields $-\phi\prime$ because of $-\frac{x'}{a}$. Subsequently, we derive 12.37 with respect to t[D]:

$$\frac{\partial h}{\partial x'} = -\frac{1}{a}\phi\prime(t-\frac{x'}{a}) + \frac{1}{a}\gamma\prime(t+\frac{x'}{a}) \tag{12.38}$$

$$\frac{\partial v}{\partial t} = -\frac{g}{a}\phi\prime(t-\frac{x'}{a}) + \frac{g}{a}\gamma\prime(t+\frac{x'}{a}) \tag{12.39}$$

The relationship between $\frac{\partial h}{\partial x'}$ and $\frac{\partial v}{\partial t}$ can easily be seen in Equations 12.38 and 12.39:

$$\frac{\partial h}{\partial x'} = \frac{1}{g}\frac{\partial v}{\partial t} \tag{12.40}$$

Similarly, we take the derivative of 12.36 with respect to t and 12.37 with respect to x', which yields:

$$\frac{\partial h}{\partial t} = \phi\prime(t-\frac{x'}{a}) + \gamma\prime(t+\frac{x'}{a}) \tag{12.41}$$

$$\frac{\partial v}{\partial x'} = \frac{g}{a^2}\phi\prime(t-\frac{x'}{a}) + \frac{g}{a^2}\gamma\prime(t+\frac{x'}{a}) \tag{12.42}$$

With these expressions, the relationship between $\frac{\partial h}{\partial t}$ and $\frac{\partial v}{\partial x'}$ becomes obvious:

$$\frac{\partial v}{\partial x'} = \frac{g}{a^2}\frac{\partial h}{\partial t} \tag{12.43}$$

Thus, we can accept that Riemann had found the correct solution. Let's describe the physical meaning of functions ϕ and γ. Jaeger [19] sends an observer with the propagation velocity a in the direction of x' on a trip. His position depends on the time travelling and his starting point x_1; here, $x' = at + x'_1$. For the passenger, the function ϕ does not change its value along x':

$$\phi(t-\frac{x'}{a}) = \phi(t-\frac{at+x'_1}{a}) = \phi(\frac{x'_1}{a}) = \text{const.} \tag{12.44}$$

Now, we send a female observer from x'_2 with a against the direction of x'. She as well does not notice any changes[E].

$$\gamma(t+\frac{x'}{a}) = \gamma(t+\frac{x'_2-at}{a}) = \gamma(\frac{x'_2}{a}) = \text{const.} \tag{12.45}$$

From the units of the functions (metre) we see that ϕ and γ must be undistorted pressure waves that propagate in the same direction as (primary wave ϕ) and opposite the direction of (reflection wave γ) the coordinate direction x'. It becomes obvious that the pressure height $h(x',t)$ consists of the steady-state condition h_0 and the superposition of

[D] Just for now, we call $\phi\prime$ and $\gamma\prime$ the derivatives of these functions since we won't need them any longer. Please don't get confused with the symbols. x' stands for the coordinate direction, whereas $\phi\prime$ denotes the (partial) derivative with respect to time.

[E] Euler, of course, sees variations of the function values x and t.

the two waves. As you can surely imagine, the functions ϕ and γ depend on the boundary conditions.
With Formula 12.36, one obtains (e. g. for a container with a free water surface at the beginning of a penstock, where $(h(L,t) = h_0 = h_o)$):

$$h(L,t) = h_0 + \phi(t - \frac{L}{a}) + \gamma(t + \frac{L}{a}) = h_o \tag{12.46}$$

We can read from Equation 12.46 that $\phi(t - \frac{L}{a}) = -\gamma(t + \frac{L}{a})$. The pressure wave, which keeps its absolute value, is being reflected at the reservoir with a negative sign (total reflection). Setting $t = t_i - \frac{L}{a}$ yields $\phi(t_i - \frac{2L}{a}) = -\gamma(t_i)$[F]. For a total reflection, the pressure wave γ corresponds to the negative wave $(-\phi)$ of the previous phase, hence we can generalise:

$$\gamma(t) = -\phi(t - \frac{2L}{a}) \tag{12.47}$$

We still follow the descriptive steps, however reduced, from Jaeger [19]. If we name the initial time step of the pressure surge $t_1 = 0$ and consider the primary time steps $t_i = (i-1)\frac{2L}{a}$ solely at $x' = 0$, we will obtain Equations 12.36 and 12.37:

$$h(t_i) = h_0 + \phi(t_i) + \gamma(t_i) \tag{12.48}$$

$$v(t_i) = v_0 - \frac{g}{a}[\phi(t_i) - \gamma(t_i)] \tag{12.49}$$

We can simplify the relationship further using formula 12.47 :

$$h(t_i) = h_0 + \phi(t_i) - \phi(t_{i-1}) \tag{12.50}$$

$$v(t_i) = v_0 - \frac{g}{a}[\phi(t_i) + \phi(t_{i-1})] \tag{12.51}$$

The example in the following Chapter 12.5 illustrates these concepts.

12.5 Joukowsky surge

The propagation of solid body waves occurs at the speed of sound. In our case with two different media, the propagation velocity is determined via the system stiffness E_{sys} (see Equation 12.22). This means that a disturbance at the end of a pipeline, which is reflected at the other end, arrives again at the place of origin after time $t_R = \frac{2L}{a}$. When the pipeline is completely closed during time $0 < t < t_R = \frac{2L}{a}$, the conditions are not affected by the reflection. In Equations 12.36 and 12.37, $\gamma(t + \frac{x'}{a})$ becomes zero and consequently the equations are:

$$h(x',t) = h_0 + \phi(t - \frac{x'}{a}) \tag{12.52}$$

$$v(x',t) = v_0 - \frac{g}{a}\phi(t - \frac{x'}{a}) \tag{12.53}$$

[F] $\frac{2L}{a}$ represents the phase or the reflection time of the pressure wave, meaning the time that it needs to travel from $x' = 0$ to $x' = L$ and back to $x' = 0$.

The expression for the function $\phi(t-\frac{x'}{a})$ is derived therefrom (Equation 12.53) and inserted into Equation 12.52. We obtain

$$\phi(t-\frac{x'}{a}) = -\frac{a}{g}\left(v(x',t)-v_0\right) \tag{12.54}$$

and for the surge height (without the steady-state piezometric pressure height h_0):

$$h(x',t) = -\frac{a}{g}\left(v(x',t)-v_0\right) \tag{12.55}$$

Equation 12.55 assumes the maximum value for $h(x',t)$ at $v(x',0)=0$, i. e. when an abrupt (at least during time $t < t_R$) complete closure of a valve occurs. The maximum pressure increase due to unsteady flow events is the so-called Joukowsky[G] surge.

$$\Delta h_{\max} = \frac{a}{g}v_0 \tag{12.56}$$

The Joukowsky surge is the maximum occurring pressure increase due to the complete stop of the fluid mass within the reflection time t_R. The same effect – but with a reversed sign – occurs when abruptly opening a closed device.

Example

Pressure surge in a pipeline

To illustrate the functions, we use an example that will be discussed starting on page 202 and that uses the method of characteristics. From the calculations therein, we bring here the propagation velocity $a = 1255\,\mathrm{m/s}$ and the steady-state flow velocity $v_0 = 0.705\,\mathrm{m/s}$. The valve at the end of the pipeline system shown in Figure 12.13 is fully open in the steady-state and is to be completely closed instantaneously (within $t_C = 0\,\mathrm{s}$). The Joukowsky surge occurs because of $t_C < t_R$, and it occurs instantly since $t_C = 0$; furthermore, $\Delta h_{\max} = \frac{a}{g}v_0 = \frac{1255}{9.81}\cdot 0.705 = 90.25\,\mathrm{m}$.
When designating $t_1 = 0$ as the point of time at which the device is completely closed instantaneously (within $t_C = 0$) and setting $v(t_1) = 0$ in Equation 12.49, we obtain for the boundary condition of the abruptly closed valve at the lower reservoir:

$$\phi(t_1) = -\left(v(t_1)-v_0\right)\cdot\frac{a}{g} + \gamma(t_1) = v_0\frac{a}{g} \tag{12.57}$$

Since $\gamma(t_1)$ comes from ϕ of the previous time step (i. e. in the steady-state), $\gamma(t_1) = 0$[H]. Thus, $\phi(t_1) = v_0\frac{a}{g}$. We obtain the pressure surge height from Equation 12.36 as sum of the function values of γ and ϕ: $h(t_1) = \gamma(t_1) + \phi(t_1) = v_0\frac{a}{g} = \Delta h_{\max} = 90.25\,\mathrm{m}$[I]. The function ϕ conveys this information involving a in the direction of x'.

[G] Nikolay Yegorovich Zhukovsky, ∗1847, Orechowo, Russia †1921, Moscow, Russia

[H] The reflection wave is not yet here!

[I] Here again, we consider only the pressure surge component and set the hydrostatic pressure height to zero.

When the high pressure in the pipe has reached the upper reservoir after $t = \frac{L}{a}$, it causes the water to return into the reservoir. The reflection of the wave ϕ at the upper reservoir is therefore effected with the sign reversed ($\gamma = -\phi$; see Equation 12.46 or e. g. [29, p. 177]) since the pressure at the free end may be released. The good news that relaxation is in sight is propagated again with a via function γ from the upper reservoir until it arrives after $t = t_R = \frac{2L}{a}$ at the closed valve. With $v(t_i) = 0$ in Equation 12.49 or 12.51 we obtain with $t_2 = 2\frac{L}{a}$ for $\phi(t_2) = v_0\frac{a}{g} + \gamma(t_2) = v_0\frac{a}{g} - \phi(t_1) = 0$. Formula 12.50 yields the pressure surge height $h(t_2) = \phi(t_2) - \phi(t_1) = -90.25\,\mathrm{m}$. The water flowing in the direction of the upper reservoir cannot further acquire any fluid at the closed valve and expands the water mass as shown by the spring in the photo sequence on page 178.
The information that nothing more can be gained at the valve is again conveyed via $\phi = 0$ at velocity a in the direction of the upper reservoir and arrives there after $t = \frac{3L}{a}$. Due to the high-pressure gradient, water flows again from the reservoir into the pipe and the negative wave is again mirrored at the free end, which is accomplished mathematically with a sign reversal by means of $\gamma = -\phi$. The wave arrives again at the valve after $t_3 = 4\frac{L}{a}$. With $\phi(t_3) = v_0\frac{a}{g} + \gamma(t_3) = v_0\frac{a}{g} - \phi(t_2) = v_0\frac{a}{g} - 0 = 90.25\,\mathrm{m}$, the surge height becomes $h(t_3) = \phi(t_3) + \gamma(t_3) = \phi(t_3) = 90.25\,\mathrm{m}$. Because of the absence of losses, the process continues indefinitely.
It is essential to take the following three issues into consideration:

1. The pressure that is described and shown corresponds only to the dynamic component. The pressure surge height $h(x,t)$ must be superimposed with the hydrostatic pressure $h_0(x)$ at the designated place.
2. Due to the assumed absence of friction in the Alliévi method, the procedure is repeated forever and a day.
3. The physical properties of water subvert our theoretical construction. Its end is reached at a pressure height of approximately $-7.5\,\mathrm{mH_2O}$ (sum of dynamic and steady-state components). Water cannot withstand tensile forces and the liquid vaporizes (see Chapter 8.7). The negative (relative) pressure is limited to the vapour pressure, which according to Table 3.2 amounts to $p_v = 2338.5\,\mathrm{N/m^2}$ at $T = 20\,^\circ\mathrm{C}$; it must be ensured that the absolute pressure is applied (i. e. the sum of atmospheric pressure and water pressure; see Chapter 7.9). It follows from $p_{\mathrm{atm}} + h \cdot \rho g \geq p_v$ that at a pressure height relative to the pipe axis of $h \cdot \rho g \geq 2338 - 101\,300 = -98\,962\,\mathrm{N/m^2}$ (from which $h = -10.09\,\mathrm{m}$), the liquid water becomes gaseous. In our specific case with the pipeline height $z_{\mathrm{valve}} = 293\,\mathrm{m.a.s.l.}$, the piezometric pressure height cannot fall below 282.91 m (see Figure 12.7). The drinking straw experiment on page 179 demonstrated the effects of negative pressure (the atmospheric pressure is higher than the pressure in the pipeline). In order to avoid such problems, vent and bleed valves are installed at critical locations in the pipeline. Preferably, you test the effect yourselves by pricking a tiny hole in the straw.

Figure 12.7 shows the piezometric pressure height over a period of 60 s.
The digression via the Riemann-Alliévi equations to the Joukowsky surge was primarily intended to create an understanding of the processes taking place. With the unsteady momentum equation that is derived in the following section, we will feed the method of characteristics (Chapter 12.7) that we make use of to calculate realistic velocity and pressure conditions when discharge changes occur in pipelines.

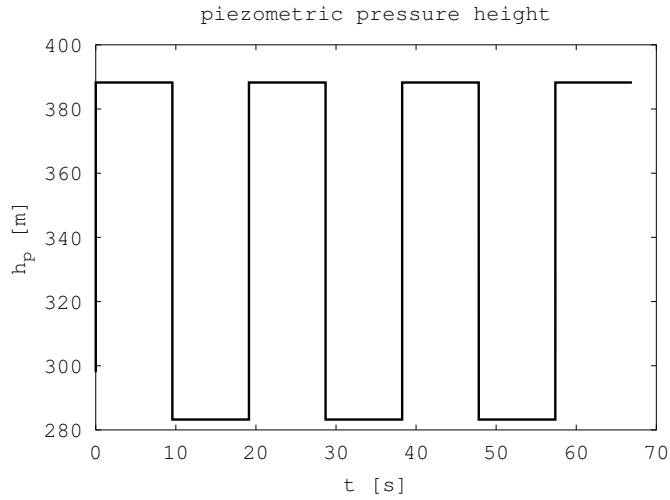

Figure 12.7: Piezometric pressure height at the valve for the pressure surge example.

12.6 Momentum equation

In this section, we derive the law of momentum for the unsteady pipe flow. Figure 12.8 shows the forces that act on a pipe section with unsteady flow.

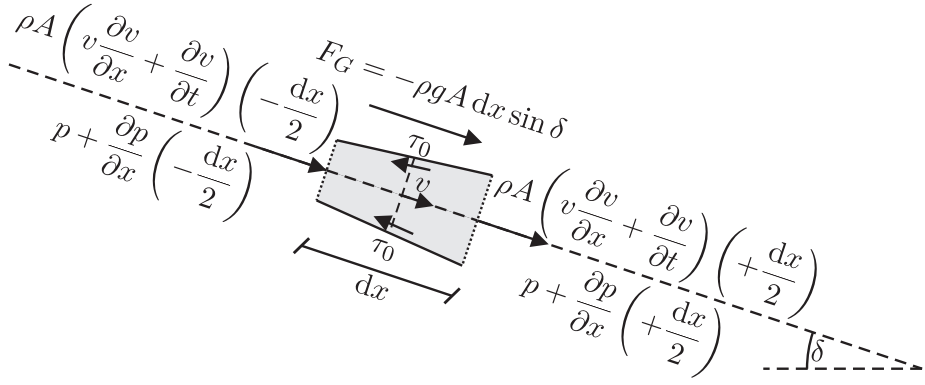

Figure 12.8: Forces on the control volume.

Pressure force:

$$F_P = -A\frac{\partial p}{\partial x}\,\mathrm{d}x \tag{12.58}$$

Gravity or downward force in the direction of the pipe axis:

$$F_G = -\rho gA\frac{\partial z}{\partial x}\,\mathrm{d}x = -\rho gA\,\mathrm{d}x\sin\delta \tag{12.59}$$

Friction force:

$$F_F = -\pi D\tau_w\,\mathrm{d}x \tag{12.60}$$

With the friction coefficient from Chapter 11 in the equation $\tau_w = \frac{\rho f_D v^2}{8}$ and the Darcy-Weisbach equation $f_D = \frac{J_E D 2g}{v^2}$, it follows that the shear stress can be expressed as $\tau_w = \frac{\rho J_E D g}{4}$. As a result, Equation 12.60 assumes the following appearance:

$$F_F = -\pi D \tau_w \, \mathrm{d}x = -\pi D \, \mathrm{d}x \frac{\rho J_E D g}{4} = -A \rho g J_E \, \mathrm{d}x \tag{12.61}$$

Inertia force:

$$F_I = \rho A \left(v \frac{\partial v}{\partial x} + \frac{\partial v}{\partial t} \right) \mathrm{d}x \tag{12.62}$$

This corresponds to the rate of change of momentum. The direction of action of the momentum fluxes at both interfaces of the control volume is "into" it (see Chapter 5.8), which is why this change also acts opposite to the direction of flow.
The sum of the forces is zero:

$$F_P + F_G + F_F + F_I = -A \frac{\partial p}{\partial x} \mathrm{d}x - \rho g A \frac{\partial z}{\partial x} \mathrm{d}x - A \rho g J_E \, \mathrm{d}x - \rho A \left(v \frac{\partial v}{\partial x} + \frac{\partial v}{\partial t} \right) \mathrm{d}x = 0 \tag{12.63}$$

We set $\mathrm{d}p = \rho \cdot g \cdot \mathrm{d}(h - z)$ (see Chapter 12.2) or rather the partial derivative with respect to x, $\frac{\partial p}{\partial x} = \rho \cdot g \frac{\partial (h-z)}{\partial x}$. We also divide Equation 12.63 by $-\mathrm{d}x$:

$$A \rho g \frac{\partial (h-z)}{\partial x} + \rho g A \frac{\partial z}{\partial x} + A \rho g J_E + \rho A \left(\frac{\partial v}{\partial t} + v \frac{\partial v}{\partial x} \right) = 0 \tag{12.64}$$

We divide this by ρA and temporarily obtain

$$g \frac{\partial h}{\partial x} - g \frac{\partial z}{\partial x} + g \frac{\partial z}{\partial x} + g J_E + \frac{\partial v}{\partial t} + v \frac{\partial v}{\partial x} = 0 \tag{12.65}$$

and ultimately the momentum equation for unsteady pipe flows:

$$g \frac{\partial h}{\partial x} + g J_E + \frac{\partial v}{\partial t} + v \frac{\partial v}{\partial x} = 0 \tag{12.66}$$

12.7 Method of characteristics

If we were to ask mathematicians about Equations 12.27 and 12.66, they would respond that they are quasilinear partial differential equations of the hyperbolic type[J] and cannot be solved as a closed system. By means of the method of characteristics, we can solve simplified equations at discrete times and places. For these equations, the boundary conditions of the steady-state flow are required. The equations allow one to successively step by the time increment Δt at specific places. The equations and the boundary conditions will be derived on the following pages before practising the method of characteristics by means of an example.

[J] In hyperbolic differential equations, disturbances propagate in two different directions; in parabolic differential equations, they propagate in one direction only, and elliptic differential equations are immune from disturbances.

We reproduce the continuity condition and the momentum equation and add to this set of equations two trivial equations that describe the total differential of h and v with chain rule (an alternative notation for e. g. $\mathrm{d}h$ appears more common: $\frac{\mathrm{d}h}{\mathrm{d}t} = \frac{\partial h}{\partial x}\frac{\mathrm{d}x}{\mathrm{d}t} + \frac{\partial h}{\partial t}$).

$$\frac{\partial v}{\partial x} + \frac{g}{a^2}\frac{\partial h}{\partial t} + \frac{vg}{a^2}\frac{\partial h}{\partial x} + \frac{vg}{a^2}\sin\delta = 0 \tag{12.67}$$

$$g\frac{\partial h}{\partial x} + gJ_E + \frac{\partial v}{\partial t} + v\frac{\partial v}{\partial x} = 0 \tag{12.68}$$

$$\mathrm{d}h = \frac{\partial h}{\partial x}\mathrm{d}x + \frac{\partial h}{\partial t}\mathrm{d}t \tag{12.69}$$

$$\mathrm{d}v = \frac{\partial v}{\partial x}\mathrm{d}x + \frac{\partial v}{\partial t}\mathrm{d}t \tag{12.70}$$

We sort and write down the following system of equations:

$$\begin{pmatrix} \frac{gv}{a^2} & 1 & \frac{g}{a^2} & 0 \\ g & v & 0 & 1 \\ \mathrm{d}x & 0 & \mathrm{d}t & 0 \\ 0 & \mathrm{d}x & 0 & \mathrm{d}t \end{pmatrix} \begin{pmatrix} \frac{\partial h}{\partial x} \\ \frac{\partial v}{\partial x} \\ \frac{\partial h}{\partial t} \\ \frac{\partial v}{\partial t} \end{pmatrix} = \begin{pmatrix} -\frac{gv}{a^2}\sin\delta \\ -gJ_E \\ \mathrm{d}h \\ \mathrm{d}v \end{pmatrix} \tag{12.71}$$

This system of equations ($A \circ x = b$) yields an unambiguous solution if $\det(A) \neq 0$, which, however, we do not aim for because then there would be no changes in space and time. Thus, we force $\det(A) = 0$.

$$\det(A) \equiv \begin{vmatrix} \frac{gv}{a^2} & 1 & \frac{g}{a^2} & 0 \\ g & v & 0 & 1 \\ \mathrm{d}x & 0 & \mathrm{d}t & 0 \\ 0 & \mathrm{d}x & 0 & \mathrm{d}t \end{vmatrix} = 0 \tag{12.72}$$

The evaluation of determinants and/or subdeterminants is described in [8, p. 269]. To make the following steps more transparent, we calculate the determinant of a matrix in Appendix A.4. Fortunately, some of the elements are zero.

$$\begin{aligned}
\det &\equiv \frac{gv}{a^2}\begin{vmatrix} v & 0 & 1 \\ 0 & \mathrm{d}t & 0 \\ \mathrm{d}x & 0 & \mathrm{d}t \end{vmatrix} - 1\begin{vmatrix} g & 0 & 1 \\ \mathrm{d}x & \mathrm{d}t & 0 \\ 0 & 0 & \mathrm{d}t \end{vmatrix} + \frac{g}{a^2}\begin{vmatrix} g & v & 1 \\ \mathrm{d}x & 0 & 0 \\ 0 & \mathrm{d}x & \mathrm{d}t \end{vmatrix} \\
&= \frac{gv}{a^2}\left(v\begin{vmatrix} \mathrm{d}t & 0 \\ 0 & \mathrm{d}t \end{vmatrix} + 1\begin{vmatrix} 0 & \mathrm{d}t \\ \mathrm{d}x & 0 \end{vmatrix}\right) - 1\left(g\begin{vmatrix} \mathrm{d}t & 0 \\ 0 & \mathrm{d}t \end{vmatrix} + 1\begin{vmatrix} \mathrm{d}x & \mathrm{d}t \\ 0 & 0 \end{vmatrix}\right) \\
&+ \frac{g}{a^2}\left(g\begin{vmatrix} 0 & 0 \\ \mathrm{d}x & \mathrm{d}t \end{vmatrix} - v\begin{vmatrix} \mathrm{d}x & 0 \\ 0 & \mathrm{d}t \end{vmatrix} + 1\begin{vmatrix} \mathrm{d}x & 0 \\ 0 & \mathrm{d}x \end{vmatrix}\right) \\
&= \frac{gv}{a^2}\left(v\left(\mathrm{d}t\,\mathrm{d}t - 0\right) + 1\left(0 - \mathrm{d}t\,\mathrm{d}x\right)\right) - 1\left(g\left(\mathrm{d}t\,\mathrm{d}t - 0\right) + 1\left(0 - 0\right)\right) \\
&+ \frac{g}{a^2}\left(g\left(0 - 0\right) - v\left(\mathrm{d}x\,\mathrm{d}t - 0\right) + 1\left(\mathrm{d}x\,\mathrm{d}x - 0\right)\right) \\
&= \frac{gv}{a^2}\left(v\mathrm{d}^2t - \mathrm{d}t\,\mathrm{d}x\right) - g\mathrm{d}^2t + \frac{g}{a^2}\left(-v\,\mathrm{d}x\,\mathrm{d}t + \mathrm{d}^2x\right) \\
&= \frac{gv^2\mathrm{d}^2t}{a^2} - \frac{gv\,\mathrm{d}t\,\mathrm{d}x}{a^2} - g\mathrm{d}^2t - \frac{gv\,\mathrm{d}x\,\mathrm{d}t}{a^2} + \frac{g\mathrm{d}^2x}{a^2} = 0
\end{aligned} \tag{12.73}$$

We multiply by $\frac{a^2}{g\mathrm{d}^2t}$ and obtain

$$v^2 - 2v\frac{\mathrm{d}x}{\mathrm{d}t} + \frac{\mathrm{d}^2x}{\mathrm{d}^2t} - a^2 = 0 \tag{12.74}$$

which is put into the form of a quadratic equation:

$$\left(\frac{\mathrm{d}x}{\mathrm{d}t}\right)^2 - 2v\frac{\mathrm{d}x}{\mathrm{d}t} + v^2 - a^2 = 0 \tag{12.75}$$

The generally known solution for a quadratic equation $x_{1,2} = \frac{-b \pm \sqrt{b^2-4ac}}{2a}$ yields:

$$\frac{\mathrm{d}x}{\mathrm{d}t} = \frac{2v \pm \sqrt{4v^2 - 4v^2 + 4a^2}}{2} = \frac{2v \pm 2a}{2} = v \pm a \tag{12.76}$$

For the condition that we established (that the determinant be 0 or that there are to be variations in space and time), the solution is valid only along the characteristic directions:

$$C_+ \equiv \frac{\mathrm{d}x}{\mathrm{d}t} = v + a \tag{12.77}$$

$$C_- \equiv \frac{\mathrm{d}x}{\mathrm{d}t} = v - a \tag{12.78}$$

Wow! Though not particularly difficult, this was time-consuming. Time for a break.
When consulting a mathematician, she or he will explain that the system provides a solution when $\det(A) = 0$ only if all determinants, which are formed by replacing an arbitrary column of the matrix by the resultant vector on the right-hand side, are also zero. We focus on the first column and replace it by the resultant vector of Equation 12.71:

$$\begin{aligned}
\det \equiv & -\frac{gv}{a^2}\sin\delta \begin{vmatrix} v & 0 & 1 \\ 0 & \mathrm{d}t & 0 \\ \mathrm{d}x & 0 & \mathrm{d}t \end{vmatrix} - 1 \begin{vmatrix} -gJ_E & 0 & 1 \\ \mathrm{d}h & \mathrm{d}t & 0 \\ \mathrm{d}v & 0 & \mathrm{d}t \end{vmatrix} + \frac{g}{a^2} \begin{vmatrix} -gJ_E & v & 1 \\ \mathrm{d}h & 0 & 0 \\ \mathrm{d}v & \mathrm{d}x & \mathrm{d}t \end{vmatrix} \\
= & -\frac{gv}{a^2}\sin\delta \left(v \begin{vmatrix} \mathrm{d}t & 0 \\ 0 & \mathrm{d}t \end{vmatrix} + 1 \begin{vmatrix} 0 & \mathrm{d}t \\ \mathrm{d}x & 0 \end{vmatrix} \right) - 1 \left(-gJ_E \begin{vmatrix} \mathrm{d}t & 0 \\ 0 & \mathrm{d}t \end{vmatrix} + 1 \begin{vmatrix} \mathrm{d}h & \mathrm{d}t \\ \mathrm{d}v & 0 \end{vmatrix} \right) \\
& + \frac{g}{a^2} \left(-gJ_E \begin{vmatrix} 0 & 0 \\ \mathrm{d}x & \mathrm{d}t \end{vmatrix} - v \begin{vmatrix} \mathrm{d}h & 0 \\ \mathrm{d}v & \mathrm{d}t \end{vmatrix} + 1 \begin{vmatrix} \mathrm{d}h & 0 \\ \mathrm{d}v & \mathrm{d}x \end{vmatrix} \right) \\
= & -\frac{gv}{a^2}\sin\delta \left(v\left(\mathrm{d}t\,\mathrm{d}t - 0\right) + 1\left(0 - \mathrm{d}t\,\mathrm{d}x\right)\right) - 1\left(-gJ_E\left(\mathrm{d}t\,\mathrm{d}t - 0\right) + 1\left(0 - \mathrm{d}t\,\mathrm{d}v\right)\right) \\
& + \frac{g}{a^2}\left(-gJ_E\left(0 - 0\right) - v\left(\mathrm{d}h\,\mathrm{d}t - 0\right) + 1\left(\mathrm{d}h\,\mathrm{d}x - 0\right)\right) \\
= & \frac{gv}{a^2}\sin\delta\,\mathrm{d}t\,\mathrm{d}x - \frac{gv}{a^2}\sin\delta v\mathrm{d}^2t + gJ_E\mathrm{d}^2t + \mathrm{d}t\,\mathrm{d}v + \frac{g}{a^2}\mathrm{d}h\,\mathrm{d}x - \frac{g}{a^2}v\,\mathrm{d}h\,\mathrm{d}t = 0
\end{aligned} \tag{12.79}$$

In the next step, we divide by d^2t:

$$\frac{gv}{a^2}\sin\delta\frac{\mathrm{d}x}{\mathrm{d}t} - \frac{gv}{a^2}\sin\delta v + gJ_E + \frac{\mathrm{d}v}{\mathrm{d}t} + \frac{g}{a^2}\frac{\mathrm{d}h}{\mathrm{d}t}\frac{\mathrm{d}x}{\mathrm{d}t} - \frac{gv}{a^2}\frac{\mathrm{d}h}{\mathrm{d}t} = 0 \tag{12.80}$$

With the first condition $\frac{\mathrm{d}x}{\mathrm{d}t} = v \pm a$, it follows that

$$\frac{gv}{a^2}\sin\delta\,(v\pm a)-\frac{gv}{a^2}\sin\delta v+gJ_E+\frac{\mathrm{d}v}{\mathrm{d}t}+\frac{g}{a^2}\frac{\mathrm{d}h}{\mathrm{d}t}\,(v\pm a)-\frac{gv}{a^2}\frac{\mathrm{d}h}{\mathrm{d}t}$$
$$=\pm\frac{gv}{a}\sin\delta+gJ_E+\frac{\mathrm{d}v}{\mathrm{d}t}\pm\frac{g}{a}\frac{\mathrm{d}h}{\mathrm{d}t}=0 \tag{12.81}$$

Finally, we obtain:

$$C_+ \Rightarrow \quad \frac{gv}{a}\sin\delta+gJ_E+\frac{\mathrm{d}v}{\mathrm{d}t}+\frac{g}{a}\frac{\mathrm{d}h}{\mathrm{d}t}=0 \tag{12.82}$$

$$C_- \Rightarrow \quad -\frac{gv}{a}\sin\delta+gJ_E+\frac{\mathrm{d}v}{\mathrm{d}t}-\frac{g}{a}\frac{\mathrm{d}h}{\mathrm{d}t}=0 \tag{12.83}$$

For the characteristic directions (12.77 and 12.78), the equations are equivalent to Equations 12.27 and 12.66, but their solution is much easier. These characteristic directions are depicted in the *x*-*t* diagram of Figure 12.9.

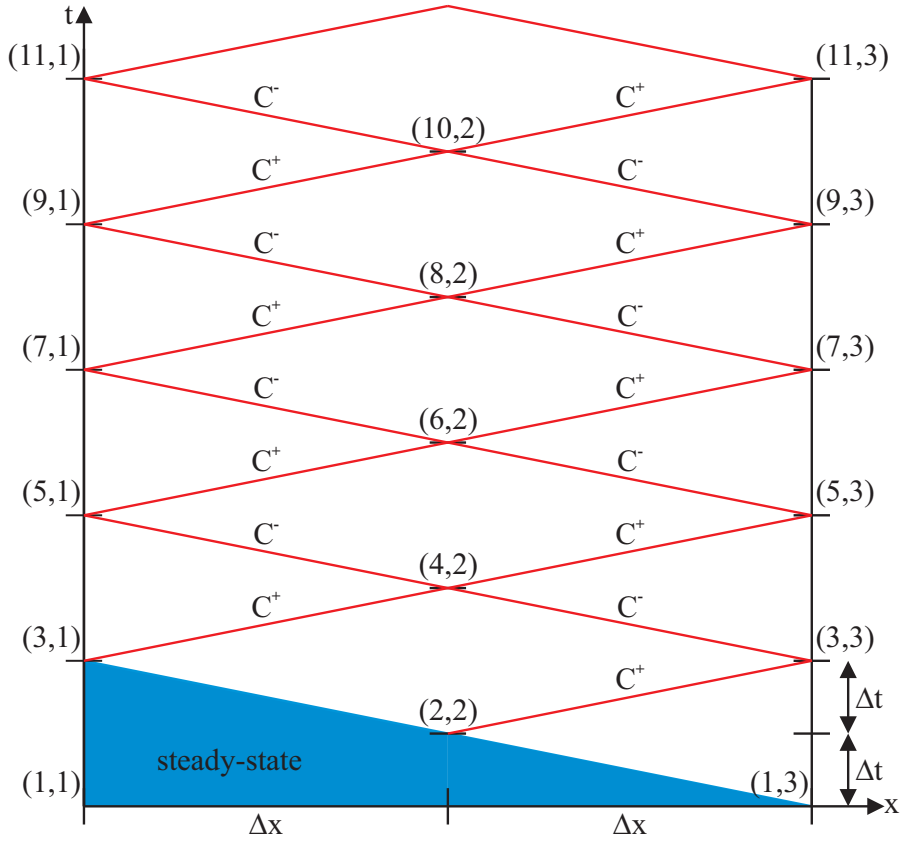

Figure 12.9: Characteristics grid.

We multiply Equations 12.82 and 12.83 by $\frac{a}{g}\,\mathrm{d}t$ and introduce difference quotients instead of the differential quotients for solving the equations on the discrete grid (see Figure 12.9). And we simplify further. The propagation velocity $a=\sqrt{\frac{\rho}{E_{\mathrm{sys}}}}$ in rigid pipes amounts to approximately 1000 m/s and the flow velocity, in general, is approximately 1.0 m/s; hence the characteristics may be approximated sufficiently accurately as $\pm a$. The term

$\frac{gv}{a}\sin\delta$ also falls victim to the same consideration, which in particular applies to pipelines normally laid horizontally (see Chapter 12.4 and [5, p. 118] or [19, p. 252]). In addition, a $\pm$ sign is smuggled into the friction term. The explanation for this is brief: because the gradient of the energy grade line was written for direction x, the C_- characteristic extends in the opposite direction. Equations 12.84 and 12.85 (below) are also referred to as compatibility conditions:

$$C_\pm = \pm a \tag{12.84}$$

$$\pm\Delta h + \frac{a}{g}\Delta v \pm a\Delta t J_E = 0 \tag{12.85}$$

We take the friction term from Chapter 11, $J_E = \mathrm{sgn}(v)\frac{f_\mathrm{D}}{D}\frac{v^2}{2g}$. Since the direction of flow may reverse in the unsteady flow, and because the velocity height is a scalar quantity, we must multiply by the sign of the velocity $\mathrm{sgn}(v)$. The gradient of the energy grade line always points in the direction of motion.

12.7.1 Initial characteristic

The initial characteristic describes the steady-state conditions. These apply at time $t = 0$, which is designated by the index $i = 1$. Information such as discharge or pressure variations is propagated at the velocity of sound waves with the characteristics C_+ in the flow direction and C_- opposite the direction of flow.
The energy loss is determined via the Darcy-Weisbach approach. A_V identifies the open valve area which is reduced in a manner similar to the outflow from openings by means of the valve coefficient μ_V (see Equations 12.109 and 12.120).

$$\Delta e = h_l - h_r = \frac{Q^2}{A_P^2 2g}\left(\frac{f_\mathrm{D}L}{D} + \sum_{i=1}^{n} K_i\right) + \Delta e_V = \frac{Q^2}{A_P^2 2g}\left(\frac{f_\mathrm{D}L}{D} + \sum_{i=1}^{n} K_i + \frac{A_P^2}{\mu_V^2 A_V^2}\right) \tag{12.86}$$

Equation 12.86 is solved for v_0, i. e. the steady-state velocity:

$$v_0 = \sqrt{\frac{(h_l - h_r)\,2g}{\frac{f_\mathrm{D}L}{D} + \sum_{i=1}^{n} K_i + \frac{A_P^2}{\mu_V^2 A_V^2}}} \tag{12.87}$$

The pressure height in the steady-state case may be determined with Equation 12.88. Compared to the pipe friction losses, minor losses are generally small. The velocity height at $v \leq 4.4\,\mathrm{m/s}$ is below $1.0\,\mathrm{m}$. Since flow velocities in pipelines are even lower in most cases, it is generally assumed in the method of characteristics that hydraulic and energy grade line coincide [5, p. 348]. The slope of the hydraulic grade line ($h_0(x)$) is therefore assumed to be constant between upper and lower reservoir levels, and the outflow loss $K_O = 1$ disappears in Equation 12.88. However, the initial velocity is determined including the minor (local) losses as shown in Equation 12.87.

$$h_0(x) = h_0 - \frac{v_P^2}{2g}\frac{f_\mathrm{D}x}{D} \tag{12.88}$$

12.7.2 Calculation modules

The following considerations on the C_+ and C_- characteristics build the foundation for the calculation of the conditions at the nodes j in a time step $i+1$. Therein, $j=1$ designates the start of the pipeline (upstream end); $j=n$ indicates the downstream end. $i=1$ identifies the start of the discharge variation. Since the equations apply only along the C_+ and the C_- characteristics, the time interval Δt between the calculation steps is dependent on the spatial resolution of the computational domain (see Figure 12.9). Principally, a distinction must be made between nodes within the grid and nodes located at the boundary.

12.7.3 Nodes within the domain

Figure 12.10 shows the conditions within the calculation domain. What happens at node j at time i is determined by the conditions conveyed by the C_+ characteristic of node $j-1$ as well as by information delivered by the C_- characteristic of node $j+1$ at time $i-1$.

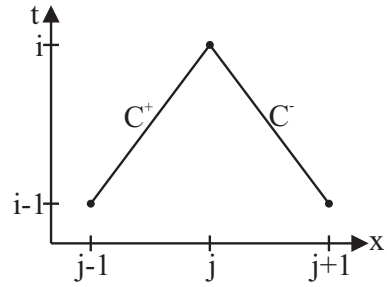

Figure 12.10: Conditions within the grid.

Let's start with the compatibility condition of the C_+ characteristic: $\Delta h+\frac{a}{g}\Delta v+a\Delta t J_E=0$. With the indexing shown in Figure 12.10, it reads:

$$h_{(i,j)}-h_{(i-1,j-1)}+\frac{a}{g}\left(v_{(i,j)}-v_{(i-1,j-1)}\right)+a\Delta t J_{E(i-1,j-1)}=0 \tag{12.89}$$

We will now go into greater detail on the C_- compatibility. The first term reads $-\Delta h=-\left(h_{(i-1,j+1)}-h_{(i,j)}\right)$, i. e. the greater x value minus the smaller one. Likewise, the velocity difference is written $\Delta v=\left(v_{(i-1,j+1)}-v_{(i,j)}\right)$. The gradient of the energy grade line is initially directed opposite to the C_- characteristic, as mentioned above, because $J_E=\frac{\Delta e}{\Delta x}$ stands for the energy grade line and therefore Δx is negative here as well as in the pressure height and velocity terms.

$$-\left(h_{(i-1,j+1)}-h_{(i,j)}\right)+\frac{a}{g}\left(v_{(i-1,j+1)}-v_{(i,j)}\right)-a\Delta t J_{E(i-1,j+1)}=0 \tag{12.90}$$

We will first equate the known quantities of Equations 12.89 and 12.90 to the auxiliary variables $K^+_{(i-1,j-1)}$ and $K^-_{(i-1,j+1)}$.

$$K^{+}_{(i-1,j-1)} = -h_{(i-1,j-1)} - \frac{a}{g} v_{(i-1,j-1)} + a\Delta t J_{E(i-1,j-1)} \tag{12.91}$$

$$K^{-}_{(i-1,j+1)} = -h_{(i-1,j+1)} + \frac{a}{g} v_{(i-1,j+1)} - a\Delta t J_{E(i-1,j+1)} \tag{12.92}$$

The two compatibility conditions C_+ and C_- may be expressed more simply with these two auxiliary variables K^+ and K^-. It is evident that two equations exist for the two unknowns $h_{(i,j)}$ and $v_{(i,j)}$. We insert K^+ and K^- into the respective Equations 12.89 and 12.90 and solve them to obtain $v(i,j)$ and $h(i,j)$.

$$v_{(i,j)} = \frac{g}{a} \frac{K^{-}_{(i-1,j+1)} - K^{+}_{(i-1,j-1)}}{2} \tag{12.93}$$

$$h_{(i,j)} = -\frac{K^{-}_{(i-1,j+1)} + K^{+}_{(i-1,j-1)}}{2} \tag{12.94}$$

12.7.4 Nodes at the left boundary

Figure 12.11 illustrates the conditions at the left boundary of the computational domain. The situation at node $j = 1$ at time i is described by the conditions of node $j+1$ (i. e. $j = 2$) conveyed by the C_- characteristic at time $i-1$. For the determination of variables $v_{(i,j=1)}$ and $h_{(i,j=1)}$, yet another equation on the prevailing boundary conditions must be added (see below).

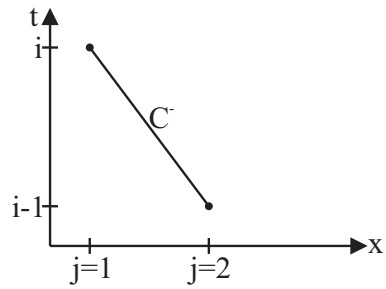

Figure 12.11: Conditions at the left boundary of the grid.

The C_- characteristic for the left node $j = 1$ generally reads:

$$-\left(h_{(i-1,j+1)} - h_{(i,j)}\right) + \frac{a}{g}\left(v_{(i-1,j+1)} - v_{(i,j)}\right) - a\Delta t J_{E(i-1,j+1)} = 0 \tag{12.95}$$

First, we sum up the known quantities of Equation 12.95 to the auxiliary variable $K^{-}_{(i-1,j+1)}$ again.

$$K^{-}_{(i-1,j+1)} = -h_{(i-1,j+1)} + \frac{a}{g} v_{(i-1,j+1)} - a\Delta t J_{E(i-1,j+1)} \tag{12.96}$$

For the C_- compatibility condition, it follows that:

$$h_{(i,j)} - \frac{a}{g} v_{(i,j)} + K^{-}_{(i-1,j+1)} = 0 \tag{12.97}$$

As already mentioned above, the boundary condition must provide the second equation (to solve the two unknowns).

12.7.4.1 Reservoir with constant water level

The boundary condition for a reservoir with constant water level is trivial:

$$h_{(i,j)} = h_l = h_{\text{container}} \tag{12.98}$$

With this condition for the reservoir at the left boundary, Equation 12.97 may be solved for $v_{(i,j)}$:

$$v_{(i,j)} = \frac{g}{a}\left(h_{(i,j)} + K^{-}_{(i-1,j+1)}\right) = \frac{g}{a}\left(h_l + K^{-}_{(i-1,j+1)}\right) \tag{12.99}$$

12.7.4.2 Reservoir with time-varying water level

The solution for the time-varying water level is similar:

$$h_{(i,j)} = h_l(t) \tag{12.100}$$

From there, the following equation for the velocity may be derived:

$$v_{(i,j)} = \frac{g}{a}\left(h_{(i,j)} + K^{-}_{(i-1,j+1)}\right) = \frac{g}{a}\left(h_l(t) + K^{-}_{(i-1,j+1)}\right) \tag{12.101}$$

12.7.4.3 Time-variable velocity

The system may also be imposed with a time-variable velocity at the boundary.

$$v_{(i,j)} = v(t) \tag{12.102}$$

Inserting Equation 12.102 into Equation 12.97 yields the pressure height:

$$h_{(i,j)} = \frac{a}{g} v(t) - K^{-}_{(i-1,j+1)} \tag{12.103}$$

12.7.4.4 Valve

Besides the water level of the reservoir, the control device is presumably the most important boundary condition. The equation for the fluid velocity at a valve generally reads:

$$v_{(i,j)} = \operatorname{sgn}(h_l - h_{(i,j)})\,\mu_V \frac{A(t)}{A_0}\sqrt{2g\left|h_l - h_{(i,j)}\right|} \tag{12.104}$$

When solving Equation 12.97 for $h_{(ij)}$ and substituting into Equation 12.104, we obtain:

$$v_{(i,j)} = \operatorname{sgn}(h_l - \frac{a}{g} v_{(i,j)} + K^-_{(i-1,j+1)}) \mu_V \frac{A(t)}{A_0} \sqrt{2g \left| h_l - \frac{a}{g} v_{(i,j)} + K^-_{(i-1,j+1)} \right|} \tag{12.105}$$

In the following steps, we omit the sign function sgn whose influence will be discussed later. Equation 12.105 is squared in order to extract the desired velocity $v_{(i,j)}$ from the root.

$$v^2_{(i,j)} = \mu_V^2 \frac{A(t)^2}{A_0^2} \left(2g \left| h_l - \frac{a}{g} v_{(i,j)} + K^-_{(i-1,j+1)} \right| \right) \tag{12.106}$$

We now extract $v_{(i,j)}$ from the absolute value expression and set the equation to zero:

$$\begin{aligned} & v^2_{(i,j)} + \frac{a}{g} v_{(i,j)} 2g\mu_V^2 \frac{A(t)^2}{A_0^2} - \mu_V^2 \frac{A(t)^2}{A_0^2} 2g \left| h_l + K^-_{(i-1,j+1)} \right| \\ & = v^2_{(i,j)} + 2a v_{(i,j)} \mu_V^2 \frac{A(t)^2}{A_0^2} - 2g\mu_V^2 \frac{A(t)^2}{A_0^2} \left| h_l + K^-_{(i-1,j+1)} \right| = 0 \end{aligned} \tag{12.107}$$

This yields a veritable quadratic equation, which may be solved via the generally known formula $x_{1,2} = \frac{-b \pm \sqrt{b^2 - 4ac}}{2a}$. With expressions $a = 1$, $b = 2a\mu_V^2 \frac{A(t)^2}{A_0^2}$ and finally $c = -2g\mu_V^2 \frac{A(t)^2}{A_0^2} \left| h_l + K^-_{(i-1,j+1)} \right|$, it follows that:

$$\begin{aligned} \left| v_{(i,j)1,2} \right| &= \frac{-2a\mu_V^2 \frac{A(t)^2}{A_0^2} \pm \sqrt{\left(2a\mu_V^2 \frac{A(t)^2}{A_0^2} \right)^2 - 4 \cdot 1 \left(-2g\mu_V^2 \frac{A(t)^2}{A_0^2} \left| h_l + K^-_{(i-1,j+1)} \right| \right)}}{2 \cdot 1} \\ &= \frac{-2a\mu_V^2 \frac{A(t)^2}{A_0^2} \pm \sqrt{4a^2\mu_V^4 \frac{A(t)^4}{A_0^4} + 8g\mu_V^2 \frac{A(t)^2}{A_0^2} \left| h_l + K^-_{(i-1,j+1)} \right|}}{2} \\ &= -a\mu_V^2 \frac{A(t)^2}{A_0^2} \pm \sqrt{a^2\mu_V^4 \frac{A(t)^4}{A_0^4} + 2g\mu_V^2 \frac{A(t)^2}{A_0^2} \left| h_l + K^-_{(i-1,j+1)} \right|} \end{aligned} \tag{12.108}$$

First, we consider the two solutions that result from the $\pm$ sign. For $A(t) = A$ and a common discharge coefficient $\mu_V = 0.98$, the absolute value of the term preceding the root is quite high. For steel pipes, a value of approximately $-1000\,\mathrm{m/s}$ is obtained. For the same opening ratio, the value under the root is greater than a^2; with respect to the absolute value, the term has the same order of magnitude as the first one. When the terms have the same sign, in this case negative, they sum up to $-2000\,\mathrm{m/s}$, which is not physically possible. The energy for accelerating the water to this velocity is not available at the pressure gradient $h_l - h_{(i,j)}$. The only valid solution is the one obtained when the root term is added.

If $v_{(i,j)} < 0$, then $\left(h_l - \frac{a}{g} v_{(i,j)} + K^-_{(i-1,j+1)} \right) > \left(h_l + K^-_{(i-1,j+1)} \right)$. In the case where $v_{(i,j)} > 0$, it follows $\left(h_l - \frac{a}{g} v_{(i,j)} + K^-_{(i-1,j+1)} \right) < \left(h_l + K^-_{(i-1,j+1)} \right)$. For the determination of the sign, the velocity term $\frac{a}{g} v_{(i,j)}$ may be readily ignored since it only moves the result of the sum further toward the sign-changing zero. Finally, we arrive at the following equation for a valve arranged at the left side of the system:

$$v_{(i,j)} = \operatorname{sgn}(h_l + K^-_{(i-1,j+1)}) \left[-\frac{\mu_V^2 A(t)^2}{A_0^2} a + \sqrt{\frac{\mu_V^4 A(t)^4}{A_0^4} a^2 + 2g\mu_V^2 \frac{A(t)^2}{A_0^2} \left| h_l + K^-_{(i-1,j+1)} \right|} \right] \tag{12.109}$$

For the pressure height, Formula 12.97 yields:

$$h_{(i,j)} = \frac{a}{g} v_{(i,j)} - K^-_{(i-1,j+1)} \tag{12.110}$$

12.7.5 Node at the right boundary

Figure 12.12 shows the conditions at the right boundary of the computational domain, i. e. at node $j = n$ for time step i. What happens there is determined only by the conditions of the node $j-1$ at time step $i-1$ conveyed by the $C+$ characteristic. We already anticipate that a further descriptive equation must be added in order to be able to calculate the two variables $v_{(i,j=n)}$ and $h_{(i,j=n)}$. The necessary information is provided via the boundary conditions.

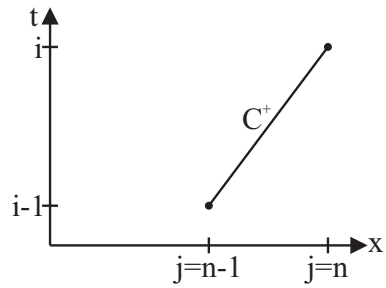

Figure 12.12: Conditions at the right boundary of the grid.

We may transfer the above considerations for the C_+ characteristic and write them down for the case of the right-hand node $j = n$.

$$h_{(i,j)} - h_{(i-1,j-1)} + \frac{a}{g} \left(v_{(i,j)} - v_{(i-1,j-1)} \right) + a\Delta t J_{E(i-1,j-1)} = 0 \tag{12.111}$$

The knowns of Equation 12.111 are used for determining the auxiliary variable $K^+_{(i-1,j-1)}$.

$$K^+_{(i-1,j-1)} = -h_{(i-1,j-1)} - \frac{a}{g} v_{(i-1,j-1)} + a\Delta t J_{E(i-1,j-1)} \tag{12.112}$$

The C_+ compatibility condition follows:

$$h_{(i,j)} + \frac{a}{g} v_{(i,j)} + K^+_{(i-1,j-1)} = 0 \tag{12.113}$$

In the following discussion, several boundary conditions will be described.

12.7.5.1 Reservoir with constant water level

The formula for a reservoir with constant water level was already given above for the left boundary.

$$h_{(i,j)} = h_r = h_{\text{container}} \tag{12.114}$$

When inserting h_r into Equation 12.113 it becomes:

$$v_{(i,j)} = -\frac{g}{a}\left(h_{(i,j)} + K^+_{(i-1,j-1)}\right) = -\frac{g}{a}\left(h_r + K^+_{(i-1,j-1)}\right) \tag{12.115}$$

12.7.5.2 Reservoir with time-varying water level

There is hardly any change in the description of the time-varying water level.

$$h_{(i,j)} = h_r(t) \tag{12.116}$$

The result for the velocity is:

$$v_{(i,j)} = -\frac{g}{a}\left(h_{(i,j)} + K^+_{(i-1,j-1)}\right) = -\frac{g}{a}\left(h_r(t) + K^+_{(i-1,j-1)}\right) \tag{12.117}$$

12.7.5.3 Time-variable velocity

The time-variable velocity for the right boundary reads:

$$v_{(i,j)} = v(t) \tag{12.118}$$

Substituting this into Equation 12.113 yields the pressure height $h_{(i,j)}$:

$$h_{(i,j)} = -\frac{a}{g}v(t) - K^+_{(i-1,j-1)} \tag{12.119}$$

12.7.5.4 Valve

The derivations of the equations for the control device installed at the right hand boundary are to be modelled after the corresponding equations for the left boundary in Chapter 12.7.4.4.

$$v_{(i,j)} = \operatorname{sgn}(-h_r - K^+_{(i-1,j-1)})\left[-\frac{\mu_V^2 A(t)^2}{A_0^2}a + \sqrt{\frac{\mu_V^4 A(t)^4}{A_0^4}a^2 + 2g\mu_V^2\frac{A(t)^2}{A_0^2}\left|-h_r - K^+_{(i-1,j-1)}\right|}\right] \tag{12.120}$$

For the pressure height, Equations 12.120 and 12.113 yield:

$$h_{(i,j)} = -\frac{a}{g}v_{(i,j)} - K^+_{(i-1,j-1)} \tag{12.121}$$

12.8 Summary: unsteady pipe flows

The acquired knowledge on unsteady pipe hydraulics is summarised in the following example.

Example

Pressure surge in a pipeline

For an illustration of the method of characteristics, we use the following example. The valve at the end of the pipeline of the system shown in Figure 12.13 is fully open in the steady-state. The valve is completely closed within $t_C = 30\,\mathrm{s}$. We assume a linear closing law and set up the computational domain with three nodes along the pipeline, allowing us to observe the unsteady pressure component at multiples of $\frac{L}{2a}$:

1. beginning of the pipeline at the upper reservoir
2. middle of the pipeline
3. end of the pipeline

You may follow the example by means of the supplied Octave routines, which run under the main program `waterHammer.m`. Insert the parameters and follow the calculation step-by-step. Vary the input values and observe the changes.

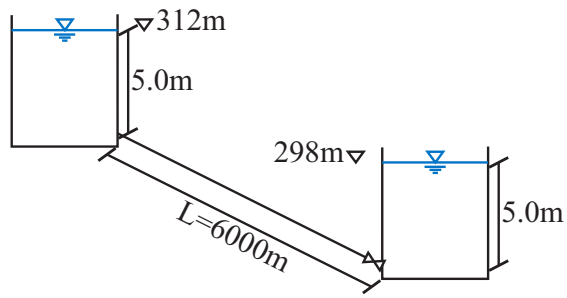

Figure 12.13: A sample pipeline.

The following is also given:

$T = 20\,^\circ\mathrm{C}$	$L = 6000\,\mathrm{m}$	$d = 0.30\,\mathrm{m}$	$E_P = 2.1 \times 10^{11}\,\mathrm{N/m^2}$
$k_S = 1.0 \times 10^{-3}\,\mathrm{m}$	$w = 8.0 \times 10^{-3}\,\mathrm{m}$	$\mu_L = 0.33$	$A_0 = A_P = 0.07069\,\mathrm{m^2}$
$h_l = 312\,\mathrm{m}$	$h_r = 298\,\mathrm{m}$	$t_C = 30\,\mathrm{s}$	$\mu_V = 0.98$

First, the propagation velocity is calculated by means of Equation 12.22.

$$a = \sqrt{\frac{\frac{E_\mathrm{F}}{\rho}}{1 + \frac{d}{w}\frac{E_\mathrm{F}}{E_\mathrm{P}}\left(1 - \mu_L^2\right)}} = \sqrt{\frac{\frac{2.1\times10^9}{\rho}}{1 + \frac{0.3}{0.008}\frac{2.1\times10^9}{2.1\times10^{11}}\left(1 - 0.33^2\right)}} = 1255\,\mathrm{m/s} \qquad (12.122)$$

Thus the time increment for the surge that propagates by half the pipe length amounts to $\Delta t = \frac{L}{2a} = \frac{6000}{2 \cdot 1255} = 2.391\,\mathrm{s}$. We see that the Joukowsky surge ($\Delta h_{\max} = v_0 \frac{a}{g}$) does not occur because $t_C > t_R = \frac{2L}{a} = 9.565\,\mathrm{s}$. The flow velocity results for the steady-state case with the opening area of the valve A_0 and the valve coefficient μ_V from the following equation.

$$h_l - h_r = \frac{v_P^2}{2g}\frac{f_D L}{d} + \frac{v_{\text{valve}}^2}{2g} = \frac{v_P^2}{2g}\frac{f_D L}{d} + \frac{v_P^2 \cdot A_P^2}{2g \cdot \mu_V^2 \cdot A_0^2} = \frac{v_P^2}{2g}\left(\frac{f_D L}{d} + \frac{A_P^2}{\mu_V^2 \cdot A_0^2}\right) \tag{12.123}$$

When solving the energy equation for the steady-state case, one obtains for the steady-state velocity in the pipeline (without considering minor losses):

$$v_0 = \sqrt{\frac{(h_l - h_r)\,2g}{\left(\frac{f_D L}{d} + \frac{A_P^2}{\mu_V^2 A_0^2}\right)}} = \sqrt{\frac{(312 - 298)\,2g}{\left(\frac{f_D \cdot 6000}{0.30} + \frac{\left(0.15^2\pi\right)^2}{0.98^2\left(0.15^2\pi\right)^2}\right)}} \tag{12.124}$$

The Prandtl-Colebrook iteration[K] yields a friction coefficient of $f_D = 0.0275$ and $v_0 = 0.705\,\mathrm{m/s}$ via $T = 20\,^\circ\mathrm{C}$ and $k_s = 1.0 \times 10^{-3}\,\mathrm{m}$. The intermediate results are:

1. $f_{D0,0} = 0.02$, $Q_0 = 0.0583\,\mathrm{m^3/s}$
2. $f_{D0,1} = 0.0275$, $Q_1 = 0.0498\,\mathrm{m^3/s}$
3. $f_{D0,2} = 0.0275$, $Q_2 = 0.0498\,\mathrm{m^3/s}$

This allows the calculation of the gradient of the energy grade line for the steady-state:

$$J_{E0} = \frac{f_D}{d}\frac{v_0^2}{2g} = 2.329 \times 10^{-3} \tag{12.125}$$

For the path of the hydraulic grade line, neglecting minor losses and velocity height, this becomes[L]:

$$h_0(x) = h_l - f_D \frac{x}{d}\frac{v_0^2}{2g} \tag{12.126}$$

$x = 0\,\mathrm{m}$	$x = \frac{L}{2} = 3000\,\mathrm{m}$	$x = L = 6000\,\mathrm{m}$
$h_0(x=0) = 312\,\mathrm{m}$	$h_0(x = \frac{L}{2}) = 305.01\,\mathrm{m}$	$h_0(x = L) = 298.03\,\mathrm{m}$

The linear closing law reads:

$$A(t) = \left(1 - \frac{t}{t_C}\right) A_0 \quad \text{for } t < t_S \text{ and } A(t) = 0 \text{ for } t \geq t_C \tag{12.127}$$

Let's get started. We scramble along the characteristics, time increment-by-time increment, from the known nodes in the steady-state. We orient ourselves at the characteristics grid illustrated in Figure 12.9. The first index corresponds to the time increment and the second one to the position. The conditions are known for the steady-state; this includes nodes (1,3), (2,2) and (3,1) because during this period, steady-state flow will still prevail there.

[K] The procedure in the Prandtl-Colebrook iteration is explained in Chapter 11.5.

[L] Note, that the calculations of v_0 and subsequently J_{E0} included the outflow-loss.

Node (3,3)

The C^+ characteristic of node (2,2) leads to node (3,3), where the valve boundary condition exists. Arriving at node (3,3), $2\Delta t$ or 4.78 s have elapsed since the beginning of the closing process. After this time, the opening area of the valve is $5.94 \times 10^{-2}\,\mathrm{m}^2$. For Equation 12.120 (the valve equation) with $A_0 = A_P$, the auxiliary variable $K^+_{(2,2)}$ is required (see Equation 12.91). Here, all quantities are known from the steady-state.

$$K^+_{(2,2)} = -h_{(2,2)} - \frac{a}{g} v_{(2,2)} + a\Delta t J_{E(2,2)} = -305.01 - \frac{a}{g} 0.705 + 1255 \cdot 2.39 \cdot 2.329 \times 10^{-3} = -388.28\,\mathrm{m} \tag{12.128}$$

Now, fully relaxed, we may solve the valve equation:

$$v_{(3,3)} = \mathrm{sgn}(-298 + 388.28) \left[-\frac{0.98^2 \cdot \left(5.94 \times 10^{-2}\right)^2}{\left(7.07 \times 10^{-2}\right)^2} \cdot 1255 + \sqrt{\frac{0.98^4 \cdot \left(5.94 \times 10^{-2}\right)^4}{\left(7.07 \times 10^{-2}\right)^4} \cdot 1255^2 + 2g \cdot 0.98^2 \frac{\left(5.94 \times 10^{-2}\right)^2}{\left(7.07 \times 10^{-2}\right)^2} |-298 + 388.28|} \right] = 0.705\,\mathrm{m/s} \tag{12.129}$$

With velocity $v_{(3,3)}$, all quantities for the determination of $h_{(3,3)}$ are now available:

$$h_{(3,3)} = -\frac{a}{g} v_{(3,3)} - K^+_{(2,2)} = -\frac{a}{g} 0.705 + 388.28 = 298.04\,\mathrm{m} \tag{12.130}$$

This wasn't that complicated, was it? We should right away calculate the gradient of the energy grade line $J_{E(3,3)}$ and $K^-_{(3,3)}$.

$$J_{E(3,3)} = \mathrm{sgn}(v_{(3,3)}) \frac{f_{\mathrm{D}(3,3)}}{d} \frac{v^2_{(3,3)}}{2g} = 2.328 \times 10^{-3} \tag{12.131}$$

We now combine the quantities to arrive at $K^-_{(3,3)}$. For the downstream boundary, the calculation of the auxiliary variable K^+ may be omitted because the C^+ characteristic moves outside the domain of the calculation.

$$K^-_{(3,3)} = -h_{(3,3)} + \frac{a}{g} v_{(3,3)} - a\Delta t J_{E(3,3)} = -214.78\,\mathrm{m} \tag{12.132}$$

Well, let's look at node (4,2) where two items meet: the C^+ characteristic from the steady-state-influenced upstream node (3,1) and the C^- characteristic from node (3,3), which was just calculated.

Node (4,2)

The two characteristics C^+ and C^- arrive at node (4,2). For this, the two following equations are to be solved:

$$v_{(4,2)} = \frac{g}{a}\frac{K^-_{(3,3)} - K^+_{(3,1)}}{2} \tag{12.133}$$

$$h_{(4,2)} = -\frac{K^-_{(3,3)} + K^+_{(3,1)}}{2} \tag{12.134}$$

We already determined the auxiliary variable $K^-_{(3,3)}$ in the previous section. For $K^+_{(3,1)}$, we must use the steady-state conditions at the upstream reservoir.

$$K^+_{(3,1)} = -h_{(3,1)} - \frac{a}{g}v_{(3,1)} + a\Delta t J_{E(3,1)} = -h_l - \frac{1255}{g}v_0 + 1255 \cdot 2.39 \cdot 2.329 \times 10^{-3} = -395.26\,\mathrm{m} \tag{12.135}$$

Thus for $h_{(4,2)}$

$$h_{(4,2)} = -\frac{-214.78 - 395.26}{2} = 305.02\,\mathrm{m} \tag{12.136}$$

and for $v_{(4,2)}$:

$$v_{(4,2)} = \frac{g}{a}\frac{-214.78 + 395.26}{2} = 0.705\,\mathrm{m/s} \tag{12.137}$$

At first sight it appears as if nothing has happened, though the decimal places are already changing. For internal nodes, it is recommended that the auxiliary variables $K^+_{(4,2)}$ and $K^-_{(4,2)}$ be calculated directly. For this purpose, we first need $J_{E(4,2)}$, which after extensive calculations hardly differs from the gradient of the energy grade line in the steady-state since $v_{(4,2)} \approx v_0$. Thus, we write $J_{E(4,2)} = 2.328 \times 10^{-3}$[M]. We obtain for $K^+_{(4,2)}$ and $K^-_{(4,2)}$:

$$\begin{aligned} K^+_{(4,2)} = -h_{(4,2)} - \frac{a}{g}v_{(4,2)} + a\Delta t J_{E(4,2)} &= -305.02 - \frac{1255}{g}0.705 + 1255 \cdot 2.39 \cdot 2.328 \times 10^{-3} \\ &= -388.28\,\mathrm{m} \end{aligned} \tag{12.138}$$

$$\begin{aligned} K^-_{(4,2)} = -h_{(4,2)} + \frac{a}{g}v_{(4,2)} - a\Delta t J_{E(4,2)} &= -305.02 + \frac{a}{g}0.705 - 1255 \cdot 2.39 \cdot 2.328 \times 10^{-3} \\ &= -221.77\,\mathrm{m} \end{aligned} \tag{12.139}$$

Slowly but surely. Now we will calculate the two boundary nodes (5,1) and (5,3) together.

Node (5,1)

After another 2.39 s, the C^- characteristic reaches node (5,1). There, the boundary condition of the constant water level h_l exists. For the left boundary, the following applies:

$$h_{(5,1)} = h_l = 312\,\mathrm{m} \tag{12.140}$$

The velocity becomes:

[M] Even though the calculation is not worked through here, you must definitely comply with the signum, i. e. the sign function, in the calculation of the gradient of the energy grade line! With flow reversal, the gradient of the energy grade line points in the other direction.

$$v_{(5,1)} = \frac{g}{a}\left(h_{(5,1)} + K^{-}_{(4,2)}\right) = \frac{g}{a}\left(312 - 221.77\right) = 0.705\,\mathrm{m/s} \tag{12.141}$$

Here again, the "dynamics" can hardly be felt. We look at the lower end at time step 5, i. e. after $4\Delta t = 9.56\,\mathrm{s}$.

Node (5,3)

The C^+ characteristic reaches node (5,3) from (4,2). The equations are available together with the valve boundary condition ($A(t = 4\Delta t) = 4.81 \times 10^{-2}\,\mathrm{m}^2$).

$$v_{(5,3)} = \mathrm{sgn}(-298 + 388.28)\left[-\frac{0.98^2 \cdot \left(4.81 \times 10^{-2}\right)^2}{\left(7.07 \times 10^{-2}\right)^2} \cdot 1255 + \sqrt{\frac{0.98^4\left(4.81 \times 10^{-2}\right)^4}{\left(7.07 \times 10^{-2}\right)^4} \cdot 1255^2 + 2g \cdot 0.98^2 \frac{\left(4.81 \times 10^{-2}\right)^2}{\left(7.07 \times 10^{-2}\right)^2}\left|-298 + 388.28\right|}\right] = 0.705\,\mathrm{m/s} \tag{12.142}$$

With velocity $v_{(5,3)}$, all quantities are now known, allowing for the determination of $h_{(5,3)}$.

$$h_{(5,3)} = -\frac{a}{g} v_{(5,3)} - K^{+}_{(4,2)} = -\frac{a}{g} 0.705 + 388.28 = 298.06\,\mathrm{m} \tag{12.143}$$

Thus, the method is straightforward. One progresses from the steady-state through the system, considering the respective boundary conditions. For the calculation of unsteady pipe flows by means of the method of characteristics, you may of course use the appropriate routines from the supplied open-source library. The results after a total of 40 time steps are listed in Tables A.1 to A.4 in Appendix A.8. Figure 12.14 shows the piezometric pressure height curves at the three spatial nodes. The pressure increases abruptly immediately after the complete closure of the pipeline. Please note that in the tables of results in Appendix A.8, the pressure cannot drop below the vapour pressure (see Chapter 8.7).

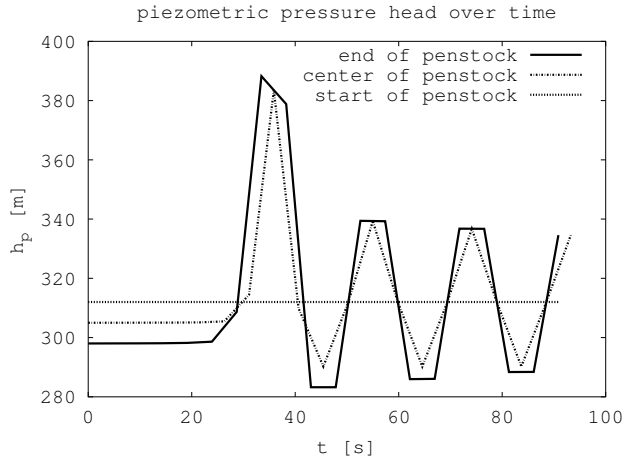

Figure 12.14: Curve of the piezometric pressure for the unsteady pipe flow example.

Chapter 13
Steady free surface flow

13.1 Flows with free surface

The fact that the Bernoulli equation does not allow any statements on flows where friction is not negligible has caused us to use semi-empirical relationships in pipe hydraulics. In open channel hydraulics, things become more complex because the Bernoulli equation permits two different flow depths for one single energy height. Before we look at the equation more thoroughly, the similarity with open channel flows will be discussed.

13.2 Dynamic similarities of open channel flows

The Navier–Stokes equation (Chapter 5.5), which is written in dimensionless form in Chapter 5.6, is of course also valid for flows with free surface. Dynamically similar flows have identical Froude and Reynolds numbers. However, these are obtained only for identical fluids and identical geometries. Generally, either the body forces or the viscous forces are dominating the flows. The driving force of an open channel flow is the body force that results from gravity. Due to the often very rough open channel wall, viscous forces are negligibly small (see Appendix A.3 and/or Chapter 11.5). Therefore, the Froude number is used for comparability with open channel flows. It is normally related to the mean flow velocity and the flow depth.

$$\mathrm{Fr} = \frac{u_{\mathrm{ref}}}{\sqrt{g_i x_{\mathrm{ref}}}} = \frac{v}{\sqrt{gy}} \tag{13.1}$$

The propagation velocity of waves may be derived by means of the Airy wave theory (see Chapter A.6). A limit value analysis leads to the distinction between shallow- and deep-water waves, though we usually deal with shallow-water waves. According to this theory, the propagation velocity of shallow-water waves is $c = \sqrt{gy}$. Thus, the Froude number specifies the ratio between the flow velocity and the propagation velocity of shallow-water waves. The following two examples clarify the relationship:

C. Rapp, *Hydraulics in Civil Engineering*,
https://doi.org/10.1007/978-3-031-54860-4_13

Let's take a look at the action scene taking place below this text. A stuntman is running along the top of a train opposite the direction of travel. In the example on the left, he's running faster than the train is travelling in the opposite direction. Not only is he moving backwards, relatively speaking, within his reference system (i. e. the roof of the train), but he's also moving opposite to the positive x-axis. His positions are indicated by $x(t_0)$ and $x(t_0 + \Delta t)$, according to the addition of the velocity vectors.

In the diagram on the right, the train moves faster than the stuntman. Though he runs relatively rearwards on the top of the train, he moves in the positive x-direction (i. e. to the right in the diagram). The addition of the velocity vectors again clearly shows the relationship.

The same conditions develop with waves, i. e. the stuntman, in an open channel with flow, i. e. the train. If the flow velocity v is lower than the propagation velocity of shallow-water waves $c = \sqrt{gy}$, then the Froude number is smaller than one ($\mathrm{Fr} < 1$); this is referred to as subcritical flow.

If the flow velocity v is greater than the propagation velocity of the waves $c = \sqrt{gy}$, the waves are carried downstream. They cannot propagate upstream and the Froude number is greater than one ($\mathrm{Fr} > 1$). Due to the high flow velocity, this is referred to as supercritical flow.

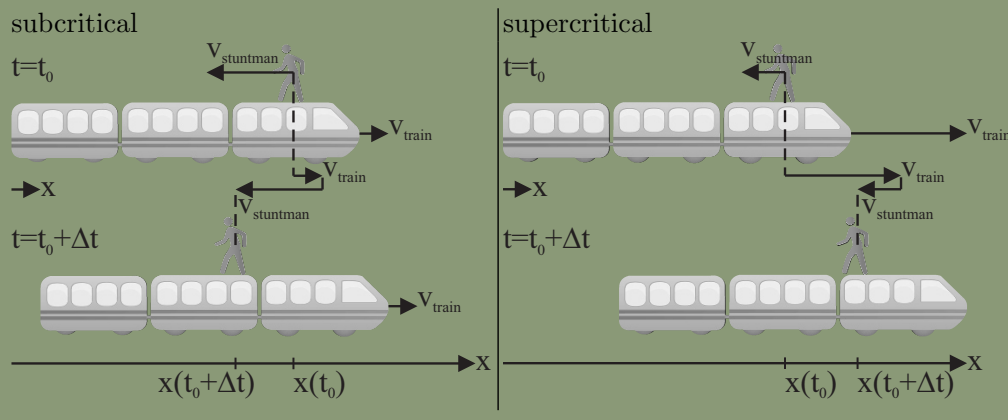

Figure 13.1: Stuntman running on a train – an analogy for the propagation of waves.

Anyone may test the propagation velocity of waves in an open channel. Just throw a stone into the water and observe the propagation of the waves. If a pattern develops like the one on the left side of Figure 13.2, i. e. if the waves propagate upstream and downstream from the point where the stone applies the disturbance onto the water surface, a subcritical flow exists. If the waves are carried downstream only, as is shown in Figure 13.2 (right), then supercritical is the characterising feature of the flow.

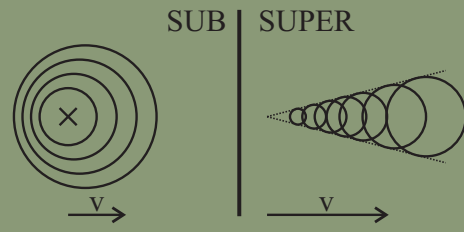

Figure 13.2: Propagation pattern of the waves in subcritical and supercritical flows.

13.3 Bernoulli equation in open channels

The Bernoulli equation (5.41) states that the sum of geodetic height, pressure and velocity height remains constant in a loss-free flow. As a consequence that losses cannot be covered by the Bernoulli equation, we relate the energy height in free surface flows to the channel bed (where $z = 0$, see Figure 13.3), and call the quantity "specific energy".

$$H = \frac{p}{\rho g} + \frac{v^2}{2g} \tag{13.2}$$

It is important that subsequent statements be made with respect to this datum (the channel bed). The Bernoulli equation "shrinks", so to speak, to the balance of the specific energies at certain cross-sections.

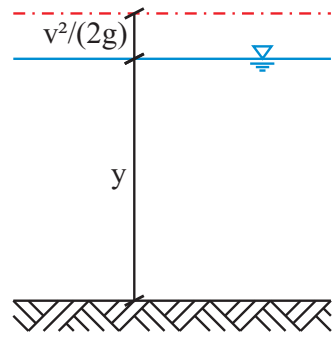

Figure 13.3: Bernoulli equation for free surface flows.

The energy balance in open channel hydraulics includes two terms: $\frac{p}{\rho g}$ and $\frac{v^2}{2g}$. At first, we assume – before thinking more thoroughly about this topic in Chapter 13.9 – that the

pressure, as in hydrostatics, increases linearly with the vertically measured depth y. Then $\frac{p}{\rho g} = y$ may be written. Upon insertion of the continuity condition (5.5), it follows that for the Bernoulli equation in open channels:

$$H = y + \frac{Q^2}{A^2 2g} \tag{13.3}$$

Requirements:

- Freedom of losses (statement on cross-section values)
- Hydrostatic pressure distribution

The following explanations are based on a rectangular open channel of width b:

$$H = y + \frac{Q^2}{b^2 y^2 2g} \tag{13.4}$$

Equation 13.4 contains three variables: H, Q and y; gravity g and width b (in the channel under consideration) are constant. In order to recognise the importance of the equation, it is recommended that one variable be set constant and that a plot of the other two, one against the other, be made in a diagram.

13.3.1 H-y diagram

First, we relate the discharge to the width of one metre (discharge per unit width: $q = \frac{Q}{b}\ [\mathrm{m}^3/(\mathrm{s\,m})]$):

$$H = y + \frac{Q^2}{b^2 y^2 2g} = y + \frac{q^2}{y^2 2g} = y + \frac{v^2}{2g} \tag{13.5}$$

Using the Bernoulli equation, we look at a constant discharge per unit width $q = \mathrm{const.}$ by plotting the specific energy and the flow depth against one another. The result is an example of a diagram, in this case shown for $q = 1.0\,\mathrm{m}^3/(\mathrm{s\,m})$ in Figure 13.4.
The flow area becomes very large for the extreme case of a very great flow depth, and from the continuity condition (5.5) it follows that the flow velocity approaches zero. The specific energy H consists of a very great proportion of the flow depth y and an extremely small proportion of the velocity height $\frac{v^2}{2g}$. In Figure 13.4, when drawing a straight line upwards from the abscissa (x-axis) at a certain specific energy (e. g. at $H = 1.6\,\mathrm{m}$), it intersects the $H - y$ function twice until it reaches the red bisector, which in turn reflects the specific energy. As we are currently interested in great flow depths, we choose the upper point of intersection, which indicates the flow depth on the ordinate (y-axis). Starting from this point to the bisector, the velocity height $\frac{v^2}{2g}$ is found again. Since it is hardly possible to read the velocity height in this illustration, we venture off to a small programming example in Octave.

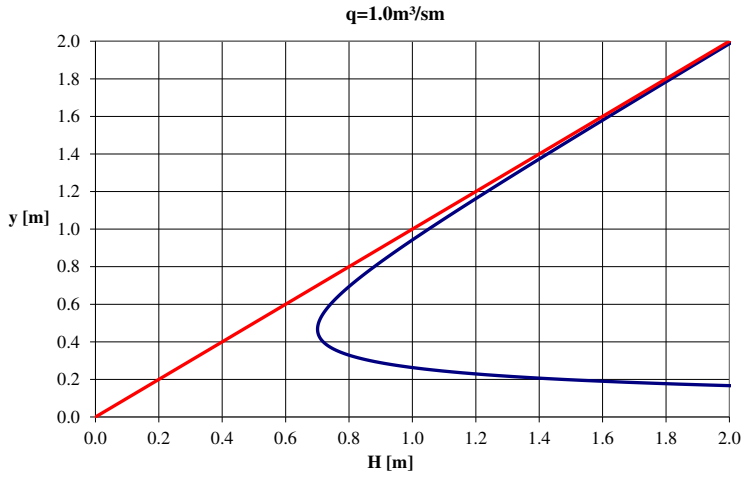

Figure 13.4: Flow depth vs. specific energy for a rectangular open channel with $q = \text{const.} = 1.0\,\text{m}^3/(\text{s}\,\text{m})$.

```
1> function H=f(y)
2> H = -1.6+y+1^2/(y^2*2*9.81);
3> endfunction
4> [y,fval,info]=fsolve(@f,1.6)
```

y is determined iteratively from Equation 13.5, which cannot be solved explicitly for y with the inserted variables for H and q as well as with the constant g. To this end, the equation is defined as H =f(y) and solved for 0.
Explanations for the individual lines `n>`

```
1> % H is a function of y.
2> % The equation must be solved for zero and termed as 'H' (see
1st line). g=9.81m/s2, H=1.6m and q=1m3/sm have already been in-
serted.
3> % ends the definition of H.
4> % solves the equation @f with the starting value 1.6.
```

Octave presents $y = 1.580\,\text{m}$ as the result. For the associated velocity height, one obtains $\frac{v^2}{2g} = H - y = 2.0\,\text{cm}$; i. e. $v = 0.633\,\text{m/s}$. To countercheck, $v \cdot y$ again results in $q = 1.0\,\text{m}^3/(\text{s}\,\text{m})$.
The same specific energy also allows a much lower flow depth. Entering `fsolve(@f,0.3)` in Octave's command line, you obtain as a result for the flow depth `0.19013` with a starting value of `0.3`. With $v = \frac{q}{y} = 5.260\,\text{m/s}$ and $\frac{v^2}{2g} = 1.410\,\text{m}$, here again it follows that $H = y + \frac{v^2}{2g} = 1.60\,\text{m}$.
The state of flow at great flow depth is referred to as **subcritical** ($y_{\text{SUB}} = 1.580\,\text{m}$) and at small flow depth as **supercritical** ($y_{\text{SUPER}} = 0.190\,\text{m}$). The flow depths at the same specific energy are referred to as **corresponding** flow depths.

Experiment

Subcritical discharge in a laboratory flume

In the experiment (as before, flow is from left to right) shown in Figure 13.5 with width $b = 4.0\,\text{cm}$, a constant discharge of $60\,\text{L/min}$, i. e. $0.025\,\text{m}^3/(\text{s m})$, has been set. Let's first look at the left part of the photo where the Pitot tube (far left – hardly recognizable in the image) indicates the specific energy $H_{\text{ups}} = 12\,\text{cm}$. As usual, it is marked on the acrylic glass wall by the red energy grade line that extends horizontally because of the lack of energy losses. In this region, the flow depth of $y = 11.77\,\text{cm}$ is somewhat lower[A].

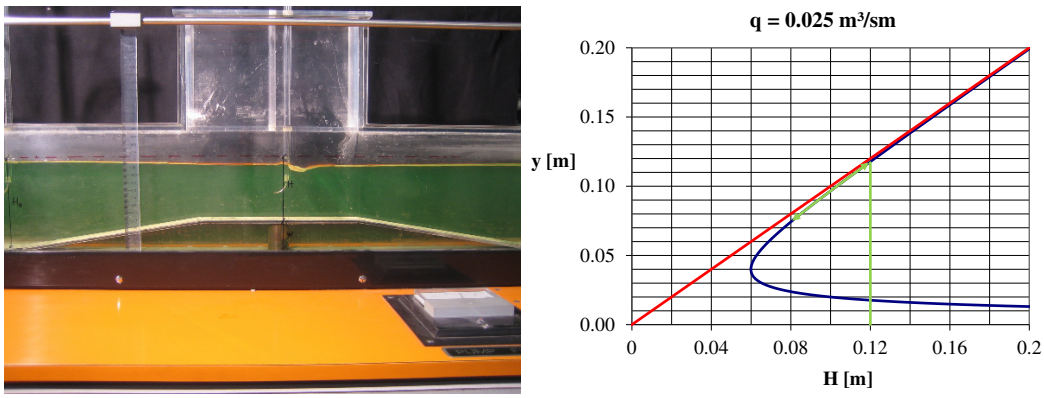

Figure 13.5: Subcritical flow in a rectangular laboratory flume with a discharge of $q = 25\,\text{L/(s m)}$.

We now let our eyes wander to the right in the direction of flow and see a ramp that heightens the bed. I hope you remember the agreement we made at the beginning of Chapter 13.3 to always relate the energy height in open channel hydraulics to the bed, i. e. applying the specific energy . When moving along the channel bed to the right, the distance to the energy grade line decreases gradually. Let's have a closer look on the right side of the $H - y$ diagram that was drawn for the constant discharge per unit width of $q = 0.025\,\text{m}^3/(\text{s m})$. We wander from the point of intersection of the green line with the flow depth along the specific energies vs. flow depths relation to the left until we have reached the specific energy $H_{\text{on the sill}} = H_{\text{upstream the sill}} - w = 0.08\,\text{m}$ on the sill with height $w = 4.0\,\text{cm}$. For $0 = y + \frac{0.025^2}{y^2 2g} - 0.08$, Octave displays $0.0742\,\text{m}$ as flow depth. And we actually see that the distance between the bed (by the bed sill) and the energy grade line has been reduced. We also see that the distance between the water level and the energy grade line increased from left to right. The velocity height increased from $12.00 - 11.77 = 0.23\,\text{cm}$ to $8.00 - 7.42 = 0.58\,\text{cm}$. This seems obvious because the flow area was significantly reduced. The Pitot tube on the bed sill again indicates the total energy at the height of the red line. Starting from the bed sill, it goes further to the right and down the ramp of the bed sill again. Since the specific energy is related to the bed, it rises again

[A] Try to solve equation $0 = y + \frac{0.025^2}{y^2 2g} - 0.12$ yourself in Octave. For a starting value, enter 0.1, i. e. `fsolve(@f,.1)`

to the right[B]. When moving to the right along the $H - y$ relation from its intersection with the specific energy $H = 0.08\,\mathrm{m}$, we find that the increase in specific energy goes along with the increase in flow depth. Exactly the same condition can be found in the photo. When looking closely at the right side of the photo, it is even discernible that the water level rises slightly in the direction of flow. And that's what must occur! The velocity is reduced with the increase of the flow depth and thus the velocity height as well. Since the distance between water level and energy grade line defines the velocity height, it must decrease because $H = \mathrm{const}$.

Experiment

Supercritical discharge in a laboratory flume

At the farthest left boundary of Figure 13.6, the water level in the Pitot tube again indicates a specific energy of $H_{\text{upstream the sill}} = 12\,\mathrm{cm}$. As in the above example, the discharge amounts to $q = 0.025\,\mathrm{m}^3/(\mathrm{s\,m})$.

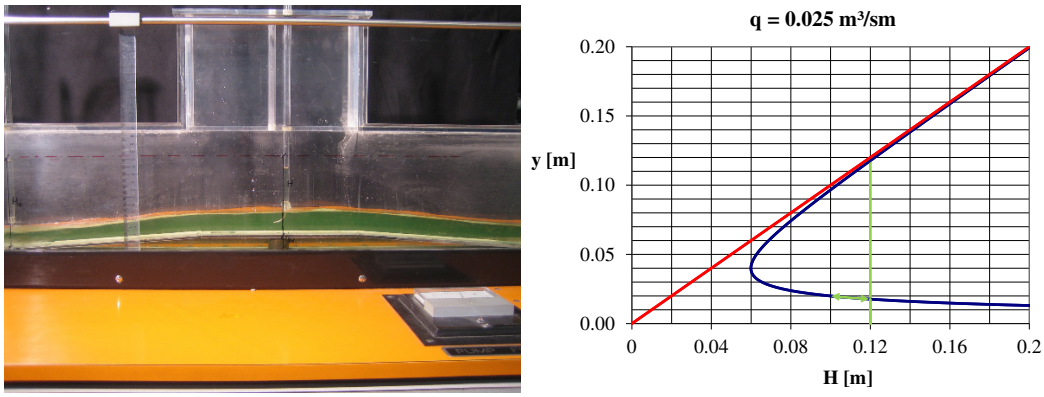

Figure 13.6: Supercritical flow in a rectangular laboratory flume with a discharge of $q = 25\,\mathrm{L}/(\mathrm{s\,m})$.

The markings on the ruler are hardly discernible in the photo; the flow depth is approximately 2.0 cm. Those who want more precise data must again rely on Octave for the solution of the Bernoulli equation:

```
function H=f(y)
H = -.12+y+.025^2/(y^2*2*9.81);
endfunction
[y,fval,info]=fsolve(@f,.02)
```

The starting value must be close to the actual solution value (here 0.02 m). Then, in this case, $y = 1.764\,\mathrm{cm}$.
Here again we turn downstream to the bed sill with height $w = 2.0\,\mathrm{cm}$. On the ramp of the bed sill, the specific energy decreases gradually until it reaches $H_{\text{on the sill}} = 12.0 - 2.0 =$

[B] After Chapter 11, everybody should be aware of the fact that the energy height cannot increase absolutely since no energy is supplied to the flow at this point.

10 cm. Let's follow the $H - y$ line in Figure 13.6. At the flow depth with supercritical flow, a decrease of the specific energy leads to an increase in flow depth. The photo shows a significant increase of the flow depth relative to the bed – and that it is even possible that the water flows "uphill". This is comparable to a roller coaster where the cars – without an engine – race at high velocity up a hill, lose kinetic energy with the increase of the potential energy and are finally pushed over the top of the hill. Using the definition for H

```
H = -.10 + y + .025^2/(y^2 * 2 * 9.81);
```

one obtains with an estimated value that is less than 4.0 cm: $y_{\text{on the sill}} = 1.995\,\text{cm}$.
Those who question the photo will see that the water level in the middle Pitot tube is not at the height of the red energy grade line, but rather approximately 1.5 cm below it. For a subcritical flow, the energy losses over such a short distance may in most cases be hidden. But due to the high velocities at supercritical flow, they cannot be disregarded. Loss-affected flows will be addressed in upcoming sections starting with 13.9. For the time being, we pretend as if no losses have occurred.
On the declining part of the bed sill, the specific energy (remark: related to the bed) increases again. When following the specific energies vs. flow depths relation starting from the point of intersection between $H = 10\,\text{cm}$ and $y = 1.995\,\text{cm}$ to the right (increasing specific energy), the flow depth must decrease. Looking more closely, one may detect (relative to the bed) a slightly dropping water level. A more distinct lowering of the flow depth is not discernible due to the occurring losses and the differences of the water levels, which are already small. Mathematically, we obtain again a flow depth of $y = 1.764\,\text{cm}$ at the prevailing specific energy ($H = 12\,\text{cm}$).

Experiment

Critical flow in a laboratory flume

We start again at the same discharge ($q = 0.025\,\text{m}^3/(\text{s m})$) with the specific energy $H_{\text{upstream the sill}} = 12.0\,\text{cm}$ (see Figure 13.7). The bed sill is now set to $w = 6.0\,\text{cm}$ so that the specific energy on the bed sill decreases to $H_{\text{on the sill}} = 6\,\text{cm}$. The flow depth upstream from the bed sill again amounts to approximately 11.8 cm. Downstream from the bed sill, however, the flow depth did not return to the original value of 11.8 cm, but rather reaches approximately 2.0 cm. The **flow transition** from subcritical to supercritical flow is forced because on the bed sill at height $w = 6\,\text{cm}$ the **critical specific energy** also known as **minimum energy** $H_{\text{min}} = H_{\text{upstream the sill}} - w = 6\,\text{cm}$ is attained (see Figure 13.7, right).
If the critical conditions, i. e. the minimum values of the $H - y$ relation, are reached, they will be passed through. In our case, the ramp again extends down to the original datum so that downstream from the sill, $H_{\text{downstream the sill}} = 12.0\,\text{cm}$. Therefore, the flow depth drops again to $y_{\text{downstream the sill}} \approx 1.8\,\text{cm}$ (see above).

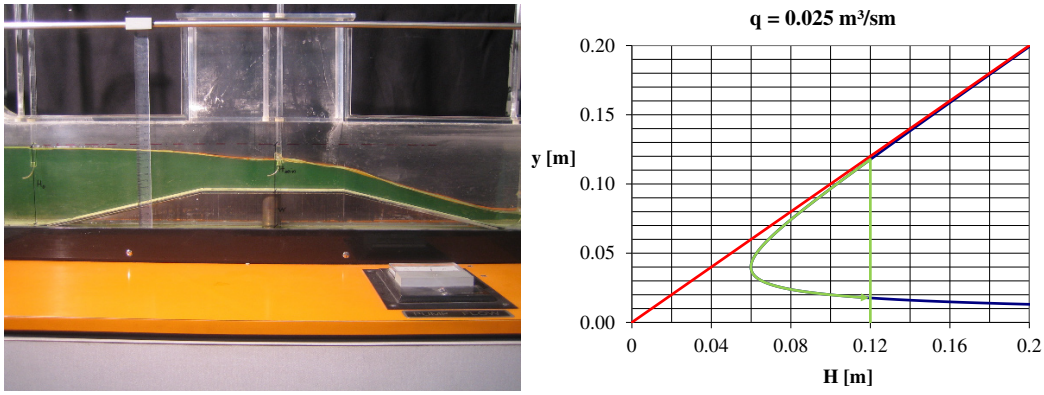

Figure 13.7: Critical flow in a rectangular laboratory flume with a discharge of $q = 25\,\mathrm{L/(s\,m)}$.

13.3.2 Mathematical description of the critical conditions

Figure 13.4 shows that at a certain specific energy, two flow depths, referred to as **corresponding flow depths**, may exist. There is no solution for the equation from $H = 0\,\mathrm{m}$ to approximately $H = 0.7\,\mathrm{m}$. In other words, at a specific energy that is smaller than a certain value (approximately 0.7 m), $q = 1.0\,\mathrm{m^3/(s\,m)}$ cannot be discharged. Minima and maxima of a function are obtained by setting the first derivative to zero. Thus the minimum energy (critical specific energy) is determined by taking the derivative of the specific energy with respect to the flow depth: $\frac{\mathrm{d}H}{\mathrm{d}y} \stackrel{!}{=} 0$. The concrete calculation steps for a rectangular cross-section are:

$$\frac{\mathrm{d}H}{\mathrm{d}y} = \left(y + \frac{q^2}{y^2 2g}\right)\frac{1}{\mathrm{d}y} = 1 + \frac{q^2 \cdot (-2)}{y^3 2g} \stackrel{!}{=} 0 \tag{13.6}$$

Solving for the flow depth y, which we designate as y_c (c stands for critical) for this extreme value, the result is:

$$y_{c,\mathrm{rectangle}} = \sqrt[3]{\frac{q^2}{g}} \tag{13.7}$$

By inserting the critical flow depth into the Bernoulli equation (13.4), the minimum energy may be determined for a rectangular cross-section:

$$\begin{aligned} H_{\min} &= y_c + \frac{q^2}{y_c^2 2g} = \sqrt[3]{\frac{q^2}{g}} + \frac{q^2}{\sqrt[3]{\frac{q^2}{g}}^2 2g} = \sqrt[3]{\frac{q^2}{g}} + \frac{q^2}{\frac{q^{\frac{4}{3}}}{g^{\frac{2}{3}}} 2g} = \\ &= \sqrt[3]{\frac{q^2}{g}} + \frac{q^{\frac{2}{3}}}{2g^{\frac{1}{3}}} = \sqrt[3]{\frac{q^2}{g}} + \frac{1}{2}\sqrt[3]{\frac{q^2}{g}} = \frac{3}{2}y_c \end{aligned} \tag{13.8}$$

Before proceeding, we will pause briefly. In Chapter 13.2, the Froude number and its importance for open channel hydraulics was discussed. It is defined as $\mathrm{Fr} = \frac{v}{\sqrt{gy}}$. From Equation 13.8 ($H_{\min} = \frac{3}{2}y_c$), it follows that $\frac{v_c^2}{2g} = \frac{1}{2}y_c$; i. e. $v_c = \sqrt{gy_c}$. By insertion of this critical velocity v_c at the critical flow depth y_c into the definition of the Froude number (Equation 13.1), $\mathrm{Fr} = \frac{v_c}{\sqrt{gy_c}} = \frac{\sqrt{gy_c}}{\sqrt{gy_c}} = 1$ is obtained. Thus, $\mathrm{Fr} = 1$ marks the boundary

between critical conditions; for $\mathrm{Fr} > 1$, supercritical conditions apply; for $\mathrm{Fr} < 1$, subcritical conditions are pertinent.

Critical conditions at arbitrary cross-sections

We may determine the critical flow depth for any cross-section of area $A(y)$ by taking the derivative of the specific energy with respect to the flow depth. The specific energy for any cross-section is:

$$H = y + \frac{Q^2}{A(y)^2 2g} \tag{13.9}$$

Taking the derivative of the specific energy with respect to the flow depth and setting it to zero:

$$\frac{\mathrm{d}H}{\mathrm{d}y} = 1 + \frac{Q^2 \cdot (-2)}{A_c^3 2g} \cdot \frac{\mathrm{d}A}{\mathrm{d}y} \stackrel{!}{=} 0 \tag{13.10}$$

In the formulation of arbitrary cross-sections, $\frac{\mathrm{d}A}{\mathrm{d}y}$ is added from use of the chain rule because $A(y)$ depends on y, as can already be seen from the expression. To gain a better understanding of this derivative, we mentally follow an image drawn by Jirka and Lang [20]. When raising the water level in an arbitrary open channel cross-section (see e. g. Figure 13.22 on page 234) by $\mathrm{d}y$, the area increases simultaneously by $\mathrm{d}A$. Thus, the increase in area of an open channel flow always takes place at the water level. Since $\frac{\mathrm{d}A}{\mathrm{d}y} = b_{\mathrm{WS}}$, then[C]:

$$\frac{\mathrm{d}H}{\mathrm{d}y} = 1 - \frac{Q^2}{A_c^3 g} \cdot b_{\mathrm{WS}} \stackrel{!}{=} 0 \tag{13.11}$$

From the underlying one-dimensional approach, it follows, strictly mathematically, that the Froude number for arbitrary cross-sections must be formed via the reference length $l_{\mathrm{ref}} = \frac{A}{b_{\mathrm{WS}}}$ (see Formula 5.33) in order to reach the critical conditions at $\mathrm{Fr} = 1$[D]. For the Froude number in any open channel, we therefore write:

$$\mathrm{Fr} = \frac{v}{\sqrt{g \frac{A}{b_{\mathrm{WS}}}}} \tag{13.12}$$

Actually, however, there will be different propagation velocities of surface waves, depending on the flow depth at their respective locations across an open channel. For those interested in the topic "one-dimensional approach to arbitrary open channel cross-sections", the standard reference by Bollrich [5] is recommended for further reading.

[C] Thus, the differential area is divided by the differential height, resulting in the width at the water surface. When verifying the statement for a rectangular open channel of width b, $\frac{\mathrm{d}A}{\mathrm{d}y} = b$, which is in accordance with the above solution. But you may well check it out yourself and derive A with respect to y, e. g. for a trapezoidal or parabolic open channel. The calculation for a partially filled circular cross-section is far more complicated. However, it will always yield $\frac{\mathrm{d}A}{\mathrm{d}y} = b_{\mathrm{WS}}$. You will find the derivations for the critical flow depths in trapezoidal, triangular and parabolic cross-sections in Appendix A.5.

[D] Let's briefly check the following: $\mathrm{Fr} = 1$ leads to $v^2 = \frac{gA}{b_{\mathrm{WS}}}$; i. e. $Q^2 = \frac{gA^3}{b_{\mathrm{WS}}}$. This is inserted into the expression for the derivative of the specific energy with respect to the flow depth: $1 - \frac{gA^3}{b_{\mathrm{WS}}} \frac{b_{\mathrm{WS}}}{A^3 g} = 0$.

13.3.3 q-y diagram

Back to Equation 13.4, in which H is set constant for the following discussion. Figure 13.8 is an example with $H = 2.0\,\mathrm{m}$ showing how the variables q and y behave at this specific energy.

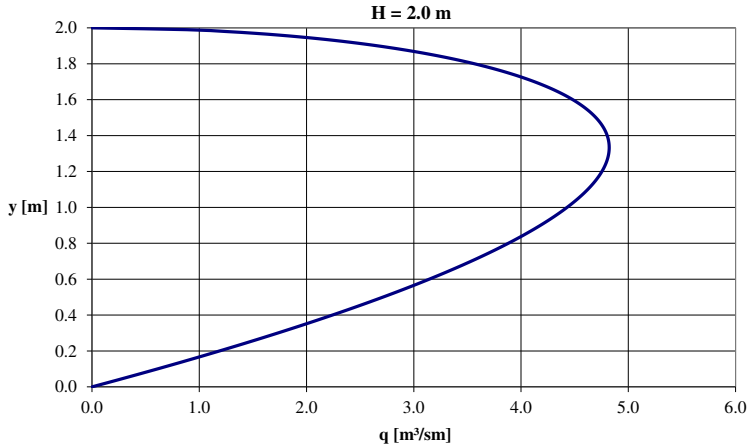

Figure 13.8: Flow depth vs. discharge per unit width for a rectangular open channel with $H = \text{const.} = 2.0\,\mathrm{m}$.

Figure 13.8 shows a curve that indicates a maximum value of the discharge per unit width. The maximum may again be determined by setting the derivative to zero. We solve the Bernoulli equation for q

$$q = \sqrt{(H-y)\cdot 2gy^2} \tag{13.13}$$

and take the derivative of it with respect to y:

$$\frac{\mathrm{d}q}{\mathrm{d}y} = \sqrt{(H-y)\cdot 2gy^2}\frac{1}{\mathrm{d}y} = \sqrt{2g}\sqrt{(H-y)}y\frac{1}{\mathrm{d}y} \overset{!}{=} 0 \tag{13.14}$$

Using the product rule $f'(x) = u'(x)\cdot v(x) + u(x)\cdot v'(x)$, as it is given in Bronstein and Semendjajew [8, S. 395], it follows that:

$$\frac{\mathrm{d}q}{\mathrm{d}y} = \sqrt{2g}\left((H-y)^{-\frac{1}{2}}\cdot\frac{1}{2}\cdot(-1)\cdot y + \sqrt{H-y}\cdot 1\right) = \sqrt{2g}\left(\sqrt{H-y} - \frac{y}{2\sqrt{H-y}}\right) \overset{!}{=} 0 \tag{13.15}$$

In order to simplify Equation 13.15, we first divide by $\sqrt{2g}$; on the right side, $\frac{0}{\sqrt{2g}}$ still equals 0. Furthermore, we move a term to the other side of the equals sign and obtain:

$$\sqrt{H-y} = \frac{y}{2\sqrt{H-y}} \tag{13.16}$$

Now we solve Equation 13.16 for y:

$$y = 2\sqrt{H-y}\sqrt{H-y} = 2(H-y) = 2H - 2y \tag{13.17}$$

With $y = \frac{2}{3}H$, which we also get from the derivative of q with respect to y, the critical conditions are in effect. In a rectangular cross-section, the maximum discharge may flow at a certain specific energy if it consists of $\frac{1}{3}$ velocity height and $\frac{2}{3}$ flow depth.
When inserting this finding into Equation 13.13, we obtain an expression for $q_{\max}$:

$$q_{\max} = \sqrt{\left(H - \frac{2}{3}H\right) \cdot 2g \left(\frac{2}{3}H\right)^2} = \sqrt{\frac{1}{3}H \cdot 2g \cdot \frac{4}{9}H^2} = \sqrt{\frac{8}{27}H^3 g} \tag{13.18}$$

Thus, no more than $q_{\max} = 4.822\,\mathrm{m^3/(s\,m)}$ may flow off at a specific energy of $H = 2.0\,\mathrm{m}$.
Let's first look at an example before we return to the $q - y$ relation in Chapter 13.8.

Example

Flow in a constriction

In an open channel, a discharge per unit width of $q = 3.0\,\mathrm{m^3/(s\,m)}$ takes place. This increases to $q = 5.0\,\mathrm{m^3/(s\,m)}$ in a lateral constriction. On the left side of Figure 13.9, we immediately see that the discharge per unit width of $q = 5.0\,\mathrm{m^3/(s\,m)}$ cannot be discharged at the available specific energy of $H = 2.0\,\mathrm{m}$; maximally, approximately $4.82\,\mathrm{m^3/(s\,m)}$ may flow. And that's how it is initially. The discharge difference ($\approx 0.18\,\mathrm{m^3/(s\,m)}$) remains upstream, the water level rises, and energy is built up until there is just enough that the arriving discharge may pass. This means again that the critical conditions (right side of Figure 13.9) are met and thus a transition from subcritical to supercritical flow occurs (see above). We may calculate the minimum required energy from Formula 13.8: $H = \frac{3}{2}\sqrt[3]{\frac{5.0^2}{g}} = 2.049\,\mathrm{m}$. When neglecting energy losses, which is well-justified by the short development length, the flow depths upstream and downstream from the constriction where a discharge per unit width of $q = 3.0\,\mathrm{m^3/(s\,m)}$ takes place may be seen on the right side of Figure 13.9. The flow depth at subcritical flow is $y_{\mathrm{upstream}} \approx 1.9\,\mathrm{m}$; the flow depth downstream may be estimated as the corresponding flow depth $y_{\mathrm{downstream}} \approx 0.55\,\mathrm{m}$.

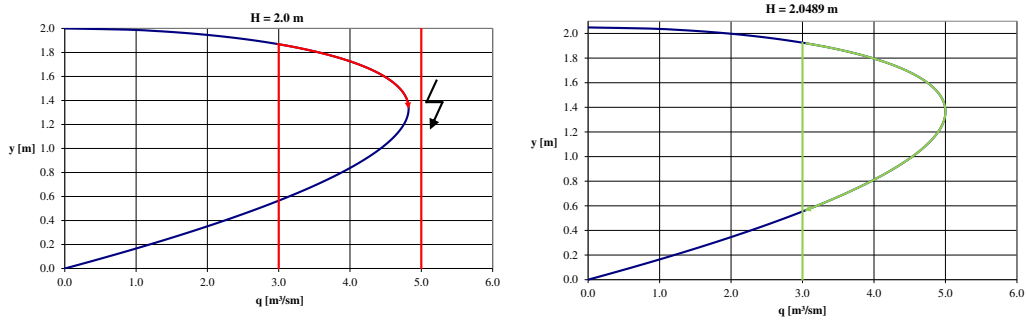

Figure 13.9: Flow through a constriction if $q > q_{\max}$.

Those who want more precise results may once again use Octave and obtain $y_{\mathrm{upstream}} = 1.925\,\mathrm{m}$ and $y_{\mathrm{downstream}} = 0.554\,\mathrm{m}$.

```
1> function H=f(y)
2> H = -2.0489+y+5^2/(y^2*2*9.81);
3> endfunction
4> [y,fval,info]=fsolve(@f,1.8)
5> [y,fval,info]=fsolve(@f,.4)
```

Enter the commands into the Octave command line. The meaning of the individual commands is:

```
4> % at the starting value of 1.8, the flow depth in the subcritical condition upstream from the constriction is obtained.
5> % with a starting value of 0.4, the iteration leads to the flow depth in the supercritical condition downstream from the constriction.
```

13.4 Flow under a sluice gate

For deriving shape parameters (e. g. [20, p. 59]), one may consider the flow under a sluice gate that is mounted at different angles against vertical. We focus on vertical sluice gates and take advantage of the Bernoulli equation following the derivation of the Torricelli equation (9.6) but consider the kinetic energy. When introducing a discharge coefficient

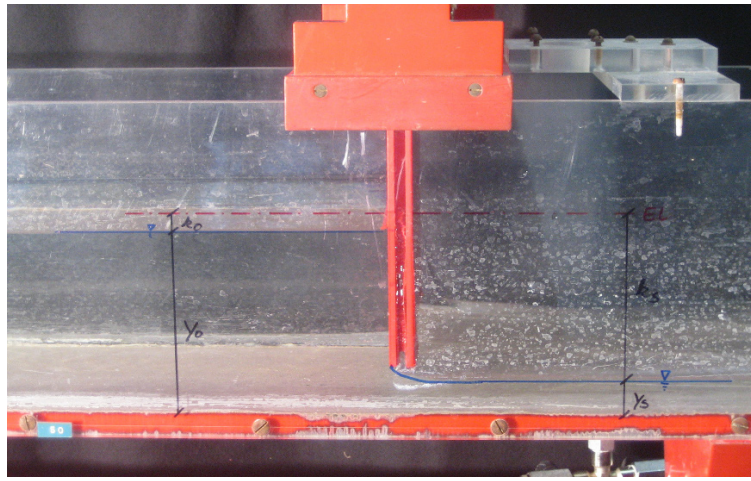

Figure 13.10: Flow under a sluice gate.

$\mu = \phi \cdot \psi$ here, as well as a combination of the loss coefficient ϕ and the contraction number ψ, the equation for the flow under sluice gates with the lifting height h_{lift} reads as follows:

$$Q = \mu \cdot h_{\text{lift}} \cdot b \cdot \sqrt{2g\,(H - y_{vc})} \quad \text{for } y_{\text{upstream}} \geq 1.5 \cdot h_{\text{lift}} \tag{13.19}$$

Also, for the flow under sluice gates, the equation is valid only if no air is sucked-in upstream (air that is sucked in would reduce the flow area). Therefore, y_{upstream} must be at least 1.5 times the lifting height h_{lift}.

We move slightly upstream, as well as downstream to the so-called vena contracta (where the least flow depth y_{vc} prevails), to find hydrostatic pressure distributions. As friction losses occur, particularly due to the high velocity downstream from the sluice gate, they will be accounted for by the coefficient μ.
Now we address the flow conditions illustrated in Figure 13.10 and determine the discharge under the sluice gate. Here, we again draw the energy diagram directly onto the acrylic glass wall. With the width of the flume $b = 20\,\text{cm}$ and the lifting height $h_{\text{lift}} = 2.6\,\text{cm}$ as well as with the discharge coefficient $\mu = 0.7$, the flow depth measurements for upstream, $y_{\text{upstream}} = 11.7\,\text{cm}$, and downstream from the sluice gate, $y_{vc} = 1.8\,\text{cm}$, lead to a discharge of $Q = 5.1\,\text{L/s}$. The result is quite close to $Q = 5.0\,\text{L/s}$, which was determined by means of a so-called magneto-inductive flow meter. Simply recalculate as follows!

```
1> function F=f(Q)
2> F = -Q+0.7*0.026*.2*sqrt(2*9.81*(0.117+Q^2/(0.117^2*.2^2*2*g)-...
> 0.018));
3> endfunction
4> [y,fval,info]=fsolve(@f,3e-3)
```

Enter the commands into the Octave command line. The dots (. . .) indicate line breaks; simply continue typing.

The discharge coefficient μ given in reference works like Bollrich [5] usually includes the influence of upstream velocity head and downstream pressure, so that the discharge under sluice gates is often calculated using the Torricelli equation (9.6). Caution is therefore required when determining the discharge coefficient. The influence of backwater is usually considered via an additional coefficient which, in this case, is obviously smaller than one.

13.5 Flow over weirs

Weirs as construction elements in hydraulic engineering are of great importance for practical applications. The flow over a weir with all relevant variables is shown in Figure 13.11.

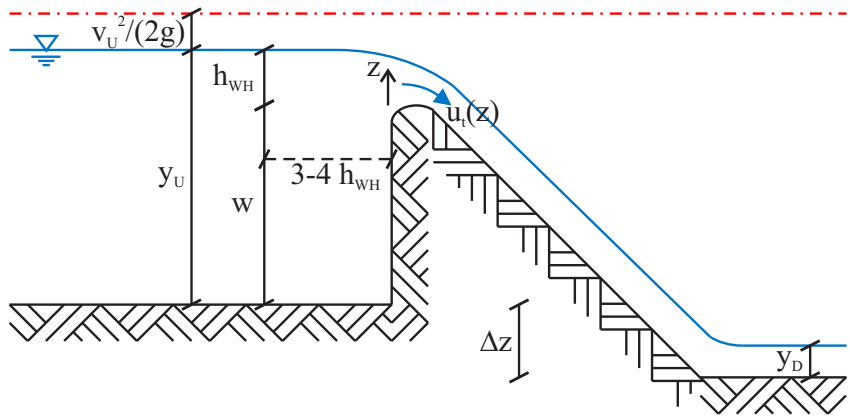

Figure 13.11: Flow over a weir.

13.5.1 Poleni equation

The fluid flows in an open channel towards a weir.

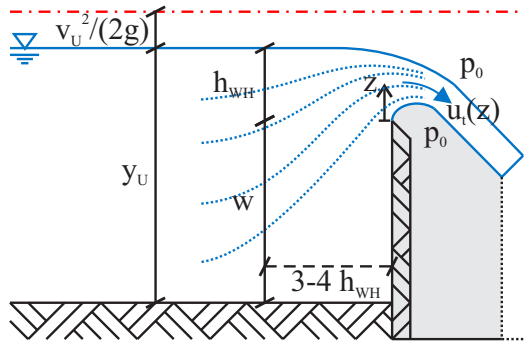

Figure 13.12: Idealised streamlines at a weir.

At a distance of 3 – 4 h_{WH}, the water level is not yet dropping; there, we may assume hydrostatic conditions. For the following considerations, our reference system has $z = 0$ (with the z-axis directed upwards) located on the weir crest, i. e. the highest point of the weir (we assume a sharp-edged weir here). The energy height may be written 3 – 4 h_{WH} upstream from the weir as $H = h_{\mathrm{WH}} + \frac{v_U^2}{2g}$ relative to $z = 0$. The streamlines that begin below $z = 0$ also meet this condition exactly; although their pressure heights $\frac{p}{\rho g}$ are greater, the geodetic heights are lower (negative) by the same degree. Stating that on the one hand the energy height along a streamline is constant (which seems not unreasonable due to the relatively short development length) and that on the other hand the pressure height on the weir is zero[E] means that each streamline on the weir exhibits the energy from the respective geodetic height z and the tangential velocity component $\frac{u_t(z)^2}{2g}$[F], while $\frac{p}{\rho g} = 0$. Thus, we may write

$$H = h_{\mathrm{WH}} + \frac{v_U^2}{2g} = z + \frac{u_t(z)^2}{2g} \tag{13.20}$$

and therefrom interpret the velocity as a function of the coordinate z as seen, for example, in Zuppke [65] or Bollrich [5, page 396]:

$$u_t(z) = \sqrt{2g\left(h_{\mathrm{WH}} - z + \frac{v_U^2}{2g}\right)} \tag{13.21}$$

The following expression for the discharge is the integral of the velocity with respect to the area. Here, the factor ζ, which is smaller than one, is meant to indicate the thickness of the water jet (also called nappe) at the respective location relative to h_{WH}.

[E] This assumption must be carefully considered. From Figure 13.12, it follows that atmospheric pressure p_0 prevails above and below the overflow jet. This also applies to fixed weirs and the design discharge (see Figure 13.13). However, the jet inside is not pressureless because the streamlines are curved and the jet is tapering.

[F] A streamline is defined such that only the tangential component exists (see Chapter 2.8).

$$Q = \int_{y=0}^{y=b} \int_{z=0}^{z=\zeta \cdot h_{\mathrm{WH}}} \sqrt{2g} \sqrt{h_{\mathrm{WH}} - z + \frac{v_U^2}{2g}} \, \mathrm{d}z \, \mathrm{d}b = b \int_{z=0}^{z=\zeta \cdot h_{\mathrm{WH}}} \sqrt{2g} \sqrt{h_{\mathrm{WH}} - z + \frac{v_U^2}{2g}} \, \mathrm{d}z \tag{13.22}$$

The integration of $\int \sqrt{-z} \mathrm{d}z$ yields $-\frac{2}{3} z^{\frac{3}{2}}$. We therefore obtain:

$$\begin{aligned} Q &= -\frac{2}{3} b \sqrt{2g} \left[\left(h_{\mathrm{WH}} - z + \frac{v_U^2}{2g} \right)^{\frac{3}{2}} \right]_0^{\zeta \cdot h_{\mathrm{WH}}} \\ &= -\frac{2}{3} b \sqrt{2g} \left[\left(h_{\mathrm{WH}} - \zeta \cdot h_{\mathrm{WH}} + \frac{v_U^2}{2g} \right)^{\frac{3}{2}} - \left(h_{\mathrm{WH}} + \frac{v_U^2}{2g} \right)^{\frac{3}{2}} \right] \\ &= \frac{2}{3} b \sqrt{2g} \left[\left(h_{\mathrm{WH}} + \frac{v_U^2}{2g} \right)^{\frac{3}{2}} - \left((1-\zeta) h_{\mathrm{WH}} + \frac{v_U^2}{2g} \right)^{\frac{3}{2}} \right] \end{aligned} \tag{13.23}$$

Neglecting the velocity height in the upstream water $\frac{v_U^2}{2g}$, which appears to be justified due to the low flow velocities there, we may further write:

$$Q = \frac{2}{3} b \sqrt{2g} \left[h_{\mathrm{WH}}^{\frac{3}{2}} - (1-\zeta)^{\frac{3}{2}} \cdot h_{\mathrm{WH}}^{\frac{3}{2}} \right] = \frac{2}{3} b \sqrt{2g} h_{\mathrm{WH}}^{\frac{3}{2}} \left[1 - (1-\zeta)^{\frac{3}{2}} \right] \tag{13.24}$$

Substituting the overflow coefficient μ for the bracketed expression $\left[1 - (1-\zeta)^{\frac{3}{2}} \right]$, we obtain the Poleni equation (13.25):

$$Q = \mu \frac{2}{3} b \sqrt{2g} h_{\mathrm{WH}}^{\frac{3}{2}} \tag{13.25}$$

The table values for μ also include the influences of friction and pressure as well as the upstream velocity height, all of which have been neglected in the derivation. μ is dependent on the design of the weir and ranges from 0.5 for wide-crested weirs to 0.75 for round-crested weirs. An advantageous flow profile was developed by the American Corps of Engineers and is internationally known as the WES profile. Design information may be found e. g. in [58, 136]. However, the equation for the discharge over a weir (13.25) is applicable only if no backwater from downstream exists (submerged flow). In this case, a reduction factor, which takes into account the influence of backwater (see Chapter 13.5.3), is introduced.

Experiment

Flow over a sharp-edged weir

Exemplary for the flow over a sharp-edged weir, we observe the development of negative pressure with insufficient aeration of the overflow jet. When aerating the region below the nappe by means of a finger held into the overflow jet, a far greater throw will form (see Figure 13.13). Sufficient aeration of the nappe must be ensured in the construction of weirs in order to prevent pulsation of the jet, which would introduce pressure fluctuations.

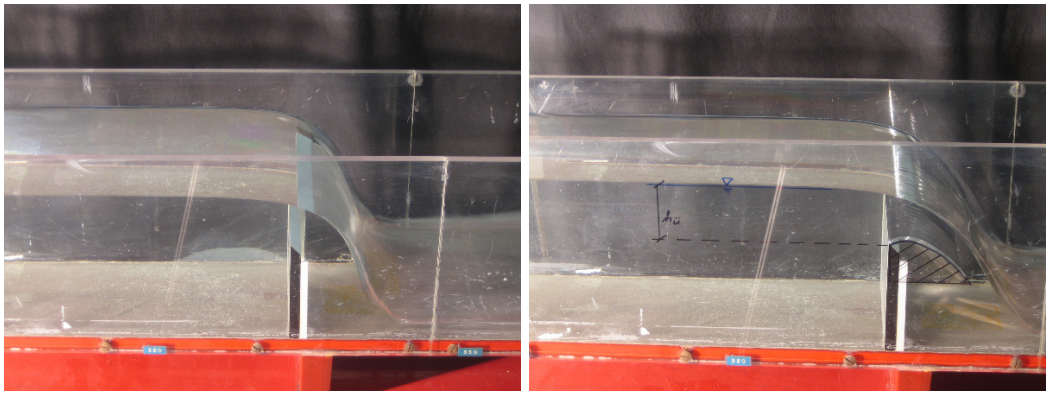

Figure 13.13: Flow over a sharp-edged weir (attached nappe on the left, aerated on the right).

In the above laboratory flume of width $b = 0.20\,\mathrm{m}$ with weir height $w = 0.10\,\mathrm{m}$ and overflow height $h_{\mathrm{WH}} = 0.053\,\mathrm{m}$, the result for the discharge coefficient, according to Rehbock[G] [49], is $\mu = 0.605 + \frac{1}{1000 \cdot h_{\mathrm{WH}}} + 0.08 \cdot \frac{h_{\mathrm{WH}}}{w} = 0.666$. From Equation 13.25, the result for the discharge is $4.8\,\mathrm{L/s}$.

13.5.2 du Buat equation

The equation according to du Buat[H] (13.26), which also explicitly indicates the upstream velocity height, is (see Equation 13.23):

$$Q = \mu_{\mathrm{du\,Buat}} \frac{2}{3} b \sqrt{2g} \left(h_{\mathrm{WH}} + \frac{v_U^2}{2g} \right)^{\frac{3}{2}} \tag{13.26}$$

Du Buat does not include the velocity height upstream from the weir in the discharge coefficient μ, which is why it differs from the Poleni coefficient and is designated as $\mu_{\mathrm{du\,Buat}}$. However, Equation 13.26 must be solved iteratively, which is why it was hardly used before the development of numeric solvers. For this reason, the pertinent tables do not contain any reference values for the discharge coefficient $\mu_{\mathrm{du\,Buat}}$. In Rössert [49], one may find only the analytically derived relation $\mu_{\mathrm{du\,Buat}} = \mu \cdot \left(1 + \frac{v_U^2}{(2gh_{\mathrm{WH}})}\right)^{-1.5}$, which consequently leads to the same result as the evaluation of Equation 13.25.

13.5.3 Submerged flow over a weir

Submerged flow over a weir occurs when the tailwater level rises up to a certain height above the weir crest. In experiments, it can be proven that the tailwater impacts the flow conditions upstream from the weir when the overflow jet separates from the weir body.

[G] Theodor Rehbock, ∗1864, Amsterdam, the Netherlands †1950, Karlsruhe, Germany

[H] "The famous researcher Chevalier du Buat shone mightily ahead . . . ", from Kreuter [24].

Initially, the pressure distribution in the crest area is changed by the rising tailwater. The occurrence of an undulating flow is typical for the separation of the jet (see Figure 13.14).

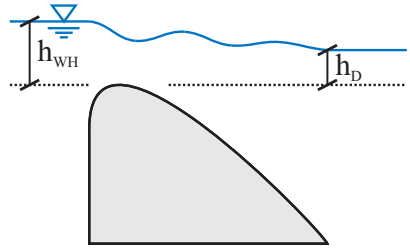

Figure 13.14: Submerged flow over a weir.

Depending on the design of the weir, various values for $\frac{h_D}{h_{WH}}$ may initiate the submerged flow. The highest degree of impounding is achievable with $\frac{h_D}{h_{WH}} \approx 0.8$ for the broad-crested weir.

13.6 Discharge through a siphon weir

A siphon weir has an appearance similar to that of a common weir with the critical difference that the discharge from the siphon takes place under pressure (or better: under negative pressure). The siphon weir has a lid, known as siphon roof, in the contour of the

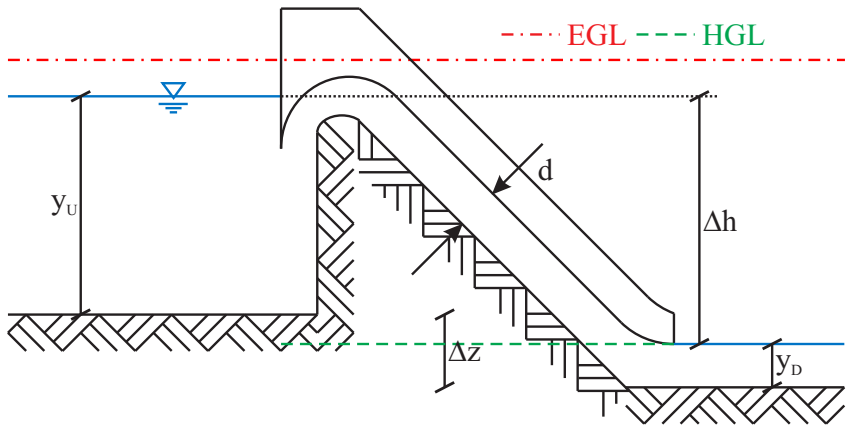

Figure 13.15: Sketch of a siphon.

weir.
But wait a minute. If the water level exceeds the height w of the siphon weir, the flow initially takes place with free surface and may be expressed via the Poleni equation (13.25). By means of priming deflectors and the high velocity at the downstream face, the air is carried out of the siphon, and the water then flows off under pressure. Hence, the energy height difference between upstream and downstream water, and no longer the overflow

height, determines the discharge. The discharge through a siphon weir is therefore described by the energy levels up- and downstream from the siphon weir, however, generally the water level difference is taken into account (see Equation 13.27). In most cases, a discharge coefficient [63] of 0.7 to 0.8 is achieved.

$$Q = \mu_{\text{siphon weir}} \cdot A_{\text{siphon weir}} \cdot \sqrt{2g\Delta h} = \mu_{\text{siphon weir}} \cdot d \cdot b_{\text{siphon weir}} \cdot \sqrt{2g\Delta z + y_U - y_D} \tag{13.27}$$

The flow stalls if the upstream water level drops below the siphon mouth or so far such that air is sucked in (see Chapter 13.4 or Equation 13.19). For the siphon weir, it must also be ensured that no cavitation occurs (see Chapter 8.7).

Example

Flow through a siphon weir

Suppose the flow through a siphon weir with a rectangular cross-section ($b = 5.0\,\text{m}$, $d = 1.0\,\text{m}$, $\mu = 0.75$, $\Delta z = 3.0\,\text{m}$) is to be determined. Furthermore, assume that the upstream flow depth is $y_U = 5.0\,\text{m}$, and downstream flow depth is $y_D = 2.0\,\text{m}$.

$$\begin{aligned} Q &= \mu_{\text{siphon weir}} A_{\text{siphon weir}} \sqrt{2g\,(\Delta z + y_U - y_D)} = 0.75 \cdot 5.0 \cdot 1.0 \sqrt{2g \cdot (3.0 + 5.0 - 2.0)} \\ &= 40.687\,\text{m}^3/\text{s} \end{aligned} \tag{13.28}$$

13.7 Flow depth at a fall

In the case of a fall, nature also demands only the energy that is absolutely necessary. Therefore, the flow depth here in subcritical flow may be derived from the minimum principle. But beware! At a fall, air can be present at the underside of the jet, which means atmospheric pressure. When viewing Figure 13.16, the experienced hydraulic engineer will notice that there is no hydrostatic pressure distribution. What we need is the law of momentum!

Let's assume that immediately upstream from the fall there are still hydrostatic conditions and that hardly any energy is dissipated over the flow distance from there to the fall. Therefore, the minimum energy $H_{\min}$ will be established just upstream from the fall; with hydrostatic conditions, this corresponds with y_c.

We will further assume that the jet behaves as if it is discharged into open air; the pressure at the fall will then become zero. The forces are plotted in Figure 13.17.

Under these conditions, the law of momentum for a rectangular open channel is established:

$$\rho Q v_c + \frac{1}{2}\rho g y_c^2 b = \rho Q v_r \tag{13.29}$$

We simplify the equation by dividing by ρ and b; Q becomes q and v is replaced with $\frac{q}{y}$:

$$q\frac{q}{y_c} + \frac{1}{2}g y_c^2 = q\frac{q}{y_r} \tag{13.30}$$

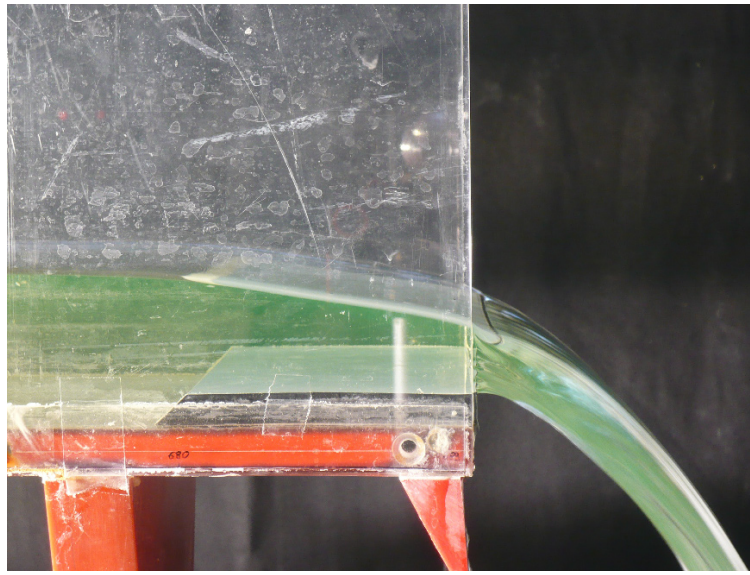

Figure 13.16: Flow depth at a fall.

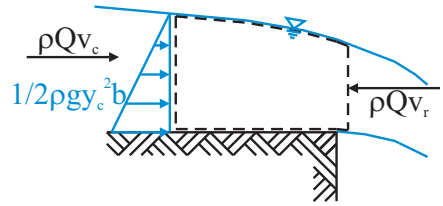

Figure 13.17: Forces at a fall.

The relationship between y_c and q for the critical conditions is known from Equation 13.7. Solving $y_c = \sqrt[3]{\frac{q^2}{g}}$ for q^2 results in:

$$q^2 = g y_c^3 \tag{13.31}$$

Inserting this result into Formula 13.30 yields Equation 13.32:

$$y_c^2 g + \frac{1}{2} y_c^2 g = \frac{y_c^3 g}{y_r} \tag{13.32}$$

When combining the terms on the left side and dividing the equation by g, the ratio becomes very clear. We obtain

$$\frac{3}{2} y_c^2 = \frac{y_c^3}{y_r} \tag{13.33}$$

which solved for y_r finally yields:

$$y_r = \frac{2}{3} \frac{y_c^3}{y_c^2} = \frac{2}{3} y_c \tag{13.34}$$

Experiment

Flow depth at a fall

While taking the photo in Figure 13.16, which shows a $b = 0.20\,\mathrm{m}$-wide flume, a discharge of $Q = 3.0\,\mathrm{L/s}$ was measured.
From Formula 13.7, the critical flow depth is $y_c = 0.0284\,\mathrm{m}$, from which $\frac{2}{3}y_c = 0.0189\,\mathrm{m}$ results. In the experiment, $y_r = 2.2\,\mathrm{cm}$, which lies between the calculated value and y_c, was measured. This is attributed to the fact that the pressure force directly at the fall is not zero; the pressure is zero at both the upper and lower side; however, the fluid in the jet itself will be subject to a certain pressure distribution. For example, Valentin [61] gives the ratio $\frac{y_r}{y_c}$ a value of approximately 0.7.

13.8 Venturi channel

The Venturi channel, as it is called, was developed by British engineers in India for measuring discharge in open channels. The measuring device is named after the Italian physicist who discovered the Venturi effect[I].
The Venturi channel makes use of the extremal principle of Bernoulli's equation: when a flow is constricted to such an extent that the discharge can no longer pass through, the flow backs up. The two functional dependencies of flow depth and specific energy (Chapter 13.3.1) as well as flow depth and discharge per unit width q (Chapter 13.3.3) have been discussed above. Wherever $q = \text{const.}$, the use of the $H - y$ relation (see Figure 13.4) is recommended. It is only the discharge that is related to the channel width that varies in such a Venturi channel, but at continuous beds (without bed sills) the specific energy stays constant ($H = \text{const.}$ or may be assumed to be constant). Therefore, the application of a $q - y$ diagram, as shown in Figure 13.8, is advantageous.
Venturi channels are very frequently employed in wastewater systems for discharge measurements because the discharge may be determined solely by measuring the flow depth upstream from the constriction. They are advantageous compared to measuring weirs because the bed sill, which may lead to sedimentation, is omitted. However, the extent of the constriction must reliably ensure the transition from sub- to supercritical flow. Therefore, we have to be careful that there is no influence from the downstream backwater into the Venturi channel. A Venturi channel is designed only for the measurement of a discharge range to be defined in advance. For a better understanding of the flow, we will briefly conduct an experiment.

[I] Giovanni Battista Venturi, ∗1746, Bibbiano, Italy †1822, Reggio nell' Emilia, Italy

Experiment

Discharge in a Venturi channel

The Venturi channel optimised by Valentin[J] (here the width of the constriction varies with height – see Figure 13.18) allows us to approximate the discharge in a laboratory flume. All we have to do is measure the cross-sectional values as well as the flow depth upstream from the constriction. The width of the channel is $b = 0.20\,\mathrm{m}$; the average width of the constriction that varies over the height is $b_{\mathrm{constriction}} = 0.085\,\mathrm{m}$. With the Venturi

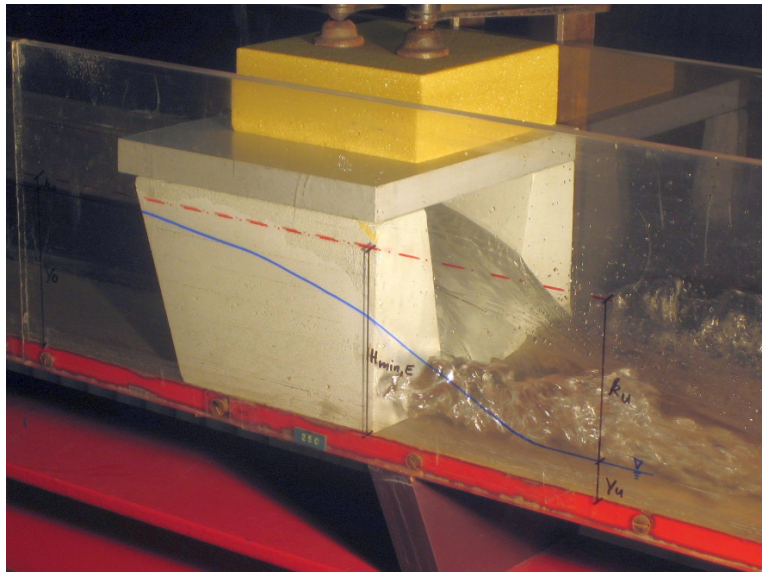

Figure 13.18: Determination of the discharge by means of a Venturi channel.

channel, it is generally assumed that energy losses are negligible; however, empirically determined loss coefficients may be applied as in DIN 19559. We equate the minimum energy at the narrowest place with the specific energy slightly upstream from the Venturi channel so that the Bernoulli equation for both cross-sections reads as follows:

$$y_{\mathrm{upstream}} + \frac{Q^2}{2gy_{\mathrm{upstream}}^2 b^2} = H_{\mathrm{min,constriction}} = \frac{3}{2}\sqrt[3]{\frac{Q^2}{gb_{\mathrm{constriction}}^2}} \tag{13.35}$$

With the measured flow depth $y_{\mathrm{upstream}} = 0.102\,\mathrm{m}$ and the cross-sectional values, Equation 13.35 reads:

$$0.102 + \frac{Q^2}{0.102^2 \cdot 0.20^2 \cdot 2g} = H_{\mathrm{min,constriction}} = \frac{3}{2}\sqrt[3]{\frac{Q^2}{g \cdot 0.085^2}} \tag{13.36}$$

For the solution, we again use Octave:

[J] Patent identification number DE19962239C2 05.12.2002.

```
1> function H=f(Q)
2> H=.102+Q^2/(.102^2*.2^2*2*9.81)-1.5*(Q^2/(.085^2*9.81))^(1/3)
3> endfunction
4> [Q,fval,info]=fsolve(@f,3e-3)
```

Octave displays $Q = 4.93\,\mathrm{L/s}$ for the discharge, which is in close agreement with the magneto-inductively measured discharge of $5.0\,\mathrm{L/s}$.

13.9 Steady-state, uniform flow (normal conditions)

Water flows in a river due to a pressure gradient caused by gravity or a water level gradient. From source to mouth, a river like the Isar or the Danube exhibits a certain water level gradient over a certain distance. We continue with the example of the Isar, which originates in the Karwendel mountains at a height of 1160 m.a.s.l. and joins the Danube after flowing for a distance of 295 km at 310 m.a.s.l. near Deggendorf. A mean water level gradient of $\frac{850}{295000} = 2.88$ results from the height difference and the flow distance. The originally existing energy has been dissipated, i. e. mostly converted into heat. By the way, the sun supplies the water with potential energy by means of evaporation and lifting vapour molecules to great heights. The rivers of the planet are fed with water and the necessary energy for the discharge is supplied by the drift of clouds and precipitation from great heights (e. g. in the Karwendel).
Open channel hydraulics deals with flows that have a free surface. In the Chapter "Hydrostatics" (7), we have also focused on (standing) water with a free water level. We found for stationary liquids that the water level is always perpendicular to the acceleration vector. If the flow depth is measured vertically – and not normally to the bed or water level – we make a small mistake. Let's look more closely at this matter:

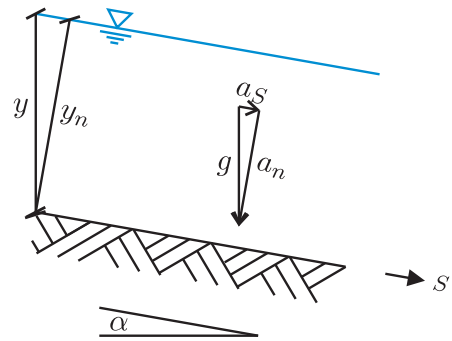

Figure 13.19: Acceleration vector and flow depth on an inclined plane.

Figure 13.19 shows a body of water on an inclined plane (the bed of our open channel). The pressure acts perpendicularly to the boundary (the river bed), and the acceleration a_s is parallel to that boundary. The component of the flow depth perpendicular to the bed corresponds to $y_n = y\cos\alpha$. In order to obtain the component a_n, which is parallel to y_n, the gravitational constant g must be multiplied by $\cos\alpha$. For the pressure, it follows that $p = \rho a_n y_n = \rho g \cos\alpha \cdot y\cos\alpha = \rho g y \cos^2\alpha$. At very steep slopes of 10 %, the cosine reaches a value of 0.995; its square is 0.99. Since the influence is negligible (1 %) even at

such steep channel beds, we will work with the vertical flow depth as pressure height $\frac{p}{\rho g}$ in the following discussion (see also [13]).

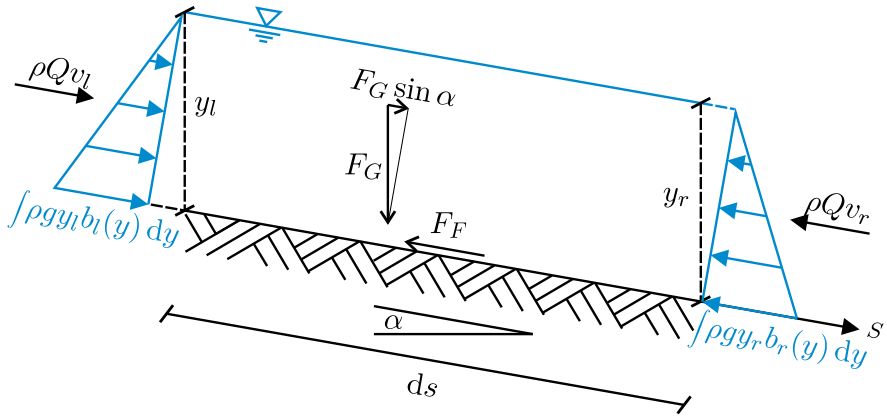

Figure 13.20: Water body on an inclined plane.

We look at the balance of forces depicted in Figure 13.20. The relationships between the quantities will be better understood if we undertake a mental bicycle tour. We mount a bike on a hill with constant gradient and roll downhill. The descent will probably take place such that we accelerate from standstill and eventually reach a velocity that does not increase further. This is the case when the downward force and the friction force are in equilibrium[K]. Flows in open channels behave in the same way. The downward force that results from gravity acting on the inclined plane accelerates the flow until a balance with the friction force is obtained. This is referred to as "normal conditions".
In the present section, we deal with these uniform conditions (see Chapter 2.7), i. e. the flow velocity does not change along the flow distance. If the velocity does not change, then the flow depth y and the velocity height $\frac{v^2}{2g}$ also do not change. As a result, the bottom gradient, the water surface gradient and the gradient of the energy grade line are identical ($J_B = J_{WS} = J_E$; see Figure 13.21).
The absolute values of the momentum flux and the force due to pressure are equal on the left- and right-hand sides of our control volume in Figure 13.20. Only the force due to mass and the friction force remain. Considering the immediately prior assumption that the flow depth may be measured vertically, it follows that for the downhill-slope force due to mass $\rho A\,\mathrm{d}s$ with acceleration a_s (see Figure 13.19) along the coordinate s:

$$F_G \cdot \sin\alpha = \rho A a_s\,\mathrm{d}s = \rho A\,\mathrm{d}s\,g\sin\alpha \tag{13.37}$$

The cross-sectional area is given by A, and the infinitesimal disk thickness in the flow direction is identified by $\mathrm{d}s$, as shown in Figure 13.20.
The friction term for the complex turbulent flow must be extremely simplified in order to be able to provide a one-dimensional solution. We benefit from the fact that the external friction is dominant and that viscous forces play a minor role – generally – in rough open channels. Therefore, only the wall shear stress, τ_W, is applied against the flow direction. It

[K] Newton stated in the lex prima, also known as the law of inertia (see Chapter 3.3), that a body remains in uniform motion if the sum of the applied forces is zero.

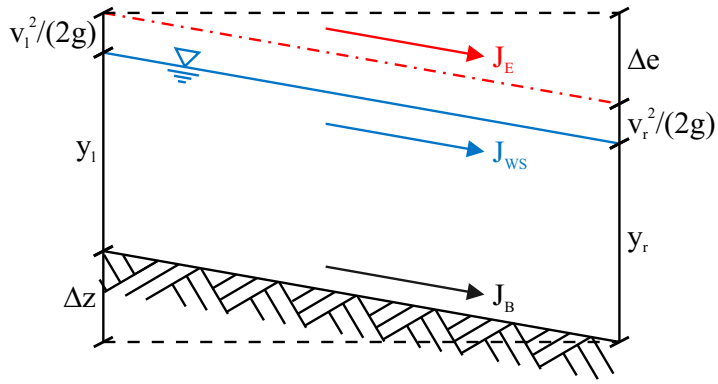

Figure 13.21: Steady-state conditions in an open channel section.

acts as a friction force F_F over the wetted perimeter P along the infinitesimal distance $\mathrm{d}s$ (see Figures 13.20 and 13.22). We may confidently assume that there is no friction with air at the free surface. From this, it follows that:

$$F_F = \tau_W P \,\mathrm{d}s \tag{13.38}$$

A check of the units signals that all is well since $\mathrm{N/m^2 \cdot m \cdot m}$ results in the unit of force N. Inserted into the momentum equation and equated with the downhill force, the result is:

$$\rho A g \sin\alpha \,\mathrm{d}s = \tau_W P \,\mathrm{d}s \tag{13.39}$$

With the hydraulic radius $R_{\mathrm{hy}} = \frac{A}{P}$ (see Figure 13.22[L]), τ_W may be written as:

$$\tau_W = \rho g R_{\mathrm{hy}} \sin\alpha \tag{13.40}$$

Since $\mathrm{d}z$ should be measured perpendicularly to $\mathrm{d}s$, we may use the small angle approximation $\sin\alpha = \tan\alpha = \frac{\mathrm{d}z}{\mathrm{d}s} = J_B$. This assumption, like the one for the pressure at the bottom, is justified[M]:

$$\tau_W = \rho g R_{\mathrm{hy}} J_B \tag{13.41}$$

When establishing a loss coefficient $\tau_W = \psi \cdot \frac{\rho}{2} v^2$, which is related to the dynamic pressure $\frac{\rho}{2} v^2$ for τ_W, it follows that:

$$R_{\mathrm{hy}} J_B = \frac{\psi v^2}{2g} \tag{13.42}$$

[L] The definition of the hydraulic radius does not lead to an ideal description of the cross-section values. For the circular cross-section, the flow area at depths $y \approx d$ increases far less than the wetted perimeter. From a purely mathematical point of view, this absurdly leads to a situation in which the cross-section at flow depths $y \geq 0.81d$ exhibits a higher capacity than when the pipe is completely full (see right-hand figure). Of course, this does not correspond to the behaviour under real conditions; therefore, it is generally calculated with the discharge at full pipe capacity starting with a filling level of $\frac{y}{d} \geq 0.81$.

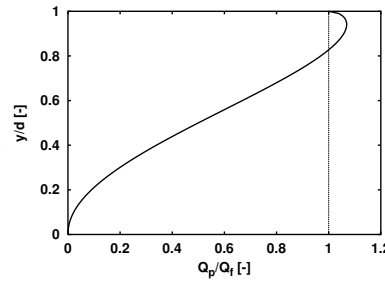

[M] Calculate the sine and the tangent for an angle of 10°. A difference of 1.5 % results.

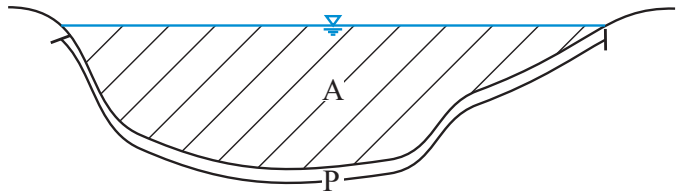

Figure 13.22: Flow area A and wetted perimeter P in an open channel.

Solved for the flow velocity in an open channel, the equation corresponds to the formula discovered by Brahms and published by Chézy [13]:

$$v = \sqrt{\frac{2g}{\psi}} \sqrt{R_{\mathrm{hy}} J_B} \tag{13.43}$$

Using the Darcy-Weisbach approach, where $\psi = \frac{f_{\mathrm{D}}}{4}$, ψ is replaced and the result is:

$$v = \sqrt{\frac{8g}{f_{\mathrm{D}}}} \sqrt{R_{\mathrm{hy}} J_B} \tag{13.44}$$

Hence, the friction coefficient may be determined with the semi-empirical Prandtl-Colebrook equations (see Equations 11.38, 11.39, 11.40 and 11.41). Equation 13.45, where log again represents the common logarithm, is mostly used in the context of questions with regard to sewers.

$$\frac{1}{\sqrt{f_{\mathrm{D}}}} = -2 \log \left(\frac{2.51}{\mathrm{Re} \sqrt{f_{\mathrm{D}}}} + \frac{k_s}{4 \cdot R_{\mathrm{hy}} \cdot 3.71} \right) \tag{13.45}$$

Under rough and highly turbulent conditions, which are usually predominant in open channels, the viscous term approaches zero so that f_{D} may be written explicitly:

$$\frac{1}{\sqrt{f_{\mathrm{D}}}} = -2 \log \left(\frac{k_s}{4 \cdot R_{\mathrm{hy}} \cdot 3.71} \right) \tag{13.46}$$

Inserting the logarithmic expression for $\frac{1}{\sqrt{f_{\mathrm{D}}}}$ into Equation 13.44, the velocity is expressed as:

$$v = -2 \sqrt{8 \cdot g \cdot R_{\mathrm{hy}} \cdot J_B} \cdot \log \left(\frac{k_s}{4 \cdot R_{\mathrm{hy}} \cdot 3.71} \right) = -2 \sqrt{8 \cdot g \cdot R_{\mathrm{hy}} \cdot J_B} \cdot \log \left(\frac{k_s}{14.84 \cdot R_{\mathrm{hy}}} \right) \tag{13.47}$$

However, because a number of scientists carried out experiments, another formula should dominate in open channel hydraulics. In generalised form, Equation 13.43 with the potencies α and β reads:

$$v = C \cdot R_{\mathrm{hy}}^{\alpha} J_B^{\beta} \tag{13.48}$$

Empirical investigations in rough pressure pipes resulted in $0.5 < \alpha < 0.75$ and $\beta = 0.5$. Then Gauckler set the values $\alpha = \frac{2}{3}$ and $\beta = \frac{1}{2}$ and limited the application range to open channels with gradients of $J_B > 7 \times 10^{-4}$. Manning suggested that the selected potencies

be assumed for all gradients, and Strickler formulated a relation between the constant C and the relevant grain diameter d_m:

$$C = \frac{K_0}{\sqrt[6]{d_m}} \tag{13.49}$$

Although Franke [13] states that $K_0 \approx 26\,\mathrm{m}^{\frac{1}{2}}/\mathrm{s}$ applies only for the range $\frac{k_s}{y} = 2 \times 10^{-3} - 3 \times 10^{-3}$, the ratio $\frac{26}{\sqrt[6]{d_m}}$ is used in a far wider roughness spectrum. In Anglo-Saxon and German-speaking regions, the Manning equation, which was derived from experiments with rough open channels, is frequently employed for the solution of one-dimensional issues. With the so-called Manning coefficient $n = \frac{\sqrt[6]{d_m}}{K_0}$[N], it reads:

$$v = \frac{1}{n}\sqrt{J_E}R_{\mathrm{hy}}^{\frac{2}{3}} \tag{13.50}$$

Thus, the normal conditions may be determined via the Manning equation (13.50) with $J_E = J_B$[O]. After inserting the continuity condition, it follows that

$$Q = \frac{1}{n}\sqrt{J_B}\frac{A_N^{\frac{5}{3}}}{P_N^{\frac{2}{3}}} \tag{13.51}$$

For a specified discharge, a certain flow depth results. This in turn leads to v_N, H_N and Fr_N in an open channel with n and J_B.

[N] In German-speaking regions, the equation is known as the Manning-Strickler equation with the roughness coefficient named after Albert Strickler. $k_{\mathrm{St}} = \frac{1}{n}$ and carries the unit $\mathrm{m}^{\frac{1}{3}}/\mathrm{s}$, in case you wonder why the author chose such weird numbers in some calculation examples.

[O] The attentive reader has noticed that the subscript of the gradient was modified from B to E. Actually, we should have written J_E from the very beginning. But for the sake of clarity between the quantity "bottom" or "bed" gradient and the identical gradients of energy grade line and water surface, it has been omitted under steady-state, uniform conditions. Chapter 13.10 explains why the Manning equation contains the gradient of the energy grade line J_E.

The provided open source library also contains a routine by means of which the normal conditions may be calculated in various shapes of open channels. The program `normalConditions.m` uses the file `dataOpenChannel.csv`, in which the input data are stored in SI units. The first two lines (`header=2`) include general details, which are not inputted. `cs` designates the shape of the cross-section in coding `1=circle` (partially filled with the diameter `d`), `2=trapezoid` (with the width of the bed `b` and the lateral gradient `m`, which for `m=0` corresponds to a rectangular cross-section) and `3=parabola` (with the parabolic parameter `a`). `eps` is the stop criterion for the iteration, `rho` the density, `JB` the bottom gradient, `g` the gravity constant and `Q` the discharge. With `ks=0` and `n` $\neq$ `0`, the program solves the Manning equation (13.50) and for `n=0` and `ks` $\neq$ `0` the Prandtl-Colebrook equation (13.45). The temperature-dependent viscosity is included in the latter equation, which is why `T` must be stated. In anticipation of Chapter 13.11, the distance between two computation nodes `dx` as well as the total distance between two open channel sections `L` are also included in the input file.

```
Geometric data for open channel hydraulics; standardised; [m]:
cs: 1=circle, 2=trapezoid, 3=parabola
eps=0.001
rho=1000
T=10
g=9.8065
n=.02
ks=0
JB=2e-2
cs=2
b=7
m=0
a=0
d=0
Q=30
dx=.5
L=200
```

13.10 Steady-state nonuniform flow

When thinking of an open channel, such as the natural course of a river, it is hardly conceivable that steady-state, uniform conditions could be found in any section. Under natural conditions, variations in cross-section and gradient as well as different degrees of roughness exist. The effects of such changes on the flow will be formally described in this section, although we will repeatedly return to the steady-state, uniform flow we just dealt with.

13.10.1 Differential equation of the water surface profile

We will use the balance of forces[P], i. e. the momentum equation in the s-direction (see Chapter 13.9). Figure 13.23 explains the generalised function for the nonuniform flow ($y_l \neq y_r$) versus that of Figure 13.20.

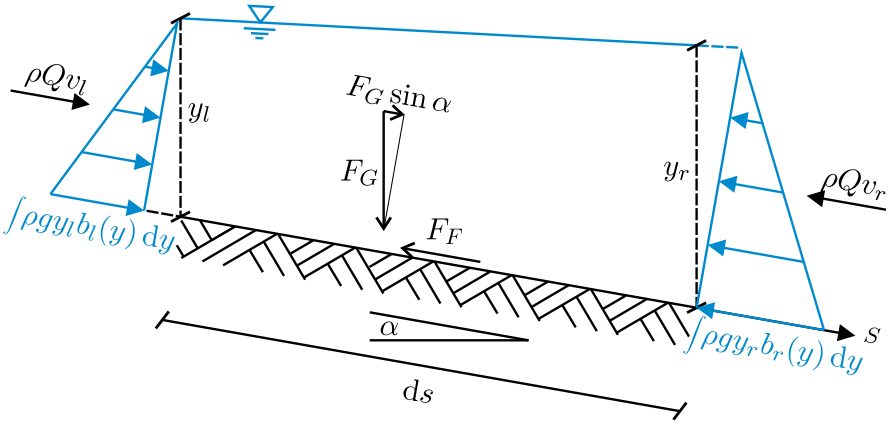

Figure 13.23: Balance of forces on a volume of water in an open channel section.

Due to the variable water level, the vertical (or rather normal to s) velocity component, is not zero. Nevertheless, we make this simplification because the influence is minimal, and it significantly facilitates the derivation of the differential equation of the water surface profile. Contrary to the result with steady-state, uniform flow, we obtain a convective acceleration that manifests as the change of the momentum flux in Figure 13.23. By multiplication with the density ρ and integration over the fluid volume with the mean cross-sectional area A and the layer thickness $\mathrm{d}s$, we obtain the force that must be applied to accelerate this volume accordingly. Here too, we can use the symbol for one-dimensional, regular differentiation d instead of that for partial differentiation ∂ while considering only one velocity component v for u_s.

$$\int \rho v \frac{\partial v}{\partial s}\,\mathrm{d}V = \rho v \frac{\mathrm{d}v}{\mathrm{d}s} A\,\mathrm{d}s \tag{13.52}$$

Next, we will deal with the pressure term $-\frac{1}{\rho}\frac{\partial p}{\partial s}$. The force due to pressure is again obtained by multiplication with the density and the integration over the control volume $\mathrm{d}V = A \cdot \mathrm{d}s$:

$$\int \rho \left(-\frac{1}{\rho}\frac{\partial p}{\partial s}\right)\mathrm{d}V = -\frac{\mathrm{d}p}{\mathrm{d}s} A\,\mathrm{d}s = -\rho g \frac{\mathrm{d}y}{\mathrm{d}s} A\,\mathrm{d}s \tag{13.53}$$

The change in pressure $\mathrm{d}p$ from the left to the right side of our infinitesimally small fluid volume with layer thickness $\mathrm{d}s$ becomes $\mathrm{d}p = \rho a_n (y_{nl} - y_{nr}) = \rho g \cdot \cos\alpha\,(y_{nl} - y_{nr})$, as already discussed in Chapter 13.9. With the assumption made therein that the flow depth may be measured vertically, it follows that $\mathrm{d}p = \rho g\,\mathrm{d}y$. The downhill and friction forces change insignificantly compared to those at the steady-state, uniform flow. In the

[P] Within this book, we deal with firm bed. Sediment transport is described splendidly by e. g. Zanke [64] for engineering applications.

calculation of the water mass, the flow area is included in the equation as mean area A and the wetted perimeter as mean wetted perimeter P.

$$F_G \cdot \sin\alpha = \int \rho a_s \, \mathrm{d}V = \rho A \, \mathrm{d}s \, g \sin\alpha = \rho A \, \mathrm{d}s \, g \frac{\mathrm{d}z}{\mathrm{d}s} \tag{13.54}$$

The friction force is again written in terms of the wall shear stress along the wetted area $P\,\mathrm{d}s$. F_F acts like the positive pressure gradient against the direction of flow; for this reason, the term representing F_F in Formula 13.56 is subtracted.

$$F_F = \tau_W P \, \mathrm{d}s \tag{13.55}$$

By substituting the derived relationships, Equation 13.56 follows:

$$\rho v A \, \mathrm{d}s \frac{\mathrm{d}v}{\mathrm{d}s} = -\rho g \frac{\mathrm{d}y}{\mathrm{d}s} A \, \mathrm{d}s - \tau_W P \, \mathrm{d}s + \rho g A \, \mathrm{d}s \frac{\mathrm{d}z}{\mathrm{d}s} \tag{13.56}$$

After dividing by $\rho g A \, \mathrm{d}s$, it may be written:

$$\frac{v}{g} \frac{\mathrm{d}v}{\mathrm{d}s} = -\frac{\mathrm{d}y}{\mathrm{d}s} + \frac{\mathrm{d}z}{\mathrm{d}s} - \frac{\tau_W P}{\rho g A} \tag{13.57}$$

In the next step, the velocity is drawn into the differential, which was already done in Chapter 5.7. We must be careful and divide by the new exponent as the differentiation factor of $\frac{\mathrm{d}v^2}{\mathrm{d}s}$ is 2 ($\frac{\mathrm{d}v}{\mathrm{d}s}$ yields 1).

$$\frac{1}{2g} \frac{\mathrm{d}v^2}{\mathrm{d}s} = -\frac{\mathrm{d}y}{\mathrm{d}s} + \frac{\mathrm{d}z}{\mathrm{d}s} - \frac{\tau_W P}{\rho g A} \tag{13.58}$$

Now the change in velocity height along the direction s is on the left side of the equals sign. The term $-\frac{\mathrm{d}y}{\mathrm{d}s}$ represents the change in water level, and $\frac{\mathrm{d}z}{\mathrm{d}s}$ may be written as the bottom gradient J_B. With $R_{\mathrm{hy}} = \frac{A}{P} = \frac{D}{4} = \frac{R}{2}$, the friction term corresponds to the gradient of the energy grade line in Equation 11.21.

Let's consider the energy diagram, or rather the energy equation, in Figure 13.24 with the marginal variations of energy $\mathrm{d}e$, velocity height $\mathrm{d}\left(\frac{v^2}{2g}\right)$ and flow depth $\mathrm{d}y$ along the infinitesimal layer thickness $\mathrm{d}s$ of our fluid volume.

The sum $\mathrm{d}z + y + \frac{v^2}{2g}$ is on the left side of the energy diagram and of our energy equation. On the right side we find y and $\frac{v^2}{2g}$ as well, with the difference that the changes relative to the conditions on the left are also listed. Compared to the conditions on the left, the flow depth y has changed by $\mathrm{d}y$ over the flow distance $\mathrm{d}s$. This coincides with the change of the velocity height $\frac{\mathrm{d}v^2}{2g}$. Moreover, the head loss $\mathrm{d}e$ is indicated on the right. The equation that reflects Figure 13.24 agrees with the result found with the balance of forces. Note that $\frac{\mathrm{d}v^2}{2g}$ is negative in the case shown in Figure 13.24.

Equation 13.59

$$\mathrm{d}z + y_l + \frac{v_l^2}{2g} = y_r + \frac{v_r^2}{2g} + \mathrm{d}e \tag{13.59}$$

becomes:

$$\mathrm{d}z = \mathrm{d}y + \frac{\mathrm{d}v^2}{2g} + \mathrm{d}e \tag{13.60}$$

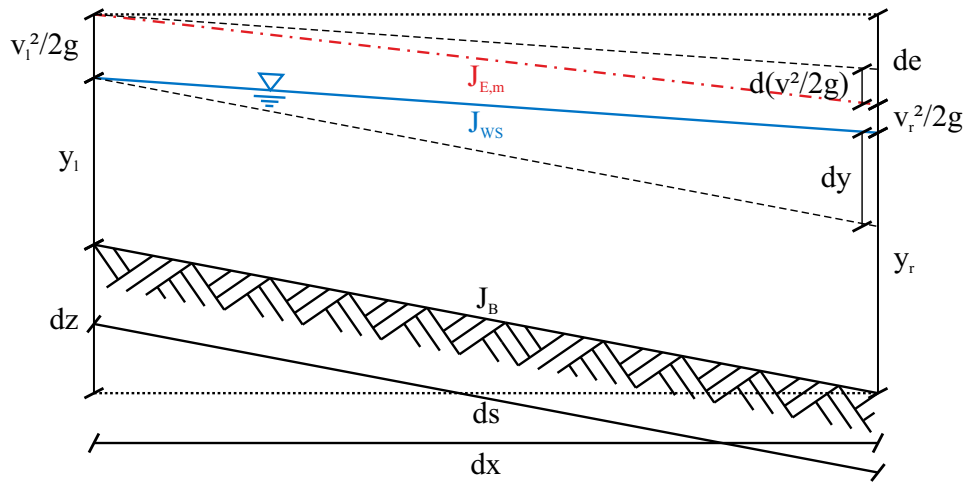

Figure 13.24: Energy diagram of a nonuniform flow in an open channel.

Dividing by ds, we obtain:

$$\frac{\mathrm{d}z}{\mathrm{d}s} = \frac{\mathrm{d}y}{\mathrm{d}s} + \frac{1}{2g}\frac{\mathrm{d}v^2}{\mathrm{d}s} + \frac{\mathrm{d}e}{\mathrm{d}s} \tag{13.61}$$

With $\frac{\mathrm{d}e}{\mathrm{d}s} = \frac{\tau_W P}{\rho g A}$, this is exactly the relationship found for the gradient of the energy grade line J_E in the balance of forces (see Equation 11.21). Rearranging Formula 13.61 and using the small angle approximation $\mathrm{d}x \approx \mathrm{d}s$ we obtain:

$$\frac{\mathrm{d}y}{\mathrm{d}x} = J_B - J_E - \frac{1}{2g}\frac{\mathrm{d}v^2}{\mathrm{d}x} \tag{13.62}$$

A clever technique enables a further simplification. We insert $v^2 = \frac{Q^2}{A^2}$ in the above equation and derive the term of the velocity height with respect to y. This results in an expression similar to that in Equation 13.11, and we write again for $\frac{\mathrm{d}A}{\mathrm{d}y} = b_{\mathrm{WS}}$: $\frac{1}{2g}\frac{\mathrm{d}}{\mathrm{d}x\mathrm{d}y}\left(\frac{Q^2}{A^2}\right) = -\frac{Q^2 b_{\mathrm{WS}}}{gA^3}\frac{1}{\mathrm{d}x}$[Q]. We shift d$y$ to the other side of the equation so that the expression becomes $\frac{1}{2g}\frac{\mathrm{d}}{\mathrm{d}x}\left(\frac{Q^2}{A^2}\right) = -\frac{Q^2 b_{\mathrm{WS}}}{gA^3}\frac{\mathrm{d}y}{\mathrm{d}x}$, which in turn may be transferred into the last intermediate step:

$$\frac{\mathrm{d}y}{\mathrm{d}x} = J_B - J_E + \frac{Q^2 b_{\mathrm{WS}}}{gA^3}\frac{\mathrm{d}y}{\mathrm{d}x} \tag{13.63}$$

After rearranging and pulling out $\frac{\mathrm{d}y}{\mathrm{d}x}$ as a common factor, the equation reads:

$$\frac{\mathrm{d}y}{\mathrm{d}x}\left(1 - \frac{Q^2 b_{\mathrm{WS}}}{gA^3}\right) = J_B - J_E \tag{13.64}$$

[Q] $\frac{\mathrm{d}}{\mathrm{d}y}\left(\frac{1}{A^2}\right) = -2 \cdot \frac{1}{A^3}\frac{\mathrm{d}A}{\mathrm{d}y} = -2 \cdot \frac{b_{\mathrm{WS}}}{A^3}$

With the Froude number $\mathrm{Fr} = \frac{v}{\sqrt{g\frac{A}{b_{\mathrm{WS}}}}}$, or the square of the Froude number $\mathrm{Fr}^2 = \left(\frac{v}{\sqrt{g\frac{A}{b_{\mathrm{WS}}}}}\right)^2 = \frac{v^2}{g\frac{A}{b_{\mathrm{WS}}}} = \frac{v^2 b_{\mathrm{WS}}}{gA} = \frac{Q^2 b_{\mathrm{WS}}}{gA^3}$, we finally arrive at the differential equation of the water surface profile:

$$\frac{\mathrm{d}y}{\mathrm{d}x} = \frac{J_B - J_E}{1 - \mathrm{Fr}^2} \tag{13.65}$$

Example

Differential equation of the water surface profile

The differential equation of the water surface profile will now be explained by means of two examples. J_B is negative in both examples. In case ①, subcritical flow takes place; in case ②, the flow is supercritical. This leads to the following discussion:

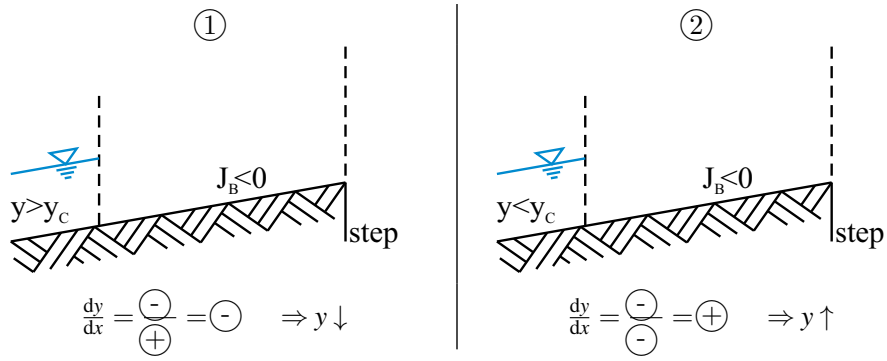

The numerator in case ① is negative because a positive number (J_E) is subtracted from a negative number (J_B). The Froude number in subcritical flow is smaller than one so that its square is also smaller than one. In this case, the denominator is positive; thus, the fraction becomes negative. This means that the flow depth in this situation must drop.

For the conditions on the right in case ②, the numerator does not change relative to case ①. However, supercritical flow is in effect here, which leads to $\mathrm{Fr} > 1$ and therefore $\mathrm{Fr}^2 > 1$. With the negative denominator, the fraction becomes positive; the flow depth rises in the flow direction (relative to the bottom).

From the differential equation of the water surface profile, it may also be concluded that the flow depth in the case of supercritical flow can decrease if the gradient of the energy grade line is smaller than the bottom gradient. With a negative denominator ($\mathrm{Fr}^2 > 1$), the fraction becomes negative only if the numerator is positive, i. e. $J_B > J_E$.

According to the differential equation of the water surface profile, the reduction in energy in subcritical flow goes along with negative $\frac{\mathrm{d}y}{\mathrm{d}x}$. For subcritical conditions, the denominator is positive; therefore, energy is reduced if $J_E > J_B$, i. e. the numerator is negative.

13.10.2 Water surface profiles

Water surface profiles are of general interest in river hydraulics. How far does backwater from a dam reach? Does water overflow in a flood event? In this chapter, we will find answers to these questions.
In Chapter 13.3, the behaviour of free surface flows with respect to the composition of the specific energy was considered. Since the Bernoulli equation (5.41) is based on the Euler equation (5.24), energy losses must be included in yet another equation. Because water may be discharged at one specific energy with two different flow depths (in subcritical and in supercritical flow), the implementation of a loss term in open channel hydraulics is not as easy as in pipe flow. The gradient of the energy grade line was introduced with the Manning equation (13.50) for open channels. The Darcy-Weisbach approach with the friction coefficient as described by the Prandtl-Colebrook equation (13.45) also contains the gradient of the energy grade line as a function of roughness and the cross-section quantities.
In this chapter, we consider water surface profiles by checking whether the two equations (friction and Bernoulli equation) can be brought into alignment.

Table 13.1: Water surface profiles – Bernoulli vs. Manning equation.

Bernoulli	Chézy or Manning	
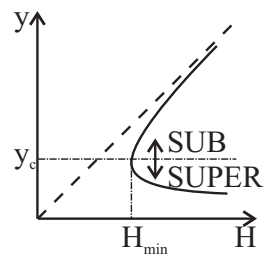		$y > y_N \rightarrow$ energy increase
		$y < y_N \rightarrow$ energy decrease

13.10.2.1 Transition subcritical – subcritical

First we assume that the normal conditions are known from the steady-state, uniform flow (see Figure 13.25). On the left side of the figure, the normal depth y_N is plotted above y_c. Subcritical flow is taking place. The centre section is marked as "smooth". According to Equations 13.50 and 13.45, a smoother boundary means a higher flow velocity. And according to the continuity condition (5.2), a higher flow velocity leads to a lower flow depth. This is marked as such in Figure 13.25 because the normal flow depth in the smooth section lies below that of the rough section but still within subcritical conditions.
At the figure's right edge, the initial conditions are once again assumed. But where do the transitions occur? The "eye" icon in each of the boxes below indicates the region that we investigate. The transition is to take place there.

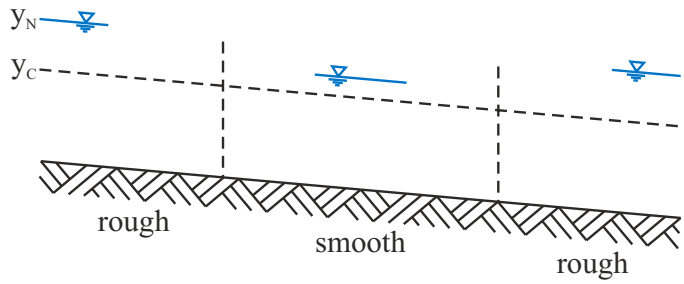

Figure 13.25: Example for the transition from sub- to subcritical flow.

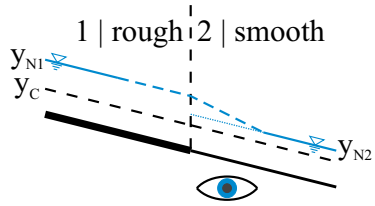	Bernoulli	$y_{\text{SUB}} \downarrow \Rightarrow H_{\text{SUB}} \downarrow$	
	Manning	$y > y_N \Rightarrow H \uparrow$	

First we consult the $H-y$ diagram in Table 13.1. We are in **subcritical** flow, i. e. on the upper branch of the specific energy vs. flow depth diagram. At a certain specific energy, we find the associated flow depth and follow the $H-y$ relation in the direction of the **decreasing** flow depth; we see that the **specific energy decreases**. This is exactly what the interrelation $y_{\text{SUB}} \downarrow \Rightarrow H_{\text{SUB}} \downarrow$ in the above table is supposed to reflect.
We now turn to the flow formulas. In the region of interest (represented by the eye), prevailing conditions permit the normal flow depth, as plotted. The flow depth in this section drops to just this water level and is therefore **above** $y_{N,\text{smooth}}$. If the flow depth is greater than y_N, then the water flows **more slowly** than normal conditions allow due to the greater cross-section at this location. At lower velocities, less energy is consumed. This is a fact known by anyone who rides a bicycle or drives a car. Thus, it follows from the flow formula that the specific energy increases.

Let's discuss the Manning equation $v = \frac{1}{n}\sqrt{J_E}R_{\text{hy}}^{\frac{2}{3}}$. The Manning coefficient n is constant in this section of the flow. With increasing y, R_{hy} increases as well[R]. If v is smaller than v_N because of the greater cross-section, then $J_E < J_B$ must also be true. Thus, energy – relative to the bottom – is built up. Since the statements resulting from the two equations are contradictory, the transition at this location is not possible.
The differential equation of the water surface profile yields the same statement[S].

$y \overset{!}{=} \downarrow$	$\frac{\mathrm{d}y}{\mathrm{d}x} = \frac{J_B - J_E}{1-\text{Fr}^2}$	$y > y_N \Rightarrow J_E < J_B \Rightarrow \frac{+}{1}$ $\text{SUB} \Rightarrow \frac{1}{+}$	$\frac{\mathrm{d}y}{\mathrm{d}x} = \frac{+}{+} \Rightarrow y \uparrow$	

[R] This applies to all cross-sections because the area increases with the flow depth faster than the wetted perimeter. The exception is the upper region of the circular cross-section (see Chapter 13.9).
[S] The author's opinion after many years of teaching experience is that the Bernoulli–Manning discussion is more descriptive than the differential equation of the water surface profile. However, the statements are identical. You may opt for either method.

The left column in the above table shows what should happen: the flow depth must decrease. For this region, $y > y_N$; this corresponds to $J_E < J_B$. Therefore, a positive numerator results. In subcritical flow, Fr < 1 and consequently $\mathrm{Fr}^2 < 1$; the denominator is positive as well. The change of the flow depth in the flow direction is positive, and according to the differential equation of the water surface profile, y must increase. The course is not possible.
We now look at a potential transition in the rough section, as symbolised by the eye icon.

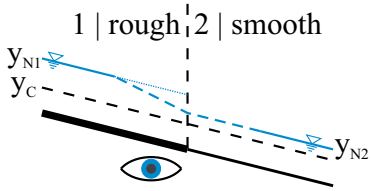	Bernoulli	$y_{SUB} \downarrow \Rightarrow H_{SUB} \downarrow$	
	Manning	$y < y_N \Rightarrow H \downarrow$	

We start again with the Bernoulli equation, which states that for this region in subcritical flow, the falling water level corresponds to a decreasing specific energy. Follow the $H - y$ curve on the upper branch along the falling water level.
In the region under observation, the water level drops below the normal flow depth of this section. This means that the water flows faster at this location than the friction, cross-section and bed gradient conditions stipulate. The flow equations also lead to an energy reduction ($y < y_N \Rightarrow H \downarrow$). Back to our mental experiment with the cycling tour: we mount the bicycle and roll downhill until the balance of downward and friction forces is established and the velocity no longer varies. If we want to accelerate ($v > v_N$), we must pedal. We burn calories, i. e. we expend additional energy.
The differential equation of the water surface profile also confirms the transition at this location:

$y \overset{!}{=} \downarrow$	$\frac{dy}{dx} = \frac{J_B - J_E}{1 - \mathrm{Fr}^2}$	$y < y_N \Rightarrow J_E > J_B \Rightarrow \frac{-}{1}$ SUB $\Rightarrow \frac{1}{+}$	$\frac{dy}{dx} = \frac{-}{+} \Rightarrow y \downarrow$	

In this case, the two equations are brought into line with each other and the **transition** occurs under **subcritical** flow conditions in the **upstream** section. The change occurs in such a manner that the normal conditions of the downstream section are in effect exactly at the boundary.

> We will refer repeatedly to this same fundamental discussion on the following pages as we successively derive various water surface profiles. This principle must be adhered to in each question and the Bernoulli vs. Manning discussion held until a consistent solution is found. And because this method is of essence in open channel hydraulics, we must practice it over and over again in the following discussion.

We will now examine the transition during the downstream change from smooth to rough conditions.

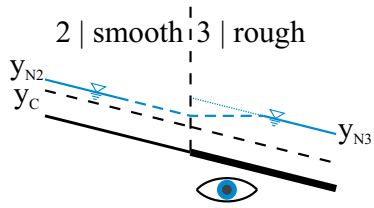	Bernoulli	$y_{SUB} \uparrow \Rightarrow H_{SUB} \uparrow$	↯
	Manning	$y < y_N \Rightarrow H \downarrow$	

With increasing flow depth in subcritical flow, the energy grade line is also increasing as can be seen from the $H - y$ diagram in Table 13.1. In the rough section, a greater normal flow depth is found; consequently, the flow depth in the transition region is smaller. But according to the continuity condition, a smaller flow depth also means that the velocity is higher than at normal conditions. Higher velocities lead to higher energy losses so that the specific energy decreases. Bernoulli and Manning do not reach a consensus.
The same result is obtained via the differential equation of the water surface profile:

$y \overset{!}{=} \uparrow$	$\frac{dy}{dx} = \frac{J_B - J_E}{1 - Fr^2}$	$y < y_N \Rightarrow J_E > J_B \Rightarrow \frac{-}{1}$ SUB $\Rightarrow \frac{1}{+}$	$\frac{dy}{dx} = \frac{-}{+} \Rightarrow y \downarrow$	↯

Therefore, we look at the transition in the section where smooth conditions are to be found:

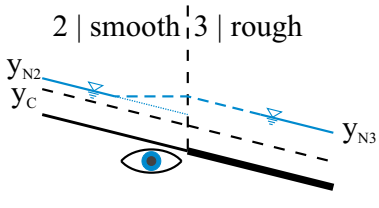	Bernoulli	$y_{SUB} \uparrow \Rightarrow H_{SUB} \uparrow$	☺
	Manning	$y > y_N \Rightarrow H \uparrow$	

With increasing flow depth in subcritical flow, the specific energy is also increasing. In this region, the flow depth is greater than the normal flow depth that is related to low roughness. The increasing area leads to lower velocities and thus to an energy buildup. Both equations state energy buildup; in subcritical flow, the transition will occur in the upstream section (see Figure 13.26). The normal flow depth of the downstream section must exist at the boundary between the different sections.
The discussion about the differential equation of the water surface profile yields the same result:

$y \overset{!}{=} \uparrow$	$\frac{dy}{dx} = \frac{J_B - J_E}{1 - Fr^2}$	$y > y_N \Rightarrow J_E < J_B \Rightarrow \frac{+}{1}$ SUB $\Rightarrow \frac{1}{+}$	$\frac{dy}{dx} = \frac{+}{+} \Rightarrow y \uparrow$	☺

Hence, we may sketch the water surface profile for the transition from sub- to subcritical flow and back in Figure 13.26.

Impacts of changes/disturbances are found upstream in subcritical flow.

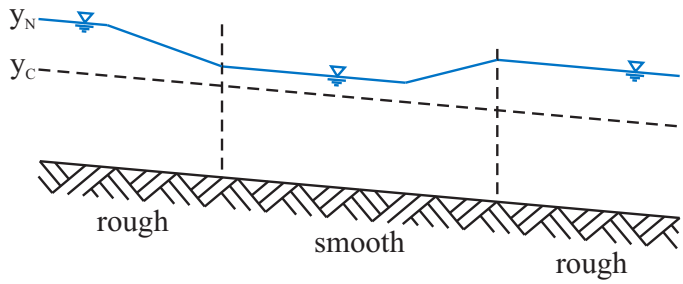

Figure 13.26: Transition from sub- to subcritical flow.

13.10.2.2 Transition supercritical – supercritical

We venture a role play in which we alternately assume the personalities of Daniel Bernoulli and Robert Manning. In the following example, the transitions between two flow sections, which are characterised by normal conditions in supercritical flow, are considered (see Figure 13.27). The normal flow depth is plotted once again in the sketch; y_N lies below y_c, which means that the discharge is in supercritical flow.

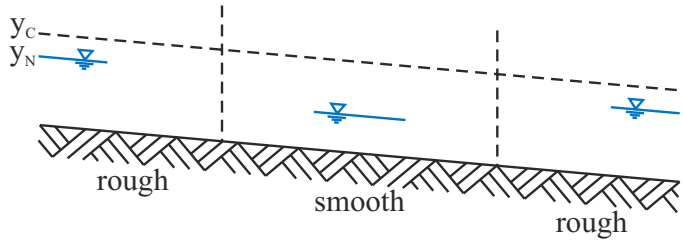

Figure 13.27: Example for the transition from super- to supercritical flow.

We begin our investigation into the transition taking place in the smooth section.

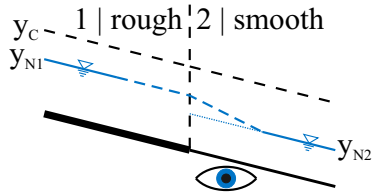	Bernoulli	$y_{\mathrm{SUPER}} \downarrow \Rightarrow$ $H_{\mathrm{SUPER}} \uparrow$	☺
	Manning	$y > y_N \Rightarrow H \uparrow$	

Daniel Bernoulli: Ladies and gentlemen, in supercritical flow we are on the lower branch of my $H - y$ relation for a constant discharge per unit metre $q = \text{const}$. When the flow depth in supercritical flow decreases, the velocity height increases faster than the flow depth decreases. From y_c onwards the specific energy increases continuously in supercritical at decreasing flow depth. $y_{\mathrm{SUPER}} \downarrow$ leads to $H_{\mathrm{SUPER}} \uparrow$! Manning: Thank you very much for your statements, Mister Bernoulli. From my point of view, I have the following to add. If the flow depth in the smooth section drops to the normal flow depth, then logically it is even greater than y_N in the transition region. According to the continuity condition,

$y > y_N$ means that $v < v_N$, which in accordance with my equation leads to an increase in specific energy. As is known, slower movements consume less energy than fast movements! Mister Bernoulli, we agree. The transition occurs in the downstream section.
Bernoulli: Of course, Mister Manning. But to be absolutely sure, we **must** check whether or not we can find another consensus in the other section.

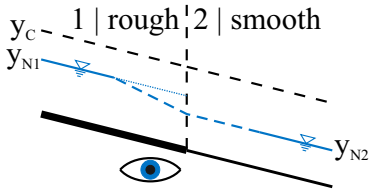	Bernoulli	$y_{SUPER} \downarrow \Rightarrow$ $H_{SUPER} \uparrow$	
	Manning	$y < y_N \Rightarrow H \downarrow$	

Bernoulli: Well, I insist. According to the equation named after me, the specific energy increases - even in the rough section - if the flow depth decreases in supercritical flow: $y_{SUPER} \downarrow \Rightarrow H_{SUPER} \uparrow$
Manning: Okay, let's enter into a scientific argumentation. When the flow depth drops in the rough section, it is lower than the existing normal flow depth there. This means that the water flows faster than during normal conditions. According to my equation, when $y < y_N$, energy is reduced. Mister Bernoulli, there won't be a deal. The transition actually takes place in the downstream section.
Bernoulli: This dispute gives me great pleasure. Let us examine how the transition takes place when it becomes rough again in supercritical flow. Once again, we begin our investigation in the downstream rough section.

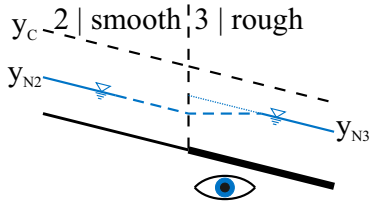	Bernoulli	$y_{SUPER} \uparrow \Rightarrow$ $H_{SUPER} \downarrow$	
	Manning	$y < y_N \Rightarrow H \downarrow$	

Bernoulli: Since we are in supercritical flow, the specific energy decreases with increasing flow depth. You see that when you move onto the lower branch of my $H - y$ relation in the direction that promises a greater flow depth. In the diagram in Table 13.1, you move only upwards on the lower branch as long as you also move to the left. I stress that point: $y_{SUPER} \uparrow \Rightarrow H_{SUPER} \downarrow$
Manning: Mister Bernoulli, indeed, I am able to follow your line of reasoning. But let me explain my standpoint. At the place of interest, we are in a region where the flow depth is lower than the normal flow depth ($y < y_N$). This means that $v > v_N$; hence, it follows that energy is reduced. Mister Bernoulli, I fully agree. The transition takes place in the downstream section. But for the sake of propriety, we should check whether a transition could not also take place in the smooth section.

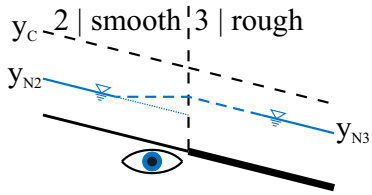	Bernoulli	$y_{\text{SUPER}} \uparrow \Rightarrow$ $H_{\text{SUPER}} \downarrow$	
	Manning	$y > y_N \Rightarrow H \uparrow$	

Bernoulli: Well, my point of view has not changed since the flow depth will increase in supercritical flow, which agrees with a decreasing specific energy: $y_{\text{SUPER}} \uparrow \Rightarrow H_{\text{SUPER}} \downarrow$
Manning: Stop! This won't work! If the flow depth already increased in the smooth section, it would be above y_N in the transition region. The flow would be slower than normal conditions allow and consequently the specific energy would increase. In this controversy, Mister Bernoulli, we won't find agreement.
The transition from super- to supercritical flow is shown in Figure 13.28.

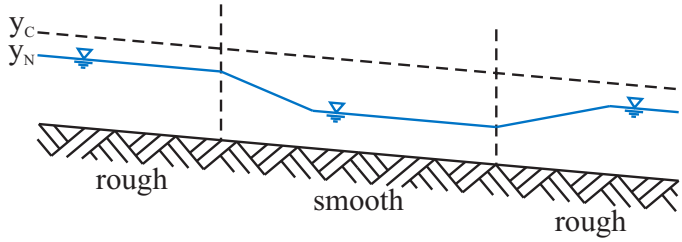

Figure 13.28: Transition from super- to supercritical flow.

Impacts of changes/disturbances are found downstream in supercritical flow.

13.10.2.3 Transition subcritical – supercritical

We now consider the transition between sub- and supercritical flow, by means of the differential equation of the water surface profile (13.65) before we work with a detailed example later. We write it down again: $\frac{\mathrm{d}y}{\mathrm{d}x} = \frac{J_B - J_E}{1 - \mathrm{Fr}^2}$
We agree that the flow depth must decrease from subcritical to supercritical flow. According to the Bernoulli equation, the specific energy also decreases in subcritical flow. The flow velocity increases, which results in a higher energy loss, i. e. $J_E > J_B$. In the differential equation of the water surface profile, the numerator is negative for this case. We turn to the denominator. Since the Froude number for conditions in subcritical flow is less than one, a positive denominator results. Consequently, the gradient of the water surface $\frac{\mathrm{d}y}{\mathrm{d}x}$ is actually negative; the water surface drops. So far so good. The flow depth cannot drop below y_c in the upstream section as the numerator is still negative, but since $\mathrm{Fr} > 1$, the denominator becomes negative, too (and therefore $\frac{\mathrm{d}y}{\mathrm{d}x}$ positive). Let's have a look at the section where supercritical flow takes place. Based on the same consideration, the differential equation of the water surface profile acquires a negative denominator. If the flow depth drops here from y_c to y_N, $v > v_N$ and therefore $J_E < J_B$. The numerator

becomes positive, and with the negative denominator we obtain a negative value for $\frac{dy}{dx}$; i. e. a decreasing flow depth.
It is obvious that we encounter a serious problem for the transition when the value of Fr approaches one since in this case the value of the denominator approaches zero. This may be investigated by means of the limit of $\frac{dy}{dx}$:

$$\text{SUB: } \lim_{Fr \to 1} \frac{dy}{dx} = -\infty \tag{13.66}$$

Consequently, the water level drops vertically at the transition from sub- to supercritical flow. In fact, the pressure conditions stabilize such that there is a continuous transition between sub- and supercritical flow. We have seen this already in Figure 13.7.

The transition between subcritical and supercritical flow is continuous; the critical conditions are passed through at the border between the sections.

13.10.2.4 Transition supercritical – subcritical: hydraulic jump

We will also analyse the transition between super- and subcritical flow, first by means of the differential equation of the water surface profile.
The flow depth must increase from super- to subcritical flow. With the limit for the Froude number approaching one in supercritical flow, the gradient of the flow depth becomes:

$$\text{SUPER: } \lim_{Fr \to 1} \frac{dy}{dx} = \infty \tag{13.67}$$

According to Equation 13.65, the water surface increases vertically at the transition between supercritical and subcritical flow. However, this wall facing opposite the flow direction falls over and a so-called hydraulic jump occurs.
With the knowledge that we have already acquired, we may even be able to interpret this phenomenon since disturbances may develop in subcritical flow upstream and in supercritical flow downstream (see Figure 13.1). A disturbance that travels upstream cannot progress beyond the hydraulic jump.

The transition between supercritical and subcritical flow occurs as a hydraulic jump.

The jet, i. e. the discharge in supercritical flow, submerges into the subcritical region near the bottom. This causes mixing and a deceleration of the jet. The water at the surface flows upstream against the flow direction; this is referred to as a recirculation zone. Such a hydraulic jump is extremely dangerous for terrestrial creatures. First, there is no escape because of recirculation and second, the water density is rather low because of the mixture with air such that one's buoyancy is poor. There is only one way out if you happen to get caught in a hydraulic jump: dive down and let yourself be carried by the jet near the wall behind the hydraulic jump.
As is shown in the photo (Figure 13.29), the flow in such a hydraulic jump is highly turbulent. The intrusion of air is mainly responsible for the dissipation of great quantities of energy in the form of sound and primarily heat, which is why the flow depths upstream and downstream from the hydraulic jump are not corresponding in terms of the Bernoulli

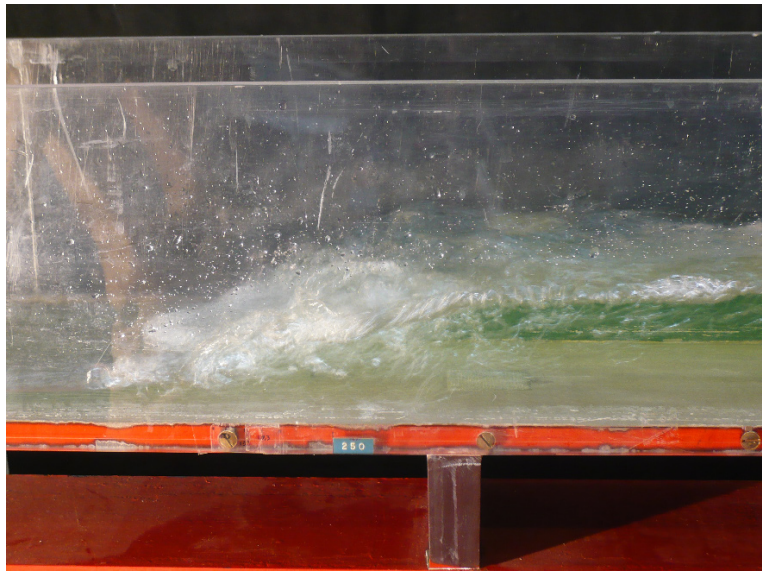

Figure 13.29: Hydraulic jump in the laboratory flume.

equation. Moreover, the dissipated energy quantity cannot be estimated a priori via an empirical equation. We are fortunate that we can resort to the law of momentum[T]!
We sketch a fluid volume in a free body diagram and plot the forces acting in the x-direction.

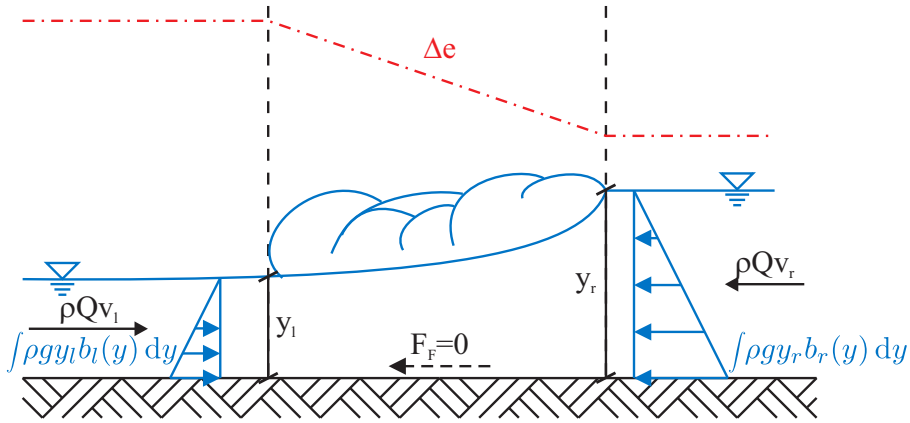

Figure 13.30: Sketch of a hydraulic jump.

The flow depths on the right and on the left of the hydraulic jump are also referred to as conjugated flow depths. For **conjugated** flow depths, the **sum of the pressure force and the momentum flux** on the left and right side of our control volume are identical. Flow depths at identical **specific energy** are referred to as **corresponding**.

[T] We remember the Prandtl quotation in Chapter 5.8 that is tailored to the hydraulic jump.

The law of momentum for an open channel flow, with the assumption already made in Chapter 13.9 regarding the small angle approximation for the forces in the x-direction, generally reads:

$$\int p_l \, \mathrm{d}A_l + \rho Q v_l = \int p_r \, \mathrm{d}A_r + \rho Q v_r \tag{13.68}$$

Therein, the friction at the bottom (the external reaction force) is neglected (see Figure 13.30). With a few mathematical techniques, this generally applicable formula may be converted to an explicitly solvable equation if it is set up for a rectangular open channel without a step. The written-out terms read as follows:

$$\frac{1}{2}\rho g y_l^2 b + \rho Q v_l = \frac{1}{2}\rho g y_r^2 b + \rho Q v_r \tag{13.69}$$

In the first step, we introduce the discharge per unit width q because we are in a rectangular open channel; we divide by the open channel width b. We also want to divide by ρg.

$$\frac{1}{2}y_l^2 + \frac{q v_l}{g} = \frac{1}{2}y_r^2 + \frac{q v_r}{g} \tag{13.70}$$

When we place the pressure forces on one side and the rate of change of momentum (or the momentum fluxes) on the other side, then the equation reads:

$$\frac{y_l^2 - y_r^2}{2} = \frac{q}{g}(v_r - v_l) \tag{13.71}$$

Using the continuity condition $v_l y_l = v_r y_r$, we solve for v_r and insert it into Equation 13.71 as follows:

$$\frac{y_l^2 - y_r^2}{2} = \frac{q}{g}\left(\frac{v_l y_l}{y_r} - v_l\right) = \frac{q}{g} v_l \left(\frac{y_l}{y_r} - 1\right) \tag{13.72}$$

We factor the left side as $(y_l + y_r)(y_l - y_r)$ and multiply the -1 in the bracketed term on the right by $\frac{y_r}{y_r}$ to obtain a common denominator.

$$\frac{1}{2}(y_l + y_r)(y_l - y_r) = \frac{q}{g} v_l \left(\frac{y_l - y_r}{y_r}\right) \tag{13.73}$$

In the next simplification step, we divide the equation by $\frac{1}{2}\left(\frac{y_l - y_r}{y_r}\right)$:

$$(y_l + y_r) y_r = 2\frac{q}{g} v_l \tag{13.74}$$

When substituting $v_l y_l$ for q and dividing by y_l^2, the major conversions will have been accomplished:

$$\frac{y_r^2}{y_l^2} + \frac{y_r}{y_l} = 2\frac{v_l^2}{g y_l} \tag{13.75}$$

The expression on the right side is equivalent to twice the square of the Froude number that we see on the left side of the hydraulic jump $\mathrm{Fr}_l = \frac{v_l}{\sqrt{g y_l}}$ (see Equation 13.1). We now make the substitution, rearrange terms, set one side of the equation to zero, and obtain:

$$\frac{y_r^2}{y_l^2} + \frac{y_r}{y_l} - 2 \cdot \mathrm{Fr}_l^2 = 0 \tag{13.76}$$

And now the ultimate sleight of hand! Equation 13.76 is a regular quadratic equation when x is substituted for the fraction $\frac{y_r}{y_l}$. Thus, we may write:

$$x^2 + x - 2 \cdot \mathrm{Fr}_l^2 = 0 \quad \text{where } x = \frac{y_r}{y_l} \tag{13.77}$$

Since the standard solution for the quadratic equation (see e. g. [8, p. 64]) $ax^2 + bx + c = 0$ is

$$x_{1,2} = \frac{-b \pm \sqrt{b^2 - 4ac}}{2a} \tag{13.78}$$

then for Equation 13.77:

$$x_{1,2} = \frac{-1 \pm \sqrt{1^2 - 4 \cdot 1 \cdot \left(-2 \cdot \mathrm{Fr}_l^2\right)}}{2 \cdot 1} = \frac{-1 \pm \sqrt{1 + 8 \cdot \mathrm{Fr}_l^2}}{2} \tag{13.79}$$

Upon substituting for the constants a, b and c in Equation 13.79, one immediately notices that the solution in which the root is subtracted is non-physical since there are no negative flow depths. We therefore write

$$\frac{y_r}{y_l} = \frac{-1 + \sqrt{1 + 8 \cdot \mathrm{Fr}_l^2}}{2} \tag{13.80}$$

and ultimately:

$$\begin{aligned} y_{r,\mathrm{HJ}} &= \frac{y_{l,\mathrm{HJ}}}{2} \left(\sqrt{1 + 8 \cdot \mathrm{Fr}_{l,\mathrm{HJ}}^2} - 1 \right) \\ y_{l,\mathrm{HJ}} &= \frac{y_{r,\mathrm{HJ}}}{2} \left(\sqrt{1 + 8 \cdot \mathrm{Fr}_{r,\mathrm{HJ}}^2} - 1 \right) \end{aligned} \tag{13.81}$$

Since formally no differences were made between the left and right sides, the same derivation may also be executed for the flow depth on the left side. Actually, only the indices are interchanged.

In the application of Equation 13.81, it is essential to ensure that the preconditions under which this equation was derived are met. When setting the pressure forces, we assumed a continuous bed[a]. The equation was derived for rectangular open channels. The friction force at the bottom was neglected, which is generally acceptable in spite of the high velocity of the jet because of the short development length.

[a] Figure 13.36 describes an approach for which no continuous bottom exists; for example, in a stilling basin.

Types of hydraulic jumps

There are different types of hydraulic jumps that are characterised by the Froude number just upstream from the jump. In the range of $\mathrm{Fr} \approx 1.7 - 2.5$ a week jump occurs, at $\mathrm{Fr} \approx 2.5 - 4.5$ it is called oscillating jump whereas only above $\mathrm{Fr} \approx 4.5$ a stable, well balanced hydraulic jump develops. The hydraulic jump is characterised by white water; the jet possesses so much energy that it submerges below the jump roller.
If the Froude number of the supercritical flow directly upstream from the hydraulic jump is smaller than 1.7, then the energy of the supercritical flow is insufficient for the jet to submerge below the jump roller. The jet is deflected upwards; this form is characterised by undulating waves.

Length of a hydraulic jump

For the length of a hydraulic jump, Franke [13] states the following relationship:

$$L_{\mathrm{HJ}} = y_{l,\mathrm{HJ}} \cdot 8.5 \left(\mathrm{Fr}_{l,\mathrm{HJ}} - 1.7\right) \quad \text{for } \mathrm{Fr} > 1.7 \tag{13.82}$$

Therein, the end of the hydraulic jump is assumed to be the cross-section where any backflow may no longer be detected at the surface.

Experiment

Hydraulic jump

We return to Figure 13.29 to look at the conditions at the hydraulic jump in an experiment. A discharge of 5.0 L/s was set in the 0.20 m-wide open channel. The flow depth directly upstream from the hydraulic jump was determined to be $y_{l,\mathrm{HJ}} = 0.018\,\mathrm{m}$, which leads to $\mathrm{Fr}_l = \frac{Q}{b \cdot y_l} \frac{1}{\sqrt{g \cdot y_{l,\mathrm{HJ}}}} = \frac{5.0 \times 10^{-3}}{0.20 \cdot 0.018} \frac{1}{\sqrt{9.81 \cdot 0.018}} = 3.305$. Equation 13.81 yields $y_{r,\mathrm{HJ}} = \frac{y_{l,\mathrm{HJ}}}{2}\left(\sqrt{1 + 8 \cdot \mathrm{Fr}_{l,\mathrm{HJ}}^2} - 1\right) = \frac{0.018}{2}\left(\sqrt{1 + 8 \cdot 3.305^2} - 1\right) = 0.0756\,\mathrm{m}$ for the conjugated flow depth in subcritical flow. By the way, the measured flow depth was 0.075 m. The interested reader may measure the water surfaces up- and downstream from the hydraulic jump from Figure 13.29 in order to check the result by means of their ratio.

13.10.2.5 Water surface profiles at the hydraulic jump

In the discussion about the water surface profiles in Chapter 13.10.2.4, we found out, why hydraulic jumps develop. The central question remains: where does this phenomenon occur? And with the highly variable normal conditions up- and downstream from the jump, it is understandable that the conjugated flow depths, which are rigidly connected via the law of momentum or via Equation 13.81, need not correspond exactly to those normal conditions. Consequently, there will be transition regions upstream or downstream from the hydraulic jump. Therefore, we distinguish between two cases: is the specific

energy of the normal conditions in supercritical greater or smaller compared to the one in subcritical flow?

In the case that the flow conditions in subcritical require more energy than those in supercritical flow, energy must be built up along a flow distance relative to the bottom. This is only feasible in subcritical flow where the velocity is low; according to Manning, energy can be built up only when $y > y_N$. Then the flow depth upstream from the hydraulic jump is the normal flow depth of the supercritical section, which may be calculated by means of the Manning equation, for example. Immediately downstream from the hydraulic jump, the water depth, which is conjugated to the normal flow depth of the supercritical section, is to be found. Subsequently, in the section where the normal conditions would permit supercritical flow, energy is built up due to the flow depth that is greater than normal. Exactly at the boundary to the downstream section, the normal flow depth (subcritical) of that section is reached.

In the case that the specific energy of the normal conditions is lower in the subcritical section than that in supercritical, energy must be reduced. Irrespective of the fact that energy is also dissipated in the hydraulic jump, the energy reduction according to Bernoulli is achieved in supercritical flow only if the flow depth increases. But in keeping with Manning, energy can be reduced only if the flow depth is less than y_N. Therefore, in order to reduce energy, the flow depth in supercritical flow may increase only in that section where the normal conditions are in subcritical. It increases until it is conjugated to $y_{N,\mathrm{SUB}}$; at that time, the hydraulic jump occurs.

Thus, we can subsume. If energy must be reduced between the two normal conditions, this is accomplished by an increasing supercritical flow depth in the section with subcritical normal conditions. As a result, y increases gradually until the conjugated flow depth of $y_r = y_{N,\mathrm{SUB}}$ is reached. At that location, the hydraulic jump occurs and subsequently $y_{N,\mathrm{SUB}}$ is attained.

If the specific energy of the normal conditions in subcritical is higher than that in supercritical flow, energy must be built up. This works only in the section where $y > y_N$, i. e. where the normal conditions allow supercritical flow.

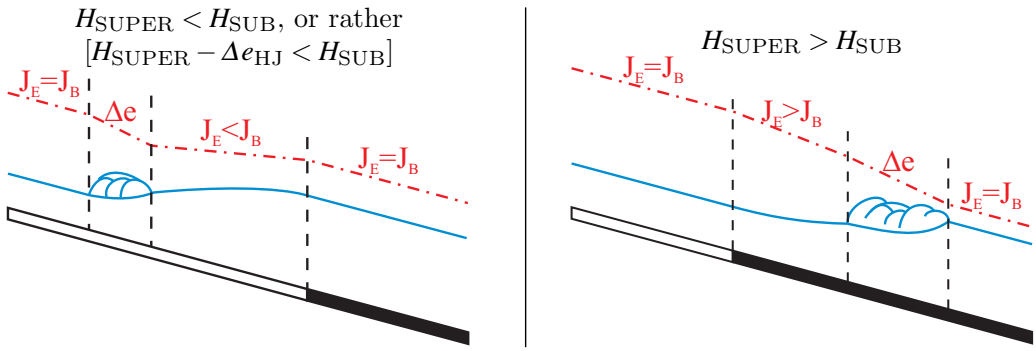

Figure 13.31: Hydraulic jumps at required energy buildup (left) and energy reduction (right).

The critical quantity in open channel hydraulics is the **specific energy**; the flow depths merely adapt to it.

Example

Transition subcritical – supercritical - subcritical flow

With the transition from sub- to supercritical and that from super- to subcritical flow, we take the Bernoulli-Manning discussion further so that we are prepared for all questions about nonuniform open channel hydraulics. In this context, it doesn't matter at all what causes the change in the normal flow depth. What is important is that it changes; how it changes is also relevant. Therefore, we consider the transition from sub- to supercritical flow and vice versa using a change of bed gradient for which we must still determine the boundary conditions.
Figure 13.32 shows an open channel with a discharge of $Q = 7.6\,\mathrm{m}^3/\mathrm{s}$ that has a bed gradient discontinuity between sections one and two before the primary conditions return in section three.

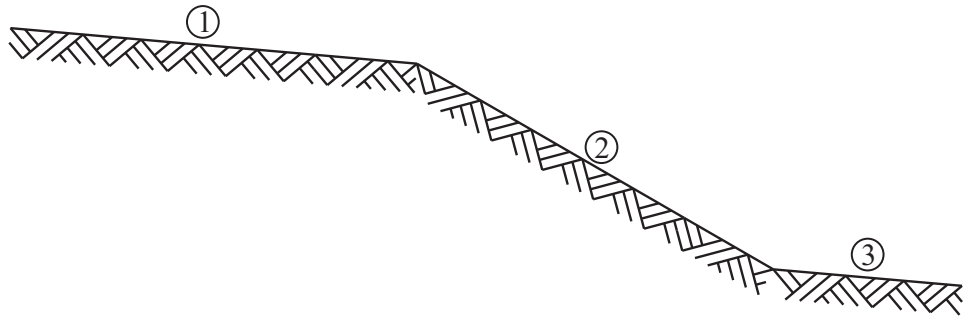

Figure 13.32: Example for the transition from sub- to super- and back to subcritical flow.

section 1	$J_{S1} = 0.30\,\%$	$n_1 = 3.33 \times 10^{-2}\,\mathrm{s/m}^{\frac{1}{3}}$	$b_1 = 6.0\,\mathrm{m}$
section 2	$J_{S2} = 2.50\,\%$	$n_2 = 2.0 \times 10^{-2}\,\mathrm{s/m}^{\frac{1}{3}}$	$b_2 = b_1 = 6.0\,\mathrm{m}$
section 3	$J_{S3} = J_{S1} = 0.30\,\%$	$n_3 = n_1 = 3.33 \times 10^{-2}\,\mathrm{s/m}^{\frac{1}{3}}$	$b_3 = b_2 = 6.0\,\mathrm{m}$

First, we must determine the normal conditions. Let´s start! Either follow the input prompts or use the routine `normalConditions.m` with the input file `dataOpenChannel.csv`, which is described on page 236.

```
1> function Q1=f(y)
2> Q1 = 7.6 - 1/(3.33e-2)*sqrt(3e-3)*(6*y)^(5/3)/(6+2*y)^(2/3);
3> endfunction
4> [y1,fval,info]=fsolve(@f,1.5)
5> v1 = 7.6/(6*y1)
6> Fr1 = v1/sqrt(9.81*y1)
7> H1 = y1+v1^2/(2*9.81)
```

Enter the commands into the Octave command line. The following lines denote their corresponding meaning:

```
1> % Q1 is a function of y.
2> % The equation is defined as Q1 = f(y) and solved for zero. The
values for n1, Q1, JS1 and b1 have already been inserted.
3> % endfunction terminates the definition of Q1.
4> % solves the equation @f with the starting value 1.5.
5> % If designating the variable to be solved in line 4 by y1, it
may be reused in this form. The same applies to v1=Q/(b*y1).
6> % The Froude number is calculated as Fr1=v1/sqrt(9.81*y1).
7> % The variables v1 and y1 are reused for calculating the spe-
cific energy.
```

It is advisable to immediately calculate all quantities under normal conditions: $\mathrm{Fr}_{N1} = 0.433 < 1$, $y_{N1} = 0.955\,\mathrm{m}$, $v_{N1} = 1.326\,\mathrm{m/s}$, $H_{N1} = 1.045\,\mathrm{m}$. We now try our hand with section two.

```
1> function Q2=f(y)[a]
2> Q2 = 7.6 - 1/0.02*sqrt(2.5e-2)*(6*y)^(5/3)/(6+2*y)^(2/3);
3> endfunction
4> [y2,fval,info]=fsolve(@f,1.5)
5> v2 = 7.6/(6*y2)
6> Fr2 = v2/sqrt(9.81*y2)
7> H2 = y2+v2^2/(2*9.81)
```

Enter the commands into the Octave command line. The following lines denote their corresponding meaning:

```
1> % Q2 is a function of y.
2> % The equation is defined as Q2 = f(y) and solved for 0. The
values for n2, Q2, JS2 and b2 have already been inserted.
3> % endfunction terminates the definition of Q2.
4> % solves the equation @f with the starting value 1.5.
5> % If designating the variable to be solved in line 4 by y2, it
may be reused in this form. The same applies to v2=Q/(b*y2).
6> % The Froude number is calculated as Fr2=v2/sqrt(9.81*y2).
7> % The specific energy is calculated with the buffered variables
v2 and y2.
```

[a] By the way, with the ↑ key, the previously typed commands may be called up again. This avoids having to type the entire equation, and only some numbers or variables may have to be changed.

For the conditions in section two, a Froude number of $\mathrm{Fr}_{N2} = 1.968$, i. e. supercritical flow, is obtained. The normal conditions for the three sections are summarised in the following table:

section 1	$y_{N1} = 0.955\,\mathrm{m}$	$v_{N1} = 1.326\,\mathrm{m/s}$	$H_{N1} = 1.045\,\mathrm{m}$	$\mathrm{Fr}_{N1} = 0.433 < 1$	**SUB**
section 2	$y_{N2} = 0.348\,\mathrm{m}$	$v_{N2} = 3.637\,\mathrm{m/s}$	$H_{N2} = 1.023\,\mathrm{m}$	$\mathrm{Fr}_{N2} = 1.968 > 1$	**SUPER**
section 3	$y_{N3} = 0.955\,\mathrm{m}$	$v_{N3} = 1.326\,\mathrm{m/s}$	$H_{N3} = 1.045\,\mathrm{m}$	$\mathrm{Fr}_{N3} = 0.433 < 1$	**SUB**

Thus, we must deal with a transition from sub- to supercritical flow between sections one and two as well as with a transition from super- to subcritical flow between sections two and three. Let's look at the details of the transitions.
We address the transition between section one and two, i. e. the change in flow from sub- to supercritical.

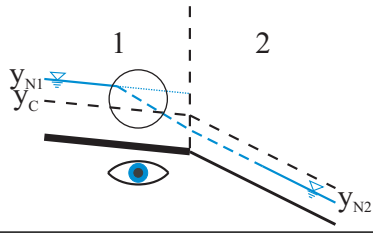

Bernoulli	$y_{\mathrm{SUB}} \downarrow \Rightarrow H_{\mathrm{SUB}} \downarrow$	☺
Manning	$y < y_N \Rightarrow H \downarrow$	

We see that the decreasing flow depth in subcritical flow occurs along with a decrease in specific energy. The same statement follows when $y < y_{N1}$, according to the Manning equation. Apparently, the transition takes place in section one. But stop! Let's take a close look at what will happen if the critical conditions are already passed through in section one. We would already be in supercritical flow in section one.

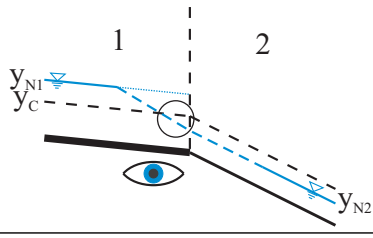

Bernoulli	$y_{\mathrm{SUPER}} \downarrow \Rightarrow$ $H_{\mathrm{SUPER}} \uparrow$	↯
Manning	$y < y_N \Rightarrow H \downarrow$	

If the flow upstream from the discontinuity in the bed gradient already changed to supercritical flow, this would mean that the specific energy increased with decreasing flow depth. However, according to Manning, this is not possible since the flow depth is smaller than the normal depth of this section.
We summarise the first considerations: the transition is possible in section one as long as subcritical flow exist.
And what about the transition in section two? We again examine both scenarios therein: 1) the decrease in the flow depth in subcritical and 2) the decrease in the flow depth in supercritical flow.

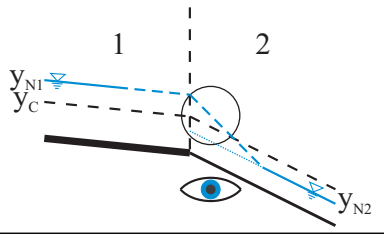	Bernoulli	$y_{SUB} \downarrow \Rightarrow H_{SUB} \downarrow$	
	Manning	$y > y_N \Rightarrow H \uparrow$	

If the flow depth drops in subcritical flow in this section, the specific energy also decreases. But this does not agree with the Manning equation because while the flow depth decreases, it is greater than the normal depth.

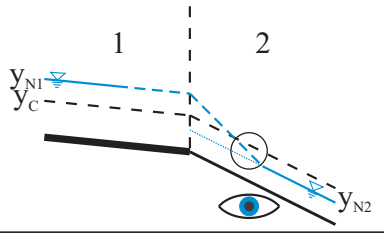	Bernoulli	$y_{SUPER} \downarrow \Rightarrow$ $H_{SUPER} \uparrow$	
	Manning	$y > y_N \Rightarrow H \uparrow$	

When we assume that we are already in supercritical flow, the decreasing flow depth leads to an increase in specific energy according to the Bernoulli equation. The flow formula also states that at $y > y_N$, the specific energy is increasing (remark: relative to the bottom).
When combining the above considerations, it follows that a decrease in flow depth in subcritical flow occurs in the upstream section, and downstream from the bed gradient discontinuity, the flow depth must drop in supercritical flow. Therefore, y_c is attained exactly at the vertex.
At the second vertex in Figure 13.32, roughness and bed gradient return to the values of section one. Consequently, a transition between super- and subcritical flow must happen somewhere. We consider first what would happen if the flow depth in section two were to increase. Since supercritical conditions are to be found in section two, we assume an increase in y in supercritical flow.

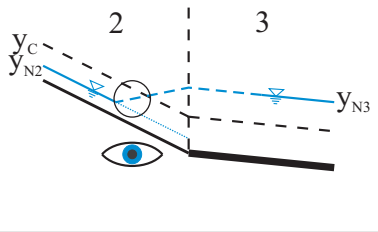	Bernoulli	$y_{SUPER} \uparrow \Rightarrow$ $H_{SUPER} \downarrow$	
	Manning	$y > y_N \Rightarrow H \uparrow$	

According to Bernoulli, H decreases when y increases in supercritical flow. As a result, $y > y_{N2}$, which, according to Manning, should lead to an increase in specific energy. But this does not happen!
In our search for the location of the transition, we will now turn to the situation in section three, where subcritical flow already exists, but y_{N3} has not yet been attained.

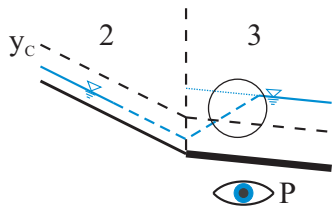	Bernoulli	$y_{SUB} \uparrow \Rightarrow H_{SUB} \uparrow$	
	Manning	$y < y_N \Rightarrow H \downarrow$	

It may feel like a curse, but it is impossible to find a system in which both equations are satisfied. A continuous transition between super- and subcritical flow is not possible[U]. Principally, the result of the discussion about the energy equation and the flow formula is that the transition between super- and subcritical must occur suddenly and not continuously, as we have already discovered above based on the differential equation for the water surface profile. A hydraulic jump occurs (see Figure 13.29).

Let's try our luck with a transition in section three. In that section, we already found that an increase in flow depth in subcritical flow is not possible (see above: $[y_{SUB} \uparrow \Rightarrow H_{SUB} \uparrow$ and $y < y_N \Rightarrow H \downarrow]$). Consequently, normal conditions (in subcritical flow) must be in effect immediately to the right of the hydraulic jump. With $y_{N3} = y_{r,\mathrm{HJ}}$, we may determine the required flow depth in supercritical flow:

$$y_{l,\mathrm{HJ}} = \frac{y_r}{2}\left(\sqrt{1+8\cdot \mathrm{Fr}_r^2}-1\right) = \frac{0.955\,\mathrm{m}}{2}\left(\sqrt{1+8\cdot 0.433^2}-1\right) = 0.278\,\mathrm{m} \qquad (13.83)$$

The flow depth to the left of the hydraulic jump would have to be smaller than the normal water depth in section two. But this is not possible because the specific energy increases with decreasing flow depth in supercritical flow, and as soon as it is below y_N energy is reduced, according to Manning.

That no transition is possible in section three could have been foreseen when considering the specific energies since $H_{N3} > H_{N2}$. Energy must be built up somewhere. Energy is dissipated in the hydraulic jump, and at a thought transition in section three, the flow depth would have to exceed y_{N3} according to the flow formulas, which is certainly not possible upstream from the hydraulic jump.

Let's look at a possible transition in section two. Since an increase in flow depth in the steep section with supercritical flow is not possible, the hydraulic jump exhibits the normal conditions on the left side. From Equation 13.81, it follows that the conjugated flow depth in subcritical flow is:

$$y_{r,\mathrm{HJ}} = \frac{y_l}{2}\left(\sqrt{1+8\cdot \mathrm{Fr}_l^2}-1\right) = \frac{0.348\,\mathrm{m}}{2}\left(\sqrt{1+8\cdot 1.968^2}-1\right) = 0.810\,\mathrm{m} \qquad (13.84)$$

Thus, we must obtain an increase in flow depth in subcritical flow in order to reach the normal flow depth of section three ($y_{N3} = 0.955\,\mathrm{m}$). Let us consider this by means of the table that is by now familiar to us:

[U] Until now, we have only considered the increase in flow depth under the conditions of the respective section. This is quite reasonable since there is no need to examine the increase in flow depth in subcritical flow in section two, and certainly not if subcritical flow is not reached. The same applies to the increase in flow depth in supercritical flow in section three. If the increase in flow depth in subcritical flow does not work in this section, then an examination of a possible increase in supercritical flow is wasted effort. Nevertheless, we will deal with this matter at a later time. Stay with it!

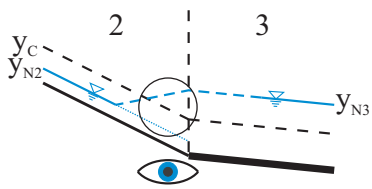	Bernoulli	$y_{SUB} \uparrow \Rightarrow H_{SUB} \uparrow$	☺
	Manning	$y > y_N \Rightarrow H \uparrow$	

Ultimately, the water surface profiles may be combined in the energy diagram in Figure 13.33.

And again, utmost attention is required. In the case that a bottom gradient of $J_B = 0.4\,\%$ exists for section one or three, the following normal conditions result:

section 2	$y_{N2} = 0.35\,\text{m}$	$v_{N2} = 3.64\,\text{m/s}$	$H_{N2} = 1.02\,\text{m}$	$\text{Fr}_{N2} = 1.97 > 1$	**SUPER**
section 3	$y_{N3} = 0.87\,\text{m}$	$v_{N3} = 1.46\,\text{m/s}$	$H_{N3} = 0.98\,\text{m}$	$\text{Fr}_{N3} = 0.50 < 1$	**SUB**

We see that $H_{N3} < H_{N2}$. This means that according to the aforementioned considerations, and because energy must be reduced, the hydraulic jump should occur in section three. When calculating the conjugated flow depth in supercritical flow, the result is $y_{\text{SUPER,conj.},N3} = 0.32\,\text{m}$, which is smaller than y_{N2}. With the understanding gained from this discussion, we will not succeed in conjuring $y < y_{N2}$ because according to Bernoulli this would necessitate an energy buildup. The case here is that the energy loss in the hydraulic jump is greater than the required energy reduction between the normal conditions in super- and in subcritical flow ($H_{\text{SUPER,conj.},N3} - H_{N3} = 1.12 - 0.98 = 0.14\,\text{m} > H_{N2} - H_{N3} = 0.04\,\text{m}$). Therefore, the transition must occur in section two. With the flow depth conjugated to y_{N2} downstream from the hydraulic jump $y_{r,\text{HJ}} = 0.810\,\text{m}$, an energy buildup from $H_{r,\text{HJ}} = 0.935\,\text{m}$ up to the specific energy of the normal conditions $H_{N3} = 0.98\,\text{m}$ takes place, still in section two. Normal conditions of section three are in effect exactly at the vertex of the bed gradient.
Sometimes you fall face-first; however, the error becomes obvious. With an incorrectly chosen section of the transition for $H_{\text{SUPER}} > H_{\text{SUB}}$, it will be noticed immediately that the flow depth in supercritical flow should become smaller than y_N for an energy buildup. Then the transition must be moved into the other section.

Example

Flow over a bed sill

This example serves to recapitulate and consolidate our knowledge. For this purpose, we will complete a task as it is executed a thousand times worldwide. The channel bed is lifted by a bed sill of height $w = 0.50\,\text{m}$ (see Figure 13.34). Additionally, we will examine what might happen if the downstream bottom is formed as in the case of a stilling basin with a negative step of $\Delta z = 0.10\,\text{m}$ (shown in broken lines). Here, the water surface profiles are of interest.

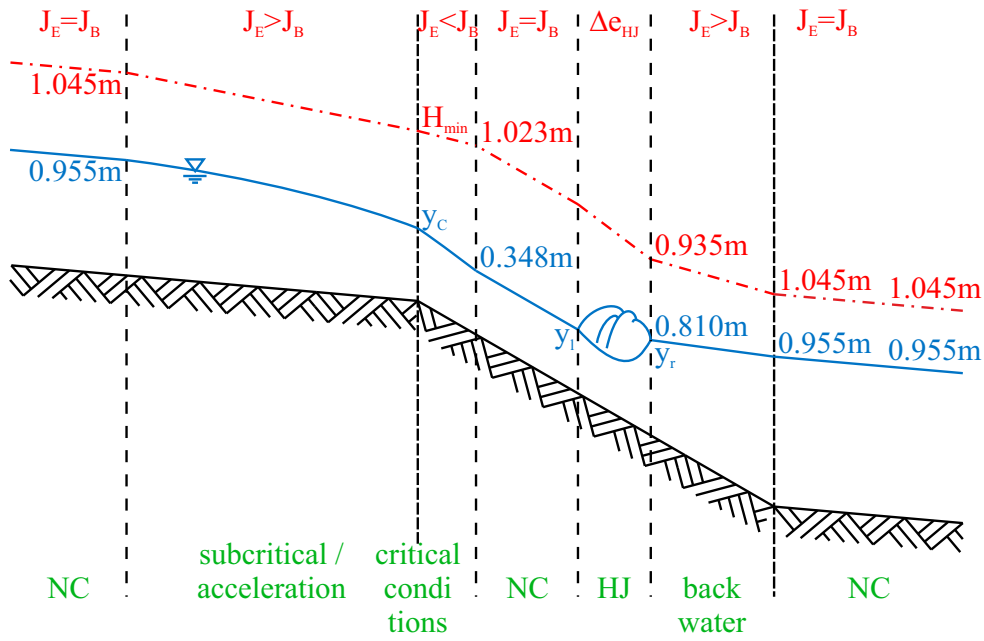

Figure 13.33: Energy diagram for a sample task with two gradient changes.

Figure 13.34: Sample task for an open channel flow with bed sill and stilling basin.

$b = 8.0\,\mathrm{m}$	$w = 0.50\,\mathrm{m}$	$Q = 25\,\mathrm{m^3/s}$	$J_B = 0.3\,\%$	$n = 2.5 \times 10^{-2}\,\mathrm{s/m^{\frac{1}{3}}}$	$\Delta z = 0.10\,\mathrm{m}$

With the input data we obtain the following[V]:

$y_N = 1.396\,\mathrm{m}$	$v_N = 2.244\,\mathrm{m/s}$	$H_N = 1.653\,\mathrm{m}$	$\mathrm{Fr}_N = 0.607 < 1$	SUB

We find normal conditions in subcritical flow. The critical quantity is the specific energy. Does the flow have sufficient energy under normal conditions to pass the bed sill? For y_c, we obtain $y_c = 0.999\,\mathrm{m}$ via Equation 13.7; or, with Formula 13.8, $H_{\min} = 1.498\,\mathrm{m}$. With a bed sill of height $w = 0.50\,\mathrm{m}$, $H_N < H_{\min} + w$. This means that upstream from the bed sill, energy up to $H_{\min} + w$ must be built up in order to reach $H_{\min}$ on the bed sill and for the critical conditions to be passed.
With knowledge of the specific energy upstream and downstream from the bed sill (energy losses are not taken into account), the flow depths upstream (subcritical) and downstream (supercritical) of the bed sill may be determined with the Bernoulli equation for $H_{\mathrm{ups}} = H_{\mathrm{downs}} = H_{\min} + w = 1.998\,\mathrm{m}$.

[V] Now, at the latest, you should consult the routine `normalConditions.m` (see page 236) for calculating the relevant values.

```
1> function H=f(y)
2> H = -1.998+y+25^2/(8.0^2*y^2*2*9.81);
3> endfunction
4> [y,fval,info]=fsolve(@f,1.8)
5> [y,fval,info]=fsolve(@f,.5)
```

Enter the commands into the Octave command line. The following denotes the corresponding meaning of the last two lines:

```
4> % with the starting value of 1.8, the flow depth in subcritical
flow upstream of the bed sill is obtained.
5> % with a starting value of 0.5, the iteration leads to the flow
depth in supercritical flow downstream from the bed sill.
```

We obtain $y_{\text{ups}} = 1.853\,\text{m}$, $y_{\text{downs}} = 0.596\,\text{m}$ and $y_c = 0.999\,\text{m}$ on the bed sill.
Together we consider how the flow depth increases upstream. Normal conditions in subcritical flow exist; the flow depth is to increase from $y_N = 1.396\,\text{m}$ to $y_{\text{ups}} = 1.853\,\text{m}$. What does Bernoulli say?

$$y_{\text{SUB}} \uparrow \Rightarrow H_{\text{SUB}} \uparrow$$

And what does Manning say?

$$y > y_N \Rightarrow H \uparrow$$

The backwater adjusts continuously upstream from the bed sill. How is the situation downstream from the bed sill?
Since subcritical flow characterises the normal conditions and the critical conditions are passed on the bed sill, a hydraulic jump must occur. With $H_{\text{SUPER}} = 1.998\,\text{m} > H_N = 1.653\,\text{m}$, it follows from Figure 13.31 that the tailwater increases in supercritical flow; then, the remaining energy difference is reduced via the hydraulic jump. Immediately downstream from the hydraulic jump, normal conditions must then prevail again[W]. The conjugated flow depth in supercritical flow is calculated by Formula 13.81:

$$y_{l,\text{HJ}} = \frac{1.396}{2}\left(\sqrt{1+8\cdot 0.607^2}-1\right) = 0.686\,\text{m} \tag{13.85}$$

This means that the flow depth increases from the downstream foot of the bed sill to the hydraulic jump; i. e. from $y_{\text{downs}} = 0.596\,\text{m}$ to $y_{l,\text{HJ}} = 0.686\,\text{m}$. A brief check shows the following:

$$y_{\text{SUPER}} \uparrow \Rightarrow H_{\text{SUPER}} \downarrow$$

$$y < y_N \Rightarrow H \downarrow$$

Thus, the task is solved, and the challenge is successfully met. The results are summarised in an energy diagram (see Figure 13.35).
As an option, one may examine in this example how conditions would develop if a stilling basin were to be placed directly downstream from the bed sill. Further effects upstream

[W] If you are still motivated, feel free to try out what would happen downstream from the hydraulic jump in subcritical flow if the flow depth were smaller or greater than y_N. For $y < y_N$, the flow depth should increase to y_N which, according to Bernoulli, should lead to an increasing specific energy. However, in line with Manning, for $y < y_N$, energy reduction takes place. So that doesn't work. We will try $y > y_N$, which would lead to a sinking water level down to y_N. In subcritical flow, a decrease in specific energy results from the Bernoulli equation. According to Manning, however, the specific energy should increase because $y > y_N$. Consequently, normal conditions result directly downstream from the hydraulic jump.

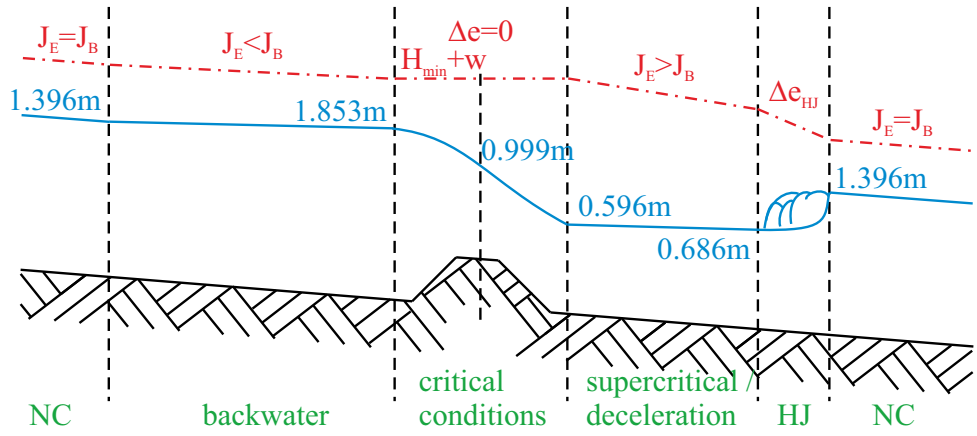

Figure 13.35: Energy diagram for the sample task with a bed sill.

may be excluded because the critical conditions and the bed sill height remain unchanged. However, the specific energy downstream from the bed sill will increase by the negative step: $H_{\text{downs}} = 2.098\,\text{m}$, which yields $y_{\text{downs}} = 0.571\,\text{m}$.
Equation 13.81 was derived for continuous bottoms; because of the forward-facing step (the positive step at the end of the stilling basin), this simple equation must not be used. The situation is described in Figure 13.36.

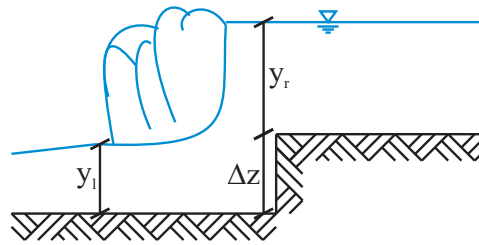

Figure 13.36: Flow depths and hydraulic jump in the stilling basin.

The law of momentum must be set anew because the pressure force on the right side includes the proportion from the forward-facing step.

$$\rho \frac{Q^2}{b \cdot y_{l,\text{HJ}}} + \frac{1}{2}\rho \cdot g \cdot y_{l,\text{HJ}}^2 \cdot b = \rho \frac{Q^2}{b \cdot y_N} + \frac{1}{2}\rho \cdot g \cdot (y_N + \Delta z)^2 \cdot b \tag{13.86}$$

We employ Octave's equation solver.

```
1> function F=f(y)
2> F = 1000*25^2/(8*y)+.5*1000*9.81*y^2*8-...
> (1000*25^2/(8*1.396)+.5*1000*9.81*(1.396+.1)^2*8);
3> endfunction
4> [yl,fval,info]=fsolve(@f,.4)
```

With $y_r = y_N$ the output for $y_{l,\mathrm{HJ}}$ is 0.603 m. The water level in the stilling basin increases from $y_{\mathrm{downs}} = 0.571\,\mathrm{m}$ to $y_l = 0.603\,\mathrm{m}$.

13.11 Computation of water surface profiles – direct step method

The computation of water surface profiles is based on the same method that was already involved in the expansion of the Bernoulli equation with the loss term according to the Darcy-Weisbach equation or in the derivation of the differential equation of the water surface profile. In German speaking countries it is known as Böß method. The energy is balanced at two open channel cross-sections (see Figure 13.37); however, we do not write differentials or infinitesimal quantities, but rather differences of "tangible" orders of magnitude. As we did with pipe hydraulics, we may also, in this case, equate the quantities on the left with those on the right side.

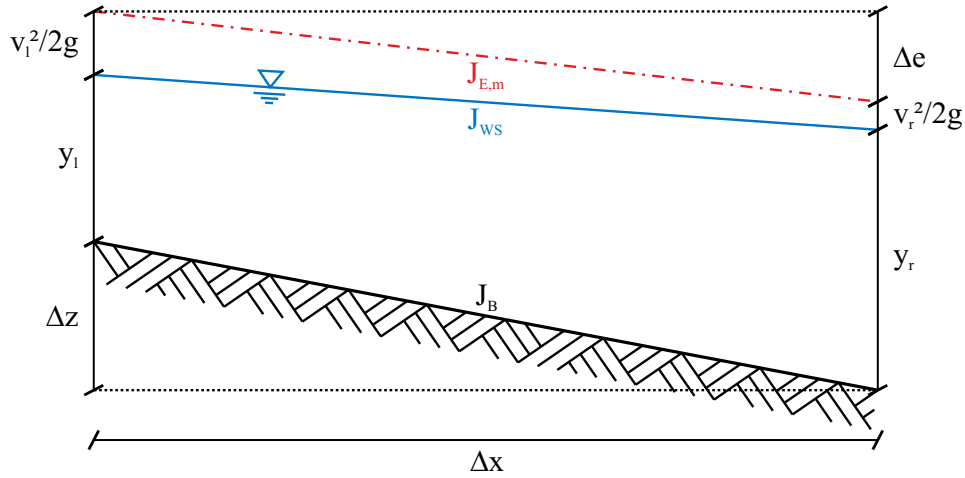

Figure 13.37: Balancing of the energy at two open channel cross-sections according to Figure 13.24.

The purely formal result is:

$$\Delta z + y_l + \frac{v_l^2}{2g} = y_r + \frac{v_r^2}{2g} + \Delta e \quad \text{with } \Delta z = J_B \Delta x \text{ and } \Delta e = J_{E,m} \Delta x \tag{13.87}$$

By means of the direct step method, the energy loss is determined for the average conditions based on the flow formulas. In this way, the distance between two flow depths Δx may be explicitly calculated, and the flow depth at any given distance may be calculated implicitly. As disturbances in supercritical flow propagate downstream only, the calculation with the direct step method in this flow condition is possible only in the downstream direction. However, in subcritical flow, the downstream conditions determine what happens upstream, which is why the direct step method (or for that matter, any other arbitrary complex method) may be applied only upstream in this case. The average conditions are determined as follows:

Table 13.2: Averagings in the direct step method.

$v_m = \frac{1}{2}(v_l + v_r)$	$R_{\mathrm{hy},m} = \frac{1}{2}\left(R_{\mathrm{hy},l} + R_{\mathrm{hy},r}\right) = \frac{A_l + A_r}{P_l + P_r}$	$J_{E,m} = \frac{v_m^2 \cdot n^2}{R_{\mathrm{hy},m}^{\frac{4}{3}}}$

The calculation of the gradient of the mean energy grade line in Table 13.2 is related to the mean velocity $v_m = \frac{1}{2}(v_l + v_r)$; however, the energy loss is dependent on the square of the velocity so that the introduced linearisation is not correct. If the cross-sections exhibit only small distances, the error is negligibly small (see example in Chapter 13.11.2).

13.11.1 Distance Δx of two flow depths

By rearranging Equation 13.87, Δx may be calculated explicitly:

$$\Delta x = \frac{H_r - H_l}{J_B - J_{E,m}} = \frac{y_r + \frac{v_r^2}{2g} - y_l - \frac{v_l^2}{2g}}{J_B - J_{E,m}} \tag{13.88}$$

13.11.2 Flow depth at distance Δx

For the calculation of the flow at a specified distance, Equation 13.87 must be solved for y_l (subcritical) or y_r (supercritical) as follows:

$$y_l = y_r + \frac{v_r^2}{2g} - \frac{v_l^2}{2g} + (J_{E,m} - J_B) \cdot \Delta x \tag{13.89}$$

By rearranging the equation, not only do the indices change, but also the signs of J_B and $J_{E,m}$:

$$y_r = y_l + \frac{v_l^2}{2g} - \frac{v_r^2}{2g} + (J_B - J_{E,m}) \cdot \Delta x \tag{13.90}$$

Since the flow depths are also included in the velocity heights, the equations cannot be solved explicitly. This means that the result must be estimated first in order to calculate $\frac{v_l^2}{2g}$ or $\frac{v_r^2}{2g}$ as well as $R_{\mathrm{hy},m}$ and $J_{E,m}$ before the values may be inserted into Equations 13.89 and 13.90. A consecutive iteration step starts with the newly obtained y_l and y_r.

Example

Calculation of the water surface profile

For a deeper understanding of the direct step method, we will again focus on the example from Chapter 13.10.2.5 on page 259. The input data are repeated in the table below. In addition, the following flow depths have been determined:

$b = 8.0\,\mathrm{m}$	$Q = 25\,\mathrm{m}^3/\mathrm{s}$	$J_B = 0.3\,\%$	$n = 2.5 \times 10^{-2}\,\mathrm{s/m}^{\frac{1}{3}}$
$y_N = 1.396\,\mathrm{m}$	$y_{\mathrm{ups}} = 1.853\,\mathrm{m}$	$y_{\mathrm{downs}} = 0.596\,\mathrm{m}$	$y_{l,\mathrm{HJ}} = 0.686\,\mathrm{m}$

The planning engineer will be interested in how far the influence of the backwater extends and how far the toe (impingement point) of the hydraulic jump is placed from the bed sill.
We calculate Δx for the upstream backwater with $y_r = y_{\mathrm{ups}} = 1.853\,\mathrm{m}$ and $y_l = y_N = 1.396\,\mathrm{m}$ and obtain explicitly $\Delta x = 341.62\,\mathrm{m}$. The distance Δx between the bed sill and the hydraulic jump is calculated with $y_l = y_{\mathrm{downs}} = 0.596\,\mathrm{m}$ and $y_r = y_{l,\mathrm{HJ}} = 0.686\,\mathrm{m}$. Since the flow depths are given, the velocity heights may also be calculated; we obtain $\Delta x = 8.43\,\mathrm{m}$. If you are interested, for example, in the flow depth at a distance of 200 m upstream from the bed sill, you must proceed iteratively.

Those who are qualified in SMS typing may carry out iterations by means of the pocket calculator. Those who enjoy programming may use the offered routines which run under `directStep.m`. Take into account the structure of the file `dataOpenChannel.csv`, which is described in Chapter 13.9 on page 236.

After a single calculation step with the Octave routine, one obtains $y_{\Delta x=200\,\mathrm{m}} = 1.530\,\mathrm{m}$ for the flow depth 200 m upstream from the bed sill. If the flow depth of the open section is iteratively calculated with 200 steps of 1.0 m in order to reduce the error from the averaging of the energy grade line gradient, $y_{\Delta x=200\,\mathrm{m}} = 1.540\,\mathrm{m}$ is obtained. The reason why the difference is not significant is because we are in the region of backwater, where the water flows slowly and the difference of the flow depths is rather small.
Let's look at the conditions in supercritical flow. But beware! The iterations in supercritical flow converge very poorly. It is best to resort to an equation solver. According to the knowledge acquired above, the supercritical jet has a length of $\Delta x = 8.43\,\mathrm{m}$. Let's calculate the flow depth at $\Delta x = 7.0\,\mathrm{m}$. For a single calculation step, the program provides a flow depth of $y_{\Delta x=7\,\mathrm{m}} = 0.670\,\mathrm{m}$. Even when dividing the calculation domain into small 10 cm disks, there is hardly any impact on the result since the section of length 7.0 m is rather short and the flow depth difference is again small; we also obtain $y_{\Delta x=7\,\mathrm{m}} = 0.670\,\mathrm{m}$.

Now you should be prepared to meet the challenges of open channel hydraulics.

Chapter 14
Unsteady free surface flow

14.1 Saint-Venant differential equations

We base the unsteady open channel hydraulics on what we have learned so far. We casually revert to the differential equation of the water surface profile (13.62) and add the normed local derivative of the velocity $\frac{1}{g}\frac{\partial v}{\partial t}$. Making use of the small-angle approximation, we set the two directions s and x equal to each other and stay in the one-dimensional context. We therefore write Equation 13.62 with the local derivative and the partial differential operator ∂ in order to be able to clearly distinguish the local ($\frac{\partial v}{\partial t}$) from the convective derivative ($v\frac{\partial v}{\partial x} = \frac{1}{2}\frac{\partial v^2}{\partial x}$):

$$\frac{\partial y}{\partial x} + \frac{1}{2g}\frac{\partial v^2}{\partial x} + \frac{1}{g}\frac{\partial v}{\partial t} = J_B - J_E \tag{14.1}$$

The continuity condition is to be described at the differential element. Generally, the discharge changed from Q by the differential quantity $\mathrm{d}Q$ to $Q + \mathrm{d}Q$. Thereby, the volume in the element under consideration must have changed to the same extent since $\rho = \text{const}$. When emptying a reservoir, for example at constant inflow Q by discharging $Q + \mathrm{d}Q$, the volume $\mathrm{d}Q\,\mathrm{d}t$ discharged over the emptying period must be missing there (we did exactly the same in Chapter 9). The discharged volume may be calculated via the change of the cross-sectional area $\mathrm{d}A$ times the length $\mathrm{d}x$. Taking into account the definition of the surface normal pointing out of the volume (just as in Chapters 5.8 and 9), the continuity condition may be written as follows:

$$\partial Q \partial t = -\partial A \partial x \quad \text{rearranging:} \frac{\partial Q}{\partial x} + \frac{\partial A}{\partial t} = 0 \tag{14.2}$$

Equations 14.1 and 14.2 are together referred to as Saint-Venant[A] differential equations.

[A] Adhémar Jean Claude Barré de Saint-Venant, ∗1797, Villiers-en-Bière, France †1886, St.-Ouen, France

C. Rapp, *Hydraulics in Civil Engineering*,
https://doi.org/10.1007/978-3-031-54860-4_14

14.2 Upsurge and downsurge

The abrupt opening and closing of regulating devices in free surface water bodies cause the occurrence of what are known as upsurge and downsurge (see Figure 14.1). The propagation velocity of these waves is approximately as high as the one derived in Chapter 13.2 ($c = \sqrt{gy}$); however, due to its magnitude, the wave height has an influence on it.

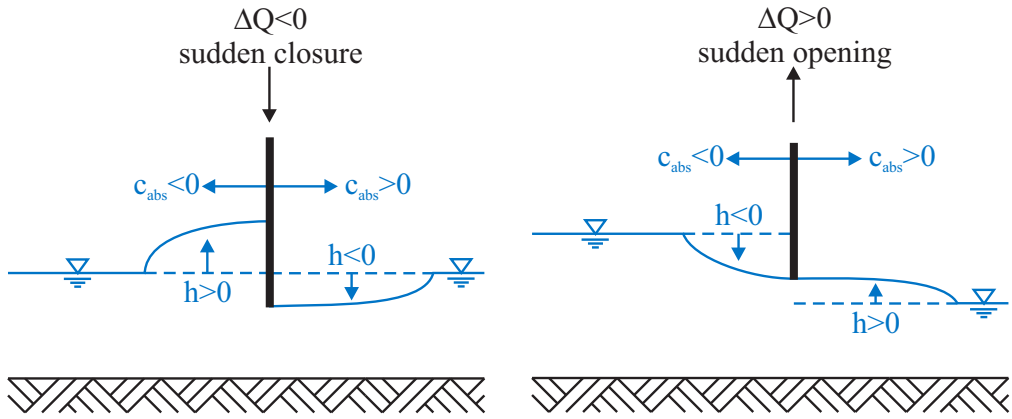

Figure 14.1: Conditions and designations during upsurge and downsurge phenomena.

We try a derivation that differs from pertinent works such as [13, 49], but accept the idea of Engels [11] that a bulkhead (in Figure 14.2, represented by a dark blue line drawn to the right of t) closing the entire cross-section of the open channel may move by a certain infinitesimal distance ds to the right. Furthermore, we look at Figure 14.3 which, for the sake of simplicity, one may imagine in a stationary coordinate system. The conditions prior to the discharge variation are in effect in the light blue coloured region; the associated water level defines the cross-sectional area A_0. Now, the bulkhead is moved within dt by the distance ds. A wave is generated; it propagates the distance dl above the original water surface at velocity c and with wave height h during the same time dt.

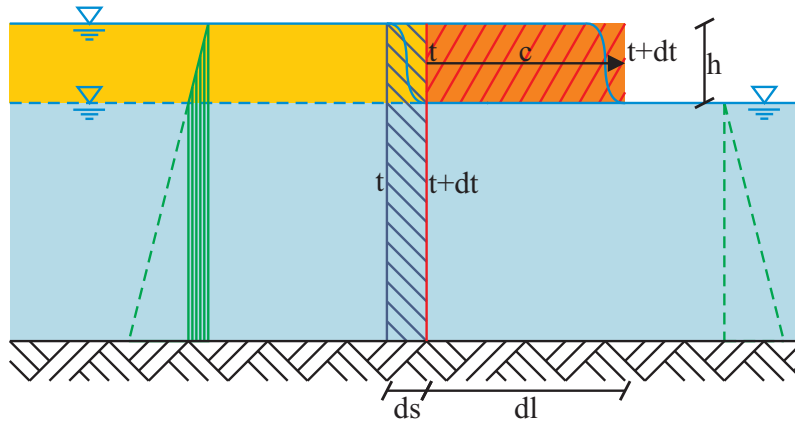

Figure 14.2: Propagation of an upsurge wave.

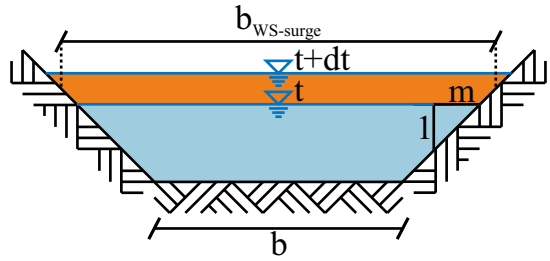

Figure 14.3: Cross-section at the propagation of a surge wave.

We approach the problem via an examination of the forces and start by considering mass conservation (see Figures 14.2 and 14.3). For continuity reasons, the water volume above the original water level (indicated by the red hatch lines //) results from the displacement that was caused by the bulkhead during the time period from t to $t + \mathrm{d}t$ (indicated by the blue hatch lines \\).

$$(A_0 + h \cdot b_{\text{WS-surge}}) \cdot \mathrm{d}s = h \cdot b_{\text{WS-surge}} \cdot \mathrm{d}l \tag{14.3}$$

We divide Equation 14.3 by $\mathrm{d}t$:

$$(A_0 + h \cdot b_{\text{WS-surge}}) \cdot \frac{\mathrm{d}s}{\mathrm{d}t} = h \cdot b_{\text{WS-surge}} \frac{\mathrm{d}l}{\mathrm{d}t} = h \cdot b_{\text{WS-surge}} \cdot c \tag{14.4}$$

The mass $\rho \cdot A_0 \cdot \mathrm{d}s$ was stationary at time t and is accelerated during time period $\mathrm{d}t$ to velocity c (the upper portion with yellow background need not be accelerated because the velocity there is already c). We already know from Chapter 3.4.1 that a mass m is accelerated by $a = \frac{\mathrm{d}c}{\mathrm{d}t}$ when a force is applied. The rate of change of momentum reads:

$$F_I = \rho A_0 \, \mathrm{d}s \, \frac{\mathrm{d}c}{\mathrm{d}t} \tag{14.5}$$

With the above considerations, this force stems from the movement of the bulkhead, but with a propagating wave in a free waterbody it results from the difference between the pressure forces to the left and right of the wave (see Figure 14.2, vertical green lines ||-lines). The pressure force is:

$$F_P = \rho g h \left(A_0 + \frac{h \cdot b_{\text{WS-surge}}}{2} \right) \tag{14.6}$$

The water must, so to speak, push itself off from the left boundary in order to be able to propagate at velocity c to the right. Taking the sign into account, terms 14.5 and 14.6 are equated as follows:

$$\rho A_0 \, \mathrm{d}s \, \frac{\mathrm{d}c}{\mathrm{d}t} = \rho g h \left(A_0 + \frac{h \cdot b_{\text{WS-surge}}}{2} \right) \tag{14.7}$$

From Equation 14.4,

$$\frac{\mathrm{d}s}{\mathrm{d}t} = \frac{h \cdot b_{\text{WS-surge}} \cdot c}{h \cdot b_{\text{WS-surge}} + A_0} \tag{14.8}$$

which, inserted into Equation 14.7, results:

$$\rho A_0 \, \mathrm{d}c \, \frac{h \cdot b_{\text{WS-surge}} \cdot c}{h \cdot b_{\text{WS-surge}} + A_0} = \rho g h \left(A_0 + \frac{h \cdot b_{\text{WS-surge}}}{2} \right) \tag{14.9}$$

Since the mass was stationary at time t (see above), the change of c ($\mathrm{d}c$) corresponds to c. Additionally, we divide by h and ρ and multiply by $A_0 + h \cdot b_{\text{WS-surge}}$, which yields:

$$c^2 \cdot b_{\text{WS-surge}} \cdot A_0 = g \left(A_0 + \frac{h \cdot b_{\text{WS-surge}}}{2} \right) \cdot (A_0 + h \cdot b_{\text{WS-surge}}) \tag{14.10}$$

Now, the right side is expanded:

$$\begin{aligned} c^2 \cdot b_{\text{WS-surge}} \cdot A_0 &= g \left(A_0^2 + A_0 \frac{h \cdot b_{\text{WS-surge}}}{2} + A_0 \cdot h \cdot b_{\text{WS-surge}} + \frac{h^2 \cdot b_{\text{WS-surge}}^2}{2} \right) = \\ &= g \left(A_0^2 + \frac{3}{2} A_0 \cdot h \cdot b_{\text{WS-surge}} + \frac{h^2 \cdot b_{\text{WS-surge}}^2}{2} \right) \end{aligned} \tag{14.11}$$

In the next step, we place A_0^2 before the bracket and divide by $A_0 b_{\text{WS-surge}}$:

$$c^2 = \frac{g A_0}{b_{\text{WS-surge}}} \left(1 + \frac{3}{2} \frac{h \cdot b_{\text{WS-surge}}}{A_0} + \frac{1}{2} \frac{h^2 \cdot b_{\text{WS-surge}}^2}{A_0^2} \right) \tag{14.12}$$

Finally, we calculate the square root in order to obtain the propagation velocity of the upsurge and downsurge waves:

$$c = \sqrt{\frac{g A_0}{b_{\text{WS-surge}}}} \sqrt{1 + \frac{3}{2} \frac{h \cdot b_{\text{WS-surge}}}{A_0} + \frac{1}{2} \left(\frac{h \cdot b_{\text{WS-surge}}}{A_0} \right)^2} \tag{14.13}$$

Perhaps you ask yourself why the cut was made exactly at this place and why, in terms of the continuity condition, part of the wave was included in the calculation while in the case of the rate of change of momentum, it was not. I appreciate that this must drive you crazy. But it must be like this. If the cut is made at the location where the wave has not yet arrived, there will be no difference in pressure forces. Therefore, this part of the wave must be included in the calculation of the mass. However, this part need not be accelerated to velocity c because it is already propagating at that velocity. The part of the mass that adds to the wave propagation results solely from that part originally flowing at velocity v_0 and with area A_0.

The first root corresponds to the propagation velocity of a shallow water wave. In physical terms only, however, this velocity depends on the respective depth at each point of the open channel cross-section, but not on the width of the water level. The second root results from the variation of the flow depth due to wave formation.
In general, the above derived movement may also be overlaid by a basic flow at velocity v_0. Even when moving the coordinate system at velocity c, in a sense "riding the wave", as Lagrange would do (see Chapter 2.3.1), the formulas will be derived in the same manner. This is because the momentum flux of an overlaid basic flow at velocity v_0 is cancelled-out since it has the same magnitude on the right and on the left in opposite directions. And

in the moving reference system too, the water for the propagation of the wave must be taken from the body of water originally moving at velocity v_0 through flow area A_0. Thereby, we obtain the absolute propagation velocity (see Figure 13.1) in the downstream direction:

$$c_{\text{abs}} = v_0 + c \tag{14.14}$$

In the upstream direction, it is:

$$c_{\text{abs}} = v_0 - c \tag{14.15}$$

Experiment

Upsurge and downsurge in a laboratory flume

We examine the propagation velocity of a surge wave that is generated by the abrupt closing of a sluice gate by means of an experiment carried out in the flume with which we are already familiar ($b = 0.20\,\text{m}$).

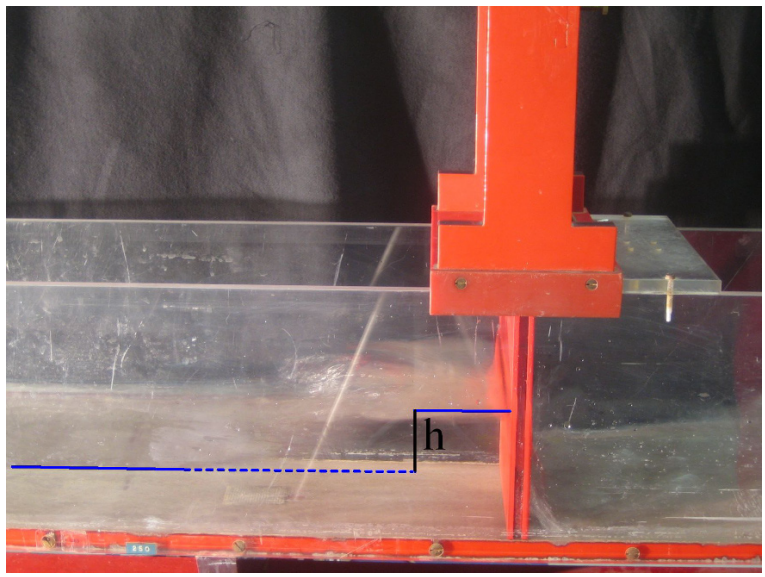

Figure 14.4: Upsurge at the abrupt closing of a sluice gate [44].

In this experiment, the original flow depth was $y_0 = 0.054\,\text{m}$ at a discharge of $Q = 6.3\,\text{L/s}$; $v_0 = 0.58\,\text{m/s}$. The height of the upsurge was determined to be $h = 0.049\,\text{m}$. The relative propagation velocity of the surge wave c may be calculated by means of Equation 14.13:

$$c = \sqrt{\frac{g \cdot 0.20 \cdot 0.054}{0.20}} \sqrt{1 + \frac{3}{2} \cdot \frac{0.049 \cdot 0.20}{0.20 \cdot 0.054} + \frac{1}{2} \left(\frac{0.049 \cdot 0.20}{0.20 \cdot 0.054} \right)^2} = 1.21\,\text{m/s} \tag{14.16}$$

The result is $c = 1.21\,\mathrm{m/s}$ and, using Equation 14.15, $c_{\mathrm{abs}} = v_0 - c = -0.63\,\mathrm{m/s}$. The variation in discharge may be verified via the continuity condition: $\Delta Q = c_{\mathrm{abs}} bh = -6.2\,\mathrm{L/s}$. This agrees quite well with the total blockage of the original discharge that was $6.3\,\mathrm{L/s}$.

Example

Hydropeaking in a headrace channel of a power plant

Let's practise using the formulas by means of a small example. In a trapezoidal headrace channel with a bottom width of $b = 6.0\,\mathrm{m}$ and a lateral inclination of $m = 1.5$, a discharge of $Q = 50\,\mathrm{m^3/s}$ flows at a depth of $y = 4.0\,\mathrm{m}$. The discharge is abruptly reduced by $\Delta Q = 25\,\mathrm{m^3/s}$, i. e. $\Delta Q = -25\,\mathrm{m^3/s}$. In the following discussion, we determine the height of the upsurge that is generated.
In the first step for calculating c, we assume that h equals zero[B]. This yields:

$$c = \sqrt{g\frac{A}{b_{\mathrm{WS}}}} = \sqrt{g\frac{48}{18}} = 5.11\,\mathrm{m/s} \tag{14.17}$$

The propagation velocity opposite to the original flow direction for the upsurge is found to be:

$$c_{\mathrm{abs}} = v_0 - c = \frac{Q}{A} - c = -4.07\,\mathrm{m/s} \tag{14.18}$$

This allows the determination of the surge height in the first iteration step:

$$h = \frac{\Delta Q}{c_{\mathrm{abs}} \cdot b_{\mathrm{WS\text{-}surge}}} = \frac{-25}{-4.07 \cdot 18} = 0.341\,\mathrm{m} \tag{14.19}$$

The propagation velocity is calculated anew with this surge height since the propagation velocity itself has changed by the surge height. Using Equation 14.13, we see that $c = 5.539\,\mathrm{m/s}$ and subsequently $c_{\mathrm{abs}} = v_0 - c = -4.50\,\mathrm{m/s}$, which leads to $h = 0.300\,\mathrm{m}$. In the next iteration step, the variations of the quantities are hardly noticeable: $c = 5.49\,\mathrm{m/s}$, $c_{\mathrm{abs}} = -4.45\,\mathrm{m/s}$, $h = 0.305\,\mathrm{m}$, all of which ultimately correspond to the converged solution. By the way, the same configuration leads to a downsurge of $h = -0.242\,\mathrm{m}$ in the tailrace channel, in case you want to check. Needless to say, you may find a script in the provided program library by means of which downsurge and upsurge waves may be calculated ;-).

Insert the required values into the file `dataSurge.csv` and save it. Then open Octave and call routine `surge.m`.

```
1> surge
```

Octave prompts you to enter the original flow depth `y` and the change of the discharge `dQ`. The command means:

```
1> % surge calls the routine surge.m, which must be present in the
active directory.
```

[B] For checking, I recommend using the routines for calculating area and width of the water surface: `flowArea('trapezoid',[6,1.5],4)` and `bWS('trapezoid',[6,1.5],4)`.

Chapter 15
Introduction to groundwater flow

Potential theory is a good choice for the calculation of groundwater flows because they are laminar due to the thin capillaries and low flow velocities. Those who want to quench their thirst for knowledge beyond the mathematical contents described herein should consult [64].

Darcy found a linear relationship between the gradient $\frac{\partial h}{\partial x}$ of the water level and the so-called filter velocity v_f by means of the filter experiment named after him (see Figure 15.1). The proportionality factor k_f is known as permeability coefficient with the unit of a velocity.

$$v_f = \frac{Q}{A_{\text{filter}}} = -k_f \frac{\partial h}{\partial x} = -k_f \frac{\Delta h}{L} \tag{15.1}$$

This law applies to creeping flows, which are characterised by a very small Reynolds number $\text{Re} = \frac{v_f \cdot d_{50}}{\nu} \leq 4$ (with the mean grain diameter d_{50}).

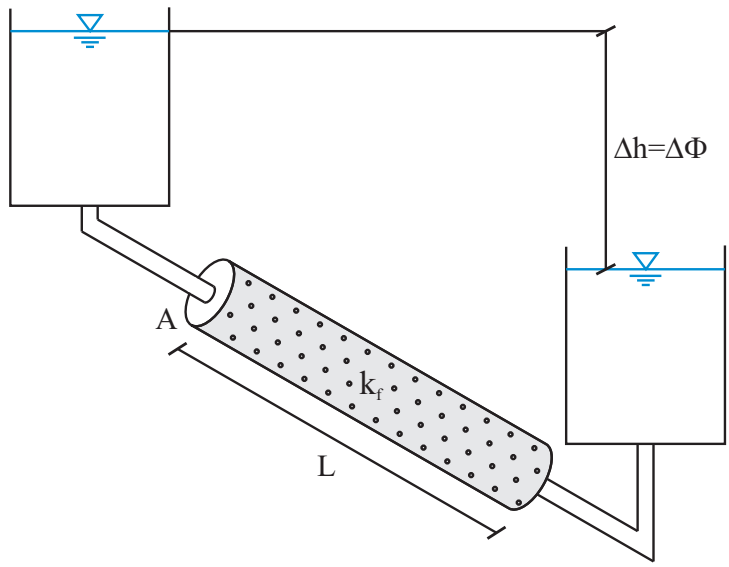

Figure 15.1: Filter experiment according to Darcy.

C. Rapp, *Hydraulics in Civil Engineering*,
https://doi.org/10.1007/978-3-031-54860-4_15

In the following discussion, we will see how Darcy's law is connected with potential theory, which was derived in Chapter 4. First, we write down Equation 15.1 with Einstein's sum convention in a general form:

$$v_{f,i} = -k_f \frac{\partial h}{\partial x_i} \tag{15.2}$$

The continuity condition must also apply to Formula 15.2, which is why the divergence of the filter velocity must be zero: $\mathrm{div}\, v_f = 0$. Written out, the divergence reads:

$$\frac{\partial}{\partial x_i} v_{f,i} = \frac{\partial}{\partial x_i} \left(-k_f \frac{\partial h}{\partial x_i} \right) = -k_f \frac{\partial^2 h}{\partial x_i^2} = 0 \tag{15.3}$$

Thus, Equation 15.3 is also a Laplace differential equation (see Chapter 4), or groundwater movements may also be interpreted as potential flows. Simultaneously, the analogy to the description of the potential function in Equation 4.1 may be noted; there, the velocity is defined as the gradient of the potential function. In groundwater flow, the filter velocity corresponds to the negative gradient of the potential function multiplied by the coefficient of permeability k_f.

$$v_{f,i} = -k_f \frac{\partial \Phi}{\partial x_i} \tag{15.4}$$

The open source library contains a code for solving potential theory questions related to groundwater flows via elementary solutions.

The program library that is provided also includes a routine in which the elementary solutions of potential theory are superimposed. The program `potential.m` uses the file `dataGW.csv` in which the input data are stored in SI units. Herein, `lx` and `ly`, in particular, signify the extension of the calculation domain in the x- and y-direction. The code `offset[x,y]` refers to the offset of the coordinate origin. At `[0,0]`, this origin lies at $\left[\frac{l_x}{2}, \frac{l_y}{2}\right]$ in the centre of the calculation domain. The notation `dx` and `dy` indicate the grid resolution of the calculation domain in the x- and y-direction. The variable `rho` is, of course, the density of the medium, `g` is the gravity constant and `kf` is the filter velocity. The number of streamlines to be drawn in the x- and y-direction are given by `numberSLx` and `numberSLy`, respectively (see routine `plotStreamlines.m`).

```
Data for Potential Flow Problems
#
lx=600
ly=400
offset=[0,0]
dx=5
dy=5
rho=1000
g=9.8065
kf=1E-3
numberSLx=10
numberSLx=20
```

The program `potential.m` searches the folder in which it is stored for files `parallel.csv`, `source.csv`, `dipol.csv` and `vortex.csv`. If these files exist, the data are read in from the third line on (`header=2`).
The meanings in `source.m` are:

```
SQ=[-.01,.01] % source/sink, negative signs correspond to a with-
drawal (sink); in m3/(sm); separated by commas, any number of
sources/sinks may be specified.
SposX=[-50,150] % x-positions of the sources/sinks.
SposY=[-50,150] % y-positions of the sources/sinks.
```

The meanings in `parallel.m` are:

```
u0 % parallel flow in the x-direction.
v0 % parallel flow in the y-direction.
```

The meanings in `dipol.m` are:

```
Dm=[.04,.05] % dipole strength in m3/s; separated by commas, any
number of dipoles may be specified.
DposX=[0,100] % x-positions of the dipoles.
DposY=[-100,0] % y-positions of the dipoles.
```

The meanings in `vortex.m` are:

```
Vgamma=[.04,.05] % vorticity in m2/s; separated by commas, any
number of potential eddies may be specified.
VposX=[-100,0] % x-positions of the eddy cores.
VposY=[0,-100] % y-positions of the eddy cores.
```

At the end, the program `potential.m` calls the routine `plotStreamlines.m`, which provides for the visualisation of the results.

Example

Extraction well and contamination

In this example, we investigate whether a drinking water well has been contaminated by oil from a car accident. The aquifer has a coefficient of permeability $k_f = 1.0 \times 10^{-3}\,\mathrm{m/s}$. The well withdrawal rate ($q = -0.02\,\mathrm{m^3/(s\,m)}$ at $(x,y) = (0,0)$) is overlaid by a parallel flow in the x-direction with velocity $u_0 = 1.0 \times 10^{-5}\,\mathrm{m/s}$. The accident occured at the coordinate $(x_0, y_0) = (300, 200)$.
For the solution of this problem, we describe the Lagrangian path of the oil contamination in the aquifer. To this end, we may use the program for the calculation of potential flows provided in the Octave library.
The Lagrangian path that a particle covers in Euler's field theory is the integral of the velocity with respect to time.

$$\vec{s} = \int \vec{u}\,\mathrm{d}t = \int\int \left(\frac{\partial \vec{u}}{\partial t} + \vec{u}\frac{\partial \vec{u}}{\partial \vec{s}} \right) \mathrm{d}t^2 \tag{15.5}$$

The result for the x- and y-directions is:

$$\begin{aligned} x &= \int\int \left(\frac{\partial u}{\partial t} + u\frac{\partial u}{\partial x} + v\frac{\partial u}{\partial y} \right) \mathrm{d}t^2 = \int \left(u_0 + \frac{\partial u}{\partial t}\,\mathrm{d}t + u\frac{\partial u}{\partial x}\,\mathrm{d}t + v\frac{\partial u}{\partial y}\,\mathrm{d}t \right) \mathrm{d}t \\ &= x_0 + u_0\,\mathrm{d}t + \frac{\partial u}{\partial t}\,\mathrm{d}t^2 + u\frac{\partial u}{\partial x}\,\mathrm{d}t^2 + v\frac{\partial u}{\partial y}\,\mathrm{d}t^2 \end{aligned} \tag{15.6}$$

$$\begin{aligned} y &= \int\int \left(\frac{\partial v}{\partial t} + u\frac{\partial v}{\partial x} + v\frac{\partial v}{\partial y} \right) \mathrm{d}t^2 = \int \left(v_0 + \frac{\partial v}{\partial t}\,\mathrm{d}t + u\frac{\partial v}{\partial x}\,\mathrm{d}t + v\frac{\partial v}{\partial y}\,\mathrm{d}t \right) \mathrm{d}t \\ &= y_0 + v_0\,\mathrm{d}t + \frac{\partial v}{\partial t}\,\mathrm{d}t^2 + u\frac{\partial v}{\partial x}\,\mathrm{d}t^2 + v\frac{\partial v}{\partial y}\,\mathrm{d}t^2 \end{aligned} \tag{15.7}$$

Due to the steadiness of the flow, the local derivatives $\frac{\partial u}{\partial t}$ and $\frac{\partial v}{\partial t}$ are zero. The velocities u_0 and v_0 are the constants of integration at location (x_0, y_0), which in turn are the constants of integration and the starting values of the path.
The two velocity components may be determined in the field $(u, v) = f(x, y)$ via the calculation of the potential and flow function (see Figure 15.2). Starting from $(x_0, y_0) = (300, 200)$, the Lagrangian path shows that the oil contamination does not reach the well (see red streamline in Figure 15.2).

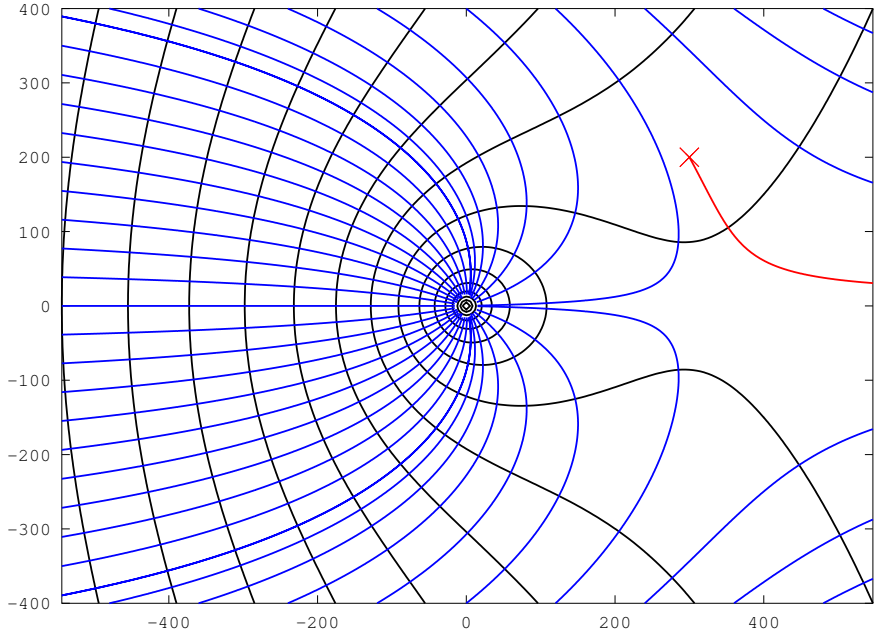

Figure 15.2: Example: Contamination of an extraction well?

Example

Cooling water extraction and injection well

For the provision of district cooling, water is to be withdrawn from an aquifer, passed through a heat exchanger and resupplied to the aquifer. In this context, the question of whether the heated and resupplied water enters the extraction well must be examined. The boundary conditions are as follows: the coefficient of permeability of the aquifer amounts to $k_f = 1.0 \times 10^{-3}\,\mathrm{m/s}$; the well withdrawal rate $q = -0.01\,\mathrm{m}^3/(\mathrm{s\,m})$ is in effect at $(x,y) = (-50,-50)$, while the same quantity $q = 0.01\,\mathrm{m}^3/(\mathrm{s\,m})$ is returned at $(x,y) = (150,150)$; the groundwater flows in the x-direction with velocity $u_0 = 1.0 \times 10^{-5}\,\mathrm{m/s}$.
Will there be a hydraulic short circuit, i. e. ingress of heated water into the extraction well? When entering the corresponding parameters, the potential and streamlines shown in Figure 15.3 result. Red streamlines with heated fluid lead from the injection well into the extraction well. Therefore, the distance that was chosen is too short.

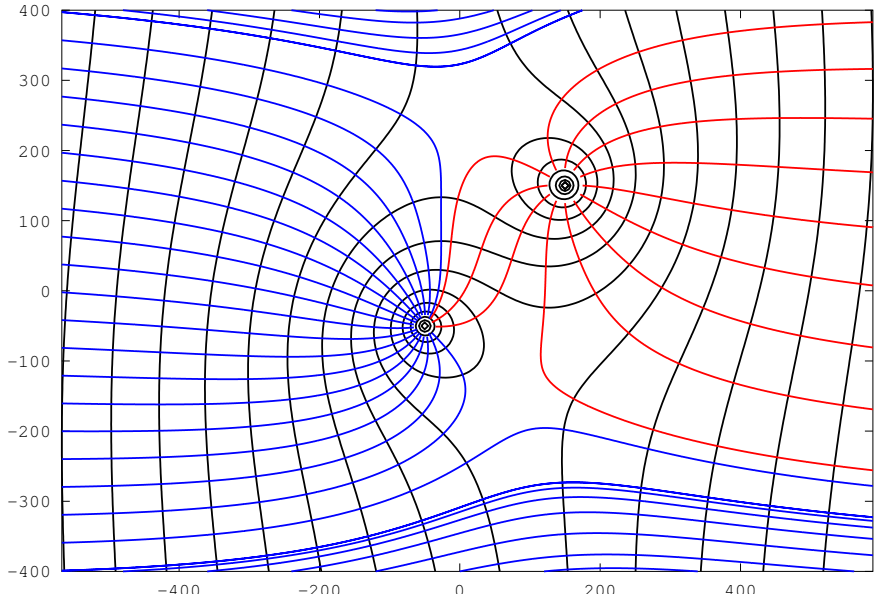

Figure 15.3: Example: Cooling water withdrawal and return via an injection well.

Part III
Excercises with solutions

Chapter 16
Exercises[A]

1 Hydrostatics

Exercise 1.1

Draw the horizontal and vertical pressure diagrams in the figures below.

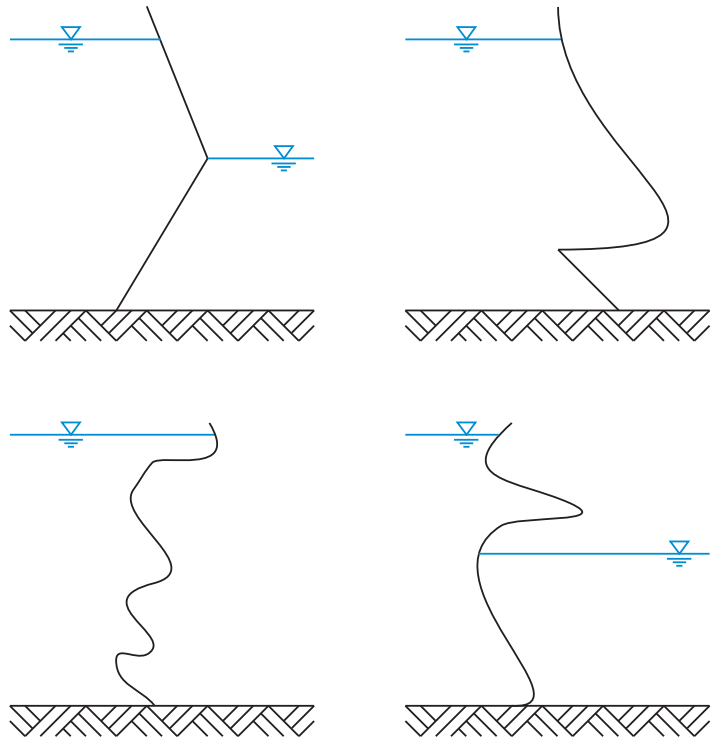

[A] The exercises were developed by the author and were set in a form similar to those in diploma examinations between 2003 and 2012 at the Technical University of Munich.

C. Rapp, *Hydraulics in Civil Engineering*,
https://doi.org/10.1007/978-3-031-54860-4_16

Exercise 1.2

A roller dam ($D = 3.0\,\mathrm{m}$) closes at an angle of $\alpha = 20°$ with respect to vertical.

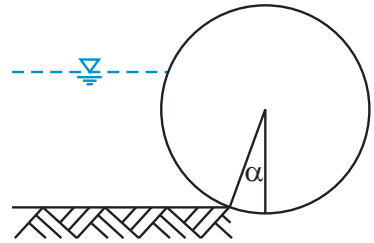

a) Draw the vertical pressure diagram for the case of maximum buoyancy.
b) Calculate the magnitude and direction of the resulting force acting on the roller.
c) Calculate the moment of force that must be counteracted by the roller axis.

Exercise 1.3

An oil-filled ($\rho_{\mathrm{oil}} = 800\,\mathrm{kg/m^3}$) rotation-symmetrical vessel with hemispherical bottom is located in a water-filled container that is also rotation-symmetrical. Answer the questions in parts a) through d) on the basis of the following values:

$$D = 4.0\,\mathrm{m},\ d = 2.5\,\mathrm{m},\ h = 5.0\,\mathrm{m}$$

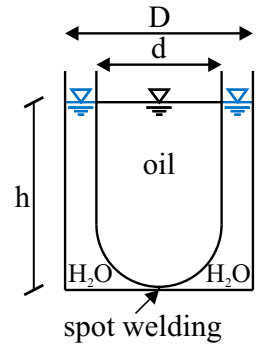

a) Draw the resulting pressure distribution on all the walls.
b) Calculate the support force of the foundation.
c) Calculate the pressure force acting on the bottom of the water-filled container.
d) Calculate the force that the weld seam must resist.

Exercise 1.4

A cylindrical glass of mass 116 g and with dimensions $R = 2.5\,\mathrm{cm}$ and $h = 10.0\,\mathrm{cm}$ is placed upside-down in a square container that is filled with water. Contact between the glass and the container is not tight; hence, water may flow in and out. The atmospheric pressure amounts to $p_0 = 101\,300\,\mathrm{N/m^2}$. Assume that the glass does not tip over.

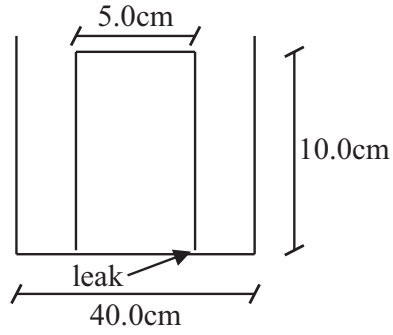

a) How much water must be poured into the container so that the glass floats?
b) Draw the pressure distribution on the glass at the moment shortly before it floats.

Exercise 1.5

The retaining wall illustrated in the sketch below is modelled by the equation $y = x^2; x \in (0 \ldots 3)$. The water level is at 9.0 m.

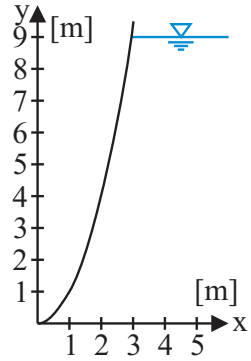

a) Draw the resulting horizontal and vertical pressure diagrams on the sketch.
b) Calculate the resulting forces per unit width in the horizontal and vertical direction.
c) Calculate the magnitude and direction of the resulting force.

Exercise 1.6

The weir shown below may turn about point A and opens clockwise. The lower part of the weir has the shape of a quadrant with radius $R = 3.0\,\text{m}$. The weight force is $F_G = 30\,\text{kN/m}$ and the centre of gravity CG of the weir is shown. Forces due to friction are assumed to be negligible.

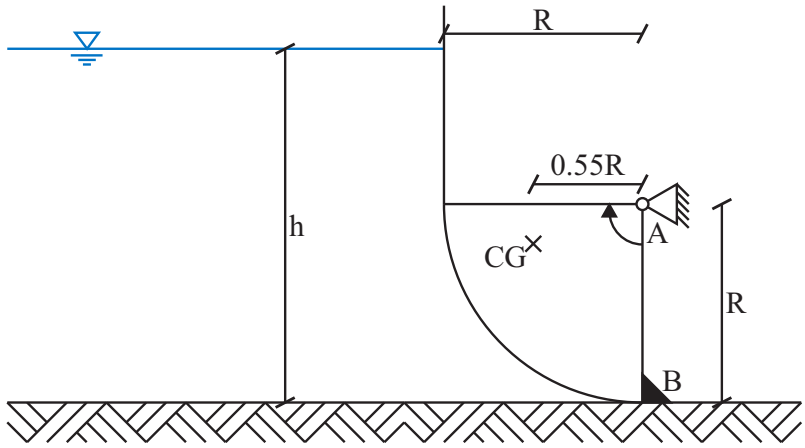

a) Draw the resulting pressure diagram at the closed weir baffle, and determine the resulting magnitude and direction of the pressure force per unit width at a water level of $h = 5.0\,\mathrm{m}$.
b) Determine the moment of force that is required to open the weir, when the water level is at $h = 5.0\,\mathrm{m}$.
c) Determine the maximum support force that the thrust bearing at point B must exert when the baffle is closed. What is the water level when this force applies?

2 Outflow through openings

Exercise 2.1

Two basins identically constructed with base area $A = 100\,\mathrm{m}^2$ are connected via a pipeline ($L = 20.0\,\mathrm{m}$; $f_\mathrm{D} = \mathrm{const.} = 0.03$; $d = 0.10\,\mathrm{m}$). Both the inlets and outlets are located at the bottom of the containers. One of the containers is situated 5.0 m higher than the other and is filled with water up to a height of $h = 2.0\,\mathrm{m}$; the lower one is completely empty. The water level of the upper basin is to be lowered to 1.0 m. How long does that take? In your calculation, neglect the acceleration of the water column as well as the water in the pipeline.

Exercise 2.2

The aeration basin of a treatment plant is to be designed for a wastewater flow rate of $0.2\,\mathrm{m}^3/\mathrm{s}$ to $1.0\,\mathrm{m}^3/\mathrm{s}$. The available base area of the basin is 20 m by 40 m. The discharge is spilled over a fixed weir ($\mu = 0.6$) along the entire short side of the basin. The minimum average dwell time of the wastewater in the basin should be assumed to be 40 min.

a) Determine the minimum required basin depth and weir height.
b) Calculate the dwell time at minimum inflow.

Exercise 2.3

A container with a constant base area $A_1 = 1.0\,\mathrm{m}^2$ is drained into an immediately adjacent container that is initially empty with cross-sectional area $A_2 = 0.5 \times A_1$. The discharge from the first container into the second is via an opening that is located $1.0\,\mathrm{m}$ above the bottom of the container (see sketch). The orifice has a cross-sectional area of $5.0\,\mathrm{cm}^2$ with a discharge coefficient of $\mu = 0.65$.

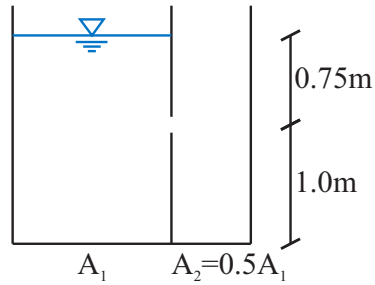

a) Where (at what height) is the balanced condition established?
b) During how much time does a free discharge take place? This may be solved without subtask a).
c) How long does it take for the balanced condition to be established?

Exercise 2.4

The completely drained rainwater retention basin in the Munich Hirschgarten is filled continuously during a heavy rain event at the rate of $10\,\mathrm{m}^3/\mathrm{s}$. Assume a constant base area $A = 2.0 \times 10^5\,\mathrm{m}^2$. The overflow (round crested weir) is located $10.0\,\mathrm{m}$ above the bottom of the basin ($b = 5.0\,\mathrm{m}$, $\mu = 0.70$). Accounting for a potential influence from backwater is not the object of this problem.

a) When does the rain-induced overflow start?
b) At what level of the water in the rainwater retention basin is a balanced condition established?
c) Calculate the time it takes for this condition to be reached.
d) How much untreated wastewater has entered the receiving water up to this point of time?

3 Momentum equation

Exercise 3.1

Calculate the horizontal support force for the Y-pipe, shown in the sketch, of a hydropower plant. At cross-section 1, the pressure height is determined to be $30\,\mathrm{mH_2O}$ and the discharge is $10\,\mathrm{m}^3/\mathrm{s}$. Furthermore, the diameters $d_1 = 1.0\,\mathrm{m}$ and $d_2 = 0.60\,\mathrm{m}$ as well as the energy loss between cross-sections 1 and 2, $\Delta e_{1-2} = 2.0\,\mathrm{m}$, are given.

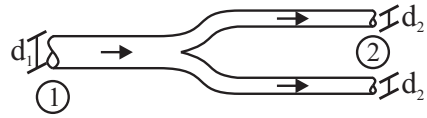

Exercise 3.2

Consider a U-pipe with a circular cross-section whose inlet diameter tapers from $d_I = 0.4\,\mathrm{m}$ to the outlet diameter $d_O = 0.2\,\mathrm{m}$. The pipe axes are spaced $0.5\,\mathrm{m}$ apart. For a discharge of $Q = 0.05\,\mathrm{m}^3/\mathrm{s}$, a pressure height of $0.5\,\mathrm{mH_2O}$ exists at the inlet.

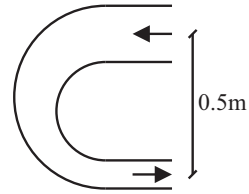

What is the magnitude of the horizontal force acting on the pipe curvature if

a) the U-pipe lies horizontally and friction losses are neglected?
b) the U-pipe stands vertically (inlet cross-section on top) and the minor (local) losses are set to $\Delta e = 0.2\left(\frac{\Delta v^2}{2g}\right)$?

Exercise 3.3

The problems below are to be solved for a water cannon used by the police. Water is withdrawn from a hydrant (location 1). Answer the following questions regarding locations 1 – 5:

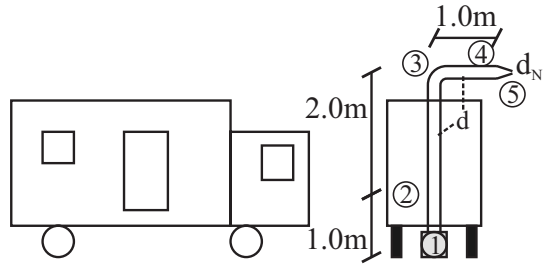

$d = 0.10\,\mathrm{m}$	$d_{\mathrm{nozzle}} = 0.01\,\mathrm{m}$	$f_{\mathrm{D}} = 0.03$	$K_{\mathrm{bend}} = 0.80$	$K_{\mathrm{nozzle}} = 0.2\frac{v^2_{\mathrm{nozzle}}}{2g}$

a) Draw a completely labelled energy diagram (locations 1 – 5).
b) Determine the discharge if the pressure is $p_2 = 4.0\,\mathrm{bar}$ at location 2.

If you have not calculated the values in subtask b), you may use the following alternative values for exercises c), d) and e): discharge $Q = 4.0\,\mathrm{L/s}$; pressure height just before the nozzle at location 4 is $p_4 = 30.0\,\mathrm{m}$

c) Calculate the resulting horizontal force acting on the police car.

d) What force is the connection between nozzle and pipe subjected to?
e) How far does the water splash? Please note the formula for the horizontal trajectory (assume a loss-free situation).

$$\vec{x}(t) = \begin{pmatrix} v_0 \cdot t \\ -\frac{1}{2} \cdot g \cdot t^2 \end{pmatrix}$$

Exercise 3.4

A horizontal pipe expansion is attached to the feed pipe by a flange. The cross-sectional area A_1, the velocity v_1 and the pressure p_1 are given.

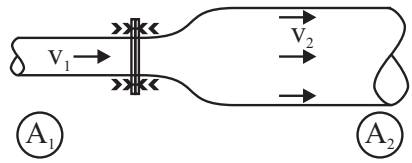

$$\boxed{A_1 = 7.00\,\text{cm}^2} \quad \boxed{v_1 = 4.00\,\text{m/s}} \quad \boxed{p_1 = 1.0 \times 10^5\,\text{N/m}^2}$$

a) First, the cross-sectional area A_2 is to be determined such that the velocity height in A_2 corresponds to one-seventh of the velocity height in cross-sectional area A_1.
b) Now calculate the pressure in cross-sectional area A_2. Take the energy losses into account: $K_{\text{exp}} = 0.5$ (related to v_2).
c) What is the magnitude of the horizontal force acting on the flange?

Exercise 3.5

Water in a channel with a circular cross-section is redirected with a deflection angle of 90° in a shaft structure. At a discharge of 40 L/s, the flow depth upstream from the shaft corresponds to the flow depth downstream. The pipe diameter is 30.0 cm and the flow depth was measured as 15.0 cm.

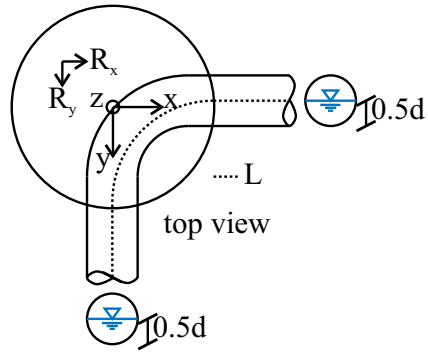

a) What type of flow exists (sub- or supercritical flow)?
b) What is the resulting horizontal force counteracted by the shaft?

4 Free surface flows

Exercise 4.1

A sketch of a rectangular open channel section with a width of 5.0 m and a discharge of $20\,\mathrm{m^3/s}$ is shown below. A stilling basin with a concrete bottom is arranged downstream from a block ramp with $w_1 = 1.5\,\mathrm{m}$. The stilling basin ends with a vertical step $w_2 = 0.50\,\mathrm{m}$.

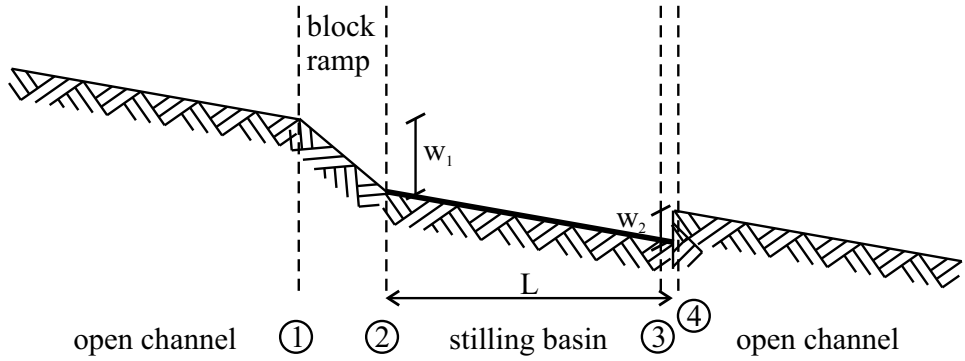

$Q = 20\,\mathrm{m^3/s}$	$w_1 = 1.5\,\mathrm{m}$	$n_{\mathrm{sb}} = 1.43 \times 10^{-2}\,\mathrm{s/m^{\frac{1}{3}}}$	$J_{B,\mathrm{sb}} = 0.8\,\%$	$\Delta e_{1-2} = \frac{v_c^2}{2g}$
$b = 5.0\,\mathrm{m}$	$w_2 = 0.5\,\mathrm{m}$	$n_{\mathrm{channel}} = 2.86 \times 10^{-2}\,\mathrm{s/m^{\frac{1}{3}}}$	$J_{B,\mathrm{channel}} = 0.8\,\%$	$\Delta e_{3-4} = \frac{0.1 \cdot v_{N,\mathrm{channel}}^2}{2g}$

a) Calculate the normal water depths, the critical depth and the corresponding specific energies in all areas.
b) Calculate the length L in such a manner that the hydraulic jump does not quite reach into the area of the block ramp.

$$L_{\mathrm{HJ}} = 8.5 y_l \left(\mathrm{Fr}_l - 1.7\right)$$

c) Draw a completely labelled energy diagram.

Exercise 4.2

The bridge over the Isar River in Munich-Thalkirchen is to be examined for a possible flood situation. In this area, the Isar may be approximated by a rectangular cross-section (width $b = 30.0\,\mathrm{m}$). Make the assumptions regarding measurements and quantities as indicated in the following sketch:

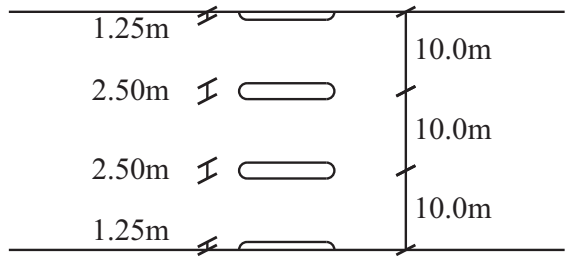

$Q = 500\,\mathrm{m^3/s}$	$b = 30.0\,\mathrm{m}$	$J_B = 0.3\,\%$	$n = 2.86 \times 10^{-2}\,\mathrm{s/m^{\frac{1}{3}}}$

a) Calculate the normal water conditions.
b) Due to a log jam in the confined area, a loss of $K = 0.5$ related to the critical velocity in the constriction, $v_{c,\mathrm{cons}}$, occurs. Determine the course of the water level and draw the energy diagram.
c) Calculate the total length of the influence of the log-jammed bridge on the flow.

Exercise 4.3

A weir ($\mu = 0.60$, $w = 1.50\,\mathrm{m}$, $\Delta z = 1.0\,\mathrm{m}$) is built in a channel with rectangular cross-section ($b = 8.0\,\mathrm{m}$) and a discharge of $Q = 40\,\mathrm{m^3/s}$. At the tail of the weir, the open channel width changes to $b = 12.0\,\mathrm{m}$. The backwater influence need not be examined. The downstream normal water flow depth amounts to $y_N = 1.35\,\mathrm{m}$.

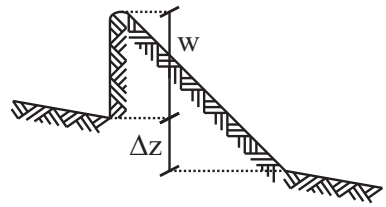

a) Calculate the overflow height as well as the flow depths both upstream and downstream from the weir.
b) A hiker measures the distance between the tail of the weir and the toe of the hydraulic jump as 20.0 m. Calculate the Manning coefficient and the gradient of the bed for this open channel section.

Exercise 4.4

An existing open channel with rectangular cross-section ($b = 5.0\,\mathrm{m}$) is to be developed over a length of 5.0 km in a more natural way (renaturated). To stabilise the bed, the original open channel has a bottom step of 1.0 m every 1000 m along its length. Assume that energy losses of $0.1 \cdot k_c$ occur in the area of the bottom step. The new open channel is to be expanded to a width of $b_{\mathrm{new}} = 8.0\,\mathrm{m}$ and provided with twice the flow length by the meanders. Secondary flows are not to be taken into account. The roughness of the bed will not change.

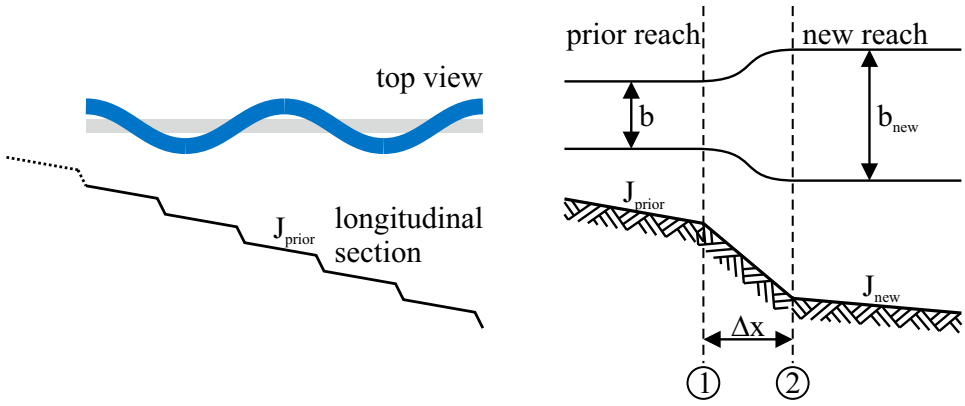

$Q = 15\,\mathrm{m^3/s}$	$b = 5\,\mathrm{m}$	$n = 2.86 \times 10^{-2}\,\mathrm{s/m^{\frac{1}{3}}}$	$J_{B,\mathrm{prior}} = 0.5\,\%$	$b_{\mathrm{new}} = 8\,\mathrm{m}$

a) Evaluate whether bottom steps are required for the new open channel. Note: the mean flow velocity must not increase; normal water conditions are to be considered.

In the following subtasks, only the transition from the existing to the renaturated open channel is to be considered (see right-hand figure).

b) Quantitatively specify the course of the water level along the illustrated flow sections (right-hand figure). There is no air entrainment at the bottom step.

c) Specify the length of the required bottom reinforcement in the renaturated section. The length of the hydraulic jump may be calculated by means of the following formula:

$$L_{\mathrm{HJ}} = 8.5 y_l \left(\mathrm{Fr}_l - 1.7\right)$$

d) Draw an energy diagram of the region where the existing geometry connects to the renaturated one (see right-hand figure).

Exercise 4.5

A channel with rectangular cross-section widens from b_1 to b_2. The first part of the open channel has gradient $J_{B1} = J_{B2}$ until point 3. From there, the open channel has slope J_{B3}. In each of the sections 1 – 3, normal water conditions are attained.

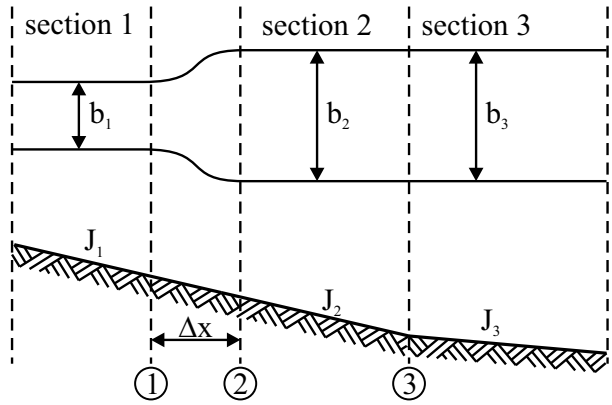

$Q = 2.0\,\mathrm{m}^3/\mathrm{s}$	$b_1 = 1.0\,\mathrm{m}$	$n_1 = 3.33 \times 10^{-2}\,\mathrm{s/m}^{\frac{1}{3}}$	$J_{B1} = 2.0\,\%$
$\Delta e_{1-2} = \Delta x \cdot J_{B1}$	$b_2 = 4.0\,\mathrm{m}$	$n_2 = 2.5 \times 10^{-2}\,\mathrm{s/m}^{\frac{1}{3}}$	$J_{B2} = 2.0\,\%$
	$b_3 = 4.0\,\mathrm{m}$	$n_3 = 2.5 \times 10^{-2}\,\mathrm{s/m}^{\frac{1}{3}}$	$J_{B3} = 1.0$

a) Calculate the normal conditions for all sections.
b) Specify the flow conditions in the individual sections. Substantiate the flow depths in cross-sections 1 – 3.
c) Draw a complete energy diagram that contains all characteristic specific energies and flow depths.

Exercise 4.6

A rectangular channel ($Q = 40.0\,\mathrm{m}^3/\mathrm{s}$) is depicted below. It tapers between cross-sections A and B (distance 5.0 m) from width b_1 to b_2. The tapering causes an energy loss of $\Delta e = 0.1 \cdot k_{N2}$ (k_{N2} = velocity height of the normal conditions in section 2). Simultaneously, slope and roughness change at cross-section A. In both sections, normal conditions occur. Complete parts a), b) and c) using the given quantities.

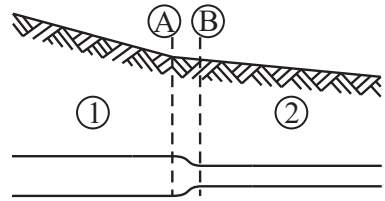

section 1	$J_{B1} = 1.5\,\%$	$n_1 = 0.025\,\mathrm{s/m}^{\frac{1}{3}}$	$b_1 = 12.0\,\mathrm{m}$
section 2	$J_{B2} = 0.3\,\%$	$n_2 = 0.020\,\mathrm{s/m}^{\frac{1}{3}}$	$b_2 = 8.0\,\mathrm{m}$

a) Calculate the normal depths with their associated specific energies and flow types in the open channel sections.
b) Determine the course of the water level.
c) Draw a complete energy diagram.

5 Pipe flow

Exercise 5.1

The sketch shows a hydropower plant. Upstream and downstream from the turbine, pipes with different diameters are installed.

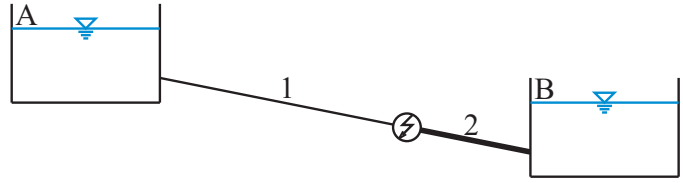

$L_1 = 2000\,\text{m}$	$d_1 = 1.0\,\text{m}$	$f_{D1} = 0.025$
$L_2 = 1000\,\text{m}$	$d_2 = 1.5\,\text{m}$	$f_{D2} = 0.020$
$H_A = 1050\,\text{m}$	$H_B = 300\,\text{m}$	$\eta_T = 0.80$

a) For what discharge does the power of the turbine P_T reach the maximum value?
b) What net head is available?
c) What power does the turbine reach?

Exercise 5.2

A pipeline is to be laid between two containers. For the transport of water from container A to container B, a pump that is to operate an average of 10 hours per day must be installed. Assume the price of electricity is 0.15 €/kWh.

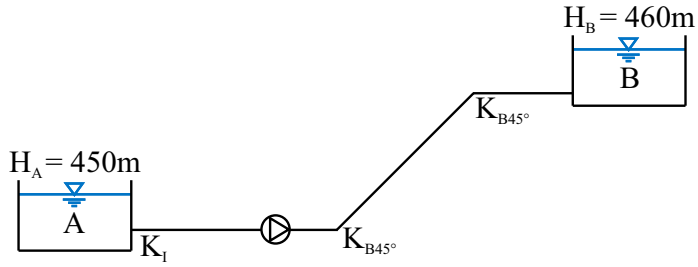

$L = 5000\,\text{m}$	$K_I = 0.5$	$K_{B45^\circ} = 0.3$	$k_s = 3.0\,\text{mm}$	$T = 10\,^\circ\text{C}$	$\eta_P = 0.80$

a) Determine the pump costs per year for a pipe with diameter $d = 1.5\,\text{m}$ and a discharge of $0.7\,\text{m}^3/\text{s}$.

The construction costs for one metre of pipeline, depending on the diameter d, amount to $d \cdot 7000\,€/\text{m}$.

b) Determine the optimum (most cost-effective) diameter of the pipe for $Q = 0.7\,\text{m}^3/\text{s}$ assuming that the construction is designed to last 30 years. The friction coefficient f_D from subtask a) may be used in subtask b) (substitute result $f_D = 0.024$).

Exercise 5.3

A pumped storage power plant is shown below.

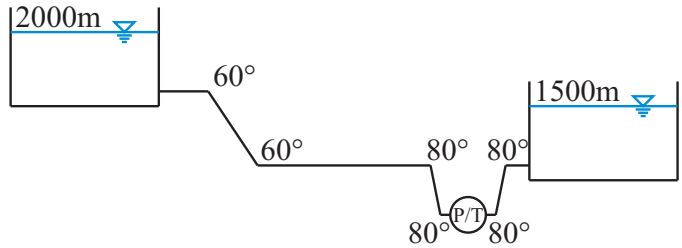

$d = 2.0\,\text{m}$	$L = 5000\,\text{m}$	$\eta_{T/P} = 0.9$	$K_{B60^\circ} = 0.5$	$K_{B80^\circ} = 0.7$	$k_s = 0.1\,\text{mm}$	$T = 5\,^\circ\text{C}$

a) Calculate the design discharge if a power of 92.9 MW is to be tapped at the turbine. Note: Start the f_D iteration with $f_{D,\,\text{step }0} = 0.01$.
b) Draw a labelled energy diagram.
c) Calculate the discharge for a pump that consumes 50 MW of electrical power using the friction coefficient of the pipe, f_D, that was determined in subtask a).
d) What is the maximum geodetic height at which the pump turbine can be installed while avoiding cavitation? Assume an energy height of 1500 m.a.s.l. and local velocities in the pump turbine of 25 m/s.

Exercise 5.4

A simplified sketch of the drinking water supply system for the city of Munich near Oberau is shown below. Water is pumped from the confined aquifer into a large tank. From there, the water, driven only by the pressure gradient, flows to the reservoir in Forstenrieder Park. Perform the calculations requested in subtasks a) and b).

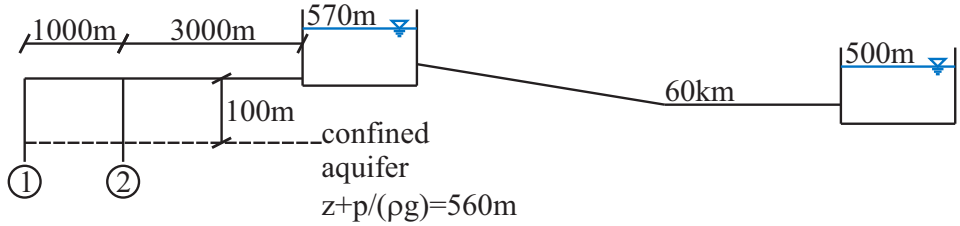

$T = 5.0\,°\text{C}$	$d_{\text{all}} = 1.40\,\text{m}$	$k_s = 0.5\,\text{mm}$	$\eta_P = 0.7$	$K_I = 0.5$

a) Calculate the steady discharge in the pipeline to Munich. Use the pipe friction coefficient determined herein for subtask b).
b) Two identical pumps that consume the same amount of power are to be employed for the two feed pipes. Calculate the partial discharges in feed pipes ① and ② as well as the power consumption of the pumps for the discharge that was determined in the previous exercise.

Exercise 5.5

A pipeline system with three containers is shown below. Water is pumped from container 2 into the two containers 1 and 3. You may refer to further data from the table below.

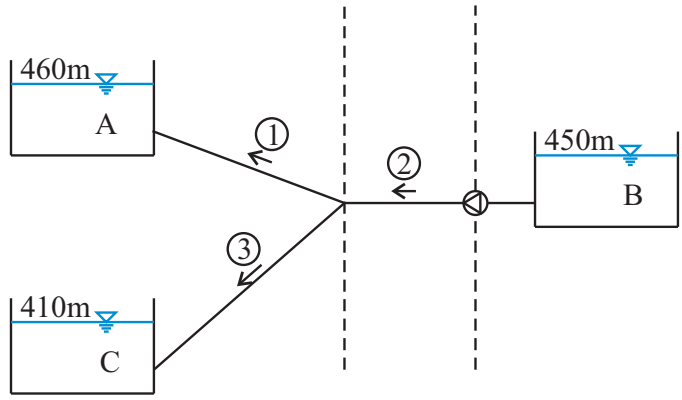

$H_1 = 460\,\text{m}$	$P_P = 500\,\text{kW}$	$l_1 = 3000\,\text{m}$	$d_1 = 1.00\,\text{m}$	$f_{D1} = 0.018$
$H_2 = 450\,\text{m}$	$\eta_P = 0.85$	$l_2 = 2000\,\text{m}$	$d_2 = 1.00\,\text{m}$	$f_{D2} = 0.020$
$H_3 = 410\,\text{m}$	$K_I = 0.5$	$l_3 = 2000\,\text{m}$	$d_3 = 0.30\,\text{m}$	$f_{D3} = 0.020$

a) Draw a complete energy diagram.
b) Specify the equations for the discharges in lines 1, 2 and 3 if the pump power consumption is $P_P = 500\,\text{kW}$. Specify the equation for the pressure height at the junction.

$10\,000\,\text{m}^3$ water per day are to be delivered into container 3.

c) How much water flows into container 1 during the operating time of the pump?
d) What are the electricity costs per day? Assume $0.20\,€$ for $1.0\,\text{kWh}$.

6 Cross-cutting issues

Exercise 6.1

The water supply for a village in the Ecuadorian rain forest is to be investigated. Consider the idealised system illustrated in the following figure. The upper tank that is initially filled up to 570 m.a.s.l. is continuously supplied with water at a rate of 0.9 L/s from a mountain spring. The discharge from tank A with base area $A_A = 1.35\,\text{m}^2$ is controlled by the consumers in the village (pipeline data: $d = 4.0\,\text{cm}$, $l = 100\,\text{m}$, $f_D = 0.02$). The water level in tank B remains constant.

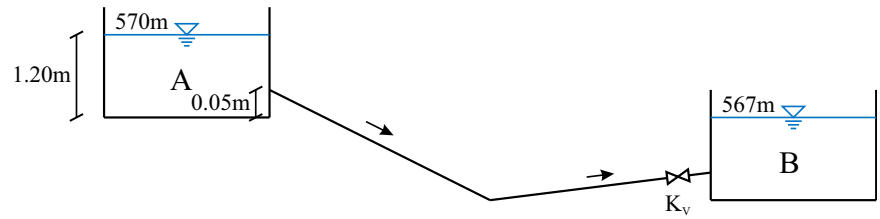

a) What loss must the valve exhibit in order to keep the water level in tank A constant?
b) Calculate the time that elapses until the water level in tank A has dropped to the inflow of the pipe when the valve is fully open ($K_V = 0$).

Exercise 6.2

For a drinking water supply, unconfined groundwater is to be accessed. Cold water at 5 °C is delivered via a pipeline of length 8.0 km into a tank.

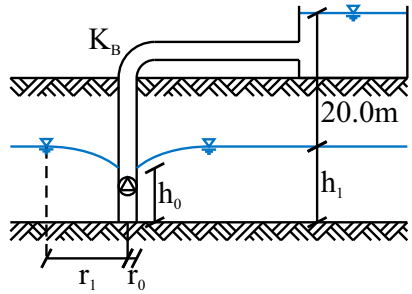

$\eta_P = 0.80$	$K_B = 0.4$	$d_{\text{pipe}} = 0.40\,\text{m}$	$k_s = 1.0\,\text{mm}$
$h_1 = 40.0\,\text{m}$	$r_0 = 0.20\,\text{m}$	$r_1 = 3000\,\text{m}$	$k_f = 1.0 \times 10^{-4}\,\text{m/s}$

a) How much water could initially be delivered (without lowering the groundwater level (that is, $h_0 = h_1$)) if the pump consumes 7.5 kW of electrical power?

Use the friction coefficient determined in question a) for the following subtasks of the problem. Bear in mind that the groundwater level decreases due to withdrawal (see following equation).

$$Q = \pi \cdot k_f \frac{h_1^2 - h_0^2}{\ln\left(\frac{r_1}{r_0}\right)}$$

b) Replace the discharge in the energy equation with the above expression.
c) How much water actually flows into the tank?
d) How far does the groundwater level drop?

Exercise 6.3

The pipeline shown below has a constant slope. The valve V of the rotation-symmetrical air vessel ($p_A = 1013\,\text{mbar}$) is initially closed. The following subtasks of the problem are to be solved for the respective steady-state cases, and $T = \text{const}$.

a) Calculate the pressure in the pipe where the air vessel is located.
b) How much would the water level in the air vessel increase if the valve were opened?
c) How does the water level change qualitatively when throttling the discharge at the lower tank?

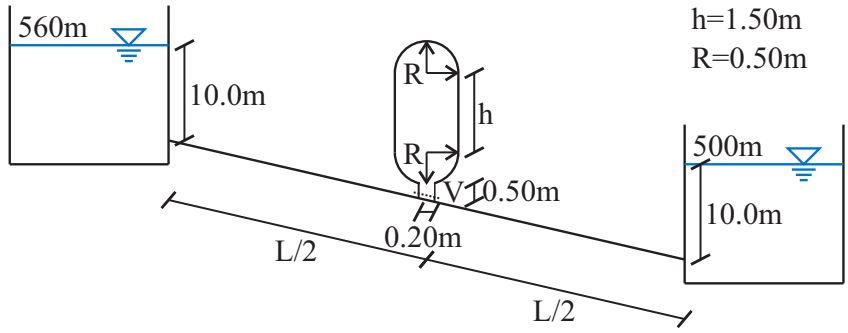

$L = 8000\,\text{m}$	$d_{\text{pipe}} = 0.50\,\text{m}$	$f_{\text{D}} = 0.020$

Exercise 6.4

A trash rack of width b is positioned at the rectangular headwater of a hydropower plant. In the upstream water, normal conditions prevail. The minor energy losses K were measured at the rack depending on v_{upstream}. Assume that the discharge per unit width does not change in the vicinity of the rack.

a) What water depth results downstream from the rack?
b) What is the magnitude of the horizontal forces acting on the rack?

$J_B = 2.0\,\%$	$b = 7.0\,\text{m}$	$Q = 30\,\text{m}^3/\text{s}$	$K = 0.2$	$n = 0.02\,\text{s}/\text{m}^{\frac{1}{3}}$

7 Unsteady free surface flows

Exercise 7.1

In a rectangular channel of width $b = 7.50\,\text{m}$, each of two gauges that are spaced $2.0\,\text{km}$ apart indicate a flow depth of $y = 2.10\,\text{m}$. Separated by a time interval of $589\,\text{s}$, both jump to $y = 2.55\,\text{m}$. Specify:

a) the propagation velocity of the disturbance;
b) the original discharge;
c) the change in the discharge;
d) the name of the phenomenon.

Exercise 7.2

At the Finsing power plant located at the Mittlere Isar Kanal, the discharge must be reduced abruptly from $55\,\text{m}^3/\text{s}$ to $30\,\text{m}^3/\text{s}$ (assume that we are dealing with an idealised rectangular cross-section). Solve the following subtasks taking into account the given conditions:

$$\boxed{Q_0 = 55\,\mathrm{m^3/s}} \boxed{\Delta Q = -25\,\mathrm{m^3/s}} \boxed{y_0 = 6.0\,\mathrm{m}} \boxed{b = 9.0\,\mathrm{m}}$$

a) Calculate the propagation velocity of the disturbance.
b) State whether the freeboard of 1.0 m is maintained during the regulation process if it was 1.5 m in the steady-state condition.
c) When does the regulation process have an influence on the water level at the weir in Oberföhring situated 8.0 km upstream?

Exercise 7.3

The following photo was taken after the sudden closure of the sluice gate in a laboratory flume (upstream from the sluice gate). The width of the open channel is 0.20 m, and the steady-state discharge was 5.0 L/s.

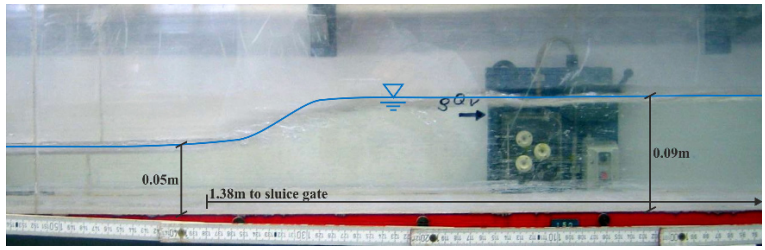

a) What was the steady-state flow velocity?
b) Record the height of the surge seen in the photo.
c) Calculate the propagation velocity of the surge wave.
d) What is the magnitude of the propagation velocity of the surge wave?
e) When was the photo taken?
f) What is the percentage of the discharge reduction?

Chapter 17
Solutions

1 Solutions: hydrostatics

Solution 1.1

Draw a vertical line from the base point as illustrated below:

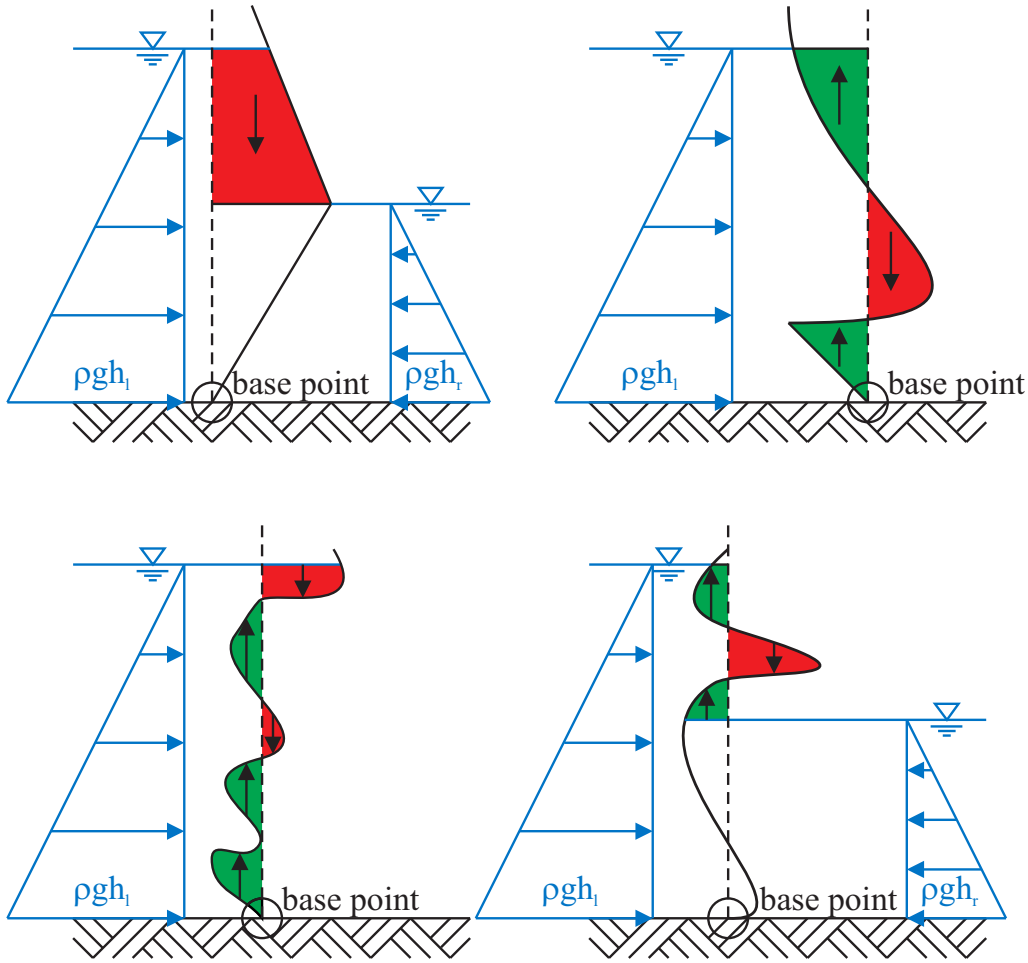

C. Rapp, *Hydraulics in Civil Engineering*,
https://doi.org/10.1007/978-3-031-54860-4_17

Solution 1.2

a) Preferably, draw a vertical line from the base point.

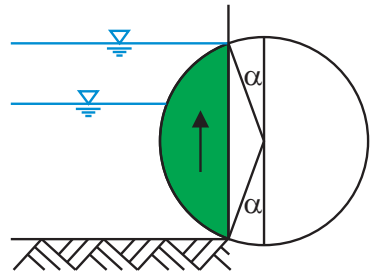

As such, it will become obvious where the maximum buoyancy results. The water level may rise up to the height where the vertical line from the base point intersects the roller dam. This is, of course, the case at an angle of 20° relative to vertical.

b) For the horizontal force, we first need the height:

$$\cos 20^\circ = \frac{h}{2 \cdot 1.5} \rightarrow h = 2.819\,\mathrm{m}$$

$$F_{H\rightarrow} = \frac{1}{2}\rho g h^2 = \frac{1}{2}\rho g \cdot 2.819^2 = 3.898 \times 10^4\,\mathrm{N/m}$$

The buoyancy area of the circle segment may be calculated via the area of the sector minus the area of the triangle; this corresponds to the green area in the diagram.

$$A_{\mathrm{segment}} = A_{\mathrm{sector}} - A_{\mathrm{triangle}} = R^2\pi\frac{140^\circ}{360^\circ} - \frac{1}{2}hR\sin 20^\circ = 2.026\,\mathrm{m}^2$$

With this, the buoyancy force is calculated:

$$F_{V\uparrow} = \rho g A_{\mathrm{segment}} = \rho g \cdot 2.026\,\mathrm{m}^2 = 1.987 \times 10^4\,\mathrm{N/m}$$

The resultant force that is applied at $\operatorname{atan}\frac{F_V}{F_H} = 27.01^\circ$ with respect to the horizontal direction has a magnitude of $|F| = \sqrt{F_V^2 + F_H^2} = 4.375 \times 10^4\,\mathrm{N/m}$.

c) The moment caused by the water pressure may be calculated via the centres of gravity of the areas that represent the vertical and the horizontal pressure force. Thereby, the lever arm of the horizontal force is spaced two thirds of the way from the water surface to the bottom, i. e. $\frac{1}{6}h = 0.470\,\mathrm{m}$ from the centre of the circle towards the bottom. The lever arm of the buoyancy area corresponds to the distance between its centre of gravity and the centre of the circle. This is (for example, as seen in [52, p. 2.12]):

$$x_{CG,\mathrm{segment}} = \frac{h^3}{12A} = 0.922\,\mathrm{m}$$

Thus, the clockwise-rotating moment of force about the centre of the circle becomes:

$$M_{\circlearrowright} = F_V \cdot x_{CG,\mathrm{segment}} - F_H\frac{1}{6}h = 0.0\,\mathrm{N\,m/m}$$

We can do without all this calculation if we just think a little. The sum of the moments about the centre is – of course – zero because the pressure is applied perpendicularly along the boundary and is therefore directed towards the centre at each point of the roller surface.

Solution 1.3

a)

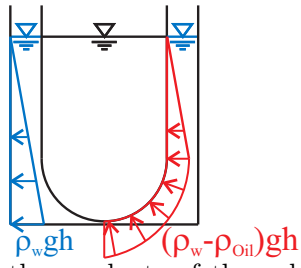

b) The weight is determined by the products of the volumes of the oil and the water with their respective densities:

$$V_{\text{oil}} = \frac{2}{3}\left(\frac{d}{2}\right)^3 \pi + \left(h - \frac{d}{2}\right)\left(\frac{d}{2}\right)^2 \pi = 22.498\,\text{m}^3$$

$$V_{\text{water}} = \left(\frac{D}{2}\right)^2 \pi \cdot h - V_{\text{oil}} = 62.832 - 22.498 = 40.333\,\text{m}^3$$

$$F_{\text{foundation}} = \rho_{\text{water}} \cdot g \cdot V_{\text{water}} + \rho_{\text{oil}} \cdot g \cdot V_{\text{oil}} = 5.722 \times 10^5\,\text{N}$$

c) The force due to pressure acting on the bottom corresponds to the pressure applied there times the area.

$$F_P = \rho_{\text{water}} \cdot g \cdot h \cdot \left(\frac{D}{2}\right)^2 \pi = 6.164 \times 10^5\,\text{N}$$

d) The weld seam must absorb the resulting force because otherwise the oil container would float.

$$F_{\text{weld seam}} = F_P - F_{\text{foundation}} = 4.415 \times 10^4\,\text{N}$$

Solution 1.4

We write down the air pressure in the glass:

$$p_1 = p_0 + \rho g \Delta h$$

The gravity force of the glass, that must be counteracted, is:

$$F_G = m \cdot g = 0.116\,\text{kg} \cdot 9.81\,\text{m/s}^2 = 1.138\,\text{N}$$

The downward-directed force due to atmospheric pressure is written as:

$$F_{p0} = p_0 A = p_0 R^2 \pi$$

The upward-directed force due to pressure within the glass is generally expressed as:

$$F_{p1} = p_1 R^2 \pi$$

a) The balance of forces for our problem reads as follows:

$$p_0 A + mg = (p_0 + \rho g \Delta h) A$$

$$\Delta h = \frac{mg}{\rho g A} = \frac{0.116}{1000 \cdot 0.025^2 \pi} = 0.0591\,\text{m}$$

This yields the pressure within the glass:

$$p_1 = 101\,300 + \rho \cdot g \cdot 0.0591 = 101\,880\,\text{N/m}^2$$

And with pressure p_1, the volume $V_1 = \frac{p_0 V_0}{p_1}$ may of course be calculated and thereby also the height of the air-filled space h_1:

$$h_1 = \frac{V_1}{A} = \frac{101\,300 \cdot 0.10 \cdot R^2 \pi}{101\,880 \cdot R^2 \pi} = 0.0994\,\text{m}$$

Thus, the water volume in the glass is:

$$V_{\text{water in the glass}} = 0.025^2 \pi\,(0.10 - 0.0994) = 1.12 \times 10^{-6}\,\text{m}^3$$

In total, the following volume must be filled; the entire area is wetted to $0.10\,\text{m} - 0.0994\,\text{m}$, additionally, the area outside of the glass is filled farther by Δh:

$$V_{\text{water total}} = 0.40^2\,(0.10 - 0.0994) + \left(0.40^2 - 0.025^2 \pi\right) \Delta h = 9.43 \times 10^{-3}\,\text{m}^3$$

b)

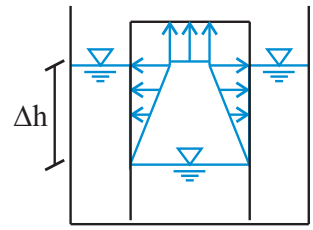

Solution 1.5

a) I'm confident that you can find the solution. Just focus on finding the **base** point.
b) You can certainly shake the horizontal pressure force out of your sleeve:

$$F_{H\leftarrow} = \frac{1}{2} \rho \cdot g \cdot 9^2 = 3.973 \times 10^5\,\text{N/m}$$

The vertical pressure force per unit width is determined via the buoyancy area:

$$F_{V\uparrow} = \rho \cdot g \cdot \frac{2}{3} \cdot 3 \cdot 9 = 1.766 \times 10^5\,\text{N/m}$$

c) The magnitude of the force and its direction are obtained via the components of the force vector:

$$|F| = \sqrt{F_V^2 + F_H^2} = 4.348 \times 10^5 \,\mathrm{N/m}$$

$$\alpha = \operatorname{atan} \frac{F_V}{F_H} = 23.96^\circ$$

Solution 1.6

a)

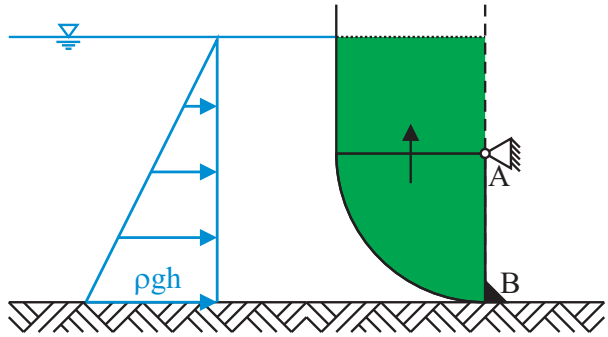

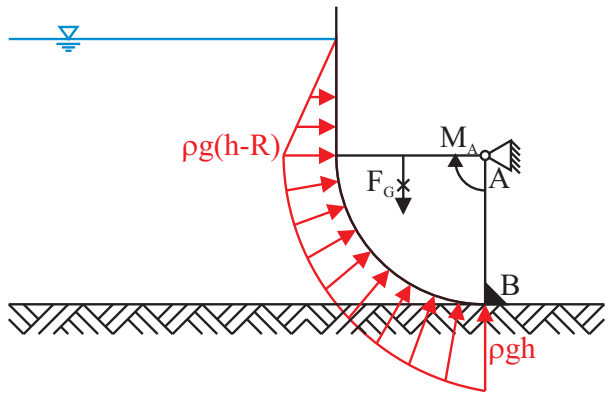

$$F_H = \frac{1}{2}\rho g h^2 = 1.226 \times 10^5 \,\mathrm{N/m}$$

$$F_V = \rho g \left(\frac{1}{4} R^2 \pi + R\,(h - R) \right) = 1.282 \times 10^5 \,\mathrm{N/m}$$

$$|F| = 1.774 \times 10^5 \,\mathrm{N/m}$$

$$\beta = \operatorname{atan} \frac{F_V}{F_H} = 46.27^\circ$$

b) The water pressure acting upon the quadrant is radial and therefore has no moment about point A; only the portion that acts on the vertical wall causes a moment.

$$\begin{aligned} M_{\circlearrowleft} &= \left(\frac{1}{2}\rho g\,(h-R)^2\right)\frac{1}{3}\,(h-R) - F_G \cdot 0.55 \cdot R \\ &= \left(\frac{1}{2}\rho g\,(5-3)^2\right)\frac{1}{3}\,(5-3) - 3.0\times 10^4 \cdot 0.55 \cdot 3.0 = -3.642\times 10^4\,\mathrm{N\,m/m} \end{aligned} \tag{17.1}$$

c) The force that must be counteracted at point B is constant for all $0 < h < R$ because the lines of action of the pressure acting on the quadrant pass through A. If the water level rises beyond the quadrant, the portion above it turns clockwise around A, which reduces the bearing force F_B. Thus, the stabilisation of the dead weight must be compensated at point B:

$$F_{B,\max} = \frac{F_G \cdot 0.55 \cdot R}{R} = 16.5\times 10^3\,\mathrm{N/m}$$

2 Solutions: outflow through openings

Solution 2.1

Well, this looks a bit difficult, although we should be happy that the container area A is constant along the height of the container. And we readily set up the discharge from the container:

$$\Delta h = \frac{Q^2}{A_{\mathrm{pipe}}^2 2g}\left(\frac{f_{\mathrm{D}} l}{d} + 1\right)$$

Δh is initially 7.0 m and is reduced with each drop that flows through the pipe. However, each drop that flows from the upper container causes a higher water level in the lower container. Therefore, we establish the following expression for Δh, noting that z is directed downward from the upper water level: $\Delta h = 7 - 2z$. For Q, it follows that:

$$Q = \sqrt{\frac{(7-2z)A_{\mathrm{pipe}}^2 2g}{\left(\frac{f_{\mathrm{D}} l}{d} + 1\right)}}$$

With it, we formulate the continuity condition which, due to the downward coordinate direction z, does not include a negative sign as in Equation 9.20:

$$t = \int_{z_t}^{z_b} \frac{A}{\sqrt{\frac{(7-2z)A_{\mathrm{pipe}}^2 2g}{\left(\frac{f_{\mathrm{D}} l}{d}+1\right)}}}\,\mathrm{d}z$$

We may move the constant part of the expression outside the integral and calculate it separately:

$$\frac{A}{\sqrt{\frac{A_{\mathrm{pipe}}^2 2g}{\left(\frac{f_{\mathrm{D}} l}{d}+1\right)}}} = \frac{100}{\sqrt{\frac{\left(7.85\times 10^{-3}\right)^2 2g}{\left(\frac{0.03\cdot 20}{0.10}+1\right)}}} = 7605.2$$

The integral now looks much more friendly:

$$t = 7605.2 \int_{z_t}^{z_b} \frac{1}{\sqrt{7-2z}}\,\mathrm{d}z = 7605.2 \left[\frac{2}{-2}\sqrt{7-2z}\right]_0^{1.0}$$
$$= 7605.2 \left[-\sqrt{7-2\cdot 1}+\sqrt{7}\right] = 3115.7\,\mathrm{s}$$

The factor 2 results from the integration of the expression with the square root in the denominator, and the division by -2 is due to the term $-2z$.

Solution 2.2

a) With a maximum discharge of $1.0\,\mathrm{m^3/s}$, an impoundment basin of $V = \int Q\,\mathrm{d}t = 1.0\,\mathrm{m^3/s} \cdot 40\,\mathrm{min} \cdot 60\,\mathrm{s/min} = 2400\,\mathrm{m^3}$ is required. With an area of $A = 40 \cdot 20 = 800\,\mathrm{m^2}$, this corresponds to a basin depth of 3.0 m.
The overflow, which must also be designed for the discharge of $1.0\,\mathrm{m^3/s}$, is determined via the Poleni equation (13.25). Solving for h_{WH}, it follows that:

$$h_{\mathrm{WH}} = \left(\frac{3}{2} \cdot \frac{1}{0.60 \cdot 20 \cdot \sqrt{19.62}}\right)^{\frac{2}{3}} = 0.0927\,\mathrm{m}$$

From that we determine the height of the weir:

$$3.0 - h_{\mathrm{WH}} = 2.907\,\mathrm{m}$$

b) The overflow height at minimum discharge is:

$$h_{\mathrm{WH}}(Q_{\min}) = \left(\frac{3 \cdot Q_{\min}}{2 \cdot \mu \cdot b \cdot \sqrt{2g}}\right)^{\frac{2}{3}} = 0.032\,\mathrm{m}$$

This results in a water depth of $h(Q_{\min}) = 2.907\,\mathrm{m} + 0.032\,\mathrm{m} = 2.939\,\mathrm{m}$. Thus, the volume is $V_{\mathrm{basin}} = 20 \cdot 40 \cdot 2.939 = 2351.2\,\mathrm{m^3}$ and:

$$t = \frac{V_{\mathrm{basin}}}{Q_{\min}} = 11\,756\,\mathrm{s} = 196\,\mathrm{min}$$

Solution 2.3

a) The balance is established as follows:

$$h = \frac{1.75 \cdot A_1}{1.5 \cdot A_1} = 1.167\,\mathrm{m}$$

b) From the continuity condition, we obtain:

$$t = -\int_{z_t}^{z_b} \frac{A}{\mu A_O \sqrt{2gz}}\,\mathrm{d}z = -\frac{A}{\mu A_O \sqrt{2g}} \int_{0.75}^{0.25} \frac{1}{\sqrt{z}}\,\mathrm{d}z$$
$$= -694.65 \left[2\sqrt{z}\right]_{0.75}^{0.25} = -694.65 \left[2\sqrt{0.25} - 2\sqrt{0.75}\right] = 508.5\,\mathrm{s}$$

c) This is a really tricky question. Preferably, you draw a coordinate system that shows the height z on the abscissa and the height difference Δh on the ordinate. At $z = 0.25\,\mathrm{m}$, $\Delta h = 0.25\,\mathrm{m}$. The point of intersection of the straight line with the abscissa, where $\Delta h = 0$, lies at $z = 0.167\,\mathrm{m}$. The line intersects the ordinate at $\Delta h = -0.50\,\mathrm{m}$ and the gradient is $3z$. And our equation is hereby established:

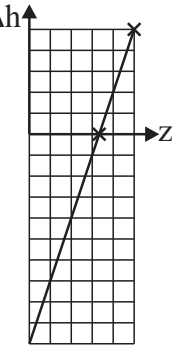

$$\Delta h = -0.5 + 3z$$

$$\begin{aligned} t &= -\int_{z_t}^{z_b} \frac{A}{\mu A_O \sqrt{2g\Delta h}}\,\mathrm{d}z = -\frac{A}{\mu A_O \sqrt{2g}} \int_{0.25}^{0.167} \frac{1}{\sqrt{-0.5+3z}}\,\mathrm{d}z \\ &= -694.65 \left[\frac{2}{3}\sqrt{-0.5+3z}\right]_{0.25}^{0.167} \\ &= -694.65 \left[\frac{2}{3}\sqrt{-0.5+3\cdot 0.167} - \frac{2}{3}\sqrt{-0.5+3\cdot 0.25}\right] = 216.9\,\mathrm{s} \end{aligned}$$

By the way, the 2 in the factor $\frac{2}{3}$ results from the division by $\frac{1}{2}$ (from the integration of $z^{-\frac{1}{2}}$) and the 3 from the term $3z$. Thus, the process takes a total of $508.5\,\mathrm{s} + 216.9\,\mathrm{s} = 725.4\,\mathrm{s}$.

Solution 2.4

a) The answer is trivial:

$$t = \frac{A \cdot h}{Q} = 200\,000\,\mathrm{s}$$

b) This is what we obtain from the rearranged Poleni equation:

$$h_{\mathrm{WH}} = \left(\frac{3}{2} \cdot \frac{10}{0.70 \cdot 5 \cdot \sqrt{19.62}}\right)^{\frac{2}{3}} = 0.978\,\mathrm{m}$$

c) Bear in mind that filling takes place in the positive z-direction. This means that the negative sign from Equation 9.19 is not written:

$$t = \int_{z_b}^{z_t} \frac{A}{10 - \frac{2}{3} \cdot \mu \cdot b \cdot \sqrt{2g} \cdot z^{\frac{3}{2}}}\,\mathrm{d}z = \int_0^{0.978} \frac{200\,000}{10 - 10.335 \cdot z^{3/2}}\,\mathrm{d}z$$

This integral may hardly be solved analytically. We use the computer and integrate numerically:

```
1> dz=1e-6;  in order to obtain a reasonable result, the selected
step must be very small.
2> T=0; % for convenience, this is the assumed constant of inte-
gration
3> for z=0:dz:.978 % the loop runs until z=.978 is reached
4> t = 200000/(10 - 10.335 * z^(3/2)) * dz; % the equation for t is
solved for each z as z increases from 0 to 0.978 by dz
5> T=T+t; % T is incremented by t
6> end
7> fname=sprintf('A total of %d s or %d min elapse.',round(T),
round(T/60));
8> disp(fname)
A total of 112305 s or 1872 min elapse.
```

We obtain 3.123×10^5 s together with the already elapsed 2×10^5 s for the time it took to fill the basin to the weir crest.

d) This is easy to calculate. The volume retained "above the weir crest" is:

$$V_{\text{above crest}} = A \cdot h_{\text{WH}} = 200\,000 \cdot 0.978 = 1.956 \times 10^5\,\text{m}^3$$

The following total volume has flowed in during the 1.123×10^5 s:

$$V_{\text{inflow}} = Q \cdot t = 10 \cdot 1.123 \times 10^5 = 1.123 \times 10^6\,\text{m}^3$$

The difference, of course, was spilled into the receiving water:

$$V_{\text{receiving water}} = V_{\text{inflow}} - V_{\text{above crest}} = 9.274 \times 10^5\,\text{m}^3$$

3 Solutions: momentum equation

Solution 3.1

$$v_1 = \frac{Q}{A} = \frac{10}{0.50^2\pi} = 12.73\,\text{m/s};\ \frac{v_1^2}{2g} = 8.26\,\text{m}$$

$$v_2 = \frac{Q}{A} = \frac{5}{0.30^2\pi} = 17.68\,\text{m/s};\ \frac{v_2^2}{2g} = 15.94\,\text{m}$$

$$EGL_1 = \frac{p_1}{\rho g} + \frac{v_1^2}{2g} = 38.26\,\text{m}$$

$$EGL_2 = EGL_1 - \Delta e_{1-2} = 38.26 - 2.0 = 36.26\,\text{m}$$

$$\frac{p_2}{\rho g} = EGL_2 - \frac{v_2^2}{2g} = 36.26 - 15.94 = 20.32\,\text{m}$$

$$\begin{aligned} F_R &= p_1 A_1 + \rho Q_1 v_1 - 2\left(p_2 A_2 + \rho Q_2 v_2\right) \\ &= 30 \cdot \rho \cdot g \cdot 0.5^2 \pi + \rho \cdot 10 \cdot 12.73 - 2\left(20.32 \cdot \rho \cdot g \cdot 0.3^2 \pi + \rho \cdot 5 \cdot 17.68\right) \\ &= 6.892 \times 10^4 \,\mathrm{N} \end{aligned}$$

Solution 3.2

a) Consider the Bernoulli equation where $z_1 = z_2$:

$$\frac{v_1^2}{2g} + \frac{p_1}{\rho g} = \frac{v_2^2}{2g} + \frac{p_2}{\rho g}$$

With this equation and the velocities from the continuity condition

$$v_1 = \frac{0.05}{0.2^2 \cdot \pi} = 0.398\,\mathrm{m/s}$$

and

$$v_2 = \frac{0.05}{0.1^2 \cdot \pi} = 1.592\,\mathrm{m/s}$$

we obtain an expression for the pressure height at the outlet:

$$\frac{p_2}{\rho g} = \frac{p_1}{\rho g} + \frac{v_1^2}{2g} - \frac{v_2^2}{2g} = 0.50 + \frac{0.398^2}{2g} - \frac{1.592^2}{2g} = 0.379\,\mathrm{m}$$

Substituting, the force balance becomes:

$$\begin{aligned} F_H &= p_1 A_1 + p_2 A_2 + \rho Q v_1 + \rho Q v_2 \\ &= 0.5 \cdot \rho \cdot g \cdot 0.2^2 \pi + 0.379 \cdot \rho \cdot g \cdot 0.1^2 \pi + \rho \frac{0.05^2}{0.2^2 \pi} + \rho \frac{0.05^2}{0.1^2 \pi} = 832.7\,\mathrm{N} \end{aligned}$$

b) The energy loss is calculated as follows:

$$\Delta e = 0.2\left(\frac{v_2^2}{2g} - \frac{v_1^2}{2g}\right) = 0.2 \cdot 0.121 = 0.0242\,\mathrm{m}$$

The energy loss must be subtracted from the pressure height calculated above. Additionally, however, the static pressure of $0.5\,\mathrm{mH_2O}$ from the curvature is in effect.

$$\frac{p_2}{\rho g} = 0.379 - 0.0242 + 0.50 = 0.855\,\mathrm{m}$$

The result for the horizontal force is:

$$\begin{aligned} F_H &= p_1 A_1 + p_2 A_2 + \rho Q v_1 + \rho Q v_2 \\ &= 0.5 \cdot \rho \cdot g \cdot 0.2^2 \pi + 0.855 \cdot \rho \cdot g \cdot 0.1^2 \pi + \rho \frac{0.05^2}{0.2^2 \pi} + \rho \frac{0.05^2}{0.1^2 \pi} = 979.3\,\mathrm{N} \end{aligned}$$

Solution 3.3

a)

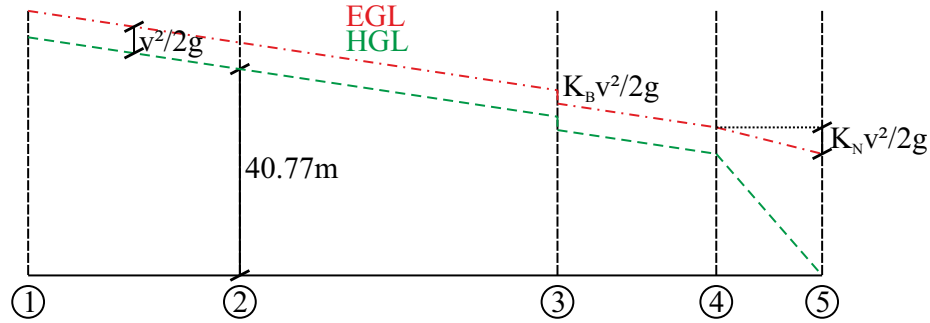

b) With $4.0\,\text{bar} = 40.77\,\text{mH}_2\text{O}$, it follows that:

$$40.77 + 1.0 + \frac{v^2}{2g} - \frac{v^2}{2g}\left(\frac{f_D l}{d} + K_B\right) - \frac{v^2_{\text{nozzle}}}{2g}\left(K_{\text{nozzle}} + 1\right) = 3.0$$

$$38.77 + \frac{Q^2}{\left(0.05^2\pi\right)^2 2g}\left(1 - \frac{f_D l}{d} - K_B\right) - \frac{Q^2}{\left(0.005^2\pi\right)^2 2g}\left(K_{\text{nozzle}} + 1\right) = 0$$

$$38.77 + \frac{Q^2}{1.21 \times 10^{-3}}\left(1 - \frac{0.03 \cdot 3}{0.10} - 0.8\right) - \frac{Q^2}{1.21 \times 10^{-7}}\left(1.2\right) = 0$$

This yields $Q = 1.977 \times 10^{-3}\,\text{m}^3/\text{s}$.

c) The force with which the nozzle must be held in place corresponds to the momentum flux:

$$F = \rho Q v_{\text{nozzle}} = \frac{1000\left(1.98 \times 10^{-3}\right)^2}{0.005^2\pi} = 49.76\,\text{N}$$

d) To find the attachment force, the pressure conditions upstream from the nozzle must also be known.

$$v = \frac{Q}{A} = 0.252\,\text{m/s};\ \frac{v^2}{2g} = 3.23\,\text{mm}$$

$$v_{\text{nozzle}} = \frac{Q}{A_{\text{nozzle}}} = 25.172\,\text{m/s};\ \frac{v^2_{\text{nozzle}}}{2g} = 32.295\,\text{m}$$

The energy height upstream from the nozzle is:

$$H_{\text{before nozzle}} = z + \frac{v^2_{\text{nozzle}}}{2g} + \Delta e_{\text{nozzle}} = 3.0 + 32.295\left(1 + 0.2\right) = 41.754\,\text{m}$$

The hydraulic grade line (or the piezometric pressure) upstream from the nozzle is:

$$HGL_{\text{before nozzle}} = H_{\text{before nozzle}} - \frac{v^2}{2g} = 41.751\,\text{m};\ \rightarrow \frac{p}{\rho g} = HGL_{\text{before nozzle}} - z = 38.751\,\text{m}$$

This allows the calculation of the force with which the nozzle must be attached to the hose:

$$
\begin{aligned}
F &= \rho Q v + pA - \rho Q v_{\text{nozzle}} \\
&= 1000 \cdot 1.98 \times 10^{-3} \cdot 0.252 + 38.702 \cdot 1000 \cdot 9.81 \cdot 7.85 \times 10^{-3} - 1000 \cdot 1.98 \times 10^{-3} \cdot 25.172 \\
&= 0.499 + 2981.9 - 49.8 = 2932\,\text{N}
\end{aligned}
$$

e) The distance traversed by the water jet depends on the time the jet is in the air.

$$3 = \frac{1}{2} g t^2$$

$$t = 0.782\,\text{s}$$

$$x = v_0 \cdot t = 25.172 \cdot 0.782 = 19.686\,\text{m}$$

Solution 3.4

a) This is our easiest exercise. We calculate the area A_2 with the velocity height and the continuity condition:

$$\frac{v_1^2}{2g} = \frac{4.0^2}{2g} = 0.815\,\text{m} \rightarrow \frac{v_2^2}{2g} = \frac{1}{7}\frac{v_1^2}{2g} = 0.116\,\text{m};\ v_2 = 1.512\,\text{m/s}$$

$$Q = v_1 A_1 = 2.8 \times 10^{-3}\,\text{m}^3/\text{s};\ A_2 = \frac{Q}{v_2} = 1.852 \times 10^{-3}\,\text{m}^2$$

b) When setting up the Bernoulli equation and accounting for energy losses, we obtain:

$$z_1 + \frac{p_1}{\rho g} + \frac{v_1^2}{2g} - \Delta e = z_2 + \frac{p_2}{\rho g} + \frac{v_2^2}{2g}$$

$$\frac{1.0 \times 10^5}{1.0 \times 10^3 \cdot g} + 0.815 - 0.5 \cdot 0.116 = \frac{p_2}{\rho g} + 0.116$$

$$\frac{p_2}{\rho g} = 10.84\,\text{mH}_2\text{O}$$

$$p_2 = 1.063 \times 10^5\,\text{N/m}^2$$

c) Ultimately, this yields the flange force:

$$
\begin{aligned}
F_H &= \rho Q v_1 + p_1 A_1 - \rho Q v_2 - p_2 A_2 \\
&= 1.0 \times 10^3 \cdot 2.8 \times 10^{-3} \cdot 4.0 + 1.0 \times 10^5 \cdot 7 \times 10^{-4} - 1.0 \times 10^3 \cdot 2.8 \times 10^{-3} \cdot 1.512 \\
&- 1.063 \times 10^5 \cdot 1.852 \times 10^{-3} = -119.885\,\text{N}
\end{aligned}
$$

Therefore, F_H acts in the direction of flow.

Solution 3.5

a) Here, the Froude number is required:

$$A = \frac{r^2\pi}{2} = 0.0353\,\mathrm{m}^2$$

$$v = \frac{Q}{A} = 1.132\,\mathrm{m/s}$$

$$\mathrm{Fr} = \frac{v}{\sqrt{g\frac{A}{b_{\mathrm{WS}}}}} = \frac{1.132}{\sqrt{g\frac{0.035}{0.30}}} = 1.054;\ \rightarrow \mathrm{SUPER}$$

b) The centre of gravity of the semicircle is spaced $0.4244 \cdot R$ from the centre of the circle.

$$h'_{\mathrm{CG}} = 0.15 \cdot 0.4244 = 0.0637\,\mathrm{m}$$

$$p_{\mathrm{CG}} = \rho g h'_{\mathrm{CG}} = 624.5\,\mathrm{N/m}^2$$

$$F_P = p_{\mathrm{CG}} A = 624.5 \cdot 0.0353 = 22.05\,\mathrm{N}$$

$$F_M = \rho Q v = 1000 \cdot 0.04 \cdot 1.132 = 45.28\,\mathrm{N}$$

$$F_{MP} = F_M + F_P = 67.33\,\mathrm{N}$$

And because the entering and leaving momentum and pressure forces act on the shaft with an angle of deflection of 90°, the reaction force to be applied is:

$$F_R = \sqrt{F_{MP}^2 + F_{MP}^2} = 95.21\,\mathrm{N}$$

4 Solutions: free surface flows

You may track the individual water level courses via the Bernoulli–Manning discussions, which are not explicitly given here.

Solution 4.1

a)

open channel	$y_N = 1.381\,\mathrm{m}$	$v_N = 2.896\,\mathrm{m/s}$	$H_N = 1.809\,\mathrm{m}$	$\mathrm{Fr}_N = 0.787$
	$y_c = 1.177\,\mathrm{m}$	$v_c = 3.398\,\mathrm{m/s}$	$H_{\min} = 1.766\,\mathrm{m}$	$\Delta e_{1-2} = 0.589\,\mathrm{m}$
stilling basin	$y_N = 0.860\,\mathrm{m}$	$v_N = 4.651\,\mathrm{m/s}$	$H_N = 1.963\,\mathrm{m}$	$\mathrm{Fr}_N = 1.601$
	$y_c = 1.177\,\mathrm{m}$	$v_c = 3.398\,\mathrm{m/s}$	$H_{\min} = 1.766\,\mathrm{m}$	$\Delta e_{3-4} = 0.0428\,\mathrm{m}$

b) At point ④, normal water conditions must exist. I leave the Manning–Bernoulli discussion to you (also, see example on page 259). The specific energy at point ③ is $H_3 = H_N + 0.1\frac{v_N^2}{2g} + w_2 = 2.352\,\mathrm{m}$; from the Bernoulli equation, the flow depth that results is $y_3 = 2.181\,\mathrm{m}$. The crucial hint for the water level course is already hidden in the specification. We would normally assume that downstream from the ramp, an increasing flow depth in supercritical flow followed by a hydraulic jump occurs. But we should first find out what's behind that hint; the hydraulic jump is to occur immediately downstream from the ramp without the section where energy decreases in supercritical flow. A specific energy of $H_{\min} + w_1 - \frac{v_c^2}{2g} = 2.677\,\mathrm{m}$ exists downstream from

the ramp[A]. With the Bernoulli equation, we obtain the flow depth in supercritical flow: $y_2 = 0.631\,\text{m}$ at $\text{Fr}_2 = 2.548$. This results in a conjugated flow depth in subcritical flow of $y_{r,\text{HJ}} = 1.980\,\text{m}$ at a specific energy of $H_{r,\text{HJ}} = 2.188\,\text{m}$. Eureka! $H_{r,\text{HJ}} < H_3$. Thus, there must be an energy build-up in the stilling basin. The length of the backwater in the stilling basin is determined by means of the direct step method (`directStepDeltaX.m`) where $y_l = y_{r,\text{HJ}} = 1.980\,\text{m}$ and $y_r = y_3 = 2.181\,\text{m}$ yield $\Delta x = 22.34\,\text{m}$. For the length of the hydraulic jump, we obtain $L_{\text{HJ}} = 4.54\,\text{m}$. The total length of the stilling basin must be $L_{\text{stilling basin}} = L_{\text{HJ}} + \Delta x = 26.88\,\text{m}$[B].

c) The complete course of the water level appears as seen below.

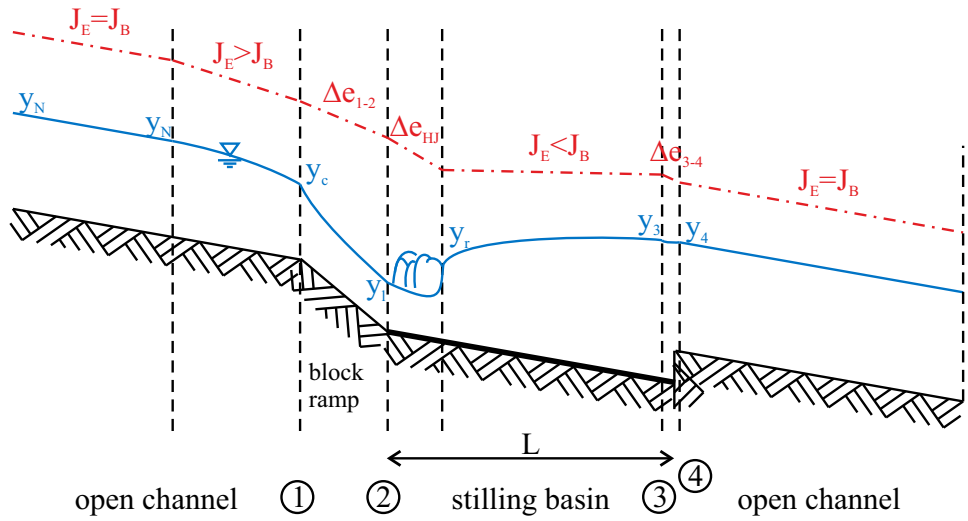

Solution 4.2

a) $\boxed{y_N = 4.026\,\text{m}} \boxed{v_N = 4.140\,\text{m/s}} \boxed{H_N = 4.900\,\text{m}} \boxed{\text{Fr}_N = 0.659}$

b) In the following steps, the characteristic specific energies and flow depths are calculated:

$$q_{\text{cons}} = \frac{Q}{3 \cdot 7.5} = 22.22\,\text{m}^3/(\text{s m})$$

$$H_{\text{min,cons}} = \frac{3}{2}\sqrt[3]{\frac{q_{\text{cons}}^2}{g}} = 5.539\,\text{m}$$

$$y_{c,\text{cons}} = 3.692\,\text{m};\ v_{c,\text{cons}} = 6.019\,\text{m/s};\ \Delta e = 0.5\frac{v_{c,\text{cons}}^2}{2g} = 0.923\,\text{m}$$

$$H_{\text{upstream}} = H_{\text{min,cons}} + \Delta e = 6.462\,\text{m} > H_N \rightarrow \text{energy build-up necessary}$$

The flow depth for $H_{\text{upstream cons}} = 6.462\,\text{m}$ in subcritical flow is obtained with the Bernoulli equation:

[A] Nature adapts to the minimum required energy. H_N is not required until the ramp is reached, but is gradually reduced to H_{min}.

[B] If it were shorter, the energy build-up for the normal water conditions at point ④ would nevertheless be required. The hydraulic jump would "travel into the ramp".

$$y_{\text{upstream cons}} = 6.079\,\text{m};\ v_{\text{upstream cons}} = 2.742\,\text{m/s}$$

As indicated, no further energy loss occurs downstream from the bridge; from the Bernoulli equation, the flow depth in supercritical flow is as follows:

$$H_{\text{downstream cons}} = H_{\text{min}} \rightarrow y_{\text{downstream cons}} = 2.00\,\text{m}$$

The specific energy downstream from the constriction is greater than H_N; therefore, energy is reduced in supercritical flow with increasing flow depth up to $y_{l,\text{HJ}}$ and y_N is in effect immediately downstream from the hydraulic jump.

$$y_{l,\text{HJ}} = \frac{y_N}{2}\left(\sqrt{1+8\text{Fr}_N^2}-1\right) = 2.245\,\text{m}$$

$$H_{l,\text{HJ}} = 5.056\,\text{m};\text{Fr}_{l,\text{HJ}} = 1.58$$

I will skip the energy diagram ;-).

c) We use the direct step method here (`directStepDeltaX.m`). The flow depth on the right corresponds to that upstream from the constriction; the normal depth is to be inserted on the left.

$$\Delta x_{\text{upstream}} = 1150.2\,\text{m}$$

The length of the supercritical section is:

$$\Delta x_{\text{downstream}} = 25.3\,\text{m}$$

Since the Froude number $\text{Fr}_l = 1.58$ upstream from the hydraulic jump is smaller than 1.7, we see an undulating hydraulic jump; here, no statement relating to the length is possible. The total length of the effect may be given as $1175.5\,\text{m} + L_{\text{pier}}$.

Solution 4.3

a) The rearranged Poleni equation reads:

$$h_{\text{WH}} = \left(\frac{3}{2}\cdot\frac{40}{0.60\cdot 8\sqrt{19.62}}\right)^{\frac{2}{3}} = 1.997\,\text{m}$$

$$y_{\text{upstream}} = h_{\text{WH}} + w = 3.497\,\text{m}$$

With this, we calculate the specific energy upstream from the weir:

$$H_{\text{upstream}} = 3.497 + \frac{\left(\frac{40}{8\cdot 3.497}\right)^2}{2g} = 3.601\,\text{m}$$

With Δz added to H_{upstream}, this corresponds to the specific energy $H_{\text{downstream}} = 4.601\,\text{m}$ downstream from the weir because no energy losses are indicated. With $b = 12.0\,\text{m}$ the flow depth in supercritical flow downstream from the weir $y_{\text{downstream}} = 0.366\,\text{m}$ follows from the Bernoulli equation.

b) We know that the additional built-up energy is dissipated again in supercritical flow and that y_N exists immediately downstream from the hydraulic jump.

$$y_{l,\mathrm{HJ}} = \frac{y_{r,\mathrm{HJ}}}{2}\left(\sqrt{1+8\cdot \mathrm{Fr}_r^2}-1\right) = \frac{1.35}{2}\left(\sqrt{1+8\cdot 0.678^2}-1\right) = 0.786\,\mathrm{m}$$

By means of the continuity condition, it follows that $v_l = v_{\mathrm{downstream}} = 9.11\,\mathrm{m/s}$ and $v_r = v_{l,\mathrm{HJ}} = 4.24\,\mathrm{m/s}$; that is, $v_m = 6.67\,\mathrm{m/s}$ and also $R_{\mathrm{hy},m} = 0.526\,\mathrm{m}$. Ultimately, $H_r = H_{l,\mathrm{HJ}} = 1.702\,\mathrm{m}$ and $H_l = H_{\mathrm{downstream}} = 4.601\,\mathrm{m}$. With the Manning equation, we formulate n for normal water conditions

$$n = \frac{\sqrt{J_B}}{Q}\cdot\frac{A^{\frac{5}{3}}}{P^{\frac{2}{3}}} = \frac{\sqrt{J_B}}{2.314}$$

and insert the expression for the coefficient into the rearranged direct step method equation; we now have an equation with one unknown, J_B:

$$\begin{aligned} H_r - H_l &= \Delta x\left(J_B - \frac{v_m^2\cdot n^2}{R_{\mathrm{hy},m}^{\frac{4}{3}}}\right) \\ &= \Delta x\left(J_B - \frac{v_m^2\cdot\left(\frac{\sqrt{J_B}}{2.314}\right)^2}{R_{\mathrm{hy},m}^{\frac{4}{3}}}\right) \\ 1.702 - 4.601 &= 20\cdot\left(J_B - \frac{6.67^2\cdot\frac{J_B}{2.314^2}}{0.526^{\frac{4}{3}}}\right) \end{aligned}$$

By means of the Octave equation solver, we obtain: $J_B = 7.79\times 10^{-3}$ and $n = 0.0381\,\mathrm{s/m^{\frac{1}{3}}}$.

Solution 4.4

a) The height difference Δz amounts to $\Delta z = J_B\cdot 5000 + 5\cdot 1.0 = 30\,\mathrm{m}$. In a new flow section of 10 km, a gradient of $J_{B,\mathrm{new}} = 0.3\,\%$ results.

$y_N = 1.331\,\mathrm{m}$	$v_N = 2.253\,\mathrm{m/s}$	$H_N = 1.590\,\mathrm{m}$	$\mathrm{Fr}_N = 0.624$
$y_{N,\mathrm{new}} = 1.086\,\mathrm{m}$	$v_{N,\mathrm{new}} = 1.726\,\mathrm{m/s}$	$H_{N,\mathrm{new}} = 1.238\,\mathrm{m}$	$\mathrm{Fr}_{N,\mathrm{new}} = 0.529$

The flow velocity is lower in the new section so that no bottom steps are required.

b) At the change in slope, critical conditions prevail with $y_c = 0.972\,\mathrm{m}$ and $H_{\min} = 1.458\,\mathrm{m}$. Downstream from the bottom step, a specific energy of

$$H_{\mathrm{downstream\ step}} = 1.458 + 1.0 - 0.1\frac{v_c^2}{2g} = 2.458 - 0.049 = 2.409\,\mathrm{m}$$

exists. Via the Bernoulli equation, this results in the flow depth $y_{\mathrm{downstream\ step}} = 0.291\,\mathrm{m}$. The supercritical flow depth increases until $y_{l,\mathrm{HJ}} = 0.434\,\mathrm{m}$ is reached.

c) The direct step method yields $\Delta x = 10.25\,\mathrm{m}$. The length of the hydraulic jump is $L_{\mathrm{HJ}} = 1.45\,\mathrm{m}$, which means that a total length of $L_{\mathrm{total}} = 11.7\,\mathrm{m}$ must be paved.

d)

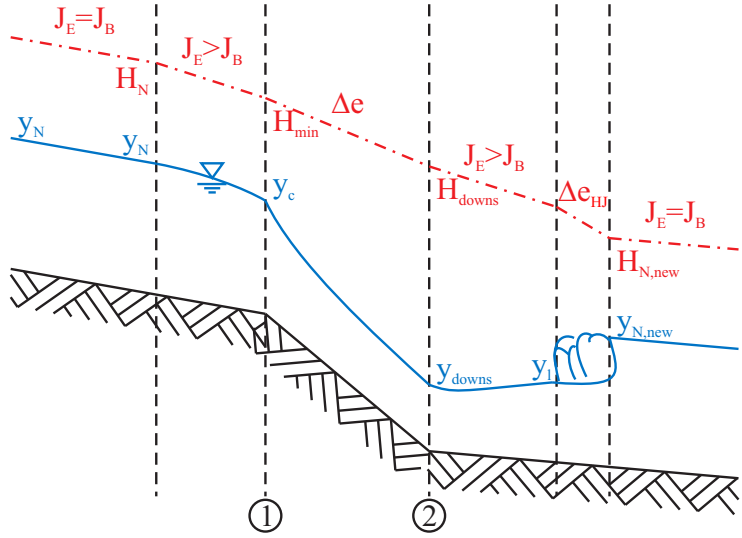

Solution 4.5

a)

section 1	$y_{N,1} = 0.984\,\text{m}$	$v_{N,1} = 2.033\,\text{m/s}$	$H_{N,1} = 1.195\,\text{m}$	$\text{Fr}_{N,1} = 0.654$
section 2	$y_{N,2} = 0.244\,\text{m}$	$v_{N,2} = 2.047\,\text{m/s}$	$H_{N,2} = 0.458\,\text{m}$	$\text{Fr}_{N,2} = 1.323$
section 3	$y_{N,3} = 0.640\,\text{m}$	$v_{N,3} = 0.781\,\text{m/s}$	$H_{N,3} = 0.671\,\text{m}$	$\text{Fr}_{N,3} = 0.311$

b) The specific energy in section 2 is lower than in section 1. This results in energy reduction. There is no reason for the specific energy to remain at $H_{N,1}$ until the end of the section; nature aims at the lowest energy state. At cross-section ①, $H_{\text{min},1} = 1.11\,\text{m}$ exists at $y_{c,1} = 0.742\,\text{m}$.

The energy loss in the expansion corresponds to the gradient at the bottom in this section. Thus, we obtain $H_2 = 1.11\,\text{m}$ for the specific energy at cross-section ②. Since the critical conditions have already been passed in cross-section ① ($H_{\text{min},1} > H_{\text{min},2}$ and thus crucial), supercritical flow with $y_2 = 0.113\,\text{m}$ is the result. The specific energy in cross-section ② is also too high for the normal conditions of this section; it is continuously reduced to $H_{N,2}$ (or, that is, to $y_{N,2}$ in supercritical flow). This flow depth remains unchanged because it is stated that normal conditions occur in all sections.

However, we see that the specific energy at normal conditions is smaller in section 2 than that in section 3. There must be an energy build-up, which is possible only in subcritical flow. In section 2, there is a hydraulic jump with $y_{N,2}$ on its left. Immediately downstream from the hydraulic jump, the flow depth $y_{r,\text{HJ}} = 0.351\,\text{m}$ is conjugated to $y_{N,2}$.

Downstream from the hydraulic jump – still in section 2 – the energy is built-up. The flow depth increases until it reaches $y_{N,3}$ precisely at the transition to section 3. From there, nothing will change.

c)

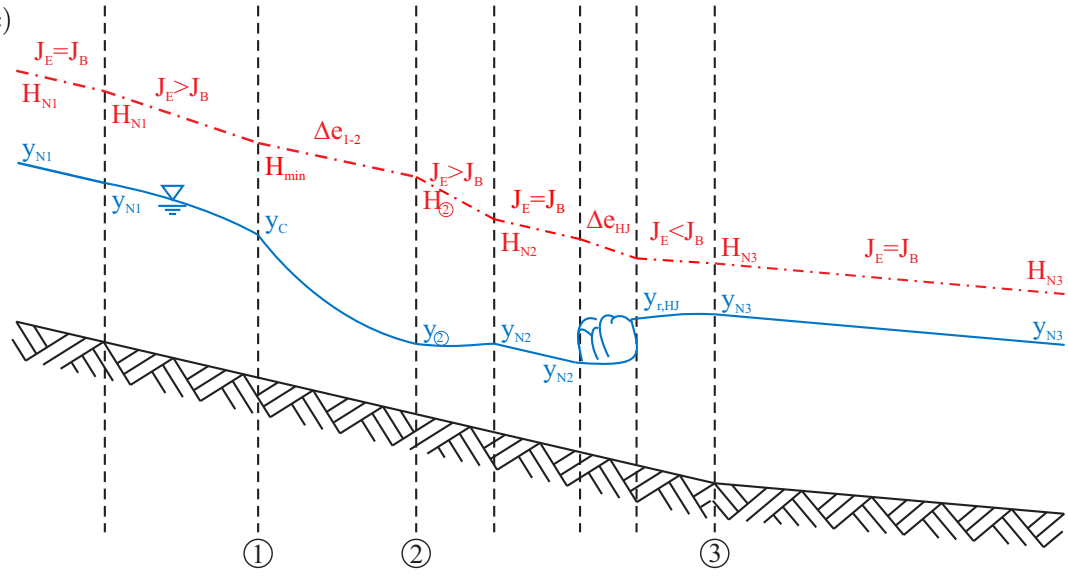

Solution 4.6

a)

section 1	$y_{N,1} = 0.836\,\text{m}$	$v_{N,1} = 3.986\,\text{m/s}$	$H_{N,1} = 1.646\,\text{m}$	$\text{Fr}_{N,1} = 1.392$
section 2	$y_{N,2} = 1.647\,\text{m}$	$v_{N,2} = 3.035\,\text{m/s}$	$H_{N,2} = 2.117\,\text{m}$	$\text{Fr}_{N,2} = 0.755$

b) Since $H_{N1} < H_{N2}$, H_{N2} is found immediately downstream from the constriction. Together with $\Delta e_{\text{cons}} = 0.0469\,\text{m}$ and $\Delta z = 5.0 \cdot J_{B2} = 0.015\,\text{m}$, this results in:

$$H_A = H_{\text{upstream cons}} = H_{N2} + \Delta e_{\text{cons}} - \Delta z = 2.149\,\text{m}$$

With this specific energy, we may calculate the flow depth upstream from the constriction by means of the Bernoulli equation: $y_{\text{upstream cons}} = y_A = 2.009\,\text{m}$.
Initially, normal conditions occur in section 1 until a transition to subcritical flow takes place ($y_{r,\text{HJ}} = 1.280\,\text{m}$). From there, energy is built-up until, immediately upstream from the constriction, $y_{\text{upstream cons}} = 2.009\,\text{m}$ (that is $H_{\text{upstream cons}} = 2.149\,\text{m}$) is reached. This is just enough for achieving normal conditions with the energy losses in the constriction immediately at the beginning of section 2.

c) I'm sure you can manage the energy diagram yourself.

5 Solutions: pipe flow

Solution 5.1

a) Initially, we establish the energy equation:

$$H_A - \frac{Q^2}{A_1^2 2g}\left(\frac{f_{\text{D1}} L_1}{d_1}\right) - \frac{Q^2}{A_2^2 2g}\left(\frac{f_{\text{D2}} L_2}{d_2} + 1\right) - H_T = H_B$$

With the specified values, it follows that:

$$H_A - \frac{Q^2}{0.785^2 2g}\left(\frac{0.025\cdot 2000}{1.0}\right) - \frac{Q^2}{1.767^2 2g}\left(\frac{0.020\cdot 1000}{1.5}+1\right) - H_T = H_B$$

With the power equation for the turbine, we may write:

$$H_T = \frac{P_T}{\eta\rho g Q} = \frac{P_T}{0.80\cdot 9.81\cdot 1000\cdot Q} = 750 - 4.131\cdot Q^2 - 0.234\cdot Q^2$$

Consequently:

$$P_T = \left(750 - 4.365\cdot Q^2\right)\cdot 7848\cdot Q = 5.886\times 10^6\cdot Q - 3.426\times 10^4\cdot Q^3$$

The maximum value of P_T is found by differentiation:

$$\frac{\mathrm{d}P_T}{\mathrm{d}Q} = 5.886\times 10^6 - 3\cdot 3.426\times 10^4\cdot Q^2 \stackrel{!}{=} 0$$

Finally, we obtain $P_{T,\max}$ when $Q = 7.568\,\mathrm{m^3/s}$.

b) The above established power equation for the turbine yields H_T:

$$H_T = 750 - 4.365\cdot Q^2 = 750 - 4.365\cdot 7.568^2 = 500.0\,\mathrm{m}$$

c) Finally, we calculate the turbine power:

$$P_T = \eta\rho g Q H_T = 0.80\cdot\rho\cdot g\cdot 7.568\cdot 500 = 29.7\,\mathrm{MW}$$

Solution 5.2

a) For determination of the pump power, we set up the energy equation and determine the pipe friction coefficient for the required discharge.

$$v = \frac{Q}{A} = 0.396\,\mathrm{m/s}$$

With `pc('circle',1.5,1.5,0.7,3e-3,10)`, we find that $f_\mathrm{D} = 0.024$.

$$H_A - \frac{v^2}{2g}\left(\frac{f_\mathrm{D} L}{d} + K_I + 2K_{45^\circ} + 1\right) + H_P = H_B$$

$$H_P = 10 + 0.656 = 10.656\,\mathrm{m};\; P_P = \frac{1}{\eta_P}\rho g Q H_P = 91.47\,\mathrm{kW}$$

This results in the pump costs per year:

$$C_P = P_P\,(10\cdot 365)\cdot 0.15 = 50080\,€/\mathrm{a}$$

b) In this case, too, we cannot bypass the energy equation.

$$H_P = 10 + \frac{16 \cdot Q^2}{d^4 \pi^2 2g}\left(\frac{f_D L}{d} + 1.1 + 1\right) = 10 + \frac{0.0405}{d^4}\left(\frac{120}{d} + 2.1\right)$$

$$P_P = \frac{1}{\eta_P}\rho g Q H_P = 8583.8 \cdot H_P$$

P_P is calculated in watts; however, the costs are indicated in €/kW/h; therefore, we must divide by 1000:

$$C_{P,30} = 0.15\frac{1}{1000}(10 \cdot 365 \cdot 30) \cdot 8583.8 \cdot H_P = 140988 \cdot H_P$$

$$C_{\text{invest}} = L \cdot 7000 \cdot d = 3.5 \times 10^7 \cdot d$$

$$C_{\text{total}} = C_{P,30} + C_{\text{invest}} = 140988\left(10 + \frac{0.0405}{d^4}\left(\frac{120}{d} + 2.1\right)\right) + 3.5 \times 10^7 \cdot d$$

$$1.410 \times 10^6 + \frac{6.852 \times 10^5}{d^5} + \frac{1.199 \times 10^4}{d^4} + 3.5 \times 10^7 \cdot d$$

The total cost must be differentiated with respect to the diameter and set to zero:

$$\frac{\mathrm{d}C_{\text{total}}}{\mathrm{d}d} = 3.5 \times 10^7 - 5 \cdot \frac{6.852 \times 10^5}{d^6} - 4 \cdot \frac{1.199 \times 10^4}{d^5} \stackrel{!}{=} 0$$

With `function C=f(d)` and the above equation, we obtain with `[d,fval,info]=fsolve(@f,.4)` an optimum diameter of:

$$d_{\text{opt}} = 0.680\,\text{m}$$

Solution 5.3

a) First, let's set up the energy equation:

$$2000 - \frac{Q^2}{A^2 2g}\left(\frac{f_D L}{d} + \sum_{i=1}^{n} K_i + K_O\right) - H_T = 1500$$

Furthermore:

$$2000 - \frac{Q^2}{3.142^2 2g}\left(\frac{f_D \cdot 5000}{2.0} + 2 \cdot K_{B,60^\circ} + 4 \cdot K_{B,80^\circ} + 1\right) - H_T = 1500$$

$$500 - \frac{Q^2}{3.142^2 2g}(2500 f_D + 4.8) - \frac{92.9 \times 10^6}{0.9 \cdot \rho \cdot g \cdot Q} = 0$$

With $f_{\text{D,step 0}} = 0.010$, we obtain a discharge of $Q_{\text{step 0}} = 27.32\,\text{m}^3/\text{s}$. From the Prandtl-Colebrook algorithm, $f_{\text{D,step 1}} = 0.0108$ results from $Q_{\text{step 0}}$. When inserted into the energy equation, Q becomes $Q_{\text{step 1}} = 29.32\,\text{m}^3/\text{s}$, with which the friction coefficient is again determined via the Prandtl-Colebrook equations. We obtain $f_{\text{D,step 2}} = 0.0108$ and may stop at this point. We calculated with the correct f_D.

b)

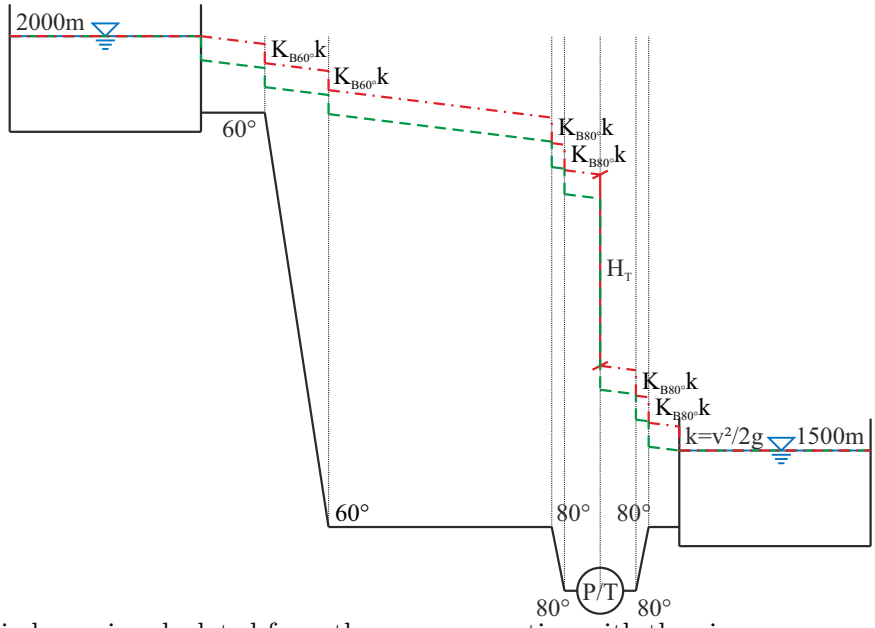

c) The discharge is calculated from the energy equation with the given pump power:

$$\frac{\eta \cdot 50 \times 10^6}{\rho \cdot g \cdot Q} = \frac{0.90 \cdot 50 \times 10^6}{1000 \cdot 9.81 \cdot Q} = 500 + \frac{Q^2}{3.142^2 2g}(2500 \cdot 0.0108 + 4.8)$$

We obtain $Q = 8.94\,\mathrm{m^3/s}$.

d) Here, the geodetic height must be taken into consideration since the total pressure (the sum of atmospheric pressure and water pressure) must not drop below the vapour pressure.

$$z_{\max} + \frac{p_{\min}}{\rho g} + \frac{v_{\max}^2}{2g} = 1500$$

With $\frac{v_{\max}^2}{2g} = 31.855\,\mathrm{m}$ and $\frac{p_{\min}}{\rho g} = -7.5\,\mathrm{mH_2O}$, we find that $z_{\max} = 1475.6\,\mathrm{m.a.s.l.}$

Solution 5.4

a) The solution starts again with the energy equation:

$$570 - \frac{Q^2}{A^2 2g}\left(\frac{f_D L}{d} + 1.5\right) = 500$$

With $f_{D,\text{step }0} = 0.020$, $Q_{\text{step }0} = 1.947\,\mathrm{m^3/s}$; subsequently, $f_{D,\text{step }1} = 0.0161$ and $Q_{\text{step }1} = 2.169\,\mathrm{m^3/s}$; $f_{D,\text{step }2} = 0.0160$ and $Q_{\text{step }2} = 2.172\,\mathrm{m^3/s}$. This confirms and ends the process because $f_{D,\text{step }3} = 0.0160$.

b) We set up the following system of equations:

$$560 + H_{P1} - \frac{Q_1^2}{A^2 2g}\left(\frac{f_D L_1}{d} - 1\right) = \mathrm{HGL}_{\mathrm{junct}}$$
$$560 + H_{P2} - \frac{Q_2^2}{A^2 2g}\left(\frac{f_D L_2}{d} - 1\right) = \mathrm{HGL}_{\mathrm{junct}}$$
$$\mathrm{HGL}_{\mathrm{junct}} - \frac{(Q_1 + Q_2)^2}{A^2 2g}\left(\frac{f_D L_3}{d}\right) = 570$$

Substituting values, and with $Q_1 + Q_2 = 2.172\,\mathrm{m}^3/\mathrm{s}$, the result is the following:

$$560 + \frac{P_{P1} \cdot 0.7}{\rho g Q_1} - \frac{Q_1^2}{1.539^2 2g}\left(\frac{0.0160 \cdot 1100}{1.40} + 1\right) = \mathrm{HGL}_{\mathrm{junct}}$$
$$560 + \frac{P_{P2} \cdot 0.7}{\rho g Q_2} - \frac{Q_2^2}{1.539^2 2g}\left(\frac{0.0160 \cdot 100}{1.40} + 1\right) = \mathrm{HGL}_{\mathrm{junct}}$$
$$\mathrm{HGL}_{\mathrm{junct}} - \frac{2.172^2}{1.539^2 2g}\left(\frac{0.0160 \cdot 3000}{1.40}\right) = 570$$

With the third equation, we may quite comfortably calculate the piezometric pressure height at the junction: $\mathrm{HGL}_{\mathrm{junct}} = 573.48\,\mathrm{m.a.s.l.}$ With $P_{P1} = P_{P2} = P_P$, we solve the first two equations for P_P, as follows, and then substitute $Q_2 = 2.172 - Q_1$ in the second equation to obtain the system as seen here:

$$P_P = \frac{\rho g Q_1}{0.7}\left(13.48 + \frac{Q_1^2}{1.539^2 2g}\left(\frac{0.0160 \cdot 1100}{1.40} - 1\right)\right)$$
$$P_P = \frac{\rho g Q_2}{0.7}\left(13.48 + \frac{Q_2^2}{1.539^2 2g}\left(\frac{0.0160 \cdot 100}{1.40} - 1\right)\right)$$
$$= \frac{\rho g\,(2.172 - Q_1)}{0.7}\left(13.48 + \frac{(2.172 - Q_1)^2}{1.539^2 2g}\left(\frac{0.0160 \cdot 100}{1.40} - 1\right)\right)$$

By equating the expressions for P_P[C], we ultimately determine that $Q_1 = 1.0748\,\mathrm{m}^3/\mathrm{s}$ and $Q_2 = 1.0972\,\mathrm{m}^3/\mathrm{s}$. Likewise, we find that $P_P = 208.12\,\mathrm{kW}$, $H_{P1} = 13.817\,\mathrm{m}$ and $H_{P2} = 13.536\,\mathrm{m}$.

[C] Preferably, use the Octave solver again and equate the two expressions for P_P since the pump powers are identical.

Solution 5.5

a)

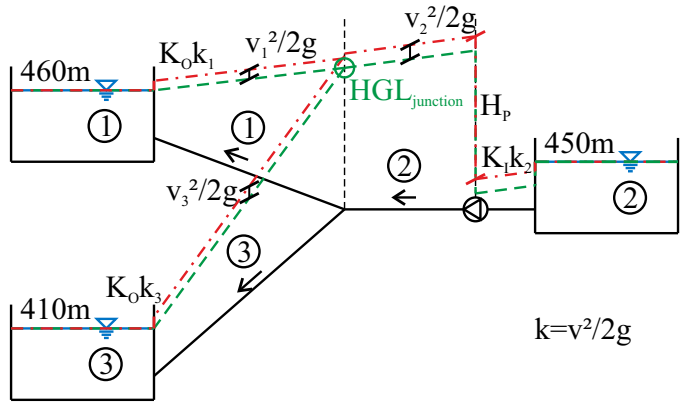

b) This is the system of equations with the boundary condition being that the hydraulic gradient lines intersect at the junction:

$$450 + H_P - \frac{(Q_1+Q_3)^2}{R_2^4\pi^2 2g}\left(\frac{f_{D2}l_2}{d_2} + K_I + 1\right) = \mathrm{HGL_{junct}}$$

$$P_P = \frac{1}{\eta_P}\rho g Q H_P$$

$$H_P = \frac{5.0\times10^5\cdot 0.85}{1.0\times10^3\cdot 9.81\cdot Q_2} = \frac{43.32}{Q_2}$$

$$450 + \frac{43.32}{Q_2} - 3.430\cdot(Q_1+Q_3)^2 = \mathrm{HGL_{junct}}$$

$$\mathrm{HGL_{junct}} - \frac{Q_1^2}{R_1^4\pi^2 2g}\left(\frac{f_{D1}l_1}{d_1}\right) = 460; \rightarrow Q_1 = \sqrt{(\mathrm{HGL_{junct}} - 460)\cdot 0.224}$$

$$\mathrm{HGL_{junct}} - \frac{Q_3^2}{R_3^4\pi^2 2g}\left(\frac{f_{D3}l_3}{d_3}\right) = 410 \rightarrow Q_3 = \sqrt{(\mathrm{HGL_{junct}} - 410)\cdot 7.35\times10^{-4}}$$

$$450 + \frac{43.32}{\sqrt{(\mathrm{HGL_{junct}}-460)\cdot 0.224} + \sqrt{(\mathrm{HGL_{junct}}-410)\cdot 7.35\times10^{-4}}} - 3.430\cdot$$
$$\cdot\left(\sqrt{(\mathrm{HGL_{junct}}-460)\cdot 0.224} + \sqrt{(\mathrm{HGL_{junct}}-410)\cdot 7.35\times10^{-4}}\right)^2 = \mathrm{HGL_{junct}} \tag{17.2}$$

When entering this equation into Octave, one thankfully obtains the following for the piezometric pressure height at the junction:

$$\mathrm{HGL_{junct}} = 468.55\,\mathrm{m}$$

This results in

$$Q_1 = \sqrt{(\mathrm{HGL_{junct}} - 460)\cdot 0.224} = 1.384\,\mathrm{m^3/s}$$

and:

$$Q_2 = \sqrt{(\mathrm{HGL_{junct}} - 410)\cdot 7.35\times10^{-4}} = 0.207\,\mathrm{m^3/s}$$

c) A rule of proportion is required.

$$\frac{1.384}{0.207} \cdot 10000 = 6.686 \times 10^4\,\mathrm{m}^3$$

d) Now the question remains: For how long must the pump operate?

$$t = \frac{V_3}{Q_3} = \frac{10000}{0.207} = 4.83 \times 10^4\,\mathrm{s} = 13.42\,\mathrm{h}$$

$$C_{\mathrm{pump}} = 500 \cdot 13.42 \cdot 0.20 = 1342.0\,€/\mathrm{d}$$

6 Solutions: cross-cutting issues

Solution 6.1

a) The energy equation is required:

$$3.0 = \frac{\left(0.9 \times 10^{-3}\right)^2}{0.02^4 \cdot \pi^2 \cdot 2g}\left(\frac{0.02 \cdot 100}{0.04} + 1 + K_V\right)$$

This results in $K_V = 63.75$.

b) We now use the continuity condition in the form $Q\,\mathrm{d}t = -A\,\mathrm{d}z$:

$$Q(z) = \sqrt{\frac{\Delta h}{1.646 \times 10^6}} = 7.794 \times 10^{-4} \cdot \sqrt{1.85 + z}$$

$$t = -\int_{1.15}^{0} \frac{A_A}{Q_{\mathrm{outflow}} - Q_{\mathrm{inflow}}}\,\mathrm{d}z = -\int_{1.15}^{0} \frac{1.35}{7.794 \times 10^{-4} \cdot \sqrt{1.85 + z} - 0.9 \times 10^{-3}}\,\mathrm{d}z = 5428\,\mathrm{s}$$

We may solve the integral numerically by means of Octave:

```
1> dz=1e-3; % the equation is solved millimetre by millimetre
2> T=0; % this is quasi the integration constant
3> for z=0:dz:1.15 % the loop runs until z=1.15 is reached
4> t = 1.35/(7.794e-4*sqrt(1.85+z)-.9e-3)*dz; % the equation is
solved for each z
5> T=T+t; % the time increment is added to T
6> end
7> fname=sprintf('A total of %d s or %d min elapse.',round(T),
round(T/60));
8> disp(fname)
A total of 5428 s or 90 min elapse.
```

Solution 6.2

a) The energy supplied by the pump must be sufficient to overcome the static head and the hydraulic losses:

$$H_P = 20 + \frac{Q^2}{A^2 2g}\left(\frac{f_D L}{d} + K_B + 1\right)$$

We proceed with the power formula for pumps:

$$\frac{7500 \cdot 0.8}{\rho g Q} = 20 + \frac{Q^2}{0.1257^2 \cdot 2g}\left(\frac{f_D \cdot 8000}{0.40} + 0.4 + 1\right)$$

For $f_{D,\text{step }0} = 0.020$, it follows that $Q_{\text{step }0} = 0.0290\,\text{m}^3/\text{s}$; then $f_{D,\text{step }1} = 0.0272$ and $Q_{\text{step }1} = 0.0285\,\text{m}^3/\text{s}$; $f_{D,\text{step }2} = 0.0272$, which confirms and ends the process, and the discharge is the same as with $f_{D,\text{step }1}$.

b) The function therefore generally reads:

$$\frac{7500 \cdot 0.8}{\rho g\left(\pi \cdot k_f \frac{h_1^2 - h_0^2}{\ln\left(\frac{r_1}{r_0}\right)}\right)} = (20 + h_1 - h_0) + \frac{\left(\pi \cdot k_f \frac{h_1^2 - h_0^2}{\ln\left(\frac{r_1}{r_0}\right)}\right)^2}{0.1257^2 \cdot 2g}\left(\frac{0.0272 \cdot 8000}{0.40} + 0.4 + 1\right)$$

Substituting values:

$$\frac{7500 \cdot 0.8}{\rho g\left(\pi \cdot 1.0 \times 10^{-4} \frac{40^2 - h_0^2}{\ln\left(\frac{3000}{0.2}\right)}\right)} = (60 - h_0) + \frac{\left(\pi \cdot 1.0 \times 10^{-4} \frac{40^2 - h_0^2}{\ln\left(\frac{3000}{0.2}\right)}\right)^2}{0.1257^2 \cdot 2g}\left(\frac{0.0272 \cdot 8000}{0.40} + 1.4\right)$$

And finally one obtains, thanks to Octave, $h_0 = 31.119\,\text{m}$.

c) We have only to insert h_0:

$$Q = \pi \cdot k_f \frac{h_1^2 - h_0^2}{\ln\left(\frac{r_1}{r_0}\right)} = 0.0206\,\text{m}^3/\text{s}$$

d) This is the difference between h_1 and h_0:

$$\Delta h = h_1 - h_0 = 8.881\,\text{m}$$

Solution 6.3

a) With

$$60 = \frac{Q^2}{A^2 2g}\left(\frac{f_D L}{d_{\text{pipe}}} + 1\right)$$

$Q = 0.376\,\text{m}^3/\text{s}$ and $v = 1.915\,\text{m/s}$; hence, $\frac{v^2}{2g} = 0.187\,\text{m}$ is the result.

$$p_{\text{piezo@air vessel}} = 500 + \frac{60 - 0.187}{2} = 529.91\,\text{m.a.s.l. at } z_{\text{pipe@air vessel}} = 520\,\text{m.a.s.l.}$$

This is to determine the total pressure in the pipe at the air vessel:

$$p_{\text{total@air vessel}} = \rho \cdot g \cdot 9.91 + p_0 = 1.9852 \times 10^5\,\text{N/m}^2$$

b) The air volume in the air vessel is:

$$V_{\text{air vessel}} = \frac{4}{3}R^3\pi + h \cdot R^2\pi + 0.1^2 \cdot \pi \cdot 0.5 = 1.717\,\text{m}^3$$

$$V_1 = \frac{p_0 V_0}{p_1} = \frac{101\,300 \cdot 1.717}{1.9852 \times 10^5} = 0.876\,\text{m}^3$$

In the upper hemisphere, the volume is $\frac{2}{3}R^3 \cdot \pi = 0.262\,\text{m}^3$; it is $0.876 - 0.262 = 0.614\,\text{m}^3$ in the remaining part. From the contact point of the upper hemisphere, $h' = \frac{0.614}{R^2\pi} = 0.782\,\text{m}$. The water level in the air vessel rises up to $520 + 0.5 + 0.5 + 1.5 - 0.782 = 521.72\,\text{m.a.s.l.}$

c) The water level rises. Due to the lower discharge, the losses in the pipe section to the valve are lower; therefore, the pressure height is greater and the air volume is further compressed.

Solution 6.4

a)

$y_N = 0.804\,\text{m}$	$v_N = 5.328\,\text{m/s}$	$H_N = 2.252\,\text{m}$
$\text{Fr}_N = 1.897$	$y_c = 1.233\,\text{m}$	$H_{\min} = 1.849\,\text{m}$

We are in supercritical flow and $H_N - K\frac{v_N^2}{2g} > H_{\min}$. Thus, there will be no backwater and the energy loss occurs at the trash rack. With $H_{\text{downs}} = H_N - K\frac{v_N^2}{2g} = 1.963\,\text{m}$, $y_{\text{downs}} = 0.972\,\text{m}$ follows (also supercritical flow).

b) Here again, the momentum equation is the means of choice. The control volume extends from upstream to downstream from the rack.

$$F + \rho \cdot \frac{Q^2}{b \cdot y_N} + \frac{1}{2} \cdot \rho \cdot g \cdot y_N^2 \cdot b = \rho \cdot \frac{Q^2}{b \cdot y_{\text{downs}}} + \frac{1}{2} \cdot \rho g \cdot y_{\text{downs}}^2 \cdot b$$

$$\rightarrow F = \rho \cdot \frac{30^2}{7 \cdot 0.972} + \frac{1}{2} \cdot \rho \cdot g \cdot 0.972^2 \cdot 7 - \rho \cdot \frac{30^2}{7 \cdot 0.804} - \frac{1}{2} \cdot \rho \cdot g \cdot 0.804^2 \cdot 7 = -1.740 \times 10^4\,\text{N}$$

7 Solutions: unsteady free surface flows

Solution 7.1

a) Velocity is distance per unit time.

$$c_{\text{abs}} = \frac{x}{t} = \frac{2000}{589} = 3.396\,\text{m/s}$$

b) We calculate the relative propagation velocity with surge height $h = 0.45\,\text{m}$.

$$c = \sqrt{\frac{g \cdot 7.5 \cdot 2.1}{7.5}} \cdot \sqrt{1 + \frac{3}{2} \cdot \frac{0.45 \cdot 7.5}{7.5 \cdot 2.1} + \frac{1}{2}\left(\frac{0.45 \cdot 7.5}{7.5 \cdot 2.1}\right)^2} = 5.26\,\text{m/s}$$

Only now we see that the absolute propagation velocity has a negative sign. This means that:

$$c_{\text{abs}} = \frac{x}{t} = \frac{-2000}{589} = -3.396\,\text{m/s}$$

But we have to go back to the calculation of the original flow velocity v_0

$$v_0 = c_{\text{abs}} + c = -3.40 + 5.26 = 1.86\,\text{m/s}$$

and to the discharge Q_0:

$$Q_0 = v_0 A_0 = 29.30\,\text{m}^3/\text{s}$$

c) The reduction in discharge results from the continuity condition:

$$\Delta Q = c_{\text{abs}} \cdot h \cdot b = -3.40 \cdot 0.45 \cdot 7.50 = -11.475\,\text{m}^3/\text{s}$$

d) It is an upsurge.

Solution 7.2

a) With the routine `surge.m`, the result reads[D]:

$$c = 8.05\,\text{m/s}$$

$$c_{\text{abs}} = -7.03\,\text{m/s}$$

b) We determine the height of the surge:

$$h_{\text{upsurge}} = 0.395\,\text{m}$$

Thus, the freeboard is maintained because $1.5 - 0.395 > 1.0$.

c) Time corresponds to distance divided by velocity.

$$t = \frac{x}{c_{\text{abs}}} = 1138\,\text{s} = 18.97\,\text{min}$$

Solution 7.3

a) And it is the continuity condition which saves us yet again:

[D] Please note that you may display the associated propagation velocities after the `while` loop via `disp(c)`; the routine displays the result for h only.

$$v_0 = \frac{Q_0}{A_0} = \frac{5.0 \times 10^{-3}}{0.20 \cdot 0.05} = 0.50\,\mathrm{m/s}$$

b) A clever technique!

$$h = 0.04\,\mathrm{m}$$

c) We once more set up the equation for the propagation velocity of shallow water waves, which are affected by the surge height h.

$$c = \sqrt{\frac{g \cdot 0.20 \cdot 0.05}{0.20}} \sqrt{1 + \frac{3}{2} \cdot \frac{0.04 \cdot 0.20}{0.20 \cdot 0.05} + \frac{1}{2} \left(\frac{0.04 \cdot 0.20}{0.20 \cdot 0.05} \right)^2} = 1.11\,\mathrm{m/s}$$

d) The propagation of the surge wave takes place opposite ($-c$) to the direction of flow $+v_0$:

$$c_{\mathrm{abs}} = v_0 - c = 0.50 - 1.11 = -0.61\,\mathrm{m/s}$$

e) time = distance / velocity:

$$t = \frac{x}{c_{\mathrm{abs}}} = \frac{-1.38}{-0.61} = 2.26\,\mathrm{s}$$

The result is 2.26 s after the closing of the open channel.

f) The continuity condition is necessary:

$$\Delta Q = 0.04 \cdot (-0.61) \cdot 0.20 = -4.88\,\mathrm{L/s}$$

The discharge reduction amounted to −97.6 %; i. e. the sluice gate was (almost) completely closed.

Part IV
Practical examples

Chapter 18
Forces and moments of force at the weir in Wieblingen

For the weir in Wieblingen at the river Neckar, which consists of roller dams, a determination of the forces and moments of force to be counteracted by the structure will be made. The width of weir field 6 is 12.94 m. Figure 18.1 is a schematic illustration of the cross-section.

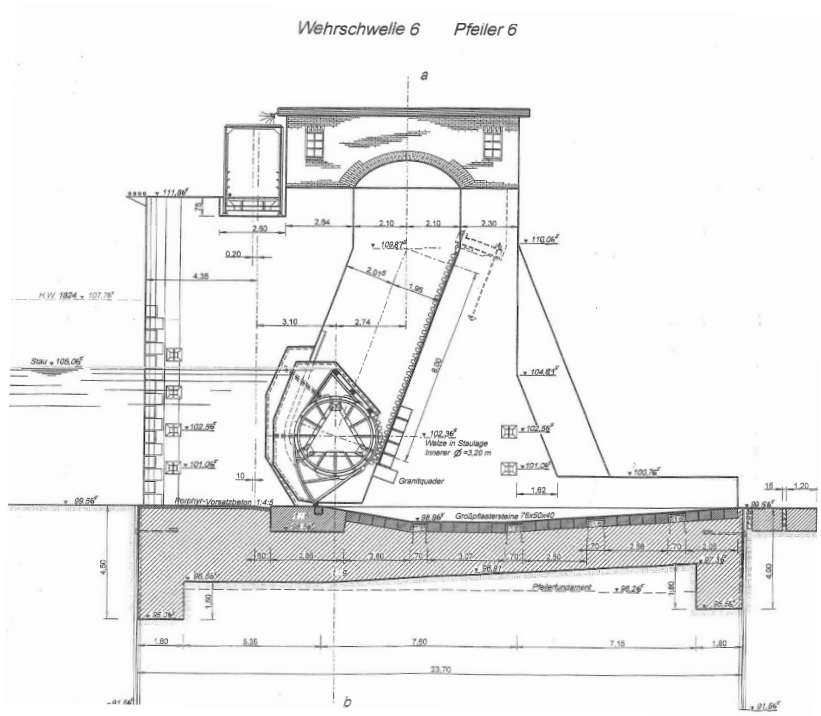

Figure 18.1: Sectional view of field 6 of the weir in Wieblingen (source: WSA Heidelberg).

The design drawing was accessed in order to be able to indicate the relevant dimensions (see Figure 18.2). The centres of gravity of the areas were calculated, transferred into the plan and the respective lever arm of the partial area was measured.
Thanks to the constant width, the horizontal force F_H is easy to calculate:

C. Rapp, *Hydraulics in Civil Engineering*,
https://doi.org/10.1007/978-3-031-54860-4_18

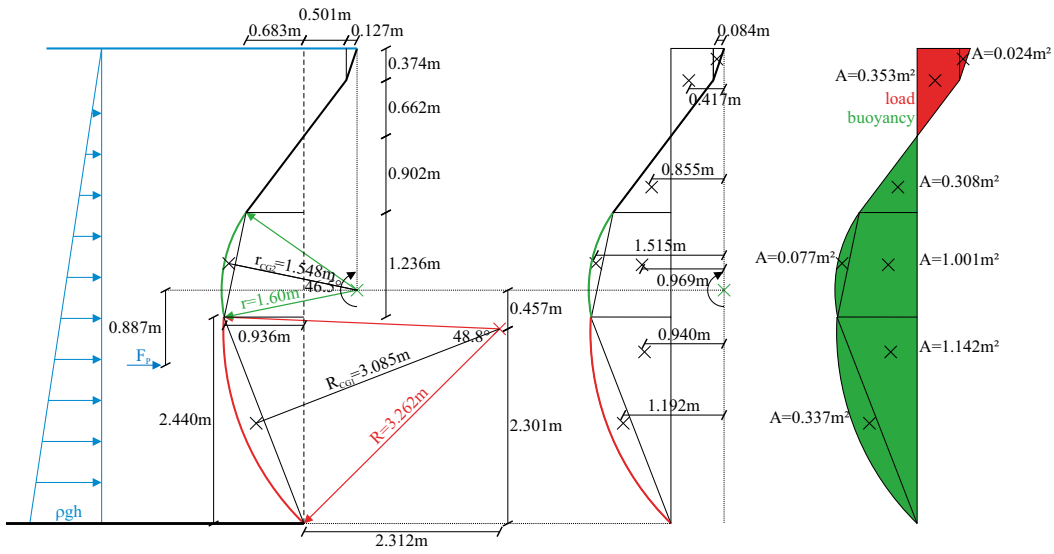

Figure 18.2: Area and lever arm calculations for the roller dam at Wieblingen.

$$F_H = \int \rho g h \, \mathrm{d}A = \frac{1}{2} \cdot \rho \cdot g \cdot h^2 \cdot b = \frac{1}{2} \cdot \rho \cdot g \cdot 5.614^2 \cdot 12.94 = 2.00 \times 10^6 \,\mathrm{N} \tag{18.1}$$

The vertical force is determined via a vertical line drawn from the base point and the resulting partial areas (or, in three dimensions, the volumes). The red areas (i. e. in three dimensions, the red volumes) of width 12.94 m result in the following downward force:

$$\downarrow F = \rho \cdot g \cdot 12.94 \cdot (0.024 + 0.353) = 4.786 \times 10^4 \,\mathrm{N} \tag{18.2}$$

The green-coloured areas are summed up to calculate the corresponding volume with width 12.94 m which results in the following upward force:

$$\uparrow F = \rho \cdot g \cdot 12.94 \cdot (0.308 + 0.077 + 1.001 + 1.142 + 0.337) = 3.637 \times 10^5 \,\mathrm{N} \tag{18.3}$$

Adding the forces vectorially, we obtain a resultant upward vertical force of $F_V = 3.158 \times 10^5$ N. The lines of action of the partial vertical forces pass through the centres of gravity of the respective areas. These may easily be determined by means of the partial areas (circular sections, triangles and trapezoids) that have already been used for calculating the vertical force.

The determination of the resultant moment of force about the pivot point is more complex; however, the essential work is already included in Figure 18.2. Rotating in a clockwise direction all buoyancy areas (volumes) with their respective lever arms, are to be specified.

$$\begin{aligned} M_{\circlearrowleft} &= (0.308 \cdot 0.855 + 0.077 \cdot 1.515 + 1.001 \cdot 0.969 + 1.142 \cdot 0.940 + 0.337 \cdot 1.192) \cdot b \cdot \rho \cdot g \\ &= 2.825 \cdot 12.94 \cdot \rho \cdot g = 3.59 \times 10^5 \,\mathrm{N\,m} \end{aligned} \tag{18.4}$$

Rotating in an anticlockwise direction, the resulting horizontal force on $\frac{2}{3}h$ at a distance of 0.887 m from the pivot point, and the load areas (volumes) with their lever arms are to be specified.

$$\begin{aligned} M_{\circlearrowleft} &= 2.00 \times 10^6 \cdot 0.887 + (0.024 \cdot 0.084 + 0.353 \cdot 0.417) \cdot b \cdot \rho \cdot g \\ &= 1.77 \times 10^6 + 1.894 \times 10^4 = 1.79 \times 10^6 \,\mathrm{N\,m} \end{aligned} \tag{18.5}$$

From that, an anticlockwise rotating moment of force results:

$$M_{\circlearrowleft \mathrm{resulting}} = M_{\circlearrowleft} - M_{\circlearrowright} = 1.79 \times 10^6 - 3.59 \times 10^5 = 1.43 \times 10^6 \,\mathrm{N\,m} \tag{18.6}$$

Please note, that only forces and moments of force induced by the water pressure were calculated. The dead loads are not to be considered here.

Chapter 19
Determination of the bearing forces in the Leitzachwerk pumped-storage power station

The Leitzachwerk is a pumped-storage power station where parts of three rivers are diverted into the upper basin, Lake Seeham, before it is used for power generation and subsequently stored in the lower basins. Later, it will probably be pumped back into Lake Seeham or released from the lower basins in the nearby river. Actually, there are two power plants with two separate penstocks. Plant 1 was first built in 1913 and completely reconstructed during the 1980s. In Plant 1, a single Francis pump turbine with vertical shaft is installed. Plant 2, which we will analyse, was built in the 1960s and comprises two ternary units. In ternary units, pump and turbine are separate from one another; however, they share a common motor generator. In pump operation, the motor drives the pump; in turbine mode, the generator converts the mechanical energy into electric power. In order to supply the two units, the penstock is split-up by a Y-pipe, which is illustrated in the left part of Figure 19.1. The two pipe strands are divided yet again to supply water to the respective turbine or to receive the water from the pump. In Figure 19.1, the left (upper) strands in the direction of flow lead to the turbine; the right (lower) strands lead to or rather come from the pump.

Inclination of the system

The upper area of Figure 19.1 shows the section of the penstock system with the vertical inclination of $5°20'$. If we intend to determine the resulting forces for the three nodes at the Y-pipes, we may apply the first simplification. With an angle of $5°20'$ with respect to the horizontal, the cosine is almost one. We therefore look at the system as if it were located on a horizontal plane.

Pressure

At a gross head of approximately $130\,\mathrm{m}$, the pressure in the penstock is about $p = \rho \cdot g \cdot 130 = 1.275 \times 10^6\,\mathrm{N/m^2}$. In the design of bearing forces, it is recommended that calculations not be made with excessive precision. The pressures may be far higher because of regulating processes (see also Chapter 12). In our case, pressures up to approximately $20\,\mathrm{bar}$ (that is, $1.962 \times 10^6\,\mathrm{N/m^2}$) are to be expected.

C. Rapp, *Hydraulics in Civil Engineering*,
https://doi.org/10.1007/978-3-031-54860-4_19

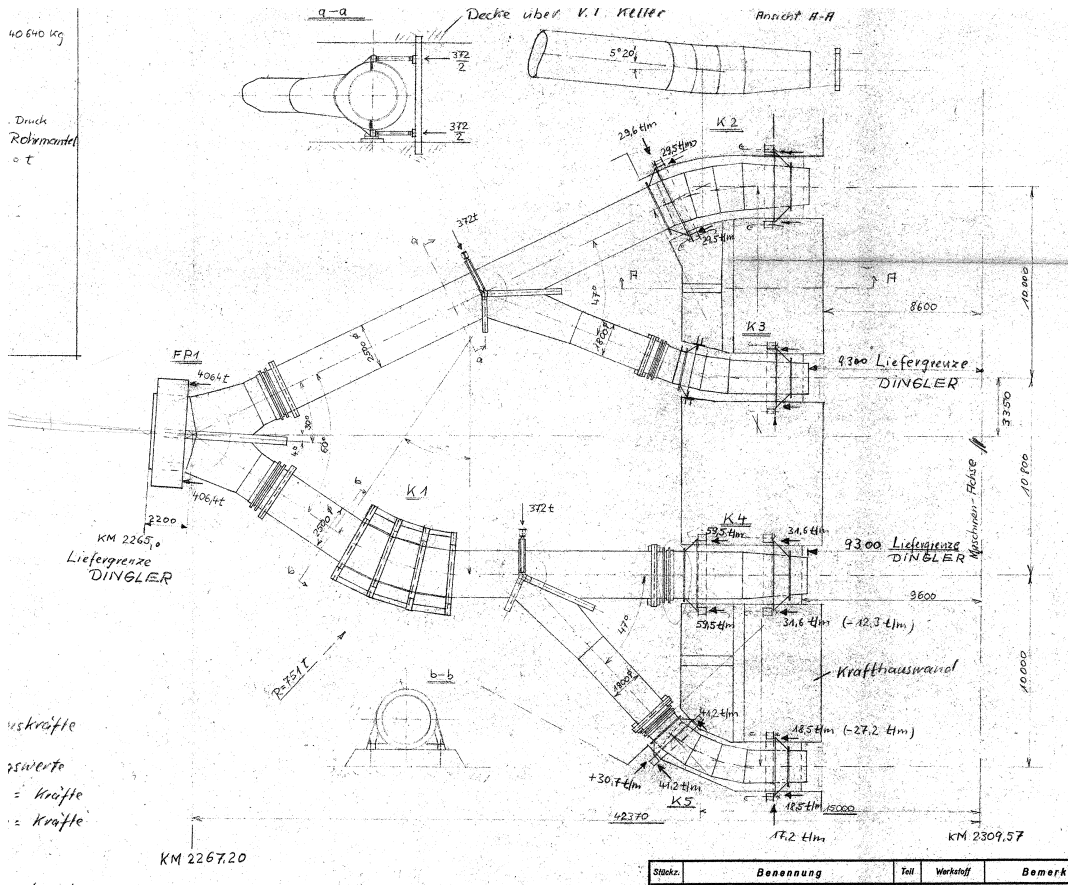

Figure 19.1: Penstock of the Leitzachwerk 2.

Momentum flux

From the discharges at various operating conditions, the maximum momentum fluxes result with the respective minimum pipe diameters:

operating mode	discharge	tightest cross-section	max. velocity	momentum flux
2 turbines	$Q = 44\,\mathrm{m^3/s}$	$A = \frac{4^2\pi}{4} = 12.57\,\mathrm{m^2}$	$v_{\max} = 3.50\,\mathrm{m/s}$	$\rho Q v_{\max} = 1.54 \times 10^5\,\mathrm{N/m^2}$
1 turbine	$Q = 22\,\mathrm{m^3/s}$	$A = \frac{2.5^2\pi}{4} = 4.91\,\mathrm{m^2}$	$v_{\max} = 4.48\,\mathrm{m/s}$	$\rho Q v_{\max} = 9.86 \times 10^4\,\mathrm{N/m^2}$
1 pump	$Q = 13\,\mathrm{m^3/s}$	$A = \frac{1.8^2\pi}{4} = 2.54\,\mathrm{m^2}$	$v_{\max} = 5.11\,\mathrm{m/s}$	$\rho Q v_{\max} = 6.64 \times 10^4\,\mathrm{N/m^2}$

It is obvious that the momentum fluxes are one order smaller than the pressure forces. Therefore, they will be neglected for the design of the bearings in the following discussion.

Decomposition of the elements

Figure 19.2 shows in more detail how the flow forces are counteracted by the system. The individual penstock elements are connected by gland packages (or stuffing boxes)

which cannot transfer axial forces (identified by ↔ in the drawing). The bearings are also identified in the drawing (movable in the direction of the pipe ≙ or unmovable ≙). It is

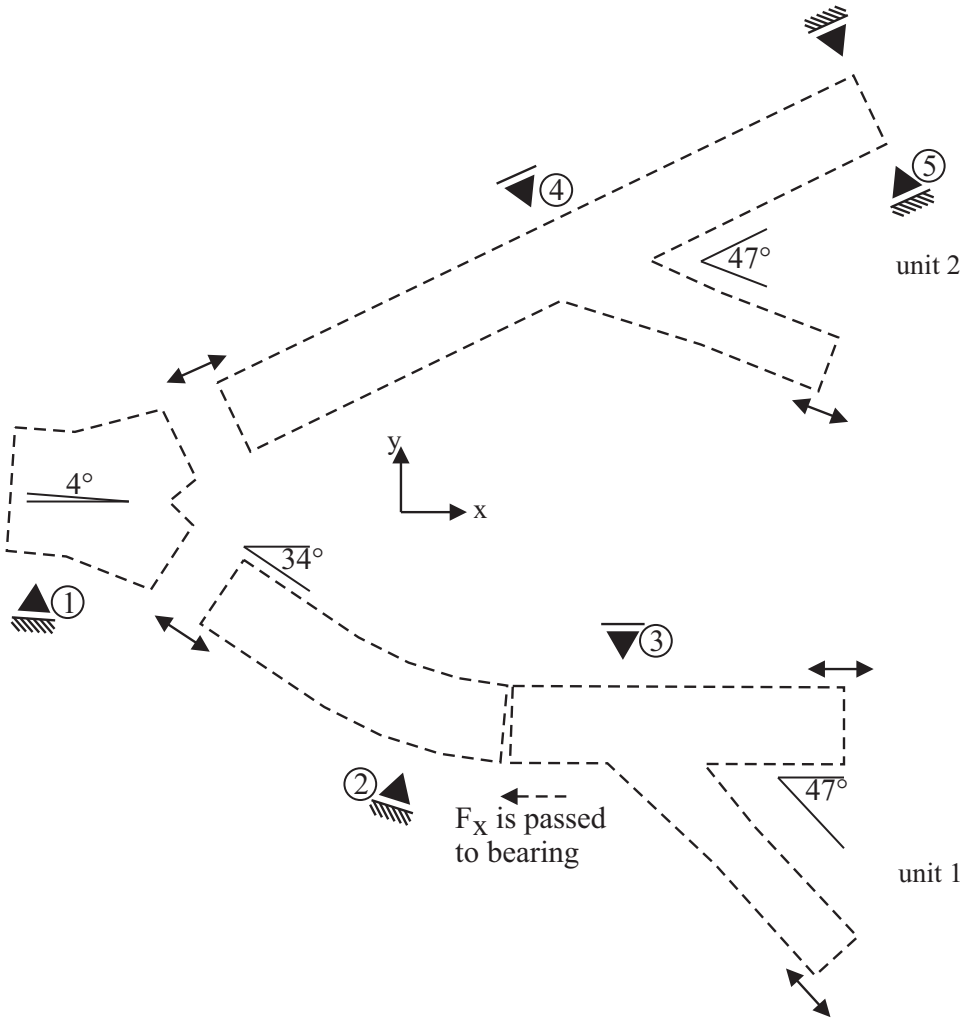

Figure 19.2: Decomposition of the support elements

evident that the bearing of the Y-pipe of unit 1 counteracts the forces in the *y*-direction and that the axial forces must be transferred in the *x*-direction to the fixed point at the bend.

Big Y-pipe

At the fixed point, the discharge is divided into two branches that are both at an angle of 30°, clockwise and anticlockwise, relative to the original direction[A]. We set up the balance of forces:

$$\begin{aligned} \leftarrow F_{x,1} &= p_l A_l - 2 \cdot p_r A_r \cos 30^\circ = 1.962 \times 10^6 \cdot \frac{4^2\pi}{4} - 2 \cdot 1.962 \times 10^6 \cdot \frac{2.5^2\pi}{4} \cdot \cos 30^\circ \\ &= 2.466 \times 10^7 - 2 \cdot 9.631 \cdot \cos 30^\circ = 2.466 \times 10^7 - 1.668 \times 10^7 = 7.974 \times 10^6\,\mathrm{N} \end{aligned} \tag{19.1}$$

Force balance at the Y-pipe of the right machine unit

The angle between the branch and the pump, relative to the x-axis, is 47°; the diameter is specified as 1.80 m.

$$\uparrow F_{y,3} = -p_r \frac{1.8^2\pi}{4} \cdot \sin 47^\circ = -3.651 \times 10^6\,\mathrm{N} \tag{19.2}$$

The force in the y-direction is applied directly. However, the bearing may not counteract forces in the x-direction. The horizontal force in the x-direction is transferred to the large bend and its bearing.

Big bend

At the bend in the lower left of the figure, the deflection is 34°. From the upstream pressure force calculated above, it follows proportionately for the x-direction $1.962 \times 10^6 \cdot \frac{2.5^2\pi}{4} \cdot \cos 34^\circ = 7.984 \times 10^6\,\mathrm{N}$; for the y-direction, we obtain $1.962 \times 10^6 \cdot \frac{2.5^2\pi}{4} \cdot \sin 34^\circ = 5.386 \times 10^6\,\mathrm{N}$.

$$\begin{aligned} \leftarrow F_{x,2} &= p_l \frac{2.5^2\pi}{4} \cdot \cos 34^\circ - p_r \frac{2.5^2\pi}{4} - p_r \frac{1.8^2\pi}{4} \cdot \cos 47^\circ \\ &= 9.631 \times 10^6 \cdot \cos 34^\circ - 9.631 \times 10^6 - 4.993 \times 10^6 \cdot \cos 47^\circ = -5.052 \times 10^6\,\mathrm{N} \end{aligned} \tag{19.3}$$

We plotted $F_{x,2}$ against the x-direction to the left. Because of the negative sign, the horizontal reaction force points in the positive x-direction to the right.

$$\uparrow F_{y,2} = p_l A_l \cdot \sin 34^\circ + p_r A_r \cdot \sin 0^\circ = 5.386 \times 10^6 + 0 = 5.386 \times 10^6\,\mathrm{N} \tag{19.4}$$

Therefore, the resultant force at the bend is:

$$\nearrow F_{RH,2} = \sqrt{(5.386 \times 10^6)^2 + (-5.052 \times 10^6)^2} = 7.384 \times 10^6\,\mathrm{N} \tag{19.5}$$

[A] The main penstock is actually rotated by 4° relative to the global x-direction, which is perpendicular to the axes of the machine sets.

Force balance at the Y-pipe of the left machine unit

The branch to the pump is tilted at an angle of 47° with respect to the main pipe and has a diameter of 1.80 m; the bearing is movable and counteracts forces perpendicularly to the main pipe only.

$$\searrow F_{\text{normal},4} = p_r \frac{1.8^2 \pi}{4} \cdot \sin 47^\circ = 3.651 \times 10^6 \,\text{N} \tag{19.6}$$

The axial force is absorbed at the right end of the pipe just upstream from the bend, which supplies the water directly to the turbine; a journal bearing with a diameter of $d = 3.75\,\text{m}$ is located there.

$$\nearrow F_{\text{axial},5} = p_r \frac{1.8^2 \pi}{4} \cdot \cos 47^\circ = 3.405 \times 10^6 \,\text{N} \tag{19.7}$$

Finally, the load acting on the journal bearing per circumferential metre is $F_{\text{bearing}} = \frac{3.405 \times 10^6}{d\pi} = 2.89 \times 10^5 \,\text{N/m}$.

Vertical forces

The vertical forces consist of the dead loads of the pipes and the weight of the water, $\rho g V$, therein.

Chapter 20
Dimensioning of an interceptor sewer in Hamburg Waltershof

We shall consider here a complex part of the sewage system in Hamburg[A]. The project comprises the construction of a waste water sewer at the Altenwerder Damm in Waltershof (see Figure 20.1). From both station 1 at 0.50 m.a.s.l. and station 2 at 0.80 m.a.s.l., water is pumped into an interceptor sewer with a water level of 3.11 m.a.s.l. The hydraulic system shown in Figure 20.2 was accessed from the planning data.
A hydrologic estimate resulted in maximum flows of $Q_1 = 0.70\,\mathrm{m}^3/\mathrm{s}$ and $Q_2 = 0.04\,\mathrm{m}^3/\mathrm{s}$ for the two pump stations (PS1 and PS2). In the calculations for sewage pipes, the kinematic viscosity is usually set at $\nu = 1.31 \times 10^{-6}\,\mathrm{m}^2/\mathrm{s}$ (see DWA-A110 [12]); this corresponds to a temperature of $T = 10\,^\circ\mathrm{C}$.

Section 1

The length of the pipe between pump station 1 and the junction of the two strands is $L_1 = 1894.91\,\mathrm{m}$; in the present example, a steel pipe lined with alumina cement and with an equivalent sand grain roughness of $k_{s1} = 3 \times 10^{-5}\,\mathrm{m}$ is to be installed[B]. The individual minor (local) losses that occur at the inlet and due to pipeline curvatures amount to $\sum K_1 = 1.463$.

Section 2

The length of the pipe between pump station 2 and the junction is $L_2 = 394.75\,\mathrm{m}$, wherein PE, with an equivalent sand grain roughness of $k_{s2} = 1 \times 10^{-5}\,\mathrm{m}$, is to be employed in this case. The minor (local) losses add up to $\sum K_2 = 0.28$.

[A] Thanks to Mrs. Dipl.-Ing. Iris Carstensen with HamburgWasser for providing the planning data.
[B] This material selection is purely fictitious. HamburgWasser uses PE pipes in accordance with the state of the art (see strand 2). These are better suited for the sometimes highly acidic environment. The alumina cement-lined steel pipe only serves to didactically process the influence of the different roughness values.

C. Rapp, *Hydraulics in Civil Engineering*,
https://doi.org/10.1007/978-3-031-54860-4_20

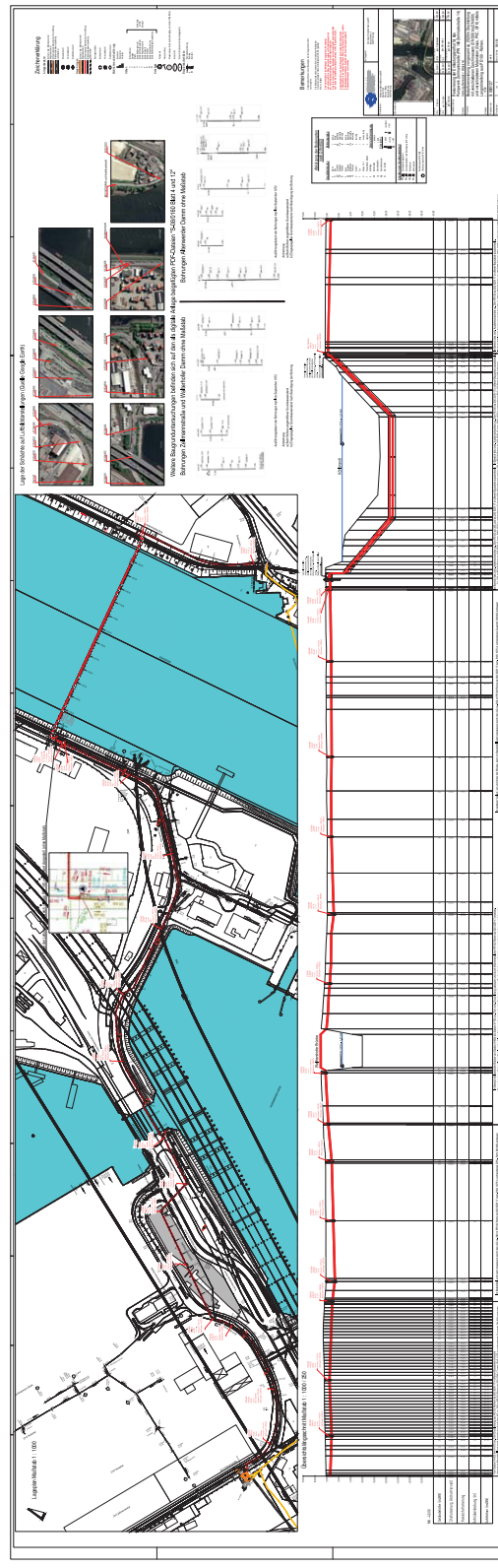

Figure 20.1: Schematic diagram of an interceptor sewer at the Altenwerder Damm in Hamburg Waltershof.

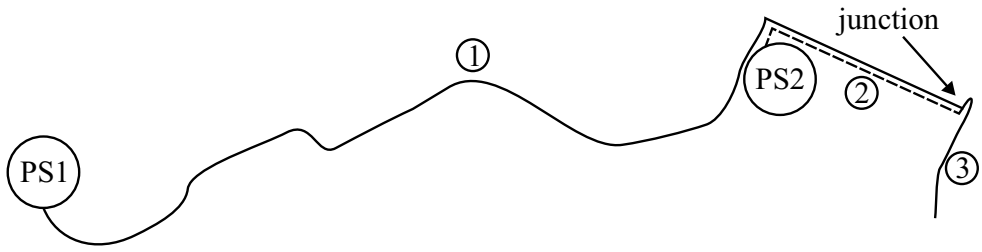

Figure 20.2: Pipeline system at the Altenwerder Damm in Hamburg Waltershof.

Section 3

The length of the pipe between section 3 and the junction is $L_3 = 225.38\,\mathrm{m}$. The minor (local) losses amount to $\sum K_3 = 0.28$. The use of an alumina cement-lined steel pipe is specified here as well ($k_{s3} = 3 \times 10^{-5}\,\mathrm{m}$); also, the diameter is to be the same as that of strand 1 $d_3 = d_1$ (as to the material selection, see strand 1).

Pump station 1

The characteristic of the identified pump in station 1 is generated from the set of points in Table 20.1:

Table 20.1: Relationship between delivery head and discharge values in pump station 1.

Q [$\mathrm{m^3/s}$]	H [m]
0	28.87
0.144	23.56
0.288	19.58
0.432	17.14
0.576	14.79
0.684	13.26
0.792	11.73
0.900	10.00
1.008	7.96
1.080	6.53

You may graph the relationship between delivery head and discharge and derive a function by means of the least squares method. When approximating the table values via a third-degree polynomial, the result for the delivery head, depending on the discharge, is:

$$H_{\mathrm{P1}} = -21.094 \cdot Q^3 + 42.311 \cdot Q^2 - 41.817 \cdot Q + 28.812 \tag{20.1}$$

For redundancy reasons, for achieving maximum discharge and for improving energy efficiency, two pumps are connected in parallel. In the parallel configuration, the characteristics, according to Figure 11.15 in Chapter 11.7.1, are such that the discharges are

"added" while the delivery head remains constant. For two pumps connected in parallel, the result from the discharges of Table 20.1, multiplied by 2, is:

$$H_{\mathrm{P1,2\,parallel\ pumps}} = -2.637 \cdot Q^3 + 10.578 \cdot Q^2 - 20.908 \cdot Q + 28.812 \tag{20.2}$$

The manufacturer of a pump that is suitable for pump station 2 indicates the relationship between discharge and delivery head in Table 20.2:

Table 20.2: Relationship between delivery head and discharge in pump station 2.

Q [m^3/s]	H [m]
0	9.00
0.0436	6.867
0.055	0

Since only three points are given, it follows that with linear approximation, for discharges less than 0.0436 m^3/s:

$$H_{\mathrm{P2}} = -48.944 \cdot Q + 9.00 \quad \text{for}\, 0 \le Q \le 0.0436\,\mathrm{m^3/s} \tag{20.3}$$

And for discharges greater than 0.0436 m^3/s, delivery head is:

$$H_{\mathrm{P2}} = -601.31 \cdot Q + 33.072 \quad \text{for}\, 0.0436 < Q \le 0.055\,\mathrm{m^3/s} \tag{20.4}$$

As in pump station 1, two pumps connected in parallel are also installed in pump station 2. Consequently, the result for the lower discharge range is

$$H_{\mathrm{P2,2\,parallel\ pumps}} = -24.472 \cdot Q + 9.00 \quad \text{for}\, 0 \le Q \le 0.0872\,\mathrm{m^3/s} \tag{20.5}$$

and for the greater one, it is:

$$H_{\mathrm{P2,2\,parallel\ pumps}} = -300.66 \cdot Q + 33.072 \quad \text{for}\, 0.0872 < Q \le 0.11\,\mathrm{m^3/s} \tag{20.6}$$

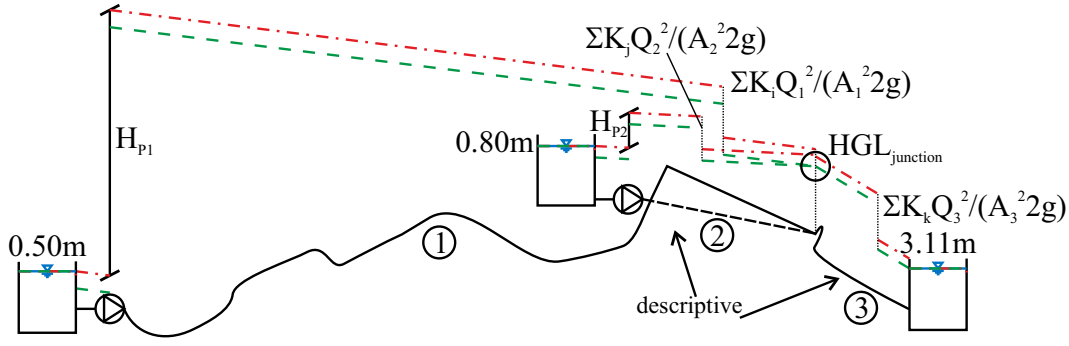

Figure 20.3: Energy diagram for the sewage system in Hamburg.

With the energy diagram in Figure 20.3, Equations 20.7 through 20.9 may be established for the three pipe sections. For the sake of clarity, no units are indicated. The result for strand 1 is:

$$0.50 + \mathrm{H_{P1}}(Q) - \frac{Q_1^2}{r_1^4 \pi^2 2g}\left(\frac{f_\mathrm{D} L_1}{d_1} + \sum K_i + 1\right) = \mathrm{HGL_{junct}} \tag{20.7}$$

From pump station 2, it follows that for the second strand:

$$0.80 + \mathrm{H_{P2}}(Q) - \frac{Q_2^2}{r_2^4 \pi^2 2g}\left(\frac{f_\mathrm{D} L_2}{d_2} + \sum K_j + 1\right) = \mathrm{HGL_{junct}} \tag{20.8}$$

From the junction to the interceptor sewer, we obtain:

$$\mathrm{HGL_{junct}} - \frac{(Q_1 + Q_2)^2}{r_3^4 \pi^2 2g}\left(\frac{f_\mathrm{D} L_3}{d_3} + \sum K_k\right) = 3.11 \tag{20.9}$$

Ideally, the equations for the delivery heads are now solved for the required maximum discharges and inserted into Equations 20.7 and 20.9. For strand 1, we obtain

$$\mathrm{H_{P1}}(Q) = -2.637 \cdot 0.70^3 + 10.578 \cdot 0.70^2 - 20.908 \cdot 0.70 + 28.812 = 18.455 \tag{20.10}$$

and for strand 2:

$$\mathrm{H_{P2}}(Q) = -24.472 \cdot 0.04 + 9.00 = 8.021 \quad \text{for } 0 \le Q \le 0.0872\,\mathrm{m^3/s} \tag{20.11}$$

Equation 20.7 reads with the results from the throttle curve of the pump for $\mathrm{H_{P1}}(Q) = 18.455\,\mathrm{m}$ from Equation 20.10 with $Q_1 = 0.70\,\mathrm{m^3/s}$:

$$0.50 + 18.455 - \frac{Q_1^2}{r_1^4 \pi^2 2g}\left(\frac{f_\mathrm{D} L_1}{d_1} + \sum K_i + 1\right) = \mathrm{HGL_{junct}} \tag{20.12}$$

And with $Q_2 = 0.040\,\mathrm{m^3/s}$, Equation 20.8 converts to (see Equation 20.11):

$$0.80 + 8.021 - \frac{Q_2^2}{r_2^4 \pi^2 2g}\left(\frac{f_\mathrm{D} L_2}{d_2} + \sum K_j + 1\right) = \mathrm{HGL_{junct}} \tag{20.13}$$

For a first approach, let's start with a diameter of $d_1 = 0.50\,\mathrm{m}$. It then follows that:

$$0.50 + 18.455 - \frac{0.70^2}{0.25^4 \pi^2 2g}\left(\frac{f_\mathrm{D} \cdot 1894.91}{0.50} + 1.463 + 1\right) = \mathrm{HGL_{junct}} \tag{20.14}$$

For the determination of f_D, the Reynolds number is required:

$$\mathrm{Re} = \frac{vd}{\nu} = \frac{0.70 \cdot 0.5}{0.25^2 \cdot \pi \cdot 1.31 \times 10^{-6}} = 1.36 \times 10^6 \tag{20.15}$$

Finally, it follows with the Prandtl-Colebrook algorithm for the smooth wall:

$$\frac{1}{\sqrt{f_\mathrm{D}}} = -2\log\left(\frac{2.5}{\mathrm{Re}\sqrt{f_\mathrm{D}}}\right) \quad \rightarrow f_\mathrm{D} = 0.011 \tag{20.16}$$

Hence, Equation 20.14, which results from 20.7, becomes:

$$0.50 + 18.455 - \frac{0.70^2}{0.25^4 \pi^2 2g}\left(\frac{0.011 \cdot 1894.91}{0.50} + 1.463 + 1\right) = \mathrm{HGL}_{\mathrm{junct}} = -9.646 \quad (20.17)$$

At this point, one may already see that the pipe that has been selected is too small. The pressure height at the place of the junction is -9.646 m.a.s.l., which is lower than the final water level of 3.11 m.a.s.l. We therefore try a DN600 pipe:

$$0.50 + 18.455 - \frac{0.70^2}{0.3^4 \pi^2 2g}\left(\frac{f_{\mathrm{D}} \cdot 1894.91}{0.60} + 1.463 + 1\right) = \mathrm{HGL}_{\mathrm{junct}} \quad (20.18)$$

We will again be in the turbulent region. The pipe friction coefficient is also determined for the smooth wall as follows:

$$\frac{1}{\sqrt{f_{\mathrm{D}}}} = -2 \cdot \log\left(\frac{2.5}{\mathrm{Re}\sqrt{f_{\mathrm{D}}}}\right) \quad \rightarrow f_{\mathrm{D}} = 0.011 \quad (20.19)$$

With $f_{\mathrm{D1}} = 0.011$, Equation 20.18 reads:

$$0.50 + 18.455 - \frac{0.70^2}{0.30^4 \pi^2 2g}\left(\frac{0.011 \cdot 1894.91}{0.60} + 1.463 + 1\right) = \mathrm{HGL}_{\mathrm{junct}} = 7.333 \quad (20.20)$$

It might work with this diameter. We may first try to see whether the energy dissipated over the distance downstream from the junction is available. With $d_3 = d_1$ and $Q_3 = Q_1 + Q_2 = 0.74\,\mathrm{m}^3/\mathrm{s}$, we also obtain $f_{\mathrm{D3}} = 0.011$ as the pipe friction coefficient for strand 3.

$$7.333 - \frac{(0.70 + 0.04)^2}{0.3^4 \pi^2 2g}\left(\frac{0.011 \cdot 225.38}{0.60} + 0.28\right) = 5.793 \quad (20.21)$$

Thus, the discharge of $Q = 0.70\,\mathrm{m}^3/\mathrm{s}$ to the junction and $Q = 0.74\,\mathrm{m}^3/\mathrm{s}$ from the junction to the interceptor sewer is possible.

Now we will deal with strand 2 and select a PE DN200 pipe ($k_{s2} = 1 \times 10^{-5}\,\mathrm{m}$). The pipe friction coefficient is to be determined by means of the equation for the smooth wall with $f_{\mathrm{D2}} = 0.016$:

$$0.80 + 8.021 - \frac{0.04^2}{0.10^4 \pi^2 2g}\left(\frac{0.016 \cdot 394.75}{0.20} + 0.28 + 1\right) = \mathrm{HGL}_{\mathrm{junct}} = 6.106 \quad (20.22)$$

In this way, the dimensioning seems to work. It is known that the required maximum discharges may be pumped through the pipes to the interceptor sewer; the exact discharge is not known. Those who want a more precise answer will have to adjust the discharges by trying some more in such a manner that, on the one hand, all three pipes at the junction exhibit the same pressure and, on the other hand, that the water level actually results in the manhole at the end of strand 3. By establishing a system of linear equations and checking the pump equation to be used (pump station 2 has two ranges of validity), the result will be obtained. The system of linear equations reads:

$$\begin{bmatrix} \frac{\left(\frac{f_{D1}\cdot L_1}{d_1}+\sum K_1+1\right)8}{d_1^4\pi^2 g} & 0 & 1 \\ 0 & \frac{\left(\frac{f_{D2}\cdot L_2}{d_2}+\sum K_2+1\right)8}{d_2^4\pi^2 g} & 1 \\ -\frac{\left(\frac{f_{D3}\cdot L_3}{d_3}+\sum K_3\right)8}{d_3^4\pi^2 g} & -\frac{\left(\frac{f_{D3}\cdot L_3}{d_3}+\sum K_3\right)8}{d_3^4\pi^2 g} & 1 \end{bmatrix} \times \begin{bmatrix} Q_1^2 \\ Q_2^2 \\ \mathrm{HGL_{junct}} \end{bmatrix} = \begin{bmatrix} 0.50+H_{\mathrm{P1,2\,parallel\ pumps}} \\ 0.80+H_{\mathrm{P2,2\,parallel\ pumps}} \\ 3.11 \end{bmatrix}$$

$$= \begin{bmatrix} 0.50-2.637\cdot Q^3+10.578\cdot Q^2-20.908\cdot Q+28.812 \\ 0.80-24.472\cdot Q+9.00 \\ 3.11 \end{bmatrix} \tag{20.23}$$

For the solution of this system of equations, one may, for example, use the code shown in Chapter A.7 to obtain:

$$Q_1 = 0.745\,\mathrm{m^3/s} \tag{20.24}$$

$$Q_2 = 0.047\,\mathrm{m^3/s} \tag{20.25}$$

$$Q_3 = 0.792\,\mathrm{m^3/s} \tag{20.26}$$

Chapter 21
Optimisation of the operation level at Uppenbornwerk 1

The two Uppenborn power plants are situated near Moosburg, Germany, at the Mittlere Isar Kanal (MIK). In addition to the upstream power stations, water is diverted from the Amper River into the Isar River and further through the so-called Alter Werkkanal (AWK) into the MIK (see Figure 21.1). The basin has no bearing on our task.

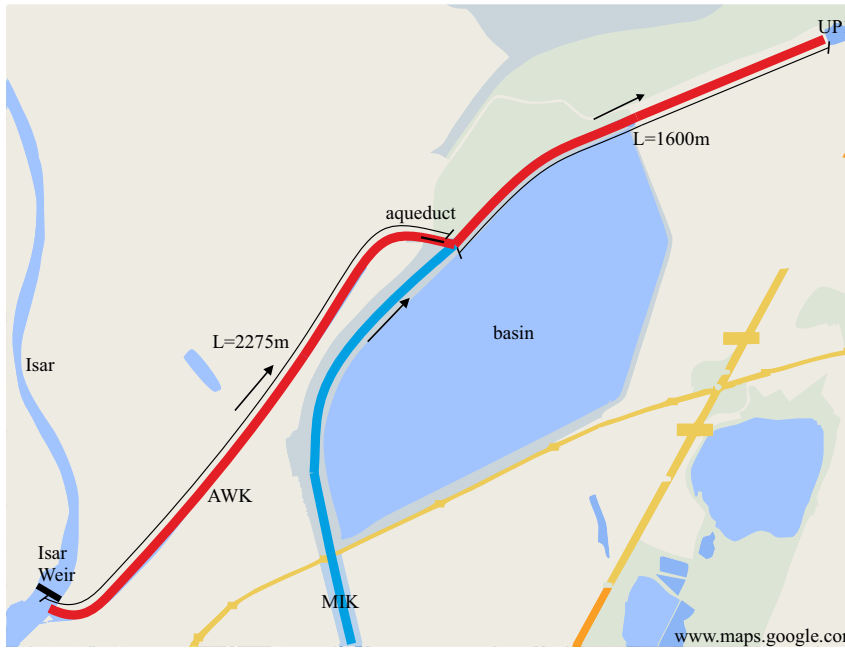

Figure 21.1: Schematic water course of the Uppenborn plants. The plant Uppenbornwerk 2 is situated approximately 8 km downstream near Landshut and not shown in the sketch.

A design discharge of 130 m^3/s flows through the MIK, while an additional 70 m^3/s may be supplied via the AWK. The maximum operation level at the hydropower plant Uppenborn 1 (UP1) is 412.47 m.a.s.l. The operation level at the Isar Weir (i. e. at the inlet structure of the AWK) is also specified as 412.47 m.a.s.l.
It is obvious that the water does not flow with a water level difference of 0.00 m. The power equation (11.54) shows that it is desirable to divert as much water as possible through the

C. Rapp, *Hydraulics in Civil Engineering*,
https://doi.org/10.1007/978-3-031-54860-4_21

turbines at the greatest feasible gross head. Depending on the available discharge at the Isar Weir, we establish a functional relationship for the optimal operation level at power plant UP1. As an example, suppose we execute the method with a discharge in the MIK of $Q_{\mathrm{MIK,total}} = 200\,\mathrm{m}^3/\mathrm{s}$ and a discharge in the AWK of $Q_{\mathrm{AWK}} = 70\,\mathrm{m}^3/\mathrm{s}$ for the operation level $h_{\mathrm{OL}} = 412.00\,\mathrm{m.a.s.l.}^{\mathrm{A}}$.
Furthermore, the following parameters of the trapezoidal channels are known from measurements, plans and other investigations:

MIK	$n = 0.02\,\mathrm{s/m}^{\frac{1}{3}}$	$J_B = 6.25 \times 10^{-5}$	$b = 19\,\mathrm{m}$	$m = 1.5$
AWK	$n = 0.02\,\mathrm{s/m}^{\frac{1}{3}}$	$J_B = 7.033 \times 10^{-4}$	$b = 12\,\mathrm{m}$	$m = 1.5$

The inlet structure is shown in Figure 21.2. It must be taken into consideration that the former log raft passage has been sealed in the meantime (crossed-out in red).

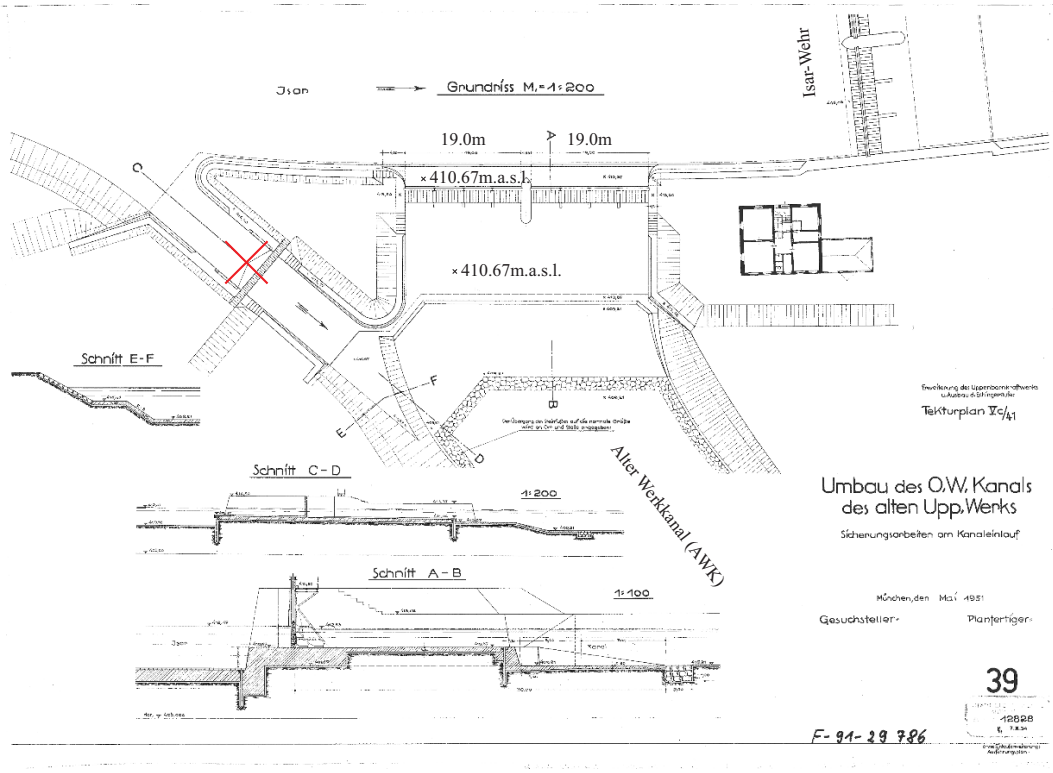

Figure 21.2: Inlet structure of the AWK.

At the end of the AWK, there is an aqueduct that introduces a higher channel bed and a constriction (see Figure 21.3). The following table lists the heights of the channel bed at the characteristic locations.

[A] Because of the three variables h_{OL}, Q_{MIK} and Q_{AWK}, we actually obtain one value for each combination, i. e. a three-dimensional matrix. To not make the matter unnecessarily complicated, we shall abandon the effort for the determination of all of the combinations; nevertheless, we will look later at the result from the comprehensive calculation (see Figure 21.5).

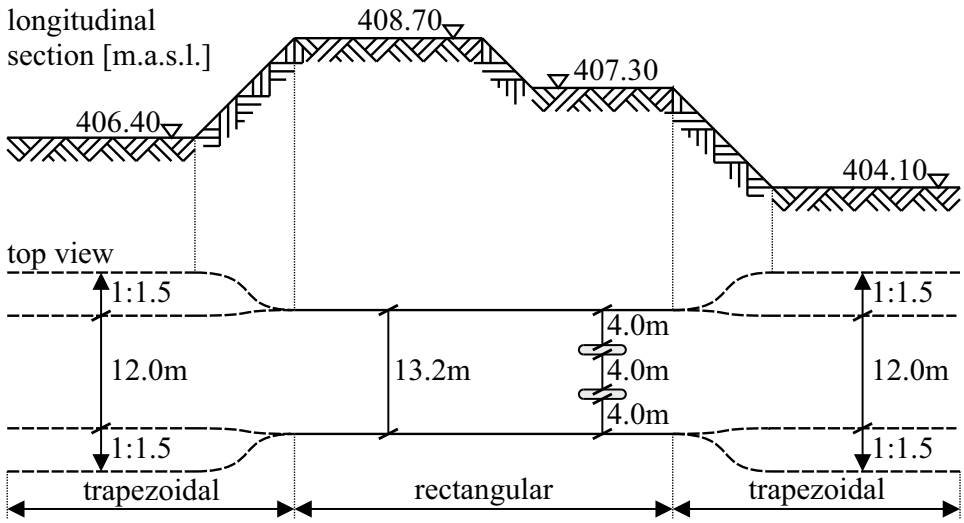

Figure 21.3: Dimensions of the aqueduct

UP1	AWK-MIK	AWK upstream from aqueduct	Isar AWK
404.00 m.a.s.l.	404.10 m.a.s.l.	406.40 m.a.s.l.	408.00 m.a.s.l.

Fundamentals

In order to discover the flow type, we calculate the normal conditions (`normalConditions.m`) in the MIK for $Q_{\mathrm{MIK}} = 200\,\mathrm{m^3/s}$; subcritical flow occurs.

Q [$\mathrm{m^3/s}$]	y_N [m]	v_N [m/s]	H_N [m]	Fr_N [−]
200	6.527	1.064	6.585	0.154

We do the same for $Q_{\mathrm{AWK}} = 70\,\mathrm{m^3/s}$. In this case, too, subcritical flow is in effect.

Q [$\mathrm{m^3/s}$]	y_N [m]	v_N [m/s]	H_N [m]	Fr_N [−]
70	2.329	1.940	2.521	0.449

This means that we are in subcritical flow everywhere[B]. We therefore calculate the flow depth at the inlet structure of the AWK, which is 1600 m away, for $h_{\mathrm{OL}} = 412.00\,\mathrm{m.a.s.l.}$ at power station UP1 by means of the direct step method.

The section within the MIK

This can be done with 10 m sections by means of a computation routine (`directStep.m`); otherwise, a computation for a single section could be made since the error is marginal due to the low flow velocity. Beginning with a flow depth of $y_{\mathrm{UP1}} = 412.00\,\mathrm{m.a.s.l.} - 404.00\,\mathrm{m.a.s.l.} = 8.0\,\mathrm{m}$ at the power station, we obtain the flow depth at the inlet structure of the AWK: 7.946 m. There, the water level is at 412.046 m.a.s.l.

[B] However, we will still have to check whether or not we reach the critical conditions on the aqueduct.

The aqueduct

Initially, we assume that the same water level is present at the end of the AWK in which $70\,m^3/s$ must flow in order to have $200\,m^3/s$ in the MIK. From the flow depth of $7.946\,m$, a flow area of $190\,m^2$ in the AWK results, which leads to a velocity height of approximately $7.0\,mm$. Since it is so small, we do not consider any proportionate loss at this point. Thus, we obtain a specific energy of $7.953\,m$ downstream from the aqueduct, which corresponds to an energy height of $412.053\,m.a.s.l.$ We see immediately that the specific energy of the normal conditions upstream from the aqueduct will definitely be insufficient ($H_N + 406.40\,m = 408.921\,m.a.s.l. \ll 412.053\,m.a.s.l.$). Backwater must occur!
Let's check the critical conditions in the area of the sill upstream from the pillars with $b = 13.2\,m$: $H_{min} = 2.131\,m$. At the pillars, with $b = 12.0\,m$, we obtain: $H_{min} = 2.271\,m$.
Thus, an energy height of $408.70 + 2.131 = 410.831\,m.a.s.l.$ is required on the front sill of the aqueduct. At the pillars, the required energy height is $407.30\,m.a.s.l. + 2.271\,m = 409.571\,m.a.s.l.$ Here, the conditions again are clear. Even with the lower discharges, the critical conditions are not passed through because the downstream energy height, which is defined by the optimal operation level of the power station, is the determining factor.
First, we estimate the flow velocity on the sill and at the pillars by solving the Bernoulli equation in order to obtain the flow depth from $H = 412.053\,m.a.s.l. - 408.70\,m.a.s.l.$: $y_{sill} = 3.214\,m$; $v_{sill} = 1.650\,m/s$; $\frac{v_{sill}^2}{2g} = 0.139\,m$. At the pillars, it follows that with $H_{pillar} = 412.053\,m.a.s.l. - 407.30\,m.a.s.l.$ and $b = 12.0\,m$, $y_{pillar} = 4.674\,m$, $v_{pillar} = 1.248\,m/s$ and $\frac{v_{pillar}^2}{2g} = 0.079\,m$.
When comparing the velocity heights on the sill and downstream from the aqueduct, the substantial difference is striking. We may assume that, except for the portion of the velocity height downstream from the aqueduct, the energy that is required for the acceleration of the water to the high velocity at the aqueduct dissipates; i. e. the difference between the velocity heights on the sill and downstream from the aqueduct is to be considered a loss. That's how we do it.

Losses at the aqueduct

Consequently, on the aqueduct and upstream from it, $H_{on/ups\ aqueduct} = 412.053\,m.a.s.l. - 7.0\,mm + \frac{v_{sill}^2}{2g}$ must be determined. We may obtain the flow depth on the sill only by an iterative approach because the losses are expressed as the difference between the velocity heights. With $\frac{v_{sill,0}^2}{2g} = 0.139\,m$, we obtain $y_{sill,0} = 3.358\,m$ thanks to the Bernoulli equation, which again leads to $\frac{v_{sill,1}^2}{2g} = 0.127\,m$. This becomes $y_{sill,1} = 3.345\,m$ and $\frac{v_{sill,2}^2}{2g} = 0.128\,m$, which may finally be confirmed by $y_{sill,2} = 3.346\,m$. With the height of the bottom, we may determine the specific energy and thus the flow depth upstream from the aqueduct: $H_{ups\ aqueduct} = 5.774\,m$; $y_{ups\ aqueduct} = 5.757\,m$.

Section to the Isar Weir

We have just determined the boundary conditions for the application of the direct step method at the AWK. With the given values we obtain a water level of $412.237\,m.a.s.l.$ at

its beginning, downstream from the inlet structure. With an area of $77.77\,\mathrm{m}^2$, the velocity head is $0.0413\,\mathrm{m}$ and the energy height $412.28\,\mathrm{m.a.s.l.}$

Inlet structure

It is obvious that the water must be accelerated towards the AWK because the diversion is perpendicular to the direction of flow of the Isar River. We assume that the water level at the Isar Weir corresponds to the energy height and calculate the velocity height at the smallest cross-section. At the sluice gates, $y = 1.528\,\mathrm{m}$ is the flow depth (obtained with the Bernoulli equation for $b = 36.2\,\mathrm{m}$ and $H = 412.28 - 410.67 = 1.61\,\mathrm{m}$), which results in a flow area of $A = 55.31\,\mathrm{m}^2$. Therefore, the water must be accelerated to $1.266\,\mathrm{m/s}$, which corresponds to a velocity height of $0.082\,\mathrm{m}$. The water level on the inlet sill sinks to $412.28 - 0.082 = 412.20\,\mathrm{m.a.s.l.}$
In effect this means that with an operation level of $412.00\,\mathrm{m}$ at power station UP1, an energy height of $412.237\,\mathrm{m.a.s.l.} + 4.13\,\mathrm{cm} = 412.28\,\mathrm{m.a.s.l.}$ must exist upstream from the Isar Weir so that an additional discharge of $Q_{\mathrm{AWK}} = 70\,\mathrm{m}^3/\mathrm{s}$ may feed into the MIK with an upstream discharge of $Q_{\mathrm{MIK}} = 130\,\mathrm{m}^3/\mathrm{s}$. Have a close look at the course of the water level in Figure 21.4 in order to comprehend the conditions.

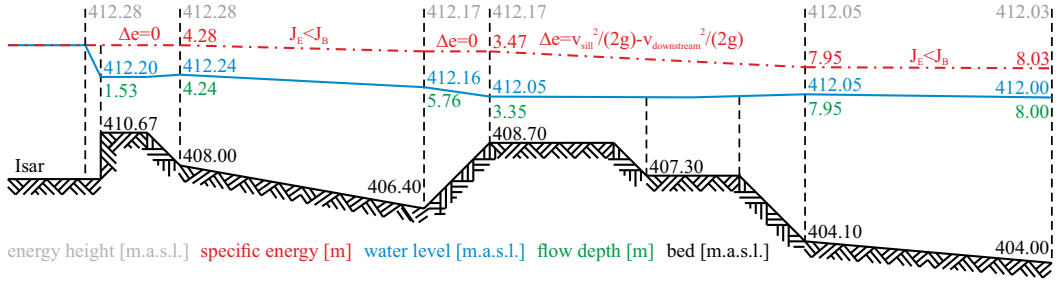

Figure 21.4: Energy diagram for the case described above.

Conclusions for multiple discharge and operation level combinations

As an example, when automating the process, which is simple with the available codes, one obtains the flow depths at the Isar Weir when $Q_{\mathrm{AWK}} = 10 \ldots 70\,\mathrm{m}^3/\mathrm{s}$, $Q_{\mathrm{MIK}} = 70 \ldots 200\,\mathrm{m}^3/\mathrm{s}$ and a range of the operation levels of $h_{\mathrm{OL@UP1}} = 412.00 \ldots 412.50\,\mathrm{m.a.s.l.}$ The blue surface in Figure 21.5 indicates the optimal operation level for the maximum power at UP1; for all these conditions, the water level at the Isar Weir is $412.47\,\mathrm{m.a.s.l.}$ By means of this graph, it is possible to optimise the operation of the power plant for various discharges in the Mittlere Isar Kanal and in the Alter Werkkanal by adjusting the operation level at power station UP1[C].

[C] A small side note: The linear dependency on the gross head follows from the power formula (Equation 11.54), which is why the optimal operation level, that depends on the discharge, is maximized. However, it is obvious that the increase in discharge exceeds by far the increase in gross head. We use as an example an operation level of $h_{\mathrm{OL@UP1}} = 412.47\,\mathrm{m.a.s.l.}$ in the AWK at a possible

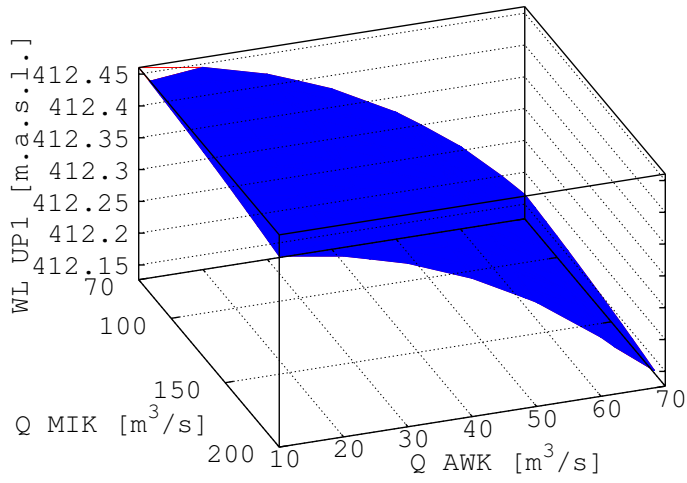

Figure 21.5: Combinations of discharge and optimal operation levels resulting in a water level of 412.47 m.a.s.l. at the Isar Weir.

discharge of $Q_{\mathrm{AWK}} = 70\,\mathrm{m}^3/\mathrm{s}$ and of $Q_{\mathrm{MIK}} = 130\,\mathrm{m}^3/\mathrm{s}$ in the MIK. Since the optimal operation levels at the Isar Weir and at power station UP1 are identical, no water flows into the AWK and we obtain $P_{\mathrm{UP1}} = \rho \cdot g \cdot 130 \cdot 13.0$ as theoretically achievable power. In comparison, an operation level of $h_{\mathrm{OL@UP1}} \approx 412.15\,\mathrm{m.a.s.l.}$ (see Figure 21.5) allows feeding an additional $Q_{\mathrm{AWK}} = 70\,\mathrm{m}^3/\mathrm{s}$ into the turbines of the power station. Nonetheless, the gross head is to be set here at only 12.68 m. The power $P_{\mathrm{UP1}} = \rho \cdot g \cdot 200 \cdot 12.68$, however, is significantly greater.

Appendix A

A.1 Dipole of a potential flow

The dipole is formed by the superposition of source and sink of identical strength and opposite sign at one point and is, in mathematical terms, a singularity. We take up the idea of Schneider [53, S. 117] and successively shift a source, located at a distance l to the left of the sink, towards this sink (see also [23]). Since the elementary solutions may be overlaid, the potential function may be transferred directly from Equation 4.13:

$$\Phi = \frac{q}{2\pi} \ln \sqrt{(x+l)^2 + y^2} - \frac{q}{2\pi} \ln \sqrt{x^2 + y^2} \tag{A.1}$$

The next step is to reduce the distance l between sink and source to zero as indicated on the x-axis. Hence, we consider the limit of a function as l approaches zero. We also use Taylor's theorem, which may be found, for example, in [8, p. 404]:

> If a function $f(x)$ is continuous in the interval $[a, a+h]$, and if it is differentiable through order n within the interval, then the function may be expressed as a Taylor series expansion:
>
> $$f(a+h) = f(a) + \frac{h}{1!}\frac{\partial f(a)}{\partial a} + \frac{h^2}{2!}\frac{\partial^2 f(a)}{\partial a^2} + \ldots + \frac{h^{n-1}}{(n-1)!}\frac{\partial^{n-1} f(a)}{\partial a^{n-1}} + \frac{h^n}{n!}\frac{\partial^n f(a+\theta h)}{\partial a^n} \tag{A.2}$$
>
> $0 < \theta < 1$; h can be positive or negative.

One can easily see that the Taylor series expansion is tailored for our problem. In our case, $a = x$ and $h = l$. Thus, we may write:

$$\begin{aligned} \Phi &= \lim_{l \to 0} \left[\frac{q}{2\pi} \ln \sqrt{(x+l)^2 + y^2} - \frac{q}{2\pi} \ln \sqrt{x^2 + y^2} \right] \\ &= \lim_{l \to 0} \left[\frac{q}{2\pi} \left(\ln \sqrt{x^2 + y^2} + \frac{l}{1!}\frac{\partial}{\partial x} \ln \sqrt{x^2 + y^2} + \ldots \right) - \frac{q}{2\pi} \ln \sqrt{x^2 + y^2} \right] \\ &= \lim_{l \to 0} \left[\frac{q}{2\pi} l \frac{\partial}{\partial x} \ln \sqrt{x^2 + y^2} \right] = \frac{q}{2\pi} l \frac{\partial}{\partial x} \ln \sqrt{x^2 + y^2} \end{aligned} \tag{A.3}$$

We terminated the Taylor series in Equation A.3 at the first derivative because the influence of higher derivations increasingly diminishes. The source and sink terms themselves

C. Rapp, *Hydraulics in Civil Engineering*,
https://doi.org/10.1007/978-3-031-54860-4

($\frac{q}{2\pi}\left(\ln\sqrt{x^2+y^2}\right)$) cancel each other out and only the term from the limit value analysis remains. By the definition of the dipole strength $m = ql$, it follows for the potential function:

$$\Phi = \frac{m}{2\pi}\frac{\partial}{\partial x}\ln\sqrt{x^2+y^2} \tag{A.4}$$

When deriving the source and sink flow by means of Equation 4.12, we integrated the expression $\frac{x}{x^2+y^2}$ with respect to x and obtained $\ln\sqrt{x^2+y^2}$. Conversely, the derivative of this result with respect to x reverses the integration, yielding once again $\frac{x}{x^2+y^2}$. Thus, the potential function reads:

$$\Phi = \frac{m}{2\pi}\frac{x}{x^2+y^2} \tag{A.5}$$

We establish the following equation for the streamlines:

$$\Psi = -\frac{m}{2\pi}\frac{y}{x^2+y^2} \tag{A.6}$$

We demonstrate via the formula indicated in [8, S.234] that the tangents of the streamlines and of the potential lines of the dipole are perpendicular to each other at one point:

$$\frac{\partial F}{\partial x}(X-x)+\frac{\partial F}{\partial y}(Y-y)=0 \tag{A.7}$$

Therein, X and Y are the moving coordinates, while the tangent equation is formulated for the point at (x,y). First, we write the tangent equation for the potential lines:

$$\begin{aligned} 0 &= \frac{\partial\Phi}{\partial x}(X-x)+\frac{\partial\Phi}{\partial y}(Y-y) = \frac{\partial}{\partial x}\frac{m}{2\pi}\frac{x}{x^2+y^2}(X-x)+\frac{\partial}{\partial y}\frac{m}{2\pi}\frac{x}{x^2+y^2}(Y-y) \\ &= \frac{m}{2\pi}\frac{-x^2+y^2}{\left(x^2+y^2\right)^2}(X-x)+\frac{m}{2\pi}\frac{-2xy}{\left(x^2+y^2\right)^2}(Y-y) \end{aligned} \tag{A.8}$$

Since the expression on the right side corresponds to zero, we may significantly simplify the equation with division by $\frac{m}{2\pi}\frac{1}{\left(x^2+y^2\right)^2}$:

$$-x^2+y^2\,(X-x) = 2xy\,(Y-y) \tag{A.9}$$

Thereby,

$$(Y-y) = \frac{-x^2+y^2}{2xy}(X-x) \tag{A.10}$$

and finally, the gradient of the tangent is:

$$\nabla(\Phi(x,y)) = \frac{-x^2+y^2}{2xy} \tag{A.11}$$

We proceed identically with the stream function:

$$
\begin{aligned}
0 &= \frac{\partial \Psi}{\partial x}(X-x) + \frac{\partial \Psi}{\partial y}(Y-y) = \frac{\partial}{\partial x}\frac{m}{2\pi}\frac{-y}{x^2+y^2}(X-x) + \frac{\partial}{\partial y}\frac{m}{2\pi}\frac{-y}{x^2+y^2}(Y-y) \\
&= \frac{m}{2\pi}\frac{0-2x(-y)}{(x^2+y^2)^2}(X-x) + \frac{m}{2\pi}\frac{-x^2+y^2}{(x^2+y^2)^2}(Y-y) \\
&= 2xy(X-x) + \left(-x^2+y^2\right)(Y-y)
\end{aligned} \tag{A.12}
$$

For $Y-y$ it follows that

$$
(Y-y) = \frac{2xy}{x^2-y^2}(X-x) \tag{A.13}
$$

and ultimately

$$
\nabla(\Psi(x,y)) = \frac{2xy}{x^2-y^2} \tag{A.14}
$$

which corresponds exactly to the negative reciprocal value of the gradient of the potential function at point (x,y). We therefore see that the streamlines and potential lines extend perpendicularly to each other.

A.2 Shear stress balance at the differential element

We establish the shear stress balance (see Figure 5.4) on a two-dimensional element (see Figure A.1) by means of an example. We may safely ignore inertia since Truckenbrodt [60] shows that the moment of force depends on the angular acceleration of the length of our minute element raised to the fifth power, while the moment of the shear stress depends on the length raised only to the third power. To exemplify the symmetry of the stress tensor [16], we sketch the shear stresses that are applied to the element in the y- (or x_2-) direction (see Figure A.1).

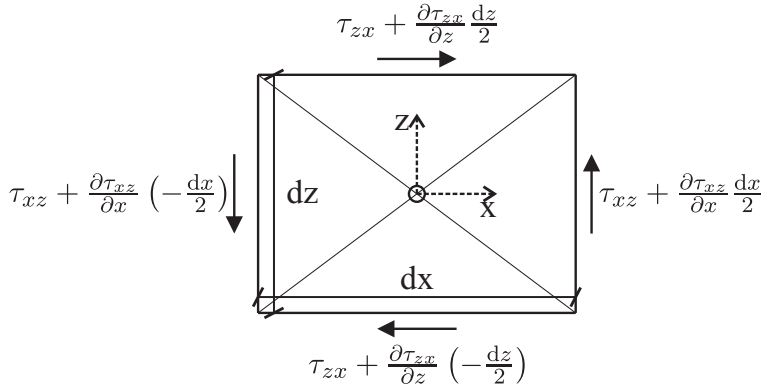

Figure A.1: Shear stresses on a two-dimensional element.

We now calculate the moment about the centre, i. e. about the y-axis pointing into the drawing plane. The lever arms are $\frac{\mathrm{d}x}{2}$ and $\frac{\mathrm{d}z}{2}$, where the signs result from the "right-hand rule" (see e. g. [15]).

$$
\begin{aligned}
M = &\left[\tau_{31} + \frac{\partial \tau_{31}}{\partial x_3}\frac{\mathrm{d}z}{2}\right]\mathrm{d}x\,\mathrm{d}y\,\frac{\mathrm{d}z}{2} + \left[\tau_{31} + \frac{\partial \tau_{31}}{\partial x_3}\left(-\frac{\mathrm{d}z}{2}\right)\right]\mathrm{d}x\,\mathrm{d}y\,\frac{\mathrm{d}z}{2} \\
&- \left[\left[\tau_{13} + \frac{\partial \tau_{13}}{\partial x_1}\frac{\mathrm{d}x}{2}\right]\mathrm{d}z\,\mathrm{d}y\,\frac{\mathrm{d}x}{2} + \left[\tau_{13} + \frac{\partial \tau_{13}}{\partial x_1}\left(-\frac{\mathrm{d}x}{2}\right)\right]\mathrm{d}z\,\mathrm{d}y\,\frac{\mathrm{d}x}{2}\right] \\
&= \tau_{31}\,\mathrm{d}x\,\mathrm{d}y\,\mathrm{d}z - \tau_{13}\,\mathrm{d}x\,\mathrm{d}y\,\mathrm{d}z
\end{aligned}
\tag{A.15}
$$

The internal forces must not lead to a moment. To achieve shear stress balance, it is necessary that $\tau_{13} = \tau_{31}$. Transferred to the spatial directions, this corresponds to $\tau_{ij} = \tau_{ji}$, which is why we may also write $\frac{\partial \tau_{ji}}{\partial x_j} = \frac{\partial \tau_{ij}}{\partial x_j}$ with Einstein's sum convention, which is the usual notation.

A.3 Derivation of the friction coefficient f_D

A.3.1 Reynolds averaging

In Chapter 6, what is known as Reynolds averaging was introduced for statistically steady flows. A time-dependent quantity $u(t)$ was divided into its time-averaged value $\langle u \rangle$ and the fluctuation u'. Even if a flow field exhibits time-converged mean values, friction is generated by the conditions that exist at any given time. Therefore, an additional term, the so-called Reynolds stress tensor $\rho\langle u_i' u_j' \rangle$ or rather its gradient $\rho\frac{\partial \langle u_i' u_j' \rangle}{\partial x_j}$ must be included when averaging the Navier–Stokes equation (see Equation A.16). The indices of the secondary diagonal elements may be interchanged (see Appendix A.2); hence, six additional unknowns are present in what is termed the Reynolds-Averaged Navier–Stokes equation (6.2).

$$
\frac{\partial \langle u_i' u_j' \rangle}{\partial x_j} = \begin{pmatrix} \frac{\partial \langle u'u' \rangle}{\partial x} & \frac{\partial \langle u'v' \rangle}{\partial y} & \frac{\partial \langle u'w' \rangle}{\partial z} \\ \frac{\partial \langle v'u' \rangle}{\partial x} & \frac{\partial \langle v'v' \rangle}{\partial y} & \frac{\partial \langle v'w' \rangle}{\partial z} \\ \frac{\partial \langle w'u' \rangle}{\partial x} & \frac{\partial \langle w'v' \rangle}{\partial y} & \frac{\partial \langle w'w' \rangle}{\partial z} \end{pmatrix}
\tag{A.16}
$$

Let's have a look on the channel with two parallel plates depicted in Figure A.2. $u'w'$

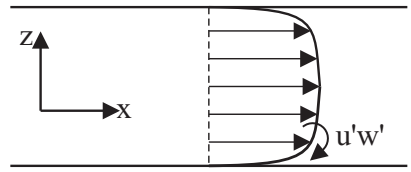

Figure A.2: $u'w'$, an eddy in the direction normal to the wall.

corresponds to an eddy that occurs in the direction normal to the wall, and $\langle u'w' \rangle$ is the time averaging of these fluctuations. Since these mean fluctuations multiplied by the density possess the unit of stress, they are referred to as "Reynolds stresses".

$$
\tau_{ij}^{\mathrm{Re}} = -\rho\langle u'w' \rangle
\tag{A.17}
$$

A.3.2 Prandtl's mixing length

Joseph Boussinesq[A] assumed that the Reynolds stresses are linearly dependent on the mean velocity gradient in the direction normal to the wall $\frac{\partial\langle u\rangle}{\partial z}$. He introduced the turbulent viscosity ν_T $\left[\mathrm{m}^2/\mathrm{s}\right]$ because the chaotic turbulences generate additional friction.

$$\tau_{ij}^{\mathrm{Re}} = -\rho\,\nu_T \frac{\partial\langle u\rangle}{\partial z} \tag{A.18}$$

The turbulent viscosity ν_T, which is also referred to as eddy viscosity, may be determined via Prandtl's mixing length approach. Prandtl developed the concept that fluid parcels vary in a turbulent flow with $\mp w'$ within $\pm l_{\mathrm{m}}$, the mixing length, until they collide with other fluid parcels[B].

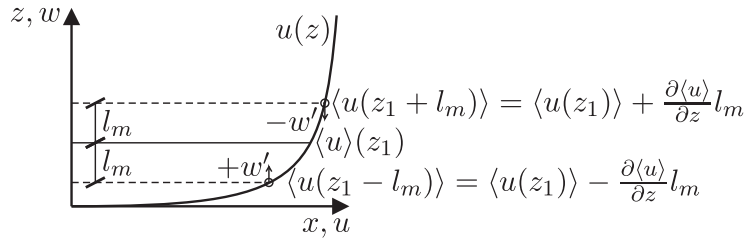

Figure A.3: Prandtl's mixing length approach.

In a manner similar to that of Adams [1], we use Figure A.3 as a reminder in order to correctly indicate the signs. On the coordinate $z_1 - l_{\mathrm{m}}$, the mean velocity in the x-direction is smaller by the velocity gradient $\frac{\partial\langle u\rangle}{\partial z}$ times $-l_{\mathrm{m}}$ (opposite the positive z-axis): $\langle u(z_1 - l_{\mathrm{m}})\rangle = \langle u(z_1)\rangle - l_{\mathrm{m}}\frac{\partial\langle u\rangle}{\partial z}$. If a fluid parcel fluctuates by $+w'$ about l_{m} to z_1, it transports fluid that is slower by $-l_{\mathrm{m}}\frac{\partial\langle u\rangle}{\partial z}$ to z_1, implying a deviation compared to the time-averaged velocity $\langle u(z_1)\rangle$ in z_1 by $u' = -l_{\mathrm{m}}\frac{\partial\langle u\rangle}{\partial z}$. We may summarise these considerations as follows:

$$u' \approx \pm l_{\mathrm{m}} \frac{\partial\langle u\rangle}{\partial z} \tag{A.19}$$

We have already stated above that $-w'$ shifts faster fluid to z_1 and $+w'$ shifts slower fluid. In order to meet the continuity condition, $|w'|$ has to adjust to the same order of magnitude as $|u'|$. The order of magnitude of w' follows in Formula A.20:

$$w' \approx \mp l_{\mathrm{m}} \frac{\partial\langle u\rangle}{\partial z} \tag{A.20}$$

Similarly, for the order of magnitude of $u'w'$:

$$u'w' \approx -l_{\mathrm{m}}^2 \left|\frac{\partial\langle u\rangle}{\partial z}\right| \frac{\partial\langle u\rangle}{\partial z} \tag{A.21}$$

[A] Joseph Valentin Boussinesq, ∗1842, Saint-André-de-Sangonis, France, †1929, Paris, France

[B] Please refer to the thought example on page 72.

This, along with Equation A.17, leads to the time-averaged velocity fluctuations $\langle u'w' \rangle$:

$$\frac{1}{\rho}\tau_{ij}^{\mathrm{Re}} \approx l_{\mathrm{m}}^2 \left| \frac{\partial \langle u \rangle}{\partial z} \right| \frac{\partial \langle u \rangle}{\partial z} \tag{A.22}$$

Via a comparison of the approximation A.22 with the Boussinesq assumption A.18, ν_T can be written as:

$$\nu_T = l_{\mathrm{m}}^2 \left| \frac{\partial \langle u \rangle}{\partial z} \right| \tag{A.23}$$

A.3.3 Law of the wall

The distribution of the shear stress for a flow without pressure gradient along a flat plate, as shown in Figure A.4, may be experimentally determined via the boundary layer thickness δ [51]. The boundary layer thickness is the extent of the region between the wall and the point at which $\langle u \rangle \approx 0.99 u_\infty$ (i. e. where 99 % of the uninfluenced velocity is to be found), as measured perpendicularly to the wall. The total stress τ_{xz}^{tot} is the sum of viscous stresses $\eta \frac{\partial u}{\partial z}$ and Reynolds stresses $-\rho \langle u'w' \rangle$.

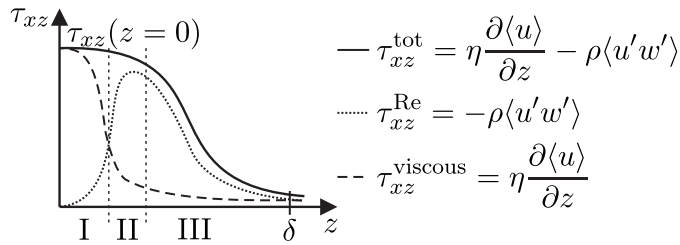

Figure A.4: Shear stress distribution in the boundary layer according to Adams [1].

Figure A.4 shows that the viscous stresses are predominant in the immediate vicinity of the wall; there, the velocity fluctuations play a minor role (region I). This region is also referred to as the viscous sublayer of thickness δ_ν. With increasing wall distance, the influence of viscosity decreases, and the Reynolds stresses dominate (region II is also referred to as the transition layer). In the outer region (region III, also known as the logarithmic layer) the influence of the viscous stresses is negligible.
Before continuing, we define two quantities by which velocity and length are divided so that these can be written in a dimensionless form. We introduce the shear stress velocity u_τ [m/s] making use of the wall shear stress τ_W. By means of Equation 11.22, where $\tau_W = \rho \frac{f_D}{8} u^2$, u_τ may also be written as:

$$u_\tau = \sqrt{\frac{\tau_W}{\rho}} = \sqrt{\frac{f_D}{8}} \cdot u \tag{A.24}$$

The turbulent length scale l_ν is likewise defined via dimensional analysis:

$$l_\nu = \nu \sqrt{\frac{\rho}{\tau_W}} = \frac{\nu}{u_\tau} \tag{A.25}$$

A.3.3.1 Region I

In the region extremely close to the wall, the viscous stresses dominate and $\tau_{xz}^{\mathrm{tot}} = \tau_W = \eta \frac{\partial \langle u \rangle}{\partial z}$. Region I is normally also referred to as a viscous sublayer. By integration with respect to z, the mean velocity in the x-direction may be expressed as follows:

$$\langle u \rangle \approx \frac{\tau_W}{\eta} z + C = \frac{\tau_W}{\eta} z \tag{A.26}$$

Here, the constant of integration C disappears with $u(z=0)=0$. When inserting the wall shear stress from Equation A.24 into Formula A.26, the result is:

$$\langle u \rangle \approx \frac{u_\tau^2}{\eta} z \rho = \frac{u_\tau^2}{\nu} z \tag{A.27}$$

The wall distance may be expressed in dimensionless form via the turbulent length scale l_ν (see Formula A.25) as $z^+ = \frac{u_\tau z}{\nu}$, which, via Equation A.27 with $u^+ = \frac{\langle u \rangle}{u_\tau}$, leads to:

$$u^+ = \frac{\langle u \rangle}{u_\tau} \approx \frac{u_\tau}{\nu} z = z^+ \tag{A.28}$$

Thus, a linear relationship between velocity and wall distance in wall units $u^+ \sim z^+$ exists in the viscous sublayer. This region in which the viscous stresses alone are dominant, extends up to $z^+ \lesssim 5$. We leave the viscous sublayer behind and focus on the description of the outer region of what is called the boundary layer.

A.3.3.2 Region II and III

It is assumed here that $\tau_{xz}^{\mathrm{tot}} \approx \tau_{xz}^{\mathrm{Re}} \approx \tau_W$ (refer again to Figure A.4). Viscosity plays only a minor role and turbulent stresses dominate. Thereby, $\tau_{xz}^{\mathrm{Re}} \approx \tau_W$ (see Equation A.18) is established as the Boussinesq assumption and inserted into the mixing length approach (Equation A.22). τ is consequently assumed to be identical with the wall shear stress τ_W and to be evenly distributed over the cross-section[C].

$$\tau_W \approx \rho l_{\mathrm{m}}^2 \left| \frac{\partial \langle u \rangle}{\partial z} \right| \frac{\partial \langle u \rangle}{\partial z} \tag{A.29}$$

Now the von Kármán[D] constant κ is introduced to indicate the linear dependency between the mixing length and the wall distance. Prandtl made this assumption, although Nikuradse had demonstrated that it is applicable at the wall only [5, p. 171].

$$\kappa = \frac{l_{\mathrm{m}}}{z} \tag{A.30}$$

This constantκ is inserted into Equation A.29, resulting in:

[C] Bollrich [5, p. 171] notes that this assumption has been made quite randomly.

[D] Theodore von Kármán, ∗1881, Budapest, Hungary, †1963, Aachen, Germany

$$\tau_W \approx \rho \kappa^2 z^2 \left| \frac{\partial \langle u \rangle}{\partial z} \right| \frac{\partial \langle u \rangle}{\partial z} \tag{A.31}$$

With the shear stress velocity u_τ and Equation A.24, it follows:

$$u_\tau^2 = \frac{\tau_W}{\rho} \approx \kappa^2 z^2 \left| \frac{\partial \langle u \rangle}{\partial z} \right| \frac{\partial \langle u \rangle}{\partial z} \tag{A.32}$$

With the reasonable assumption of a positive mean velocity gradient in a boundary layer $\frac{\partial \langle u \rangle}{\partial z}$, which means that the mean velocity $\langle u \rangle$ in the z-direction increases, we write:

$$u_\tau \approx \kappa z \frac{\partial \langle u \rangle}{\partial z} \quad \text{hence,} \quad \frac{\partial \langle u \rangle}{\partial z} = \frac{u_\tau}{\kappa z} \tag{A.33}$$

In order to obtain $\langle u(z) \rangle$, we must integrate. With $\int \frac{1}{z} \, \mathrm{d}z = \ln |z|$, where ln is the natural logarithm, it follows that:

$$\langle u(z) \rangle = \int \frac{\partial \langle u \rangle}{\partial z} \, \mathrm{d}z = \int \frac{u_\tau}{\kappa z} \, \mathrm{d}z = \frac{u_\tau}{\kappa} \ln |z| + C = \frac{u_\tau}{\kappa} \ln z + C \tag{A.34}$$

For the determination of the integration constant C, Equation A.34 with the boundary condition $u(z = z_W) = 0$ is solved. z_W is a small wall distance, and so this condition is still met (see Figure A.5).

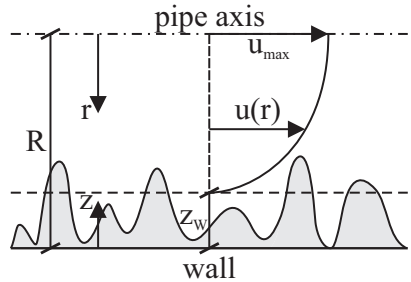

Figure A.5: Explanation of coordinates z and r, the radius R as well as the wall distance z_W at which the velocity becomes zero; i. e. $u(z = z_W) = 0$, according to Bollrich [5].

$$C = -\frac{u_\tau}{\kappa} \ln z_W \tag{A.35}$$

With this constant of integration C inserted into Equation A.34, we obtain:

$$\langle u(z) \rangle = \frac{u_\tau}{\kappa} \ln z - \frac{u_\tau}{\kappa} \ln z_W = \frac{u_\tau}{\kappa} \ln \frac{z}{z_W} \tag{A.36}$$

Next, we introduce the radial coordinate $r = R - z$ and thereby replace z with $R - r$ in Expression A.36. A.37 is also referred to as the von Kármán-Prandtl equation:

$$\langle u(r) \rangle = \frac{u_\tau}{\kappa} \ln \frac{R - r}{z_W} \tag{A.37}$$

It is obvious that the maximum velocity $\langle u_{\max}\rangle$ occurs at the centre of the pipe, i. e. at $r = 0$:

$$\langle u_{\max}\rangle = \frac{u_\tau}{\kappa} \ln \frac{R}{z_W} \tag{A.38}$$

We eliminate z_W by means of a smart technique:

$$\langle u(r)\rangle - \langle u_{\max}\rangle = \frac{u_\tau}{\kappa} \ln \frac{R-r}{z_W} - \frac{u_\tau}{\kappa} \ln \frac{R}{z_W} = \frac{u_\tau}{\kappa} \ln \left(\frac{R-r}{z_W} \cdot \frac{z_W}{R} \right) = \frac{u_\tau}{\kappa} \ln \frac{R-r}{R} \tag{A.39}$$

This leads to an expression for $\langle u(r)\rangle$:

$$\langle u(r)\rangle = \langle u_{\max}\rangle + \frac{u_\tau}{\kappa} \ln \frac{R-r}{R} \tag{A.40}$$

We proceed stepwise, following the same process as Bollrich [5]. Next, we want to determine the mean velocity in the pipe cross-section; therefore we must integrate $\langle u(r)\rangle$ with respect to the cross-section and divide it by the area. In the following steps, the time- and space-averaged velocity $\langle \bar{u}\rangle$ in the direction of the pipe axis is expressed as u. The Jacobian factor r should be borne in mind.

$$\begin{aligned} u = \langle \bar{u}\rangle &= \frac{1}{A} \int_0^{2\pi} \int_0^R \langle u(r)\rangle r \,\mathrm{d}r \,\mathrm{d}\phi = \frac{1}{R^2\pi} \int_0^R 2\pi \langle u(r)\rangle r \,\mathrm{d}r \\ &= \frac{2\pi}{R^2\pi} \int_0^R \left(\langle u_{\max}\rangle + \frac{u_\tau}{\kappa} \ln \left(\frac{R-r}{R} \right) \right) r \,\mathrm{d}r = \frac{2}{R^2} \int_0^R \langle u_{\max}\rangle r \,\mathrm{d}r + \frac{2}{R^2} \int_0^R \frac{u_\tau}{\kappa} \ln \left(\frac{R-r}{R} \right) r \,\mathrm{d}r \\ &= \frac{2}{R^2} \langle u_{\max}\rangle \frac{R^2}{2} + \frac{2u_\tau}{\kappa R^2} \int_0^R \ln \left(\frac{R-r}{R} \right) r \,\mathrm{d}r = \langle u_{\max}\rangle + \frac{2u_\tau}{\kappa R^2} \int_0^R \ln \left(\frac{R-r}{R} \right) r \,\mathrm{d}r \end{aligned} \tag{A.41}$$

An attempt to solve the integral in Equation A.41 means virtually insurmountable problems for a non-mathematician. In a first step we prepare the integral to make it suitable for integral tables:

$$\int \ln \left(\frac{R-r}{R} \right) r \,\mathrm{d}r = \int r \ln \left(-\frac{r-R}{R} \right) \mathrm{d}r \tag{A.42}$$

Herein the integration limits are to be omitted for the sake of clarity. We continue with partial integration $\int \Phi' \Gamma \,\mathrm{d}r = \Phi\Gamma - \int \Phi\Gamma' \,\mathrm{d}r$, where $\Phi' = r$ and $\Gamma = \ln\left(-\frac{r-R}{R}\right)$ (see, for example, [8, p. 446]). These become $\Phi = \frac{r^2}{2}$ and $\Gamma' = \frac{1}{r-R}$, respectively[E].

$$\int \Phi' \Gamma \,\mathrm{d}r = \Phi\Gamma - \int \Phi\Gamma' \,\mathrm{d}r = \frac{r^2}{2} \ln \left(-\frac{r-R}{R} \right) - \int \frac{r^2}{2\,(r-R)} \,\mathrm{d}r \tag{A.43}$$

After we got rid of the logarithm in the integral, we have "only" to solve the simple integral.

$$\int \frac{r^2}{2\,(r-R)} \,\mathrm{d}r = \frac{1}{2} \int \frac{r^2}{r-R} \,\mathrm{d}r \tag{A.44}$$

[E] Γ is derived via the chain rule (see e. g. [8, p. 396]):

$$\frac{\mathrm{d}\left(\ln\left(-\frac{r-R}{R}\right)\right)}{\mathrm{d}r} = \left(-\frac{1}{\frac{r-R}{R}} \right) \cdot \frac{\mathrm{d}}{\mathrm{d}r} \left(-\frac{r-R}{R} \right) = -\frac{R}{r-R} \cdot \left(-\frac{\frac{\mathrm{d}}{\mathrm{d}r}(r) + \frac{\mathrm{d}}{\mathrm{d}r}(-R)}{R} \right) = -\frac{R\left(-\frac{1-0}{R}\right)}{r-R} = \frac{1}{r-R}$$

With the substitution $s = r - R$, it follows that $\frac{\mathrm{d}s}{\mathrm{d}r} = 1$ and $r = s + R$ (see e. g. [8, p. 446]). Equation A.44 becomes:

$$\begin{aligned}\frac{1}{2}\int \frac{r^2}{r-R}\,\mathrm{d}r &= \frac{1}{2}\int \frac{(s+R)^2}{s}\,\mathrm{d}s = 0.5\left[\int\left(s+\frac{R^2}{s}+2R\right)\mathrm{d}s\right] \\ &= 0.5\int s\,\mathrm{d}s + 0.5R^2\int\frac{1}{s}\,\mathrm{d}s + R\int 1\,\mathrm{d}s \\ &= \frac{0.5}{2}s^2 + 0.5R^2\ln s + Rs\end{aligned} \tag{A.45}$$

To be quite honest, the goal will ultimately be reached only gradually. We resubstitute $s = r - R$ in Equation A.44:

$$\frac{1}{2}\int \frac{r^2}{r-R}\,\mathrm{d}r = \frac{0.5}{2}s^2 + 0.5R^2\ln s + Rs = 0.25\,(r-R)^2 + 0.5R^2\ln(r-R) + R(r-R) \tag{A.46}$$

Thereby, we return to Expression A.42:

$$\begin{aligned}\int \ln\left(\frac{R-r}{R}\right) r\,\mathrm{d}r &= \frac{r^2}{2}\ln\left(-\frac{r-R}{R}\right) - \int\frac{r^2}{2\,(r-R)}\,\mathrm{d}r \\ &= \frac{r^2}{2}\ln\left(-\frac{r-R}{R}\right) - 0.25\,(r-R)^2 - 0.5R^2\ln(r-R) - R(r-R)\end{aligned} \tag{A.47}$$

We now place the entire expression inside square brackets and write the integration limits 0 and R[F].

$$\begin{aligned}&\left[\frac{r^2}{2}\ln\left(-\frac{r-R}{R}\right) - \frac{R^2}{2}\ln(r-R) - 0.25\,(r-R)^2 - R(r-R)\right]_0^R \\ &= \left[\frac{R^2}{2}\ln\left(-\frac{R-R}{R}\right) - \frac{R^2}{2}\ln(R-R) - 0.25\,(R-R)^2 - R(R-R)\right] \\ &- \left[\frac{0^2}{2}\ln\left(-\frac{0-R}{R}\right) - \frac{R^2}{2}\ln(0-R) - 0.25\,(0-R)^2 - R(0-R)\right] \\ &= \left[\frac{R^2}{2}\ln\left(-\frac{R-R}{R}\cdot\frac{1}{R-R}\right) - 0.25\,(0)^2 - R(0)\right] \\ &- \left[0 - \frac{R^2}{2}\ln(-R) - 0.25R^2 - R(-R)\right] \\ &= \left[\frac{R^2}{2}\ln\left(-\frac{1}{R}\right)\right] - \left[-\frac{R^2}{2}\ln(-R) - 0.25R^2 + R^2\right] \\ &= \frac{R^2}{2}\ln\left(-\frac{1}{R}\right) + \frac{R^2}{2}\ln(-R) + 0.25R^2 - R^2 \\ &= \frac{R^2}{2}\ln\left(-\frac{1}{R}\cdot -R\right) + 0.25R^2 - R^2 = \frac{R^2}{2}\ln(1) - 0.75R^2 = 0 - 0.75R^2\end{aligned} \tag{A.48}$$

[F] The mathematical rampage, dividing by zero, is spared only if we formally integrate to $R - z_W$ (and not to R, see Figure A.5).

It is unbelievable that nothing but $-0.75R^2$ remains after the nasty integration. We return to Equation A.41 and set the von Kármán constant to $\kappa = 0.4$:

$$u = \langle u_{\max} \rangle - \frac{2u_\tau}{\kappa R^2} \cdot 0.75R^2 = \langle u_{\max} \rangle - \frac{1.5 \cdot u_\tau}{0.4} = \langle u_{\max} \rangle - 3.75 \cdot u_\tau \tag{A.49}$$

By inserting Equation A.24 ($u_\tau = u\sqrt{\frac{f_D}{8}}$) into the Expression A.40, the velocity distribution with $\kappa = 0.4$ becomes:

$$u(r) = \langle u_{\max} \rangle + \frac{u}{\kappa} \cdot \sqrt{\frac{f_D}{8}} \cdot \ln\left(1 - \frac{r}{R}\right) = \langle u_{\max} \rangle + u \cdot 0.884 \cdot \sqrt{f_D} \cdot \ln\left(1 - \frac{r}{R}\right) \tag{A.50}$$

We also combine Equations A.24 and A.49:

$$u = \langle u_{\max} \rangle - 3.75 \cdot u_\tau = \langle u_{\max} \rangle - 3.75 \cdot u\sqrt{\frac{f_D}{8}} = \langle u_{\max} \rangle - 1.326 \cdot u\sqrt{f_D} \tag{A.51}$$

For u and $\langle u_{\max} \rangle$, we obtain:

$$u = \frac{\langle u_{\max} \rangle}{1 + 1.326 \cdot \sqrt{f_D}} \quad \text{alternatively: } \langle u_{\max} \rangle = u\left(1 + 1.326 \cdot \sqrt{f_D}\right) \tag{A.52}$$

The result of Equation A.52 inserted into A.50 yields

$$u(r) = \langle u_{\max} \rangle + \frac{\langle u_{\max} \rangle}{1 + 1.326 \cdot \sqrt{f_D}} \cdot 0.884 \cdot \sqrt{f_D} \cdot \ln\left(1 - \frac{r}{R}\right) \tag{A.53}$$

and furthermore:

$$\frac{u(r)}{\langle u_{\max} \rangle} = 1 + \frac{0.884 \cdot \sqrt{f_D}}{1 + 1.326 \cdot \sqrt{f_D}} \cdot \ln\left(1 - \frac{r}{R}\right) \tag{A.54}$$

A.3.4 Smooth conditions

For smooth walls (in particular, see Figure 11.3), the wall distance z_W, where $u(z_W) = 0$, was experimentally determined to be $z_W = \frac{1}{9}\frac{\nu}{u_\tau}$ [5][G]. We refer back to Equation A.38 and insert into it $\kappa = 0.4$ and the experimentally determined expression for the wall distance $z_W = \frac{1}{9}\frac{\nu}{u_\tau}$:

$$\begin{aligned} \langle u_{\max} \rangle &= \frac{u_\tau}{\kappa} \ln \frac{R \cdot u_\tau}{\frac{1}{9} \cdot \nu} = \frac{u_\tau}{0.4}\left(\ln \frac{R \cdot u_\tau}{\nu} - \ln \frac{1}{9}\right) = 2.5u_\tau \cdot \left(\ln \frac{R \cdot u_\tau}{\nu} + \ln 9\right) \\ &= u_\tau\left(2.5 \cdot \ln \frac{R \cdot u_\tau}{\nu} + 2.5 \cdot 2.197\right) = u_\tau\left(2.5 \cdot \ln \frac{R \cdot u_\tau}{\nu} + 5.5\right) \end{aligned} \tag{A.55}$$

The constant 5.5 is explicitly used elsewhere without the detour via z_W. When inserting the expression given above for the maximum velocity $\langle u_{\max} \rangle$ into the equation for the mean cross-sectional velocity A.49, we obtain:

[G] Malcherek [27, p. 159] indicates a value of $z_W = \frac{1}{9{,}535}\frac{\nu}{u_\tau}$.

$$u = u_\tau \left(2.5 \cdot \ln \frac{R \cdot u_\tau}{\nu} + 5.5 \right) - 3.75 \cdot u_\tau = u_\tau \left(2.5 \cdot \ln \frac{R \cdot u_\tau}{\nu} + 1.75 \right) \tag{A.56}$$

From $u_\tau = u\sqrt{\frac{f_D}{8}}$, i. e. $\frac{u}{u_\tau} = \sqrt{\frac{8}{f_D}}$, we furthermore obtain:

$$\sqrt{\frac{8}{f_D}} = 2.5 \cdot \ln \frac{R \cdot u_\tau}{\nu} + 1.75 \tag{A.57}$$

We divide by $\sqrt{8}$:

$$\frac{1}{\sqrt{f_D}} = 0.884 \cdot \ln \frac{R \cdot u_\tau}{\nu} + 0.619 \tag{A.58}$$

By means of Equation A.24, we modify the argument of the logarithm:

$$\frac{R u_\tau}{\nu} = \frac{D}{2} \cdot \frac{u}{u} \cdot \frac{u_\tau}{\nu} = \frac{uD}{\nu} \cdot \frac{u_\tau}{2u} = \mathrm{Re} \frac{u_\tau}{2u} = \mathrm{Re} \sqrt{\frac{f_D}{8}} \cdot \frac{u}{2u} = \frac{1}{5.66} \cdot \mathrm{Re} \cdot \sqrt{f_D} \tag{A.59}$$

Inserting A.59 into A.58 yields:

$$\begin{aligned} \frac{1}{\sqrt{f_D}} &= 0.884 \cdot \ln \frac{\mathrm{Re} \cdot \sqrt{f_D}}{5.66} + 0.619 = 0.884 \cdot \ln \left(\mathrm{Re} \cdot \sqrt{f_D} \right) + 0.884 \cdot \ln \frac{1}{5.66} + 0.619 \\ &= 0.884 \cdot \ln \left(\mathrm{Re} \cdot \sqrt{f_D} \right) - 0.913 \end{aligned} \tag{A.60}$$

In the next step, the natural logarithm is replaced by the common logarithm. The relevant conversion may be found, for example, in [8, p. 10] as $\log(x) = \frac{\ln(x)}{\ln(10)}$ or, rearranged, as $\ln(x) = \log(x) \cdot \ln(10)$:

$$\begin{aligned} \frac{1}{\sqrt{f_D}} &= 0.884 \cdot \ln(10) \cdot \log \left(\mathrm{Re} \cdot \sqrt{f_D} \right) - 0.913 = 2.035 \cdot \log \left(\mathrm{Re} \cdot \sqrt{f_D} \right) - 0.913 \\ &= 2.035 \left(\log \left(\mathrm{Re} \cdot \sqrt{f_D} \right) - \frac{0.913}{2.035} \right) = 2.035 \left(\log \left(\mathrm{Re} \cdot \sqrt{f_D} \right) - 0.449 \right) \\ &= 2.035 \log \left(\frac{\mathrm{Re} \cdot \sqrt{f_D}}{10^{0.449}} \right) = 2.035 \log \left(\frac{\mathrm{Re} \cdot \sqrt{f_D}}{2.81} \right) \end{aligned} \tag{A.61}$$

Bollrich [5, p. 177] notes that the numeric values differ slightly from those that were determined experimentally due to the assumptions that were made ($\kappa = \frac{l_m}{z}$ and $\tau(r) = \tau_W = \text{const.}$). When inserting these values into Equation A.61, one obtains the well-known law for the friction coefficient for hydraulically smooth conditions:

$$\frac{1}{\sqrt{f_D}} = 2.0 \log \left(\frac{\mathrm{Re} \cdot \sqrt{f_D}}{2.5} \right) = -2.0 \log \left(\frac{2.5}{\mathrm{Re} \cdot \sqrt{f_D}} \right) \tag{A.62}$$

A.3.5 Rough conditions

In experiments for rough conditions, Nikuradse determined a wall distance $z_W = \frac{k_s}{30}$ by adhering grains of sand onto smooth pipe walls, for which $u(z_W) = 0$ applies. We insert this expression for z_W into Equation A.38:

$$\begin{aligned}\langle u_{\max}\rangle &= \frac{u_\tau}{\kappa}\ln\frac{30\cdot R}{k_s} = 2.5\cdot u_\tau\left(\ln\left(\frac{D}{k_s}\right)+\ln 15\right)\\ &= u_\tau\left(2.5\cdot\ln\left(\frac{D}{k_s}\right)+2.5\cdot\ln 15\right) = u_\tau\left(2.5\cdot\ln\left(\frac{D}{k_s}\right)+6.77\right)\end{aligned} \tag{A.63}$$

This maximum velocity is substituted into Equation A.49, which is $u = \langle u_{\max}\rangle - 3.75\cdot u_\tau$, resulting in:

$$u = u_\tau\left(2.5\cdot\ln\left(\frac{D}{k_s}\right)+6.77-3.75\right) = u_\tau\left(2.5\cdot\ln\left(\frac{D}{k_s}\right)+3.02\right) \tag{A.64}$$

We continue the calculation with $\frac{u_\tau}{u} = \sqrt{\frac{f_D}{8}}$ (see Equation A.24):

$$\frac{u}{u_\tau} = \sqrt{\frac{8}{f_D}} = 2.5\cdot\ln\left(\frac{D}{k_s}\right)+3.02 \tag{A.65}$$

At this point, we again divide by $\sqrt{8}$ and introduce the common logarithm as in Equation A.61:

$$\begin{aligned}\frac{1}{\sqrt{f_D}} &= \frac{2.5}{\sqrt{8}}\cdot\ln(10)\cdot\log\left(\frac{D}{k_s}\right)+\frac{3.02}{\sqrt{8}} = 2.035\cdot\left(\log\left(\frac{D}{k_s}\right)+\frac{1.07}{2.035}\right)\\ &= 2.035\cdot\log\left(\frac{D}{k_s}\cdot 10^{\frac{1.07}{2.035}}\right) = 2.035\cdot\log\left(3.36\cdot\frac{D}{k_s}\right)\end{aligned} \tag{A.66}$$

The equation for the rough region is also adjusted on the basis of the constants that were found empirically. We ultimately obtain:

$$\frac{1}{\sqrt{f_D}} = 2.0\cdot\log\left(3.7\cdot\frac{D}{k_s}\right) = -2.0\cdot\log\frac{k_s}{3.7\cdot D} \tag{A.67}$$

A.3.6 Transition region

The transition region between smooth and rough conditions, where influences of viscosity and roughness are in effect, was proposed by Colebrook on the basis of measurements. The above derived Expressions A.62 and A.67 result from the limit value analyses $k_s \to 0$ and $\mathrm{Re} \to \infty$, respectively, of Equation A.68.

$$\frac{1}{\sqrt{f_D}} = -2.0\cdot\log\left(\frac{2.5}{\mathrm{Re}\sqrt{f_D}}+\frac{k_s}{3.7\cdot D}\right) \tag{A.68}$$

Oumeraci [33] specifies the validity range for Equation A.68 as $65 \leq \mathrm{Re}\frac{k_s}{D} \leq 1300$. Sigloch [57, p. 139] sees the transition region at $25 \leq \mathrm{Re}^{0.875}\frac{k_s}{D} \leq 350$. The widely quoted validity limit between transition region and rough behaviour is, according to Blasius (who was Prandtl's assistant), $\mathrm{Re}\cdot\sqrt{f_D}\cdot\frac{k_s}{D} = 200$ (see for example [5, p. 179]). We rely on Schlichting [51, p. 573] and indicate the validity limit between hydraulically smooth conditions and the transition region as $\frac{k_s\cdot u_\tau}{\nu} \leq 5$, which, via the turbulent length scale $l_\nu = \frac{\nu}{u_\tau}$ (see Equation A.25), corresponds to the thickness of the viscous sublayer of $\delta_\nu \approx 5l_\nu$ (see Equation A.28 with $z^+ \lesssim 5$)[H]. From $k_s \approx 5\frac{\nu}{u_\tau}$ and using Expression A.24, the final result is $k_s \approx 5\frac{\nu}{u\cdot\sqrt{\frac{f_D}{8}}}$. The introduction of the Reynolds number $\frac{\nu}{u} = \frac{D}{\mathrm{Re}}$ results in $k_s \approx \frac{5\cdot D}{\mathrm{Re}\cdot\sqrt{\frac{f_D}{8}}} = \frac{5\cdot\sqrt{8}\cdot D}{\mathrm{Re}\sqrt{f_D}}$. From this, the Inequality A.69 follows as the validity limit between smooth conditions and the transition region:

$$\mathrm{Re}\sqrt{f_D}\frac{k_s}{D} \leq 5\cdot\sqrt{8} = 14.14 \tag{A.69}$$

In Schlichting [51, p. 573], it is stated further that the validity limit between the transition region and the rough conditions is at $\frac{k_s\cdot u_\tau}{\nu} \leq 70$ which, in a manner similar to the above approach, leads to Inequality A.70:

$$\mathrm{Re}\sqrt{f_D}\frac{k_s}{D} \leq 70\cdot\sqrt{8} \approx 198.0 \approx 200 \tag{A.70}$$

It should be noted here that these considerations are of an academic nature. The equation for the transition region (A.68) is often used universally since the deviations from the smooth and rough laws are marginal. The influence of assumptions concerning the condition of the pipe wall, the laying technique or the like is far greater.

A.4 Calculation of the determinant of a matrix

The determinant of a matrix is evaluated by successively multiplying the elements of the first row by their corresponding subdeterminants and adding the results of each such operation. Thereby, the column and the line (the first line) of the element are omitted and the matrix is reduced to the remaining elements. This has to be repeated until a scalar remains. However, care must be taken with the signs of each multiplication. Multiplications by elements of the first row in uneven columns are added positively, whereas multiplications by elements of the first row in even columns are added negatively. By the way, in the case of a 2×2 matrix, the subdeterminant is a scalar.

$$\begin{aligned}\det(A) \equiv \begin{vmatrix} a_1 & a_2 & a_3 \\ b_1 & b_2 & b_3 \\ c_1 & c_2 & c_3 \end{vmatrix} &= a_1 \begin{vmatrix} b_2 & b_3 \\ c_2 & c_3 \end{vmatrix} - a_2 \begin{vmatrix} b_1 & b_3 \\ c_1 & c_3 \end{vmatrix} + a_3 \begin{vmatrix} b_1 & b_2 \\ c_1 & c_2 \end{vmatrix} \\ &= a_1\,(b_2c_3 - b_3c_2) - a_2\,(b_1c_3 - b_3c_1) + a_3\,(b_1c_2 - b_2c_1)\end{aligned} \tag{A.71}$$

[H] For the determination of the thickness of the viscous sublayer, various equations can be found in the reference literature.

A.5 Derivation of the critical conditions for selected cross-sections

A.5.1 Trapezoid

The Bernoulli equation for a trapezoidal open channel with the bank slope m and area $A = (b + my)\, y$ reads:

$$H = y + \frac{Q^2}{2gA^2} = y + \frac{Q^2}{2g\left[(b+my)\, y\right]^2} \tag{A.72}$$

The derivative of y is first taken with respect to y, yielding one. It then follows "from the outside to the inside" that $\left(by + my^2\right)^{-2}$ yields $-2 \cdot \left(by + my^2\right)^{-3}$ (for the derivative inside the bracket) and $\cdot\,(b + 2my)$ (for the derivative of $\left(by + my^2\right)$.

$$\frac{\mathrm{d}H}{\mathrm{d}y} = \left(y + \frac{Q^2}{\left[(b+my)\, y\right]^2 2g} \right) \frac{1}{\mathrm{d}y} = 1 + \frac{Q^2}{2g} \frac{-2\,(b+2my)}{\left(by + my^2\right)^3} \stackrel{!}{=} 0 \tag{A.73}$$

The equation cannot be solved explicitly for the desired variable. We obtain an implicit solution:

$$\frac{g}{Q^2} = \frac{b + 2my_{c,\mathrm{trapezoid}}}{\left(by_{c,\mathrm{trapezoid}} + my_{c,\mathrm{trapezoid}}^2\right)^3} \tag{A.74}$$

We check the equation for a rectangular open channel with $m = 0$:

$$\frac{g}{Q^2} = \frac{b + 2 \cdot 0 \cdot y_c}{\left(by_c + 0 \cdot y_c^2\right)^3} = \frac{b}{\left(by_c\right)^3} = \frac{1}{b^2 y_c^3} \tag{A.75}$$

Solving for y_c, we obtain the same expression as that of Equation 13.7:

$$y_c = \sqrt[3]{\frac{Q^2}{b^2 g}} \tag{A.76}$$

A.5.2 Triangle

For the special case of a trapezoid with $b = 0$, i. e. for a triangle, it follows that

$$\frac{g}{Q^2} = \frac{0 + 2 \cdot my}{\left(0 \cdot y + m \cdot y^2\right)^3} = \frac{2my}{\left(my^2\right)^3} = \frac{2}{m^2 y^5} \tag{A.77}$$

and thus for y_c,

$$y_{c,\mathrm{triangle}} = \sqrt[5]{2\frac{Q^2}{gm^2}} \tag{A.78}$$

A.5.3 Parabola

A parabola is generally described by:

$$y = ax^2 \tag{A.79}$$

Solving for x yields:

$$x = \sqrt{\frac{y}{a}} \tag{A.80}$$

The area of the right-hand branch is obtained by integration with respect to y:

$$A = \int \sqrt{\frac{y}{a}}\,\mathrm{d}y = \int \frac{y^{\frac{1}{2}}}{\sqrt{a}}\,\mathrm{d}y = \frac{2}{3}\frac{y^{\frac{3}{2}}}{\sqrt{a}} \tag{A.81}$$

Inserted as $(2 \cdot A)^2$ (for the two branches at the right- and left-hand side of the coordinate origin) in the Bernoulli equation, the result is:

$$H = y + \frac{Q^2}{\frac{16}{9}\frac{y^3}{a}2g} \tag{A.82}$$

To find the minimum value of H, take its derivative with respect to y and set it equal to zero:

$$\frac{\mathrm{d}H}{\mathrm{d}y} = 1 + \frac{Q^2 \cdot (-3)}{\frac{16}{9}\frac{2g}{a}y^4} = 1 - \frac{27}{32}\frac{aQ^2}{y^4 g} \stackrel{!}{=} 0 \tag{A.83}$$

Solving for y, which we again designate as y_c, we obtain:

$$y_{c,\mathrm{parabola}} = \sqrt[4]{\frac{27}{32}\frac{aQ^2}{g}} \tag{A.84}$$

A.6 Wave theory

The description of water waves dates back to George Airy[I]. In the linear wave theory[J] named after him, a frictionless, incompressible and irrotational flow of average depth is assumed. Therein, the fluid particles move on elliptical paths about their centres, as shown in Figure A.6, while the wave propagates at velocity c. The maximum wave height $\xi_{\max}$ that is measured from the undisturbed water level $z = 0$ is to be small relative to both the wavelength λ_{wave} and the depth of the water body h ($\frac{\xi_{\max}}{\lambda_{\mathrm{wave}}} \ll 1$ and $\frac{\xi_{\max}}{h} \ll 1$) in order to be able to describe the problem linearly [25].
According to the Airy theory, the fluid particles oscillate about their centre positions; their mean velocity is zero. To satisfy the continuity condition, they move towards the wave crest and move away from the wave trough. The radius of movement of the particles at

[I] George Biddell Airy, ∗1801, Alnwick, England †1892, Greenwich, England

[J] A more detailed derivation of the equations may be found in [25, p. 219 ff.] or in [28, p. 117]; at this point, the relationships will be mentioned briefly and placed into the context of open channel hydraulics.

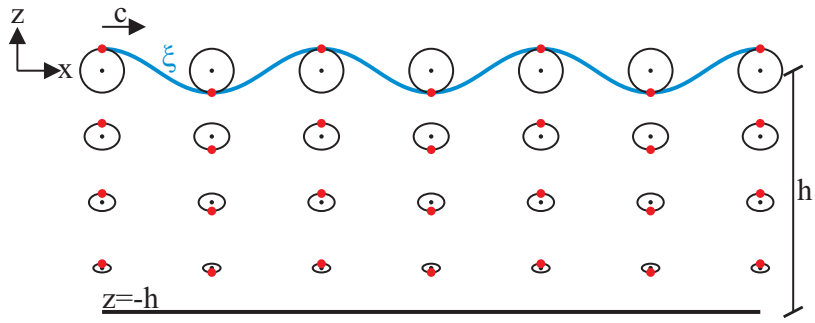

Figure A.6: Sketch of the wave movement and the elliptical particle paths.

the bottom is very small compared to the range at the water surface. By the way, Bollrich [5] indicates that waves surge at a proportion $h < 1.3\xi$ because of their translational movement.
The above assumptions of a frictionless, incompressible and irrotational flow permit the definition of a velocity potential (see Chapter 4):

$$u = \frac{\partial \Phi}{\partial x}; \quad w = \frac{\partial \Phi}{\partial z} \tag{A.85}$$

Thus, Laplace's equation reads:

$$\frac{\partial^2 \Phi}{\partial x^2} + \frac{\partial^2 \Phi}{\partial z^2} = 0 \tag{A.86}$$

Due to the freedom of rotation and friction, we may use the Bernoulli equation (5.41). With the local derivative that is integrated along the streamline $\int \frac{\partial u}{\partial t} \mathrm{d}s = \frac{\partial \Phi}{\partial t}$, it reads:

$$\frac{\partial \Phi}{\partial t} + \frac{1}{2}\left(u^2 + w^2\right) + \frac{p}{\rho} + gz = f(t) \tag{A.87}$$

We may derive the boundary conditions for Laplace's equation (A.86) from this equation. When generally setting up a cosine function with the wave number $k = \frac{2\pi}{\lambda_{\text{wave}}}$ and the rotational frequency ω for the description of the water surface, the result is:

$$\xi(x,t) = \xi_{\max} \cos(kx - \omega t) \tag{A.88}$$

Kundu and Cohen [25] indicate the solution for the associated velocity potential as follows:

$$\Phi(x,z,t) = \frac{\xi_{\max}\omega}{k} \cdot \frac{\cosh(k \cdot (z+h))}{\sinh(kh)} \sin(kx - \omega t) \tag{A.89}$$

Equations A.88 and A.89, with the boundary conditions of the velocity potential [25], result in:

$$\omega = \sqrt{gk \tanh(kh)} \tag{A.90}$$

With the propagation velocity $c = \frac{\omega}{k}$, Equation A.90 may be written as:

$$c = \sqrt{\frac{g}{k} \tanh(kh)} = \sqrt{\frac{g\lambda_{\text{wave}}}{2\pi} \tanh\left(\frac{2\pi}{\lambda_{\text{wave}}} h\right)} \tag{A.91}$$

Now there must be a case-by-case analysis because for small values of the argument of the hyperbolic tangent function, the value of the function approximates the argument itself, whereas when the argument of the function x approaches ∞, the value of the function approaches 1; i. e. $\lim_{x\to\infty} \tanh(x) = 1$.

A.6.1 Deep water waves

For example, for $\frac{h}{\lambda_{\text{wave}}} = 0.25$, one obtains $\tanh(2 \cdot \pi \cdot 0.25) = 0.917 \approx 1$, and for $\frac{h}{\lambda_{\text{wave}}} = 0.4$, the result is $\tanh(2 \cdot \pi \cdot 0.4) = 0.987 \approx 1$. One may therefore confidently refer to "deep-water waves" when the water depth is greater than approximately one-third of the wavelength. With the assumption that $\tanh\left(\frac{2\pi h}{\lambda_{\text{wave}}}\right) \approx 1$, it follows for the propagation velocity of deep-water waves:

$$c = \sqrt{\frac{g}{k}} = \sqrt{\frac{g\lambda_{\text{wave}}}{2\pi}} \tag{A.92}$$

The propagation velocity of deep-water waves is dependent on the wavelength λ_{wave}.

A.6.2 Shallow-water waves

On the other hand, for $h \ll \lambda_{\text{wave}}$, the hyperbolic tangent becomes $\tanh\left(\frac{2\pi h}{\lambda_{\text{wave}}}\right) \approx \frac{2\pi h}{\lambda_{\text{wave}}}$. With a ratio of $\frac{h}{\lambda_{\text{wave}}} = 0.1$, the result is $\tanh(2 \cdot \pi \cdot 0.1) = 0.557$, whereas $\frac{2\pi h}{\lambda_{\text{wave}}}$ itself has the value 0.628. If the water depth is $\frac{1}{20}$ of the wavelength, then one obtains $\tanh(2 \cdot \pi \cdot 0.05) = 0.304$, whereas $2 \cdot \pi \cdot 0.05$ itself is approximately 0.314.
By means of the limit value analysis for $\tanh\left(\frac{2\pi h}{\lambda_{\text{wave}}}\right) \approx \frac{2\pi h}{\lambda_{\text{wave}}}$, the propagation velocity of shallow-water waves is obtained:

$$c = \sqrt{\frac{g\lambda_{\text{wave}}}{2\pi}\left(\frac{2\pi}{\lambda_{\text{wave}}}h\right)} = \sqrt{gh} \tag{A.93}$$

The propagation velocity of shallow-water waves is dependent on the depth of the water body h. This velocity plays a particularly important role, especially when focusing on the Froude similarity, where it may be directly read from the dimensionless Navier–Stokes equation (5.33).

A.6.3 Capillary waves

For capillary waves, the surface tension of the water is the determining force (per unit meter). Although line forces are not considered in this book, the capillary waves shall be mentioned briefly. When setting up the Bernoulli equation along the water surface with the surface tension height $\frac{\sigma}{r\rho g}$ as an additional term (with surface curvature r), one arrives at the description of the propagation velocity of a capillary wave:

$$c = \sqrt{\frac{g\lambda_{\text{wave}}}{2\pi} + \frac{2\pi\sigma}{\rho\lambda_{\text{wave}}}} \tag{A.94}$$

With wavelength $\lambda_{\text{wave}} = 1.71\,\text{cm}$, the minimum propagation velocity of a capillary wave is found to be $c_{\text{min,capillary}} = 0.231\,\text{m/s}$. The influence of the surface tension relative to gravity decreases considerably with increasing wavelength. According to Kallenrode [22, p. 166], it is already negligibly small (less than 3 %) with a wavelength of $\lambda_{\text{wave}} = 10\,\text{cm}$. When projecting this ratio onto the propagation velocity of a disturbance with surface tension, one obtains a propagation velocity of $c_{\text{capillary}} = 0.401\,\text{m/s}$; without surface tension, the propagation velocity is $c = 0.395\,\text{m/s}$ at this wavelength. This means that the capillary effects play a minor role at water depths greater than $h = \frac{c^2}{g} = 1.6\,\text{cm}$ or propagation velocities above $c = 0.40\,\text{m/s}$.

A.7 Solution for the practical example of the Hamburg interceptor sewer

```
% Program for the solution of the set of equations of the pipeflow example 'Hamburg
sewer'
%%%%%%%%%%%%%%%%%%%%%%%%%%%%%%%%%%%%%%%%%%%%%%%%%%%%%%%%
% % % Copyright (C) <2016>  <Christoph Rapp>

% % % This program is free software: you can redistribute it and/or modify
% % % it under the terms of the GNU General Public License as published by
% % % the Free Software Foundation, either version 3 of the License, or
% % % (at your option) any later version.

% % % This program is distributed in the hope that it will be useful,
% % % but WITHOUT ANY WARRANTY; without even the implied warranty of
% % % MERCHANTABILITY or FITNESS FOR A PARTICULAR PURPOSE.  See the
% % % GNU General Public License for more details.

% % % You should have received a copy of the GNU General Public License
% % % along with this program.  If not, see <http://www.gnu.org/licenses/>
%%%%%%%%%%%%%%%%%%%%%%%%%%%%%%%%%%%%%%%%%%%%%%%%%%%%%%%%
% input
file='dataHH.csv';
delimiter='=';
header=2;
dataInput(file,delimiter,header);
% input
% cross sections
if cs==1
    cs='circle';
    csP1=d1;
    csP2=d2;
    csP3=d3;
else
    error('Valid for circular cross sections only.')
end
% crosssections

Q3=Q1+Q2; % [m3/s]
% INITIAL VALUE ONLY
Q3=1; % [m3/s] INITIAL VALUE ONLY
% INITIAL VALUE ONLY
k=0;
while abs(Q1-(Q3-Q2))>1E-3
    Q3=Q1+Q2;
    Hp1=-2.6368*Q1^3+10.578*Q1^2-20.908*Q1+28.812; % throttle curve for 2 parallel
    pumps
    if Q2<0.0872
        Hp2=-24.472*Q2+9; % throttle curve for 2 parallel pumps
    elseif Q<.11
        Hp2=-300.66*Q2+33.072; % throttle curve for 2 parallel pumps
    else
        error('Pumps in pump station 2 are to small.')
    end
    fD1=pc(cs,csP1,csP1,Q1,ks1,T); % fD via subroutine pc
    fD2=pc(cs,csP2,csP2,Q2,ks2,T); % fD via subroutine pc
    fD3=pc(cs,csP3,csP3,Q3,ks3,T); % fD via subroutine pc
```

```
    % set of equations
    A = [(fD1*L1/d1+sumK1+1)/(d1^4*pi^2*g/8),0,1;
    0,(fD2*L2/d2+sumK2+1)/(d2^4*pi^2*g/8),1;
    -1*(fD3*L3/d3+sumK3+1)/(d3^4*pi^2*g/8),-1*(fD3*L3/d3+sumK3+1)/(d3^4*pi^2*g/8),1];
    % set of equations
    % solution matrix
    E = [.5+Hp1;.8+Hp2;3.11];
    % solution matrix
    X=A\E; % solving of the set of equations
    Q1=sqrt(X(1)); % solving of the substitution
    Q2=sqrt(X(2)); % solving of the substitution
    DlKn=X(3);
end
fname=sprintf('Q1 = %1.3f m3/s,\nQ2 = %1.3f m3/s,\nQ3 = %1.3f m3/s',Q1,Q2,Q3);
disp(fname) % display of the results
```

The program uses data from file `dataHH.csv`. It contains the following entries line-by-line:

```
# Data for the sewer in Hamburg
# qs: 1=circle, 2=trapezoid, 3=parabola
eps=0.0001
rho=1000
g=9.8065
qs=1
d1=.6
d2=.2
d3=.6
Q1=.7
Q2=.04
T=10
L1=1894.91
sumK1=1.463
ks1=3E-5
L2=394.75
sumK2=.28
ks2=1E-5
L3=225.38
sumK3=.28
ks3=3E-5
```

A.8 Results for the example of the unsteady pipe flow from page 202

Table A.1: Results for the example of the unsteady pipe flow from page 202.

i	$(i-1)\,\Delta t$ [s]	$J_E(i,1)$ [ ]	$J_E(i,2)$ [ ]	$J_E(i,3)$ [ ]	$v(i,1)$ [m/s]	$v(i,2)$ [m/s]	$v(i,3)$ [m/s]
1	0.00	2.33×10^{-3}	2.33×10^{-3}	2.33×10^{-3}	0.7054	0.7054	0.7054
2	2.39	NaN	2.33×10^{-3}	NaN	NaN	0.7054	NaN
3	4.78	2.33×10^{-3}	NaN	2.33×10^{-3}	0.7054	NaN	0.7053
4	7.17	NaN	2.33×10^{-3}	NaN	NaN	0.7053	NaN
5	9.56	2.33×10^{-3}	NaN	2.33×10^{-3}	0.7052	NaN	0.7052
6	11.96	NaN	2.33×10^{-3}	NaN	NaN	0.7051	NaN
7	14.35	2.33×10^{-3}	NaN	2.32×10^{-3}	0.7050	NaN	0.7048
8	16.74	NaN	2.32×10^{-3}	NaN	NaN	0.7047	NaN
9	19.13	2.32×10^{-3}	NaN	2.32×10^{-3}	0.7044	NaN	0.7038
10	21.52	NaN	2.32×10^{-3}	NaN	NaN	0.7036	NaN
11	23.91	2.31×10^{-3}	NaN	2.29×10^{-3}	0.7030	NaN	0.7001
12	26.30	NaN	2.29×10^{-3}	NaN	NaN	0.6997	NaN
13	28.69	2.27×10^{-3}	NaN	1.81×10^{-3}	0.6970	NaN	0.6201
14	31.09	NaN	1.82×10^{-3}	NaN	NaN	0.6233	NaN
15	33.48	1.48×10^{-3}	NaN	0.00	0.5602	NaN	0
16	35.87	NaN	-7.23×10^{-6}	NaN	NaN	-0.0377	NaN
17	38.26	-1.70×10^{-3}	NaN	0.00	-0.6008	NaN	0
18	40.65	NaN	-1.39×10^{-3}	NaN	NaN	-0.5434	NaN
19	43.04	-1.15×10^{-3}	NaN	0.00	-0.4931	NaN	0
20	45.43	NaN	-7.44×10^{-5}	NaN	NaN	-0.1207	NaN
21	47.82	2.50×10^{-4}	NaN	0.00	0.2265	NaN	0
22	50.22	NaN	2.42×10^{-4}	NaN	NaN	0.2227	NaN
23	52.61	2.35×10^{-4}	NaN	0.00	0.2191	NaN	0
24	55.00	NaN	-2.51×10^{-8}	NaN	NaN	-6.88×10^{-4}	NaN
25	57.39	-2.26×10^{-4}	NaN	0.00	-0.2150	NaN	0
26	59.78	NaN	-2.19×10^{-4}	NaN	NaN	-0.2116	NaN
27	62.17	-2.13×10^{-4}	NaN	0.00	-0.2085	NaN	0
28	64.56	NaN	1.95×10^{-8}	NaN	NaN	5.33×10^{-4}	NaN
29	66.95	2.05×10^{-4}	NaN	0.00	0.2045	NaN	0
30	69.34	NaN	2.00×10^{-4}	NaN	NaN	0.2016	NaN
31	71.74	1.94×10^{-4}	NaN	0.00	0.1988	NaN	0
32	74.13	NaN	-1.47×10^{-8}	NaN	NaN	-4.04×10^{-4}	NaN
33	76.52	-1.87×10^{-4}	NaN	0.00	-0.1950	NaN	0
34	78.91	NaN	-1.82×10^{-4}	NaN	NaN	-0.1925	NaN
35	81.30	-1.78×10^{-4}	NaN	0.00	-0.1900	NaN	0
36	83.69	NaN	1.07×10^{-8}	NaN	NaN	2.94×10^{-4}	NaN
37	86.08	1.71×10^{-4}	NaN	0.00	0.1864	NaN	0
38	88.47	NaN	1.67×10^{-4}	NaN	NaN	0.1841	NaN
39	90.87	1.64×10^{-4}	NaN	0.00	0.1819	NaN	0
40	93.26	NaN	-7.32×10^{-9}	NaN	NaN	-2.01×10^{-4}	NaN

Table A.2: Results of the exercise example related to nonstationary pipe hydraulics.

Index i	$t=(i-1)\,\Delta t$ [s]	$K^+(i,j=1)$ [m]	$K^+(i,j=2)$ [m]	$K^+(i,j=3)$ [m]
1	0	−395.26	−388.28	−381.29
2	2.39	NaN	−388.28	NaN
3	4.78	−395.26	NaN	−381.29
4	7.17	NaN	−388.28	NaN
5	9.56	−395.25	NaN	−381.30
6	11.96	NaN	−388.27	NaN
7	14.35	−395.22	NaN	−381.29
8	16.74	NaN	−388.25	NaN
9	19.13	−395.16	NaN	−381.29
10	21.52	NaN	−388.21	NaN
11	23.91	−395.00	NaN	−381.32
12	26.30	NaN	−388.12	NaN
13	28.69	−394.36	NaN	−382.71
14	31.09	NaN	−388.89	NaN
15	33.48	−379.25	NaN	−388.89
16	35.87	NaN	−379.27	NaN
17	38.26	−240.22	NaN	−379.27
18	40.65	NaN	−244.39	NaN
19	43.04	−252.35	NaN	−244.39
20	45.43	NaN	−252.57	NaN
21	47.82	−340.23	NaN	−252.57
22	50.22	NaN	−339.51	NaN
23	52.61	−339.33	NaN	−339.51
24	55.00	NaN	−339.33	NaN
25	57.39	−285.17	NaN	−339.33
26	59.78	NaN	−285.83	NaN
27	62.17	−285.97	NaN	−285.83
28	64.56	NaN	−285.97	NaN
29	66.95	−337.55	NaN	−285.97
30	69.34	NaN	−336.96	NaN
31	71.74	−336.85	NaN	−336.96
32	74.13	NaN	−336.85	NaN
33	76.52	−287.61	NaN	−336.85
34	78.91	NaN	−288.15	NaN
35	81.30	−288.23	NaN	−288.15
36	83.69	NaN	−288.23	NaN
37	86.08	−335.33	NaN	−288.23
38	88.47	NaN	−334.83	NaN
39	90.87	−334.78	NaN	−334.83
40	93.26	NaN	−334.78	NaN

Table A.3: Results of the exercise example related to nonstationary pipe hydraulics.

Index i	$t=(i-1)\,\Delta t$ [s]	$K^-(i,j=1)$ [m]	$K^-(i,j=2)$ [m]	$K^-(i,j=3)$ [m]
1	0	−228.74	−221.75	−214.76
2	2.39	NaN	−221.75	NaN
3	4.78	−228.74	NaN	−214.78
4	7.17	NaN	−221.77	NaN
5	9.56	−228.75	NaN	−214.82
6	11.96	NaN	−221.80	NaN
7	14.35	−228.78	NaN	−214.90
8	16.74	NaN	−221.87	NaN
9	19.13	−228.84	NaN	−215.11
10	21.52	NaN	−222.06	NaN
11	23.91	−229.00	NaN	−215.94
12	26.30	NaN	−222.82	NaN
13	28.69	−229.64	NaN	−234.85
14	31.09	NaN	−240.32	NaN
15	33.48	−244.75	NaN	−388.89
16	35.87	NaN	−388.87	NaN
17	38.26	−383.78	NaN	−379.27
18	40.65	NaN	−375.10	NaN
19	43.04	−371.65	NaN	−283.24
20	45.43	NaN	−283.02	NaN
21	47.82	−283.77	NaN	−283.24
22	50.22	NaN	−283.97	NaN
23	52.61	−284.67	NaN	−339.51
24	55.00	NaN	−339.51	NaN
25	57.39	−338.83	NaN	−339.33
26	59.78	NaN	−338.67	NaN
27	62.17	−338.03	NaN	−285.83
28	64.56	NaN	−285.83	NaN
29	66.95	−286.45	NaN	−285.97
30	69.34	NaN	−286.56	NaN
31	71.74	−287.15	NaN	−336.96
32	74.13	NaN	−336.96	NaN
33	76.52	−336.39	NaN	−336.85
34	78.91	NaN	−336.31	NaN
35	81.30	−335.77	NaN	−288.15
36	83.69	NaN	−288.15	NaN
37	86.08	−288.67	NaN	−288.23
38	88.47	NaN	−288.73	NaN
39	90.87	−289.22	NaN	−334.83
40	93.26	NaN	−334.83	NaN

Table A.4: Results of the exercise example related to nonstationary pipe hydraulics. The coloured cells identify values that were limited to the the vapour pressure.

Index i	$t=(i-1)\Delta t$ [s]	A_t [m^2]	$h_p(i,j=1)$ [m]	$h_p(i,j=2)$ [m]	$h_p(i,j=3)$ [m]
1	0	7.07×10^{-2}	312	305.01	298.03
2	2.39	6.51×10^{-2}	NaN	305.01	NaN
3	4.78	5.94×10^{-2}	312	NaN	298.04
4	7.17	5.38×10^{-2}	NaN	305.02	NaN
5	9.56	4.81×10^{-2}	312	NaN	298.06
6	11.96	4.25×10^{-2}	NaN	305.03	NaN
7	14.35	3.69×10^{-2}	312	NaN	298.10
8	16.74	3.12×10^{-2}	NaN	305.06	NaN
9	19.13	2.56×10^{-2}	312	NaN	298.20
10	21.52	2.00×10^{-2}	NaN	305.13	NaN
11	23.91	1.43×10^{-2}	312	NaN	298.63
12	26.30	8.71×10^{-3}	NaN	305.47	NaN
13	28.69	3.08×10^{-3}	312	NaN	308.78
14	31.09	0	NaN	314.61	NaN
15	33.48	0	312	NaN	388.89
16	35.87	0	NaN	384.07	NaN
17	38.26	0	312	NaN	379.27
18	40.65	0	NaN	309.74	NaN
19	43.04	0	312	NaN	283.24
20	45.43	0	NaN	290.24	NaN
21	47.82	0	312	NaN	283.24
22	50.22	0	NaN	311.74	NaN
23	52.61	0	312	NaN	339.51
24	55.00	0	NaN	339.42	NaN
25	57.39	0	312	NaN	339.33
26	59.78	0	NaN	312.25	NaN
27	62.17	0	312	NaN	285.83
28	64.56	0	NaN	290.24	NaN
29	66.95	0	312	NaN	285.97
30	69.34	0	NaN	311.76	NaN
31	71.74	0	312	NaN	336.96
32	74.13	0	NaN	336.90	NaN
33	76.52	0	312	NaN	336.85
34	78.91	0	NaN	312.23	NaN
35	81.30	0	312	NaN	288.15
36	83.69	0	NaN	290.24	NaN
37	86.08	0	312	NaN	288.23
38	88.47	0	NaN	311.78	NaN
39	90.87	0	312	NaN	334.83
40	93.26	0	NaN	334.80	NaN

References

[1] Adams NA (2008) Fluidmechanik I, Einführung in die Dynamik der Fluide. Technische Universität München, München
[2] Ball P (2001) Biographie des Wassers, 2nd edn. Piper
[3] Beffa CJ (1994) Praktische Lösung der tiefengemittelten Flachwassergleichungen. PhD thesis, ETH Zürich
[4] Beitz W, Grote KH (eds) (2001) Dubbel - Taschenbuch für den Maschinenbau. Springer, Berlin
[5] Bollrich G (2013) Technische Hydromechanik 1, Grundlagen, vol 1, 6th edn. Beuth Verlag GmbH, Berlin
[6] Breuer M, Peller N, Rapp C, Manhart M (2009) Flow over periodic hills - numerical and experimental study over a wide range of Reynolds numbers. Computers and Fluids 38(2):433–457
[7] Brockhaus (1971) Brockhaus der Naturwissenschaften und der Technik, 7th edn. F. A. Brockhaus, Wiesbaden
[8] Bronstein I, Semendjajew K (2001) Taschenbuch der Mathematik, 5th edn. Verlag Harri Deutsch, Thun and Frankfurt (Main)
[9] on Climate Change IP (2007) Fourth Assessment Report - Working Group 1; Report on Physical Science. IPCC
[10] Eckelmann H (1997) Einführung in die Strömungsmesstechnik, Leitfaden der angewandten Mathematik und Mechanik, vol 74. Teubner, Stuttgart
[11] Engels H (1914) Handbuch des Wasserbaues, vol 1. Wilhelm Engelmann, Leipzig and Berlin
[12] Flick KH, Billmeier E, Engel N, Hager W, Koch F, Krier H, Mehler R, Schmidt H, Strahlendorff J, Valentin F, Wallisch S, Weiß G (2006) Arbeitsblatt DWA-A 110 - Hydraulische Dimensionierung und Leistungsnachweis von Abwasserleitungen und -kanälen. Arbeitsblatt 110, Deutsche Vereinigung für Wasser, Abwasser und Abfallwirtschaft
[13] Franke PG (1974) Hydraulik für Bauingenieure. Walter de Gruyter, Berlin, New York
[14] Fröhlich J (2006) Large Eddy Simulation turbulenter Strömungen. Teubner, Wiesbaden
[15] Grehn J, von Hessberg A, Holz HG, Krause J, Krüger H, Schmidt HK (1992) Metzler Physik. Grehn, J., Hannover
[16] Gummert P, Reckling KA (1986) Mechanik, 3rd edn. Vieweg, Wiesbaden
[17] Hawking S (2001) Eine kurze Geschichte der Zeit. Deutscher Taschenbuchverlag

C. Rapp, *Hydraulics in Civil Engineering*,
https://doi.org/10.1007/978-3-031-54860-4

[18] Herwig H (2006) Strömungsmechanik, 2nd edn. Springer, Berlin, Heidelberg, New York
[19] Jaeger C (1949) Technische Hydraulik. Springer Basel AG
[20] Jirka GH, Lang C (2009) Einführung in die Gerinnehydraulik. Universitätsverlag Karlsruhe
[21] Kaiser W, König W (eds) (2006) Geschichte des Ingenieurs. Hanser
[22] Kallenrode MB (ed) (2003) Ozeane und Küsten. Universität Osnabrück, Skript
[23] Kornev N (2008) Grundlagen der Schiffstheorie. Universität Rostock, Rostock, Skript
[24] Kreuter F (1906) Der Wasserbau in Bayern. In: Darstellungen aus der Geschichte der Technik, Industrie und Landwirtschaft in Bayern., pp 91–109
[25] Kundu PK, Cohen IM (2004) Fluid Mechanics, 3rd edn. Elsevier Academic Press
[26] Lindner H (1979) Grundriss der Festkörperphysik. No. 75 in Mitteilungen, Vieweg, Braunschweig / Wiesbaden
[27] Malcherek A (2004) Hydromechanik für Bauingenieure, 6th edn. Skript, Universität der Bundeswehr München, München
[28] Malcherek A (2010) Gezeiten und Wellen - Die Hydromechanik der Küstengewässer, 1st edn. Praxis, Vieweg + Teubner, Wiesbaden
[29] Martin H, Pohl R (2014) Technische Hydromechanik 3, Aufgabensammlung, 4th edn. Beuth, Berlin, Wien, Zürich
[30] Mosonyi M (1987) Low-Head Power Plants, 3rd edn. Akadémiai Kiadó, Budapest
[31] Orsenna E (2010) Die Zukunft des Wassers. C. H. Beck
[32] Örtel H, Prandtl L (2002) Prandtl - Führer durch die Strömungslehre, 12th edn. Vieweg, Berlin
[33] Oumeraci H (2015) Hydromechanik. Universität Braunschweig
[34] Pope SB (2000) Turbulent Flows. Cambridge University Press, Cambridge
[35] Rapp C (2004) Hydraulic Engineering. Jordan University of Science and Technology, Irbid, Jordan, Skript
[36] Rapp C (2004) Hydraulik Übung I. Technische Universität München, Skript
[37] Rapp C (2004) Hydraulik Übung II. Technische Universität München, Skript
[38] Rapp C (2004) Hydromechanik Übung. Technische Universität München, Skript
[39] Rapp C (2005) Hydromechanics Exercises. Technische Universität München, Skript
[40] Rapp C (2006) Education in Hydraulic Engineering. In: Rutschmann P (ed) Flood or Draught? In the MENA Region, pp 99–106
[41] Rapp C (2006) Free Surface Flows. Technische Universität München, Skript
[42] Rapp C (2007) Hydromechanics of Free Surface Flows. Jordan University of Science and Technology, Irbid, Jordan, Skript
[43] Rapp C (2009) Experimentelle Studie der turbulenten Strömung über periodische Hügel. No. 75 in Mitteilungen, Fachgebiet Hydromechanik, TUM, München
[44] Rapp C (2012) Forschung und Lehre im Laboratorium für Hydromechanik der Technischen Universität München. No. 77 in Mitteilungen, Fachgebiet Hydromechanik, TUM, München, 2. überarbeitete und erweiterte Auflage
[45] Rapp C, Pfleger F (2009) Skriptum Hydraulik Praktikum. Fachgebiet Hydromechanik, Technische Universität München, Skript
[46] Rapp C, Zeiselmair A (2014) Educational Concept Supporting a Renewable Energies School in Africa. IAHR HydroLink (4):110–113
[47] Rapp C, Le Duc A, Pfleger F (2009) Skriptum Fluid Mechanics Laboratory. Fachgebiet Hydromechanik, Technische Universität München, Skript
[48] Rodi W (1993) Turbulence models and their application in hydraulics - a state of the art review, 3rd edn. International Association for Hydraulic Research, Delft

[49] Rössert R (1964) Hydraulik im Wasserbau. R. Oldenburg
[50] Schade H, Kunz E, Kameier F, Paschereit CO (2013) Strömungslehre. de Gruyter Lehrbuch, Walter de Gruyter & Co., Berlin, New York
[51] Schlichting H (1964) Grenzschicht-Theorie. Braun, G., Göttingen
[52] Schneider KJ (ed) (1998) Schneider Bautabellen, 13th edn. Werner-Verlag, Düsseldorf
[53] Schneider W (ed) (1978) Mathematische Methoden der Strömungsmechanik. Vieweg, Braunschweig
[54] Schwertfirm F (2005) Skriptum Hydromechanik III. Fachgebiet Hydromechanik, Technische Universität München, Skript
[55] Schäffler U, Jud M, Bierhance D, Schilcher M, Schwertfirm F, Rapp C (2011) GIS-gestütztes Preprocessing zur Generierung der Inputdatensätze für ein Computational Fluid Dynamics-basiertes hydrodynamisches Modell. In: DWA-Tagung Kassel: GIS und GDI in der Wasserwirtschaft, DWA, Kassel
[56] Siegerstetter L (2006) Instationäre Strömung in Druckleitungen. Skript, Fachgebiet Hydromechanik, TUM, München
[57] Sigloch H (2012) Technische Fluidmechanik. Springer, Berlin, Heidelberg
[58] Strobl T, Zunic F (2006) Wasserbau. Springer-Verlag, Berlin, Heidelberg, New York
[59] Szabó I (1975) Einführung in die Technische Mechanik, 8th edn. Springer
[60] Truckenbrodt E (1989) Fluidmechanik: Band 1, 3rd edn. Springer Handbook, Springer, Heidelberg
[61] Valentin F (2003) Skriptum Hydraulik II, Angewandte Hydromechanik. Lehrstuhl für Hydraulik und Gewässerkunde, Technische Universität München, Skript
[62] Vismann U (2015) Wendehorst Bautechnische Zahlentafeln. Springer Vieweg, Berlin
[63] Zanke UCE (2002) Hydromechanik der Gerinne und Küstengewässer. Parey, Berlin
[64] Zanke UCE (2013) Hydraulik für den Wasserbau, 3rd edn. Springer-Vieweg, Berlin
[65] Zuppke B (1988) Hydromechanik im Bauwesen, 3rd edn. Bauverlag, Wiesbaden